2011 Southern California Earthquake Center Annual Meeting

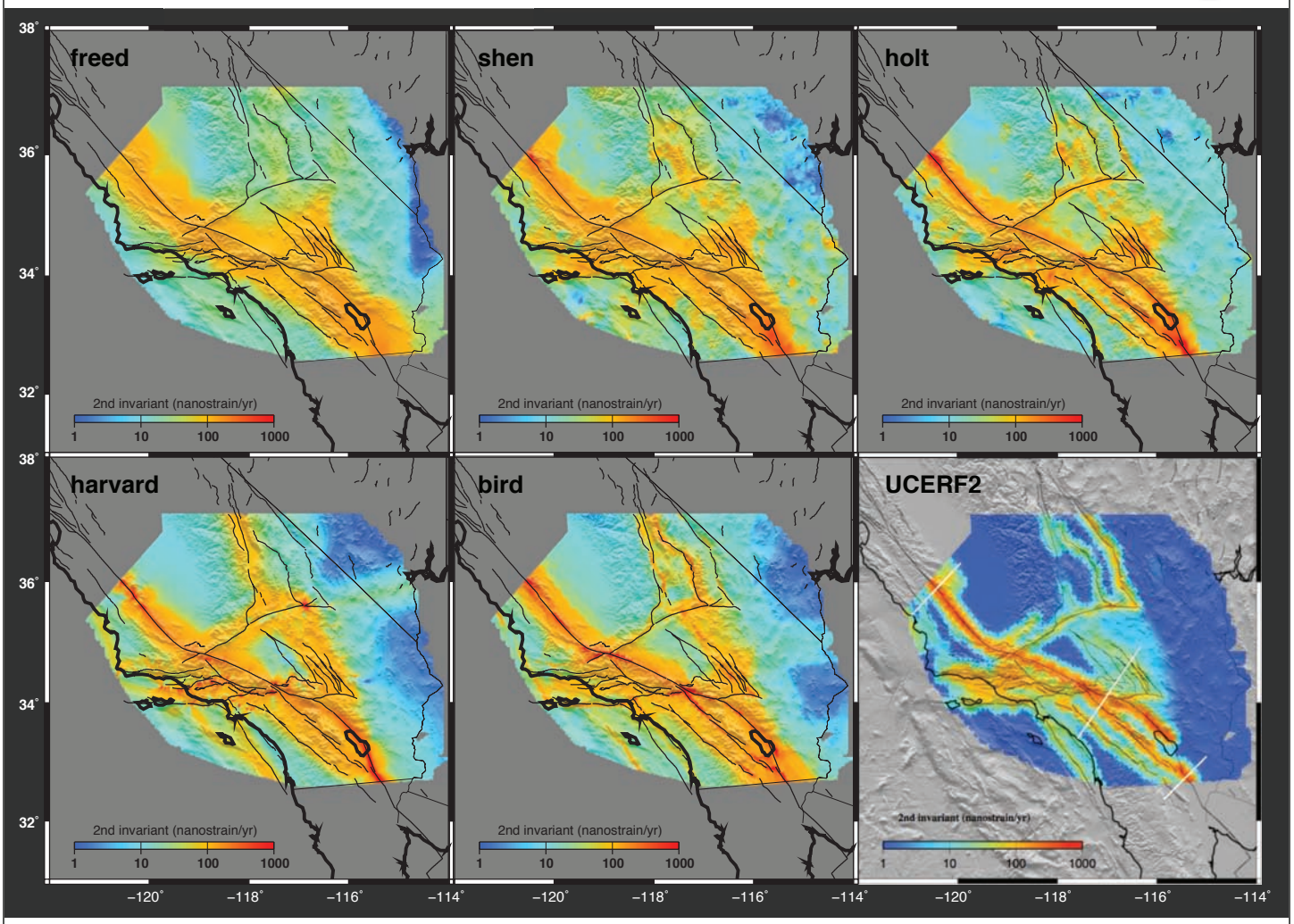

Proceedings and Abstracts, Volume XXI

September 11-14, 2011

SCEC

an NSF+USGS center

SCEC3 ORGANIZATION

Center Director, *Tom Jordan*

Deputy Director, *Greg Beroza*

Associate Director for Administration, *John McRaney*

Associate Director for Communication, Education, & Outreach, *Mark Benthien*

Associate Director for Information Technology, *Phil Maechling*

Special Projects & Events Coordinator, *Tran Huynh*

Research Contracts & Grants Coordinator, *Karen Young*

Administrative Coordinator, *Deborah Gormley*

Education Programs Manager, *Robert de Groot*

Digital Products Manager, *John Marquis*

Research Programmers, *Scott Callaghan, Sandarsh Kumar, Maria Liukis, Kevin Milner, Patrick Small*

Systems Administrator, *John Yu*

SCEC3 PLANNING COMMITTEE

Chair, *Greg Beroza*

Seismology, *Egill Hauksson, Elizabeth Cochran*

Tectonic Geodesy, *Jessica Murray-Moraleda, Rowena Lohman*

Earthquake Geology, *Mike Oskin, James Dolan*

Unified Structural Representation, *John Shaw, Kim Olsen*

Fault and Rupture Mechanics, *Judith Chester, Ruth Harris*

Crustal Deformation Modeling, *Liz Hearn, Kaj Johnson*

Lithospheric Architecture & Dynamics, *Paul Davis, Thorsten Becker*

Earthquake Forecasting & Predictability, *Terry Tullis, Jeanne Hardebeck*

Ground Motion Prediction, *Brad Aagaard, Rob Graves*

Seismic Hazard & Risk Analysis, *Paul Somerville, Nico Luco*

Southern San Andreas Fault Evaluation, *Tom Rockwell, Kate Scharer*

Working Group on California Earthquake Probabilities, *Ned Field*

Collaboratory for the Study of Earthquake Predictability, *Tom Jordan, Danijel Schorlemmer*

Extreme Ground Motion, *Tom Hanks*

Community Modeling Environment, *Phil Maechling*

SCEC3 ADVISORY COUNCIL

Jeffrey Freymueller, *Chair, U. Alaska*

Gail Atkinson, *U. Western Ontario*

Roger Bilham, *U. of Colorado*

Donna Eberhart-Phillips, *UC Davis*

John Filson, *U.S. Geological Survey (Emeritus)*

Jim Goltz, *CalEMA*

Bob Lillie, *Oregon State University (new member 2011)*

Anne Meltzer, *Lehigh University*

Dennis Mileti, *U. Colorado (Emeritus)*

M. Meghan Miller, *UNAVCO*

Farzad Naeim, *John A. Martin & Associates*

John Vidale, *U. Washington*

Andrew Whittaker, *U. Buffalo*

SCEC3 BOARD OF DIRECTORS

Tom Jordan, *Chair, USC*

Lisa Grant-Ludwig, *Vice-Chair, UCI (At-Large Member)*

Ralph Archuleta, *UCSB*

Peter Bird, *UCLA*

David Bowman, *CSUF (At-Large Member)*

Tom Brocher, *USGS Menlo Park*

Emily Brodsky, *UCSC*

Glenn Biasi, *UNR*

Steve Day, *SDSU*

James Dieterich, *UCR*

Yuri Fialko, *UCSD*

Tom Herring, *MIT*

Ken Hudnut, *USGS Pasadena*

Nadia Lapusta, *CalTech*

Jim Rice, *Harvard*

Paul Segall, *Stanford*

Bruce Shaw, *Columbia*

Jill McCarthy, *USGS Golden*

Cover Image: Southern California deviatoric strain rate fields generated by five models compared against earthquake probabilities from the Uniform California Earthquake Rupture Forecast, Version 2 (UCERF2). Geodetic surface deformation data will be incorporated in the next generation California earthquake hazard assessment (UCERF3). [*Figure from David Sandwell (UCSD) with contributions from the UCERF3/GPS Technical Activity Group.*]

Table of Contents

SCEC Annual Meeting Program

Sunday, September 11th

07:00 – 18:30 Registration Check-In (Hotel Lobby)

07:00 – 08:00 Breakfast (*Poolside*)

08:00 – 12:00 **WORKSHOP: Source Inversion Validation**

Conveners: *P. Martin Mai (KAUST), Morgan Page (USGS), and Danijel Schorlemmer (USC/GFZ)*

Location: *Palm Canyon Room*

The 2011 Source Inversion Validation (SIV) workshop will focus on the inversion results for the first test inversion problem, which is based on a dynamic rupture for an M ~6.6 strike-slip earthquake, embedded in a layered media. Synthetics at 40 sites are to be used for the inversion, forward-prediction from the obtained model at additional 16 sites are required to help assess the quality and robustness of the solution. Additionally, we will discuss the modelers experience with the SIV-wiki and the newly created benchmarking site in order to streamline the dissemination of future exercises (data and descriptions) and the upload and automated analysis and comparison capacities of the online toolbox.

We hope that many source-modeling teams will present their results and experience with the SIV exercise. However, general contributions on recent developments for source-inversion strategies are welcome as well. We also encourage presentations on finite-fault source studies for recent well-recorded earthquakes that highlight the challenges in kinematic rupture inversions.

08:00 Introduction

08:10 Recent Developments in the SIV Portal and Its Benchmarking Tools (*M. Mai, KAUST*)

08:20 SIV Modeling Teams on Their Results for Exercise: in1_dip (15 minutes per group)

09:20 Discussion: SIV Portal, Exercise inv1_dip, Future SIV Exercises

10:00 *Break*

10:15 Source Studeis of the Sept 2010 M 7.1 and Feb M 6.3 Earthquakes in New Zealand (*GNS Researchers*)

10:45 High Frequency Aspects of Earthquake Rupture Imaged By Back-Projection of Seismic Array Data (*J.-P. Ampuero, Caltech*)

11:15 Discussion: Back-Projection Constraints for Finite-Fault Inversion, New Data for SIV Exercises

12:00 *Adjourn*

08:00 – 12:00 **WORKSHOP: El Mayor-Cucapah Science and Earthquake Response**

Conveners: *Mike Oskin (UC Davis), Sinan Akciz (UC Irvine), and Ramon Arrowsmith (ASU)*

Location: *Horizon Ballroom*

More than a year has passed after the M7.2 El Mayor Cucupah earthquake. The event provided a view of a major earthquake in Southern California and opportunities for new discoveries in earthquake science and for reflection on future earthquake response activities. The event also engendered important cross border scientific collaborations. Our goals for this workshop are to review the recent research results as well as to take away lessons for the next major Southern California earthquake. Strict time constraints for the presentations will be enforced with 10 minutes on science and 3 minutes on lessons for response.

<u>Introduction</u>

08:05 The 4 April 2010 El Mayor-Cucapah earthquake source, from initial glimpse to synoptic overview (*K. Hudnut, USGS*)

<u>Seismology</u>

08:20 The 4 April 2010 El Mayor - Seismological evidence and dynamic model of reverse rupture propagation during the 2010 M7.2 El Mayor Cucapah earthquake (*L. Meng, Caltech*)

08:35 Seismic field response to the El Mayor - Cucapah earthquake (*E. Cochran, USGS*)

08:50 Spatial distribution of the 4 April, 2010 (Mw7.2) El Mayor-Cucapah seismic sequence using a local network (*R. Castro, CICESE*)

GPS/InSAR Geodesy

09:05 Postseismic deformation following the El Mayor-Cucapah earthquake from GPS and InSAR (*A. Gonzalez, CICESE*)

09:20 Crustal deformation associated with the Mw7.2 2010 El Mayor-Cucapah earthquake from GPS geodesy (*J. Spinler, Arizona*)

09:35 Satellite SAR geodetic imaging response and joint geodetic-teleseismic inversion for fault slip evolution models of the El Mayor-Cucapah earthquake (*E. Fielding, JPL*)

09:50 *Break*

LiDAR and UAVSAR

10:00 Airborne lidar of the El Mayor-Cucapah surface rupture: Rapid fault mapping and discovery of hidden structures and distributed deformation (*M. Oskin, UC Davis*)

10:15 Horizontal and vertical deformation induced by the 2010 El-Mayor-Cucapah earthquake, as observed from SPOT and LiDAR imagery using COSI-Corr (*S. Leprince, Caltech*)

10:30 Assessment of coseismic slip variation from terrestrial LiDAR scans of the El Mayor-Cucapah surface rupture (*P. Gold, UC Davis*)

10:45 UAVSAR Observations of the 2010 M 7.2 El Mayor-Cucapah Earthquake (*A. Donnellan, JPL*)

Surface Rupture Mapping

11:00 UAVSAR as an Aid to Fault Rupture Mapping in the Yuha Desert (*J. Treiman, CGS*)

11:15 Structural Controls on the Surface Rupture Associated with the Mw7.2 El Mayor-Cucapah Earthquake of 4 April 2010: A Comparative Analysis of Scarp Array Kinematics, Orientation, Lithology and Width (*O. Teran, CICESE*)

11:30 Rupture Pattern of the 1892 Laguna Salada Earthquake: A precursor to 2010 El Mayor-Cucapah (*K. Mueller, U Colorado*)

11:45 Discussion

12:00 *Adjourn*

12:00 – 13:00 Lunch (*Poolside / Terrace*)

12:00 – 15:00 SCEC Board of Directors Lunch Meeting (*Tapestry Room*)

13:00 – 17:00 SCEC CME Leadership Meeting (*Oasis Room III*)

13:00 – 17:00 Teacher Workshop (*Oasis Room II*)

13:00 – 17:00 WORKSHOP: Automating the Transient Detection Process

Conveners: *Rowena Lohman (Cornell) and Jessica Murray-Moraleda (USGS)*

Location: *Palm Canyon Room*

The next phase of the Transient Detection effort within SCEC addresses the goal of implementing a geodetic transient detector by the end of SCEC III. In this workshop we will demonstrate the use of the CSEP-style infrastructure that can be used by Transient Detection participants once their code has been automated. Participants are encouraged to discuss any automated or retrospective algorithms that they've developed, as well as the results from these on the synthetic test data sets or on real geodetic data. Discussions will focus on the issues that face researchers who seek to automate their approaches, as well as the priorities for the next year.

13:00 Introduction (*R. Lohman, Cornell*)

13:30 Presentations on Individual Algorithms

15:00 *Break*

15:15 Introduction to the Automatic Testing Facility and Example Algorithm and Codes

16:00 Discussion 1: Barriers in the Way of Implementing Codes, Suggestions for Changes to the Testing Facility

16:30 Discussion 2: What are Our Priorities for the Next Several Years?

17:00 *Adjourn*

13:00 – 17:00 **WORKSHOP: Southern San Andreas Fault Evaluation (SoSAFE)**

Conveners: *Kate Scharer (USGS) and Ramon Arrowsmith (ASU)*

Location: *Horizon Ballroom*

The primary goal of the Southern San Andreas Fault Evaluation (SoSAFE) project is to understand the timing of and slip due to earthquakes that occurred along the southern San Andreas and San Jacinto faults over the last 2000 years. This workshop will combine both individual presentations summarizing major SoSAFE research results and group discussion about the implications and use of these results. Discussions are designed to address field- and technology-related challenges in paleoseismology and slip rate studies, as well as wider discussion on the scope and priorities of SoSAFE in future years.

13:00 Introduction

13:15 Talk 1: Evidence from Parkfield Study: Implication of Extreme Events (*N. Toke, Utah Valley*)

13:30 Group Discussion

13:40 Talk 2: New Work on the San Jacinto (*N. Onderdonk, CSULB*)

13:55 Group Discussion

14:05 Talk 3: Long-Term Slip Rates on the San Jacinto (*K. Blisniuk, UC Davis*)

14:20 Group Discussion

14:30 Talk 4: Short-Term Slip Rates on the San Jacinto (*J. Spinler, Arizona*)

14:45 Group Discussion

14:55 *Break*

15:10 Talk 5: Slip/Event Data Compilation: What Do We Know About the Slip History of the SAF System? (R. Arrowsmith, ASU and R. Weldon, Oregon)

15:30 Group Discussion

- Is the SAF/SJF system generally characteristic in slip at a point?
- Are these faults really segmented?
- What is the largest earthquake that can occur along the system based on the paleoseismic record?
-What do geomorphic offsets represent, or more importantly, how we can use such data to develop rupture histories when it can be shown that not all earthquakes are clearly recorded as separate offsets.

15:45 Talk 6: Earthquake Response Given Large Southern California Event – Background and Existing Plans: USGS (*K. Hudnut*), CGS Plans (*J. Treiman*), CalEMA (*J. Goltz*) - 15 minutes each

16:30 Group Discussion

- Given experience in recent earthquakes, what technologies should be adopted?
- Should we assign areas or other coordination given likely limitations to internet access?
-Coordination with other groups/agencies?

16:45 Discussion and Feedback

- What are the priorities for SoSAFE for the next several years?
- How shall we coordinate field review?

17:00 *Adjourn*

13:00 – 17:00 Poster Set-Up: Group A (*Plaza Ballroom*)

17:00 – 18:00 **SPECIAL INVITED TALK**: **The Great 2011 Tohoku, Japan Earthquake (Mw9.0) – An Unexpected Event**

Presenter: *James Mori (DPRI, Kyoto University)*

Location: *Horizon Ballroom*

On March 11, 2011, the northeast coast of Honshu experienced the largest historical earthquake for Japan (Mw9.0). Based on about 400 years of historical records that included 18 M7 to 8 earthquakes, there was thought to be fairly good knowledge of the expected sizes and locations of expected large events in the Tohoku region of Japan. So this event was a shocking surprise to the seismological community. The unprecedented size of the earthquake caused very large tsunamis that inundated coastal regions, which were probably among the best tsunami-prepared regions in the world. Tsunami heights of 15 to 30 meters topped sea walls that were typically about 10 meters high. The effects of the tsunami were amplified by large subsidence of much of the coastal areas by up to 2 meters. Most of the extensive damage (US$200 to 300 billion) and loss of lives (over 27,000) that occurred on the east coast of Honshu were due to the tsunami and not the strong shaking.

There is a strong frequency dependence to the spatial distribution of the radiation of seismic waves. The largest slip and source of the long-period waves originate on the shallow portion of the thrust plane close to the Japan trench. In contrast, the short-period radiation has strong sources deeper on the fault plane to the west of the hypocenter.

The mainshock has triggered other earthquake activity across Japan with increases in seismicity in many regions, including 13 volcanoes. There have been at least 8 crustal earthquakes in the M5.0 to M6.7 range outside of the immediate aftershock zone, which are apparently related to the Tohoku earthquake. These events are likely due to both static and dynamic stress changes caused by the mainshock.

The society and infrastructure of Japan is struggling to recover from the widespread effects of this earthquake. Power shortages, nuclear power plant issues, and the large number of displaced people have caused severe problems for the country.

18:00 – 20:00 SCEC Annual Meeting Welcome Dinner (*Poolside / Terrace*)

18:30 – 20:30 SCEC Advisory Council Dinner Meeting (*Tapestry Room*)

20:00 – 22:30 **POSTER SESSION I: Group A** (*Plaza Ballroom*)

Monday, September 12th

07:00 – 08:00 Registration Check-In (*Hotel Lobby*)

07:00 – 08:00 Breakfast

08:00 – 10:30 **PLENARY SESSION I: State of the SCEC**
Location: *Horizon Ballroom*

08:00 Welcome and State of the Center (*T. Jordan, SCEC/USC*)

08:30 Report from NSF (*J. Whitcomb, NSF*)

08:45 Report from USGS (*M. Blanpied/E. Lemersal, USGS*)

09:00 Communication, Education, and Outreach Highlights (*M. Benthien, SCEC/USC*)

09:30 SCEC3 Science Accomplishments (*G. Beroza, Stanford*)

10:30 – 11:00 Break

10:30 – 18:30 Registration Check-In (*Hotel Lobby*)

11:00 – 13:00 **PLENARY SESSION II: Science and Engineering Issues from Earthquake and Tsunami Hazards Along the California Coast**
Moderator: *J. Baker (Stanford)*
Location: *Horizon Ballroom*

11:00 **Offshore Faulting and Associated Hazards Along the Southern California Coast** (*J. Shaw, Harvard*)

Over the past decade, SCEC researchers have contributed to a growing understanding of the complex systems of active faults that lie offshore along the southern California coast. In particular, acquisition and analysis of marine seismic reflection data has helped to identify and map a series of large strike- and oblique-slip faults, including the Newport-Inglewood-Rose Canyon, Palos Verdes, San Pedro Bay, San Diego Trough, San Clemente, Santa Catalina, and other systems. In addition, these data have been used to identify and describe a series of emergent and blind-thrust faults in the Santa Barbara Channel and Santa Monica Bay (e.g., Pitas Point, Channel islands, Anacapa-Dume) and in the Inner Borderlands (e.g., Oceanside, Thirtymile Bank, Carlsbad). The offshore thrust systems, in particular, may pose significant seismic hazards that have not yet been assessed comprehensively. Thrust faults generally represent large, moderately dipping surfaces that form large earthquake source areas capable of generating moderate to large (M≥7) earthquakes. Coseismic uplift patterns and accelerations, which are often most intense in the hanging walls of dip slip systems, could produce hazardous ground shaking along much of the southern California coastline. Many of these individual structures are aligned along strike with other thrust faults, such as the Channel Islands and Anacapa-Dume faults, and/or interact with strike-slip fault systems within the seismogenic crust. These cases present the possibility of larger (M 7.5 to 8+) and more complex multi-segment ruptures. Such events, while perhaps rare, would likely present extreme levels of ground shaking for coastal southern California, and may also cause seafloor displacements that generate tsunamis. Despite these potential hazards, there is much that we do not know about these fault systems that is necessary to properly characterize them. In particular, we lack definitive late Quaternary and Holocene slip rates, as well as displacements and ages of past earthquakes, on most of these systems.

11:20 **Seismic Hazards along the California Coast: Issues for California's Nuclear Power Plants**
(*N. Abrahamson, PG&E*)

Following the 2011 Tohoku earthquake, there has been increased concern with the seismic safety of the California's nuclear power plants located along the California coast. At low probability levels important for critical structures, the seismic hazard along the central and southern California coast is dominated by a system of strike-slip faults located 0-10 km offshore and by thrust faults located both onshore and offshore within 10 km of the coastline.

Because the large magnitude of the Tohoku earthquake was not considered as part of the design basis for Japanese nuclear plants, there has been a focus on possible large magnitude earthquakes in California. This has focused concern on earthquakes with larger magnitudes than considered in developing the design ground motions for California nuclear power plants that could occur for multi-segment ruptures. This focus on earthquake magnitude is missing the key issue for seismic safety at nuclear power plants. Structures are designed for ground motions, not earthquake magnitudes. This sounds circular because the design ground motion is developed considering earthquake magnitude, but the distinction is important. The safety related systems, structures, and components at nuclear power plants are stiff and respond to high frequency ground motions (typically in the 3-30 Hz range). Both empirical observations and numerical

simulations of ground motions have shown that, for sites located close to faults, the high frequency ground motion scales only weakly with magnitude for magnitudes greater than 6.5. For probabilistic hazard, the decreased rate for larger magnitudes required to balance the moment-rate on the fault leads to lower overall hazard (and risk of core damage) if larger magnitudes are included in the source characterization. Unusually large high frequency ground motions that would exceed the design basis of nuclear power plants are most likely to come from nearby M6.5-M7 earthquakes that are unusually energetic (ground motions more than 2 standard deviations above the median) rather than from unusually large magnitudes. In contrast to ground motions, tsunami waves heights scale strongly with earthquake magnitude or slide dimension. For tsunamis hazard, the possibility of larger magnitude events is a key factor.

11:40 Group Discussion

12:00 **Tsunami Interaction with Nearshore Infrastructure** (*P. Lynett, USC*)

In this talk, the well-established approaches of coupling tsunami generation to seismic seafloor motion and the following trans-oceanic wave propagation will be briefly introduced. The focus of the presentation will be on the complex transformation of the tsunami as it approaches very shallow waters, as well as how these possibly large and fast-moving water waves interact with coastal infrastructure. Two examples of coastal impact will be discussed. First, a simulation of a tsunami flooding an urban coastal town will be shown, and we the creation and behavior of the many turbulent wakes that form behind each structure will be discussed. A conclusion of this example is that it is possible to achieve very high fluid forces away from the immediate shoreline; having a row of structures seaward of a given location does not necessarily protect against the flow. The second example will look at tsunami-induced currents in ports and harbors. Tsunamis, or "harbor waves" in Japanese, are so-named due to the common observation of enhanced damage in harbors and ports. However, the dynamic currents induced by these waves, while regularly observed and known to cause significant damage, are poorly understood. We will show that the strongest currents in a port are governed by horizontally sheared and rotational shallow flow with imbedded turbulent coherent structures. Without proper representation of the physics associated with these phenomena, predictive models may provide drag force estimates that are an order of magnitude or more in error. Such an error can mean the difference between an unaffected port and one in which vessels 300 meters in length drift and spin chaotically through billions of dollars of infrastructure.

12:20 **Seismic Risk Challenges at Nuclear Power Plants** (*G. Hardy, SGH*)

Recent earthquakes in Japan have exceeded their seismic design basis. The 2007 Niigataken Chuetsu-Oki Earthquake (NCO) earthquake affected the Kashiwazaki nuclear power plant with exceedances of more than a factor of two on the design in-structure accelerations. The process that Japanese utility Tokyo Electric Power has undergone to establish the seismic safety of the Kashiwazaki plants (largest nuclear plant in the world with 7 units) has ramifications for all nuclear plants, including SONGS and Diablo Canyon in California. Likewise, the 2011 Tohoku earthquake resulted in ground motions at several of the Japanese nuclear power plants that exceeded their new seismic design basis which had been increased following the NCO earthquake. The Nuclear Regulatory Commission as well as the nuclear utility industry are studying the results of the Tohoku earthquake and the resulting tsunami on the nuclear power industry. Lessons learned will help reduce risks in the US in the future.

This presentation will focus on the lessons learned from these recent earthquakes affecting nuclear power plants in Japan. The focus will be on characterizing the nature of the design basis exceedances, the seismic upgrades that were required at these Japanese plants, and the expected ramifications for US nuclear power plants.

12:40 Group Discussion

13:00 – 14:30 Lunch (*Poolside / Terrace*)

13:00 – 14:30 "What's Next?" Student Luncheon (*Tapestry Room*)

14:30 – 16:00 **POSTER SESSION II: Group A** (*Plaza Ballroom*)

16:00 – 18:00 **PLENARY SESSION III: Are We Properly Characterizing Extreme/Rare Events?**

Moderator: *J. Hardebeck (USGS)*

Location: *Horizon Ballroom*

16:00 **22 February 2011 Christchurch Earthquake** (*B. Bradley, Cantebury*)

An overview of the 22 February 2011 Christchurch earthquake is presented in the context of characterization of extreme/rare events. Focus is given to the earthquake source, observed near-source strong ground motions, and effects of site response, while structural response and consequences are mentioned for completeness. For each of the above topics comparisons and discussions are made with predictive models for each of phenomena considered. In light of the

observations and predictive model comparisons, the author's opinion on improving the characterization of such extreme/rare events, and their appropriate consideration in seismic design is presented.

16:30 **Structural Linkage of Onshore and Offshore Thrust Systems Across the Ventura Fault and Prospects for Large Earthquakes in the Transverse Ranges** (*J. Hubbard, Harvard*)

The Ventura Avenue anticline, western Transverse Ranges, is one of the fastest uplifting structures in southern California, rising at ~5 mm/yr (Rockwell et al., 1988). However, there is disagreement about whether this structure poses a seismic hazard, due to uncertainty about the nature of the Ventura fault, which lies along its southern margin. Either the Ventura fault extends to seismogenic depth beneath the anticline (e.g. Sarna-Wojcicki et al., 1976), or it is a shallow, bending-moment fault that does not pose a hazard (e.g. Yeats, 1982). Seismic data across the tip of the fault suggest that it deforms late Pleistocene and younger strata, implying that the fault is active. Given that the fault trace extends directly through Ventura, CA, distinguishing between these two interpretations is very important for seismic hazard assessment.

We use well data, industry seismic reflection profiles, and two seismic profiles acquired by our group in 2010, to construct a more complete 3D model of the system. Based on dipmeter logs and seismically-imaged stratigraphic cutoffs, we show that the N-dipping Ventura fault extends to seismogenic depth beneath the anticline. Fault offset increases with depth, implying that the fault has propagated upward over time. We interpret the Ventura Avenue anticline to be a fault-propagation fold underlain by an active thrust ramp. A decrease in the uplift rate at 30 ka (Rockwell et al., 1988) is consistent with a breakthrough of the fault at that time, although it is still buried by sedimentary cover.

The Ventura fold trend continues offshore and coincides with a set of oil fields. A 3D seismic dataset across the Dos Cuadras field, which lies along the trend, shows that it is a fault-propagation fold, underlain by the N-dipping Pitas Point thrust. Based on our and others' mapping, the Ventura and Pitas Point faults form an en echelon system that extends >40 km offshore. Other regional faults, including the San Cayetano and Red Mountain faults, link with this system; we suggest that at 15 km depth, these faults may form a continuous surface. Linkage of the Ventura/Pitas Point fault could generate a M7.3 earthquake, while rupture with other regional faults could produce larger events. We provide 3D models of these faults and estimate the magnitudes of potential multi-segment earthquakes. Finally, we show that GPS data are consistent with a high shortening rate (>6 mm/yr) across the anticline, reinforcing its hazardous nature.

17:00 **Large Co-Seismic Uplift of Coastal Terraces Across the Ventura Avenue Anticline: Implications for the Size of Earthquakes and the Potential for Tsunami Generation** (*T. Rockwell, SDSU*)

Much of the crustal shortening in the western Transverse Ranges near Ventura is accommodated by the Ventura Avenue anticline, a propagation thrust that deforms every geomorphic landform into the late Holocene. A sequence of late Pleistocene fluvial terraces are folded across the anticline along Ventura River and record uplift for the past ~100 ka. The "bedrock" itself that forms the core of the fold are marine sediments that are as young as 200-300 ka, and these sediments have experienced as much as 2.7 km of structural relief, making this one of the fastest growing folds in southern California. At Pitas Point, the presence of 4-5 emergent Holocene marine terraces, with the highest reaching an elevation of nearly 40 m, demonstrate that fold growth has continued to the present. The first emergent terrace has a back-edge (paleo-shoreline) at about 8-9 m elevation, whereas the modern shoreline reaches to about 1-2 m. This requires uplift of 6-8 m of this paleo-shoreline. Radiocarbon dates from an archeological site with house structures on the paleo-shoreface show that the site and associated beach date to about 0.5-0.9 ka B.P. and were abandoned after emergence. An older, abandoned village site sits on the fore-edge of the 2nd emergent terrace at about 15-20 m elevation, and radiocarbon ages place the age of this terrace at about 2-2.2 ka. These observations argue that the Holocene terraces record discrete uplift events, accompanied by village abandonment, with uplift in the range of 6-8 m per event. The recurrence for such events appears to be on the order of 1 ka. For a 45° dipping fault at depth, this requires displacements to be in the range of 8-10 m, which are typical for earthquakes in the M7.5-7.8 range but suggests that the VAA may not act alone. As the anticline trends offshore at Pitas Point, such co-seismic uplift events will directly displace large volumes of water and potentially generate tsunamis with wave heights that are similar in magnitude to the uplift; this tsunami would be focused southward towards Los Angeles. This may constitute an extreme event if it were to occur today, but appears to be typical for this structure.

17:30 Group Discussion

16:00 – 21:00 Poster Removal: Group A / Poster Set-Up: Group B (*Plaza Ballroom*)

19:00 – 21:00 SCEC Honors Banquet (*Poolside*)

21:00 – 22:30 POSTER SESSION III: Group B (*Plaza Ballroom*)

Tuesday, September 13th

07:00 – 08:00 Breakfast

08:00 – 09:00 **PLENARY SESSION IVA: Operational Earthquake Forecasting - State of Knowledge and Issues for Implementation**

Moderator: *A. Michael (USGS)*

Location: *Horizon Ballroom*

08:00 **Operational Earthquake Forecasting and Decision-Making in a Low-Probability Environment: Lessons from L'Aquila and Application in California** (*T. Jordan, SCEC/USC*)

Operational earthquake forecasting (OEF) is the dissemination of authoritative information about the time dependence of seismic hazards to help communities prepare for potentially destructive earthquakes. Most previous work on the public utility of OEF has anticipated that forecasts would deliver high probabilities of large earthquakes; i.e., deterministic predictions with low error rates (false alarms and failures-to-predict) would be possible. This expectation has not been realized; the seismic cycle is very unsteady, and the search for diagnostic precursors has not yet produced successful short-term prediction schemes. An alternative to deterministic prediction is probabilistic forecasting based on empirical statistical models of aftershock triggering and seismic clustering. During periods of high seismic activity, short-term earthquake forecasts can attain prospective probability gains in excess of 100 relative to long-term forecasts. The utility of such information is by no means clear, however, because even with hundredfold increases, the probabilities of large earthquakes typically remain small, rarely exceeding a few percent over forecasting intervals of days or weeks. Civil protection agencies have been understandably cautious in implementing OEF in this sort of "low-probability environment."

The need to move more quickly has been underscored by recent seismic crises, such as the 2009 L'Aquila earthquake sequence, in which an anxious public was confused by informal and inaccurate earthquake predictions. After the L'Aquila disaster, the Italian Department of Civil Protection appointed an International Commission on Earthquake Forecasting (ICEF), which I chaired, to review the state of knowledge and recommend guidelines for OEF utilization. Our report has just been published (Ann. Geophys., 54, 4, 2011; doi: 10.4401/ag-5350; http://www.annalsofgeophysics.eu/index.php/annals/article/view/5350). This presentation will review the ICEF guidelines and comment on their application in California. I will emphasize how authoritative statements of increased hazard, even when the absolute probability is low, can provide a psychological benefit to the public by filling information vacuums that lead to informal predictions and misinformation. Formal OEF procedures based on probabilistic forecasting appropriately separate hazard estimation by scientists from the decision-making role of civil protection authorities. The prosecution of seven Italian scientists on manslaughter charges stemming from their actions before the L'Aquila earthquake makes clear why this separation should be explicit in defining OEF protocols.

08:30 Group Discussion

09:00 – 10:00 **PLENARY SESSION IVB: Ground Motion Simulation Validation**

Moderators: *N. Luco (USGS) and K. Olsen (SDSU)*

Location: *Horizon Ballroom*

SCEC has established a Technical Activity Group (TAG) focused on Ground Motion Simulation Validation (GMSV) in order to develop and implement testing/rating methodologies via collaboration between ground motion modelers and engineering users. A SCEC workshop was held in January 2011 to kick off the GMSV TAG. During this workshop, the discussion included selection of ground motion simulation scenarios, simulation models, goodness-of-fit methodologies and metrics, engineering application targets, archival and distribution of the simulations/validations, appropriate platform(s) for the validations, and operational issues (including funding issues and possible coordination with OpenSees and NGA-E). During this plenary session the recommendations from the workshop will be reviewed and opened up for additional input from interested SCEC participants.

10:00 – 10:30 Break

10:30 – 12:30 **PLENARY SESSION V: How Do We Develop the Community Stress Model?**

Moderator: *T. Becker (USC)*

Location: *Horizon Ballroom*

10:30 **Fault Stress Heterogeneity and Implications for Rupture Dynamics** (*J.-P. Ampuero, Caltech*)

I will present and discuss theoretical constraints and observational evidence on the spatial distribution of stress in active fault zones, with emphasis on the statistical description of stress heterogeneities over a broad range of length scales. I will illustrate through dynamic rupture simulations the possible implications of such heterogeneities on the

evolution of earthquake rupture and on the induced strong ground motions. One of the key issues raised by the recent Tohoku-Oki earthquake is the possibility of a very different frequency content of slip in different areas of a fault. I will offer an interpretation of this observation, although non-unique, in terms of rupture proagation through the residual stress field left by previous seismicity.

11:00 **Earthquake Focal Mechanisms Imply Homogeneous Stress at Seismogenic Depths** (*J. Hardebeck, USGS*)

Stress at seismogenic depths is often thought to be heterogeneous, based on the variety of earthquake focal mechanisms present in some catalogs. However, when differences in tectonic regime and the sizable focal mechanism uncertainties are accounted for, the focal mechanisms appear more uniform. On average, the closer two events are in space, the more similar their focal mechanisms, so comparing events over a large area increases the apparent heterogeneity. Additionally, even relatively well-constrained focal mechanisms may have uncertainties of 25° or more; these errors increase the apparent focal mechanism variability, especially for similar mechanisms. It has been proposed that homogeneous focal mechanisms could be compatible with an extremely heterogeneous crustal stress field. The hypothesis is that the stress field contains significant heterogeneity in stress orientation, and earthquakes preferentially occur where the local stress tensor aligns with the stressing rate tensor, which loads the faults that are well-oriented in those areas. Earthquake focal mechanisms would reflect the stressing rate tensor, and uniform tectonic loading would produce relatively uniform focal mechanisms. A testable prediction of this model is that focal mechanisms before and just after a large earthquake should align with different stress fields: the tectonic loading and the mainshock static stress perturbation, respectively. I test this prediction using aftershocks of the Landers earthquake. The observed rotation of focal mechanisms near the mainshock rupture could represent a true coseimic stress rotation, so I limit my test to aftershocks far enough away from the mainshock that the stress change is too small to rotate the stress field. I identify the aftershock zone as the region where post-Landers events are significantly more consistent with triggering by the Landers-induced static stress perturbation than the pre-Landers events. I find that these aftershocks also align with the same stress field as the pre-Landers mechanisms, contradicting the heterogeneous stress model. The aftershocks occurred on faults that were well oriented for failure in the pre-Landers background stress field and further loaded by the Landers-induced static stress change. The heterogeneous stress model, if it applies anywhere, should apply to the complex active fault system in southern California. This counterexample is evidence that the heterogeneous stress model is not widely applicable.

11:30 **Strain-Based Interpretation of Southern California Focal Mechanism Data and Implications for a Community Stress Model** (*I. Bailey, USC*)

The observations based on recorded motion (e.g. seismograms and geodetic data) that are typically used to constrain the crustal stress field are more directly related to strain. Studying these data directly in terms of strain can help to better understand the degree to which we can constrain crustal stress. Here, we examine characteristics of focal mechanisms of small earthquakes (ML<5), which sample coseismic strain throughout the seismogenic crust. Considering southern California as a whole, the average properties of focal mechanisms are remarkably consistent with the orientation of relative plate motion. This is most simply interpreted in terms of an overlying homogeneous stress field driven by plate tectonics. At the scale of large (~50-250 km) fault zones, average properties reflect the dominant surface trace orientation of the fault zones. While a stress based analysis may interpret these orientations in terms of spatial variation of the stress field, distinct structural properties of the individual fault zones are likely to account for much of this signal. Within individual fault zones, there is a large amount of focal mechanism heterogeneity that can generally be related to geometrical complexities. This may be interpreted as heterogeneity of the stress field related to concentrations of stress at fault terminations, but can also be interpreted as the interaction of a smooth stress field with rheological complexity. Given the wide range of earthquake and fault length-scales, we can make an intuitive argument that the stress field has a hierarchical nature with different amplitude variations over a wide range of length-scales. However, limitations in the resolution and accuracy of the strain-based data, or knowledge of the pre-existing fault structures and rheology, will limit the smallest scale to which we can constrain the stress field. Hence, it is important to understand the length scales over which a community stress model can explain the strain-based observations and the limiting factors of its resolution.

12:00 Group Discussion

12:30 – 14:00 Lunch (*Poolside / Terrace*)

12:30 – 14:00 SCEC Advisory Council Executive Session – Working Lunch (*Executive Boardroom*)

14:00 – 15:30 **DISCUSSION: Special Fault Study Areas**
Moderator: *M. Oskin (UC Davis)*
Location: *Palm Canyon Room*

14:00 – 15:30 **POSTER SESSION IV: Group B** (*Plaza Ballroom*)

15:30 – 17:00 **PLENARY SESSION VIA: New Directions in Earthquake Forecasting**

Moderator: *I. Zaliapin (UNR)*

Location: *Horizon Ballroom*

15:30 **UCERF3 – Progress on an Operational Earthquake Forecast for California** (*E. Field, USGS*)

The Working Group on California Earthquake Probabilities (WGCEP) is actively building the 3rd Uniform California Earthquake Rupture Forecast (UCERF3). The main innovations for this model will be: 1) the relaxation of fault segmentation assumptions and the inclusion of multi-fault ruptures; and 2) the addition of spatiotemporal clustering (earthquake triggering and aftershocks), which will form the basis of an operational earthquake forecast. Our plan for both these enhancements was bolstered tragically by the 2011 Tōhoku, Japan and Christchurch, New Zealand earthquakes. In addition to giving an overview and progress report on the UCERF3 development, this talk will strive to emphasize the following more general themes: a) building a useful, state-of-the-art, system-level model inevitably leads to unearthing deep and interesting scientific questions; b) object-oriented design and programming, plus high performance computing, are key to success; c) physics-based simulators are becoming more and more critical to the forecasting enterprise; and d) none of this could happen without SCEC (including the intern program).

16:00 Group Discussion

16:15 **The Future of Earthquake Forecasting: The Role of Earthquake Simulators** (*J. Dieterich, UCR*)

Earthquake simulators provide a physics-based and self-consistent framework for generating region-specific models of earthquake occurrence. Simulations typically consist of ≥100,000 events and span tens of thousands of years. Earthquake simulation capabilities are rapidly evolving – current capabilities now include detailed portrayals of geometrically complex fault systems at regional scales that incorporate physics-based representations of earthquake slip (including space-time clustering effects) slow slip events, and continuous fault creep. Some areas where simulators may make unique contributions to earthquake forecasting include 1) deterministic modeling of short-term clustering of large events that is linked to material parameters and evolving stress conditions; 2) integration of the short-term (minutes to years) predictability of earthquakes, and long-term processes (100-1000 years) that condition fault systems to fail in great earthquakes; 3) characterization of possible location-specific interactions that control the statistics of earthquake occurrence; 4) statistical characterizations of earthquake occurrence over time scales that greatly exceed our observational record (which is short compared to the typical recurrence times for large and great earthquakes); 5) possible precursory, or triggering, interactions between slow slip events and great earthquakes in subduction zones; 6) generation of multiple synthetic catalogs to test proposed forecasting algorithms.

16:45 Group Discussion

17:00 – 18:30 **PLENARY SESSION VIB: SDOT Interdisciplinary Group - What Is Needed To Make Progress On Understanding Stress Transfer From Plate Motion To Crustal Faults?**

Moderator: *K. Johnson (Indiana)*

Location: *Horizon Ballroom*

17:00 **An Integrated View of the Mw 6 Earthquake Sequence at Parkfield** (*S. Barbot, Caltech*)

Advances in geophysical monitoring now provide an extensive set of observations of all aspects of the earthquake cycle. Yet, unifying physical models that connect these observations into a coherent picture are lacking. At the same time, laboratory experiments and theoretical developments provide an increasingly detailed understanding of the fault physics, offering the basis for an extrapolation to natural conditions.

In this study, we bridge the gap between observations and fault physics by developing the first model of the full earthquake cycle that explains a number of interesting and robust observations of the crustal dynamics at Parkfield. Despite the similarities between the repeating Mw 6 earthquakes and their short recurrence times (from 12 to 32 years for 5 events until 1966), the latest rupture of 2004 defied the odds by taking place a decade later than anticipated and initiating at the south end to propagate northward, contrarily to all previous events.

We build our model of fault friction using the spatial patterns of microseismicity, the time series of GPS displacements in the 1999-2010 period, the InSAR data, and the GPS offsets of the 2004 earthquake. We also consider the slip distribution of the 1966 event and the historical catalog of recurrence times and hypocenter locations. We show the special role of microseismicity, which marks the transition between stable and unstable friction and circumscribes the seismogenic zone. We use the program BICYLE (Boundary Integral Cycles of Earthquakes) of Lapusta & Liu (2009) to solve the elasto-dynamic equations that govern the fault slip evolution. We obtain a sequence of Mw~6 earthquakes that can explain the observed variability of hypocenters and reproduce the geodetic observations of surface deformation in the co- and postseismic periods associated with the 2004 event. The change of hypocenter between 1966 and 2004 and the delay of the latest event is consistent with the occurrence of a swarm of smaller-magnitude earthquakes during the 1992-1994 period and these two locations being close to the boundary of the seismogenic zone. Our study introduces a methodology capable of integrating seismological and geodetic observations into a coherent physical model of the earthquake cycle. Our approach can serve as an important tool to investigate the effect of other components of earthquake physics and to help understand and mitigate seismic hazards around active faults.

17:20 **Dramatic Lithospheric Thinning Beneath Rifted Regions of Southern California** (*V. Lekic, Brown*)

Although rifting is fundamental to the evolution of the continental lithosphere, what happens to the underlying mantle lithosphere during rifting is poorly known, in large part because seismologists have yet to directly image lithospheric variations across an active rift system. Indeed, constraints on the kinematics and dynamics of rifting are almost exclusively provided by surface geologic and geochemical observations combined with geophysical imaging of the crust. Here, we detect mode conversions of teleseismic shear waves (Sp phases) across the lithosphere-asthenosphere boundary (LAB) beneath Southern California, and present maps of lithospheric thickness that resolve variations on lengthscales relevant for constraining continental rifting. LAB depth varies from ~90 to ~40 km below the region, with thick lithosphere present beneath the Peninsular and Transverse Ranges, and thin lithosphere beneath the Salton Trough and the Continental Borderland. Although variations in LAB depth appear to occur across some major faults, particularly those associated with extension at some point in their history, no discernible change in LAB depth is observed across many faults in the region.

In the Salton Trough, assuming that pre-rift lithosphere exists, apparent mantle lithospheric thinning is substantially greater than crustal thinning. The two can be reconciled if either substantial loss of mantle lithosphere or crustal addition through mafic underplating / intrusion and/or metamorphosis of sediment into basement rock has occurred. On the other hand, if the thinned regions represents newly formed lithosphere, our results imply ~150 km of opening across the Salton Trough in the direction of present-day extension. Shallow LAB depths beneath the Inner Continental Borderland are consistent with a deformation history that involves substantial extension, which likely occurred during the Miocene in wake of the rotation of the Western Transverse Range block.

Our results demonstrate that lithospheric thinning occurs over very similar lengthscale as and is not systematically offset with respect to surficial and crustal expressions of rifting, consistent with a mode of deformation that is either pure-shear or simple-shear along steeply dipping shear zones. Furthermore, rapid horizontal variations in lithospheric thinning suggest efficient strain localization within the lithosphere, which may point to the role of a strain-weakening rheology or active asthenospheric upwelling.

17:40 **Long-Term Fault Strength Evolution: The Examples of Subduction Zones and Ductile Shear Zone** (*L. Lavier, UT Austin*)

We present 2 examples of fault strength evaluation to foster discussions on long-term fault strength evolution. 1- Frictional resistance to the relative motion between the upper and lower plates at subduction zones generates great earthquakes along the subduction interface. It has been noted that regions with a negative trench-parallel gravity anomaly are more likely to have great earthquakes. It is believed that strong coupling along the subduction interface drags down the fore-arc region of the overriding plate. This generates the observed gravity and topography anomalies, and possibly stores more strain energy to be released during a great earthquake. We developed a 2D numerical thermo-mechanical code for modeling subduction. The cohesion and friction angle are reduced with increasing plastic strain after yielding. To track different petrologic phases, Lagrangian particles are distributed in the domain. Interestingly, our numerical models show that the degree of coupling negatively correlates with the coefficient of friction. For t low friction, the subduction interface has very shallow dipping angle, which helps to couple plastically the upper and lower plates. The topography and gravity anomalies of the low friction case are consistent with observations indicate strong coupling between plates. 2- Geological observations point to variations in fault slip rate over paleoseismological (10^3 yrs) and midterm geomorphological (10^4 to 10^5 yrs) time-scales. We present a model for fault zone dynamics in which longtime scale changes in fault strength and slip rate arise as a consequence of shear failure in brittle-ductile shear zones. These faults extend through the brittle plastic transition through zones of anastomosing narrow ductile shear zones behaving in a semi-brittle manner. We show that a shear stress drops (fracture) generated by elastic unloading in the rigid brittle parts of the media results in transient slip events. These slip events are damped by viscoelastic flow in the ductile viscous part of the shear zone. We apply this model to well documented slip rate variations occurring over long time scales along the Wasatch fault zone. We show that slow fracture events occurring in ductile shear zone at the brittle-plastic transition can reproduce large variations in strain accumulations on a 10 kyr timescale with low strain accumulation rates on the 100 kyr timescale.

18:00 Group Discussion

19:00 – 21:00 Dinner (*Poolside / Terrace*)

20:00 – 22:00 SCEC Advisory Council Executive Session (*Executive Boardroom*)

21:00 – 22:30 **POSTER SESSION V: Group B** (*Plaza Ballroom*)

Wednesday, September 14th

07:00 – 08:30 Breakfast

07:00 – 08:30 SCEC Planning Committee Breakfast Meeting (*Palm Canyon A*)

07:00 – 08:30 SCEC Board Breakfast Meeting (*Palm Canyon B*)

07:00 – 08:30 Remove Posters (Group B)

08:30 – 10:00 PLENARY SESSION VII: How Can Increasingly Complex Community Models Continue To Evolve?

Moderator: *B. Aagaard (USGS)*

08:30 **The Salton Seismic Imaging Project (SSIP): Active Rifting and Strike-Slip Faulting in the Salton Trough, California** (*J. Hole, Virginia Tech*)

The Salton Seismic Imaging Project (SSIP) acquired seismic data in and across the Salton Trough in southern California and northwestern Mexico in March 2011. SSIP is investigating both rifting processes at the northern end of the Gulf of California extensional province and earthquake hazards at the southern end of the San Andreas Fault system. SSIP acquired seven lines of land refraction and low-fold reflection data in the Coachella, Imperial, and Mexicali Valleys, airguns and OBS data in the Salton Sea, onshore-offshore data, and a line of broadband stations across the trough. Seismometers were temporarily deployed at over 4200 onshore locations at 50-500 m spacing, and at 78 locations on the floor of the Salton Sea. Broadband seismometers have been deployed for 18 months at 42 sites along one of the controlled-source lines. These arrays and permanent network seismographs recorded up to 126 large explosive shots onshore and 2300 airgun shots offshore. Data were acquired inline for dense 2-D coverage and in grids for 3-D coverage. The project utilized over 130 field personnel from 31 colleges and universities, a majority of whom were student volunteers.

Previous studies suggest that North American lithosphere has been rifted completely apart in the Salton Trough. Based primarily on a 1979 seismic refraction project, the ~22 km thick crust is apparently composed entirely of new crust added by magmatism from below and sedimentation from above. Between the major transform faults, active rifting is manifested by faults observed in modern sediment, seismicity in the Brawley seismic zone, volcanism at the Salton Buttes, very high heat flow and geothermal energy production. The new data will constrain the style of continental breakup, the role and mode of magmatism, the effects of rapid Colorado River sedimentation upon extension and magmatism, and the partitioning of oblique extension. To improve earthquake hazard models, SSIP is producing images of the geometry of the San Andreas, Imperial and other faults; the structure of sedimentary basins in the Salton Trough; and three-dimensional seismic velocity of the crust and uppermost mantle. Preliminary results of seismic velocity analyses will be presented.

09:00 **Mechanical Investigations of 3D Fault Complexity in Southern California** (*M. Cooke, UMass*)

Fault geometry has a first-order influence on the partitioning of deformation among faults and as off-fault deformation. By creating a Community Fault Model, SCEC has been a leader in assembling an open repository of community vetted three-dimensional surfaces of active faults in southern California [Plesch et al, 2007]. The CFM provides a tremendous opportunity to investigate the role of fault geometry on fault system deformation. However, the primary challenge to using the CFM remains implementing the 3D surfaces into an appropriate model. Finite Element Method models require volumetric meshes that struggle with some of the more complex fault shapes within the CFM. Meanwhile block models, which are very well-suited for incorporating GPS data, require connected faults that bound closed volumes; an unnatural fault configuration in some complexly faulted regions. Several advantages of the Boundary Element Method (BEM) code Poly3D for examining issues of fault complexity include: 1) only the fault surfaces are meshed into triangular elements that preserve fault surface complexity 2) faults need not be connected and 3) faults slip in response to both applied loading and mechanical interaction with each other. Since the start of the CFM development ~11 years ago, my students, colleagues and I have been using CFM-based BEM models to investigate the effects of fault geometry on deformation associated with both geologic and interseismic time scales [e.g. Cooke & Marshall, 2006; Marshall et al., 2009]. Our studies of the Los Angeles basin, Ventura basin, San Gorgonio Pass region and Eastern California Shear Zone have revealed that variations to fault geometry and connectivity produce observable differences in uplift pattern and fault slip rates [Griffith & Cooke, 2004; Meigs et al. 2008; Marshall et al , 2008; Dair & Cooke, 2009; Cooke & Dair, 2011; Herbert & Cooke, SCEC 2011]. These studies show that we should expect slip rates to vary with position, even along any one fault segment. Consequently, a characteristic slip rate for each fault segment may be both difficult to determine from only one site investigation and potentially misleading for seismic hazard analysis. The studies also demonstrate that models with over-connected and over-simplified faults will produce slip rates that are too high. This has important implications for block models that in their goals of modeling large areas, compromise accuracy by connecting and smoothing fault surfaces. The current CFM is a representation of the active fault configuration in southern California but is probably incorrect in many places. To avoid propagating the errors of fault geometry into

seismic hazard analysis of southern California, SCEC should continue to test the CFM and alternatives to the presently preferred CFM geometry and we should gather new data to constrain fault geometry.

09:30 Group Discussion

10:00 – 10:30 Break

10:30 – 12:00 **PLENARY SESSION VIII: Wrap-Up**
Location: *Horizon Ballroom*

10:30 2012 Science Collaboration and RFP (*G. Beroza, Stanford*)

11:00 Report from the SCEC Advisory Council (*J. Freymueller, Alaska*)

11:30 Concluding Remarks (*T. Jordan, SCEC/USC*)

12:00 *Adjourn*

12:30 – 14:00 Lunch (*Tapestry Room / Terrace*)

13:00 – 17:00 **WORKSHOP: Strategies for Implementing a Community Stress Model**
Conveners: *Bruce E. Shaw, Jeanne L. Hardebeck, Brad Aagaard, John H. Shaw, and Thorsten W. Becker*
Location: *Horizon Ballroom*

The community stress model is one of the more high risk targets of SCEC IV but its hypothetical end-product, a model or suite of models for the 4D stress tensor in the California lithosphere, might be useful for a range of SCEC core science issues. This workshop is intended to kick-start the discussion between observationalists and modelers as to how a long term strategy can be implemented, which short-term achievable goals can be implemented via an RFP, and what kinds of stress models are desired by the users.

13:00 Introduction

13:10 Talk 1: Stress Required for Rupture Dynamics Models (*B. Aagaard, USGS*)

13:25 Talk 2: Stress Required for Fault Loading Models (*B. Meade, Harvard*)

13:40 Talk 3: Stress Required for Simulators (*K. Richards-Dinger, UCR*)

13:55 Group Discussion and 5-Minute Presentations

14:45 *Break*

15:00 Talk 4: Alternative Stress Observations from Boreholes, etc. (*N. Davatzes, Temple*)

15:15 Talk 5: Stress Observations from Seismicity (*E. Hauksson, Caltech*)

15:30 Talk 6: Connecting Stress Models to Real World Measurements (*D. Sandwell, UCSD*)

15:45 Discussion

- What Do Users Want?
- How Do We Implement the Database?
- Can We Self-Organize into Smaller Working Groups?
- What are CSM Targets for 2012?

17:00 *Adjourn*

State of SCEC, 2011

Thomas H. Jordan
SCEC Director

Welcome to the 2011 Annual Meeting

The next five-year phase of the Southern California Earthquake Center (SCEC4) will officially begin on February 1, 2012. The 21st SCEC Annual Meeting will therefore be a transitional meeting with two main goals: to share research results related to the SCEC3 science objectives, and to incorporate new ideas and collaboration plans into the preparations for SCEC4.

The SCEC Planning Committee, under the leadership of our Deputy Director, Greg Beroza, has put together an outstanding program that features some thought-provoking talks by keynote speakers, discussion sessions on major science themes, poster sessions on research results, technical demonstrations, education & outreach activities, and social gatherings. Five workshops and several project-coordination sessions are scheduled before and after the main meeting. Be prepared for a busy few days!

Much has happened in the world of earthquakes since our last meeting, and the agenda reflects these events. Sunday afternoon, Professor Jim Mori of Kyoto University's Disaster Prevention Research Institute will kick off the program with a plenary presentation on the Great Tohoku Earthquake of March 11, 2011. Monday features two related sessions, *Science and Engineering Issues from Earthquake and Tsunami Hazards Along the California Coast* and *Are We Properly Characterizing Extreme/Rare Events?*, followed on Tuesday by two sessions on the science and practice of earthquake forecasting.

The week's activities will bring together one of the largest collaborations in geoscience: over 560 people have pre-registered (Figure 1), and almost 300 poster abstracts have been submitted. This year's pre-registrants include more than 160 first-time attendees, so we will welcome many new scientists and proto-scientists!

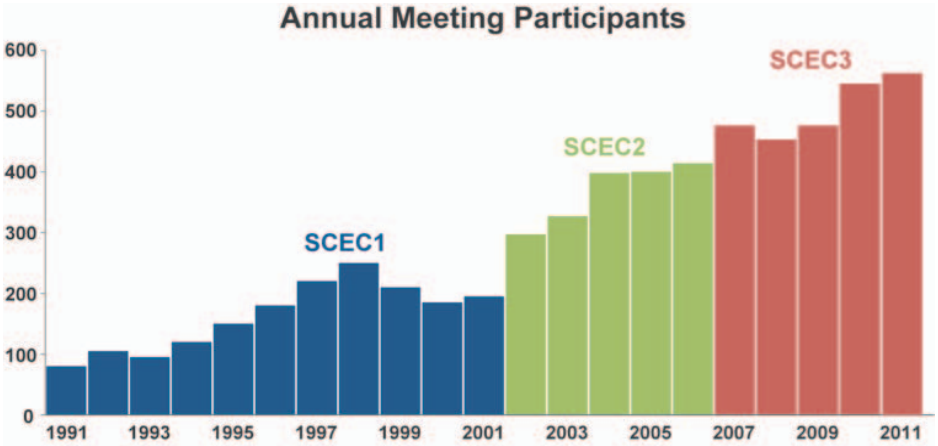

Figure 1. Registrants at SCEC Annual Meetings 1991-2011. Number for 2011 (562) is pre-registrants.

SCEC3 Accomplishments

Greg and the PC have put together an impressive annual research report, which is included in your online meeting volume, highlighting the science projects supported by SCEC during the past year. This annual report demonstrates substantial progress in attaining the basic SCEC3 objectives. Greg will summarize the research results in his plenary address on Monday morning. The poster presentations at the Annual Meeting will provide a forum for more detailed discussions and interchange of ideas.

The SCEC4 Transition

A primary focus of this transition meeting will be on long-range planning for the five-year SCEC4 program. Thanks to tremendous efforts by many people, the SCEC4 proposal process, which began in 2009, was very successful. At last year's Annual Meeting, we were informed by our agency representatives that, based on a rigorous sequence of mail and panel

reviews, both the National Science Foundation and U.S. Geological Survey were going to commit substantial resources to the next five years of the SCEC program.

In late May, we were given the panel reviews and official agency letters of commitment. Our NSF program officer Greg Anderson stated:

> "I am very pleased to inform you that your proposal 'The Southern California Earthquake Center, Phase 4 (SCEC4): Tracking Earthquake Cascades' has successfully undergone review by NSF, in cooperation with our USGS partners… I intend to recommend funding for this proposal as a cooperative agreement with a five-year duration beginning 1 February 2012, at an annual anticipated funding level of $3,000,000 (total of $15,000,000 over the award duration)."

UGSG contracting officer Margaret Eastman stated:

> "Your proposal submitted to USGS for support of SCEC4 has been favorably reviewed and is recommended for five years of funding at the requested level of $1,340,000 for the first year, pending availability of funds. USGS may not be able to support the requested inflationary increases in years two through five as our budgets typically do not include such inflationary increases."

Separate panel reviews were conducted by the NSF and USGS. The review summaries, which totaled 26 pages, contain detailed and generally favorable evaluations of SCEC3 progress and the SCEC4 proposal. The panels made a series of thoughtful recommendations to improve SCEC interactions, especially with groups external to SCEC. For example, the NSF panel recommended that a special advisory structure be created to help our well-regarded Communication, Education, and Outreach (CEO) program set up and evaluate progress toward new milestones and measures-of-success. CEO Associate Director Mark Benthien and I have asked the SCEC Advisory Council to consider what type of structure under its umbrella would be most appropriate to implement this recommendation.

From the perspective of this meeting, the most important conclusion of the reviews was the acceptance by both panels of the science plan articulated in the SCEC4 proposal. The SCEC4 scientific program is framed in terms of a very challenging, long-term research goal: *to understand how seismic hazards change across all time scales of interest, from millennia to seconds*. This problem is well suited to SCEC's integrated approach to earthquake system science. Earthquakes emerge from complex, multiscale interactions within active fault systems that are opaque, and are thus difficult to observe. They cascade as chaotic chain reactions through the natural and built environments, and are thus difficult to predict. The practical goals of SCEC4 research program are focused on time-dependent seismic hazard analysis—the geoscience required to "track earthquake cascades" (Figure 2).

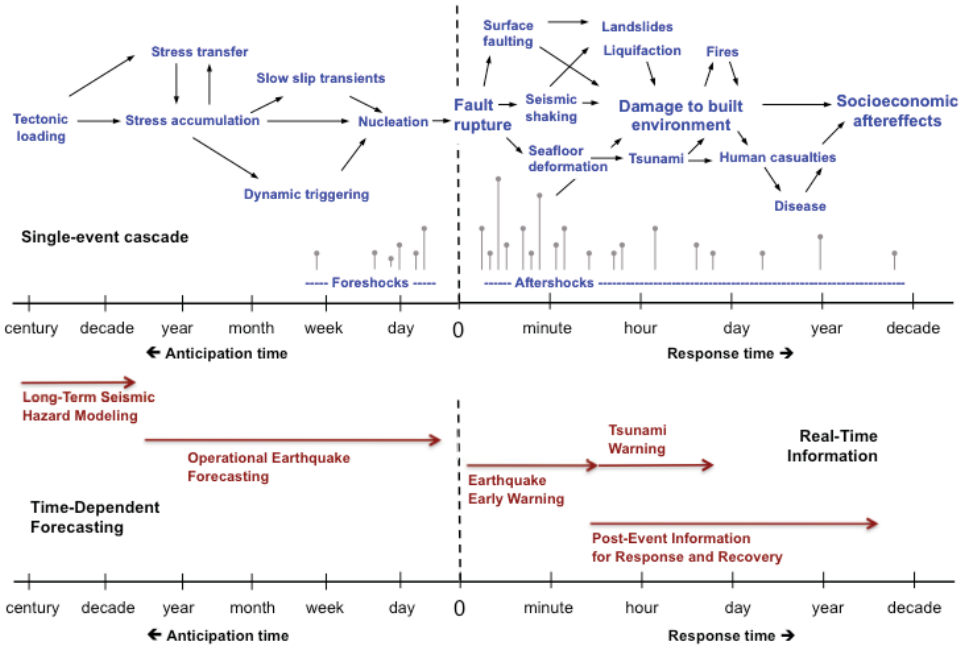

Figure 2. Earthquake processes (in blue) cascade through the natural and built environments, depicted here for a single damaging event on a nonlinear time line. Advancing the science behind long-term hazard modeling, operational earthquake forecasting, earthquake early warning, and delivery of post-event information (in red) will help reduce seismic risk and improve community resilience.

The SCEC4 science plan was developed by the Center's Board of Directors and Planning Committee with broad input from the SCEC community. A committee chaired by Nadia Lapusta assessed the basic research that will be needed to move towards the Center's scientific goals, identifying six fundamental problems in earthquake physics (Table 1).

These problems are interrelated and require an interdisciplinary, multi-institutional approach. Each was described in the proposal by a short problem statement, a set of SCEC4 objectives, and a listing of priorities and requirements (a copy of the complete SCEC4 proposal can be downloaded from *http://www.scec.org/aboutscec/documents/index.html*).

Table 1. Fundamental Problems of Earthquake Science for SCEC4

1. Stress transfer from plate motion to crustal faults: long-term fault slip rates
2. Stress-mediated fault interactions and earthquake clustering: evaluation of mechanisms
3. Evolution of fault resistance during seismic slip: scale-appropriate laws for rupture modeling
4. Structure and evolution of fault zones and systems: relation to earthquake physics
5. Causes and effects of transient deformations: slow slip events and tectonic tremor
6. Seismic wave generation and scattering: prediction of strong ground motions

We developed a coherent set of interdisciplinary research initiatives that will focus on special fault study areas, the development of a Community Geodetic Model for Southern California (which will combine GPS and InSAR data), and a Community Stress Model. The latter will provide a new platform for the integration of various constraints on earthquake-producing stresses. Improvements will be made to SCEC's unified structural representation and its statewide extensions.

Our organizational structure, reformulated in accordance with the overall SCEC4 research plan, comprises disciplinary working groups, interdisciplinary focus groups, special projects, and technical activity groups (Figure 3). A set of special projects funded separately by the NSF, USGS, and other agencies (the pink boxes in Figure 3) will continue to leverage core research support.

The Planning Committee has organized a series of talks coupled with group discussions that emphasize new elements in the SCEC research program and are designed to encourage SCEC4 planning. The SCEC4 objectives will be incorporated into the 2012 Science Plan. A draft of this plan prepared by Deputy Director Greg Beroza and the Planning Committee is included in the online meeting volume. An objective of this meeting is to get community input into this plan, which will be finalized by the beginning of October.

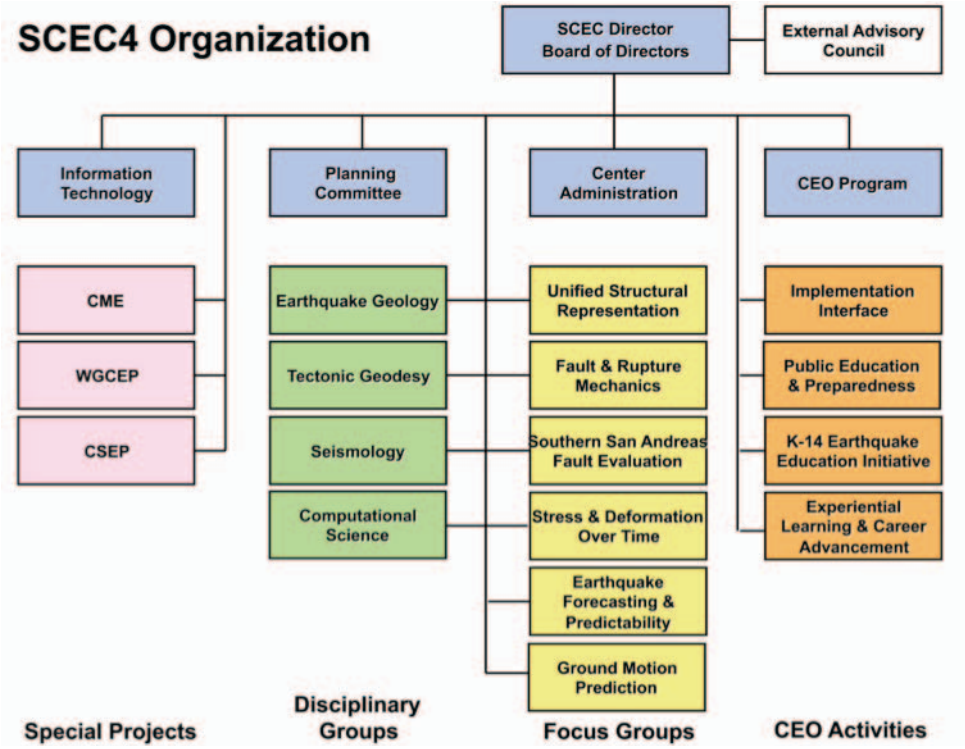

Figure 3. The SCEC3 organization chart, showing the disciplinary committees (green), focus groups (yellow), special projects (pink), CEO activities (orange), management offices (blue), and the external advisory council (white).

Organization and Leadership

SCEC is an institution-based center, governed by a Board of Directors, who represent its members. The membership currently stands at 17 core institutions and 58 participating institutions (Table 2). SCEC currently involves more than 800 scientists and other experts in active SCEC projects. A key measure of the size of the SCEC community—registrants at our Annual Meetings—is shown for the entire history of the Center in Figure 1. By this measure, participation in SCEC has grown by one-third during the five years of SCEC3.

The current core institutions have all committed resources to SCEC4. The California Geological Survey (CGS), a long-standing participant in SCEC, was admitted as a new core institution at the February meeting of the Board of Directors. A consortium of California State Universities (members of the nation's largest university system) is being formed as a "distributed" core institution in SCEC4. The CSU initiative, led by Prof. David Bowman of CalState Fullerton, will benefit an outstanding group of faculty and students who have contributed substantially to the SCEC research program.

Table 2. SCEC Institutions (June 1, 2011)

Core Institutions (16)	Participation Institutions (58)
California Geological Survey California Institute of Technology Columbia University Harvard University Massachusetts Institute of Technology San Diego State University Stanford University U.S. Geological Survey, Golden U.S. Geological Survey, Menlo Park U.S. Geological Survey, Pasadena University of California, Los Angeles University of California, Riverside University of California, San Diego University of California, Santa Barbara University of California, Santa Cruz University of Nevada, Reno University of Southern California (lead) Proposed: CalState Consortium	Appalachian State University; Arizona State University; Berkeley Geochron Center; Boston University; Brown University; Cal-Poly, Pomona; Cal-State, Chico; Cal-State, Long Beach; Cal-State, Fullerton; Cal-State, Northridge; Cal-State, San Bernardino; California Geological Survey; Carnegie Mellon University; Case Western Reserve University; CICESE (Mexico); Cornell University; Disaster Prevention Research Institute, Kyoto University (Japan); ETH (Switzerland); Georgia Tech; Institute of Earth Sciences of Academia Sinica (Taiwan); Earthquake Research Institute, University of Tokyo (Japan); Indiana University; Institute of Geological and Nuclear Sciences (New Zealand); Jet Propulsion Laboratory; Los Alamos National Laboratory; Lawrence Livermore National Laboratory; National Taiwan University (Taiwan); National Central University (Taiwan); Ohio State University; Oregon State University; Pennsylvania State University; Princeton University; Purdue University; SUNY at Stony Brook; Texas A&M University; University of Alaska; University of Arizona; UC, Berkeley; UC, Davis; UC, Irvine; University of British Columbia (Canada); University of Cincinnati; University of Colorado; University of Illinois; University of Massachusetts; University of Miami; University of Missouri-Columbia; University of New Hampshire; University of Oklahoma; University of Oregon; University of Texas-El Paso; University of Utah; University of Western Ontario (Canada); University of Wisconsin; University of Wyoming; URS Corporation; Utah State University; Woods Hole Oceanographic Institution

Board of Directors. Under the SCEC3 by-laws, each core institution appoints one member to the Board of Directors, and two at-large members are elected by the Board from the participating institutions. The Board is chaired by the Center Director, who also serves as the USC representative; the Vice-Chair is Lisa Grant Ludwig. The complete Board of Directors is listed on page ii of the meeting volume. Policies regarding the at-large members for SCEC4 will be discussed at the Board of Directors meeting on Wednesday, and your thoughts about this representation would be valued.

Advisory Council. The SCEC4 external Advisory Council will be chaired by Dr. Jeffrey Freymueller of the University of Alaska. The AC is charged with developing an overview of SCEC operations and advising the Director and the Board. Since the inception of SCEC in 1991, the AC has played a major role in maintaining the vitality of the organization and helping its leadership chart new directions. A verbatim copy of the AC's 2010 report follows this report in the meeting volume.

Kudos go to our distinguished colleagues who are rotating off the AC Members, Dennis Mileti (emeritus professor of the University of Colorado) and Stephen Mahin (director of the Pacific Earthquake Engineering Research Center). We also welcome Bob Lillie (Oregon State), who will be joining the AC this year.

Working Groups. The SCEC organization comprises a number of disciplinary committees, focus groups, special project teams, and technical activity groups. These working groups have been the engines of its success. The discussions organized by the working-group leaders at the Annual Meeting provide critical input to the SCEC planning process. The structure proposed for SCEC4 is shown in Figure 3.

The Center supports disciplinary science through standing committees in Seismology, Tectonic Geodesy, and Earthquake Geology. A new disciplinary committee in Computational Science has been added for SCEC4. These groups (green boxes of Figure 3) are responsible for disciplinary activities relevant to the SCEC Science Plan, and they make recommendations to the Planning Committee regarding the support of disciplinary research and infrastructure.

SCEC coordinates earthquake system science through interdisciplinary focus groups (yellow boxes). Four of these groups existed in SCEC3: Unified Structural Representation (USR), Fault & Rupture Mechanics (FARM), Earthquake Forecasting & Predictability (EFP), and Ground Motion Prediction (GMP). The Southern San Andreas Fault Evaluation (SoSAFE) project, funded by the USGS Multi-Hazards Demonstration Project for the last four years, has been transformed into a standing interdisciplinary focus group to coordinate research on the San Andreas and the San Jacinto master faults. A new focus group called Stress and Deformation Through Time (SDOT) will merge the activities of two SCEC3 focus groups, Crustal Deformation Modeling and Lithospheric Architecture and Dynamics. Research in seismic hazard and risk analysis will be bolstered through a reconstituted Implementation Interface (an orange box in Figure 3) that will include educational as well as research partnerships with practicing engineers, geotechnical consultants, building officials, emergency managers, financial institutions, and insurers.

Table 3. SCEC4 Working Group Leadership

Disciplinary Committees	
Geology	Lisa Grant Ludwig*
	Mike Oskin
Seismology	Egill Hauksson*
	Cochran
Geodesy	Jessica Murray-Moraleda*
	Dave Sandwell
Computational Science	Yifeng Cui*
	Eric Dunham
Focus Groups	
Structural Representation	John Shaw*
	Brad Aagaard
Fault & Rupture Mechanics	Judi Chester*
	Jean-Paul (Pablo) Ampuero
Southern San Andreas Fault Evaluation	Kate Scharer*
	Ramon Arrowsmith
Stress & Deformation Over Time	Kaj Johnson*
	Thorsten Becker
Earthquake Forecasting & Predictability	Jeanne Hardebeck*
	Ilya Zaliapin
Ground Motion Prediction	Kim Olsen*
	Rob Graves
Engineering Implementation Interface	Jack Baker*
	Jacobo Bielak
Special Project Groups	
Community Modeling Environment	Phil Maechling*
WG on Calif. Earthquake Probabilities	Ned Field*
Collaboratory for Study of Earthquake Predictability	Tom Jordan
	Danijel Schorlemmer*

* *Planning Committee members*

SCEC sponsors Technical Activity Groups (TAGs), which self-organize to develop and test critical methodologies for solving specific problems. TAGs have formed to verify the complex computer calculations needed for wave propagation and dynamic rupture problems, to assess the accuracy and resolving power of source inversions, and to develop geodetic transient detectors and earthquake simulators. TAGs share a *modus operandi:* the posing of well-defined "standard problems", solution of these problems by different researchers using alternative algorithms or codes, a common cyberspace for comparing solutions, and

meetings to discuss discrepancies and potential improvements. An important new TAG in SCEC4 will be the Ground Motion Simulation Validation (GMSV) group, led by Nico Luco, which began to develop plans for the validation of numerical earthquake simulations last January.

The SCEC4 Leadership Group is listed in Table 3. We welcome the new members with high hopes for the future and thank those who are rotating off with a deep appreciation of their service and accomplishments on behalf of the SCEC community.

Planning Committee. The SCEC Planning Committee (PC) is chaired by the SCEC Deputy Director, Greg Beroza, and comprises the leaders of the SCEC science working groups—disciplinary committees, focus groups, and special project groups—who together with their co-leaders guide SCEC's research program (Table 3).

The PC has the responsibility for formulating the Center's science plan, conducting proposal reviews, and recommending projects to the Board for SCEC support. Its members will play key roles in formulating the SCEC4 proposal. Therefore, I urge you to use the opportunity of the Annual Meeting to communicate your thoughts about future research plans to them.

Center Budget and Project Funding

In 2011, SCEC received $3.0M from NSF and $1.1M from the USGS under the fifth year of the current cooperative agreements with these two agencies. These agreements will be renewed for SCEC4 next year. Supplementing the $4.1M in base funding was $240K from the USGS Multi-Hazards Demonstration Project for SoSAFE and $40K from Pacific Gas & Electric Company for the rupture dynamics project. Other funds available for core projects included $100K from the geodesy royalty funds and $111K from the UCERF3 project. Therefore, SCEC core funding for 2011 totaled $4,591K, down slightly from $4,778K in 2010.

The base budget approved by the Board of Directors for this year allocated $3,272K for science activities managed by the SCEC Planning Committee; $35K (including $25K for intern programs) for communication, education, and outreach activities, managed by the CEO Associate Director, Mark Benthien; $200K for information technology, managed by Associate Director for Information Technology, Phil Maechling; $304K for administration and $250K for meetings, managed by the Associate Director for Administration, John McRaney; and $130K for the Director's reserve account.

Structuring of the SCEC program for 2011 began with the working-group discussions at our last Annual Meeting in September, 2010. An RFP was issued in October, 2010, and 172 proposals (including collaborative proposals) requesting a total of $5,270K were submitted in November, 2010. All proposals were independently reviewed by the Director and Deputy Director. Each proposal was also independently reviewed by the leaders and/or co-leaders of three relevant focus groups or disciplinary committees. (Reviewers were required to recuse themselves when they had a conflict of interest.) The Planning Committee met on January 13-14, 2011, and spent two days discussing every proposal. The objective was to formulate a coherent, budget-balanced science program consistent with SCEC's basic mission, short-term objectives, long-term goals, and institutional composition. Proposals were evaluated according to the following criteria:

1. Scientific merit of the proposed research
2. Competence and performance of the investigators, especially in regard to past SCEC-sponsored research
3. Priority of the proposed project for short-term SCEC objectives as stated in the RFP
4. Promise of the proposed project for contributing to long-term SCEC goals as reflected in the SCEC3 science plan
5. Commitment of the P.I. and institution to the SCEC mission
6. Value of the proposed research relative to its cost
7. Ability to leverage the cost of the proposed research through other funding sources
8. Involvement of students and junior investigators
9. Involvement of women and underrepresented groups
10. Innovative or "risky" ideas that have a reasonable chance of leading to new insights or advances in earthquake physics and/or seismic hazard analysis.
11. The need to achieve a balanced budget while maintaining a reasonable level of scientific continuity given very limited overall center funding.

The recommendations of the PC were reviewed by the SCEC Board of Directors at a meeting on January 23-24, 2011. The Board voted unanimously to accept the PC's recommendations. After minor adjustments and a review of the proposed program by the NSF and USGS, I as Center Director approved the final program in March 2011. This year proved more difficult than usual to manage as final funding from NSF did not come through until July.

Communication, Education, and Outreach

Through its CEO Program, SCEC offers a wide range of student research experiences, web-based education tools, classroom curricula, museum displays, public information brochures, online newsletters, workshops, and technical publications. Highlights of CEO activities for the past year are reported in the meeting volume by the Associate Director for CEO, Mark Benthien, who will present an oral summary on Monday morning.

SCEC has led the development of the Earthquake Country Alliance (ECA), an umbrella organization, now statewide, that includes earthquake scientists and engineers, preparedness experts, response and recovery officials, news media representatives, community leaders, and education specialists. The ECA has become our primary framework for developing partnerships, products, and services for the general public. SCEC maintains the ECA web portal (*www.earthquakecountry.org*), which provides multimedia information about living in earthquake country, answers to frequently asked questions, and descriptions of other resources and services provided by ECA members. Mark is the ECA Executive Director.

A major focus of the CEO program since 2008 has been organizing the *Great California ShakeOut* drills and coordinating closely with ShakeOuts in other states and countries. The purpose of the Shakeout is to motivate all Californians to practice how to protect ourselves during earthquakes ("Drop, Cover, and Hold On"), and to get prepared at work, school, and home. 7.9 million people participated in the 2010 ShakeOut, up from 6.9 million in 2009. More than 500 TV and radio news stories across the state and country aired in the days surrouding the drill, including a lengthy story on CBS Sunday Morning, and over 300 print stories appeared, including a front-page photo in the New York Times. Recruitment is well underway for the 2011 ShakeOut, with over 7.1 million participants registered as of August 31; the goal is to exceed 9 million. I would like to encourage California members of the SCEC community to register for the ShakeOut (at *www.shakeout.org*) and to encourage their institutions to join USC and others that are already registered.

ShakeOut has spread across the country and around the world. In October 2010 Nevada and Guam joined with California. In January 2011, Oregon and British Columbia held drills to commemorate the anniversary of the 1700 Cascadia earthquake. In April 2011, eleven states of the Central and Southern U.S. commemorated the 1811-1812 New Madrid earthquake bicentennial with a ShakeOut drill involving 3 million participants. Idaho will hold its first ShakeOut in October 2011 and Utah in April 2012. Other areas considering ShakeOut drills include Washington (2012), Alaska (2014), as well as Hawaii, Puerto Rico, New Zealand (2012), and Turkey. The ECA is now collaborating with colleagues in Tokyo, to help them coordinate their first ShakeOut on the one-year anniversary of the great Tohoku earthquake and tsunami of March 11, 2011.

SCEC CEO staff continues to work with museums and other informal education venues to develop content and programs for earthquake education and to distribute SCEC resources, such as the extensive set of publications that has grown out of *Putting Down Roots in Earthquake Country*. In 2008, SCEC organized a group of museums and other locations interested in earthquake education into a network of *Earthquake Education and Public Information Centers* (Earthquake EPIcenters), which has since been expanded to over 60 venues distributed throughout California. The EPIcenters are essential partners in the ShakeOut, as many hold public events on drill day, and help promote participation.

SCEC is very active in the earth science education community, participating in organizations such as the National Association of Geoscience Teachers, the Coalition for Earth System Education, and local and national science educator organizations (e.g. NSTA). SCEC Education Programs Manager Bob de Groot leads these efforts and runs the SCEC Teacher Workshops and K-12 partnerships. SCEC is collaborating with IRIS and EarthScope in developing the content for the San Andreas fault Active Earth Kiosk, building on a workshop SCEC co-organized in 2009. Last year Arizona State University, the OpenTopography Facility, and SCEC developed three earth science education products to inform students and other audiences about LiDAR and its application to active tectonics research.

Bob de Groot is also skillfully leading SCEC's Office for Experiential Learning and Career Development. His office manages two SCEC intern programs: Summer Undergraduate Research Experiences (SURE, 221 interns since 1994), Undergraduate Studies in Earthquake Information Technology (UseIT, 167 interns since 2002). The ELCA office promotes diversity in the scientific workforce and the professional development of early-career scientists (Figure 4). As someone very involved in these intern programs, I really enjoy seeing the students grapple with the tough but engaging problems of cutting-edge earthquake science. For example, the "grand challenge" for this year's UseIT program was to *develop a Seismic Sequence Visualization System based on SCEC-VDO and GIS that can display earthquake sequences, monitor their evolution in space and time, and assess their hazards and risks*. Many of the summer interns will be presenting their work at this meeting, and I hope you'll have the opportunity to check out their posters and demos.

Figure 4. This "Brady Bunch" picture shows the students from around the country who participated in the 2011 UseIT summer program at USC. Many will be attending the Annual Meeting to present posters, demos, and animations.

A Word of Thanks

As SCEC Director, I want to express my deep appreciation to all of you for your attendance at the Annual Meeting and your sustained commitment to the collaboration. Greg Beroza and the PC have developed an outstanding program, so the entire meeting should be a pleasant experience. I'd especially like to thank Tran Huynh, the SCEC Special Projects and Events Coordinator, and her diligent associates, Deborah Gormley, John Marquis, and Matt Goldberg, for their hard work and exceptional skill in organizing this meeting and arranging its many moving parts. Please do not hesitate to contact me, Greg, Tran, or other members of the SCEC team if you have questions or comments about our meeting activities and future plans. Now please enjoy the sessions, the meals, and the pool in the spectacular tectonic setting of Palm Springs!

Report of the Advisory Council

Southern California Earthquake Center

2010 SCEC Annual Meeting

Advisory Council Membership*

Mary Lou Zoback, Chair, Risk Management Solutions-RMS

Gail Atkinson, University of Western Ontario

Roger Bilham, University of Colorado

John Filson, USGS (Emeritus)

Jeffrey T. Freymueller, University of Alaska

Jim Goltz, CA Emergency Management Agency

Anne Meltzer, Lehigh University

Dennis Mileti, University of Colorado, Boulder (Emeritus)

Steve Mahin, Pacific Earthquake Engineering Research Center (PEER)

Farzad Naeim, John A. Martin & Associates

John Vidale, University of Washington

Andrew Whitaker, University of Buffalo

Members highlighted in bold attended the 2010 Annual Meeting and contributed to this report. Gail Atkinson was unable to attend but did contribute to the report.

Introduction

The Advisory Council of the Southern California Earthquake Center (SCEC) met during the 2010 SCEC Annual Meeting, held in Palm Springs, California, 12-15 September 2010. The principal meeting of the Advisory Council (AC) was during the afternoon and early evening of 14 September; an earlier session was held prior to the start of the Annual Meeting on 12 September to outline areas of focus. The incoming Council chair, Jeff Freymueller, summarized the principal Council findings and recommendations in an oral report delivered during the closing session of the Annual Meeting on the morning of 15 September.

Prior to the Annual Meeting on 10 September the SCEC Director circulated to the Advisory Council a confidential report summarizing how SCEC had responded to Advisory Council recommendations from the previous year and raised a number of new and continuing issues warranting Council attention. Those issues included:

- Evaluation of the Communication, Education, and Outreach (CEO) Program
- Input on Collaboratory for the Study of Earthquake Predictability (CSEP) and operational earthquake forecasting
- Advice on initiatives in earthquake simulation and ground motion prediction and interface with the earthquake engineering community
- Documenting SCEC earthquake system science accomplishments in an integrated report
- Advisory Council structure/representation
- Input and reaction to the SCEC4 proposal
- Advice on leadership development and succession planning within SCEC
- SCEC's role in international collaborations

After some general introductory remarks, we provide input on these issues raised by the Director. We also comment on some topics raised by the AC--some are new and some are recurring:

- Increasing the visibility of workshops within SCEC and awareness of their outcomes
- Input on the effectiveness of annual meeting sessions for science planning
- Reflections on the size of the annual meeting

Finally, we note that in this year's AC report we include some recommendations for the USGS in areas where their programmatic interests strongly overlap with those of SCEC.

Some General Impressions

Congratulations are in order on multiple fronts. Foremost, at the 2010 meeting we celebrated SCEC's 20th anniversary and were thrilled to learn that both the USGS and NSF have agreed to fund SCEC4. We applaud the herculean scientific planning and proposal writing effort produced an on time submittal despite the occurrence of the M7 Haiti earthquake in January and the M9.2 Chile earthquake just days before the deadline. By all accounts the June site visit to SCEC by both USGS and NSR review panels was extremely well organized and succeeded in portraying the many facets of SCEC and hence was critical in assuring the continued funding.

We also applaud the SCEC CEO's initiative in building a statewide coalition of regional earthquake alliances that helped plan and promote an all-California ShakeOut drill in October 2010 which engaged more than 7.9 million state residents. In addition, the Earthquake Country Alliance, under Mark Benthien's able leadership, is actively exporting the ShakeOut exercise to both other regions of the U. S. and to at least one international site, New Zealand. We view the ShakeOut exercise as a unique scientific leadership and effective outreach outcome that was only possible as a result of the shared vision, the stature, strong participatory spirit, and integrative organization of SCEC as a dedicated science center.

We also want to strongly commend the outstanding, on-going commitment to involving undergrads in SCEC research through intern programs under the leadership of Bob de Groot. The enthusiasm, breadth and diversity of the outstanding undergrads getting an opportunity to participate directly in earth science research are inspiring. The entire SCEC community benefits from energy and stimulation these students bring to the Annual Meeting through their participation and presentation posters on their work.

All these CEO efforts were all highlighted in a very positive review of the effectiveness of the CEO program conducted by an independent review panel in the fall of 2009. The review panel's report was included in the SCEC4 proposal.

Since members of the Advisory Council are not members of SCEC, the Annual Meeting provides an important opportunity for Council members to assess the community's annual progress on the Center's goals and programs. The 2010 meeting and associated workshops proved again to be impressive demonstrations of the energy and enthusiasm of the SCEC community. The 160 registrants who were attending their first SCEC Annual Meeting (nearly 30% of the 545 total registrants), including many students and interns, provided heartening evidence of the center's growing participation and its compelling mission.

The Advisory Council also lauds the entire SCEC membership for its persistently selfless community spirit which enables considerable progress in developing communal, system-level models and representations that are advancing the goals of both fundamental and applied earthquake system science. In particular, we would like to recognize Deputy Director Greg Beroza's superb leadership of the science collaboration process. Beroza's kickoff keynote on SCEC scientific accomplishment did a superb job of highlighting breakthrough science and the progress made towards SCEC3 goals.

Finally, the Advisory Council would like to particularly acknowledge Tom Jordan's exemplary leadership of SCEC over the past 10 years. Tom arrived in 2000 and brought an infusion of energy and creative ideas to SCEC as it went into its SCEC2 planning process. Under his direction the SCEC2 proposal was funded and numerous new research directions were launched. Tom's vision and ability to cultivate and seize funding opportunities outside of the core support has brought new perspectives, expertise and tools to address earthquake system science. Under Tom's initiative and leadership, SCEC now leads the earthquake science community in active engagement of the high performance computing community. The California Earthquake Authority was so impressed with the joint SCEC-USGS-CGS' UCERF2 uniform statewide assessment of earthquake likelihood analysis that they have funded a UCERF3 proposal to address a number of key issues and uncertainties leading to an improved assessment.

As Tom is always the first to admit, the outstanding staff support provided by John McRaney, SCEC's Associate Director of Administration and Tran Huynh, Special Project Manager, are vital to the success of SCEC. John and Tran keep SCEC running smoothly and money flowing to researchers in a timely fashion, and they make sure workshops are easy to organize and run flawlessly. We especially thank them for providing all manner of cheerful and indefatigable assistance while managing all the details involved in carrying out another highly successful Annual Meeting.

Evaluation of the Communication, Education and Outreach (CEO) Program

The Advisory Committee makes a number of recommendations regarding the CEO program:

1. Carry out a "forward-looking" Phase II CEO Review
2. Develop SCEC4 CEO Program targets and create metrics to track program progress toward targets
3. Expand oversight of and input to the SCEC CEO program
4. Deepen the CEO's relationship with FEMA.
5. Institute risk communication training for SCEC members likely to speak with the media
6. Bring the latest social science research on risk communication to operational earthquake forecasting and the Collaboratory for the Science of Earthquake Prediction (CSEP) activities

Each of the six recommendations is discussed in more detail below.

Carry out a" forward-looking" Phase II CEO Review

The Advisory Council continues to call for a "forward-looking " Phase II review of the SCEC CEO Program (as opposed to the retrospective review carried out in the Fall of 2009). We recommend the review panel be comprised of a broad range of disciplinary experts, e.g. marketing and/or advertising, psychology, risk communication, and more. The purpose of the review would be to detect and explore potential new ideas for the SCEC4 CEO workplan, activities and directions. This review might best occur if it were phased as follows: (1) add a new disciplinary member to the Advisory Council as described in a later section, (2) involve new and existing Advisory Council members in planning the review, and (3) conduct the review in a meeting format and compile its results. The critical time issue is that the Phase II review happens in time to have the maximum impact on all of SCEC4 CEO activities.

Develop SCEC4 CEO program targets and create metrics to track program progress toward targets

The Advisory Committee recommends that the CEO program develop a comprehensive list of SCEC4 targets—those that are "social process orientated" as well as those with more readily quantified targets. The targets should first be generated and then metrics should be developed to measure progress toward them. This could be done by SCEC CEO staff with input from external outreach experts (including social scientists, practitioners, and education experts). It would ideally be informed by the forward-looking review recommended above.

Examples of such targets include:

- Prepare and Distribute a "Baseline Public Preparedness Summary". The State of California funded a recently completed scientifically-based study to measure the state of adoption by households of 40+ SCEC CEO-recommended preparedness and mitigation actions for earthquakes. Data was gathered on three California populations: (1) high risk southern California counties, (2) high risk northern California counties, and (3) the rest of the state. This study was intended to provide a baseline against which the impact of the 2008 Shake Out and others could be assessed. SCEC CEO should synthesize, distribute, and use this baseline against which to evaluate past, present and future Shake Out and other public information dissemination activities. The distribution of these baseline data could be used to motivate others to provide or procure funds to replicate the study to determine the impacts of subsequent efforts to motivate household preparedness and mitigation action-taking.

- Prepare, Distribute and Use a "Motivating Public Preparedness Metric". A definitive study of what factors motivate public preparedness and mitigation has recently been funded by the Department of Homeland Security. It produced clear, certain, and replicated scientific conclusions for all hazards on the entire population of the U.S., high risk cities,

and the nation's major racial and ethnic minority groups. This study's findings about "what works" and "what does not work" to motivate public preparedness and mitigation should be clearly synthesized into a metric. This metric(s) should be disseminated, and used to inform choices about future SCEC outreach activities.

Many other SCEC CEO public information and education targets should be catalogued and metrics developed to track progress toward them. Among these is clarification regarding the program's mission in southern California versus in other regions.

Expand oversight of and input to the SCEC CEO Program

The Advisory Council recommends that SCEC incorporate a broader range of disciplines to better evaluate SCEC CEO activities and potentially to provide input more frequently. Specific recommendations are:

- Expand Disciplinary Membership by adding an additional Advisory Council member, to represent other CEO-relevant disciplines beyond those of the disciplines of sociology and emergency management currently on the AC. SCEC might also consider an advisory committee specifically for CEO activities, involving, but not exclusive to, AC members. Suggested additional disciplines include:
    - advertising and/or marketing
    - the psychology of risk communication
    - public science education
- Expand CEO Oversight. Structure whereby an increased number and more diverse set of outreach and education experts can offer advice and oversight to the SCEC CEO Program more than once a year as is now the case. This could possibly be done through a dedicated subcommittee reporting to the AC.

Deepen the CEO Program's Relationship with FEMA

The Advisory Council notes that SCEC's CEO Program is likely the most successful CEO Program in the nation, and perhaps the world. We are proud of the progress that its Director has made in the last year to increase funding for CEO activities from groups such as FEMA. But we recommend that a more aggressive set of activities be put in place to cultivate SCEC CEO relationships with FEMA. There are a number of possible projects that might be appropriate to pursue with FEMA. However, the following ShakeOut related projects are "prime candidates" and should be pursued first.

- Leverage the SCEC ShakeOut with FEMA as a Best Practice. The ShakeOut model is now being emulated by other places, states, nations, and other hazards (the Great Hurrican Blowout is being run for hurricane awareness, see *http://www.greathurricaneblowout.org*). A long-standing practice in FEMA is to identify "a national best practice" and then export it. This is already underway at FEMA but could be upgraded. First, SCEC CEO should seek FEMA funding for an individual to distinguish and write-up the ShakeOut's design parameters and implementation procedures to enhance its export by FEMA to other entities (e.g.,produce a briefing book to spread the ShakeOut approach as a FEMA "best practice"). This project should be pursued with the endorsement and cooperation of the USGS and Cal-EMA.
- Rigorously evaluate the effectiveness of the ShakeOut program. SCEC CEO should s FEMA to evaluate the effectiveness of the ShakeOut program to determine what about it works best and what does not. This would be easy to accomplish because of the baseline data described above. Such an evaluation would enable the Shake Out to adjust its approach, if needed, and fine-tune details about its export to other places so that its effectiveness is maximized.

Institute risk communication training for SCEC members likely to speak with the media

The Advisory Council continues to recommend that risk communication training be sought and delivered to SCEC members likely to talk about earthquakes or earthquake hazard in southern California on the radio, in front of a television camera, or on other public media. It would be appropriate to involve new Advisory Council or subcommittee member(s) in the discipline of risk communication to help organize this training. Different levels and types of training are likely appropriate for different types and levels of SCEC participants.

Bring latest social science research on risk communication to operational earthquake forecasting and the Collaboratory for the Science of Earthquake Prediction (CSEP) activities

Two areas of knowledge in the social sciences can inform CSEP and operational earthquake forecasting activities. The Advisory Council recommends an active two-part role for CEO in helping craft operational earthquake forecasting communication for both SCEC and the USGS:

- Transfer of existing knowledge and stimulating new research. There is a rich research literature in the social and behavioral sciences regarding risk communication (including changed probabilities and public warning statements) conducted primarily in this nation, but also internationally. The topics covered include:
    - public warning information system design to assure that rarely used systems are highly reliable
    - public messaging and the importance of the words that are made public to maximize societal benefits and minimize societal disruptions
    - the best methods to accomplish public education activities to upgrade what the public know about such topics

  The CEO should explore formats to isolate applicable knowledge from this research and to clarify new formal social science research needed to support the emergence of operational earthquake forecasting (OEF) practices. Possible formats include:
    - request that either NEHRP or the USGS fund an NRC/NAS Committee to review the relevant literature and make recommendations on needed research (e.g., a study similar to the NRC effort evaluating the National Tsunami Warning Program, report released September 27, 2010).
    - Alternatively, a group of social science experts on these topics could be assembled for a workshop.

  The range of research topics that might emerge are likely to be varied including message testing in psychological laboratories, the role of social media in influencing what people hear, think, and do, and many more.

- Take advantage of cutting edge research in peripheral fields. Public risk communication is in a state of rapid change related to the advent of Web 2.0 and rapidly expanding use of social media (e.g., people are warning themselves and their friends). The role of social media in the domain of risk communication is one of the hottest research topics in risk communication today, well-funded by the Department of Homeland Security. SCEC and the USGS would do well to reach out to researchers in this field to be informed by new discoveries applicable to CSEP/OEF. A key research center is the START Center of Research Excellence at the University of Maryland at College Park. There is no reason to duplicate this research, but there is strong reason to know what their research is revealing.

Input on the Collaboratory for the Study of Earthquake Predictability (CSEP) and Operational Earthquake Forecasting

We applaud SCEC for its continued progress in developing CSEP and in promoting test centers in other countries--special congratulations are due for establishing a CSEP test center in China. CSEP uniquely fulfills the role of open, scientifically rigorous and consistent evaluation of earthquake prediction methodologies.

Despite its successes, the enterprise is currently at risk, as the Keck seed funding expired in 2010 and funding is scarce in the USGS, the natural home for the operational side of this effort.

The Advisory Council recommends the following actions to the SCEC leadership:

1. The AC strongly endorses the continuation of the CSEP, as this program is a well- conceived, well-executed, and critical step toward quantifying the temporal variations in earthquake hazard. It is particularly critical as prediction methodologies are far from mature, and new evidence such as deformation and paleoseismology are continually expanding the measurements being monitored, and early warning systems and aftershock probabilities estimates are coming to fruition.
2. CSEP should continue to avoid monitoring responsibilities and focus only on evaluation of forecasts.

3. CSEP should evolve from its current development phase to one of sustained operations as a matter of economy. This may involve reducing or curtailing of investment of resources in international collaborations. Nevertheless, CSEP is to be strongly commended for having helped to launch a suite of international efforts with similar goals.
4. As the goals of CSEP are directly aligned with NEHRP statutory evaluation of hazard and public safety responsibilities, we strongly urge USGS take a leadership role within NEHRP in securing funding to sustain CSEP operations.
5. CSEP should be the scientific element of an end-to-end operational earthquake forecasting system that is informed by risk communication science (see specific recommendations in the CEO section). CSEP should work with USGS and state agencies to implement an OEF plan.

Advice on initiatives in earthquake simulation and ground motion prediction and building collaboration with the earthquake engineering community

The Advisory Council commends SCEC for its continued progress in broadband and large-scale ground motion simulations. Significant progress has been made in confirmation of these simulations through comparison with recorded data and through assessments of the consistency and accuracy of results from various investigators.

The scientific foundations and methods used in this work are solid and the potential applications, as a supplement to recorded data, are significant. With regard to the science, the Advisory Council notes that studies of recent earthquakes in Haiti, Chile, and northwestern Mexico (Sierra El Mayor) discovered unexpected complexities of the earthquake source. Such complexities may be necessary to take into account in ground motion simulations and the study of the variability in these simulations.

The utilization of ground motion simulations within engineering practice remains a challenge. Despite the wide range of scenarios for which simulations can be computed, far exceeding the number of events with recorded data, their acceptance by the engineering community has remained muted. Without general acceptance by the engineering profession, the ground motion simulation projects of SCEC will remain an exercise of great interest to some but will not realize their full potential. The reservations of the engineering profession regarding simulated ground motions may have several causes, including:

- The difficulty in assuring practitioners of the consistency of the simulations with existing recordings of strong motions.
- The difficulty in capturing the sensitivity of simulations to the range of unpredictable parameters, i.e., quantifying the uncertainty in a useful way.
- Lack of knowledge of the scientific underpinnings of the simulation methods.
- Lack of awareness of recent advances in simulation studies.
- Lack of general availability of "user-friendly" access and well-documented sets of simulations that are readily useable by the research engineering community in comparative studies of the applicability of such simulations relative to "real" recordings.

The needed level of engineering acceptance would be accelerated by proactive outreach, indeed a campaign, by SCEC to engage the engineering community to address these issues.

The Advisory Council recommends the following actions to the SCEC leadership:

1. Create a technical activity group (TAG) specifically charged to engage the engineering community. This group should be comprised of ground motion model developers and earthquake engineers. The TAG should convene, early on, a topical workshop on engineering needs, the status of ground motion simulation, and means to establish a sustained and energetic dialog between the scientific and engineering interest in this topic. One promising mechanism for this dialog of might be for SCEC to participate in the Ground Motion Selection and Modification group at PEER.
2. Investigate methods of delivering and promoting simulations to the engineering community by making them more comprehensive and accessible. As an example, a recent PEER initiative provides a web tool by which engineers can

search and/or scale a database of time histories to match given target scenarios and conditions. Perhaps a similar database could be compiled (and accessed through the same or similar tool) for simulated time histories; this would make it apparent how these simulations "fleshed out" the recorded time histories, and also enable comparisons. It would also provide a good vehicle for collaboration with PEER.

3. Motivate and facilitate active participation of members of the engineering community in the Advisory Council. A meeting of the Advisory Council at a different time from the Annual Meeting to discuss means of building rapport with the engineering community may be necessary.
4. Actively seek to involve young engineering students in SCEC's student intern programs to build more integration into the next generation of engineers.

Documenting SCEC earthquake system science and outreach accomplishments in an integrated report

The Advisory Council was asked to consider how the SCEC story might be told, and how its findings might be integrated in an appropriate publication.

The two decades of SCECs unique existence have resulted in a sequence of findings that many perceive justifies an equally unique report. This report will be eagerly awaited by not only by the SCEC community and by funding bodies, but also by the international science community. The success or otherwise of SCEC's systems approach to science and embedded outreach justifies a full account - what worked, what didn't, and where would earthquake science be without SCEC.

The committee discussed conventional journal reporting versus a monograph, or possibly a book. The anticipated scope was considered inappropriate and too wide ranging for most journals, with the possible exception of Reviews of Geophysics, but a length limitation in that journal would restrict a full treatment of the motivation behind, and the successes ensuing from SCEC's unusual interdisciplinary collaboration and its system-level approach to earthquake science.

The Advisory Committee recommends:

1. SCEC consider a full length monograph, e.g. AGU's Geodynamic series, or a dedicated book as the best setting for telling the integrated story of SCEC - from conception, to evolution, to results. Such a comprehensive report would be a formidable undertaking for SCEC leadership, but it should be possible to lessen the burden through shared authorship and dedicated editing.

Advisory Council

In past years, the Advisory Council has done essentially all its business at the SCEC Annual Meeting. As SCEC has grown, this model has been increasingly strained. Given the time constraints at the meeting, it is difficult for the AC to do more than discuss items brought to it by the SCEC leadership, plus a few of the most pressing issues that may be raised or observed at the meeting. Probably we could do a bit more if we received some materials farther in advance of the meeting, but this would only reduce rather than eliminate the time crunch. It may be time to augment the AC meeting at the Annual Meeting with a shorter, focused meeting at USC during a less hectic period. Ideally, this would also mean a lighter workload for the AC at the Annual Meeting.

There has been a pattern of irregular AC attendance in certain disciplines (for example, engineering). Holding a ~1-day meeting at USC in addition to the Annual Meeting might help reduce this problem, especially if the time of the meeting was flexible. Other suggestions outlined earlier in this report may also help as well. The suggested Technical Activity Group on ground motion simulations and their use may also provide an additional hook to draw further participation from the engineering community. Providing progress reports and soliciting specific advice from the AC on this endeavor may be an effective way to increase participation (if not, you may need to choose different people from the engineering community).

As mentioned before, the SCEC AC could use additional expertise on CEO matters. Adding several CEO-focused members would result in a lack of balance in the AC, but adding one more would be a positive step. Through the forward-looking CEO evaluation that we have recommended, SCEC has an opportunity to engage experts in a broader range of disciplines and these people could be asked to provide advice on an ongoing basis to SCEC (directly or through the AC) on specific CEO-related topics.

Input and reaction to the SCEC4 Proposal

We thank SCEC for the copy of the SCEC4 proposal, and we congratulate SCEC on another success! Time has not yet allowed us to make serious comments about the final submitted proposal, which we received in the packet for the Annual Meeting. In any case, it may be more important for SCEC to get our input to the proposal once the peer and panel reviews have been received. We recommend that SCEC ask for further input in the spring once these reviews have been received.

Most likely, SCEC will have to make some difficult choices in its prioritization of activities under SCEC4, given that the funding level will be lower than requested. In 2008 the Advisory Council was told that the SCEC Planning Committee would be tracking progress toward the achievement of the 19 SCEC3 research objectives. We have yet to receive the results of this tracking or a report on the status of progress on the various SCEC3 goals. We suggest again that such a report be generated, not as a bean-counting exercise but as a helpful self-assessment of SCEC3 successes (and remaining challenges) that will aid in the prioritization of SCEC4 research priorities. To some extent this self-assessment was done in the SCEC4 planning process. We recommend:

1. An annual report tracking progress toward the achievement of the SCEC4 research objectives, even if only for internal use.

Advice on Leadership Development and Succession Planning within SCEC

The AC was delighted that Tom Jordan committed to continue to lead SCEC through the SCEC4 proposal process. However, with Tom Jordan's stated desire to step down from the directorship, the challenges of attracting a new director remain. The AC strongly recommends that a plan be defined as soon as possible for recruiting a new director with a specific time table. The plan should also include strategies for cultivating a pool of potential candidates such as engaging them in SCEC by inviting potential candidates to serve on the Advisory Council, or by inviting them to attend SCEC meetings and workshops. It will also be important to consider alternate leadership structures for the future as an element of this succession planning. For example, the leadership should consider the possibility that there could be separate directors of special projects that are not funded through the core science budget. This kind of thinking might be important both to the future growth of SCEC and to attracting a new director with management strengths different from the current director.

Defining SCEC's role in international collaborations

The Advisory Council was asked to consider when it might be appropriate for SCEC to expand its research activities beyond the confines of California.

The AC recommends that SCEC should clearly focus its international efforts on partnerships that support its core science mission. Although it is tempting to export SCEC findings to address similar tectonic settings elsewhere in the world, SCEC's motivation in such involvement should lie in identifying opportunities that are perceived to complement or advance ongoing SCEC research tasks. Examples include:

- Fault networks in Southern California that extend beyond the US national border. One cannot conceive of studying the fault systems of southern California in isolation. Ties and collaborative projects with Mexican scientists should be pursued with vigor especially in the aftermath of the El Mayor-Cucapah earthquake. Methods to exchange seismic and fault slip data transparently and in a timely fashion are recognized as especially important.
- Partnerships with other organizations working on operational earthquake forecasting are clearly beneficial to SCEC. In this case the societal complexities of "uncertain information" communication have common ground in numerous countries.
- One can envisage that future opportunities may arise to study scientific problems that SCEC cannot solve locally – in these instances international partnerships would be of benefit. An example might be the availability of deep boreholes elsewhere in the world that might illuminate the physics of hypocentral processes, or the physics of fault slip.

- SCEC provides an unusual but exemplary template for innovative coordinated science that might benefit other regions. SCEC may thus have an international role in showcasing its methodology to a worldwide scientific community.
- SCEC may have an important advisory role in guiding international efforts at the design stage (e.g., acquisition of new forms of remotely sensed data suited to the study of earthquake processes).

Increasing the visibility of workshops within SCEC and awareness of their outcomes

SCEC fills a tremendous need of the community by facilitating easy-to-convene topical workshops in a short time frame. The Advisory Council has noted that while many SCEC members are aware of recent workshops in a related area, in general they are not very aware of the workshop outcomes if they did not personally attend. These workshops are a tremendous resource for the entire community, and the benefit will be enhanced if the outcomes are better publicized.

Expanding on the AC focus on this issue for the past two years, we recommend:

1. Continue SCEC-wide promotion of workshop opportunities (this part of the process seems to be working well)
2. Provide brief oral summaries of outcomes of the pre-annual meeting workshops as part of each Annual Meeting program
3. Provide a tab on the SCEC website to provide easy access to information upcoming as well as past workshops.

4. Require all SCEC workshop conveners to submit a brief summary of workshop outcomes for posting online within 45 days of the workshop. An email notification to the SCEC community to alert them to the posting with a link to the summary would enhance the impact of the workshop discussions on the broader SCEC community.

Input on the effectiveness of science planning at annual meeting sessions

The SCEC annual meeting exists as a forum for presenting cutting edge scientific results and for planning future year's activities. The advisory committee was asked to comment on the success of the meeting format for addressing those two goals.

During the 2010 meeting a number of the plenary sessions were organized to focus on emerging new results and potential future science directions. The keynote presentations in these discussion sessions were uniformly interesting and informative. There was, however, more variability in the 1.5 hour science planning discussion sessions that followed.

The discussions that were most successful were those that placed the scientific presentation and issues raised in it directly in the context of a SCEC planning process. The most effective of these discussions were those that followed a template of prearranged questions designed to seed and stimulate audience participation. Plenary sessions that were aimed at general science topics rather than focused SCEC collaboration goals, though interesting, were perceived to be less successful.

Size of the annual meeting

The SCEC meeting is very popular, and continues to grow in size each year. On the positive side, this reflects the steady growth in interest in SCEC and SCEC activities. On the negative side, the meeting is already much larger than a "small

meeting", and if the meeting grows too much larger it may be difficult to manage. Yet any attempt to limit the size of the meeting would require difficult and awkward choices.

When thinking about the size and scope of the annual meeting the most critical question to keep in mind is whether this meeting continues to meet the focused needs of the SCEC collaboration. In our assessment, it still does even at the present size, although science planning sessions are difficult with such a large group. That was not a serious problem this year, but because the next meeting or two will focus on SCEC4 plans and priorities it will be important to ensure that there is still an effective forum for participating SCEC scientists to provide input and feedback on the collaboration science plans and priorities. Otherwise, the general participants could begin to feel that these are set behind closed doors rather than in an open process.

Final Comments

It is the current sense of the Advisory Council that the researchers and, particularly, the senior leadership of SCEC are doing an outstanding job. The many individuals now leading committees and focus groups constitute a broadly diverse, extremely able, and committed group. The Advisory Council applauds SCEC's continued role in catalyzing and supporting special projects such as UCERF3, high performance computing, and CSEP. Developing new support for these kinds of activities are essential to growing the community of scientists who are engaged in earthquake science and to leverage the knowledge and understanding developed in SCEC.

The Advisory Council is pleased to continue to provide assistance to SCEC in its efforts to formulate and accomplish the center's major goals. At any time the Council welcomes comments, criticism, and advice from the SCEC funders as well as the seismological community, including individuals and groups both inside and outside SCEC membership, on how best to provide that assistance.

The Advisory Council welcomes new members Roger Bilham, University of Colorado; Meghan Miller, UNAVCO; Farzad Naeim, John A. Martin & Associates; John Vidale, University of Washington; Andrew Whitaker, University of Buffalo. We regretfully say goodbye to Patti Guatteri, Swiss Re; John Rudnicki, Northwestern University; and Lloyd Cluff; Pacific Gas and Electric. Patti and John in particular have been very active members of AC for a number of years and we will miss their input and perspective. We all look forward to working with SCEC leadership in helping successfully launching SCEC4 and in helping ensure that the products and accomplishments of the center are well-documented and widely disseminated.

Finally, on a personal note, as of this meeting Mary Lou Zoback is stepping down from the AC and as the chair. This transition is bittersweet; I am balancing the value of rotational leadership with the opportunity to be part of the exciting scientific dialog that is the SCEC collaboration. It has been an honor and a privilege to serve SCEC in this capacity. I depart the AC knowing I leave it in the very able hands of Jeff Freymueller.

SCEC Communication, Education, and Outreach

Mark Benthien / Robert de Groot

CEO Director for SCEC | CEO Education Programs Manager

Introduction

The SCEC Communication, Education, and Outreach (CEO) program has four long-term goals:

- Coordinate productive interactions among a diverse community of SCEC scientists and with partners in science, engineering, risk management, government, business, and education;
- Increase earthquake knowledge and science literacy at all educational levels, including students and the general public;
- Improve earthquake hazard and risk assessments; and
- Promote earthquake preparedness, mitigation, and planning for response and recovery.

These goals are pursued through activities organized within four CEO focus areas: ***Research Partnerships*** coordinated within the SCEC Seismic Hazard & Risk Analysis focus group; ***Knowledge Transfer*** activities with practicing professionals, government officials, scientists and engineers; ***Public Outreach*** activities and products for the general public, civic and preparedness groups, and the news media; ***Education*** programs and resources for students, educators, and learners of all ages, including the Experiential Learning and Career Advancement office which coordinates undergraduate and graduate internships and support for early career scientists. Many activities span more than one CEO focus area.

Partnerships are key to achieving SCEC's mission, research objectives, and outreach goals. These partners include other science organizations (e.g. IRIS, EarthScope, and UNAVCO), engineering organizations (e.g. PEER and EERI), education organizations (e.g. Los Angeles County Unified School District, California Department of Education, museums, and the National Association of Geoscience Teachers), and public service / risk management organizations (e.g. California Emergency Management Agency, the California Earthquake Authority, FEMA, and the American Red Cross).

Immediately following the 2009 SCEC Annual Meeting, a major review meeting was held of the SCEC CEO program. An extensive evaluation document was prepared in summer 2009 by evaluation consultants, which an external review panel used as the basis of its analysis. The review panel's report was quite thorough and provided several excellent recommendations. Overall, they concluded that "It is the strong consensus of the review committee that the SCEC CEO program has been an overwhelming success both in terms of breadth and impact." The SCEC Advisory Council commented that "the review strongly indicates that SCEC has demonstrated success in meeting the Broader Impacts criterion of NSF reviews, has become a leading force in education and outreach efforts related to earthquake science in Southern California, and has set a standard for others to emulate in all of California or elsewhere." The review was very important to the SCEC4 proposal process and was supported with funding from the NSF.

The following are highlights of SCEC's Public Outreach and Education activities in the last year.

Public Outreach Activities

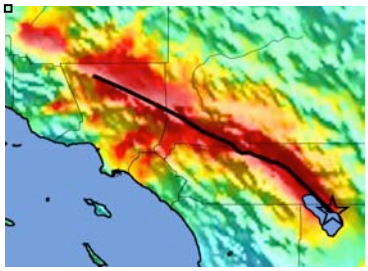

Great (Southern & Statewide) California ShakeOut. A major focus of the CEO program since 2008 has been organizing the Great California ShakeOut drills and coordinating closely with ShakeOuts in other states and countries. The purpose of the Shakeout is to motivate all Californians to practice how to protect ourselves during earthquakes ("Drop, Cover, and Hold On"), and to get prepared at work, school, and home.

Immediately following the 2008 ShakeOut (initially conceived as a "once-in-a-lifetime"

event), participants began asking for the date of the 2009 ShakeOut. After significant discussion among ECA partners and state agencies, the decision was made to organize an annual, statewide Shakeout drill to occur on the third Thursday of October (October 20th1in 2011). This date is ideal for our school partners and follows National Preparedness Month in September, which provides significant exposure prior to the drill (in 2011 we are partnering with FEMA for a "National ShakeOut Registration Week" at the end of September, to encourage participation in all planned ShakeOuts).

The initial statewide expansion was more complicated than simply deleting the word "Southern" from all materials and webpages. The 2008 ShakeOut was based on a single earthquake scenario, which does not apply to the entire state. Thus, 11 "ShakeOut Information Areas" were created, based on earthquake hazards, geography, media markets, and other factors, to provide local hazard information for participants throughout California. The redesigned ShakeOut.org website contains a description of each area's earthquake hazard and ShakeOut registration statistics down to the county level.

In addition, expanding statewide required considerable partnership development with state agencies and regional alliances. As described below, the Earthquake Country Alliance, which has also expanded statewide, is the primary organization behind the ShakeOut, connecting four regional alliances. The group works together to coordinate messaging and develop resources.

7.9 million people participated in the 2010 ShakeOut, up from 6.9 million in 2009. Many participants renew their participation each year, with nearly 5.5 million being staff and students from K-12 schools. The rest are people and organizations that typically do not have earthquake drills. . In addition to registered participants, millions more see or hear about the ShakeOut via the news media. A list of over 300 print and online news stories is available on the ShakeOut web page, which in 2010 included a front-page photo in the New York Times. More than 500 TV and radio news stories across the state and country aired in the days surrouding the drill. A lengthy story on CBS Sunday Morning featured the ShakeOut.

Recruitment is well underway for the 2011 ShakeOut, with over 7.1 million participants registered as of August 31. The goal is to exceed at least 9 million.

The ShakeOut's impact has been more than just as a one-day event. Each registered participant receives periodic reminders leading up to the ShakeOut as well as drill instructions, preparedness information and access to a host of resources available on the ShakeOut website. Participants can download a soundtrack to play during their Drop, Cover, and Hold On Drill, ShakeOut posters and flyers, and web banners to place on their own websites encourage others to participate. ShakeOut flyers are available in many versions including custom flyers for schools, individuals and families, businesses, state and local government, retirement communities, museums and libraries and many other participant categories. We have also made information available in Spanish, Korean, Vietnamese, and Chinese. The ECA has also created several drill manuals for schools, non-profits, businesses, and government agencies, respectively. Each version of the manual has information specific to the type of institution and has multiple drill levels, from a simple drill, to an advanced emergency simulation drill. These manuals include topics for discussion among the organizations leaders, evacuation procedures, and suggestions for making the simulation more engaging for employees or students.1Access to these important earthquake resources is one of the most important benefits of being involved in the ShakeOut.

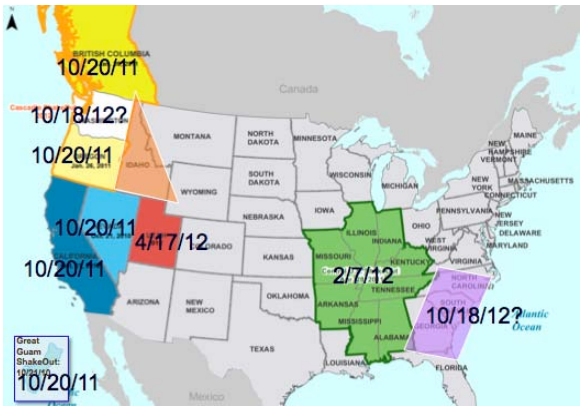

The ShakeOut has been so successful that it has spread across the country, and even around the world. In October 2010 Nevada (110,000 participants) and Guam (38,000) joined with California, In January 2011, Oregon (38,000) and British Columbia (470,000) held drills to commemorate the anniversary of the 1700 Cascadia earthquake, and in April 2011 eleven states of the Central and Southern U.S. (Alabama, Arkansas, Georgia, Illinois, Indiana, Kentucky, Mississippi, Missouri, Oklahoma, South Carolina, and Tennessee) commemorated the 1811-1812 New Madrid earthquake bicentennial with a ShakeOut drill that grew to 3 million participations. Idaho will hold its first ShakeOut in October 2011 and Utah in April 2012. All of these areas are now holding ShakeOut drills annually (see www.shakeout.org/regions). Other areas considering ShakeOut drills include Washington (2012), Alaska (2014), and also Hawaii, Puerto Rico, New Zealand (2012), and Turkey. The ECA is now collaborating with colleagues in Tokyo, to help them coordinate their first ShakeOut on the one-year

anniversary of March 2011 devastating earthquake and tsunami. ShakeOut is changing the way people and organizations are approaching the problems of earthquake preparedness.

The ShakeOut has been the focus of significant media attention and has gone a long way to encourage dialogue about earthquake preparedness in California. Through the ShakeOut, the ECA does more than simply inform Californians about their earthquake risk. The ShakeOut teaches people a life-saving response behavior while fostering a sense of community that facilitates further dialogue and preparedness, and as such is an effective structure for advocacy of earthquake preparedness and mitigation.

Putting Down Roots in Earthquake Country. In 1995 SCEC, the USGS, and a large group of partners led by Lucy Jones (USGS) developed and distributed 2 million copies of a 32-page color handbook on earthquake science, mitigation and preparedness. Funding was primarily from the National Science Foundation and USGS. The booklet was distributed through libraries, preparedness partners, cities, companies, and directly to individuals through SCEC.

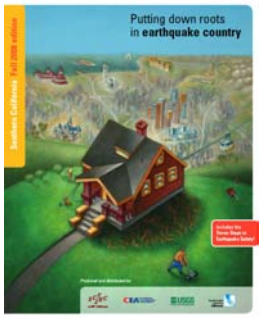

The creation of the Earthquake Country Alliance in 2003 was concurrent with the desire to update Putting Down Roots in advance of the 10th anniversary of the Northridge earthquake. The process brought the ECA together to develop consensus messaging and notably introduced the "Seven Steps to Earthquake Safety," which has become a standard approach to organizing earthquake preparedness messaging. Since 2004, the booklet has undergone six additional revisions and printings. The Fall, 2008, version included the ShakeOut Scenario and an overview of the Uniform California Earthquake Rupture Forecast study led by SCEC. The April, 2011, version includes new tsunami science and preparedness content.

Putting Down Roots has been widely distributed through newspaper inserts, museums, schools, at events organized by SCEC and ECA partners, and via an online order form. Over 2.5 million copies have been distributed since 2004, and an additional 1.25 million copies in Spanish have been distributed. Printing and distribution of the booklet was made possible by generous support of the California Earthquake Authority and additional funding from the Federal Emergency Management Agency (FEMA), and the USGS. The handbook is available at www.earthquakecountry.info/roots as an online version and downloadable PDF, and printed copies can be ordered for free through an online request form.

Putting Down Roots is the principal SCEC framework for providing earthquake science, mitigation, and preparedness information to the public. The "Roots" framework extends beyond the distribution of a printed brochure and the online version. For example, the Birch Aquarium in San Diego developed an earthquake exhibit that featured a "Seven Steps" display, similar to SCEC's "ShakeZone" exhibit at the Fingerprints Youth Museum in Hemet, CA. The Emergency Survival Program (managed by LA County) based its 2006 and 2009 campaigns around the "Seven Steps."

The new version of Putting Down Roots was designed to allow other regions to adopt and adapt its structure to create additional versions. The first is a Greater San Francisco Bay Area version produced by a partnership led by the USGS with SCEC, local and state emergency managers, the Red Cross and many other organizations. Over 2.3 million copies have been printed, many distributed in newspapers, with funding from the California Earthquake Authority, USGS, FEMA, Red Cross, OES, CGS, and several others). In addition, a new booklet, Protecting Your Family From Earthquakes–The Seven Steps to Earthquake Safety, was produced in 2006 as part of the Putting Down Roots series, in two versions - English and Spanish in one booklet, and English, Chinese, Korean, and Vietnamese in another booklet. All Bay Area booklets can also be accessed from www.earthquakecountry.info/roots. All printings of the Bay Area version to date have been coordinated through SCEC.

Other versions have also been produced, and can be downloaded from the Roots website:

- The Utah Seismic Safety Commission in 2008 produced the first version of *Putting Down Roots* outside of California, which in turn was adapted in 2010 by the State of Idaho for their version of *Putting Down Roots*.1Also in 2010, the USGS developed a1Central United States version in time for the New Madrid Bicentennial.

- *Living on Shaky Ground*, an update to the well-known earthquake booklet for California's North Coast, now including the Seven Steps to Earthquake Safety, has been in development for several years and is subtitled "Part of the *Putting Down Roots* in Earthquake Country Series."1This booklet has also been adapted by Oregon.1

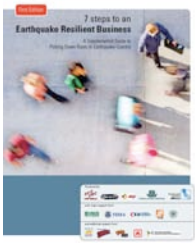

Finally, SCEC and ECA partners have developed a new supplement to Putting Down Roots (and the Living on Shaky Ground booklets as well), titled The Seven Steps to an Earthquake Resilient Business, an exciting new 16-page guide for businesses to develop comprehensive earthquake plans, printed in Fall, 2008. This booklet is the first non-regional publication, created as a supplement to all Putting Down Roots or other materials that include the Seven Steps to Earthquake Safety. It can be also downloaded and ordered from www.earthquakecounty.info/roots.

Earthquake Country Alliance. The ECA is a public-private partnership of people, organizations, and regional alliances, each of which are committed to improving preparedness, mitigation, and resiliency.1The ECA was created in 2003 to coordinate efforts in southern California, and grew statewide in early 2009 in partnership with similar groups in the Bay Area and North Coast. People, organizations, and regional alliances of the ECA collaborate in many ways: sharing resources; committing funds; and volunteering significant time towards common activities.1ECA's mission is to support and coordinate efforts that improve earthquake and tsunami resilience. The Earthquake Country Alliance is now the primary SCEC mechanism for maintaining partnerships and developing new products and services for the general public.

SCEC has played a key role in the development of the ECA, beginning in 2003 when SCEC convened formative meetings with many key partners at USC and created the original ECA website, in advance of the ten-year anniversary of the Northridge earthquake. This role has continued as materials, activities, and new partnerships have been developed and expanded.1SCEC develops and maintains all ECA websites (*www.earthquakecountry.org*, *www.shakeout.org*, *www.dropcoverholdon.org*, and *www.terremotos.org*), has managed the printing of the "Putting Down Roots" publication series throughout the state, and coordinated key aspects of ShakeOut recruitment, content development, and customer support, including support for ShakeOut efforts in other regions.

Feedback from selected ECA members collected through interviews in 2009 indicate that the foundation and development of the ECA benefited greatly from SCEC's leadership, credibility and reputation as a trusted science and research consortium. As a non-governmental entity, SCEC is viewed as a 'neutral' and trusted leader, who employs a collaborative model for organizing stakeholders around a common cause. SCEC brings value to the collaborative by providing science-based information about earthquakes, incorporating this information in the development of materials and tools, and contributing human and material resources.

ECA members have also commented that the grassroots approach employed by SCEC in the development of the ECA has created a 'flexible' environment, with added value for its members that include: a) networking, b) coordination, c) ability to participate at different levels and in varying roles over time (fluid participation), d) opportunities to contribute to the dialogue about hazard preparedness, response and mitigation, e) ability to adapt information and materials to local contexts and for local audiences, f) and publicity.

In November 2010, the ECA held a Strategic Planning Workshop to discuss next steps for the organization's expanding programs and to increase engagement in the planning, management, and funding of initiatives. In this Workshop, the five researched solutions presented and discussed included the ECA becoming a 1) 501(c)(3) non-profit; 2) a 501(c)(4) non-profit; 3) a 501(c)(6) non-profit; 4) remaining as the same structure- a loosely organized confederation that cannot accept/administer grant funds directly; or, 5) becoming a program of SCEC under as part of SCEC's USC-based structure. Pros and cons were listed for all options looking at management, funding/budget, legal, governmental requirements, and other implications. The unanimous consensus of ECA leadership was to organize the ECA at USC to be administered by SCEC, under the direction of a statewide Steering Committee made up of regional ECA leaders, with these considerations:

- Recognize the diverse and voluntary nature and size of ECA's component organizations and allow participation by the widest possible net of stakeholders, with an emphasis on regional groupings;
- Acknowledge that although most ECA Associates represent organizations, certain organizations need a role in the management structure;

- Minimize the size and role of the statewide effort in favor of supporting and connecting component organizations and regional alliances;
- Foster information sharing and provide effective and direct means of communication within and among ECA groups.

ECA Associates benefit from their participation by coordinating their programs with larger activities to multiply their impact; being recognized for their commitment to earthquake and tsunami risk reduction; having access to a variety of resources on earthquake and tsunami preparedness; networking with earthquake professionals, emergency managers, government officials, business and community leaders, public educators, and many others; and connecting with ECA sector-based committees to develop customized materials and activities. To participate, visit *www.earthquakecountry.org/alliance/join.html*.

Media Relations. SCEC engages local, regional and national media organizations (print, radio and television) to jointly educate and inform the public about earthquake-related issues. The goal has been to communicate clear, consistent messages to the public–both to educate and inform, and to minimize misunderstandings or the perpetuation of myths. SCEC CEO encourages scientists who are interested in conducting interviews with media reporters and writers to take advantage of short courses designed and taught by public information professionals.

Education Program

SCEC and its expanding network of education partners are committed to fostering increasing earthquake knowledge and science literacy at all grade levels and in a variety of educational environments.

The SCEC Education program uses the research literature (science education, learning psychology, sociology, etc.) and evaluation methodology to:

- Develop new materials and products (e.g. lesson plans, evaluation instruments, websites) where needed.
- Collaborate with partner organizations to enhance existing materials or products to meet the needs for SCEC's Earthquake Program mission.
- Utilize and promote existing materials that coincide with or complement SCEC's earthquake K-12 Education Program mission.
- Provide innovative experiential learning opportunities to undergraduate and graduate students during the summer and year-round.

SCEC Education programs include internship programs, facilitated activities at museum exhibits, earthquake education workshops, public earthquake talks, and activities at conferences such as the National Science Teachers Association. SCEC Education programs and products are implemented in a variety of educational environments- any place, situation, or context where the transmission of knowledge to learners is taking place.

SCEC Experiential Learning and Career Advancement Programs

Since 1994, SCEC has provided 457 internships to undergraduate and graduate students (some students participate in multiple years and are counted each time), with 384 internships since 2002 (charts included here are for 2002-2009 only). SCEC currently offers two summer internship programs (SCEC/SURE and SCEC/UseIT) and in 2010 completed a year-round program for both undergraduate and graduate students (ACCESS). These programs are the principal framework for undergraduate student participation in SCEC, and have common goals of increasing diversity and retention. In addition to their research projects, participants come together several times during their internship for orientations, field trips, and to present posters at the SCEC Annual meeting. Students apply for both programs at www.scec.org/internships.

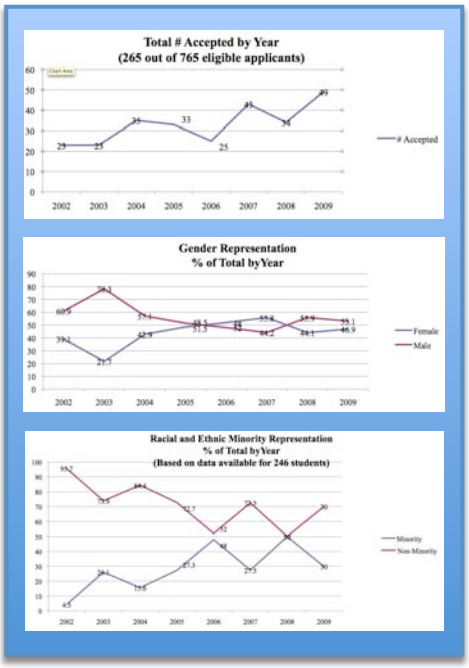

The SCEC Summer Undergraduate Research Experience (SCEC/SURE) has supported 221 students to work one-on-one as student interns with1SCEC scientists since 1994 (150 since 2002). SCEC/SURE has supported students working on numerous projects in earthquake science, including the history of earthquakes on faults, risk mitigation, seismic velocity modeling, science education, and earthquake engineering.

The SCEC Undergraduate Studies in Earthquake Information Technology (SCEC/UseIT) program, unites undergraduates from across the country in an NSF REU Site at USC. SCEC/UseIT interns interact in a team-oriented research environment with sme of the nation's most distinguished geoscience and computer science researchers. Since 2002, 167 students have participated. Research activities are structured around "Grand Challenges" in earthquake information technology. Each summer the interns build upon the foundation laid by previous intern classes to design and engineer increasingly sophisticated visualization tools.

Our UseIT and CME experience identified a "weak link" in cyberinfrastructure (CI)-related career pathways: the transition from discipline-oriented undergraduate degree programs to problem-oriented graduate studies in earthquake system science. We worked to address this educational linkage problem through a CI-TEAM implementation project entitled the Advancement of Cyberinfrastructure Careers through Earthquake System Science (ACCESS) which ended in late 2010 with 29 internships having been awarded. The objective of the ACCESS project was to provide a diverse group of students with research experiences in earthquake system science that will advance their careers and encourage their creative participation in cyberinfrastructure development. Its overarching goal was to prepare a diverse, CI-savvy workforce for solving the fundamental problems of system science. Undergraduate (ACCESS-U) internships support CI-related research in the SCEC Collaboratory by undergraduate students working toward senior theses or other research enhancements of the bachelor's degree. Graduate (ACCESS-G) internships supported up to one year of CI-related research in the SCEC Collaboratory by graduate students working toward a master's thesis.

Earthquake Exhibits and Museum Partnerships

Recognizing the key role that museums have in engaging communities not often reached by schools, SCEC facilitates a network of museums and other locations interested in providing earthquake education programming. These organizations also serve as a distribution point for SCEC resources such as Roots. SCEC has worked with some of these partners for many years, and in summer 2008 they have been organized as Earthquake Education and Public Information Centers (Earthquake EPIcenters). The concept emerged during the planning of the 2008 Great Southern California ShakeOut, and the need to organize museums for the ShakeOut has evolved into a year-round interaction with the ShakeOut being the culminating community event for the year. The ShakeOut has provided a basis for institutions to share resources and expertise

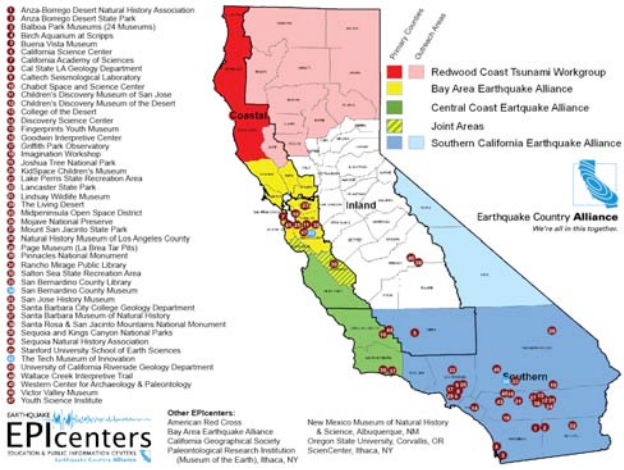

EPIcenters share a commitment to demonstrating and encouraging earthquake preparedness. They help coordinate Earthquake Country Alliance activities in their county or region (including the ShakeOut), lead presentations or organize events in their communities, or in other ways demonstrate leadership in earthquake education and risk reduction. EPIcenters are found in a variety of public meeting places such as museums, science centers, libraries, and universities. Just as the ShakeOut became a statewide effort in 2009 so did the EPIcenter Network. Currently over 60 free-choice learning institutions statewide participate in the ShakeOut and other activities throughout the year. The statewide Network is coordinated by SCEC Education Program Manager Robert de Groot with Kathleen Springer (San Bernardino County Museum) and Candace Brooks (The Tech Museum) coordinating Network activities in Southern and Northern California respectively.

SCEC's first major project in the development of a free choice-learning venue was the Wallace Creek Interpretive Trail. In partnership with the Bureau of Land Management (BLM), SCEC designed an interpretive trail along a particularly spectacular and accessible 2 km long stretch of the San Andreas Fault near Wallace Creek. Wallace Creek is located on the Carrizo Plain, a 3-4 hour drive north from Los Angeles. The trail opened in January 2001. The area is replete with the classic landforms

produced by strike-slip faults: shutter ridges, sag ponds, simple offset stream channels, mole tracks and scarps. SCEC created the infrastructure and interpretive materials (durable signage, brochure content, and a website at *www.scec.org/wallacecreek* with additional information and directions to the trail). BLM has agreed to maintain the site and print the brochure into the foreseeable future.

The *ShakeZone Earthquake Exhibit* at Fingerprints Youth Museum in Hemet, CA was developed originally in 2001, was redesigned in 2006, and was retired from display in 2011. The redesigned version of the exhibit is based on SCEC's *Putting Down Roots in Earthquake Country* handbook. Major partners involved in the exhibit redesign included Scripps Institution of Oceanography and Birch Aquarium at Scripps. With funding from the United Way and other donors ShakeZone will be expanded in 2010 to include a section on Earthquake Engineering.

In 2006 SCEC has embarked on a long-term collaboration with the San Bernardino County Museum (SBCM) in Redlands, California. SCEC participated in the development and implementation of Living on the Edge Exhibit. This exhibit explains and highlights natural hazards in San Bernardino County (e.g. fire, floods, and earthquakes). SCEC provided resources in the development phase of the project and continues to supply the exhibit with copies of *Putting Down Roots in Earthquake Country*.

As a result of the successful collaboration on *Living on the Edge*, SCEC was asked to participate in the development of SBCM's *Hall of Geological Wonders*. To be completed in 2012, the Hall is a major expansion of this important cultural attraction in the Inland Empire. One of the main objectives of the Hall is to teach about the region from a geologic perspective. The museum is devoting a large space to the story of Southern California's landscape, its evolution and dynamic nature. SCEC has played an ongoing advisory role, provided resources for the development of the earthquake sections of the exhibit, and will have an ongoing role in the implementation of educational programming

The most recent debut of an EPIcenter earthquake display is the *Earthquake Information Center* at the Rancho Mirage Public Library in Rancho Mirage, CA. This exhibit, created in partnership with the City of Rancho Mirage, features a computer screen showing recent worldwide and local earthquakes. Located in the computer resource room this exhibit also displays the seven steps to earthquake safety and components of a basic earthquake disaster supply kit. Many hundreds of local residents from the desert communities pass by the exhibit every day on their way to accessing other resources in the library. Recently, the1Development of other EPIcenter exhibits and resource areas are occurring at the The California Science Center, Los Angeles, and the Natural History Museum of Los Angeles County.

K-12 Education Partnerships and Activities

Partnerships with Science Education Advocacy Groups and Organizations with Similar Missions. SCEC is an active participant in the broader earth science education community including participation in organizations such as the National Association of Geoscience Teachers, the Coalition for Earth System Education, and local and national science educator organizations (e.g. NSTA). Improvement in the teaching and learning about earthquakes hinges on improvement in earth science education in general. Hence, SCEC contributes to the community through participation on outreach committees wherever possible, co-hosting meetings or workshops, and building long-term partnerships. An example of a current project is a partnership with EarthScope to host a San Andreas Fault workshop for park and museum interpreters that was held in Spring 2009. In 2010 SCEC is collaborating with IRIS and EarthScope in developing the content for the San Andreas fault Active Earth Kiosk. The Active Earth Kiosk is an interactive website where visitors learn about earth hazards in a particular region. EarthScope is creating an Active Earth Kiosk for each of the regions covered by its Interpretive Workshops. Also in 2010 Arizona State University, the OpenTopography Facility, and SCEC developed three earth science education products to inform students and other audiences about LiDAR and its application to active tectonics research. First, a 10-minute introductory video titled LiDAR: *Illuminating Earthquakes* was produced and is freely available online. The second product is an update and enhancement of the Wallace Creek Interpretive Trail website. LiDAR topography data products have been added along with the development of a virtual tour of the offset channels at Wallace Creek using the B4 LiDAR data within the Google Earth environment. Finally, the virtual tour to Wallace Creek is designed as a lab activity for introductory undergraduate geology courses to increase understanding of earthquake hazards through exploration of the dramatic offset created by the San Andreas Fault (SAF) at Wallace Creek and Global Positioning System-derived displacements spanning the SAF at Wallace Creek. This activity is currently being tested in courses at Arizona State University. The goal of the assessment is to measure student understanding of plate tectonics and earthquakes after completing the activity. Including high-

resolution topography LiDAR data into the earth science education curriculum promotes understanding of plate tectonics, faults, and other topics related to earthquake hazards.

Teacher Workshops. SCEC offers teachers 2-3 professional development workshops each year with one always held at the SCEC Annual Meeting. The workshops provide connections between developers of earthquake education resources and those who use these resources in the classroom. The workshops include content and pedagogical instruction, ties to national and state science education standards, and materials teachers can take back to their classrooms Workshops are offered concurrent with SCEC meetings, at National Science Teachers Association annual meetings, and at the University of Southern California. In 2003 SCEC began a partnership with the Scripps Institution of Oceanography Visualization Center to develop teacher workshops. Facilities at the Visualization Center include a wall-sized curved panorama screen (over 10m wide). The most recent teacher workshop held in partnership with Mt. San Antonio College was held in April 2010 at the GSA Cordilleran Section meeting.

Since 2009, SCEC has been collaborating with the Cal State San Bernardino/EarthScope RET program led by Sally McGill. During the course of the summer 7-10 high school teachers and their students conduct campaign GPS research along the San Andreas and San Jacinto faults. SCEC facilitates the education portion of the project through the implementation of the professional development model called Lesson Study. This allows for interaction with the teachers for an entire year following their research. For the second year all of the members of the RET cohort participate in the SCEC Annual Meeting by doing presentation of their research, participating in meeting activities such as talks and works culminating in presenting their research at one of the evening poster sessions.

Sally Ride Science Festivals. Attended by over 1000 middle school age girls (grades 5–8) at each venue, Sally Ride Science Festivals offer a festive day of activities, lectures, and social activities emphasizing careers in science and engineering. Since 2003, SCEC has presented workshops for adults and students and participated in the Festival's "street fair," a popular venue for hands-on materials and science activities. At the street fair SCEC demonstrates key concepts of earthquake science and provides copies of *Putting Down Roots in Earthquake Country*. The workshops, presented by female members of the SCEC community share the excitement and the many career opportunities in the Earth sciences.

National Science Teachers Association and California Science Teachers Association. Earthquake concepts are found in national and state standards documents. For example, earthquake related content comprises the bulk of the six grade earth science curriculum in California. SCEC participates in national and statewide science educator conferences to promote innovative earthquake education and communicate earthquake science and preparedness to teachers in all states.

Development of Educational Products

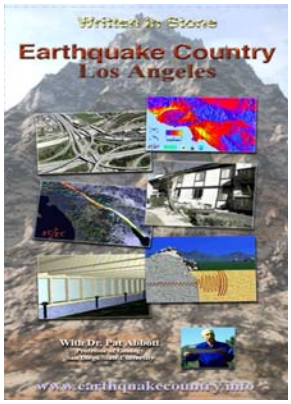

Earthquake Country - Los Angeles Video Kit. The video, produced by Dr. Pat Abbott of SDSU, tells the story of how the mountains and valleys of the Los Angeles area formed, and the important role of earthquakes. The video features aerial photography, stunning computer animations (some produced by SCEC's USEIT interns), and interviews with well-known experts. SCEC developed an educator kit for school and community groups, available online and provided at SCEC's teacher workshops.

Plate Tectonics Kit. This new teaching tool was created to make plate tectonics activities more accessible for science educators and their students. SCEC developed a user-friendly version of the *This Dynamic Earth* map, which is used by many educators in a jigsaw-puzzle activity to learn about plate tectonics, hot spots, and other topics. At SCEC's teacher workshops, educators often suggested that lines showing the location of plate boundary on the back of the maps would make it easier for them to correctly cut the map, so SCEC designed a new (two-sided) map and developed an educator kit.

Research Accomplishments

Southern California Earthquake Center

2011 Annual Report

This section summarizes the main research accomplishments and research-related activities during 2009 and the early months of 2010. The research reported here was funded by SCEC with 2010 research funds. While the presentation is organized sequentially by disciplinary committees, focus groups, and special project working groups, it is important to note that most SCEC activities are crosscutting and could be presented under multiple focus groups.

Disciplinary Activities

The following reports summarize recent progress in the three main infrastructural activities and the discipline-oriented research, *Seismology, Geodesy,* and *Geology*.

Seismology

The objectives of the Seismology group are to gather data on the range of seismic phenomena observed in southern California and to integrate these data into physics-based models of fault slip. Researchers investigate seismicity across the network of southern California faults to explore spatial and temporal distribution of earthquakes and tremor, associated stress drops, and triggering etc. New methods are being developed to search for unusual signals using combined seismic, GPS, and borehole strainmeter data. In addition, near-fault crustal properties, fault structural complexity, and constraints on crustal structure and the state of stress are being explored. The seismology group is committed to the enhancement and continued operation of the SCEDC and other existing SCEC facilities particularly the near-real-time availability of earthquake data from SCEDC and automated access. Related work includes the enhancement of capability for earthquake early warning (EEW) systems and densification of seismic instrumentation. Below we highlight a subset of the recent research accomplishments.

Seismicity Studies

Figure 1. Major earthquake swarms in the Salton Trough since 1981. Examples of estimated seismicity migration vectors are plotted in red. These generally trend SW– NE at velocities of 0.1 to 0.5 km/hr.

Shearer and Hauksson are producing an updated relocated reference catalog that will include accurate error estimates. More than 500,000 earthquakes are included between 1981-2010. The effort required the development of new analysis methods to mine efficiently the large dataset. Shearer et al. also explored major earthquake swarms that occurred in the Salton Trough since 1981. They found that swarms typically last 1-20 days and that seismicity during a swarm migrates with time. Analysis of the migration shows that swarm migrations typically trend SW-NE at a rate of 0.1 to 0.5 km/hr (Figure 1).

Hauksson et al. examine the Mw7.2 El Mayor-Cucapaph mainshock and aftershock sequence that began on 4 April 2010. They found that the mainshock was complex and triggered earthquakes to the north along the Elsinore and San Jacinto faults (Figure 2). The focal mechanisms of the mainshock and M4+ aftershocks exhibit mostly northwest to west- northwest-striking dextral strike-slip faulting, although the faulting in the Yuha basin is in a region of northwest and northeast striking faults.

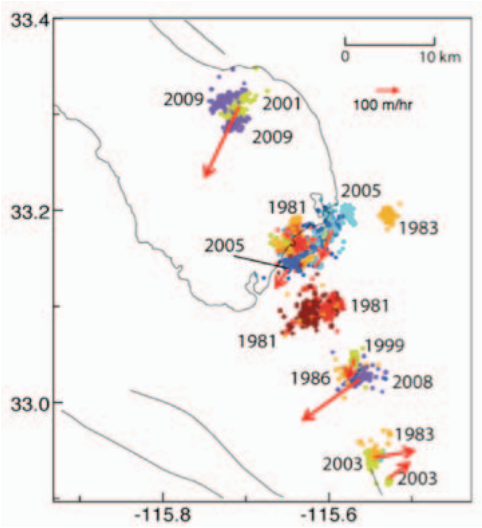

Figure 1. Major earthquake swarms in the Salton Trough since 1981. Examples of estimated seismicity migration vectors are plotted in red. These generally trend SW–NE at velocities of 0.1 to 0.5 km/hr.

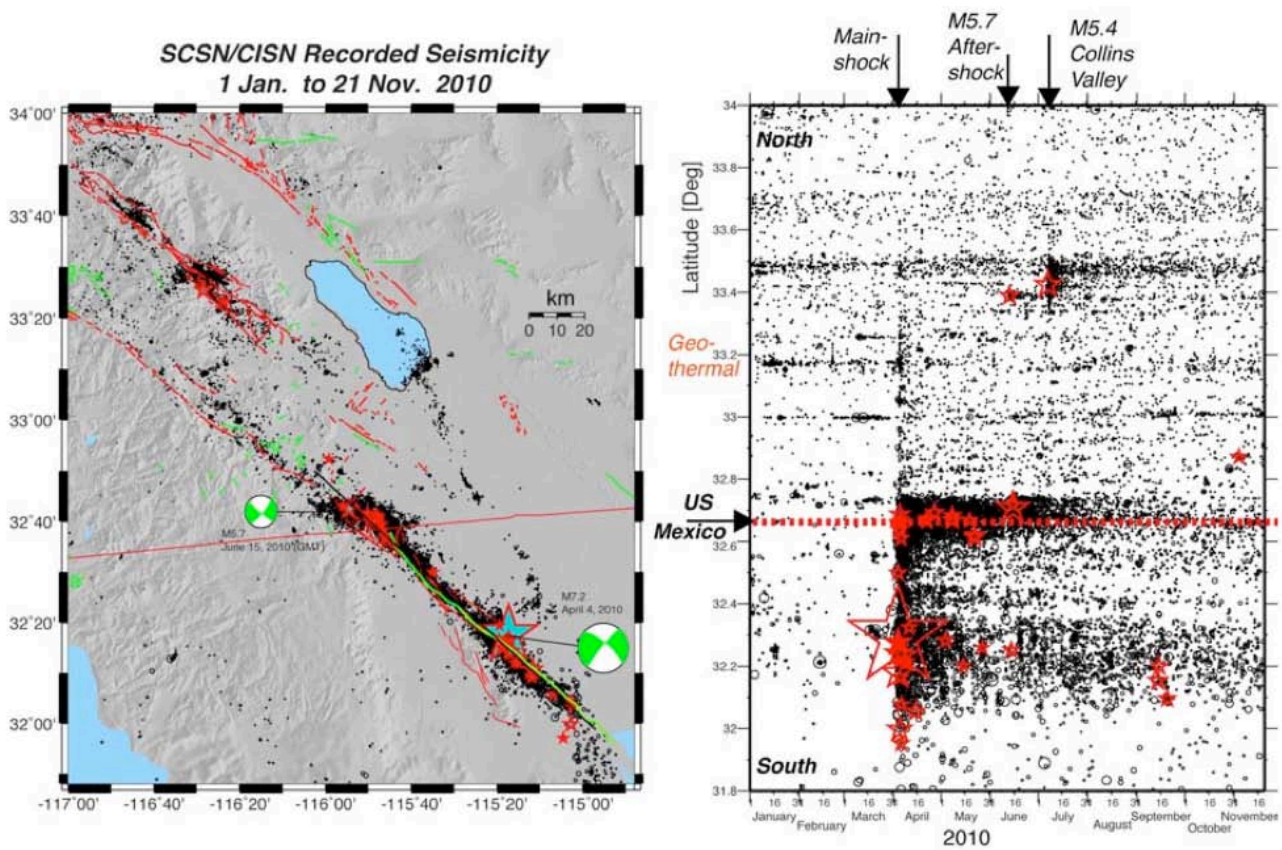

Figure 2. (Left) Map of El Mayor sequence and the background seismicity from 1 Jan. to 21 Nov. 2010. (Right) Time-space plot of latitude versus time of El Mayor aftershocks triggered earthquakes to the north along the San Jacinto and Elsinore fault zones.

Observations of Tremor in California

Bürgmann et al. examine triggering of tremor and repeating earthquake sequences (RES) at Parfield. They explore whether tidal triggering of tremor occurs by comparing the timing of 600,000 low-frequency earthquakes (LFEs) reported in the Shelly and Hardebeck [2010] catalog. They find that the shear stress perturbations correlate with tremor occurrence better than normal stress perturbations (Figure 3). They also find that short-term triggering may occur between neighboring events as shown by the joint occurrence of RES and nearby background earthquakes. The immediate triggering of few second to minutes can happen when the separation distance is within a few km. When earthquakes are farther apart, triggering is less efficient.

Peng et al. explore and compare triggered tremor in California. They find that along the San Andreas fault triggering generally occurs after the S-wave arrival with the most intense triggering during large-amplitude

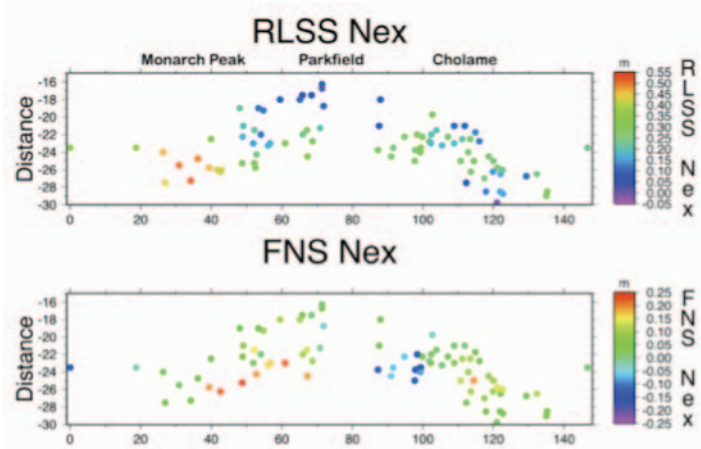

Figure 3. Along-fault section near Parkfield showing LFE locations colored by the percent excess value (Nex), the difference between the actual and expected number of events that occur under a particular tidal loading condition divided by the expected number of events. Positive Nex values indicate a surplus of events and negative values, a deficit. Values representing correlation of LFE occurrence with right-lateral shear stress (RLSS, top) and fault normal stress (FNS, bottom) are shown.

surface wave arrivals. They find an apparent migration of triggered LFEs along strike at 80 km/hr. The observation of triggered tremor on northern and southern California faults is less frequent and these tremor episodes have lower amplitudes (Figure 4).

Cochran et al. are developing a neural network approach to detect tremor within continuous data. The approach uses Self Organizing Maps (SOMs) based on the work of Köhler et al [2009] to classify the time-series data into prototype vectors based on waveform characteristics including frequency content, amplitude, and polarization. These prototype vectors can then be associated with different signal types including earthquakes, tremor, and noise. The method is being applied to data collected during a temporary deployment of broadband instruments near Cholame, California.

Fault Structure and Damage Zones

Li et al. completed a detailed study of the on- and near-fault damage and healing at the San Andreas fault (SAF) Parkfield and the Longmen-Shan Fault (LSF) in Sichuan, both of which ruptured in the recent major earthquakes. Along the SAF, they find a waveguide that is interpreted to be a damage zone of reduced seismic velocities with a width of 100-200 m that extend to at least 7 km depth (Figure 5). The Wenchuan fault is found to have a 200-400 m wide damage zone with velocities reduced by up to 50% at shallow depths.

Ma modeled the effect of heterogeneity of fault geometry on rupture dynamics in three dimensions with off-fault plasticity (Figure 6). He finds that fault roughness results in irregular rupture fronts that could result in greater high-frequency radiation. In addition, he finds that fault roughness results in more pulse-like ruptures due to rapid healing. Duan models the effect of off-fault damage and pore-pressure variations on the dynamics of parallel strike-slip faults. He finds that when effects of off-fault plastic yielding and time-dependent pore pressure changes are combined, the effect of time-dependent pore-pressure dominates, while off-fault plastic yielding only exerts a second-order effect.

References

Aiken, C., Z. Peng, and C. Wu (2011), Dynamic triggering of microearthquakes at three geothermal regions in California, Seismological Society of America Annual Meeting, Memphis, TN.

Aguiar, A. C., J. R. Brown, and G. C. Beroza (2009), Non-volcanic tremor near the Calaveras Fault Triggered by Mw~8 Teleseisms, Eos Trans. AGU, 90(54), Fall Meet. Suppl., Abstract T23E-06.

Chao, K., Z. Peng, A. Fabian, and L. Ojha (2011), Comparisons of Triggered Tremor in California, Seis. Res.

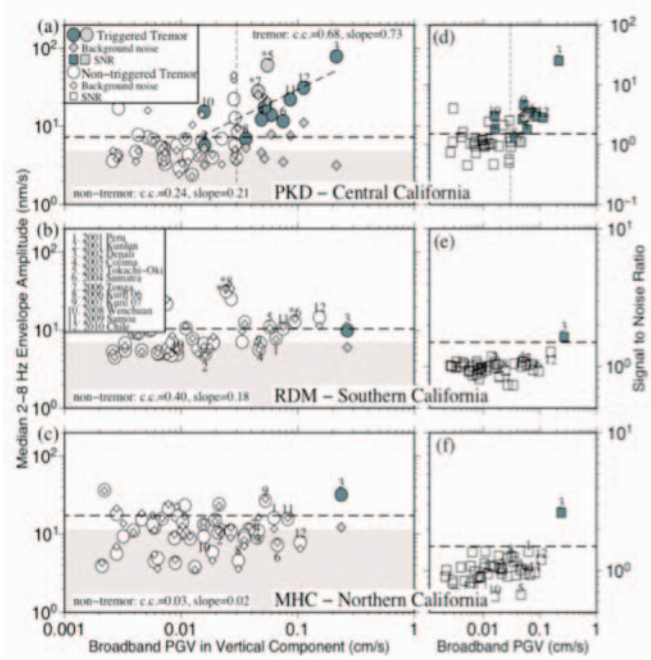

Figure 4. Median amplitude of the high-frequency envelope functions versus the peak surface wave amplitudes measured at the broadband station PKD in central California for teleseismic earthquakes. The values measured during the surface waves and before the P-wave.

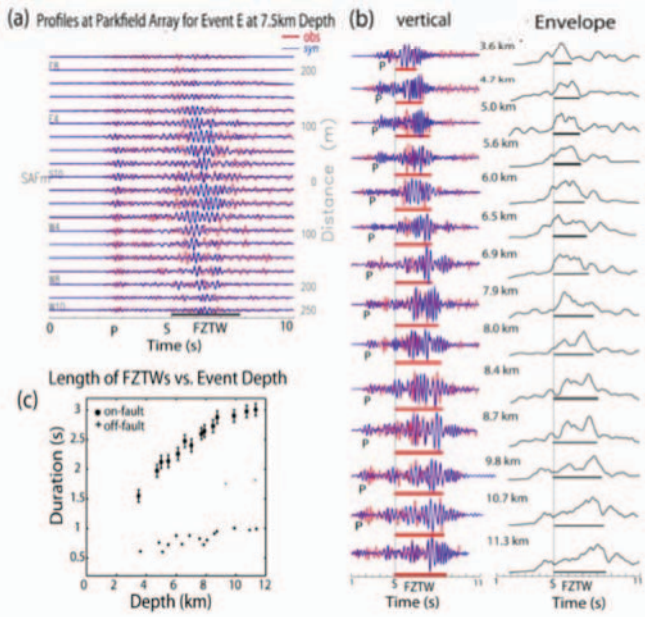

Figure 5. (a) Observed and synthetic vertical-component seismograms for an on-fault aftershock recorded at an array near Parkfield, showing fault-zone guided waves. Seismograms have been <6 Hz filtered. (b) Observed and synthetic vertical-component seismograms and envelopes at on-fault station ST0 for 14 on-fault aftershocks that occur at a range of depths (c) The measured FZTW wavetrain lengths versus focal depths for the 14 aftershocks recorded at on-fault (black circles) and off-fault (grey crosses) stations.

Lett., Seismological Society of America Annual Meeting, Memphis, TN.

Chen, K. H., Bürgmann, R., and Nadeau, R. M. (2010), Triggering effect of M 4-5 earthquakes on the earthquake cycle of repeating events at Parkfield, Bull. Seism. Soc. Am., 100, 2, doi:10.1785/0120080369.

Fabian, A., L. Ojha, Z. Peng, and K. Chao (2009), Systematic search of remotely triggered tremor in Northern and Southern California, Eos Trans. AGU, 90(54), Fall Meet. Suppl., Abstract T13D-1916.

Hauksson, E., J. Stock, K. Hutton, W. Yang, A. Vidal, and H. Kanamori, The 2010 Mw7.2 El Mayor-Cucapah Earthquake Sequence, Baja California, Mexico and Southernmost California, USA: Active Seismotectonics Along the Mexican Pacific Margin, Pure Appl. Geophys, Topical Issue: Geodynamics of the Mexican Pacific Margin, DOI 10.1007/s00024-010-0209-7, 2010.

Horstmann, T., Harrington, R.M., Cochran, E.S., Wang, T., Potier, C.E. (2010), Automatic tremor detection and waveform component analysis using a neural network approach, Abstract S23A-2122, 2010 Fall Meeting, American Geophysical Union.

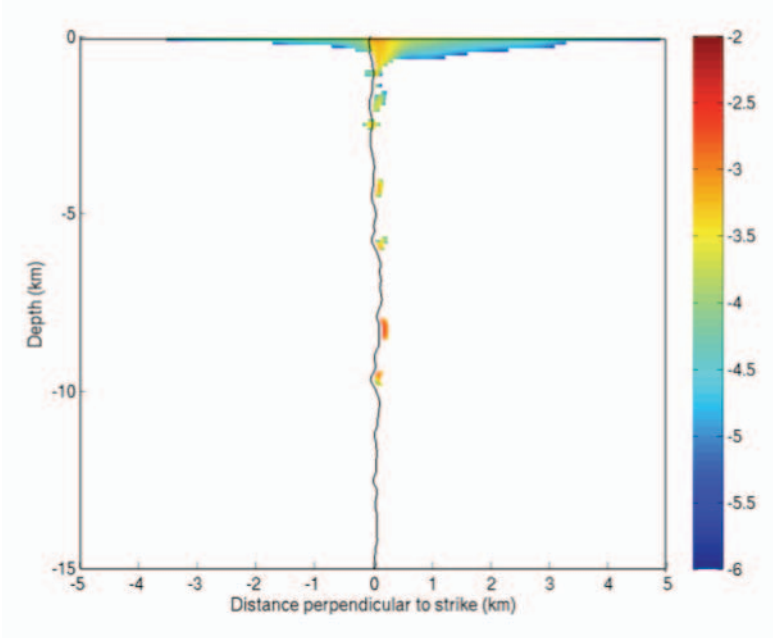

Figure 6. Accumulated plastic strain in logarithmic scale at a cross section 15 km from the epicenter from a model using a fractal fault geometry. The curved black line shows the fault trace at this cross section. The right side of the fault is a extensional regime, where the plastic strain is larger.

Li, Y. G., P. Malin, and E. Cochran, High-Resolution Characterization of the Damage Zone on the Parkfield San Andreas Fault at Depth from Fault-Zone Trapped Waves, Book of Frontiers in Seismology, China High-Education Press, Beijing , in press, 2011

Ma, S., and D. J. Andrews (2010), Inelastic off-fault response and three-dimensional earthquake rupture dynamics on a strike-slip fault, J. Geophys. Res., 115, B04304, doi:10.1029/2009JB006382.

Peng, Z., D. P. Hill, D. R. Shelly and C. Aiken (2010), Remotely triggered microearthquakes and tremor in Central California following the 2010 Mw8.8 Chile Earthquake, Geophys. Res. Lett., 37, L24312, doi:10.1029/2010GL045462.

Peng, Z., C. Wu, and C. Aiken (2011), Delayed triggering of microearthquakes by multiple surface waves circling the Earth, Geophys. Res. Lett., Geophys. Res. Lett., 38, L04306, doi: 2010GL046373.

Shelly, D. R., Z. Peng, D. P. Hill and C. Aiken (2011), Delayed dynamic triggering of tremor and implications for triggered creep and earthquakes, Nature Geosci., accepted.

Shelly, D. R., and J. L. Hardebeck (2010), Precise tremor source locations and amplitude variations along the lower␣crustal central San Andreas Fault, Geophys. Res. Lett., 37, L14301, doi:10.1029/2010GL043672.

Tectonic Geodesy

Introduction

The tectonic geodesy community within SCEC has again focused its efforts on inter-related combinations of data gathering and interpretation. The validation and application of transient detection algorithms was again a major effort, with a wide range of algorithms being tested against real and synthetic data. We are currently on track to having several detectors running in a SCEC-supported testing framework before the end of the year.

Transient Detection

Duncan Agnew made his FAKENET software available to the community, both for internal testing of detection algorithms as well as for the generation of new synthetic test data. Some of the major changes this year allowed inclusion of more realistic, non-sinusoidal seasonal signals and volume sources that imitate the effects of groundwater withdrawal and recharge. Herring

also supported the effort through the ongoing generation of a merged geodetic data product. The initial phase of "automated" detections will be performed on the PBO data product.

Approaches used in transient detection fall generally into strain-based, "menu function"-based (i.e., various flavors of Kalman filters), and eigenvector/principle component decomposition-based families. Holt's strain-based approach uses a polynomial interpolation and appears to be fairly sensitive to the background strain field used in the analysis and to variations in temporal coverage caused by stations coming in and out of the network. However, it did detect some signals that were not found by other approaches. Segall et al's Network Inversion Filter performed well on the blind test exercise this year, and they continue to work on rigorously assessing the statistical significance of detections. McGuire, Wei and Segall apply their Network Strain filter to data from the Tohoku earthquake and find that their approach would have detected slow slip in the 48 hours before the mainshock. They also suggest that offshore pressure gauge data may have allowed further confidence in identifying the precursory slip.

Ji and Herring's principal component approach has been, in general, the most successful of the decomposition-based approaches, and they have applied it to real data from Akutan Volcano, in Alaska. They perform their PCA analysis on data that has already been filtered using a state estimation that is part of a Kalman filter. Lipovsky & Funning use eigenfunctions with and without filtering of the noise and find that they are unable to detect most of the synthetic test signals (Figure 7). They also apply their approach to InSAR data in the Bay Area, and find that it is very sensitive to seasonal, aquifer-related signals. Empirical Mode Decomposition and autoregressive processes are explored by Becker et al., but to date they have not proved useful for applications on large networks with real data. Kreemer et al. use a decomposition into piecewise-linear segments, which may potentially be very efficient. However, they do not think that their approach will be viable for automatic detections, as it does still require some manual intervention and is not ideal in regions with a large station spacing.

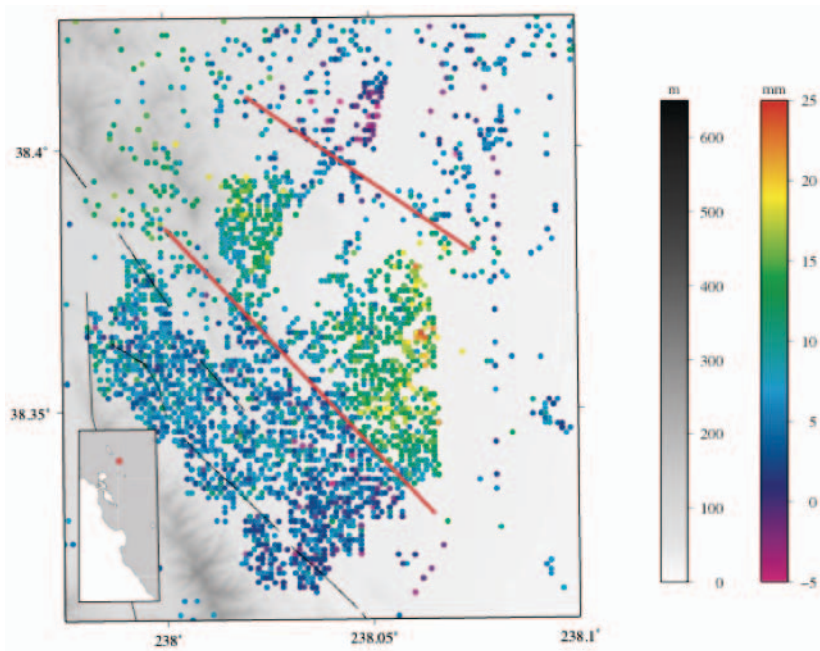

Figure 7. Seasonal deformation from a subset of the ERS T70 InSAR dataset. The deformation pattern shows a confined aquifer that is bounded by two previously unknown faults. Known faults are shown with thin, black lines. (Funning and Lipovsky, 2010)

Data Collection and Analysis

Marshall et al. continued development of a GPS dataset for the Western Transverse Ranges by filtering data to remove offsets and seasonal signals. They are currently processing InSAR data, which will be used to identify and mitigate any remaining signals in the GPS data related to anthropogenic sources, such as aquifer draw-down. These observations, along with geologic slip rates, will be used to constrain Boundary Element Method models of the Ventura basin (employing the CFM) that account for the different geodetic and geologic time scales.

Sandwell et al. continued rapid-static GPS surveys of the Brawley seismic zone in order to understand better how strain is partitioned in this region. The growing dataset records the 2005 Obsidian Buttes earthquake swarm, highlighting a northeast striking fault at the location of the observed strain anomaly. If the swarm were due to slip on this fault, the data suggest that 9 mm/yr of left lateral motion occurred between 2003 and 2009. The dense geodetic array developed for this work also has provided the opportunity to observe triggered slip due to the El Mayor Cucapah earthquake. In addition to this work, Sandwell et al. have established 17 new GPS monuments across the Imperial fault and launched an intense field effort to collect data both north and south of the Mexico border following the El Mayor Cucapah event, building on an existing collaboration with scientists at CISESE through which they were already collecting interseismic data in this region (Figure 8).

Funning et al. resurveyed 19 GPS sites in the Anza gap region along the San Jacinto fault and processed these data to extend position time series for these sites. These data have made possible new or revised velocity calculations for GPS sites in this region. In the event of a San Jacinto fault earthquake, these velocities will be required in order to obtain accurate coseismic and postseismic displacement measurements. Improved interseismic velocities will also prove valuable for refining models strain accumulation, and thus seismic hazard, in the vicinity of the San Jacinto fault.

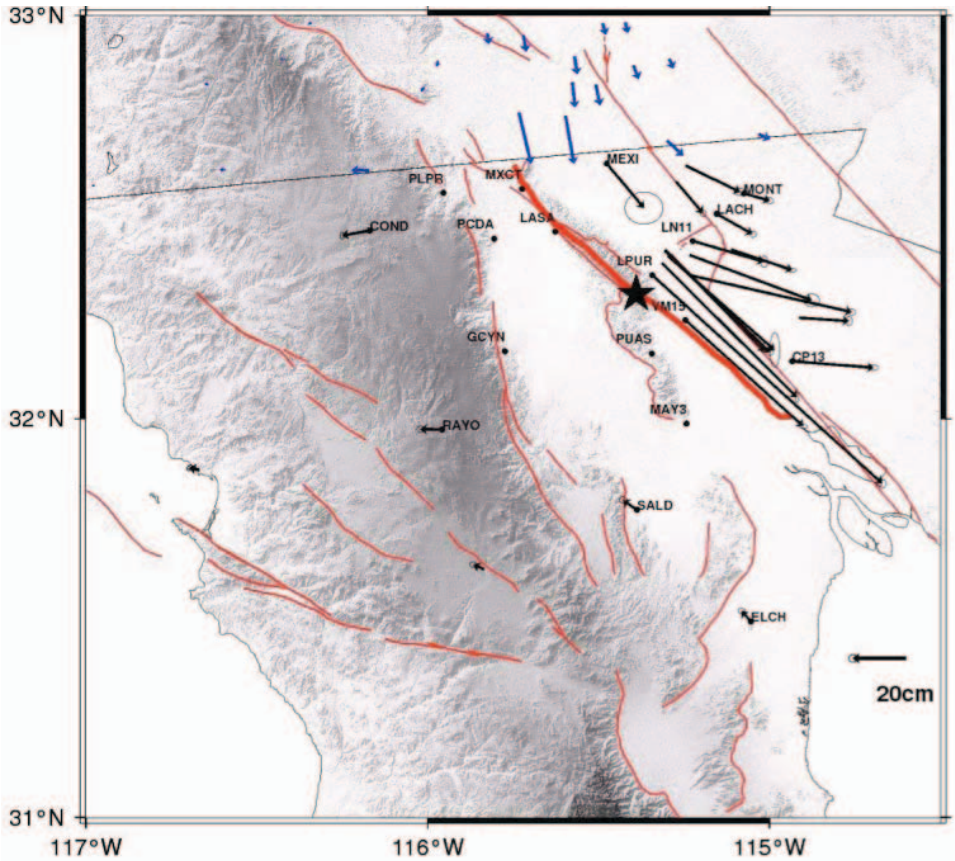

Figure 8. M7.2 El Mayor-Cucupah coseismic displacements (black arrows) from campaign GPS surveys.(Sandwell et al., 2010)

GPS data collection in the Anza gap region is complemented by the variety of observations recorded at the Piñon Flat Observatory (PFO). With partial support from SCEC, Wyatt et al. maintained and operated the PFO, which includes a longbaseline strainmeter, assisted other groups with operation and testing of various seismic instruments, and continued processing and archiving longbaseline strain data. These data show intriguing trends during the initial months following the El Mayor Cucapah earthquake that may reflect slow slip on the San Jacinto fault.

Oskin et al. developed a test to distinguish between two end-member models of long-term earthquake temporal clustering and applied it to the southern San Jacinto fault. One end-member is that clustering occurs due to changes in the brittle fault strength, and this would predict anti-correlated slip rate behavior of individual fault strands. Alternatively, clustering can result from changes in loading by the ductile lower crust which would predict correlated slip rate behavior of fault strands. To test these models they estimated slip rates at six sites along strands of the San Jacinto fault using two independent dating techniques to reduce potential bias in the results. Their results indicate there is a strong slip rate gradient along the San Jacinto fault with the slip rate decreasing to the southeast where slip is transferred from the Clark fault strand to the Coyote Creek fault and Salton Trough. The slip rates estimated for the Clark and Coyote Creek faults both show an increase over time suggesting that the change is due to an increase in fault zone loading.

Weldon et al. completed mapping of the north branch of the San Andreas fault in the San Bernardino Valley and prepared for sample collection for cosmogenic dating to be conducted in the summer of 2011. These data will be used to determine the slip rate on this fault branch, a structure for which little slip rate information exists despite its important role in assessing the geodetic/geologic slip rate discrepancy and seismic hazard in this region.

Kilb inspected the spectra for triggered earthquakes in the wavetrain of large amplitude teleseismic events and demonstrated that these triggered events are similar to typical shallow earthquakes in the same region (the Salton Sea) rather than having frequency characteristics expected of triggered tremor.

San Andreas Fault System Modeling

Figure 9. Interseismic stressing rate and seismicity on San Andreas fault derived from estimated slip rates for all southern California faults. Seismicity correlates with sections of fault for which neighboring faults make substantial contribution to interseismic stressing. (Meade et al., 2010)

Platt and Becker used GPS data to investigate strain partitioning around the Garlock fault as a pilot study designed to understand better the mechanics of sinistral faults that occur in the dominantly dextral San Andreas Fault system. They found that the Garlock Fault slips left-laterally at ~7.5 mm/yr and rotates counterclockwise at 5.2°/m.y.

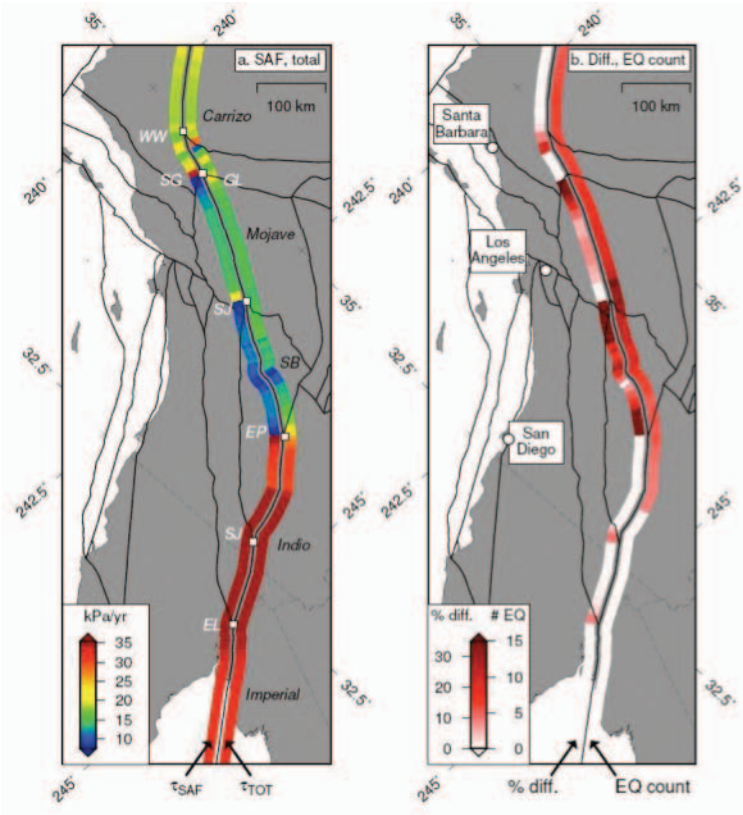

Figure 9. Interseismic stressing rate and seismicity on San Andreas fault derived from estimated slip rates for all southern California faults. Seismicity correlates with sections of fault for which neighboring faults make substantial contribution to interseismic stressing. (Meade et al., 2010)

Hooks et al. developed a new 3D finite difference model for the southern San Andreas Fault system in order to investigate vertical deformation. The SCEC geological vertical motion database provided long-term vertical deformation rates to refine the model. The resulting model successfully reproduces the general patterns of horizontal velocity (from the PBO data) and strain rate. Current work is focused on assessing the model resolution and influence of boundary conditions. They plan to integrate the results from the dynamic model with the results from their semi-analytic crustal deformation models.

Bennett et al. developed geodetically-constrained block models to investigate four possible fault-block geometries in the Eastern Transverse Ranges in an effort to constrain better slip-rate estimates for the southernmost San Andreas Fault (SSAF). While no model provided a statistically better fit to the data than the others, for all geometries considered, the results suggest that the SSAF has a strong along-strike slip rate gradient with rates decreasing from ~23 mm/yr to < 10 mm/yr as one moves northwest while the estimated San Jacinto slip rate is ~12 mm/yr.

In another application of block modeling, Meade et al. used southern California fault slip rates estimated from a geodetically constrained block model that includes all major regional fault structures to calculate fault stressing rates resulting from interseismic fault system interactions (Figure 9). Their results suggest that interseismic stressing over the course of the earthquake cycle is as significant as co-seismic and postseismic stress changes and that seismic hazard assessment should consider stressing due to interseismic fault interactions rather than simply the slip rates on individual faults.

Modeling Fault Zone Behavior

Efforts at modeling more realistic fault zone behaviors, such as damage regions, progressed significantly this year, with codes including fault stepovers and dipping faults instead of the simple straight, vertical strike slip faults examined previously. Hearn &Vaghri explore the effects of lateral rheological contrasts in suites of strike-slip faults as well as deep, viscous shear zones and their effects on modeling of interseismic geodetic data. Duan et al., 2011, find that triggered elastic and inelastic deformation on nearby fault zones can occur coseismically when the pre-seismic stress level is comparable to the strength of the fault zones, and that the sense of inelastic deformation can be the opposite from the elastic deformation that would be predicted based on the coseismic Coulomb stress change (Figure 10). Fialko et al. explore 2D numerical models that investigate the origin of shallow slip deficits that appear in many inversions of coseismic data associated with large strike-slip

earthquakes. They find that plastic yielding can produce a shallow slip deficit, although they also find that the inversion approaches used on the coseismic data need further analysis. Fialko and Barbot continue development of their semi-analytical approach to modeling time-dependent deformation, which reproduces fairly similar results to ABAQUS for a simple strike-slip case. Meade et al. explored how the quasi-static earthquake cycle modeling that is now commonplace may be biased when inaccurate fault models are used or viscoelastic deformation is neglected. Geologic/geodetic slip discrepancies in the San Bernadino region are a key motivation for this study.

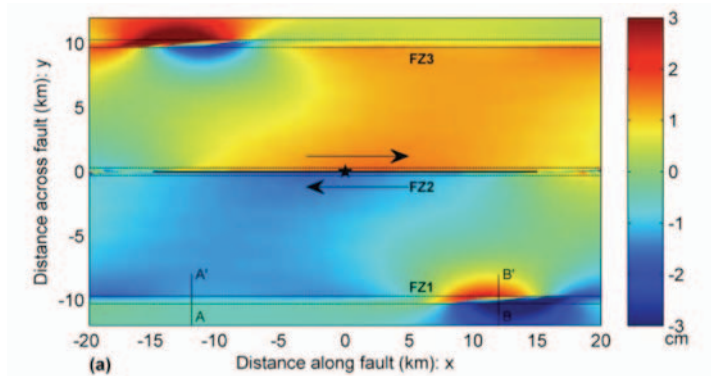

Figure 10. Fault-parallel component of the residual displacement field after an earthquake on the fault (solid black line) within a low-velocity fault zone FZ2. Motion across FZ1 is retrograde along AA', while it is sympathetic along BB'. They correspond to elastic and inelastic response of FZ1 to the rupture, respectively. (Duan et al., 2011)

Seismic Hazard Assessment

With 2010 SCEC funding, Thatcher et al. held the first of several workshops focusing on how GPS constraints on strain rates and fault slip rates can be more directly incorporated in the UCERF3 seismic hazard assessment. During this workshop, participants reviewed existing studies and developed a consensus assessment of which results were sufficiently well-developed and accepted to be included in UCERF3. They also identified new SCEC research objectives that would result in additional geodetically constrained rate estimates being usable for UCERF3. These research directions included extension of strain and slip rate modeling to additional regions of California, better assessment of rate uncertainties (including epistemic uncertainty), and quantification of postseismic effects on rate estimates.

Ward has further developed approaches to incorporating geodetic data in seismic hazard assessment both through new methods for estimating the strain rate from GPS velocities and new ways to incorporate geodetic data into earthquake simulators. This year's work has employed the CMM4 velocity field, and a focus of current work is transitioning to using a new, more physically realistic and detailed, fault model in the ALLCAL earthquake simulator as well as testing and tuning ALLCAL. This work was highlighted in presentations in Italy and Japan during 2010.

Publications and Presentations of Results

Barbot, S. and Y. Fialko, Constraints on rheological structure of the lithosphere from geodetic observations of postseismic transients due to the Landers and Hector Mine earthquakes, Southern California, submitted.

Barbot, S. and Y. Fialko, A unified continuum representation of postseismic relaxation mechanisms: Semi-analytic models of afterslip, poroelastic rebound and viscoelastic flow, Geophys. J. Int., 182, 1124-1140, 2010.

Barbot, S. and Y. Fialko, Fourier-domain Green function for an elastic semi-infinite solid under gravity, with applications to earthquake and volcano deformation, Geophys. J. Int., 182, 568-582, 2010.

Cooke, M.L., Herbert, J., Marshall, S.T., 2010. Spatially Varying Slip Rates on the Southern San Andreas Faults Reflect Fault Geometry and Interaction. Southern California Earthquake Center Workshop on Integrating Geodesy into the UCERF3, Pomona, CA

Del Pardo, C., B.P. Hooks, B.R. Smith-Konter, L. Serpa, and T.L. Pavlis, 2010, Three-dimensional thermo-mechanical modeling of the Death Valley Fault Zone, Southern California Earthquake Center Annual Meeting, Proceedings and Abstracts, v. 20 p. 206.

Del Pardo, C., B. P. Hooks, B. Smith-Konter, L. Serpa, and T.L. Pavlis, Numerical modeling of strain accumulation within the Death Valley Fault Zone, to be submitted to J. Geophys. Res.

Doran, A.K., Z. Peng, C. Wu, and D. Kilb (2010). Dynamic Triggering of Shallow Earthquakes in the Salton Sea Region of Southern California, SCEC Annual Meeting 2010, poster 2-099.

Doran, A., X. Meng, Z. Peng, C. Wu, D. L. Kilb, (2010). Dynamic Triggering of Earthquakes in the Salton Sea Region of Southern California from Large Regional and Teleseismic Earthquakes. American Geophysical Union, Fall Meeting 2010, Abstract #S33B-2104.

Doran, A. K., Z. Peng, X. Meng, C. Wu, D. Kilb (2011). Dynamic Triggering of Earthquakes in the Salton Trough of Southern California, Seis. Research Letters, 82.

Duan, B. (2010), Inelastic response of compliant fault zones to nearby earthquakes, Geophys. Res. Lett., 37, L16303, doi:10.1029/2010GL044150.

Duan, B., J. Kang, and Y.-G. Li (2011), Deformation of compliant fault zones induced by nearby earthquakes: Theoretical investigations in two dimensions, J. Geophys. Res., 116, xxxxxx, doi:10.1029/2010JB007826, in press.

Fialko, Y., A. Gonzalez, J J Gonzalez-Garcia, S. Barbot, S. Leprince, D. T. Sandwell, D. Agnew, Static Rupture Model of the 2010 M7.2 El Mayor-Cucapah Earthquake from ALOS, ENVISAT, SPOT and GPS Data, Abstract T53B-2124, presented at 2010 Fall Meeting, AGU, San Francisco, Calif., 13-17 Dec.

Hooks, B.P., B.R. Smith-Konter, 2010, Numerical Modeling of the San Andreas Fault System: Comparison with analytical solutions and geological observations, Southern California Earthquake Center Annual Meeting, Proceedings and Abstracts, v. 20, p. 226.

Hooks, B.P., B.R. Smith-Konter, 2010, Preliminary strain results from 3D continuum mechanics models (FLAC3D) of the San Andreas Fault System , Southern California Earthquake Center Workshop on Incorporating Geodetic Surface Deformation Data into UCERF3, Pomona, CA, 1-2 April 2010.

Hooks, B.P., and B.R. Smith-Konter, 2010, 3D numerical mechanical modeling of the southern San Andreas Fault system, 2010 Workshop on Crustal Deformation Modeling, sponsored by Southern California Earthquake Center and Computational Infrastructure for Geodynamics, Golden, CO. 18 June 2010.

Hooks, B.P., and B. Smith-Konter, Dynamic 3D mechanical numerical modeling of the long-term evolution of the Southern San Andreas Fault System, to be submitted to J. Geophys. Res.

Gonzalez, A, J J Gonzalez-Garcia, D T Sandwell, Y Fialko, D Agnew, B. Lipovsky, J. Fletcher, F. A. Nava Pichardo, GPS coseismic and postseismic surface displacements of the El Mayor-Cucapah earthquake, Abstract T53B-2125, presented at 2010 Fall Meeting, AGU, San Francisco, Calif., 13-17 Dec.

Kaneko, Y. and Y. Fialko, Shallow slip deficit due to large strike-slip earthquakes in dynamic rupture simulations with elasto-plastic response, Geophys. J. Int., submitted.

Kaneko, Y. and Y. Fialko, Modeling shallow slip deficit in large strike-slip earthquakes using simulations of spontaneous earthquake sequences in elasto-plastic media, Eos Trans. AGU, 91(55), T33B-2248, 2010.

Kaneko, Y. and Y. Fialko, Modeling shallow slip deficit in large strike-slip earthquakes using simulations of spontaneous earthquake sequences in elasto-plastic media, SCEC annual meeting, 2010.

Marshall, S.T., Owen, S.E., Funning, G.J. 2010 The Ups and Downs of Geodetically-Derived Deformation Rates in the Western Transverse Ranges Region, CA. Eos, Transactions of the American Geophysical Union.

Marshall, S.T., Owen, S.E., Funning, G.J. 2010 Separating Seasonal, Anthropogenic, and Tectonic Deformation in the Western Transverse Ranges Region, CA. Southern California Earthquake Center Annual Meeting, Palm Springs, CA.

Marshall, S.T., Cooke, M.L. 2010. Interseismic Deformation along Finite and Intersecting Faults: Application to the Los Angeles and Ventura Regions, CA. Southern California Earthquake Center Workshop on Integrating Geodesy into the UCERF3, Pomona, CA.

Morris, A.C., Marshall, S.T. 2010 Spatial Variations in Slip on Corrugated Reverse Fault Surfaces. Eos, Transactions of the American Geophysical Union.

Sandwell, D., T. Becker, P. Bird, J. Bormann, A. Freed, M. Hackl, B. Meade, W. Holt, B. Hooks, S. Kedar, C. Kreemer, R. McCaffrey, T. Parsons, F. Pollitz, Z-K. Shen, B. Smith-Konter, C. Tape, and Y. Zeng, 2010, Comparison of 16 strain rate maps for southern California, Southern California Earthquake Center Annual Meeting, Proceedings and Abstracts, v. XX, p. 271.

Sandwell, D T , R. Mellors, X. Tong, M. Wei, P. Wessel, GMTSAR Software for Rapid Assessment of Earthquakes, G13A-0651, presented at 2010 Fall Meeting, AGU, San Francisco, Calif., 13-17 Dec.

Spinler, J. C., R. A. Bennett, M. L. Anderson, S. F. McGill, S. Hreinsdóttir, and A. McCallister (2010), Present-day strain accumulation and slip rates associated with southern San Andreas and eastern California shear zone faults, J. Geophys. Res., 115, B11407, doi:10.1029/2010JB007424.

Wei, M., D. Sandwell, Y. Fialko, and R. Bilham Slip on faults in the Imperial Valley triggered by the 4 April 2010 Mw 7.2 El Mayor-Cucapah earthquake revealed by InSAR, Geophys. Res. Lett., doi:10.1029/2010GL045235, in press. (accepted 19 November 2010).

Earthquake Geology

The SCEC geology disciplinary group coordinates diverse field-based investigations of the Southern California natural laboratory. The majority of Geology research accomplishments fall under two categories: (1) focused studies of the southern San Andreas and San Jacinto faults in coordination with the SoSAFE (Southern San Andreas Fault Evaluation) special project; and (2) studies of other portions of the southern California fault network aimed at a better understanding fault system behavior. Geology also contributes to earthquake response efforts and supports field observations related to several focus-group activities (e.g., USR, WGCEP, FARM, GMP, LAD, CDM). Additional goals include longer-term slip rates and long, multi-event paleoseismologic records that have a high impact on seismic hazard assessments. In support to these efforts the Geology group coordinates geochronology infrastructure resources that are shared among various SCEC-sponsored projects.

SoSAFE Special Project

The primary goal of the SoSAFE project is to document the timing of large paleoearthquakes and amount of slip released by the southern San Andreas and San Jacinto faults over the past 2000 years. Additional goals include examination of longer-term slip rates and modeling studies that directly impact seismic hazard assessments. The SoSAFE project has become the dominant focus of geological investigations under SCEC3. The numerous accomplishments of this program are described in detail in the Special Projects section, below.

Fault System Behavior

A major emphasis of the Geology group has been to characterize patterns in fault system behavior that could significantly affect earthquake hazards. Recent efforts, focused on the San Cayetano-Ventura reverse fault system, aim to understand fault linkage and potential earthquake magnitude along the rapidly converging northern margin of the Ventura basin. Analysis of well data, industry seismic reflection profiles, and four high-resolution seismic profiles acquired in 2010 have allowed Hubbard, Shaw, Dolan, McAuliffe and Pratt to construct a more complete 3D model of the system (Figure 11). These data suggest that the Ventura Fault, previously interpreted by some as a shallow, bending-moment fault that does not pose a seismic hazard, is in fact a major, through-going thrust ramp that extends to seismogenic depths. Slip on the Ventura ramp has generated the prominent Ventura Avenue anticline, which Hubbard et al. (in prep.) interpret as a fault-propagation fold. Moreover, the structural similarity of the Ventura Avenue anticline and the Dos Cuadras structure offshore to the west suggests that these major structures form an en echelon system that could potentially link together to form large-magnitude thrust earthquakes. Similarly, the southern, blind San Cayetano Fault to the east of Ventura is a north-dipping thrust ramp overlain by a large anticline that appears to be part of this same system. Rupture of this entire system could generate a very large-magnitude event, similar to the 2008 Mw 7.9 Wenchuan earthquake. Significant portions of such a rupture would lie offshore, resulting in the potential for generation of large, near-shore tsunamis that could affect coastlines throughout southern California. Ongoing analysis of the 2010 high-resolution seismic reflection data, coupled with shallow borehole data collected during Summer 2011 across the locus of active folding above the Ventura and western San Cayetano anticlines, should reveal the ages and displacements of recent earthquakes on these major thrust ramps, which will in turn allow the evaluation of possible multi-segment ruptures and correlation to the uplifted Holocene marine terrace record documented by T. Rockwell.

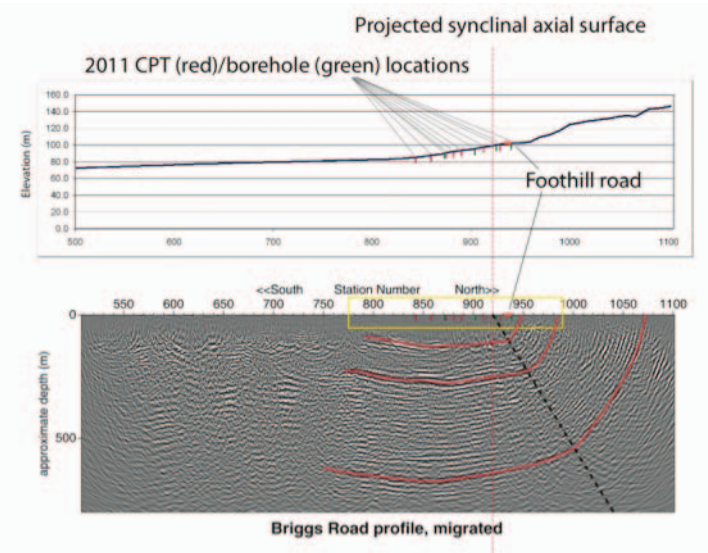

Figure 11. High-resolution seismic profile acquired across the active fold limb and synclinal axial surface associated with the tipline of the blind, southern San Cayetano Fault along the northern edge of the Ventura basin. The upper figure shows the locations of continuously cored boreholes and cone-penetration tests drilled across the zone of active folding during Summer 2011 to define precisely the geometry of strata folded in recent earthquakes and to sample dateable material to define paleo-earthquake ages.

El Mayor-Cucapah Earthquake

Investigations are maturing in response to the 4 April 2010 El Mayor-Cucapah earthquake in northernmost Baja California. This is the first earthquake where comprehensive lidar topographic surveys and differential lidar have been available to map the rupture and constrain near-field deformation (Figure 12). Lidar data collection was supported by an NSF-RAPID grant, supplemented by SCEC funds that allowed for expansion of the survey. Oskin et al. (in review) describe the collection and

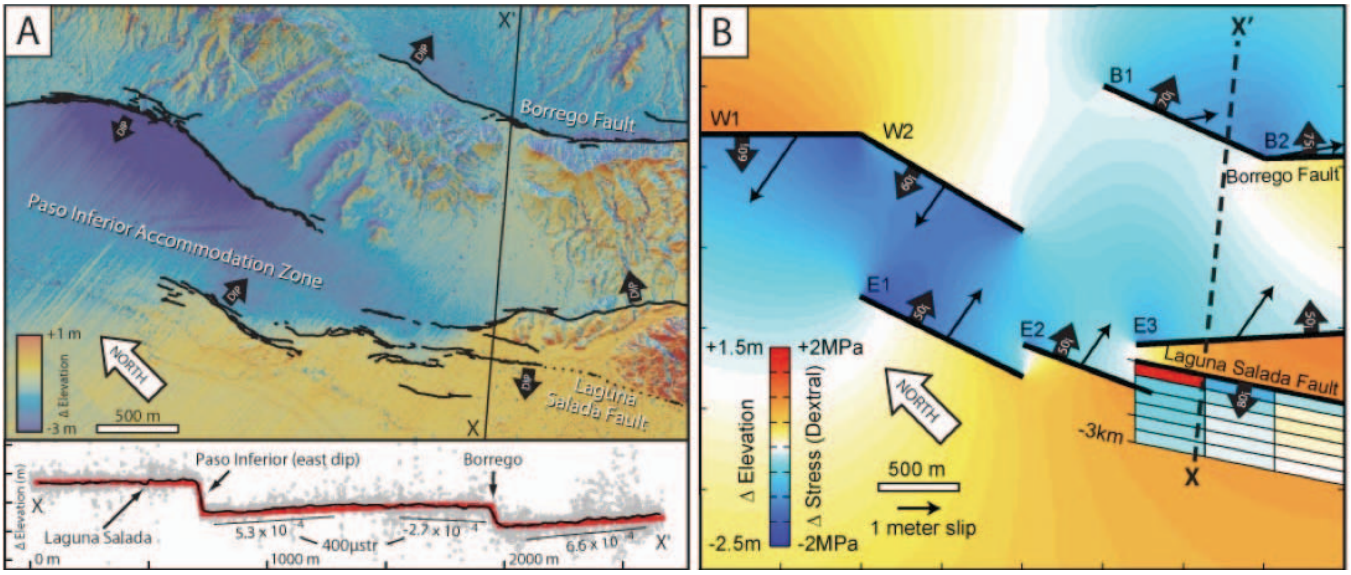

Figure 12. A. Elevation difference map (post-pre) generated from lidar surveys obtained before and after the 2010 El Mayor-Cucapah earthquake. Cross-section shows folding between two dextral oblique normal faults that slipped in this earthquake. B. Elastic model of the Paso Inferior Accommodation Zone, based on observed fault offsets. Note how the model reproduces observations well along the cross-section in A (model shown as red dashed line).

first results of this survey, highlights of which include large near-field strains (~10-3) that appear to be elastically generated, and evidence for a blind strike-slip fault system that slipped beneath the Colorado River delta. Overall, the El Mayor Cucapah earthquake represents the latest of a class of distributed, multi-fault earthquake ruptures that present difficult-to-quantify, distributed seismic hazard. Rupture mapping led by a joint USA-Mexico team of Fletcher and Rockwell, has revealed up to seven fault segments that slipped in this earthquake. A paper summarizing the numerous measurements and lidar-assisted rupture mapping will soon be submitted for publication. Efforts are ongoing to compare this rupture to previous events, including the immediately adjacent rupture generated by the 1892 Laguna Salada earthquake. That two earthquakes of similar size occurred within a few kilometers of each other challenges the role that elastic rebound may play in reducing earthquake hazard immediately after a nearby event. The latest and ongoing research from the El Mayor-Cucapah earthquake, including results from analysis of both airborne and terrestrial lidar, will be presented at a workshop at the upcoming 2011 SCEC annual meeting. Current registration for this workshop already exceeds 100 persons.

Shallow Slip Deficits

SCEC researchers are also attempting to determine how representative geologic slip rates are of the true slip rate of fault slip at depth. Although surface fault slip measurements are commonly used to infer seismic hazard, it has long been noted that surface slip during earthquakes is often smaller than slip at depth determined from inversion of geodetic and seismologic data. If this shallow slip deficit is due to significant off-fault deformation in the near-surface region, as suggested by earlier SCEC-supported studies (e.g. Shelef and Oskin, 2010), then geological surface slip measurements will systematically underestimate fault slip at depth. Consequently, seismic hazard inferred from these measurements will also be underestimated. In an effort to determine if this shallow slip deficit varies as a function of measureable fault characteristics such as total fault slip or near-surface geology, Haravitch and Dolan (in prep.) have systematically compared the co-seismic surface displacements in six, large-magnitude (Mw ≥7) strike-slip earthquakes with static inversions of geodetic data for slip at 3-6 km depth. Their study reveals a striking correspondence between the degree to which fault slip remains localized to the surface and the structural maturity of the fault, as defined by cumulative fault displacement. For example, ruptures on faults with ≤10 km of cumulative fault slip typically manifest only ~40-60% of slip at 3-6 km depth as discrete surface fault slip, in contrast to ruptures on structurally mature faults, which manifest 80-95% of slip at depth as discrete surface fault slip (Figure 13). This pattern extends to smaller scales, and comparisons of slip at the surface with slip at depth for any point along these ruptures reveals the same basic trend when structurally simple and structurally complicated sections of the surface ruptures are examined separately. These observations have basic implications for probabilistic seismic hazard assessment, which depends strongly on geologic fault slip rates as a primary input, and provide a way forward to potentially defining a multiplier based on measurable fault parameters (e.g., cumulative fault slip) that can be used to correct geologic slip rates to account for the amount of deep fault slip that is distributed in the near surface.

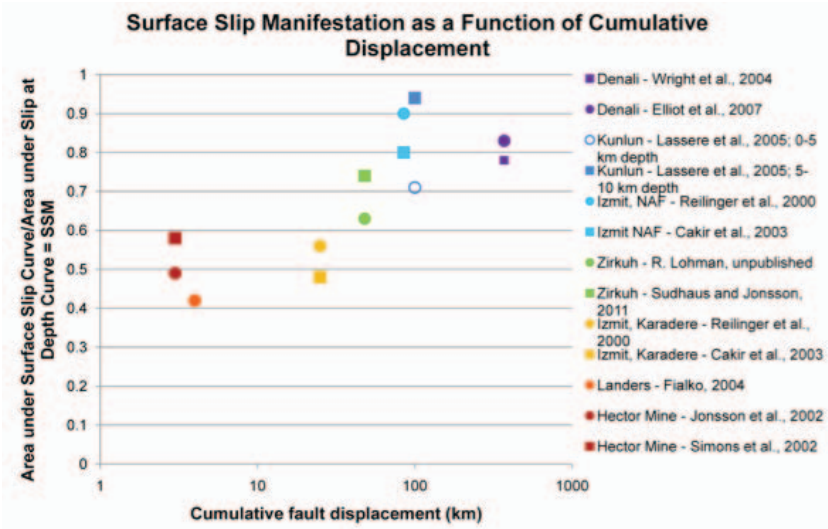

Figure 13. Comparison of Surface Slip Ratio (SSR) with cumulative displacement of six faults that produced earthquakes M≥7. Comparisons are based on geologic surface offset data, geodetic estimations of slip at depth and geologic estimation of cumulative displacement.

Geochronology Infrastructure

The geochronology infrastructure program pools dating funds at various participating laboratories. This approach leads to greater efficiency in allocating resources, as most projects cannot fully anticipate their dating requirements ahead of time. Nearly 900 geochronology analyses have been completed thus far under the SCEC3 program. 600 of these have been 14C, spread roughly equally between Lawrence Livermore National Lab (LLNL) and U.C. Irvine labs. Cosmogenic 10Be (measured at LLNL) comprises most of the remaining analyses (227 dates) followed by optically stimulated luminescence (52 OSL dates, measured at University of Cincinnati and Utah State). 76% of 14C, 65% of 10Be, and 60% of OSL dates have been expended on SoSAFE projects, reflecting the high impact this special program has had on SCEC3 geology. The geochronology program has also spawned new collaborations to advance dating methodologies. One rapidly advancing technique melds the 10Be and U-series dating approaches to date alluvial fans. This has been applied to date offsets along the San Andreas Fault at Biskra Palms (Behr et al., 2010; Fletcher et al., 2010) and at several sites along the southern San Jacinto Fault (Blisniuk et al., in preparation).

Figure 14. Sampling profile and shape model for Grass Valley Rock GV-2. Modeling the 3-D exposure history reveals that this rock has been precarious for 18.0 ± 2.5 kyr.

Another advance has been the application of multiple 10Be surface exposure dates to model the onset of fragility of precariously balanced rocks (Figure 14), recently published in Quaternary Geochronology (Balco et al., 2011).

References

Balco, G., Purvance, M., and Rood, D. (2011) Exposure dating of precariously balanced rocks, Quaternary Geochronology, v. 6, p. 295-303.

Behr, W., Rood, D., Fletcher, K., Guzman, N., Finkel, R., Hanks, T., Hudnut, K., Kendrick, K., Platt, J., Sharp, W., Weldon, R., and Yule, J. (2010) Uncertainties in slip-rate estimates for the Mission Creek strand of the southern San Andreas fault at Biskra Palms Oasis, southern California, Geological Society of America Bulletin, vol. 122, p. 1360-1377.

Fletcher, K., Sharp, W., Kendrick, K., Behr, W., Hudnut, K., and Hanks, T. (2010) 230Th/U dating of a late Pleistocene alluvial fan along the southern San Andreas fault, Geological Society of America Bulletin, v. 122, p. 1347-1359.

Oskin, M., Arrowsmith, J., Hinojosa, A., Elliott, A., Fletcher, M., Fielding, E., Gold, P., Gonzalez, J, Hudnut, K., Liu-Zheng, J., and Teran, O., (2010) Near-field deformation from the El Mayor-Cucapah earthquake quantified with airborne LiDAR, submitted to Nature Geoscience.

Shelef, E., and Oskin, M., (2010) Deformation processes adjacent to active faults: Examples from Eastern California, Journal of Geophysical Research – Solid Earth, Vol. 115, B05308, 24 pp., doi:10.1029/2009JB006289.

Disciplinary Activities

Within the SCEC structure, the focus groups are responsible for coordinating interdisciplinary activities in six major areas of research: *Unified Structural Representation*, *Fault and Rupture Mechanics*, *Crustal Deformation Modeling*, *Lithospheric Architecture and Dynamics*, *Earthquake Forecasting and Predictability*, *Ground Motion Prediction*, and *Seismic Hazard and Risk Analysis*. The following sections summarize the year's activities in each of these areas.

Unified Structural Representation

The Unified Structural Representation (USR) Focus Area develops models of crust and upper mantle structure in California for use in a wide range of SCEC science, including strong ground motion prediction, earthquake hazards assessment, and fault systems analysis. These efforts include the development of Community Velocity Models (CVM-S, CVM-SI, & CVM-H) and Community Fault Models (CFM, CFM-R, SCFM), which together comprise a USR. In partnership with other working groups in SCEC, the USR Focus Area also helps support the evaluation and improvement of these models through ground motions simulations, 3D waveform tomography, earthquake relocations, and fault systems modeling.

1. This past year's accomplishments include:
2. Development of new versions of the SCEC Community Velocity Model (CVM-H 11.2 and 11.9), which include new representations of the San Bernardino and offshore Santa Maria basins;
3. Development of a new version of the SCEC Community Velocity Model (CVM-SI), which includes perturbations to an existing model (CVM-S) as a result of iterative inversion simulations by Chen et al (2011) and Lee et al (2010). A similarly refined CVM-H model was released as versions 11.2 to 11.9, and is currently being updated.
4. Support for the development of the statewide UCVM by the SCEC CME group, which includes these latest southern California model versions (CVM-S, CVM-SI, CVM-H) along with other alternative and complimentary regional velocity models in a common delivery platform.
5. Implementation of a new CVM evaluation system by the SCEC CME that uses wave propagation simulations of moderate magnitude historical earthquakes and goodness-of-fit (GOF) measurements that compare simulated and

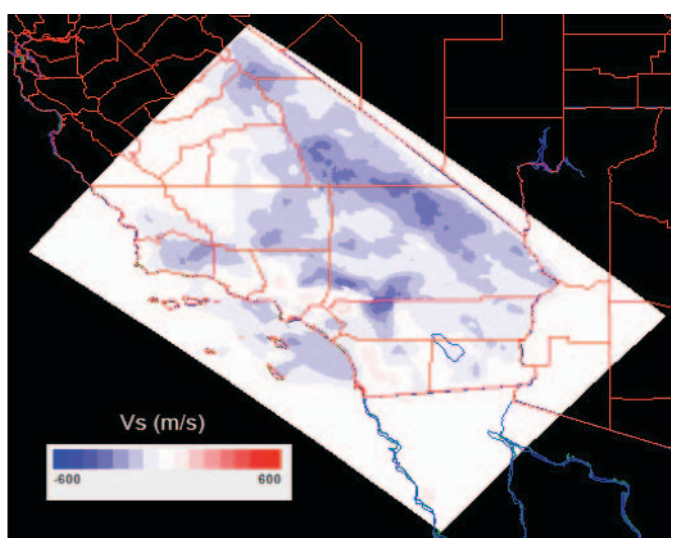

Figure 15. Map of difference in Vs between CVM-SI i5-i0 and CVM-S

observed waveforms (after Olsen and Mayhew, 2010).

6. Development of a new version of the SCEC Community Fault Model (CFM 4.0) for southern California that includes updates based on relocated seismicity catalogs and detailed fault traces in the USGS Quaternary Fault and Fold database.
7. Development of a new version of the statewide Community Fault Model (SCFM 2.0) in coordination with the California Geological Survey and the USGS in support of the UCERF3 project.

Community Velocity Models (CVM, CVM-SI, CVM-H)

A series of improvements were made to the SCEC Community Velocity Models this past year to improve their performance in strong ground motion simulations and a range of other applications. These efforts included 3D waveform tomographic inversions using the F3DT scattering integral method that evaluated the longstanding CVM-S model (Chen et al., 2011, and Lee et al., 2010). Based on comparisons of observed and synthetic waveforms, perturbations were applied to this model to generate a revised velocity description (Figure 15). The model is expressed as a 3D grid of 1536 x 992 x 100 cells with a grid spacing of 500 m and is available as a C/Fortran code and associated files that are downloaded, compiled, and run locally. This improved model has been imported into UCVM and is referenced with the model label CVM-SI.

In addition, we developed updated versions of the CVM-H (11.2 and 11.9) that are also released as part of UCVM. The latest version of this model includes a newly compiled Moho surface, addition of the offshore Santa Maria basin, a new detailed representation of the San Bernardino basin, and much smoother transitions between low and high resolution regions of the model. The new Moho surface was compiled by Carl Tape from a large number of data sources, including receiver functions and active-source studies. Improvements to the offshore Santa Maria basin representation in the CVM-H included a revised definition of the basement surface using reflection seismic data that extends to the western margin of the model. The new model also includes a representation for the San Bernardino basin that was developed using gravity (Anderson, 2000) and seismic reflection data (Stephenson et al., 2002). The velocity structure (Vp) in the basin is defined by stacking velocities (Stephenson et al., 2004) and a 1D velocity profile (Graves, 2008) combined to a basin thickness-depth-velocity function. Finally, the transitions from the high to the low resolution models were revised by introducing a new smoothing velocity gradient. This latest model version is being quantitatively assessed by performing seismic wavefield simulations based on unstructured hexahedral meshing (GEOCUBIT) and the spectral-element method (SPECFEM3D) using a database of synthetic seismograms for 234 reference earthquakes in southern California (Tape et al., 2011). These synthetic seismograms are filtered over different period ranges and then compared with observed seismograms using a variety of misfit functions. The misfit analysis provides an earthquake-based perspective of the quality of CVM-H, and will be used to revise the velocity parameterizations in future model releases.

Planning for the future of SCEC Community Velocity Models

Comparisons of observed and synthetic waveforms for earthquakes in southern California demonstrate that the SCEC Community Velocity Models (Magistrale et al., 2000; Süss and Shaw, 2003; Plesch et al., 2009) perform much better than simple 1-D velocity models in accurately simulating seismic wave propagation and forecasting the distribution of hazardous ground shaking (e.g., Komatitsch et al., 2004; Chen et al., 2007; Olsen and Mayhew, 2010). Furthermore, the new 3D waveform tomographic inversion methods that are being used to evaluate and improve the current velocity models offer great promise of offering further improvements in model performance. To help facilitate the process of evaluating and improving these models, the USR Focus Area has worked closely with SCEC CME group over this past year to coordinate model releases, enhance the code that delivers the models, and provide tools that can help in evaluating model performance.

Specifically, the UCVM framework now provides a common platform that can be used to access all of community velocity model versions (CVM-S, CVM-SI, CVM-H), along with other alternative and complementary regional velocity models. This helps to facilitate direct comparisons between models, as well as use of alternative models in various seismological and hazard assessment studies that explore the significance of differences between current model versions. In addition, the CME group has implemented a CVM evaluation system that uses wave propagation simulations of moderate magnitude historical earthquakes and goodness-of-fit (GOF) measurements that compare simulated and observed waveforms (Figure 16). The system is designed to automate running of multiple earthquake wave propagation simulations, keeping all-aspects of the simulations identical except the velocity model used. CVM evaluations are run prior to release of new version of CVM-H, or

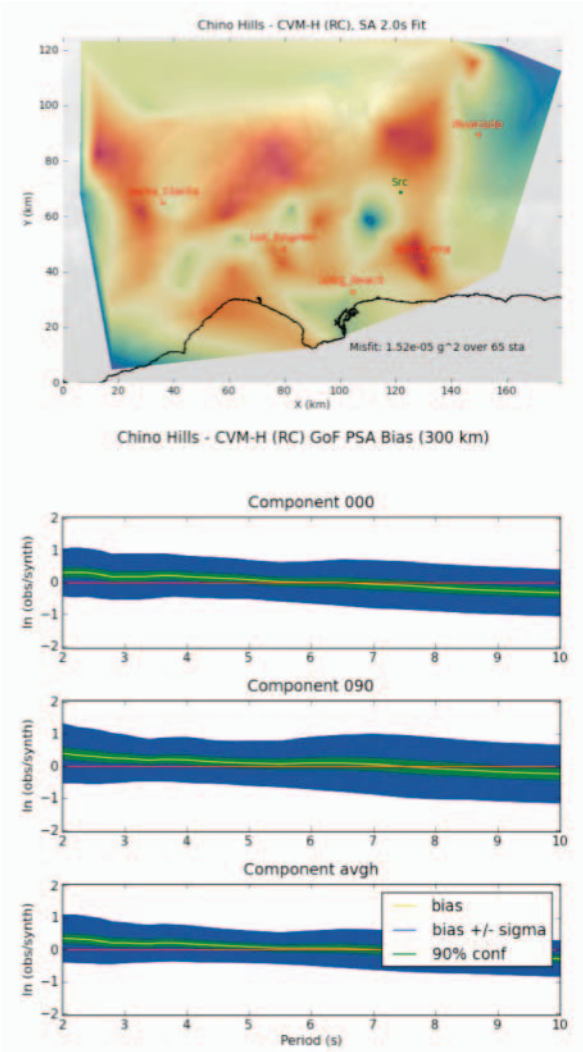

Figure 16. Example of CVM evaluation, using the 2008 Chino Hills earthquake. (top) Map-based GOF for SA-2s, and (bottom) bias of spectral accelerations at 65 stations for periods 2-10s.

other SCEC CVM's. Multiple CVM's are evaluated at one time, so that performance of a new CVM can be compared to existing, or prior, CVM versions. The GOF method includes a series of metrics, such as PGA, PGV, and spectral accelerations (SA) at various periods (Olsen and Mayhew 2010).

Finally, we recognize that state-of-the-art velocity models do not resolve small-scale amplification effects in the near-surface sediments, possibly introducing bias in earthquake ground motion simulations, as frequencies increase. Preliminary analysis shows that even simple and rather weak fractal stochastic inhomogenities imply significant variations in ground motion amplifications (up to a factor of six or more) as well as de-amplification, including bands of strong amplification aligned along the average ray path from a 0-2 Hz horizontally propagating SH-wave source. Simulations with vertically incident planar SH-wave sources show that the small-scale heterogeneities included in the upper ~100m of the sediment column contribute more to the site effects, as compared to small-scale heterogeneities buried deeper in the sediments. Thus, the USR Focus Area is supporting efforts to explore how to establish a realistic stochastic model of near-surface inhomogeneities by comparison of earthquake ground motion simulations to data and by directly mapping the statistical properties of shallow Vs estimates. If incorporated in the CVMs, such models may improve deterministic ground motion prediction as supercomputers allow the highest frequency to increase.

Community Fault Model (CFM)

The SCEC Community Fault Model (CFM) is an object-oriented, 3D representation of more than 140 active faults in Southern California, and includes direct contributions from more than twenty SCEC investigators (Plesch et al., 2007). The model consists of triangulated surface representations (T-surfs) of major faults, which are defined by surface geology, seismicity, well logs, seismic reflection profiles, and geologic cross sections. These 3D fault representations are intended to support SCEC research efforts in fault system modeling and earthquake rupture propagation, as well as to serve as a basis for regional seismic hazards assessment.

This past year, we completed a major update of the model (CFM v.4.0), which incorporates improvements in 3D fault representations, a detailed fault surface trace layer, and a new naming and numbering scheme for individual 3D fault models that allows for direct connections to the USGS/CGS Quaternary Fault database (Qfaults) and other SCEC data sets (Nicholson et al., 2011). Fault representations in CFM are now referenced to the modern WG84 datum and the new surface layer in CFM allows 3D fault models to be registered to the more detailed Qfaults digital trace maps. Systematic revision of CFM 3D fault segments was required to ensure compatibility between some previous CFM fault representations and the newer Qfaults surface traces, as well as by the availability of extensive catalogs of relocated earthquake hypocenters to define better the subsurface geometry of active faults. New 3D fault representations for major fault zones include the San Andreas from San Gorgonio Pass to the Salton Sea, the Mecca Hills, San Jacinto, Elsinore-Laguna Salada (including El Mayor-Cucapah), and an Fernando/Sierra Madre fault systems. In addition, a new SCEC fault database hierarchical naming and numbering scheme is implemented that provides unique identifiers (number, name, abbreviation) for each level of the fault hierarchy under which a particular fault segment is classified. Levels of fault hierarchy include Fault Area, Fault Zone or System, Fault Section, Fault Name, Fault Strand or Model, and Fault Component. These additional fault hierarchical levels allow for more flexible

database searches and easier identification of fault components, alternative representations, and possible system-level associations of individual 3D fault elements that comprise CFM.

Finally, we also completed a second version of the statewide Community Fault Model (SCFM 2.0), which includes updates in the southern California model along with more than 150 new fault representations in northern California (Figure 17). In conjunction with the California Geological Survey and USGS, the model inventory was expanded to include all of the priority faults defined by the Uniform California Earthquake Rupture Forecast (UCERF 3) working group. We are currently coordinating our formal evaluation of the SCFM with the UCERF 3 effort. This will involve a virtual workshop in which participants evaluate the SCFM 2.0 using the SCEC VDO visualization software and be asked to assess the accuracy and completeness of the representations. This will involve assigning a quality ranking to each fault representation based on criteria used to evaluate the SCEC CFM. These rankings, which largely reflect the amount of data available to directly constrain the interpretations, will be used to rank alternative fault representations, with the highest ranked alternative being used to compose the preferred (versioned) fault model.

Figure 17. Perspective view of the Statewide CFM (SCFM 2.0), which includes more than 300 fault representations. Earthquakes are shown from Shearer et al., (2005).

References

Anderson, M. L., C. W. Roberts, and R. C. Jachens, 2000, Principal facts for gravity stations in the vicinity of San Bernardino, southern California, U.S. Geol. Surv. Open-File Rept. 00-193, 32 pp.

Chen, P., Lee, E., Jordan, T. H., Maechling, P. J., Denolle, M., & Beroza, G. C., 2011, Full-3D Waveform Tomography for Southern California, 2011 SSA Annual Meeting, Memphis, TN.

Chen, P., L. Zhao, Li, T. H. Jordan, 2007, Full 3D tomography for the crustal structure of the Los Angeles region, Bulletin of the Seismological Society of America, vol.97, no.4, pp.1094-1120.

Graves, R., 2008, The Seismic Response of the San Bernardino Basin Region during the 2001 Big Bear Lake Earthquake, Bulletin of the Seismological Society of America, Vol. 98, No. 1, pp. 241–252.

Komatitsch, D., Q. Liu, J. Tromp, P. Süss, C. Stidham, and J. H. Shaw, (2004), Simulations of strong ground motions in the Los Angeles basin based upon the spectral element method, BSSA, Vol. 94, No. 1, pp. 187–206.

Lee, E., Chen, P., Jordan, T. H., Maechling, P. J., Denolle, M., & Beroza, G. C., 2010, Full-3D Waveform Tomography for Southern California, 2010 AGU Fall Meeting, San Francisco, CA.

Magistrale, H., S. Day, R. W. Clayton, and R. Graves, 2001, The SCEC Southern California Reference Three-Dimensional Seismic Velocity Model Version 2: Bulletin of the Seismological Society of America, v. 90, no. 6B, p. S65-S76.

Mayhew, J.E., and K.B. Olsen (2009). Goodness-of-fit criteria for broadband synthetic seismograms, with application to the 2008 Mw5.4 Chino Hills, CA, earthquake, submitted to Seism. Res. Lett.

Nicholson, C., A. Plesch, J.H. Shaw, 2011, CFM v.4.0: Continued upgrades and improvements to the SCEC Community Fault Model and its associated databases, 2011 SCEC Annual Meeting, Palm Springs, CA.

Olsen, K. B., and J. E. Mayhew (2010), Goodness-of-fit criteria for broadband synthetic seismograms, with application to the 2008 Mw 5.4 Chino Hills, California, earthquake, Seis. Res. Lett., 81 (5), 715–718.

Plesch, A., John H. Shaw, Christine Benson, William A. Bryant, Sara Carena, Michele Cooke, James Dolan, Gary Fuis, Eldon Gath, Lisa Grant, Egill Hauksson, Thomas Jordan, Marc Kamerling, Mark Legg, Scott Lindvall, Harold Magistrale, Craig Nicholson, Nathan Niemi, Michael Oskin, Sue Perry, George Planansky, Thomas Rockwell, Peter Shearer, Christopher Sorlien, M. Peter Süss, John Suppe, Jerry Treiman, and Robert Yeats, 2007, Community Fault Model (CFM) for Southern California, Bulletin of the Seismological Society of America, v. 97, no. 6.

Plesch, A., C. tape, and J.H. Shaw, 2009, CVM-H 6.0: integration of adjoint-based tomography, the San Joaquin basin and other advances in the SCEC community velocity model, SCEC Annual Meeting, Palm Springs, CA.

Shearer, P., E. Hauksson, and G. Lin, Southern California hypocenter relocation with waveform cross correlation: Part 2. Results using source-specific station terms and cluster analysis, Bull. Seismol. Soc. Am., 95, 904-915, doi: 10.1785/0120040168, 2005.

Stephenson, W. J., J. K. Odum, R. A.Williams, and M. L. Anderson, 2002, Delineation of faulting and basin geometry along a seismic reflection transect in urbanized San Bernardino valley, California, Bull. Seismol. Soc. Am. 92, 2504–2520.

Süss, M. P., and J. H. Shaw, 2003, P-wave seismic velocity structure derived from sonic logs and industry reflection data in the Los Angeles basin, California, Journal of Geophysical Research, 108/B3.

Tape, C., Q. Liu, A. Maggi, and J. Tromp, 2010, Seismic tomography of the southern California crust based on spectral-element and adjoint methods, Geophys. J. Int., 180, 433–462.

Tape, C., Q. Liu, A. Maggi, and J. Tromp, 2009, Adjoint tomography of southern California, Science, vol 325, p. 988-992.

Fault and Rupture Mechanics

The primary mission of the Fault and Rupture Mechanics Focus Group is to develop physics-based models of the nucleation, propagation, and arrest of dynamic rupture to understand earthquakes in Southern California. Specific research goals of FARM are to investigate the relative importance of different dynamic weakening mechanisms, characterize the constitutive behavior of faults and develop a capability to incorporate the behavior into dynamic rupture models, discover the relation of fault zone structure and earthquake mechanics at all scales, and determine the extent and causes of rupture directivity. Over the past year a large number of funded projects have addressed the research priorities of FARM using a variety of techniques. For the purpose of reporting research accomplishments, the projects are loosely categorized into the themes of fault-slip behavior, the micromechanics of faulting, the constitutive behavior of fault materials, advanced dynamic rupture modeling, and the characteristics of fault-slip and fault structure through observational studies in the field and laboratory. This section provides a brief summary of some accomplishments and research-related activities reported in March of 2011. Additional accomplishments are reviewed in other sections of this report. For a complete review of all FARM-related activities please see the annual reports for the individual projects posted on the SCEC website.

Mechanics-based Analysis of Fault Slip Behavior

Building off of earlier work of Shearer et al. (2005), Bird recomputed Brune-type stress drops of magnitude 1.5-3.1 earthquakes occurring in southern California from 1989 to 2001 to test hypotheses relating stress drops to hypocentral

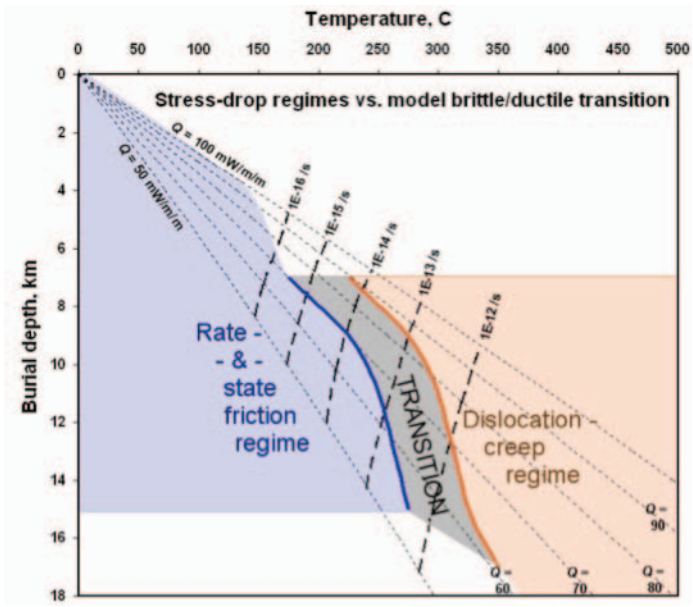

Figure 18. Interpreted stress-drop regimes, based on temperature- and depth-systematics (from Fig. 3 in SCEC Report #10025). Dotted lines show steady-state geotherms for various heat-flows, based on the assumed crustal conductivity and radioactivity. Long-dashed curves show model brittle/ductile transition conditions (for strain rates varying over 4 orders of magnitude) in the homogeneous crustal rheology assumed by Liu & Bird [2002], whose models used the same thermal

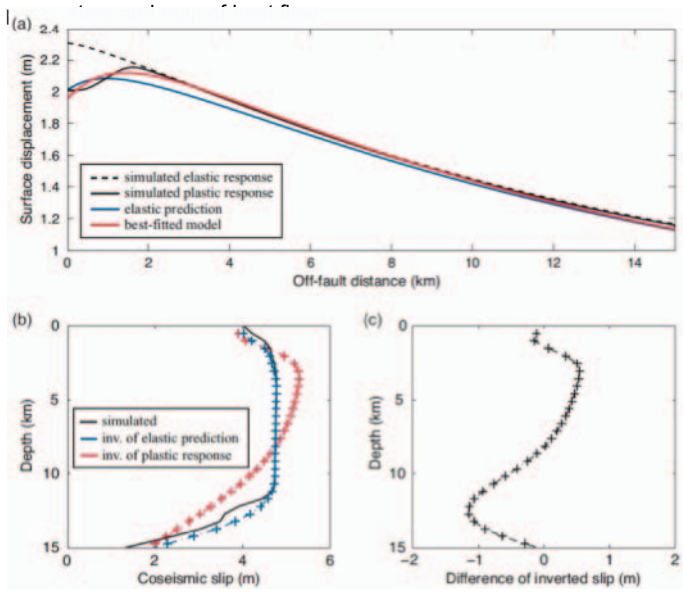

Figure 19. (a) The profiles of coseismic displacement on the Earth surface for the elastic simulation, a plastic simulation, an elastic prediction for the simulated slip distribution shown in panel b, and the best fitting model to the plastic response in the inversion. (b) The slip distribution in the plastic simulation and slip inversions of the surface displacements. The blue curve is the inverted slip of the surface displacement of the elastic prediction. The red curve is the inverted slip of the surface displacement of the simulated plastic response. (c) Difference between the inverted slip distributions shown in panel b, indicating that 10% (0.5 m) of the coseismic slip at 3-4 km depths is

burial depth, long-term tectonic strain-rate, and terrane composition. He found that stress drops increase with temperature up to 250 degrees C and are independent of depth, whereas they decrease above 300 degrees C, showing a positive correlation with depth. He interprets the low temperature data to reflect a proportional relation between shallow-crustal stress drop and interseismic fault healing, consistent with rate and state theory. In contrast, he suggests that the higher temperature data reflect preseismic shear stresses controlled by dislocation creep and mean composition (Figure 18). To investigate the slip deficit suggested by inversions of geodetic data, Kaneko and Fialko (2011; 2010) investigated the effect of inelastic deformation in simulations of dynamic rupture on a planar, vertical strike-slip fault in 2-D numerical models following previous studies [e.g., Templeton and Rice, 2008; Ma, 2008]. Kaneko and Fialko's simulations suggest that shallow slip is overestimated by as much as 10% of the coseismic slip at depth if inelastic deformation is ignored (Figure 19), supporting the need to reinterpret existing geodetic data through forward modeling. Also exploring the effects of inelastic deformation, Duan (2010) and Duan et al. (2011) use dynamic models to investigate the response of the damage zone of one fault to an earthquake occurring along a nearby fault. For the case of parallel strike-slip faults, a heterogeneous distribution of triggered elastic and inelastic strain develops, where locally the inelastic and elastic shear strains can be of opposite sign (Figure 20). These results also have implications for the interpretation of geodetic (e.g., InSAR) data, and may provide some constraints on absolute stress levels along faults. Important to understanding slip gradients and slip deficits are sound techniques to estimate surface slip. Shaw (2011) has developed a new

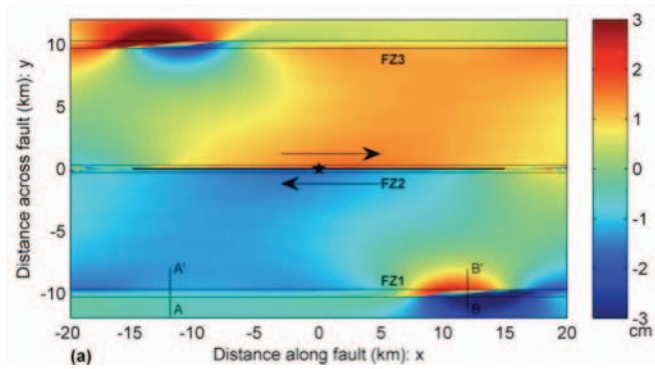

Figure 20. Fault-parallel component of the residual displacement field after an earthquake on the fault (solid black line) within a low-velocity fault zone FZ2. Motion across FZ1 is retrograde along AA', while it is sympathetic along BB'. They correspond to elastic and inelastic response of FZ1 to the rupture, respectively (shown in Fig. 2 of SCEC Report #10191). (From Duan et al., 2011)

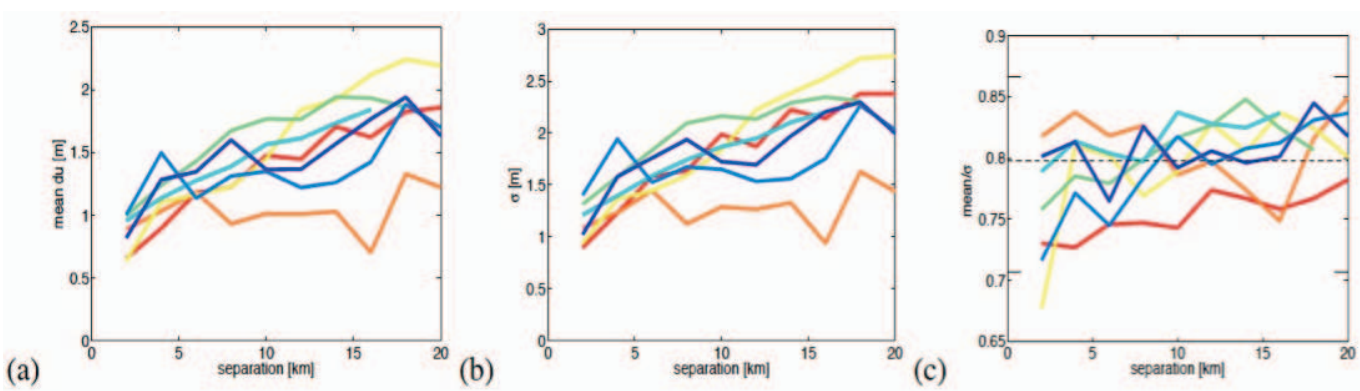

Figure 21. Averaging over slip differences as a function of separation. The different color curves are for each different earthquake. (a) Mean. (b) Standard deviation. (c) Mean/Standard deviation. The dashed black line shows the ratio for a normal distribution, which is seen to be a much better fit than either the tick mark below for a heavier tailed exponential distribution, or the tick mark above for a lighter tailed box-car function. From [Shaw, 2011].

statistical method to infer slip gradients from noisy signals associated with large earthquakes. One important observation is that the average slip differences increase linearly to length scales of the seismogenic crust, yet when extrapolated back to zero separation a nonzero intercept results (Figure 21). Shaw's results are consistent with constant stress drop at length scales smaller than event size.

Several SCEC researchers continue to explore tectonic tremor. Through analysis of small-aperture seismic arrays, Ampuero, in collaboration with Steidl and Vernon, confirmed a deep origin for tremor signals near the Anza gap on the San Jacinto fault and suggest that tremor swarms migrate rapidly in this region. To understand these migration patterns, and in particular, the rapid tremor reversals noted by Houston et al. (2011), Ampuero developed numerical simulations of slow slip and tremor swarms assuming a fault with heterogeneous frictional properties that is populated by a system of brittle asperities. When

subjected to transient creep, asperity failure occurs, initiating tremor sequences. Parametric studies are underway to define the properties that control the propagation velocity and distance.

Pollard and Madden investigated the effects of non-planar and non-vertical fault geometry on aftershock focal mechanisms and fault slip distributions for the 1992 Landers earthquake. They analyzed slip distributions compiled and digitized by the California Geological Survey (CGS) (Bryant, 1992, 1994, 2004; CGS, 2002), used the HASH (Hardebeck and Shearer, 2002) algorithm and aftershocks relocated by Zanzerkia (2003), and performed numerical modeling using the quasi-static, linear elastic, boundary element program Poly3D (Thomas, 1993; Maerten et al., 2005). Their 3D characterization suggests that the orientations of focal mechanisms may reflect the local stress field produced by slip during the main shock and are sensitive to fault geometry. They show that failure is predicted on non-planar faults having a wide range of orientations (Figure 22 and Figure 23), not all consistent with the orientation of and sense-of-slip on the mainshock faults if they were assumed to be vertical and planar. Also exploring aspects of fault complexity, Cooke performed claybox models to study fault formation and demise in restraining stepovers along strike-slip faults. Part of her efforts focused on characterizing the rheologic properties of wet kaolin (in collaboration with van der Elst and Brodsky) demonstrating that below the yield stress wet kaolin displays elastic-plastic behavior, and at failure exhibits velocity weakening rate-and-state behavior, thereby serving as a sufficient analog material for upper crustal deformation.

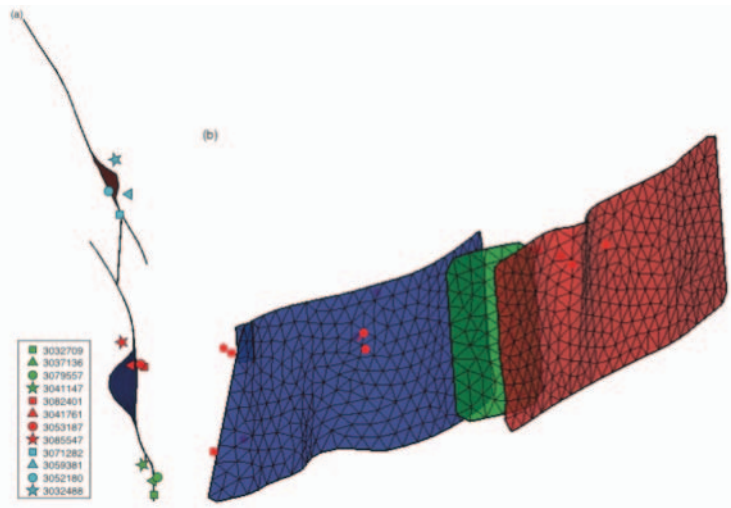

Figure 22. Preferred model geometry in (a) map view with icons showing the locations of the analyzed aftershocks, and (b) oblique view, looking northwest. Vertical bars indicate fault extents.

Micromechanics and Constitutive Behavior

Using micromechanical damage mechanics, Sammis et al. have extended their investigation of the effect of strain rate on the generation of off-fault damage in the process zone of faults. They demonstrate direct agreement with laboratory data on fracture strength as a function of slip rate from quasistatic to coseismic rates (Figure 24), and are working to extend their analysis to address the relation of off-fault damage to earthquake rupture mechanics specifically for the case of a large fault subjected to multiple earthquakes. Oglesby and Beeler are investigating the dependence of fault strength on rapid changes in normal stress and their implications for dynamic rupture in the laboratory by shearing bare granite surfaces at normal stress between 5 and 7 MPa. They find that the response of shear stress to changes in normal stress evolves with time or displacement, therefore more closely resembling the results of Prakash (1998) and that constitutive relationship of Prakash (1998) provides the best model of the results (Figure 25). Oglesby and Beeler interpret these results to reflect the enhanced resolution and digital recording capabilities that were not available at the time of the Linker and Dieterich (1992) study. Continuing their work investigating plastic deformation and strain localization and their implications for dynamic rupture, Carlson et al. are generalizing their STZ

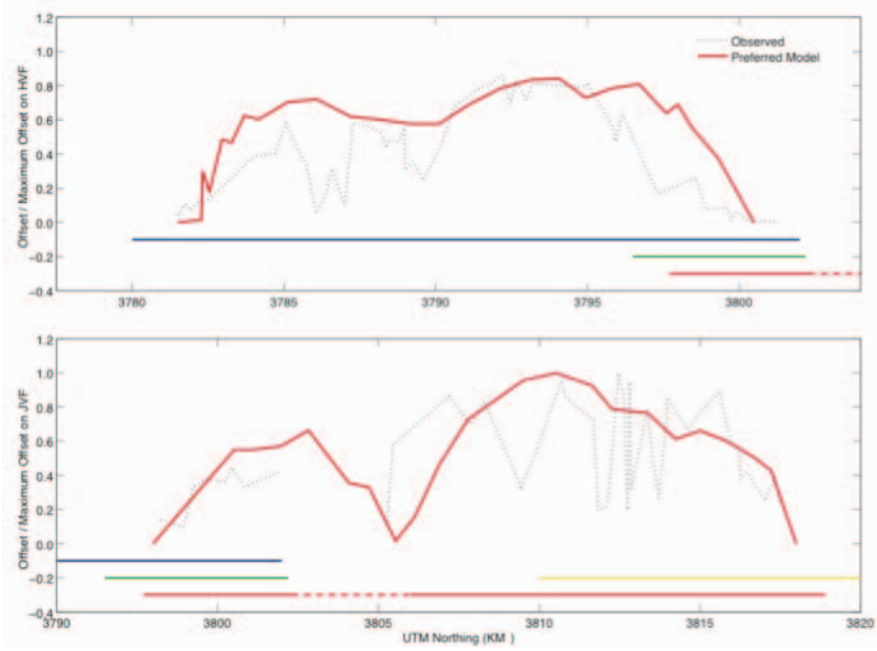

Figure 23. Normalized preferred model slip distributions along the (a) Johnson Valley fault, JVF and (b) Homestead Valley fault, HVF. Horizontal bars below the slip distributions show the extents of faults, as in Figs. 1 and 2 of SCEC Report #10035.

theory to include grain fracture and a broad distribution of particle sizes to better represent the microphysical processes important during formation and shear of fault gouge (Bouchbinder and Langer 2011a;b).

Dynamic Rupture Modeling

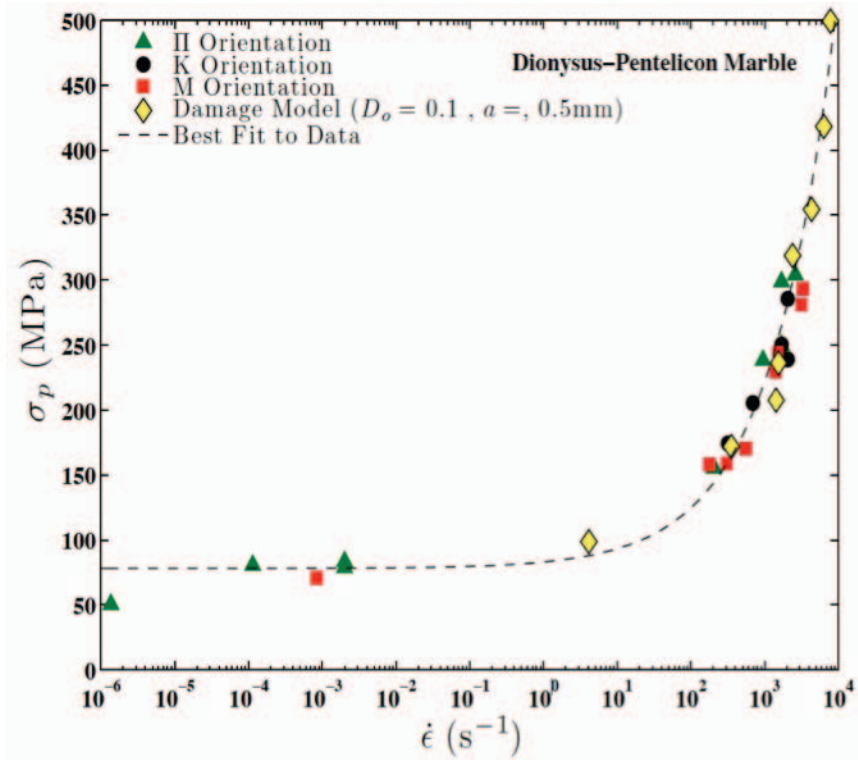

Figure 24. Comparison between experimental measurements of the strength of Pentelicon marble as a function of loading rate and the predictions of their dynamic damage mechanics model (Bhat, Rosakis, and Sammis, 2011, in prep.).

Numerous research groups are exploring various topics through dynamic rupture modeling. Segall and Dunham continued their analysis of thermal pressurization, analyzing its effect through all phases of nucleation and into the early stage of dynamic rupture using rate and state friction with the aging form of the state evolution law on an infinitely thin fault. Their simulations begin using a quasi-static nucleation code and switch to an elastodynamic code just before seismic radiation becomes significant (Schmitt et al. 2011). When they compare purely quasi-dynamic simulations to those incorporating elastodynamics, they find that the slip distributions are the same, but rupture propagation is about 2.5 times faster in the quasi-dynamic case. Incorporating elastodynamics slows crack growth to the P-wave speed. For an infinitely thin slip surface, they find that thermal pressurization begins to dominate fault-weakening at 0.06 mm/s, and once a maximum velocity of 0.2 mm/s is reached, thermal pressurization is the only important weakening term (Figure 26). Inconsistent with observations, incorporating thermal pressurization in the dynamic simulations results in a total loss of shear strength, an artifact that they attribute to the spatially uniform stress and shear resistance. They have begun to explore models with two types of

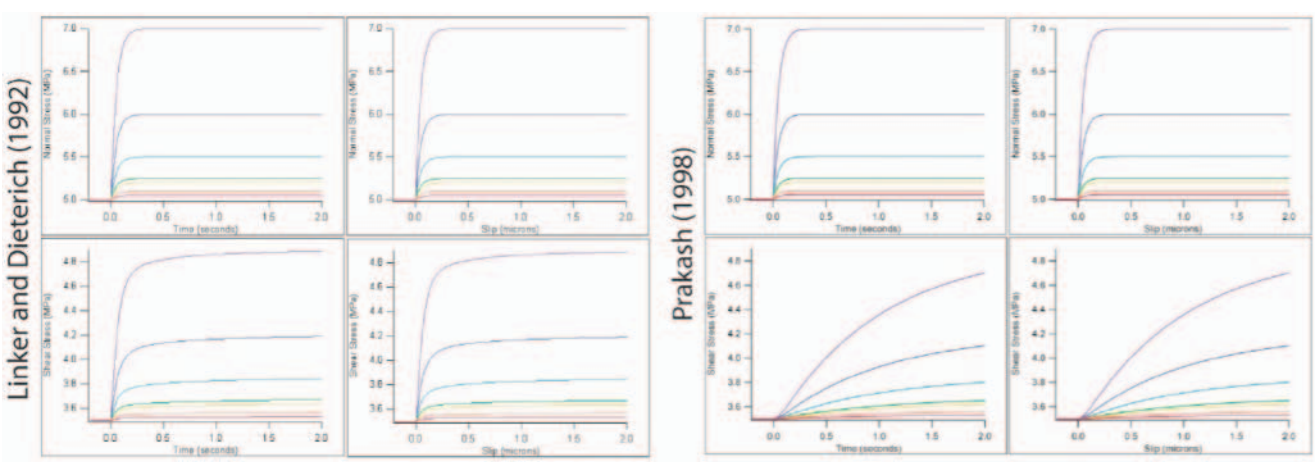

Figure 25. Simulations of the normal stress changes and shear stress response in the experiments that are shown in Fig. 2 of SCEC Report #10145. The left 4 panels are using the constitutive relations of Linker and Dieterich (1992), arranged in the same order as in Fig. 2. Right 4 panels are using the constitutive relations of Prakash (1998).

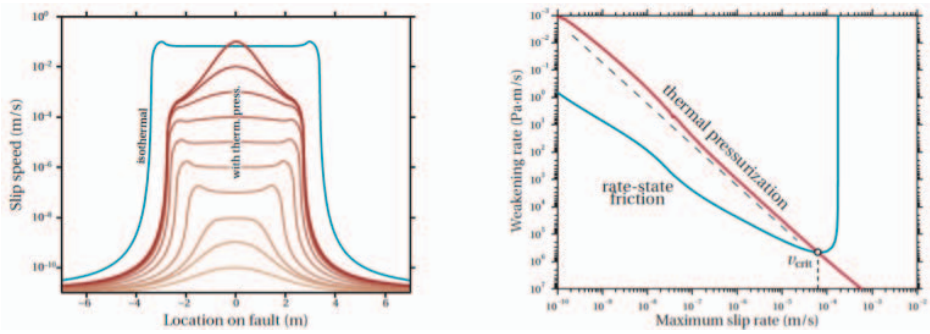

Figure 26. Left: The effect of thermal pressurization on aging law nucleation. Lines are snapshots of slip speed on the fault. In red, snapshots for every 10-fold increase in vmax are shown for nucleation with thermal pressurization. The nucleation zone starts as a growing crack, then shrinks. For comparison, the isothermal profile for a maximum velocity of 100 mm/s is shown; crack growth continues in this case. Right: Critical velocity. The two weakening terms (averaged over the slipping zone) are plotted against the maximum velocity. Rate/state friction dominates the weakening until a critical velocity of 0.06 mm/s, at which point thermal pressurization becomes the dominant weakening term in the equation of motion. By the time the maximum velocity reaches 0.2 mm/s, thermal pressurization becomes the only weakening term. Rate/state friction becomes strengthening because of its direct velocity-strengthening component. The dashed line is a reference line with slope -3/2.

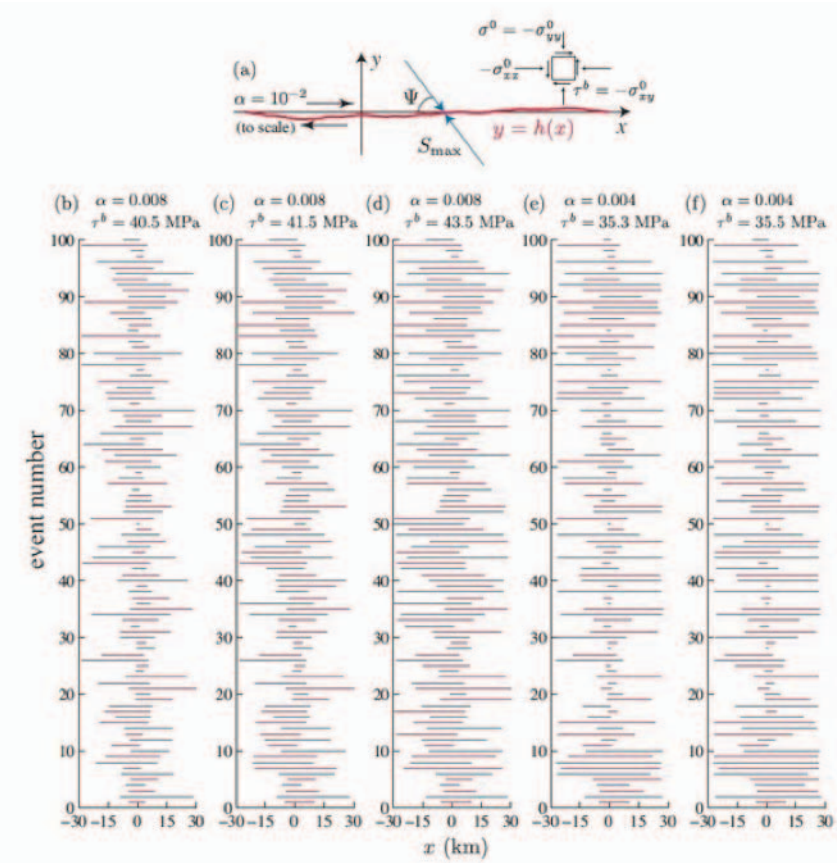

Figure 27. (a) Spatially uniform prestress field with ψ being the angle between the maximum principal compressive stress and the surface y = 0. (b)-(f) Ensemble simulations showing extent of earthquake ruptures on 100 randomly generated self-similar faults under different background stress levels. Colors alternate to distinguish ruptures. Ruptures stop naturally at unfavorable fault bends or reach the end of the simulation domain. At the lower background stress levels, like in (a), most ruptures arrest soon after nucleation and large events are the exception.

heterogeneity, a high shear stress region and a low effective normal stress region to address this issue, and intend to incorporate more realistic conditions to generate stress heterogeneities and weakness into their simulations in the future. Dunham et al. (2010; 2011a; 2011b) continued their studies of rupture along planar and nonplanar faults governed by strongly rate-weakening friction and off-fault plasticity. They find that the average rupture length increases with increasing shear stress and decreases with increasing roughness, and that a critical background stress level is required for self-sustaining rupture propagation (Figure 27). At this stress level, rupture velocity fluctuates significantly and propagation becomes notably sensitive to roughness. Currently, this group is developing a time-stepping methodology to explore the evolution of stress states over the interseismic period and plan to simulate earthquake cycles with multiple rupture events. Following Dunham's work in 2D, Ma (2010) studied the effects of heterogeneous fault geometry on rupture dynamics in 3D with off-fault plasticity. Using his previously developed finite element code (Ma, 2008; Ma and Andrews, 2010) and a slip-weakening law he calculated the rupture dynamics and seismic radiation, demonstrating that fault roughness causes small wavelength irregularity in the rupture fronts that can serve as a potential source of high-frequency radiations (Figure 28). Furthermore, rapid healing produces a more pulse-like rupture that is characterized by significant heterogeneous changes in shear and normal stress. Higher resolution simulations to resolve the distributions of plastic yielding currently are underway. Duan and colleagues (2010) have continued their investigation of the effect of off-fault plastic yielding and time-dependent pore pressure variations on dynamic rupture propagation through step-over regions between parallel strike-slip faults using the finite element dynamic code EQdyna. When compared to simulations in elastic

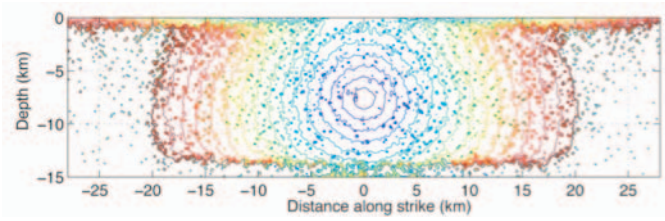

Figure 28. Rupture contours every 0.5 s are mapped on the fault.

medium (Harris and Day, 1993), they find that plastic yielding has little influence on compressional step-over ruptures, but significantly reduces the along strike overlap required for jumping and allows for a wider stepover region along dilatation stepovers (Figure 29). Time-dependent pore-pressure changes allow rupture jumping over wider compressional stepovers, but significantly reduce the ability for rupture jumping at dilatational stepovers. When considered together, time-dependent pore-pressure changes have the greatest effect on the resultant behavior (Figure 30). Several research groups examined rupture propagation along branching faults. Rice and colleagues address the physical and modeling issues associated with rupture propagation through branched triple junctions using 2D finite element methods (DeDontney et al., 2011). When a non-cohesive elastic-plastic material is employed, the elevated stresses around the rupture tip and at the branch junction promote material failure and inhibit opening, especially in the damage zones of mature faults (Figure 31). Opening may occur in intact crystalline rock and deformed zones that have experienced significant cementation (i.e., rocks having large cohesive strength), but is accompanied by significant material softening, decreasing the material strength with shear. Off-fault-plasticity also promotes rupture of extensional side branches and inhibits rupture on compressional side branches. Oglesby and Bowman continue to use the finite-element method to model the dynamics of branched faults, extending the work of King et al. (2005). Over the past year, SCEC intern Jennifer Tarnowski, investigated how the size and shape of the barrier on the vertical fault affected rupture propagation to the dipping fault. Her results suggest that the barrier on the vertical fault must be larger than some minimum area for the rupture to move to the dipping fault (Figure 32). To test the hypothesis that rupture propagation preferentially occurs in the direction of the more compliant side of a bi-material interface, producing greater damage on the stiffer side, and to understand the influence of material contrast on fault branching in 2D, DeDontney et al. (2011 in press; 2011; 2011 submitted) examined the role of stress state on the distribution of plastic strain and the direction of rupture propagation. Their results suggest several factors contribute to determining rupture directivity and branch location. For plastic deformations, the most critical parameter is the orientation of the greatest compressive stress. DeDontney et al. demonstrate that plastic yielding is predicted in both the stiff and compliant sides, depending on the stress orientation, and rupture propagation can occur in the direction of slip displacement in the stiffer material if the most compressive stress is at a low angle to the master fault. Furthermore, fault branches are more likely to rupture when the branch is in the more compliant material, regardless of the stress state (Figure 33). Returning to the theme of planar faults and bimaterials (e.g., Andrews and Ben-Zion, 1997; Harris and Day, 1997), Rubin and Wang use observations to test the hypothesis that directivity is related to across-fault contrast in elastic properties. They (Wang and Rubin, 2011) performed inversions of spectral ratios of microearthquakes on the northern creeping section of the SAF to determine if SE propagation is favored. The spectral ratio data were fit with the moving point source model to give estimates of rupture lengths. The data suggest that of the 40% of earthquake events that can be classified as bilateral ruptures, the rupture length of the SE end is longer in ~67% of the cases, and for rupture segments that can be defined as more nearly unilateral, more than ~75% propagate to the SE, and when defined, have approximately 10% faster propagation velocities. They conclude that the asymmetry in aftershock occurrence and SE directivity reflect the across-fault material contrast. Although the inversion results show that the directivity is somewhat broadly scattered, their analysis clearly demonstrates that several SE-propagating, strongly unilateral events do not have NW-propagating counterparts, regardless of the model

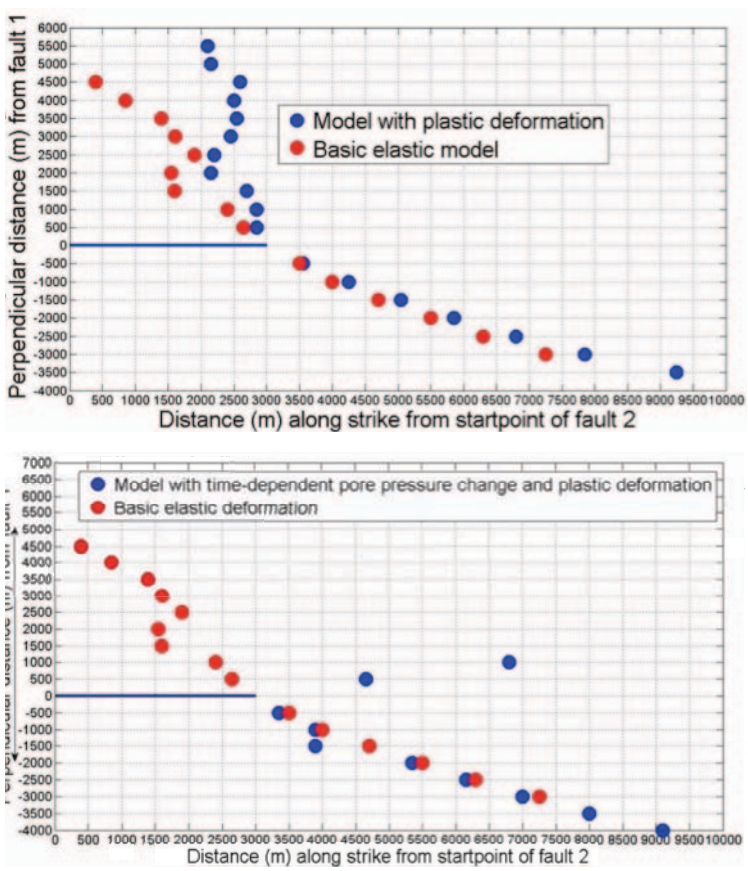

ıure 30. Combined effects of off-fault plastic yielding and time-dependent
:e-pressure on the ability of rupture jumping across a stepover

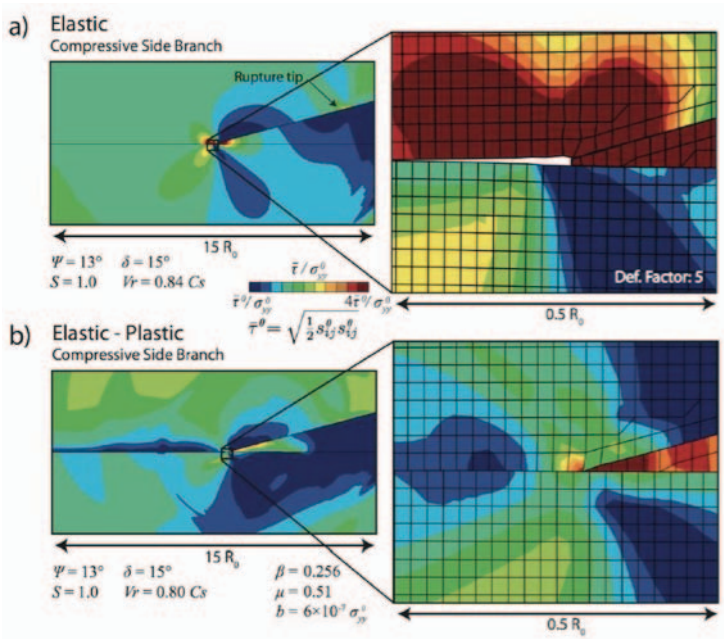

Figure 31. Image of the branching junction some time after the rupture has propagated onto the compressive side branch and a small distance along the main fault. Contours show the shear stress level. (a) Opening occurs at the junction for an elastic off-fault material. (b) Opening does not occur for an incohesive elastic-plastic material.

parameterization (Figure 34). When all well-resolved events are considered, the data suggest that the tendency for SE propagation increases with event size (Figure 35).

An additional interesting result is that events with nearby foreshocks tend to propagate away from their foreshocks. The multi-investigator Rupture Dynamics Code Validation project continued to make excellent progress, and the group's work on verifying the code used to predict extreme ground motions at Yucca Mountain is being published this September (Harris et al., 2011). In early 2011, group members, along with a stealth international following, tackled a 2D thermal pressurization benchmark. The results matched well when the codes used an element spacing smaller than 100 m. The group also worked on two branched-fault benchmarks, each in 2D and 3D versions. These latter exercises were the first non-planar fault geometries to be treated. The results were that the 2D codes generated better matches than the 3D codes did, and that some modelers were unable to execute the 3D benchmarks because of limitations in the computational capacities of their research institutions. Part of the challenge with the fault-branch benchmarks was that different codes assume different locations for edges and ends of faults. Whereas this was less of an issue when simulating ruptures that nucleate in the middle of planar faults, the fault branch case includes a fault intersection. How to numerically handle fault intersections (and what they look like in nature) is a topic of discussion in our community that will likely continue into SCEC4. DeDontney et al. (2011 submitted) discusses some of the challenges of fault-intersection simulations, in 2D. Upcoming Dynamic Rupture group plans include exploring 2D and 3D fault branches with off-fault yielding, in addition to rupture simulations on a vertical strike-slip fault with a heterogeneous initial on-fault stress condition. The heterogeneous initial conditions, planar-fault benchmark(s) will once again unify the group's efforts in that all of the participating dynamic earthquake rupture codes can simulate earthquakes on vertical faults. In addition, describing and quantifying fault stress heterogeneity is an important topic that spans multiple SCEC groups, demonstrating that we are continuing to address critical earthquake-science topics.

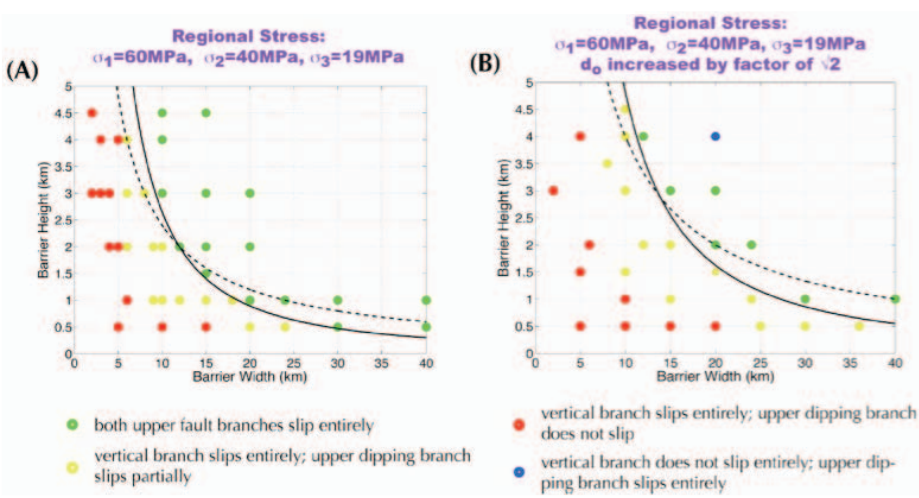

Figure 32. Ability of rupture to propagate from the vertical to the dipping fault as a function of the height and width of the barrier on the vertical fault. Dashed curve: best-fitting curve of constant barrier area, signifying the minimum barrier size for rupture propagation to the dipping fault. Solid curve: best-fitting curve that separates the part of phase space with dipping fault slip from the part with only vertical fault slip. A comparison of a) and b) shows that multiplying the slip-weakening distance by /2 causes the minimum barrier area to double, in agreement with the idea that the barrier needs to cause a patch of critical area on the dipping fault to exceed its static frictional stress in order to nucleate spontaneous rupture on the dipping fault.

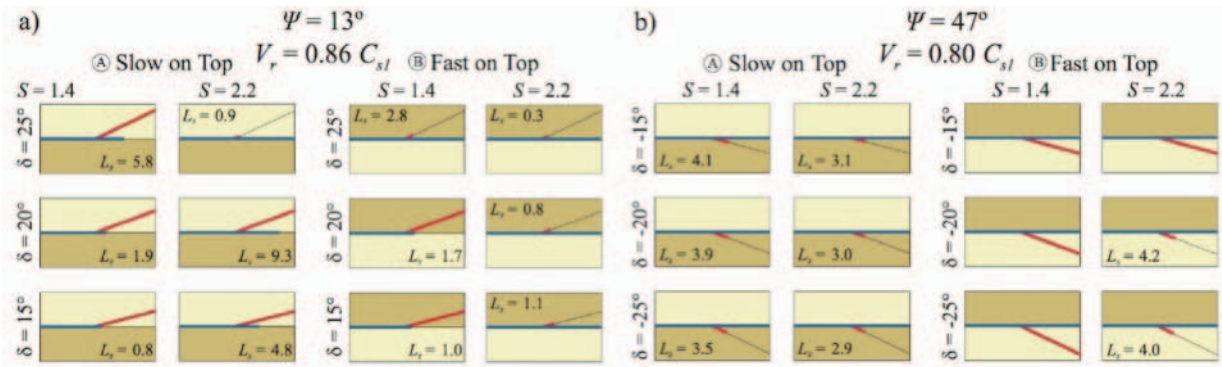

Figure 33. Branch activation results. Both compressional side branches (a) and extensional side branches (b) are more likely to rupture when the branch is in a more compliant ("slower") material.

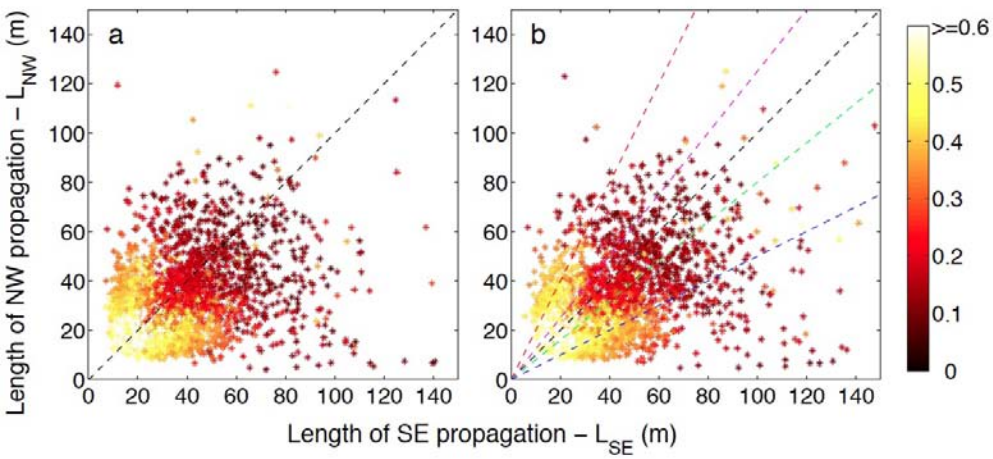

Figure 34. Inversion results for the directivity of 3103 earthquakes. (a) Central points of the posterior pdfs, color-coded according to the resolution of directivity (the width of the 90% confidence interval of LSE/[LSE + LNW]). Only events for which this resolution is < 0.6 are shown. (b) The same but for an inversion where the a priori distribution of rupture propagation velocities to the SE is 10% faster than that to the NW.

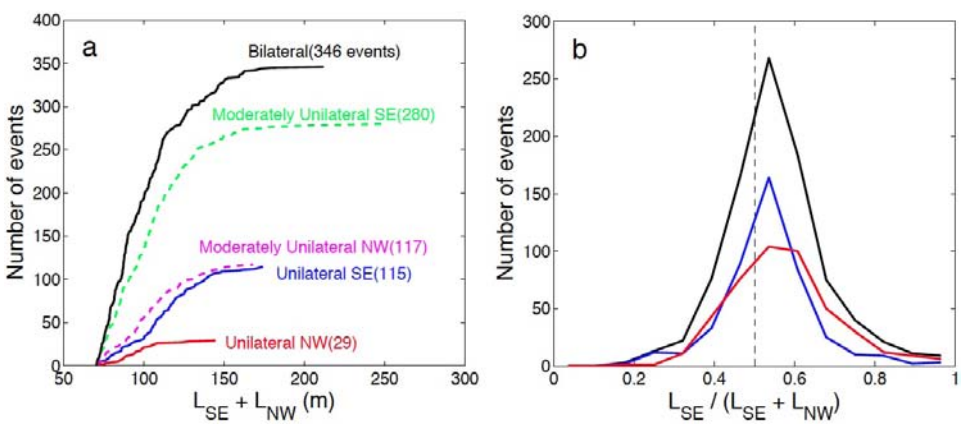

Figure 35. (a) Cumulative number of the 887 well-resolved events in five different regions of Figure FARM16b, indicated by the dashed lines in that figure. The cumulative events are plotted as function of total inverted rupture length LSE +LNW. (b) Histograms of LSE/(LSE +LNW) for all the well-resolved events in Figure FARM16b (black) and for those with total inverted length smaller than 100 m (blue, 444 events) and larger than 100 m (red, 443 events).

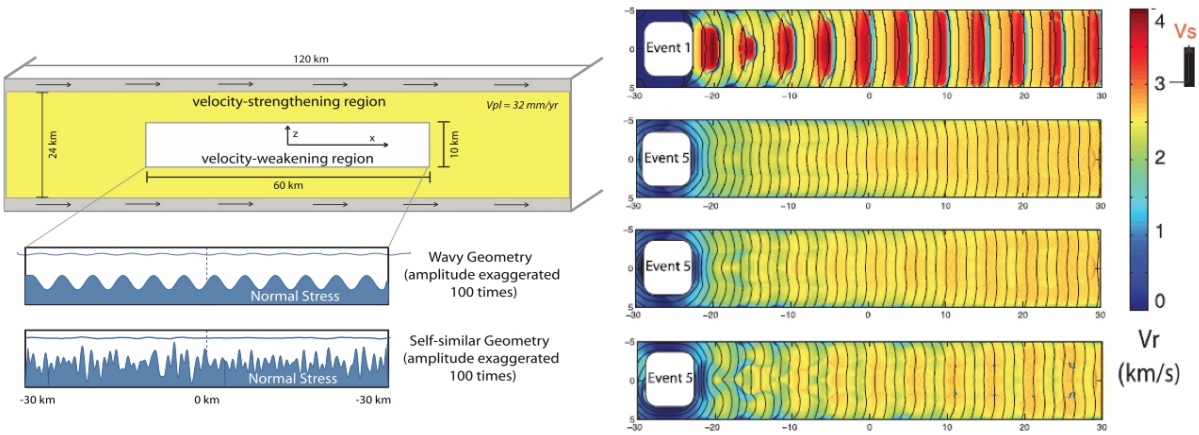

Figure 36. Stress redistribution on faults with heterogeneous strength significantly affects the long-term seismic fault behavior. Left: Model of a rate-and-state fault with non-uniform distribution of normal stress motivated by fault nonplanarity. Right: Distribution of rupture speeds over the fault for selected events. When the initial shear prestress is arbitrarily chosen to be uniform, the rupture speed in the 1st event varies significantly over the fault (top panel, the case of 10% normal stress variation). However, the 5th event of the same simulation (second panel) has nearly constant rupture speed, similar to the case with uniform normal stress (not shown). The other panels show the 5th events for cases with 20% and 40% variation.

Large-scale dynamic rupture simulations carried out by SCEC teams have the potential to provide novel and critical information for the assessment of seismic hazard in Southern California. It is important to understand how to assign initial conditions for these simulations that are consistent with other assumed ingredients for dynamic rupture simulations, including fault geometry, materials, initial stresses, and friction (e.g., Harris, 2004). Several groups are focusing on these critical issues. As an example, Lapusta and colleagues are studying how dynamic rupture interacts with fault heterogeneity over many earthquake cycles, taking into account the effect of prior fault slip. Dynamic rupture simulations suggest that both variations in fault strength and fault prestress can strongly influence the development of dynamic ruptures, e.g. induce or suppress supershear rupture speeds (e.g., Day, 1982; Madariaga et al., 1998; Madariaga and Olsen, 2000; Fukuyama and Olsen, 2002; Dunham et al., 2003; Liu and Lapusta, 2008). Two distributions – of fault strength and shear stress – are often assumed independently, but they are related due to prior fault slip. To assess how the distribution of fault strength affects typical fault prestress before large events, Lapusta's group simulates long-term slip on a fault segment that includes multiple earthquake cycles and (i) resolves all the stages of every single earthquake in detail, including earthquake nucleation, dynamic rupture propagation and arrest, and (ii) reproduces post-seismic slippage and interseismic creep (Lapusta et al., 2000; Lapusta and Liu, 2009). These simulations of faults with heterogeneous normal stress distributions motivated by non-planar faults (Jiang and Lapusta, AGU, 2010) show that the RMS mismatch between the representative static fault strength and prestress before model-spanning events evolves to near-constant values in the long-term history of the fault. In a set of models, comparison between the first simulated earthquake and subsequent events shows that shear stress redistribution over time at least partially compensates for the heterogeneity in fault strength, diminishing its effect on seismic events (Figure 36). Quantifying the long-term mismatch between strength and prestress in terms of the model parameters, such as the degree of fault heterogeneity, could provide physically based guidance for assigning initial conditions in simulations of single dynamic earthquake ruptures.

Observational Studies of Fault Slip and Fault Structure

Wechsler et al. (2011) characterize the composition, structure and particle size distribution (PSD) of pulverized and damaged granitic rocks in a 42-m-deep core adjacent to the San Andreas Fault near Littlerock, CA. The cored section is composed of pulverized granites and granodiorites, and is cut by numerous mesoscopic secondary shears. The most pronounced fault-related alteration occurs along the shears, and is a function of both composition and depth. Alteration to clay appears to be the result of fluid–rock interaction and brittle deformation under low temperature conditions, rather than of surface-related weathering. The zones of pulverization that lack significant weathering likely reflect repeating episodes of dynamic dilation and contraction. The mean particle size for the majority of pulverized and cataclastic samples falls between 50 and 470 μm, and PSDs can be fit by a power law, with D-values ranging between 2.5 and 3.1. To better understand the response of damage

zones to movement through bends in fault surfaces, Becker et al. are characterizing the structure and intensity of damage along the North Branch of the San Gabriel fault, and Evans is focusing on defining deformation mechanisms and slip processes at high temperature conditions.

References

Andrews, D. J., and Y. Ben-Zion (1997), Wrinkle-like slip pulse on a fault between different materials, J. Geophys. Res., v. 102, 553-571, doi:10.1029/96JB02856

Bouchbinder, E., ,and J. S. Langer (2011), Shear-Transformation-Zone Theory of Linear Glassy Dynamics, Phys. Rev. E 83, 061503. ArXiv:1101.2015

Bouchbinder, E., and J. S. Langer, Linear Response Theory for Hard and Soft Glassy Materials (2011), Phys. Rev. Lett. 106, 148301. ArXiv:1101.3539

Bryant, W. A. (1992), Surface rupture along the Johnson Valley, Homestead Valley, and related faults associated with the M7.5 28 June 1992 Landers Earthquake, Div. of Mines & Geology Fault Evaluation Report 234, 239, CA Dept of Conservation, Sacramento.

Bryant, W. A. (1994), Surface fault rupture along the Homestead Valley, Emerson, and related faults associated with the M7.3 28 June 1992 Landers Earthquake, Div. of Mines & Geology Fault Evaluation Report 239, CA Dept of Conservation, Sacramento.

Bryant, W. A. (2004), Surface rupture associated with the June 28, 1992, Mw 7.3 Landers earthquake, Iron Ridge, Fry Mountain, and Camp Rock Mine 7.5 minute quadrangles, San Bernardino, CA, CA Geological Survey unpublished digital mapping for the Pacific Earthquake Engineering Research Center, Sacramento.

California Geological Survey (2002), GIS files of official maps of Alquist-Priolo earthquake fault zones, southern region, CA Geological Survey CD 2001-05, Sacramento.

Day, S. M. (1982), Three-dimensional simulations of spontaneous rupture: The effect of nonuniform prestress. Bull. Seismol. Soc. Am., 72, 1881–1902.

DeDontney, N., E. L. Templeton-Barrett, J. R. Rice, and R. Dmowska (2011, in press), Influence of Plastic Deformation on Bimaterial Fault Rupture Directivity, J. Geophys. Res., doi:10.1029/2011JB008417, in press.

DeDontney, N., J. R. Rice, and R. Dmowska (2011), Influence of material contrast on fault branching behavior, Geophys. Res. Lett., 38, L14305, doi:10.1029/2011GL047849.

DeDontney, N., J. R. Rice, and R. Dmowska (2011, submitted), Finite element model of branched ruptures including off-fault plasticity, Bull. Seism. Soc. Am.

Duan, B. (2010), Inelastic response of compliant fault zones to nearby earthquakes, Geophys. Res. Lett., 37, L16303, doi:10.1029/2010GL044150.

Duan, B., J. Kang, and Y.-G. Li (2011), Deformation of compliant fault zones induced by nearby earthquakes: Theoretical investigations in two dimensions, J. Geophys. Res., vol. 116, B03307, doi:10.1029/2010JB007826.

Dunham, M., P. Favreau, and J. M. Carlson (2003), A supershear transition mechanism for cracks, Science, 299, 1557–1559.

Dunham, E. M., D. Belanger, L. Cong, and J. E. Kozdon (2011), Earthquake ruptures with strongly rate-weakening friction and off-fault plasticity: 1. Planar faults, Bull. Seism. Soc. Am., in press.

Dunham, E. M., D. Belanger, L. Cong, and J. E. Kozdon (2011), Earthquake ruptures with strongly rate-weakening friction and off-fault plasticity: 2. Nonplanar faults, Bull. Seism. Soc. Am., in press.

Fukuyama, E., and K.B. Olsen (2002), A condition for supershear rupture propagation in a heterogeneous stress field. Pure. Appl. Geophys., 157, 2047–2056.

Hardebeck, J. L., and P. M. Shearer (2002), A new method for determining first-motion focal mechanisms, Bull. Seism. Soc. Am., v. 92; no. 6; p. 2264-2276; DOI: 10.1785/0120010200.

Harris, R. A. (2004), Numerical simulations of large earthquakes: dynamic rupture propagation on heterogeneous faults, Pure and Applied Geophysics, vol. 161, No.11/12, pp. 2171-2181, DOI: 10.1007/s00024-004-2556-8.

Harris, R. A., and S. M. Day (1993), Dynamics of fault interaction: Parallel strike-slip faults, J. Geophys. Res., 98, 4461-4472.

Harris, R. A., and S. M. Day (1997), Effects of a low-velocity zone on a dynamic rupture, Bull. Seism. Soc. Am., v. 87; no. 5, p. 1267-1280.

Harris, R. A., M. Barall, D. J. Andrews, B. Duan, E. M. Dunham, S. Ma, A.-A. Gabriel, Y. Kaneko, Y. Kase, B. Aagaard, D. Oglesby, J.-P. Ampuero, T. C. Hanks, and N. Abrahamson (2011), Verifying a computational method for predicting extreme ground motion, Seism. Res. Lett., Vol. 82, No. 5, September/October 2011.

Hillers, G., and J.-P. Ampuero (2011), Spontaneous harmonic tremors on the San Jacinto fault, southern California, submitted to Nature Geoscience.

Houston, H., B. G. Delbridge, A. G. Wech and K. C. Creager (2011), Rapid tremor reversals in Cascadia generated by a weakened plate interface, Nature Geoscience 4, 404–409, doi:10.1038/ngeo1157.

Jiang, J., and N. Lapusta (2010), Dynamic rupture on faults with heterogeneous strength due to non-uniform normal stress: The effect of stress redistribution by prior events, Abstract S33E-05 presented at 2010 Fall Meeting, AGU, San Francisco, Calif., 13-17 Dec.

Kaneko, Y., and Y. Fialko (2011), Shallow slip deficit due to large strike-slip earthquakes in dynamic rupture simulations with elasto-plastic response, Geophysical Journal International, doi:10.1111/j.1365-246X.2011.05117.x

Kaneko, Y., and Y. Fialko (2010), Modeling shallow slip deficit in large strike-slip earthquakes using simulations of spontaneous earthquake sequences in elasto-plastic media, Abstract T33B-2248 presented at 2010 Fall Meeting, AGU, San Francisco, Calif., 13-17 Dec.

King, G. C. P., Y. Klinger, D. Bowman, and P. Tapponnier (2005). Slip-partitioned surface breaks for the Mw 7.8 2001 Kokoxili Earthquake, China, Bulletin of the Seismological Society of America 95, 731-738, doi:10.1785/0120040101.

Lapusta N., J. R. Rice, Y. Ben-Zion, and G. Zheng (2000), Elastodynamic analysis for slow tectonic loading with spontaneous rupture episodes on faults with rate- and state-dependent friction, J. Geophys. Res., 105, 23,765-23,789.

Lapusta, N, and Y. Liu (2009), Three-dimensional boundary-integral modeling of spontaneous earthquake sequences and aseismic slip, J. Geophys. Res., 114, B09303, doi:10.1029/2008JB005934.

Linker, M .F., and J. H. Dieterich (1992), Effects of variable normal stress on rock friction: Observations and constitutive relations, Journal of Geophysical Research, 97 (B4), 4923-4940.

Liu, Y., and N. Lapusta (2008), Transition of mode II cracks from sub-Rayleigh to intersonic speeds in the presence of favorable heterogeneity. J. Mech. Phys. Solids, 56, 25–50, doi:10.1016/j.jmps.2007.06.005.

Ma, S. (2008), A physical model for widespread near-surface and fault zone damage induced by earthquakes, Geochem. Geophys. Geosyst., 9, Q11009, doi:10.1029/2008GC002231.

Ma, S., and D. J. Andrews (2010), Inelastic off-fault response and three-dimensional earthquake rupture dynamics on a strike-slip fault, J. Geophys. Res., 115, B04304, doi:10.1029/2009JB006382.

Madariaga, R., K. B. Olsen, and R. J. Archuleta (1998), Modeling dynamic rupture in a 3-D earthquake fault model. Bull. Seismol. Soc. Am., 88, 1182–1197.

Madariaga, R., and K. B. Olsen (2000), Criticality of rupture dynamics in 3D. Pure. Appl. Geophys., 157, 1981–2001.

Maerten, F., P. Resor, D. D. Pollard and L. Maerten (2005). Inverting for slip on three-dimensional fault surfaces using angular dislocations, Bull. Seismo. Soc. Am. 95 1654-1665.

Prakash, V. (1998), Frictional response of sliding interfaces subjected to time varying normal pressures, Journal of Tribology, 120, 97-102.

Schmitt, S. V., P. Segall, and T. Matsuzawa (2011), Shear heating-induced thermal pressurization during earthquake nucleation, J. Geophys. Res, 116, B06308, doi:10.1029/2010JB008035

Shaw, B.E. (2011), Surface Slip Gradients of Large Earthquakes, Bulletin of the Seismological Society of America, 101, 792.

Shearer, P., E. Hauksson, and G. Lin (2005), Southern California hypocenter relocation with waveform cross-correlation: Part 2. Results using source-specific station terms and cluster analysis, Bull. Seismol. Soc. Am., 95, 904-915, doi:10.1785/0120040168.

Templeton, E. L., and J. R. Rice (2008), Off-fault plasticity and earthquake rupture dynamics, 1. Dry materials or neglect of fluid pressure changes, J. Geophys. Res., 113.

Thomas, A. L. (1993), Poly3D: a three-dimensional, polygonal element, displacement discontinuity boundary element computer program with applications to fractures, faults, and cavities in the Earth's crust, Master's Thesis, Stanford University, Stanford, CA.

Wang, E., and A. M. Rubin (2011), Rupture directivity of microearthquakes on the San Andreas Fault from spectral ratio inversion, Geophys. J. Int., 186, *Wechsler, N., E. E. Allen, T. K. Rockwell, G. Girty, J. S. Chester, Y. Ben-Zion (2011), Characterization of pulverized granitoids in a shallow core along the San Andreas Fault, Little Rock, CA, Geophys. J. Int., V.186, Issue 2, doi: 10.1111/j.1365-246X.2011.05059.x.

Zanzerkia, E. (2003), Towards an understanding of seismic triggering through precise earthquake locations, PhD Thesis, Stanford University, Stanford, CA.

Zhao, P., Z. Peng, Z. Shi, M. A. Lewis, and Y. Ben-Zion (2010), Variations of the velocity contrast and rupture properties of M6 earthquakes along the Parkfield section of the San Andreas Fault, Geophys. J. Int., 180, 765–780, doi:10.1111/j1365-246X.2009.04436.x.

Crustal Deformation Modeling

The goal of the SCEC Crustal Deformation Modeling (CDM) focus group is gaining an understanding of how faults work mechanically, during the interseismic interval and over geological time. This provides insights on absolute stresses and stressing rates in the Earth's crust (and along active faults in particular). We also use our deformation models to estimate fault slip rates and other parameters from surface velocity data (e.g. the SCEC GPS velocity field), for the UCERF rupture forecasting process. For 2010, forty SCEC proposals were flagged by the PI's as fitting into the CDM Focus Area, though perhaps half of these related directly to modeling static deformation of the Earth's crust. Our activities for 2010 may be divided loosely into four categories (there is some overlap): (i) conducting workshops, (ii) block and boundary-element modeling, (iii) modeling long-term deformation (at the regional scale or within individual fault systems), and (iv) modeling earthquake-cycle deformation. Developing earthquake simulators is a joint undertaking with EFP, so we will summarize just the workshop here.

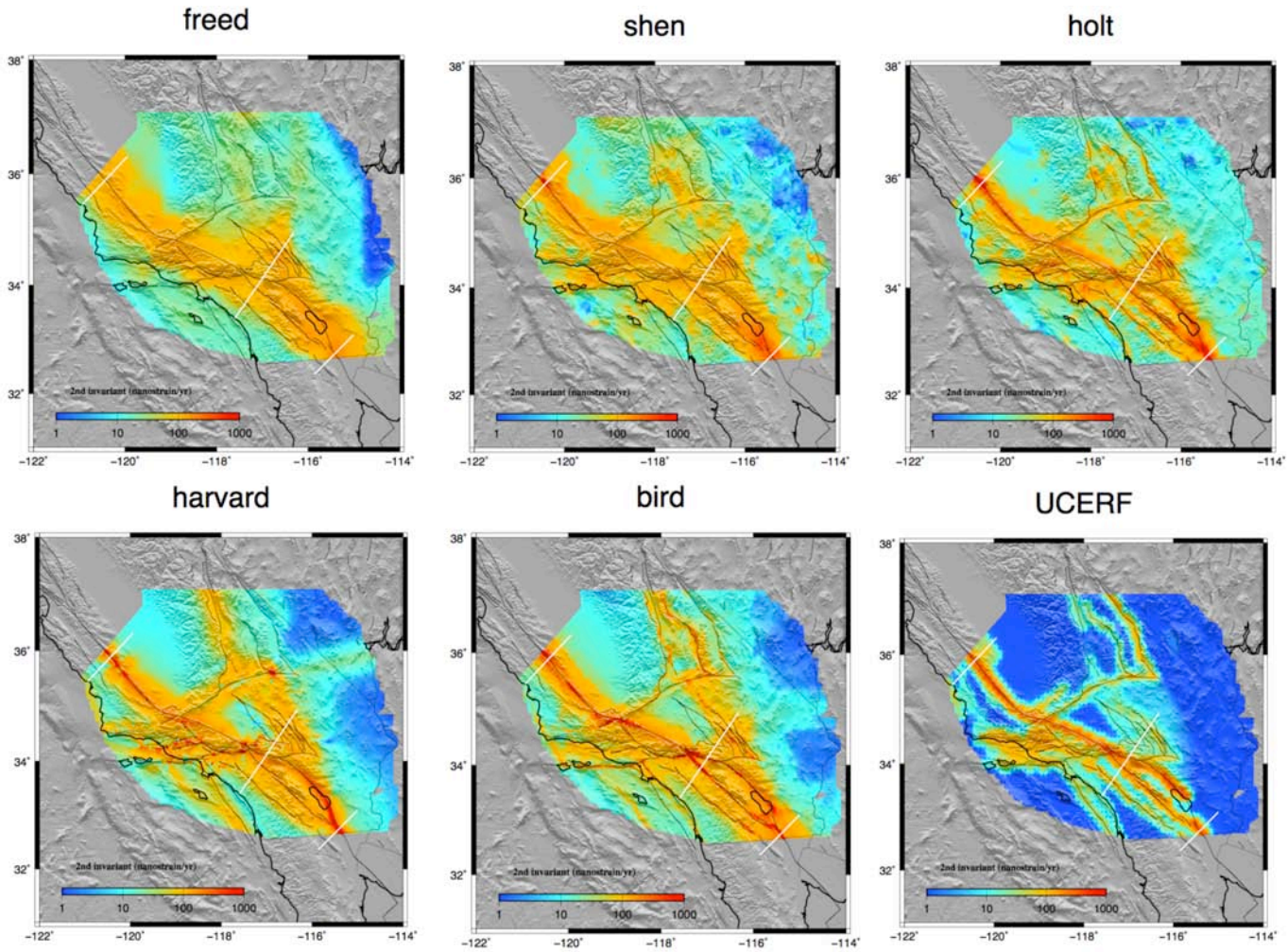

Figure 37. Second invariant of the 2D horizontal strain rate tensor, derived from GPS velocity measurements using a variety of approaches. The original references may be found in the following URL: http://sceccore.usc.edu/proposalfiles/2010reports/Thatcher_10082_report.pdf. The area shown here is limited to the union of the coverage of all 15 strain rate maps that were submitted by GPS-UCERF workshop participants. For comparison purposes only, the area distribution of the earthquake probability P of the UCERF-2 earthquake forecast ("UCERF, bottom right panel) was scaled into strain rate using the following ad-hoc formula: $d\varepsilon/dt = 10P + 3.4$. The 3.4 factor was selected so the variance on the UCERF2 strain rate matched the median variance of the 15 strain rate maps. From David Sandwell.

Workshops

SCEC supported three workshops related to crustal deformation modeling in 2010, covering (i) finite-element deformation modeling, (ii) integrating GPS into the UCERF3 process, and (iii) comparing earthquake simulators.

The ninth annual Workshop on Crustal Deformation Modeling (June 14-18, 2010, in Golden Colorado) was co-sponsored by SCEC and the Computational Infrastructure for Geodynamics (CIG), and attracted 68 participants. The first two days were dedicated to training in the use of state-of-the-art finite-element codes for modeling crustal deformation with the remaining three days filled with science talks and discussions. See *http://www.geodynamics.org/cig/workinggroups/short/workshops/cdm-10/agenda* for the complete agenda and slides for all of the presentations. This year's workshop included several presentations on the recent Haiti, Chile, and El Mayor-Cucapah earthquakes along with talks on fault and bulk rheologies with a focus on the base of the seismogenic zone. A discussion at the end of the workshop indicated overwhelming support for continuing the series of annual workshops. In early 2011 the organizing committee decided that in order to keep the scientific agenda fresh and increase interest among leading researchers, we will switch to biannual meetings and skip holding a workshop in 2011. Instead we will hold a virtual (online) workshop in 2011 focused solely on training users in the use of PyLith and related codes for modeling crustal deformation. This experiment with online training should enable us to determine if this approach is effective and how to distribute our efforts in the future between in-person training at workshops versus online training.

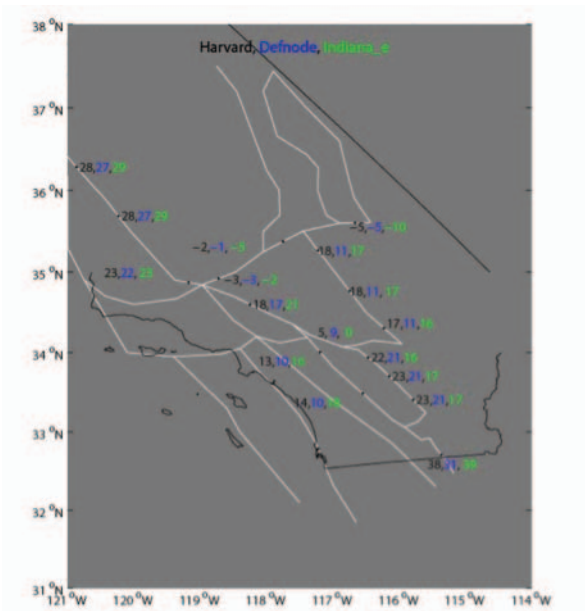

Figure 38. Slip rate estimates on some fault segments from elastic block models, supplied by GPS-UCERF workshop participants. Right-lateral is positive. Left-lateral is negative. Results shown here were provided by Rob McCaffrey; Brendan Meade and Jack Loveless; and Kaj Johnson and Raymond Chuang. From Kaj Johnson. (This exercise has been superceded by a new block modeling test exercise, developed in 2011 by Kaj Johnson.)

In April 2010, the inaugural workshop on incorporating geodetic surface deformation data into UCERF3 was held in Pomona, California (42 attendees, by invitation). A number of goals potentially achievable within a year were identified including (1) slip rate estimates—with uncertainties or ranges—for all major and some minor faults of the extended San Andreas system; (2) strain rate estimates or bounds on rates for selected regions lying off the major faults of the San Andreas system; and (3) corrections or bounds on perturbing effects of post-seismic deformation and elastic crustal moduli heterogeneities on the observed GPS velocity field. Test exercises related to these items included a comparison of southern California strain rate fields generated by several researchers (coordinated by David Sandwell, Scripps), a block modeling test exercise, using the SCEC GPS velocity field (version 3) and a specified block model geometry (coordinated by Kaj Johnson, Indiana U), and an exercise exploring the range of fault slip rates, locking depths, interseismic moment accumulation that might be inferred from a GPS velocity profile across a single fault (coordinated by Elizabeth Hearn, UBC). The results of the former two activities (Figures 37 and Figure 38) indicated large discrepancies, which need to be understood before we provide information to WGCEP.

Immediate follow-on activities were identified to begin implementing the goals enumerated here. These include tightly focused mini- and micro- workshops of 5 to 20 participants each that would be oriented along the same niche specialist lines as the 3 main Pomona workshop sessions. The first of these workshops was held in Golden, Colorado in July (a micro-workshop with just the four organizers of the main workshop, Ned Field (USGS/WGCEP), and a few other participants) and a mini-workshop with some 20 attendees at the SCEC Annual Meeting in September 2010. In 2011, micro-workshops will focus on a revised block model comparison exercise, and a range of GPS-inferred slip rates will be delivered to WGCEP well in advance of the final due date for UCERF3. A detailed summary of the April 2010 GPS-UCERF3 workshop is here: (*http://sceccore.usc.edu/proposalfiles/2010reports/Thatcher_10082_report.pdf*). A shorter version of this appeared in Transactions of the AGU (Hearn et al., 2010).

In July 2010, Terry Tullis lead a workshop for 25 attendees (by invitation). The principal purposes of the workshop were to allow the participants 1) to compare the results from the first simulations to use our common input and output formats and

output processing tools, and 2) to determine how well the tools are working with a view to improving and adding to them, and 3) to see what preliminary conclusions we could reach about the ways in which the simulator results are similar and in what ways they are different, and, if possible, why differences exist, and 4) to plan the next steps in comparing the simulators,

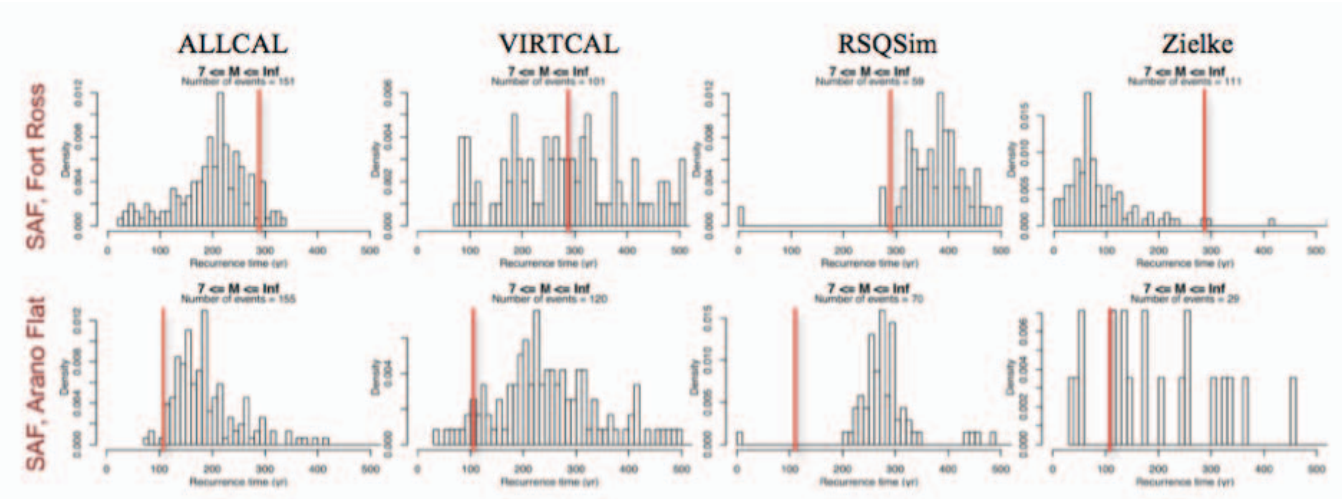

Figure 39. Frequency-magnitude plots for five simulators for the norcal1 model. Workshop participants are still evaluating what factors make the simulators have the magnitude distributions shown. For example, in the case of VIRTCAL (Virtual California, Yikilmaz et al., 2010), the lack of small events is due to the intentional use of a dynamic stress concentration factor that makes it easier for adjacent elements to slip if an event is underway. From Terry Tullis.

in particular what new problems we should consider and how earthquake simulators might help the ongoing UCERF3 process. The simulator comparison exercises demonstrated that the input and output formats that had been prepared by Michael Barall, after an iterative process via several conference calls and numerous emails, were very useful. They allowed analysis tools that were created by Keith Richards-Dinger to process the output of all the many-fault simulations done by the participants. For the first time they were able to make side-by-side comparisons of the various results (Figure 39 and Figure 40) show such a comparison for their northern California fault system test model "NorCal"). Details of all of the results can be found in the presentations made at the workshop at: (*http://scec.usc.edu/research/eqsims/workshop_2010_07_20.html*).

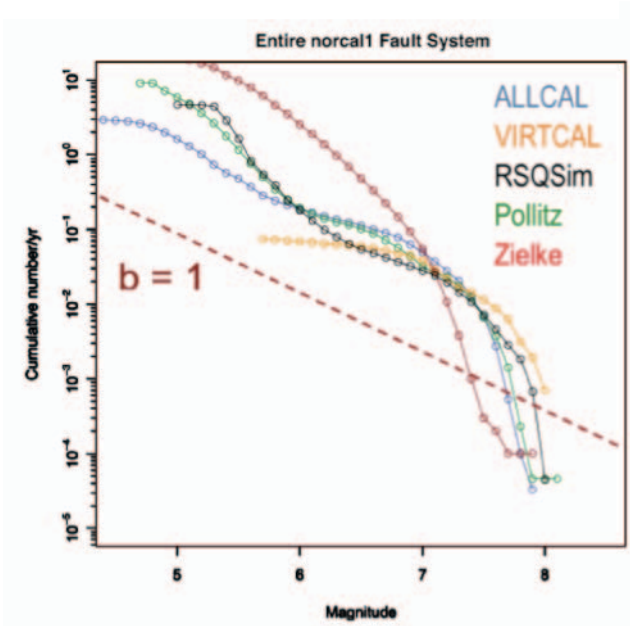

Figure 40. PDFs of recurrence intervals for four simulators for the norcal1 model, at two of the six locations having paleoseismic data. Such plots were generated for many magnitude ranges, but only this one for M > 7 is shown since smaller events may not show up in trenches. The red lines show the preferred inter-event time for these locations from Appendix C of the UCERF2 report (Field et al., 2008). From Terry Tullis.

Block and Boundary Element Modeling

3D Fault Kinematics and Geologic Slip Rates

Michelle Cooke and Scott Marshall continued their work on using elastic boundary-element models to assess whether the SCEC CFM geometry is kinematically consistent with geological slip rates on individual fault segments (which may vary along strike). Scott Marshall and collaborators focus on the Ventura Basin region, and combine this modeling with geodetic data analysis (InSAR and GPS). They have completed an analysis of GPS data from 53 sites in the region and have removed seasonal, anthropogenic, and earthquake-related perturbations to the position time seres. They are currently processing InSAR scenes to locate localized regions of deformation due, for example, to groundwater pumping, and to correct the GPS data in these areas or remove them from the velocity field. Their preliminary boundary element deformation models have addressed whether the CFM fault geometry and velocity boundary conditions are consistent with geological slip rates on individual faults, and they

plan to continue this work with a revised version of their boundary element model which generates surface velocities that may be compared with GPS velocities.

Inferring fault slip and stressing rates from the Southern California GPS Velocity Field

Brendan Meade and Kaj Johnson continued their research using block models based on the SCEC CFM to infer fault slip and moment accumulation rates on active faults in southern California. Both of these PI's have also begun to tackle the problem of how viscoelastic relaxation could affect their results. Direct, analytical calculation (Okada, 1992) of stress rates along the SAF (in the context of a block model) inherently incorporates kinematically consistent fault slip rates and the influence of all fault segments considered in the analysis. Brendan Meade and his student John Loveless (Harvard) have applied this strategy to the SAF, determining the shear and Coulomb stressing rates both due to slip on SAF segments alone ("self stress") and due to slip on all segments in the block model ("total stress") (Figure 41). Comparing the self and total shear stress rates, τSAF and τTOT, respectively, provides indication of how structures nearby and intersecting the SAF influence patterns of stress accumulation (Figure 41). The shear stress rate difference, defined as $\Delta\tau = (\tau TOT - \tau SAF)/\tau TOT \times 100$, reaches values of up to +30% along the Mojave and San Bernardino segments of the SAF and is nearly zero to the north along the Carrizo segment and to the south along the Indio and Imperial segments, except near the isolated fault junctions. The enhanced stressing rate along Big Bend segments demonstrates that interseismic activity on structures that intersect the SAF, including the San Gabriel, Garlock, North Frontal, and Eureka Peak faults, act to increase the likelihood and/or frequency of seismic failure as compared to estimates based on τSAF alone. Interpretations of paleoseismic offset data suggest that Big Bend segments have ruptured in roughly twice the number of earthquakes as the more isolated Carrizo and Indio segments (Weldon et al., 2004), illustrating a correlation between long-term, macro-scale seismicity and interseismic stress enhancement due to off-SAF processes (Figure 41).

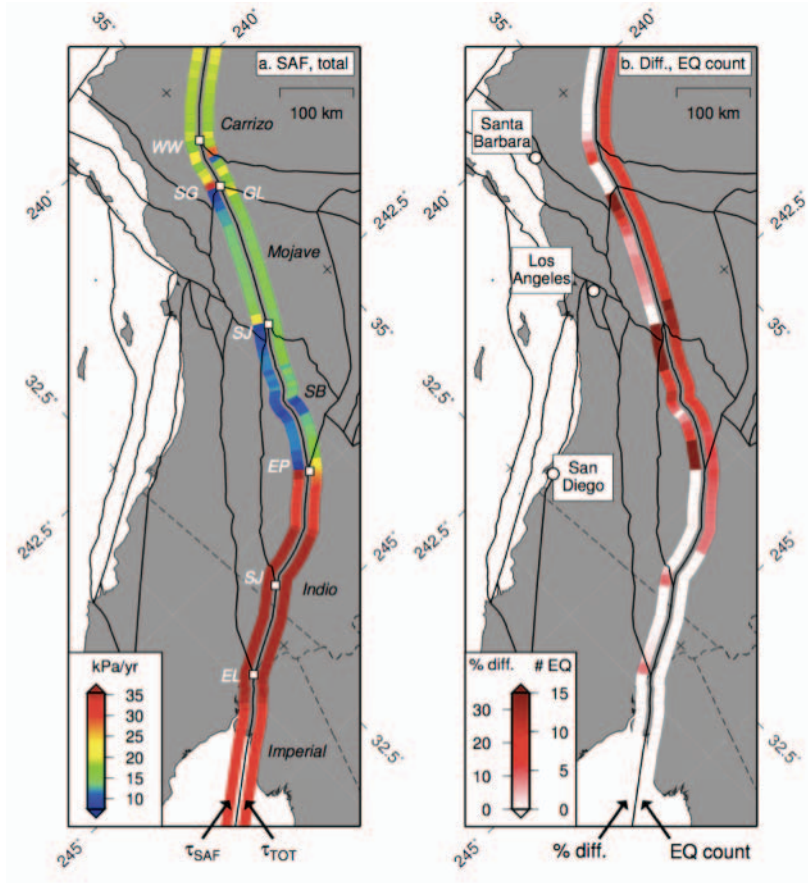

Figure 41. Modeled shear stress accumulation rates along the SAF (left panel), with and without contributions from activity on other faults (left and right color traces, respectively). The difference reaches values of up to 30% along the Mojave and San Bernardino segments of the SAF and is nearly zero to the north along the Carrizo segment and to the south along the Indio and Imperial segments, except near the isolated fault junctions. The enhanced stressing rate along the Big Bend segments demonstrates that interseismic activity on structures that intersect the SAF, including the San Gabriel, Garlock, North Frontal, and Eureka Peak faults, may act to increase the likelihood and/or frequency of seismic failure as compared to estimates based on the SAF shear alone. Interpretations of paleoseismic offset data suggest that Big Bend segments have ruptured in roughly twice the number of earthquakes as the more isolated Carrizo and Indio segments (Weldon et al., 2004), illustrating a correlation between long-term, macro-scale seismicity and interseismic stress enhancement due to off-SAF processes (right panel). From Brendan Meade.

Long-term deformation with large strains and plastic deformation

Regional Scale Models

Benjamin Hooks (UT Martin) and Bridget Smith-Konter (UT El Paso) are developing regional-scale numerical models of long-term deformation associated with the SAF system and its surroundings.They use FLAC, a 3-D dynamic numerical model (e.g. Cundall and Board, 1988) to reproduce the first-order vertical deformation associated with the Southern San Andreas Fault

System (from the SCEC Geological Vertical Motion Map). Their models are driven by applied basal forces, and they incorporate layered viscoelasticity and realistic geometries to model the deformation of the SAFS over the past million years (a schematic is shown on Figure 42). The crust is either treated as fault-bounded elastic blocks, or as an elastic-plastic continuum, in which faults are allowed to develop in response to imposed velocities at the edges of the model (so far, the former approach works best). Comparisons show horizontal strain rates and long-term uplift rates that are broadly consistent with observations (Figure 43). The models developed to date are a preliminary step towards a more complete model of the long-term development of the western North American plate boundary over the last 10 Ma.

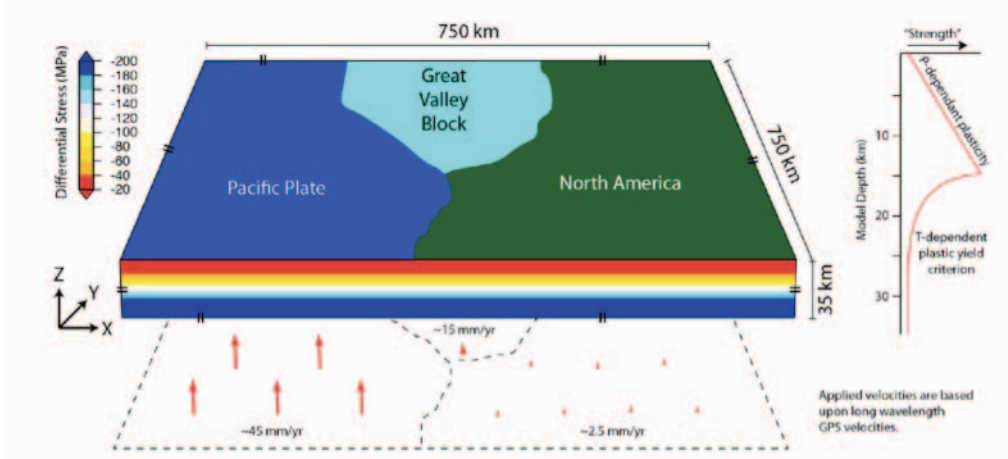

Figure 42. Schematic showing the geometry, applied basal kinematic driving force, rheological stratification, and boundary conditions for Benjamin Hooks' regional-scale, long-term deformation model. The model encompasses an area of 750 km by 750 km centered on southern California. A relative velocity of 45 mm/yr across the model is assumed. The model incorporates a pressure-dependent upper crust rheology (coefficient of friction angle of = 35° with strain-softening conditions), and a plastic-yield lower crust rheology (based upon published flow laws, e.g. Mackwell et al., 1998). From Benjamin Hooks.

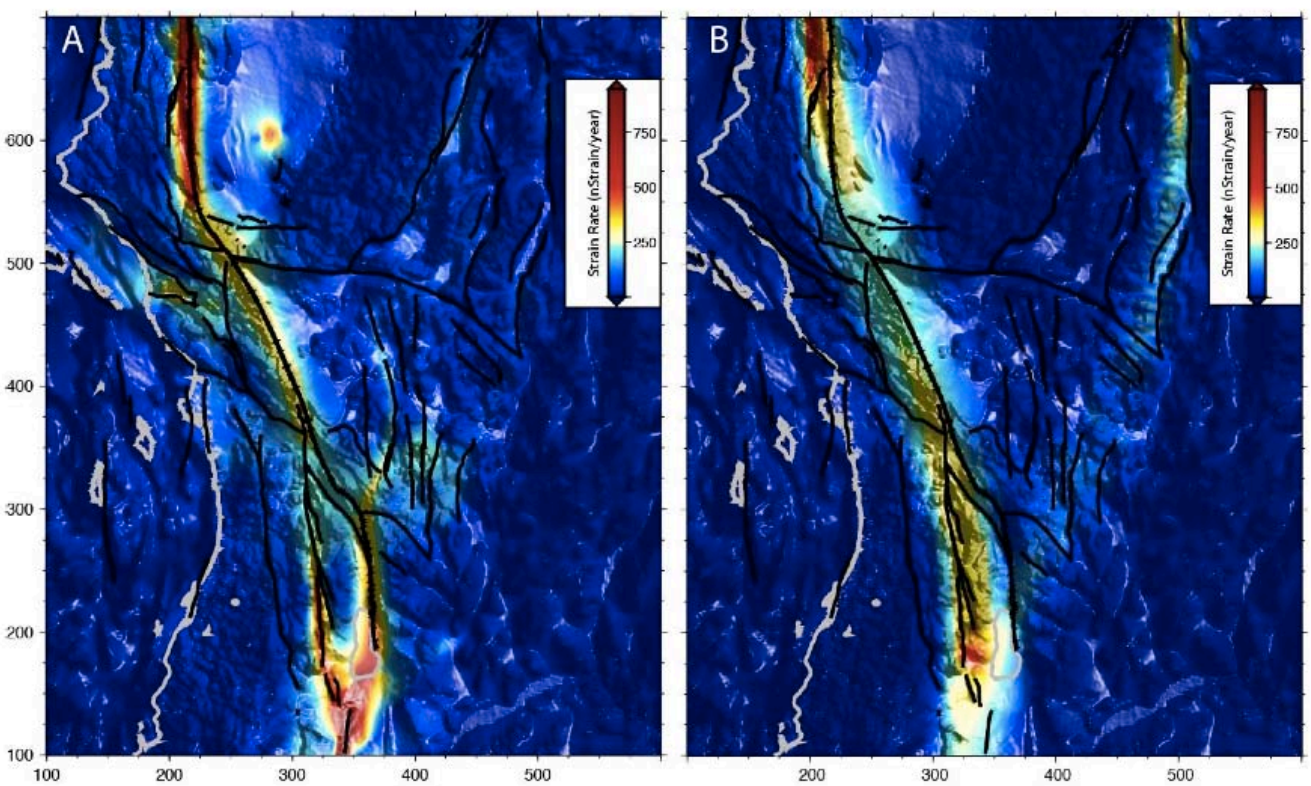

Figure 43. Color contour plots of A) semi-analytical (Smith-Konter and Sandwell, 2009) and B) dynamically modeled strain rate (nanoStrain/yr) of the San Andreas Fault System. Color scale is saturated at 500 nanoStrain/yr. Black lines indicate the location of major faults for spatial reference. Coastlines are shown in white. From Benjamin Hooks.

Local-Scale Models

CDM group researchers are also developing highly focused numerical models of long term deformation and fault system development, taking into account plastic deformation and damage generation. In his research project, which straddles the FARM and CDM research areas, Benchuan Duan (TAMU) models plasticity evolution due to earthquake shaking. He neatly illustrates how this results in a component of coseismic strain in nearby fault damage zones which is consistent with the background stress, rather than the coseismic stress change (Figure 44; Duan et al., 2011). Together with earlier SCEC-funded work (Hearn and Fialko, 2009), this work highlights the possibility that absolute stress levels in the upper crust might be inferred from the coseismic deformation of fault damage zones. Yuri Fialko and Yoshi Kaneko (Scripps) have also been looking into whether inelastic failure in the shallow crust due to dynamic earthquake rupture can explain the apparent deficit in shallow slip which is often noted in coseismic ruptures. They find that the amount of shallow slip deficit is indeed proportional to the amount of inelastic deformation near the Earth's surface. However, the largest magnitude of slip deficit in models accounting for off-fault yielding is 2-4 times smaller than that inferred from kinematic inversions of geodetic data (Kaneko and Fialko, 2011).

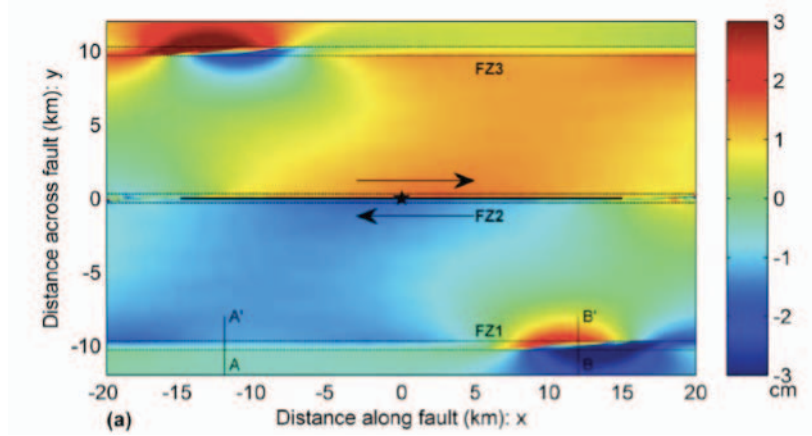

Figure 44. Fault-parallel component of the residual displacement field after an earthquake on the fault (solid black line) within a low-velocity fault zone FZ2. Motion across FZ1 is retrograde along AA', while it is sympathetic along BB'. They correspond to elastic and inelastic response of FZ1 to the rupture, respectively. From Duan et al., 2011.

In addition to the aforementioned numerical studies, Michele Cooke (U M Amherst) is continuing her work with wet kaolin (clay) analogue models of fault system development, with the goal of understanding the complex geometry of the SAF system in the Big Bend region. Her models show how faults form and are abandoned at restraining bends under progressive (oblique) shear strain, and she makes the argument that the chronology of fault formation and abandonment (i.e. development of secondary faults at progressively increasing distances from the original SAF bend) is consistent with the geologic record.

Viscoelastic models of the earthquake cycle

Two CDM research groups (Brendan Meade at Harvard and Elizabeth Hearn at UBC) tackled the question of how fault slip rates inferred from classical elastic half-space dislocation models might be affected by viscoelastic earthquake cycle effects, using earthquake-cycle models. To evaluate the magnitude of the viscoelastic deformation effects, both groups used forward models of two-dimensional faults with Maxwell and other rheologies to model velocity profiles at different times in the interseismic interval. These profiles were inverted for slip rates on a buried dislocation in an elastic halfspace, providing an effective means of assessing the predicted range of variability in fault slip rate estimates due to an idealized rheological parameterization. Both groups have found that if earthquake cycle variability is assumed to take place entirely within the upper mantle as a result of stress relaxation, then certain Burgers rheologies can simultaneously explain the general agreement between geologic and geodetic

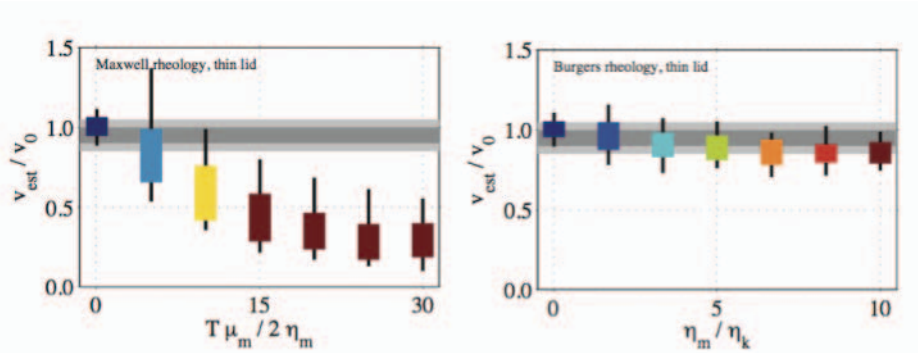

Figure 45. Predicted and observed variation in geologic/geodetic slip rate estimates as a function of upper mantle rheology. Left- and right-hand panels are Maxwell and Burgers rheologies, respectively. Hotter colors indicate larger postseismic deformation signals. Of the models considered here, only those to the far right hand side of the rightmost figure are consistent with both the general agreement of between geologic and geodetic slip rate estimates and the observed magnitude of postseismic deformation. From Brendan Meade.

slip rate estimates and large postseismic transients, while the widely used Maxwell models appear to be less applicable. Figure 45 (from Brendan Meade) is a compact illustration of these results: it clearly shows that inferred slip rates late in the interseismic interval are too low for models with a large savage parameter (long recurrence interval relative to the Maxwell time). Hearn and Vaghri note this same effect: early in the cycle, most of their Maxwell viscoelastic models produce velocity profiles that cannot be fit to elastic dislocation solutions; later, inferred slip rates are too small and locking depths too large to be even broadly consistent with typical observations (Vaghri and Hearn, 2011, Tables 1-3). Burgers rheology models with a large evolution in effective viscosity following a stress step can explain both a large transient and stationary and localized interseismic deformation.

The UBC group has also investigated the effect of a contrast in viscosity structure on earthquake-cycle deformation across a strike-slip fault (Vaghri and Hearn, 2011). This was motivated by the fact that though elasticity variations for different rock types under similar ambient conditions are generally modest, effective viscosity of the crust and mantle may vary over orders of magnitude. They found that asymmetric surface deformation is greatest for large contrasts in plate thickness (or in viscosity structure) across the fault, and for low viscosities. However, these models produce time-varying and broadly distributed interseismic deformation, inconsistent with observations from faults such as the SAF. Not only that, but the sense of asymmetry in the velocity profiles (relative to a point on the fault) reverses partway through the cycle (Figure 46). Models that could produce localized interseismic deformation around the fault (i.e., those with high substrate viscosities) produced only very modestly asymmetric interseismic surface deformation. Lateral contrasts in viscosity or effective plate thickness cannot produce observed, dramatic asymmetries in GPS surface velocity profiles across some major strike-slip faults. Large apparent contrasts are more likely due to small offsets between the mapped fault trace and the fault's creeping extension at depth. Deviations from a vertical fault geometry need not be great to produce this effect, and could easily be missed by conventional geophysical studies (e.g. seismic profiles or hypocenter locations). This finding is of obvious importance to inferring slip rates from block models in areas with many closely-spaced faults.

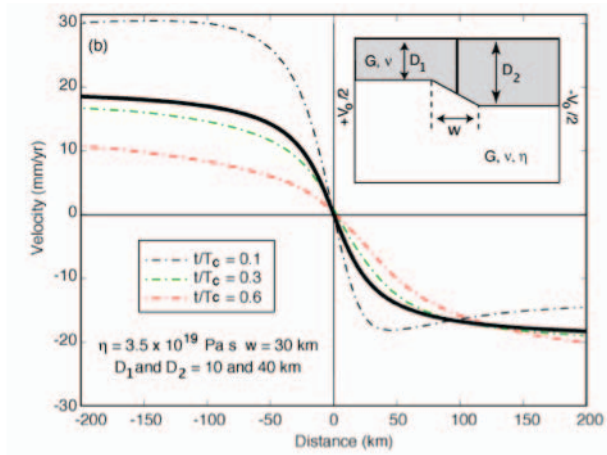

Figure 46. Velocity profiles at different times in the interseismic interval, from an earthquake-cycle model with a plate-thickness contrast across a vertical strike-slip fault. Velocities are plotted relative to a point on the fault trace. Note the reversal in the sense of velocity profile asymmetry with time. The heavy line shows a velocity profile due to a dislocation creeping at the a rate of Vo (40 mm/yr) below a depth of 17.5 km (D for this suite of asymmetric models). t is time since the last major earthquake and Tc is the recurrence interval. From Vaghri and Hearn, 2011.

References

Cundall, P. A., and J. Board (1988) A microcomputer program for modeling large-strain plasticity problems, in Swododa, C., editor, Numerical Methods in Geomechanics, Proceedings 6th International Conference on Numerical Methods in Geomechanics, Innsbruck, Austria, April 11– 15: Rotterdam, Balkema, p. 2101–2108.

Duan, B., J. Kang and Y. Li (2011) Inelastic response of compliant fault zones to nearby earthquakes, J. Geophys. Res., 116, B03307, 22 PP., 2011 doi:10.1029/2010JB007826.

Field, E. H., et al. (2008), The Uniform California Earthquake Rupture Forecast, Version 2 (UCERF 2), , USGS Open File Report 2007-1437.

Hearn, E. H. and Y. Fialko (2009) Can compliant fault zones be used to measure absolute stresses in the upper crust?, J. Geophys. Res.,114, B04403, doi:10.1029/2008JB005901.

Hearn, E., K. Johnson and W. Thatcher (2010) Space geodetic data improve seismic hazard assessment in California, EOS Trans. Am. Geophys. Union, 91, 336.

Kaneko, Y. and Y. Fialko (2011) Shallow slip deficit due to large strike-slip earthquakes in dynamic rupture simulations with elasto-plastic response, Geophys. J. Int., submitted.

Mackwell, S.J., M.E. Zimmerman, and D.E. Kohlstedt (1998) High temperature deformation of dry diabase with application to tectonics on Venus, J. Geophys. Res., v. 103, pp. 975– 984.

Okada, Y. (1992) Internal deformation due to shear and tensile faults in a half-space, BSSA, 82, 1018-1040.

Smith-Konter, B., and D. T. Sandwell (2009), Stress evolution of the San Andreas Fault System: recurrence interval versus locking depth, Geophys. Res. Lett., 36, doi:10.1029/2009GL037235.

Vaghri, A. and E. Hearn (2011) Can lateral viscosity contrasts explain asymmetric interseismic deformation around strike-slip faults?, Bull. Seis. Soc. Am., MS D-10-00347, in press.

Yikilmaz, B., D. L. Turcotte, G. Yakovlev, J. B. Rundle, and L. H. Kellogg (2010), Virtual California earthquake simulations: Simple models and their application to an observed sequence of earthquakes, Geophys. J. Int., 180(2), 734-742.

Weldon, R., K. Scharer, T. Fumal and G. Biasi (2004), Wrightwood and the earthquake cycle: What a long recurrence record tells us about how faults work, GSA Today, 14(9), 10.1130/1052-5173.

Lithospheric Architecture and Dynamics

Section CLM Tomography

3D P S Vp/Vs Tomography Using Body and Surface Waves

Gene Humphreys' group have performed Body Surface wave inversions of the 3D P and S wave structure of the western US (Figure 47) and confirm the presence of the now-well known high-velocity deep anomalies: the Isabella anomaly, the Transverse Ranges, and the Escalante anomaly. Inversions using Rayleigh waves tend to place the anomaly depths shallower than those based on body waves. However the lateral positions are generally consistent.

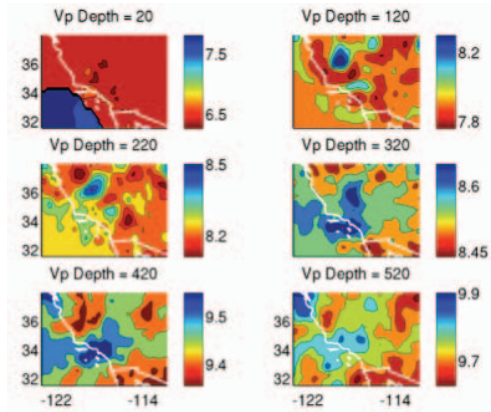

Figure 47. California Lithosphere Model (CLM) tomography.

California Lithosphere Model

The California Lithospheric Model CLM is a working ascii file model of crustal, mantle lithosphere and asthenospheric velocities including anisotropy (Figure 47). It can be downloaded from *http://quake.ess.ucla.edu/CLM*. For the crust it uses the Harvard SCEC Velocity model, whereas in deeper regions it uses the tomographic results from Schmandt and Humphreys (2010). The anisotropy model has been determined from the surface wave studies of Lin et al., (2011), Prindle and Tanimoto (2006), Alvizuri and Tanimoto (2011) and the SKS splitting results of Kosarian et al., (2011).

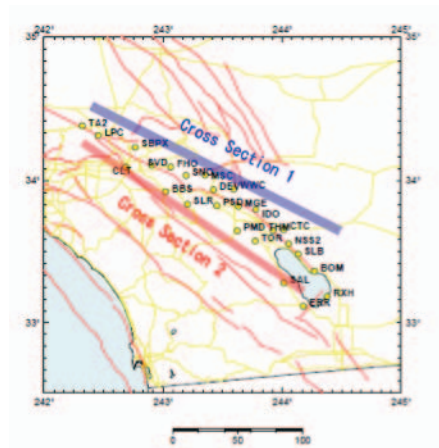

Figure 48. Map of cross-sections.

Fault Related Lithospheric Offsets

Search for Fault-Related Moho Offsets

After the discovery of Moho offsets by Yan and Clayton (2007a,b) at TA2 (station Table Mountain) receiver functions have been analyzed as a function of azimuth for stations along the major California faults (Clayton 2011). This has included all available data from new stations installed along the southern San Andreas Fault (SAF). While azimuthal variation is seen in the data, whether is it is due to offset, dip or anisotropy is difficult to determine. If due to offset, the amount of offset is less than observed at TA2 and Moho depth appears to deepen to the East and to decrease southwards towards the Salton Sea (Figure 48 and Figure 49). The receiver function tau-X stacking method developed by Helffrich and Thompson, (2010) is used to determine Vp/Vs ratio and Moho depth, but owing to the azimuthal complexity of the multiples that go into the stack, the method appears to work on limited azimuthal ranges only. Using S-receiver functions Meghan Miller's group have identified a step in the lithosphere-asthenosphere boundary near the San Jacinto fault (Figure 50 and Figure 51) at a

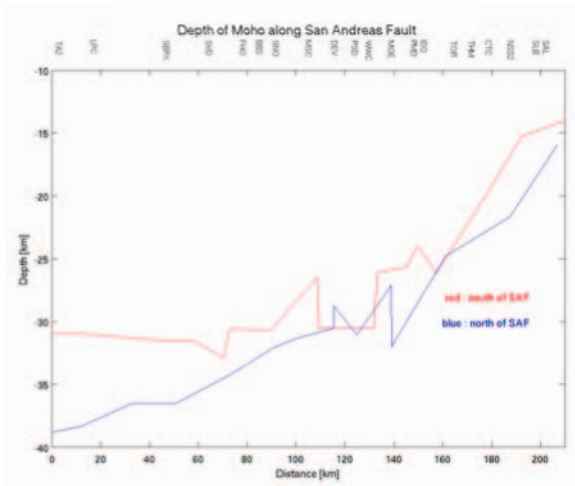

Figure 49. Moho Offsets from Receiver Functions.

depth of about 70 km (Miller 2011), adding evidence to the notion that the faulting is localized from the surface expression through the lithosphere.

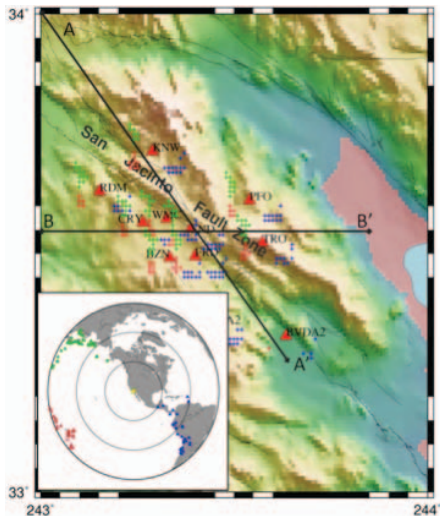

Figure 50. Map of sections where receiver functions are calculated.

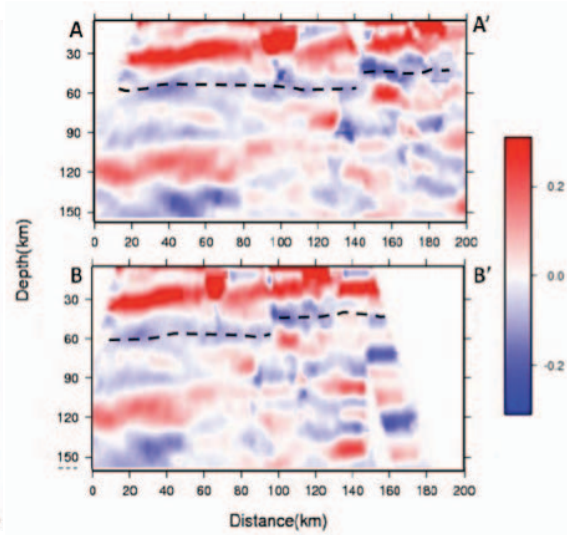

Figure 51. Inferred offset of lithosphere beneath the San Jacinto fault from receiver functions.

Lithospheric Scatttering

Role of Seismic Scattering and the Development of Coda

Seismic scattering has been analyzed at CI stations with a view to examining how lithospheric structure contributes to coda (Davis and Zeng 2011). A full-space scattering model developed by Hoshiba (1991) has been applied to coda from stations from the CI network and compared with results from the half-space layer model developed by Yoshimoto (2000). A comparison has been made between data from Peru, Mexico and California to assess the role of earthquake depth and lithospheric structure on inferred properties such as scattering, albedo, and mean free path. The methods seek to separate scattering from intrinsic attenuation (Figure 52 and Figure 53). Intrinsic attenuation (Figure 53) is significantly less-frequency dependent than scattering attenuation (Figure 52) and may even be frequency-independent. Scattering parameters at each station can be used to predict the stochastic part of coda.

Anisotropy

Anisotropy from Mantle Flow Appears Decoupled from Lithospheric Deformation

The CLM contains estimates of S wave anisotropy to a depth of 635 km derived from (1) radial anisotropy in the mantle and crust from surface wave studies (Moschetti et al., 2010) (2) azimuthal anisotropy in the crust and lithosphere from noise correlation and surface waves (Lin et al., 2011) and (3) Interpolated SKS estimates in the asthenosphere and lower (Kosarian et al., 2011). In general SKS directions are parallel to absolute plate motion directions.

Lithospheric azimuthal anisotropy is shown in Figure 54 along withe SKS splitting. The two disagree in both direction and amplitude with SKS anisotropy several times larger suggesting splitting originates deeper. The surface wave anisotropy directions west of the SAF are parallel to the SAF. This suggests that transpression that has given rise to the San Gabriel Mts in the big bend region has generated anisotropy in the mantle lithosphere, but deeper down, absolute plate motion aligns olivines in the asthenosphere. Figure 55 shows CLM asthenospheric azimuthal anisotropy that has been extrapolated from the SKS data. Figure 56 (Zandt 2011) is a map of the southwestern US showing lower crust anisotropy orientations calculated using receiver functions. Black lines are anisotropy orientations, and red lines are quaternary fault locations. Blues lines are SKS measurements compiled in Zandt and Humphreys (2008). Rose diagram shows anisotropy azimuths for stations in southern California. The length of the lines are related to the plunge of the fast axis. These data are not yet in the CLM.

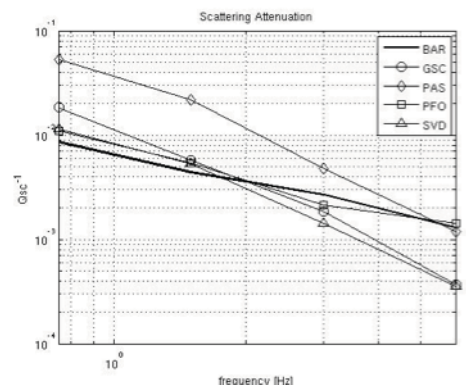

Figure 52. Scattering attenuation from coda

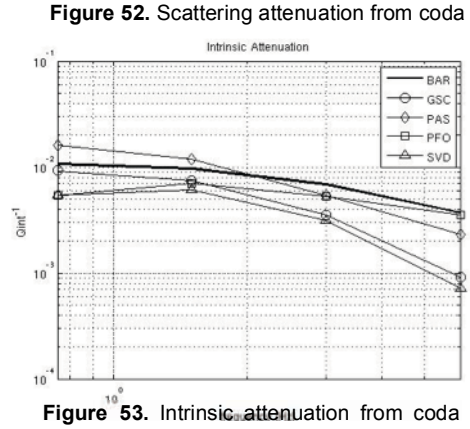

Figure 53. Intrinsic attenuation from coda showing less dependence on frequency than scattering Q.

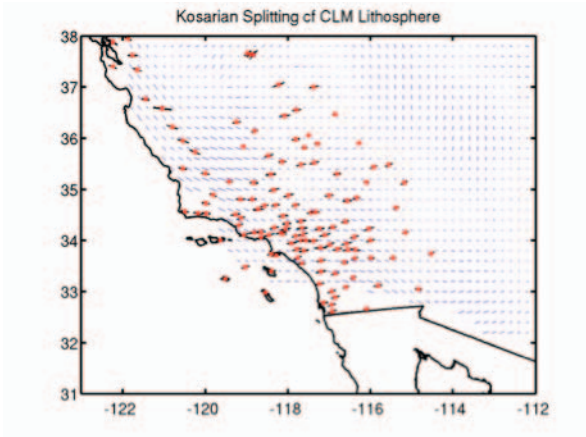

Figure 54. CLM splitting from mantle lithosphere compared with observations showing splitting signal arises from deeper than 100 km.

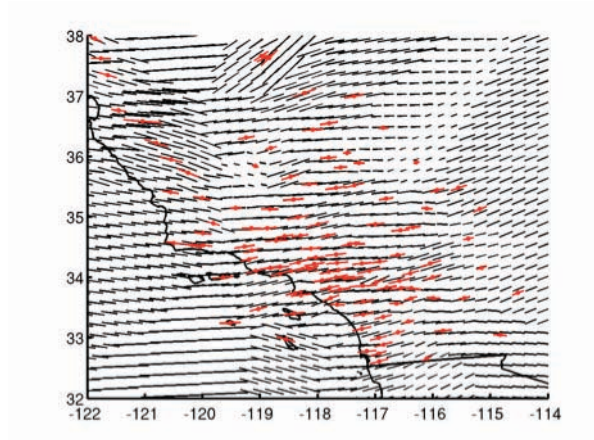

Figure 55. CLM splitting from mantle asthenosphere Z>100 km compared with observations.

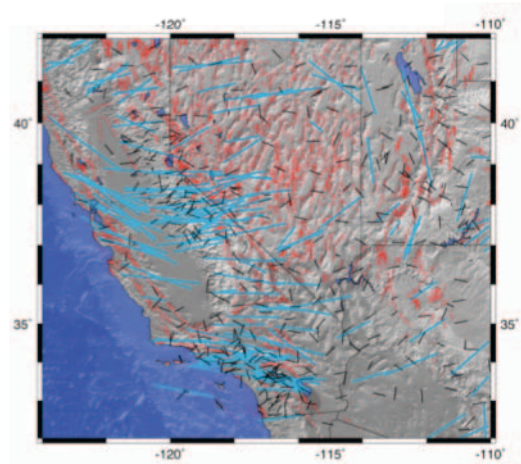

Figure 56. Plunge of anisotroic slow axes in lower crust from receiver function anisotropy (Zandt 2011).

Salton Seismic Imaging Project

The LAD group participated in both the active and passive parts of the Salton Seismic Imaging Project (SSIP) (Figure 57). Fuis et al (2011 AGU abstract) describes the project: Seismic data were acquired from 2 to 18 March 2011. One hundred and twenty-six borehole explosions (10-1400 kg yield) were detonated along seven profiles in the Salton Trough region, extending from area of Palm Springs, California, to the southwestern tip of Arizona. Airguns (1500 and 3500 cc) were fired along two profiles in the Salton Sea and at points in a 2-D array in the southern Salton Sea. Approximately 2800 seismometers were deployed at over 4200 locations throughout the Salton Trough region, and 48 ocean-bottom seismometers were deployed at 78 locations beneath the Salton Sea. Many of the onshore explosions were energetic enough to be recorded and located by the Southern California Seismograph Network. A line of passive broadband stations will run for a year.

References

Alvizuri, C., and T. Tanimoto, (2011), Azimuthal anisotropy from array analysis of Rayleigh waves in Southern California, Geophys. J. Int. (2011) 186, 1135–1151.

Clayton, R., (2011), Adding the Moho and Anisotropy to the SCEC Community Velocity Model via the CLM, SCEC Annual Report 2010.

Davis, P.M. and Y. Zeng, (2011), The dependence of coda on anisotropic scattering and intrinsic attenuation, SCEC 2010 Annual Report.

Helffrich, G., Thompson (2010), D. A stacking approach to estimate Vp/Vs from receiver functions. Geophys. J. Int., v. 181, 899-902.

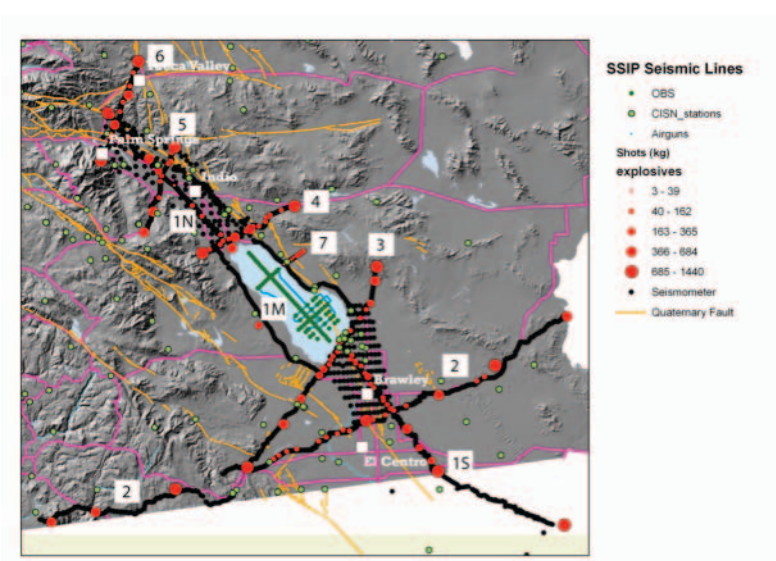

Figure 57. Salton Seismic Imaging Project SSIP March 2011.

Kosarian, M., P. Davis, T. Tanimoto, and R. Clayton (2011), The relationship between upper mantle anisotropic structures beneath California, transpression and absolute plate motions, J. Geophys. Res., doi:10.1029/2010JB007742.

Lin, F., Michael H. Ritzwoller, Yingjie Yang, Morgan P. Moschetti & Matthew J. Fouch, (2011), Complex and variable crustal and uppermost mantle seismic anisotropy in the western United States, Nature Geoscience 4, 55–61 (2011) doi:10.1038/ngeo1036.

Miller, M.,(2011) Systematic mapping of the Moho beneath southern California: Towards an understanding of crustal architecture and strain localization, SCEC Annual Report, 2010.

Moschetti, M.P., M.H. Ritzwoller, F. Lin and Y. Yang, (2010) Seismic Evidence for widespread western-US deep-crustal deformation caused by extension, Nature, 464,8 April 2010, 885-889.

Prindle, K., and T. Tanimoto (2006), Teleseismic surface wave study for S-wave velocity structure under an array: Southern California, Geophys. J. Int., 166(2), 601-621.

Schmandt, B., and E. Humphreys (2010), Seismic heterogeneity and small-scale convection in the southern California upper mantle, Geochem. Geophys. Geosyst., 11, Q05004, doi:10.1029/2010GC003042.

Yoshimoto K. (2000). Monte Carlo simulation of seismogram envelopes in scattering media. J. Geophys. Res 105, no. B3, 6153-6161.

Zandt, G., (2011), Lithospheric Anisotropy in Southern California From Receiver Functions: Identification of the Decoupling Zone. SCEC Annual Report 2010.

Zeng, Y., F. Su, and K. Aki, (1991),Scattering wave energy propagation in a medium with randomly distributed isotropic scatterers, I, Theory, J. Geophys. Res., 96, 607-619.

Zeng,Y., and Y. Jing, (2009), A new interpretation on the scattering origin of seismic coda, SCEC 2009 Annual Meeting, Proceedings and Abstracts, XIX, 238.

Earthquake Forecasting and Predictability

The Earthquake Forecasting and Predictability (EFP) focus group coordinates four types of research projects: (1) the development of earthquake forecasting methods to the point that they can be moved to testing within the framework of the Collaboratory for the Study of Earthquake Predictability (CSEP), (2) the development of testing methodologies for evaluating the performance of earthquake forecasts, (3) studies that aim to obtain fundamental knowledge of earthquake behavior that may be relevant for forecasting earthquakes, and (4) the development and use of earthquake simulators to understand predictability in complex fault networks.

Earthquake Forecasts

The largest earthquakes on mid-ocean ridge transform faults occur very regularly, and published prospective forecasts of the time of the next event on transform fault segments have been quite successful so far (e.g. McGuire, 2008; Figure 58). These forecasts appear to be the most successful time-dependent earthquake forecasts currently being made, aside from aftershock rate models. Boettcher et al. ("CSEP Testing of Seismic Cycles and Earthquake Predictability on Three Mid-Ocean Ridge Transform Faults") moved the testing of these forecasts from informal forecasts in published papers to the more formal testing framework of CSEP. They developed simple renewal models for five mid-ocean ridge transform fault segments for testing in CSEP. The targeted transform faults have short recurrence times, from 5 to 20 years, and four of the segments are expected to produce an earthquake within the next 5 years. Very narrow recurrence distributions, with coefficients of variation from 0.05 to 0.2, are being used. The combination of the short recurrence times and the narrow forecasts

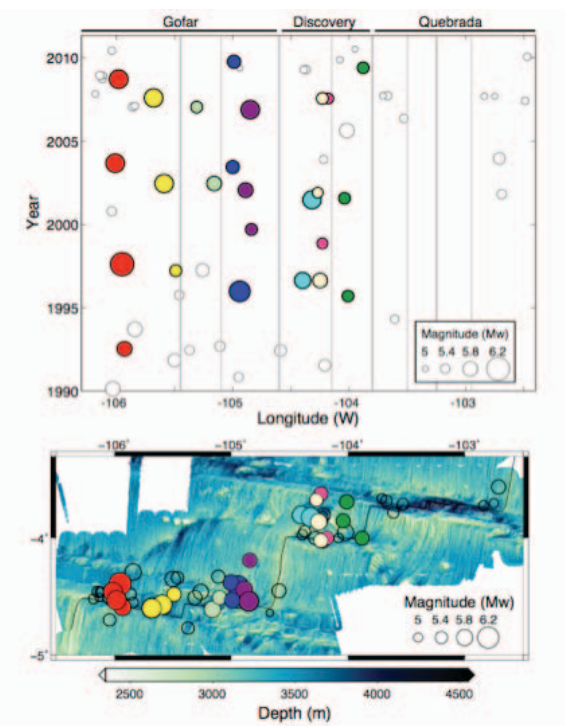

Figure 58. Global CMT catalog events that occurred on Quebrada, Discovery, and Gofar transform faults for the time period from 1/1990 to 4/2010. Earthquakes are plotted at their CMT estimated longitude in the upper panel and both latitude and longitude in

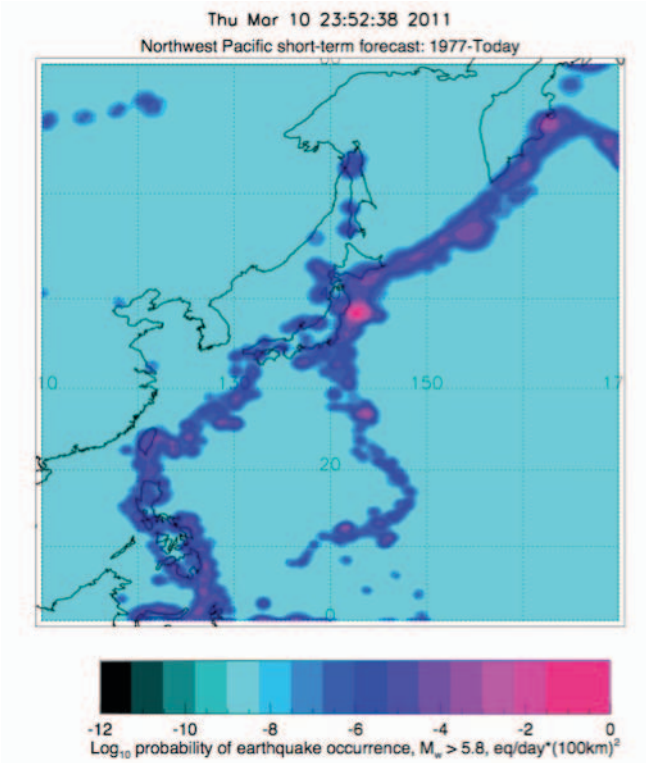

Figure 59. The short-term rates after 2011/03/09 MW7.5 foreshock and before the MW9.1 Tohoku event – at the foreshock epicenter the short-term rates are about 100 times higher than the long-term rates. From annual report of Kagan.

windows mean that the CSEP tests should produce meaningful results in a reasonable time frame. Kagan ("Testing Global Long-Term Earthquake Forecasts") produced an improved global earthquake forecast that is updated daily. This model is based on smoothed seismicity, and includes focal mechanism forecasts. Because of the daily update of the model, it successfully forecast a high earthquake probability at the location and time of the 2011 M9.0 Tohoku, Japan, earthquake, based on the occurrence of the M7.5 foreshock two days earlier (Figure 59). This model is less successful for great earthquakes that were not preceded by foreshocks, such as the 2004 M9.3 Sumatra earthquake.

Testing Methodology

One of the concerns about CSEP, particularly for the regional testing areas such as California, is that the relatively low rate of earthquakes means that it could take a long time to accumulate enough events to meaningfully distinguish between models. Gerstenberger et al. ("How Long Will it Take to Obtain Meaningful Test Results (and Distinguish Models) in CSEP?") quantified how long it would take to distinguish between the 5-year RELM models for southern California, and find that it would take between 5 and 13 M≥4.95 earthquakes to distinguish between the spatial distributions of two models, depending on which two models are being compared, implying that a 5-year testing period is not enough. They also find that catalog variations between different 5-year (or longer) testing periods may lead to substantially different results. These are important considerations for interpreting the results of the RELM and CSEP tests.

Schoenberg et al. ("Evaluating and improving models for seismicity forecasting using modern residual analysis techniques") explored several residual analysis techniques, which are well-suited to exploring where and when an earthquake forecast model over- or under-predicts the observed earthquake rate. They found that some residual analysis techniques have more power than the existing CSEP tests. With the large number of earthquake forecasts that are being submitted to CSEP, it's important to be able to evaluate the relative strengths and weaknesses of each model. The current tests implemented in CSEP provide an assessment of the overall performance of each model, while the residual analysis techniques could give the developers more detailed feedback on how the next generation of their models could be improved.

Additionally, SCEC supported travel for international participants in CSEP to attend SCEC and CSEP activities, collaborate with SCEC scientists, and work on CSEP development in collaboration with the Southern California CSEP testing center. SCEC supported travel for Gerstenberger and Rhoades of the New Zealand CSEP testing center ("CSEP Forecast Test Methodology: Development and Participation") and Werner et al. of the European CSEP testing center in Switzerland ("Travel Funds for CSEP Integration and Development").

Observational Constraints

Earthquake forecasts, particularly frequently-updated time-dependent forecasts, could be improved through a better understanding of what triggers earthquakes. Bürgmann et al. ("Static vs. Dynamic Triggering of Earthquakes and Tremor at Parkfield") found that repeating earthquakes at Parkfield tend to be preceded, at higher rates that expected, by up to several days by earthquake that transfer >1 kPa of static stress. Immediate triggering, within a few seconds to minutes, can happen when the separation distance is within a few km. Short-term triggering only occurs when the triggered repeating event is already late in its recurrence cycle, so the regularity of the repeating events is not substantially impacted. Dahmen and Ben-Zion ("Earthquake nucleation mechanisms and damage healing in heterogeneous fault zones") studied earthquake triggering

by periodic loading, such as tidal stresses or seasonal stress loads. They find a theoretical frequency-dependent threshold amplitude for triggering, which agrees with lab experiments. While the over-all behavior of aftershocks sequences is generally predictable, the behavior of swarms is not. Shearer ("Analysis of Triggering Models and Earthquake Stress Drops in Southern California") studied swarms in southern California, in particular identifying characteristic swarm migration rates that might be useful to distinguish between slow slip and fluid diffusion as triggering mechanisms. They also identify low stress drops in the Salton Sea area, where swarms are prevalent.

Earthquake Simulators

Earthquake simulators are numerical models aimed at generating catalogs of simulated earthquakes over a variety of spatial and temporal scales. The aim of these studies is to gain new insight into the behavior of real earthquakes by studying the behavior of simulated earthquakes. For example, one line of inquiry is to see if patterns of simulated seismicity in space and time occur that might also be discovered in real seismicity. If so, forecasting future earthquakes might be done by recognizing ongoing patterns in past and current seismicity.

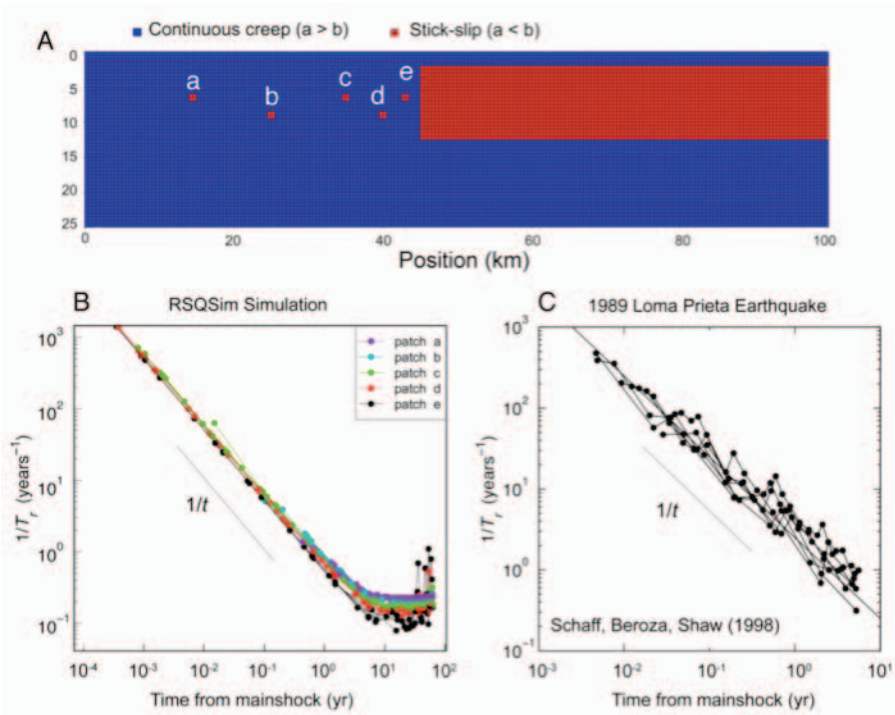

Figure 60. Simulation of earthquake repeaters. (A) Model of fault with repeating earthquakes on small patches (red) that are surrounded by fault sections that creep (blue). Fault creep drives recurring slip on the repeater patches a-e. Hence, accelerated afterslip, which decays with the logarithm of time following mainshocks on the large seismogenic patch in the right half of the model, result in accelerated rates of earthquakes on repeater patches. (B) Rates of occurrence of earthquakes on the repeater patches (as the reciprocal of recurrence time) on the patches following mainshocks on the large patch. (C) Rates of occurrence on repeaters following the 1989 Loma Prieta Earthquake from Schaff and others (1998). From annual report of Richards-Dinger.

The Earthquake Simulator Comparison Project (Tullis and Ward, "A Collaborative Project: Comparison and Validation of Earthquake Simulators") has recently focused on comparing the results of different simulators for two problems: (1) a single fault with different strength on its two halves, with different strength ratios producing different modes of behavior, and (2) two faults that are offset, with the goal of studying under what conditions a rupture can jump the gap, a problem that has previously been analyzed with dynamic rupture models, while none of the simulators include fully dynamic ruptures. The collaboration has also developed a fault model for all of California to be used in simulations, and standardized input/output formats, to ease comparison between different simulators.

Additional progress has been made on individual simulators. Richards-Dinger ("Application of a Physics-Based Earthquake Simulator to Southern California") added creeping faults to the rate-and-state friction-based simulator RSQSim, and modeled repeating earthquakes as stick-slip patches embedded in a creeping fault (Figure 60). Ward ("ALLCAL – An Earthquake Simulator for All of California","Geodetic Inputs to Seismic Hazard Estimation") is working to incorporate geodetic data into the simulator ALLCAL.

Workshops

The "Workshop on Earthquake Simulators, Number 4" was held in July 2010 (Tullis "2010 Earthquake Simulators Workshop Report"). At this workshop, participants compared the results of their simulators for two benchmark problems outlined at the previous workshop (a single fault with different strength on its two halves, and a simplified version of the northern California fault network), and discussed future benchmark tests and standardized input/output formats.

A "Workshop on Satellite Observations and Earthquake Predictability" was held in July 2011. This workshop brought together two separate communities that are active in attempting to understand how and whether it is possible to predict earthquakes. One is a group of space scientists involved in making satellite-based observations of anomalous electromagnetic and thermal signals that may be associated with earthquakes. The other consists of earthquake scientists involved in making seismological and geodetic observations, many of whom are involved with SCEC. These communities have had insufficient communication or collaboration, and bringing them together may help each understand better each other's data and perspectives.

References

McGuire, J. J. (2008), Seismic Cycles and Earthquake Predictability on East Pacific Rise Transform Faults, Bull. Seis. Soc. Am., 98(3), 1067-1084, doi: 10.1785/0120070154.

Ground-Motion Prediction

The primary goal of the Ground-Motion Prediction focus group is to develop and implement physics-based simulation methodologies that can predict earthquake strong-motion waveforms over the frequency range 0-10 Hz. At frequencies less than 1 Hz, the methodologies deterministically predict the amplitude, phase and waveform of earthquake ground motions using fully three-dimensional representations of Earth structure, as well as dynamic or dynamically compatible kinematic representations of fault rupture. At higher frequencies (1-10 Hz), the methodologies predict the main character of the amplitude, phase and waveform of the motions using a combination of deterministic and stochastic representations of fault rupture and wave propagation.

Rupture characterization plays a vital role in ground-motion prediction and significant progress has been made in the development of more realistic implementations of dynamic and dynamically compatible kinematic representations of fault rupture within ground-motion simulations. Verification (comparison against theoretical predictions) and validation (comparison against observations) of the simulation methodologies continues to be an important component of this focus group with the goal being to develop robust and transparent simulation capabilities that incorporate consistent and accurate representations of the earthquake source and three-dimensional velocity structure. The products of the Ground-Motion Prediction group are designed to have direct application to seismic hazard analysis, both in terms of characterizing expected ground motions in future

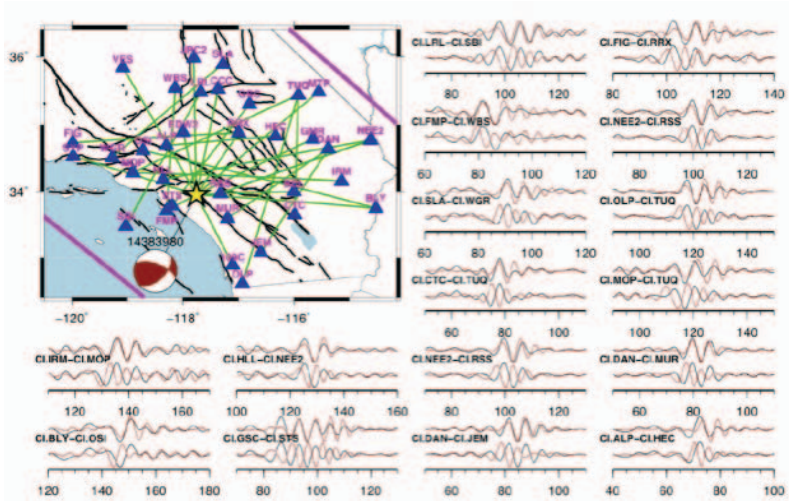

Figure 61. Examples of Green's functions derived from abient noise analysis (black) and synthetic ones from the SCEC CVM 4.0 (lower traces) and the model revised using full waveform tomography (CVM4SI2). The map shows the epicenter (start) and CMT solution (red beachball) of the Chino Hills earthquake and the inter-station paths (green lines) for the Green's functions.

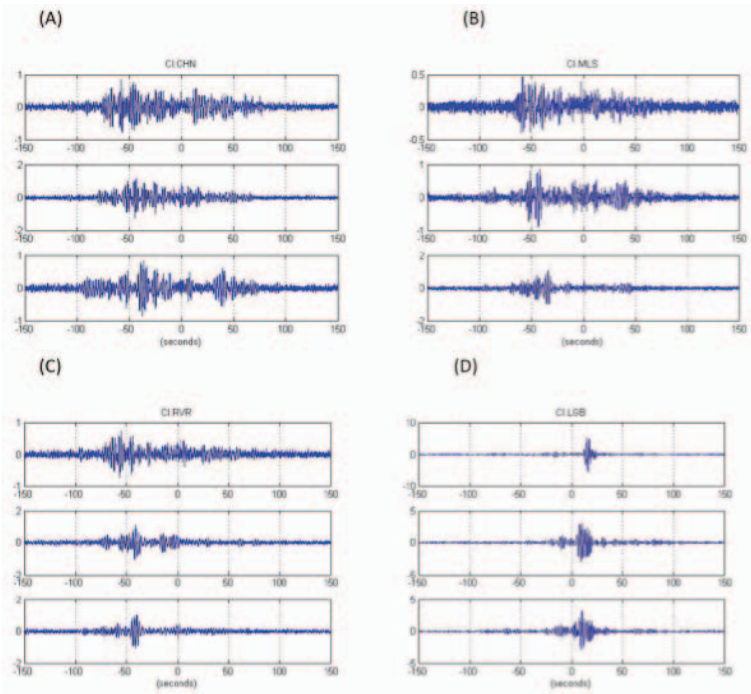

Figure 62. Three component (transverse: top, radial: middle, vertical: bottom) Green's functions for three paths within the waveguide (A-C) and one outside the waveguide (D). The Green's functions relatively impulsive for the path outside the waveguide, whereas the Green's functions contain long duration reverberations for paths within the waveguide, supporting its presence in the SCEC Community Velocity Model.

earthquakes, and in terms of directly interfacing with earthquake engineers in the analysis of built structures. Activities in these areas are highlighted by the projects described below.

Model Validation

Precariously Balanced Rocks

Recent activity in studying precariously balanced rocks has shifted towards quantifying the dates of the rocks in order to facilitate comparison with fault behavior. Grant-Ludwig et al. are using Be-10 dating techniques to constrain the ages of precariously balanced rocks at several locations along the San Andreas and San Jacinto faults. Analysis of one of the Grass Valley rocks in the western San Bernardino mountains, which lies near the intersection of the San Andreas and San Jacinto faults, supports the assessment by Bryant (1987) that the Cleghorn fault has not ruptured in the Holocene. Furthermore, Grant-Ludwig et al. hypothesize that the Grass Valley and other precariously balanced rocks near Silverwood Lake may indicate that ground motions have been relatively lower near the stepover between the San Andreas and San Jacinto faults near Cajon Pass as a result of earthquake ruptures jumping between these two faults. If corroborated with additional observations, these results would directly impact the development of earthquake rupture scenarios and forecasts for these two major faults as well as the corresponding ground motions.

Ambient Noise Analysis

Several SCEC researchers continue to exploit ambient noise analysis in validating SCEC Community Velocity Models as a complement to ground-motion recordings from earthquakes. Chen and Olsen demonstrated improvements made to the SCEC Community Velocity Model 4.0 via full waveform tomography analysis through comparison of synthetic Green's functions derived from the seismic velocity model and those from ambient noise observations (Figure 61). These results suggest that the revised seismic velocity model will yield more accurate travel times and shaking duration for sites throughout southern California. Hirakawa and Ma evaluated whether observations derived from ambient noise support the waveguide along a chain of sedimentary basins from San Bernardino to Los Angeles identified in the TeraShake simulations (Olsen et al., 2006). From four years of ambient seismic noise correlations for 50 station pairs, they generated 570 Green's functions separated into four frequency bands. Hirakawa and Ma found reverberations for Green's functions involving propagation paths across the basins, consistent with the waveguide (Figure 62). However, they caution that these Green's functions also contain noise, which must be reduced to reach a more definitive conclusion about the the presence or absence of the waveguide.

Nonlinear Site Response

Focus group activities have continued to include efforts to understand the physics involved in ground motion at high frequencies. Wu and Peng are applying a technique developed using Japanese KIK-Net data to determine the peak ground acceleration at which nonlinear site response becomes significant. In Japan they found that the threshold appears to be in the range of 60-100 gal with a logarithmic recovery in time. They hypothesize that smaller nonlinear responses below this threshold with near instantaneous recovery coincide with pre-existing levels of damage, where as the nonlinear responses above this threshold reflect development of further damage during strong shaking. Wu and Peng are currently applying this technique to the El Mayor-Cucapah earthquake sequence to determine if the threshold observed in the KIK-Net data applies to California as well. These results will have a direct impact on further development of the SCEC Broadband Platform, which relies on stochastic methods and nonlinear site corrections to produce broadband synthetic ground motions.

Ground-Motion Simulations

Broadband Simulations

As described in Section SPECIAL PROJECTS, Community Modeling Environment, the recently released Broadband Platform provides scientists with a suite of tools to compute broadband synthetic ground motions, including the effects of heterogeneous rupture propagation and nonlinear site effects. These capabilities continue to be refined as additional studies provide improved methodologies. Research activities within the last year have focused on nonlinear site response (as described earlier and in the next paragraph) and rupture model characterization.

Assimaki et al. developed Site 1D as a component of the Broadband Platform in order to provide a more realistic model of damping in the nonlinear response. Site 1D uses a viscoelastic formulation for frequency-independent Q with a hysteretic damping scheme. (Li and Assimaki, 2010). In addition to the implementation of the nonlinear site response, the code uses the peak ground acceleration on rock and a frequency index (FI, a dimensionless quantity that describes the alignment of the site

response peaks to the incident ground motion) to indicate the potential presence of nonlinear effects (Figure 63); this can be used to a priori determine whether nonlinear site response should be employed for a given synthetic ground-motion record. Archuleta et al. continue to refine their tools to construct earthquake rupture models for large scenario earthquakes. Their most recent work has focused on quantifying the autocorrelation of parameters in spontaneous rupture models in order to construct kinematic rupture models with the same properties. Using the autocorrelation of slip as a reference, they found (Figure 64) initial stress is less correlated than final slip, rise time correlates with slip, and rupture speed and peak slip time only weakly depend on the final slip. Additional analysis also revealed that only the most highly correlated stress fields produced supershear rupture and these same ruptures also produced the largest slip amplitudes and slip rates.

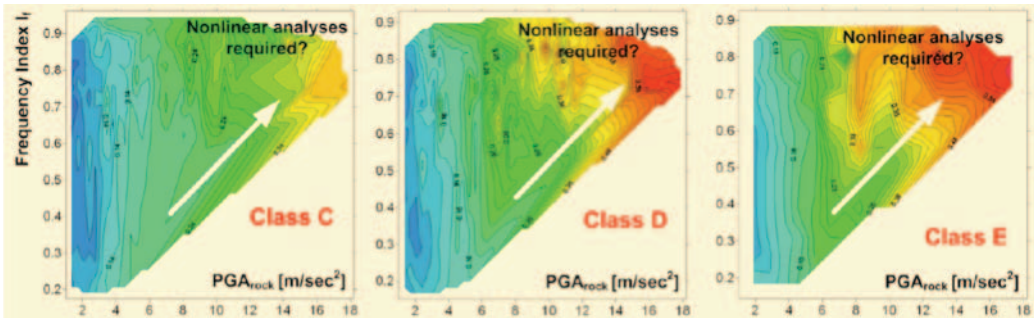

Figure 63. Deviation of linear elastic predictions from nonlinear site-specific response predictions at three sites (Class C: stiff soil, Class D: medium stiff soil, and Class E: soft soil) in the Los Angeles basin for a series of broadband ground-motion synthetics. Large values of the peak ground acceleration and values of the frequency index close to unity imply the empirical amplification factors do not adequately describe the site response, and siste-specific analyses should be used.

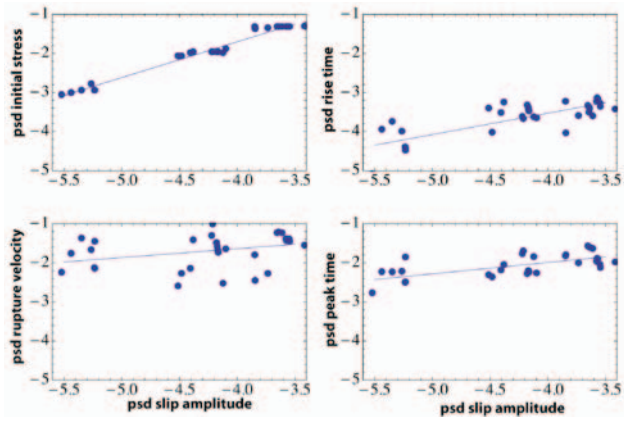

Figure 64. 2D power spectral decay (slope of the power spectrum) for initial stress, rise time, rupture velocity, and peak slip time as a function of the spectral decay for final slip. The power spectral decay for initial stress and rise time exhibit strong correlations with power spectral decay for final slip, whereas the spectral decay for rupture speed and peak slip time show much weaker correlations.

Large-Scale Simulations

The Mw 7.2 El Mayor-Cucapah earthquake generated shaking that was recorded by over 200 strong motion instruments throughout northern Baja California and southern California. This earthquake provides an important opportunity to test our ability to use scenario rupture models and the SCEC Community Velocity Models to generate synthetic ground motions consistent with those observed. Graves and Aagaard generated synthetic long-period (T > 2 s) ground motions using the methodology proposed by Graves and Pitarka (2010) and two seismic velocity models (CVM-4m and CVM-H62), as would be done for a scenario event. For the non-basin regions, simulations with the CVM-H62 model perform significantly better than those of CVM-4m, which we attribute to the inclusion of the Tape et al. (2009) tomographic updates within the background crustal velocity structure of CVM-H62 (Figure 65 and Figure 66). Within the greater Los Angeles basin, the CVM-4m model generally matches the level of observed motions whereas the CVM-H62 model over-predicts the motions in the southernmost portion of the basin. This over-prediction is created by the sharp impedance contrast along the southern margin of the Los Angeles basin in the CVM-H62 model. Overall, these results are encouraging and provide confidence in the predictive capabilities of the simulation methodology, while also suggesting some regions where the seismic velocity models may need

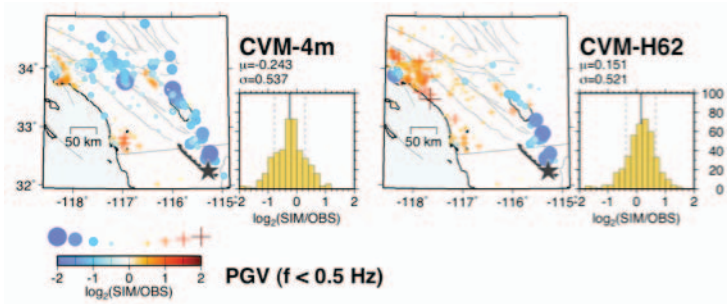

Figure 65. Residuals of simulated PGV for one rupture scenario using seismic velocity models CVM-4m (left column) and CVM-H62 (right column). Residuals are displayed as the base 2 logarithm of the ratio of the simulated-to-observed value computed for each recording site. The mean (μ) and standard deviation (σ) of the residuals are indicated above the histogram and are also shown by the solid and dashed lines, respectively.

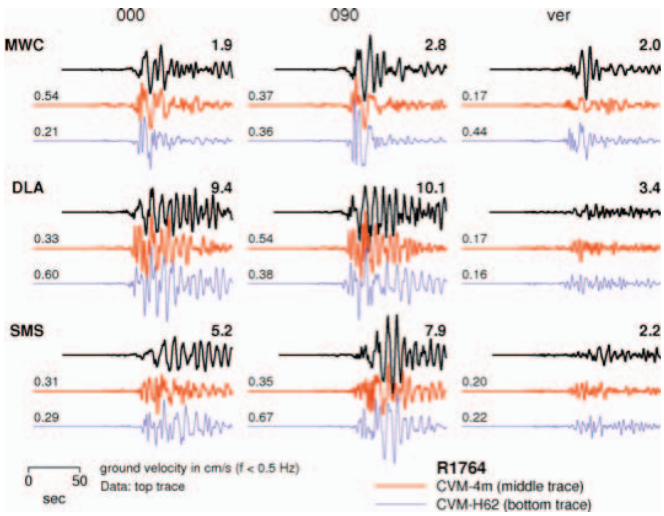

Figure 66. Comparison of observed and simulated three-component ground velocity waveforms for selected sites in the Los Angeles basin region for one rupture model (same scenario as in FIGURE_GMP5). All waveforms have been low-pass filtered at f < 0.5 Hz. For each site waveforms are scaled to the absolute maximum amplitude observed at that site; the peak amplitude (in cm/s) for each component (simulated or observed) is indicated at the top right of the observed trace, and the waveform correlation coefficient computed for the simulated and observed motion is at left edge of the synthetic traces.

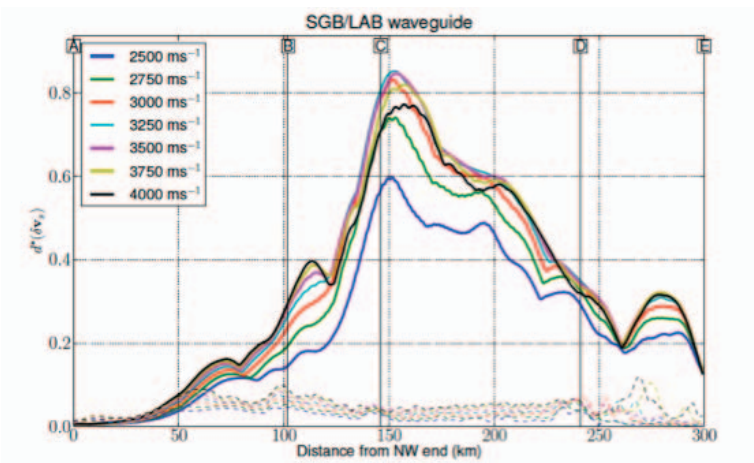

Figure 67. Los Angeles basin excitation sensitivity for slip perturbations to the ShakeOut rupture scenario that are parameterized by location (distance along SAF from NW to SE along the SAF) and rupture velocity. Curves are solid for rupture from SE to NW, dashed for rupture from NW to SE.

improvement. Simulations of earthquake rupture on the southern San Andreas fault (SAF) reveal large amplifications in the San Gabriel and Los Angeles basins (SGB and LAB) apparently associated with long-range path effects. Day et al. have developed a method for rapid calculation of the sensitivity of such predicted wave-field features to perturbations of the source kinematics, using a time-reversed (adjoint) wave-field simulation. The calculations are analogous to those done in adjoint tomography, and the same time-reversed calculation also yields path-sensitivity kernels that give further insight into the excitation mechanism. For rupture on the southernmost 300 km of SAF, LAB excitation is greatest for slip concentrated between the northern Coachella Valley and the Transverse Ranges, propagating to the NE, and with rupture velocities between 3250 and 3500 m/s along that fault segment (Figure 67 and Figure 68). That is within or slightly above the velocity range (between Rayleigh and S velocities) that is energetically precluded in the limit of a sharp rupture front, highlighting the potential value of imposing physical constraints (such as from spontaneous rupture models) on source parameterizations. LAB excitation is weak for rupture to the SW and for ruptures in either direction located north of the Transverse Ranges, while the Ventura Basin is preferentially excited by NE ruptures situated north of the Transverse Ranges. Olsen et al. have continued to analyze the results from the 0-2 Hz simulation of a Mw 8 San Andreas rupture (see also SPECIAL PROJECTS, Community Modeling Environment). The 3-D simulations include strong directivity, rupture complexity, and basin effects resulting in a much more complex spatial variation in shaking compared with empirical ground-motion prediction equations that estimate median levels of shaking across an ensemble of events (Figure 69). At rock sites (Vs30 > 1.0 km/s) the synthetic ground motions exhibit a similar decay in peak ground velocity with distance from the rupture as the Boore and Atkinson (2008) and Campbell and Bozorgnia (2008) ground-motion prediction equations (Vs30 = 760 m/s). In another study Olsen et al. have started examining the effects of including small-scale stochastic variations in elastic properties in seismic velocity models. Preliminary results indicate that weak fractal spatial variations can generate spatial variations in peak velocity (both amplification and de-amplification) by up to a factor of six. Figure 70 shows snapshots for a purely elastic (infinite Q), 0-2 Hz simulation of a horizontally incident SH plane wave propagating through a velocity structure containing fractal inhomogeneities having a Hurst exponent of 0 and a standard deviation of 10%. This structure is imposed on a background 1D velocity profile taken from the SCEC CVM-S4 for a typical Los Angeles basin site. Ongoing work will examine the tradeoff between scattering associated with this stochastic variation and intrinsic attenuation associated with anelastic attenuation.

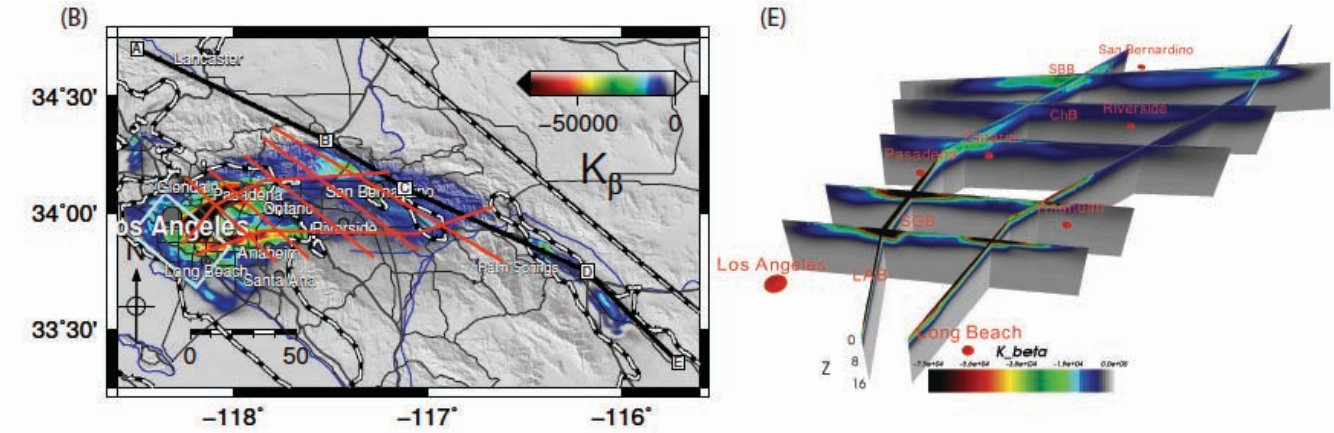

Figure 68. One-km horizontal depth slices (left) and cross-sections (right) of the path sensitivity kernel for S-wave speed in the Los Angeles basin region. Red lines in the left panel show the cross section locations for the corresponding fence diagrams in the right panel. Since these kernels are indices of the sensitivity of the LAB excitation to wave-speed perturbations, they illuminate the predominant pathways of seismic energy entering the basin in the reference scenario.

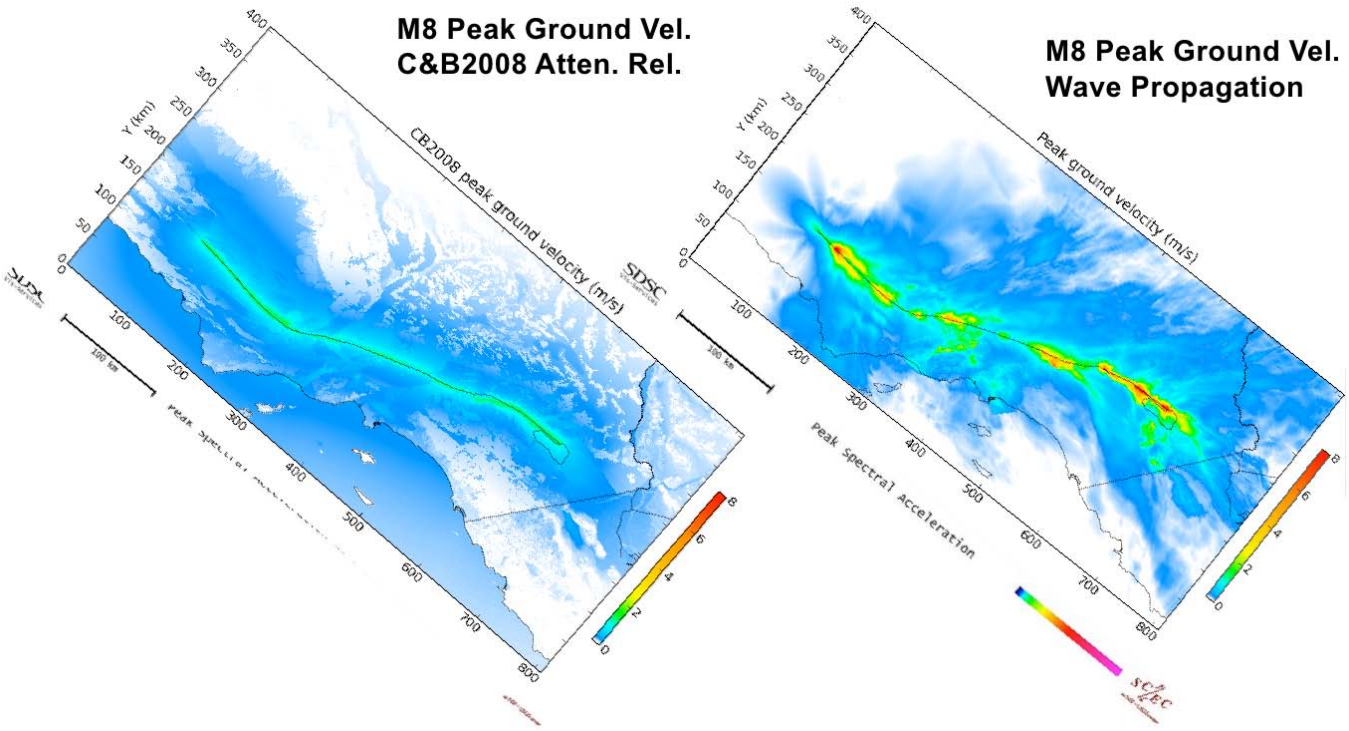

Figure 69. Peak ground velocity for the Mw 8 San Andreas simulation (right) and Campbell and Bozorgnia (2008) empirical ground-motion prediction equation (left). The simulation produces complex spatial variations in amplitude associated with heterogeneous slip and rupture propagation, rupture directivity, and basin effects, whereas the empirical relation provides the median value (including site effects) across an ensemble of earthquakes.

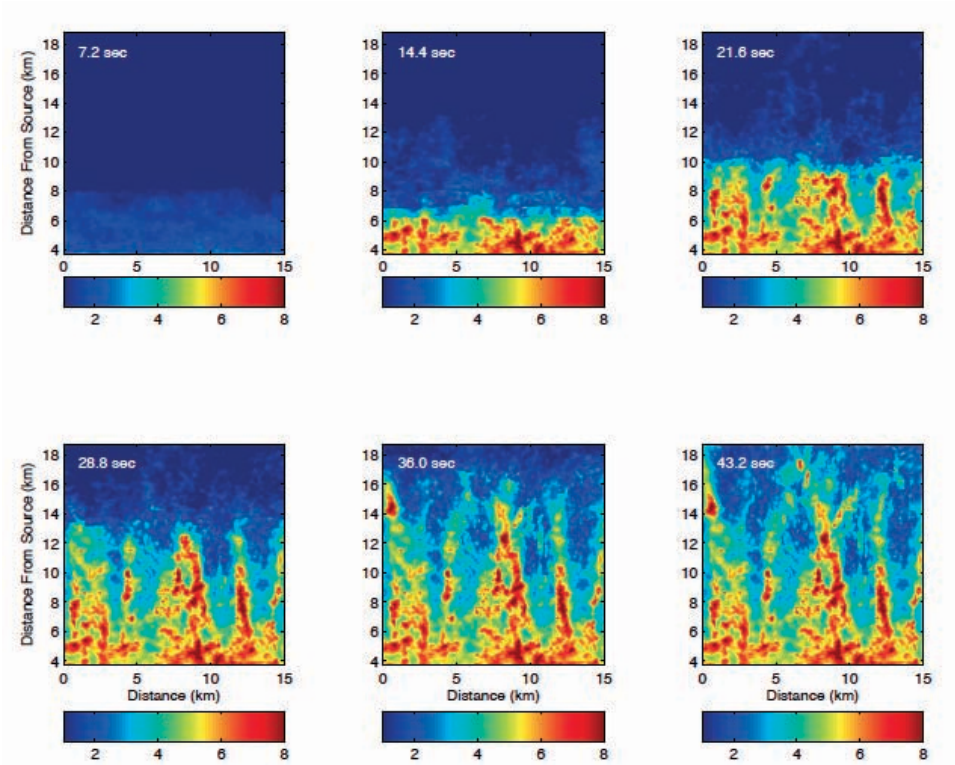

Figure 70. Snapshots of cumulative velocity vector magnitude for a simulation with fractal inhomogeneities having a Hurst value of 0 and standard deviation of 10%. Bands of amplified/deamplified motions develop as the SH/Love waves sweep through the inhomogeneities and the wave field is locally focused/defocused.

References

Boore, D. M., and G. M. Aktinson (2008). Ground-motion prediction equations for the average horizontal component of PGA, PGV, and 5%-damped PSA at spectral periods between 0.01 s and 10.0 s, Earthq. Spectra 24, no. 1, 99–138, doi 10.1193/1.2830434.

Bryant, W.A., 1987, Cleghorn and related faults, San Bernardino County: California Division of Mines and Geology Fault Evaluation Report FER-187, microfiche copy in California Division of Mines and Geology Open-File Report 90-14, 9 p., scale 1:24,000.

Campbell, K. W., and Y. Bozorgnia (2008). NGA ground motion model for the geometric mean horizontal component of PGA, PGV, PGD and 5% damped linear elastic response spectra for periods ranging from 0.01 to 10 s, Earthq. Spectra 24, no. 1, 139–171, doi 10.1193/1.2857546.

Graves, R. W., and A. Pitarka (2010) Broadband ground-motion simulation using a hybrid approach, Bull. Seismol. Soc. Am. 100, 2095–2123, doi: 10.1785/0120100057.

Li, W. & Assimaki, D. (2010) Site- and Motion-Dependent Parametric Uncertainty of Site-Response Analyses in Earthquake Simulations, Bull. Seismol. Soc. Am. 100, 995-1009, doi: 10.1785/0120090030.

Olsen, K. B., S. M. Day, J. B. Minster, Y. Cui, A. Chourasia, M. Faerman, R. Moore, P. Maechling, and T. Jordan (2006), Strong shaking in Los Angeles expected from southern San Andreas earthquake, Geophys. Res. Lett., 33, L07305, doi:10.1029/2005GL025472.

Tape, C., Q. Liu, A. Maggi, and J. Tromp (2009). Adjoint tomography of the southern California crust, Science 325, 988–992.

Seismic Hazard and Risk Analysis

This report highlights the results of five projects that made significant contributions to seismic hazard and seismic risk analysis.

Non-Linear Structural Simulations using SCEC Simulated Ground Motions

Although substantial progress has been made in physics-based ground motion simulations in the recent years, the engineering community is still reluctant to use simulated time series for design. One of the reasons for this is a lack of understanding of how simulated ground motions compare to recorded ground motions, especially when it comes to their impact on structural response. There are on-going efforts at validation and verification of simulated ground motions, but these tend to be focused on record properties or on the response of single-degree-of-freedom systems. Goulet, Haselton and Bayless (2011) used a different approach by comparing the nonlinear structural response of buildings subjected to recorded and simulated ground motions, given that both sets had similar response spectral shapes.

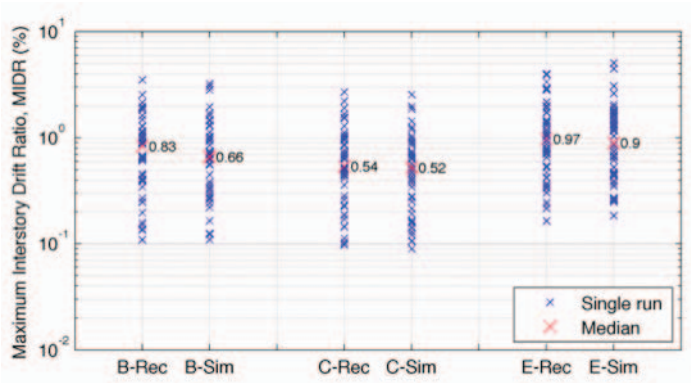

Figure 71. Summary of structural simulation results for buildings B (12 stories), C (20 stories) and E (4 stories) and for both the recorded (Rec) and simulated (Sim) acceleration time series.

The responses of buildings to recorded motions were already been processed in a project recently completed by the PIs. The recorded set is representative of a magnitude 7 earthquake, rupturing within 20 km from a site in a shallow crustal tectonic environment such as California. The SCEC simulated records were selected for the same type of event and distance with spectral shapes that were consistent with the recorded set. Structural simulations were then performed for three computer-modeled concrete structures, and the response results from both sets of time series were compared. Figure 71 shows a summary of the maximum inter-story drift ratio (MIDR) results obtained from the structural simulations. The vertical data stripes correspond to the MIDR results for all three buildings, for both the recorded and simulated time series. For each stripe, the maximum and minimum values were removed. For all three buildings, the ranges of MIDR values are similar, but the overall distribution of values for the recorded and simulated sets tend to differ for a given building. This leads to a large difference in the median MIDR estimate for building B, but to no statistical difference for building C. The preliminary conclusion based on the two datasets used is that the simulated ground motions led to structural response that were consistent with those derived from recorded motions.

Validation of End-to-End Simulation of Building Response using Ground Motion Simulations

This study had the objective of validating the use of simulated ground motions by integrating physics-based ground motion simulation and performance-based damage estimates and examining, probabilistically, building response due to both simulated and recorded ground motions. The research involved the comparison of building response to two earthquake scenarios: the 7.8Mw Los Angeles region ShakeOut scenario developed by Graves et al. (2008), a repeat of the 1906 San Francisco earthquake generated by Aagaard et al. (2009), and the Puente Hills scenario developed by Graves et al. (2006).

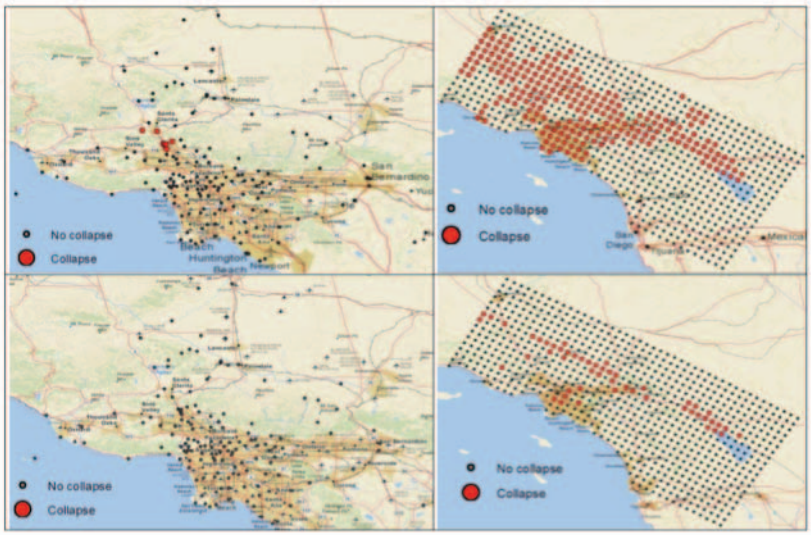

Figure 72. Collapse results of older (top) and modern (bottom) 8-story RC frame for (left) Northridge earthquake recorded ground motions and (right) ShakeOut scenario simulated ground motions. Source: Liel and Rowe (2010).

This analysis considered 735 evenly spaced sites for the hypothetical ShakeOut scenario earthquake and 157 sites where the Northridge earthquake was recorded. As a preliminary check on the simulation results, geographic trends of areas high

collapse risk for both the Northridge and ShakeOut earthquakes were identified as those sites where building simulation models collapsed, as shown in Figure 72. These figures reveal that, for both the Northridge earthquake and the simulated LA ShakeOut scenario, the older RC frame building is more likely to collapse than the modern building. This study predicts 12 collapses for the older RC frames during the Northridge earthquake (concentrated in the region shown on the map) and no collapses for the modern building subjected to the same ground motions. For the ShakeOut scenario, the study predicts 231 failures for the older RC frame and only 51 for the modern building. This difference between older and modern buildings is expected, due to the stricter building codes governing the seismic detailing of RC structures after 1970, and is consistent with observed results during the Northridge earthquake, during which very few modern RC buildings collapsed.

Loss Estimates for Kinematic and Dynamic ShakeOut Earthquake Scenarios

The goal of this project was to compare HAZUS®-estimated economic loss and population impacts for six San Andreas Fault (SAF) scenarios. Long period ground motions for the SAF ruptures were simulated using dynamic rupture propagation. Five realizations of the "ShakeOut" scenario with dynamic rupture propagation were analyzed. The synthetic ground motions provided for the loss estimation within HAZUS® were 0-10Hz broadband synthetics generated by combining long-period (0-1Hz) finite-difference synthetics with high-frequency scattering operators.

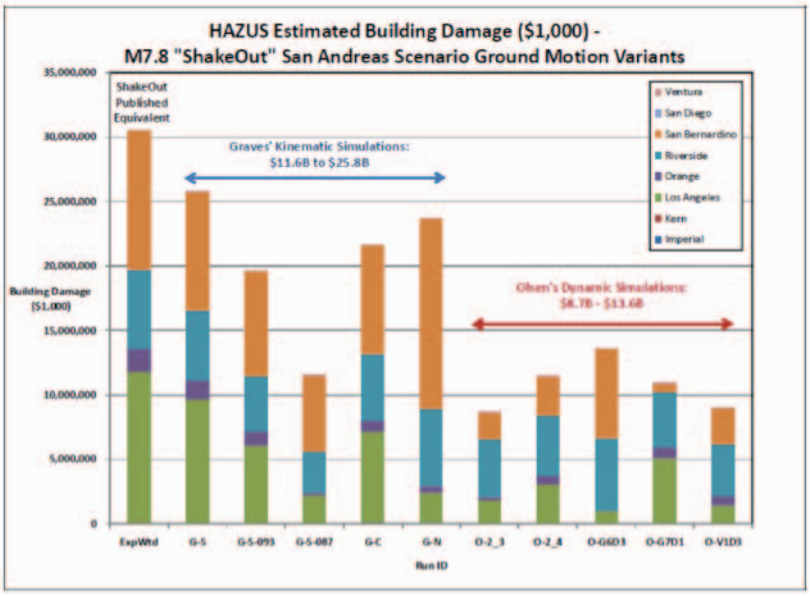

Figure 73. HAZUS® Estimates of Building Damage for the ShakeOut Ground Motion Scenarios. Source: Seligson and Olsen (2010).

Each M7.8 scenario variant was a 300-km S-N rupture on the southernmost San Andreas Fault, with dynamic source descriptions; the variants are designated as 2_3, 2_4, G6D3, G7D1 and V1D3. HAZUS® analyses were conducted for each of these five scenario variants, for comparison with the kinematic results. All "ShakeOut" HAZUS® analyses were conducted with enhanced inventory data. Database enhancements included improvements to the underlying building inventory data as well as to information utilized by HAZUS® on construction patterns throughout the eight county study area. As shown in Figure 73, the kinematic simulations produce larger loss estimates than do the dynamic simulations.

A Nonlinear Site Response Computer Application for the SCEC Broadband Ground Motion Simulation Platform

This project involved the implementation of a nonlinear site response computer application in the SCEC Braodband Ground Motion Simulation Platform. The site response model was developed for nonlinear site response analyses based on a viscoelastic formulation for frequency-independent Q and a hysteretic model. The model can simulate close to frequency-independent viscous damping in the strain range below the linear threshold, and match the nonlinear dynamic soil properties of soils (G/Gmax and damping) in the intermediate to high strain range (>10-3). The model was implemented into the 1D site response computational tool "Site1D" of the SCEC Broadband Ground Motion Simulation Platform.

Figure 74 shows the deviation of linear elastic prediction from site-specific nonlinear predictions as a function of (PGAROCK, FI) for three sites in the LA Basin: a stiff (Class C), a medium stiff (Class D) and a soft (Class E) site. As can be seen, the trend is the same for all three sites. Large PGAROCK and FI close to unity imply that empirical amplification factors do not adequately describe the site response, and that site-specific analyses should be employed.

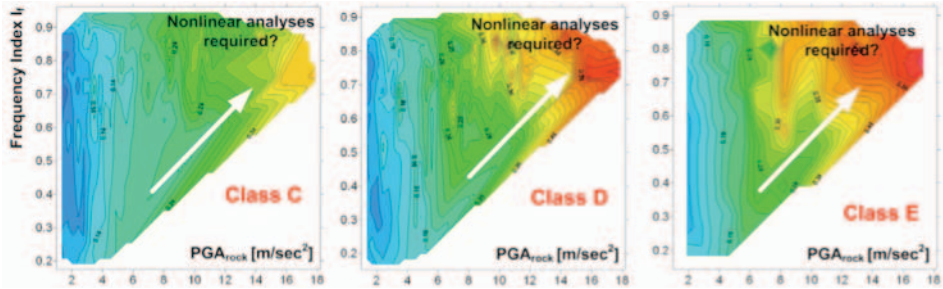

Figure 74. (PGA, FI) criteria implementation at three sites (Class C, D and E) in the Los Angeles basin for a series of broadband ground motion synthetics. The contour plots indicate the deviation of linear elastic predictions from nonlinear site-specific response predictions. Source: Assimaki (2010).

Implementation of a generalized conditional intensity measure (GCIM) approach in OpenSHA

The fundamental basis of the GCIM approach is that for a given earthquake scenario (Rup) the joint distribution of a vector of intensity measures (i.e. IM | Rup) has a multivariate lognormal distribution [1]. Characterisation of IM | Rup, therefore requires the marginal distributions, IMi | Rup and correlations between IMi and IMj for which several prediction equations already exist. The total probability theorem can then be used to construct the conditional distribution of any intensity measure given the occurrence of a specific value of another intensity measure. Figure 75 illustrates the conditional spectral acceleration and Arias Intensity distributions given Sa(1.0) with an annual exceedance probability of 1/475. This project involved the implementation of this generalized conditional intensity measure (GCIM) approach in OpenSHA.

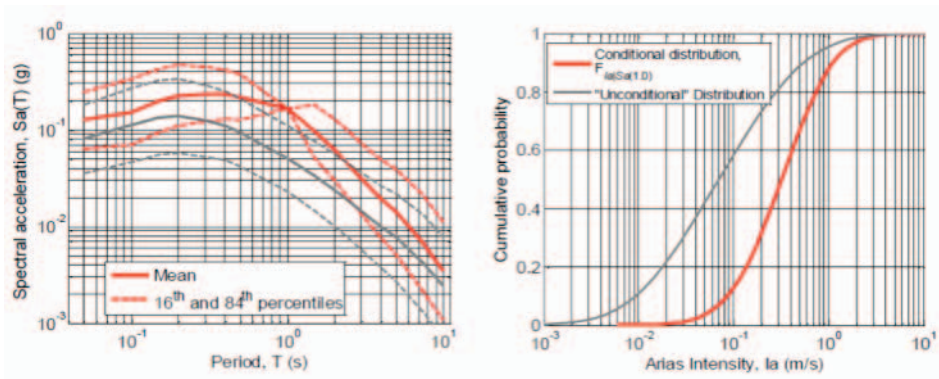

Figure 75. Example conditional distributions for a site in Christchurch, New Zealand. Source: Bradley (2010).

References

Assimaki, D. (2010). A Nonlinear Site Response Computer Application for the SCEC Broadband Ground Motion Simulation Platform. Report to SCEC.

Bradley, B. (2010). Implementation of a generalized conditional intensity measure (GCIM) approach in OpenSHA. Report to SCEC.

Goulet,C., K. Haselton and J.Bayless (2011). Non-linear structural simulations using SCEC simulated ground motions – one-to-one comparisons. Report to SCEC.

Liel, A.B. and K.L. Rowe (2010). Integration of Physics-Based Ground Motion Simulation and Performance-Based Building Damage Estimates for Improved Assessment of Seismic Risk. Report to SCEC.

Seligson, H. and K.B. Olsen (2010). HAZUS® Loss Estimates for Six Large San Andreas Fault Earthquake Scenarios, including the Mw8.0 "Wall to Wall." Report to SCEC.

Special Projects

In addition to the disciplinary groups, and cross-cutting focus groups, SCEC has undertaken a number of special projects, which are focused on problems with well-defined short-term research objectives, but are nevertheless consistent with SCEC goals. These include the *Southern San Andreas Fault Evaluation (SoSAFE)*, *Collaboratory for the study of Earthquake Predictability (CSEP)*, *Working Group on California Earthquake Probabilities (WGCEP)*, and *Community Modeling Environment (CME)*.

Southern San Andreas Fault Evaluation

The primary goal of the SoSAFE project is to document the timing of large paleoearthquakes and amount of slip released by the southern San Andreas and San Jacinto faults over the past 2000 years. Additional goals include examination of longer-term

slip rates and modeling studies that directly impact seismic hazard assessments. Research includes earthquake trenching studies, radiocarbon dating supported through the geochronology infrastructure funding, geomorphic studies using lidar and other aerial imagery data in tandem with field measurements, and examination of new methods for analyzing and incorporating neotectonic data. The annual SoSAFE workshop, highlighting the 2010-2011 accomplishments was held during the SCEC Annual Meeting in September, and attracted over 120 attendees. This workshop helps to maintain the focused objectives of the SoSAFE special project, and we anticipate that these activities will continue as SoSAFE is incorporated as a focus group under SCEC4.

San Jacinto - San Andreas Interaction

SCEC researchers continue to make significant progress at several sites along the southern San Jacinto fault. Slip rate studies by Blisniuk et al. (2010), Janecke et al. (2010) and in progress efforts by several researchers indicate that the San Jacinto fault slips at a rate approaching that of the San Andreas fault in the Salton Trough. The surprising rapidity of slip on this system (10-14 mm/yr) has several implications. For one, because the San Jacinto fault is more complex and segmented than the San Andreas fault, it may produce more earthquakes in the mid to low magnitude 7 range, thus increasing its contribution to hazard regionally. Whether some of these earthquakes propagate onto the San Andreas fault at Cajon Pass is one of the outstanding questions facing SoSAFE, motivating efforts to uncover the timing of earthquakes at the Mystic Lake paleoseismic site on the Claremont fault. On-going work by Onderdonk, Rockwell and McGill at Mystic Lake shows that ground-rupturing earthquakes repeat at an average interval of ~180 years since ca. 500 A.D., and preliminary dating suggests a few events with strong temporal correlation to published San Andreas fault records from the Mojave section. These few events do not have strong temporal correlation with the Hog Lake record, (Rockwell and others) indicating that the northern San Jacinto periodically interacts with the San Andreas fault.

Substantial effort by three groups is underway to study the region around the intersection of the San Andreas and San Jacinto faults, where these faults become multi-stranded and poorly expressed, respectively. Along the North Branch of the San Andreas fault (Weldon) and the Claremont fault (McGill, Onderdonk and Rockwell), fieldwork and sampling for cosmogenic dates of geomorphic surfaces has been completed and should yield new insight into the distribution of slip rates; current slip rate studies have been inconclusive in these areas. In San Gorgonio Pass, trenching investigations by Heermance and Yule at key points along this complex fault network indicate that fault slip rates are low, but preliminary dating and vertical separation on the thrust faults of 2 m per event, or approximately 5 m of slip, suggest that infrequent large slip events can rupture through the pass.

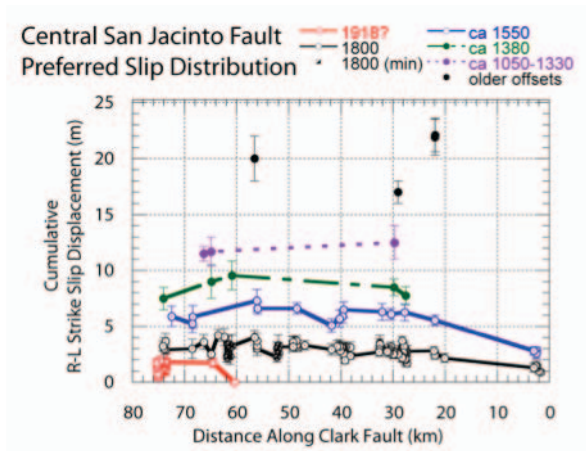

Figure 76. Slip distribution graph for the most recent events on the Clark strand of the central San Jacinto fault. Data points represent the most reliable and best-preserved features (good and excellent) to estimate displacement. We attribute the 3-4 m offsets through the Anza region to the most recent, large- scale rupture event on the Clark fault (black line). We also recognize the likely rupture from the 21 April 1918 earthquake, which broke a short ~15-20 km section of the fault (with an average of 1.25 m of right-lateral displacement - red line) in Blackburn Canyon, apparently due to lower displacement in that area in the ca. 1800 event.

Slip-per-event and Slip Rate Implications

New data on the frequency of earthquakes on the San Andreas fault in the Carrizo Plain (Akciz et al., 2010) have motivated additional reexamination of the slip rate and slip per earthquake record there. The paradigm of infrequent, 10 m slip events (Sieh, 1978; Liu et al., 2003) was overturned with new geomorphic offsets of 5 m found by Zielke et al. (2010). Even this lower slip-per-event value has been subject to reexamination because it would imply slips of 5 m approximately every 100 years (Akciz et al., 2010), yielding a slip rate of 50 mm/yr for this stretch of fault. It is likely that even these smaller offsets are sometimes a composite of more than one earthquake, too closely spaced in time to be differentiated in the geomorphic record (Grant-Ludwig et al., 2010). It is also possible that the long-term slip rate on the San Andreas fault in the Carrizo plain is higher than the 34 mm/yr found by Sieh and Jahns (1984) at Wallace Creek. The spectacular 127 m offset of this creek is not in question, but the timing obtained from conventional radiocarbon could be affected by inherited (older) charcoal. New efforts by Grant-Ludwig and Arrowsmith are underway to re-date this site, and to date other, nearby stream offsets, using modern single-sample AMS techniques.

Two new regions with geomorphic offsets were studied in 2011. Salisbury et al. (in review) compared field and lidar-based measurements of hundreds of offsets along the Clark fault, and found that the geomorphic record of slip events favors fairly regular offsets with maximum displacement near Anza of 3-4 m, and possible evidence for surface rupture associated with the historical (1918) earthquake, which they relocate to the Clark strand of the San Jacinto fault (Figure 76). New trenching to the northwest of Hog Lake may support this interpretation. On the San Andreas fault, Williams completed terrestrial lidar scans of a dozen offset gullies along the Mission Creek section. These offsets are also fairly regularly spaced, lending additional support for repetition of similar-sized earthquakes along the southernmost San Andreas fault and preference for rupture on the Mission Creek fault over the San Gorgonio section in most events based on the recurrence data from nearby Thousand Palms (Fumal et al., 2002).

Synthesis and Proposal Activities

This year the SoSAFE community developed and submitted an NSF Tectonics proposal geared to exploring the spatio-temporal behavior of the San Andreas and San Jacinto fault systems. A team of PIs from nine institutions worked collaboratively to identify key gaps in existing coverage of the SAF/SJF system, such as spatial gaps where lower (M7) events could be overlooked and temporal gaps produced by insufficient dating or stratigraphic context in past projects, with the goal of developing a full rupture history for the system. Modeling efforts were also included to explore the stress changes over several earthquake cycles as constrained by paleoseismic data. This proposal received high marks from the external reviews. Although declined for funding, the actualization of this proposal served to invigorate the SoSAFE community, aided in identification of new ways to integrate paleoseismic data with other geophysical approaches, and fostered new collaborations between researchers.

References

Blisniuk, K., Rockwell, T., Owen, L., Oskin, M., Lippincott, C., Caffee, M., and Dorch, J., (2010): Late Quaternary slip-rate gradient defined using high-resolution topography and 10Be dating of offset landforms on the southern San Jacinto fault, California, Journal of Geophysical Research – Solid Earth, Vol. 115, B08401, doi:10.1029/2009JB006346

Janecke, S., Dorsey, R., Forand, D., Steely, A., Kirby, S., Lutz, A., Housen, B., Belgarde, B., Langenheim, V., Rittenour, T. (2010) High Geologic Slip Rates since Early Pleistocene Initiation of the San Jacinto and San Felipe Fault ZOnes in the San Andreas Fault System: Southern California, USA, Geological Society of America Special Paper 475.

Zielke, O., Arrowsmith, J., Grant-Ludwig, L., and Akciz, S. (2010) Slip in the 1857 and earlier large earthquakes along the Carrizo Plain, San Andreas fault, Science, v. 327, p. 1119-1121.

Grant-Ludwig, L., Akciz, S., Noriega, G., Zielke, O., and Arrowsmith, J. (2010) Climate-modulated channel incision and rupture history of the San Andreas fault in the Carrizo Plain, Science, v. 327, p. 1117-1119.

Akciz, S., Grant-Ludwig, L., Arrowsmith, J., and Zielke, O. (2010) Century-long average time intervals between earthquake ruptures of the San Andreas fault in the Carrizo Plain, California, Geology, v. 38, p. 787-790.

Working Group on California Earthquake Probabilities

The Working Group on California Earthquake Probabilities (*http://www.WGCEP.org*) is actively building the 3rd Uniform California Earthquake Rupture Forecast (UCERF3). The main innovations for this model will be: 1) the relaxation of fault segmentation assumptions and the inclusion of multi-fault ruptures; and 2) the addition of spatiotemporal clustering (earthquake triggering and aftershocks), which will form the basis of an operational earthquake forecast. Our plan for both these enhancements was bolstered tragically by the 2011 Tōhoku, Japan and Christchurch, New Zealand earthquakes.

The main accomplishment over the last year was the development of our Proposed UCERF3 Plan, which also includes prototype model components (*http://www.wgcep.org/sites/wgcep.org/files/UCERF3_Project_Plan_v52.pdf*).

This was reviewed by the general scientific community at a marathon series of workshops in June, 2011, and a formal review was conducted by our Scientific Review Panel [1] on June 13th and 14th, 2011. The Final UCERF3 Plan is due at the end of September, 2011, and the final model is due June 30, 2012. The many details of this project can be found in the preliminary plan referenced above.

Collaboratory for the Study of Earthquake Predictability

Controversies have clouded research on earthquake prediction and forecasting for at least a century (Hough, 2009). Many have stemmed from the lack of community standards and an inadequate infrastructure for conducting scientific prediction experiments (Wyss and Booth, 1997; Jordan, 2006). To improve earthquake forecasting in California, the USGS and SCEC set up a Working Group on Regional Earthquake Likelihood Models. The five-year RELM project, which began in 2006 (Field, 2007), has compared the performance of 19 earthquake forecasting models in California using standardized testing procedures that assess forecast reliability and skill (Schorlemmer et al., 2010). The RELM mid-term results have been published (Schorlemmer et al., 2010), and a final report is in preparation (Schorlemmer et al., 2011).

RELM's success encouraged SCEC to initiate CSEP (Jordan, 2006). Support was provided by a $1.2M, 3-year grant from the W. M. Keck Foundation, which began on 1 Jan 2006. In the first year, a computational system comprising four subsystems was developed (Figure 77), and all of the RELM forecasts were registered into the nascent W. M. Keck Testing Center at SCEC. On 1 Sept 2007, CSEP began operational prospective testing at SCEC using an automated scientific workflow (Zechar et al., 2009). Since then, updates to the operational system have been installed at SCEC and released to the other testing centers on a quarterly basis. Careful management of the Keck funds and leveraging through the SCEC base program have allowed the continuation of CSEP development and operations through the first half of 2011.

Since it began operations in 2007, CSEP has grown into a global collaboratory with testing activities in a variety of tectonic environments, maintained through a series of international agreements. As currently configured, its infrastructure comprises four primary components:

- **Testing regions:** natural laboratories comprising active fault systems with adequate, authoritative data sources for conducting prediction experiments.
- **Community standards:** rules for the registration and evaluation of scientific prediction experiments.
- **Testing centers:** facilities with validated procedures for conducting and evaluating prediction experiments.
- **Communication protocols:** procedures for conveying scientific results and their significance to the scientific community, government agencies responsible for earthquake hazard information, and the general public.

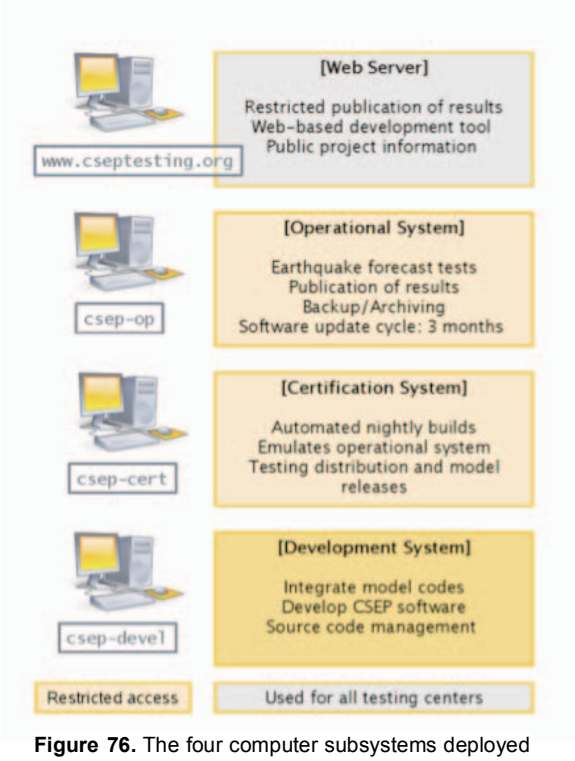

Figure 76. The four computer subsystems deployed within the W.M. Keck CSEP Testing Center at SCEC are configured to support the development of new earthquake forecast models (csep-devel), certification of these models into a formal testing environment (csep-cert), operational testing of registered algorithms (csep-op), and dissemination of testing results (www.cseptesting.org). The CSEP cyberinfrastructure is described in more detail by Zechar et al. (2009).

Current Status

Regional experiments are now underway in California (Zechar et al., 2009), New Zealand (Gerstenberger & Rhoades, 2010), Italy (Marzocchi et al., 2010), and Japan (Nanjo et al., 2011) and will soon be started in China (Figure 78). A program for global testing has also been initiated. The testing centers run forecasting experiments using a common software system that automatically updates short-term, seismicity-based models and evaluates the forecasts on a regular (quarterly) schedule. Both likelihood-based tests (Schorlemmer et al., 2007) and alarm-based tests (Zechar and Jordan, 2007) have been implemented.

In each of the testing regions, both time-independent and time-dependent models are being evaluated using standardized seismicity catalogs collected from authoritative sources. For example, CSEP uses the Advance National Seismic System

(ANSS) catalog in California, the Japan Meteorological Agency (JMA) catalog for Japan, and the Global Centroid Moment Tensor (CMT) catalog in the Western Pacific testing region. The CMT catalog is also used for global testing.

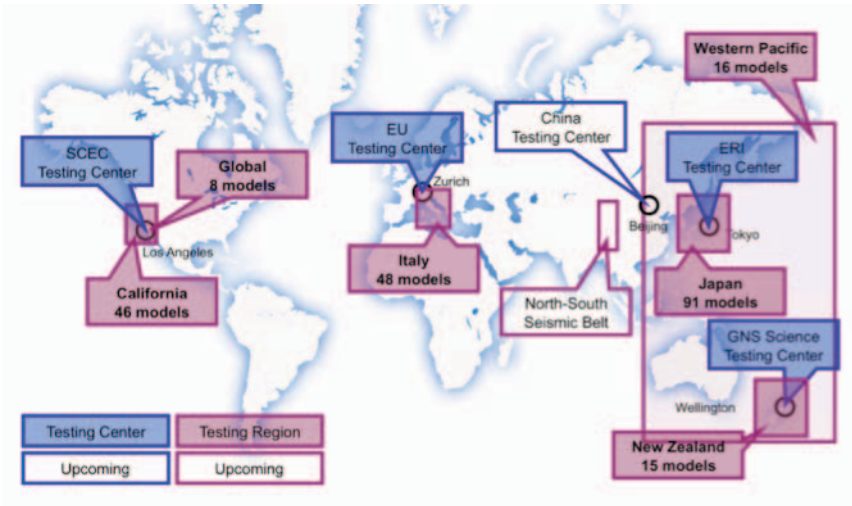

Figure 78. CSEP testing centers and testing regions as of June 1, 2011, showing the number of earthquake forecasting models under test in each region.

Today, 224 forecasting experiments are being tested worldwide (Figure 79). Two regions of current interest are New Zealand, where 15 models were being tested by CSEP at the time of the 4 Sept 2010 Darfield earthquake (M7.1), and Japan, where 91 models were under CSEP testing at the time of the 11 Mar 2011 Tohoku earthquake (M9.0). The Darfield and Tohoku earthquake sequences are being observed by high-quality seismic networks, and they may lead to a better understanding about how such sequences could unfold along other active zones like those in the western United States.

The CSEP testing procedures follow strict "rules of the game" that adhere to the principle of reproducibility: the testing region, the authoritative data sources, including the seismicity catalog, and the conventions for model evaluation are established before and maintained throughout an experiment. An experiment can be re-run at any time by any researcher, and it will produce the same results. All models submitted to CSEP are required to be properly documented (preferably in the form of source code for the executable model), and they can be calibrated using retrospective data for each region; however, any data used for calibrating the models retrospectively are not employed in model evaluations.

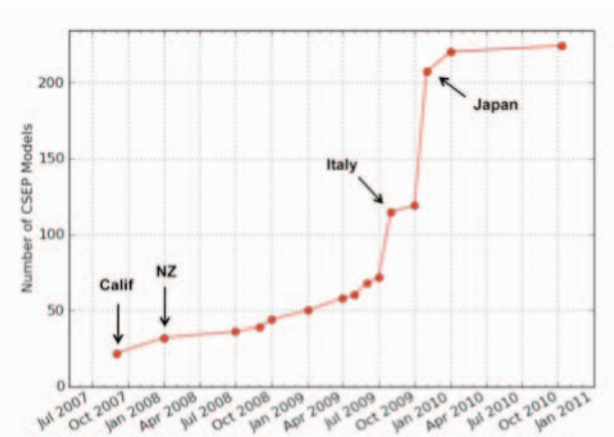

Figure 79. Number of earthquake forecasting experiments under test in CSEP testing regions worldwide as a function of time from the initiation of the SCEC Testing Center in September, 2007, through November, 2010. Annotation indicate when new testing regions were initiated.

The catalog latency is variable but generally exceeds the updating intervals of the shortest-term forecasts; therefore, current CSEP testing is not strictly prospective. However, the model and any updating methods are fixed; authors cannot modify or interact with their models after an experiment has begun, and they are not involved in conducting the statistical tests. Thus, the forecasts are truly blind. Although the main focus is on this quasi-prospective testing, the reproducibility of CSEP experiments provides a unique capability for retrospective testing.

Examples of CSEP Results

Assessing the quality of a method is a multifaceted problem that can involve many attributes of performance (e.g., Jolliffe and Stephenson, 2003). The attributes of forecast quality emphasized in the current CSEP testing procedures are reliability and skill. Reliability is an absolute measure of performance; it evaluates the statistical agreement between the forecast probabilities of target events and the observed frequencies of those events (e.g., the mean observation conditional on a particular forecast). Skill, on the other hand, assesses the performance of one method relative to another. Measures of skill can be used to evaluate a candidate method relative to a standardized reference method; e.g., a short-term earthquake forecast relative to a long-term forecast. To be useful for operational purposes, a method must demonstrate both reliability and skill.

Figure 80 and Figure 81 illustrate CSEP evaluations of reliability and skill for short-term forecasting models. An important result is the high performance of the STEP model of Gerstenberger et al. (2005, 2007) in the California testing region, which supports the USGS use of STEP as an operational forecasting model for California.

Interesting results have also been obtained for the seismic sequence in the Canterbury region of New Zealand, which began with the MW 7.1 Darfield earthquake of 3 Sept 2010. The time-dependent ETAS model out performs the PPE and other time-independent models; probability gains above 1000 have been achieved by ETAS during the Darfield sequence.

New data are also coming in rapidly from the Japan testing region. The aftershock numbers predicted by ETAS models for the Tohoku sequence are under-estimates of the actual number (Figure 82). These results indicate that the ETAS updating interval of 1 day is too long to capture the aftershock activity, which decays rapidly after the mainshock. (This conclusion has also been drawn from the California experiments.) Figure 6 also shows that the aftershock number is higher during the post-interval relative to pre-event intervals, which may be related to artificially high magnitude cutoffs in the ETAS model of aftershock productivity.

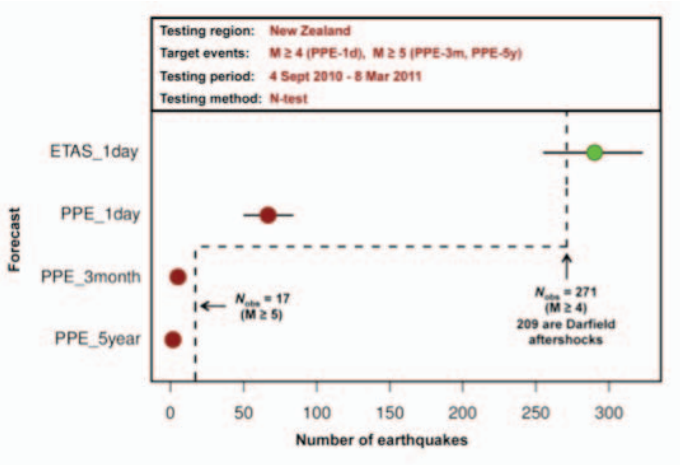

Figure 80. Examples of CSEP results that assess the absolute reliability of four models by testing the number of earthquakes forecast (dots with 95% confidence intervals) against the number observed (dashed lines) in the New Zealand testing region during the interval 4 Sept 2010 – 8 Mar 2011. ETAS_1day is a time-dependent (Omori-Utsu) Epidemic Type Aftershock Sequence model, updated daily, which passes the test (indicated by green dot). PPE_3month, PPE_1day, and PPE_5year are time-independent (Poisson) Proximity to Past Earthquakes models with updating intervals 1 day, 3 months, and 5 years, respectively, which fail the test (indicated by red dots). The ETAS and PPE_1day tests comprised 271 events with M ≥ 4, whereas the PPE_3month and PPE_5year test comprised 17 events with M ≥ 5. (209 of the 271 events in the former set were aftershocks of the 3 Sept 2010 Darfield earthquake.) Results from the New Zealand Testing Center are courtesy of D. Rhoades and M. Gerstenberger of GNS Science.

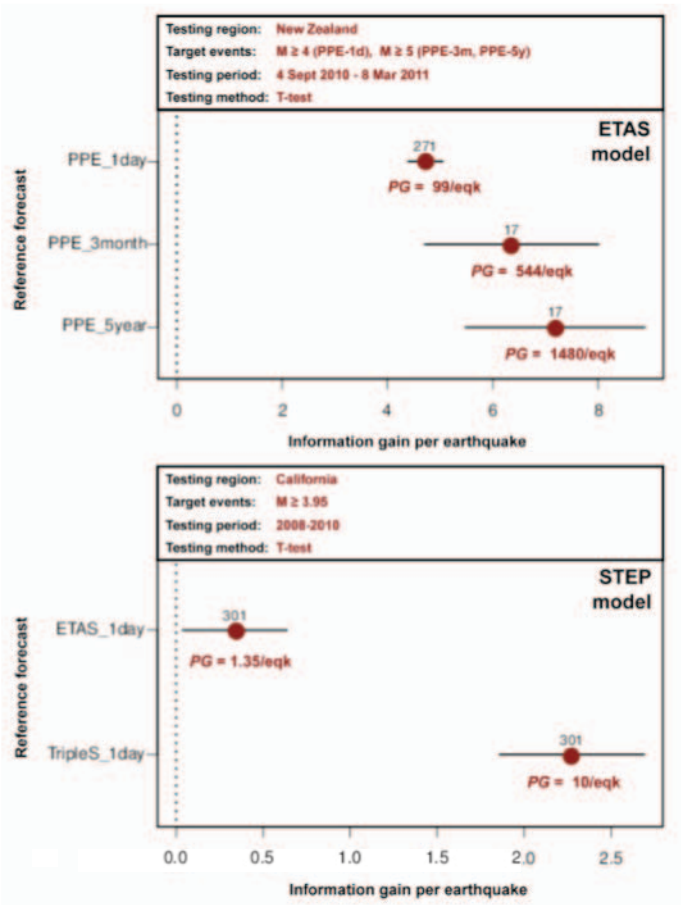

Figure 81. Examples of CSEP testing results that assess the relative skill of forecasting models. Upper panel: Information gain (IG) per earthquake of the ETAS_1day model relative to three PPE models for target events recorded in the New Zealand testing region during the interval 4 Sept 2010 – 8 Mar 2011. The PPE_1day comparison comprised 271 events with M ≥ 4, whereas the PPE_3month and PPE_5year comparisons comprised 17 events with M ≥ 5. (209 of the 271 events in the former set were aftershocks of the 3 Sept 2010 Darfield earthquake.) In this experiment, ETAS_1day achieved a probability gain (PG) of 99/eqk relative to PPE_1day and 1480/eqk relative to PPE_5year, and the null hypothesis of no probability gain can be rejected (indicated by red dots with 95% confidence intervals). Results from the New Zealand Testing Center are courtesy of D. Rhoades and M. Gerstenberger of GNS Science. Lower panel: IG per earthquake of Gerstenberger's STEP_1day model relative to Zuang's ETAS_1day model and Zechar & Jordan's TripleS_1day model for 301 target events with M ≥ 3.95 recorded in the California testing region during the 3-year interval 2008-2010. All three of the forecasting models were updated on a daily basis. In this experiment, STEP_1day achieved a PG of 1.35/eqk relative to ETAS_1day and 10/eqk relative to TripleS_1day, and the null hypothesis of no probability gain can be rejected (indicated by red dots with 95% confidence intervals). STEP and ETAS are time-dependent (Omori-Utsu) models; TripleS and PPE are time-independent (Poisson) models. All models were evaluated using a paired T test, developed by D. Rhoades based on the student's t distribution. Information gain is the natural logarithm probability gain.

References

Gerstenberger, M. C., L. M. Jones, and S. Wiemer (2007). Short-term aftershock probabilities: Case studies in California, Seismol. Res. Lett., 78, 66-77.

Gerstenberger, M.C. & D. A. Rhoades (2010), New Zealand Earthquake Forecast Testing Centre, Pure Appl. Geophys., 167, 877-892.

Gerstenberger, M. C., S. Wiemer, L. M. Jones, and P. A. Reasenberg (2005). Real-time forecasts of tomorrow's earthquakes in California, Nature, 435, 328-331.

Field, E. H. (2007). Overview of the working group for the development of regional earthquake likelihood models (RELM), Seismol. Res. Lett., 78, 7-16.

Jolliffe, I. T., and D. B. Stephenson (2003). Forecast Verification – A Practitioner's Guide in Atmospheric Science, John Wiley & Sons, Chichester, 254pp.

Jordan, T. H. (2006). Earthquake predictability, brick by brick, Seismol. Res. Lett., 77, 3-6.

Marzocchi, W., D. Schorlemmer & S. Wiemer, eds. (2010), An Earthquake Forecast Experiment in Italy, Special volume, Ann. Geofisica, 53 (3), 163 pp.

Nanjo, K. Z., H. Tsuruoka, N. Hirata & T. H. Jordan (2011), Overview of the first earthquake forecast testing experiment in Japan, Earth Planets Space, 63, 159–169, doi:10.5047/eps.2010.10.003.

Schorlemmer, D., M. C. Gerstenberger, S. Wiemer, D. D. Jackson, and D. A. Rhoades (2007). Earthquake likelihood model testing, Seismol. Res. Lett., 78, 17-29.

Schorlemmer, D., J. D. Zechar, M. J. Werner, E. H. Field, D. D. Jackson, T. H. Jordan, and the RELM Working Group (2010). First results of the Regional Earthquake Likelihood Models experiment, Pure Appl. Geophys., 167, 859-876, doi:10.1007/s00024-010-0081-5.

Wyss, M., and D. C. Booth (1997). The IASPEI procedure for the evaluation of earthquake precursors, Geophys. J. Int., 131, 423-424.

Zechar, J. D., and T. H. Jordan (2008). Testing alarm-based earthquake predictions, Geophys. J. Int., 172, 715-724.

Zechar, J. D., D. Schorlemmer, M. Liukis, J. Yu, F. Euchner, P. J. Maechling, and T. H. Jordan (2010). The Collaboratory for the Study of Earthquake Predictability perspective on computational earthquake science, Concurr. Comput.-Pract. Exp., 22, 1836-1847, doi:10.1002/cpe.1519.

Community Modeling Environment

The SCEC Community Modeling Environment (CME) collaboration conducts earthquake system science and computational science research with funding from the National Science Foundation (NSF), the U.S. Geological Survey (USGS), and other sources. Many important seismic hazard data products are computationally intensive and computational improvements can lead to improved seismic hazard information. CME researchers are developing new ways to use high performance computing to advance seismic hazard research. The CME research program provides an avenue through which basic SCEC research advancements can be implemented in computational form and integrated into standard, broad-impact, ground motion forecast calculations. More than thirty researchers, graduate students, and staff participated in this year's CME collaborative research activities. The following sections summarize several CME research accomplishments between August 2010 and August 2011. More detailed information about these, and other, CME research accomplishments are presented in the SCEC Annual Meeting poster sessions.

California 3D Velocity Model Development

Earthquake simulations require accurate 3D seismic velocity models to produce accurate ground motion estimates. To support quantitative comparison between alternative CVM's, we established a standardized and automated velocity model evaluation system, and we used this system to evaluate existing SCEC CVM models. Our CVM evaluation system uses wave propagation simulations to evaluate 3D velocity models in the following way. Our CVM evaluation system builds a 3D velocity mesh using the CVM under test, runs a forward wave propagation simulation at 1Hz for a well-recorded southern California earthquake. The simulated ground motion records (seismograms) are compared to observed seismograms for the event using standard goodness of fit metrics including map-based plots that show geographical variations in goodness of fit results.

With a CVM evaluation system in place, we developed, evaluated, and released an updated version of CVM-H. Released in February 2011, CVM-H v11.2 updates an earlier version of the CVM-Harvard velocity model called CVM-H v6.3. CVM-H

v11.2 includes an expanded coverage region and a standardized 350-m geotechnical layer based on the California Geologic Survey's statewide mapping of VS30 (average shear velocity in the upper 30 m). This improved geotechnical layer is expected to improve the modeling of near-surface scattering in high-frequency ground motion simulations.

To support current and future SCEC CVM developments, we have developed an integrated software framework, the Unified Community Velocity Model (UCVM) framework, to support the assembly of a statewide California velocity model from existing regional models. The UCVM software framework enables users to quickly build, visualize, and validate meshes from alternative velocity models through an standardized CVM query interface, and it integrates regional 3D models with selected statewide topography and bathymetry data sets and with the standardized, VS30-based geotechnical layer described above. The UCVM platform accepts input of material properties in multiple formats, including raster, voxel, and Octree, and it can export models in multiple formats, including Octree and NetCDF.

Tera3D

A CME group led by P. Chen used the scattering integral method of full-3D tomography to validate and improve CVM-SCEC v4 (CVM-S4), a widely used SCEC 3D community velocity model for Southern California. The CME Tera3D project has produced a series of CVM-S improvements, including refinements based on waveform data from moderate California earthquakes, as well as Green-function time series derived from ambient-noise cross-correlation at station pairs in California. The Tera3D software has also been applied to the inversion of waveform data to obtain refined estimates of centroid moment tensors (CMTs) of the earthquake sources, which are then used to produce improved synthetics for structure inversions. These source inversions have also been extended to finite-source (2nd-moment) parameterizations. One important result has been a CMT catalog that resolves the fault-plane ambiguity for 40 small earthquakes in Southern California. This catalog is being used to improve tectonic interpretations of the seismicity.

By combining progress on our UCVM framework, with Tera3D model improvements, an updated version of the CVM-S4 velocity model, currently labeled CVM4-SI5, is now available through the SCEC web site. This is an important advance because it provides the SCEC research community with access to the results of the Tera3D inversion performed on the CVM-S4 velocity model.

Broadband Platform

The scientific and engineering need for higher frequency ground motion simulations has led to the development of the SCEC broadband platform. The SCEC broadband platform is a software integration effort in which multiple SCEC scientific codes have been integrated together into a "software system", that is, a single software distribution capable of calculating ground motions for arbitrary ruptures up to 10Hz. Because of the tremendous computational requirements for 10Hz deterministic simulations, the SCEC Broadband platform calculates low frequency deterministic seismograms (0Hz – 1Hz) and adds stochastic high frequencies (>1Hz – 10Hz) to produce broadband (0-10Hz) seismograms.

CME researchers released a software distribution of the SCEC Broadband platform v11.2 in February 2011. The Broadband Platform integrates several scientific software elements—pseudo-dynamic rupture generators, deterministic and stochastic seismogram synthesis codes, and non-linear site effect modeling codes—into a single software distribution capable of calculating broadband seismograms (0-10 Hz) for kinematic finite-source models. The Broadband Platform distribution contains a set of earthquake source models of historic validation events including Northridge, Loma Prieta, and Landers. It can also generate broadband seismograms using user-defined source descriptions of scenario earthquakes. The Broadband platform was designed for portability and ease-of-use by non-experts, including geoscientists and earthquake engineers. Users may select among various codebases for rupture generation, 1D low-frequency synthesis, high-frequency synthesis, and incorporation of non-linear site effects, with the option of running goodness-of-fit comparisons against observed or other simulated seismograms. The platform produces a variety of ground motion-related data products, including broadband seismograms, rupture visualizations, and goodness-of-fit plots.

CyberShake Platform

During this year, we continued development of the CyberShake hazard model. The CyberShake platform calculates physics-based probabilistic seismic hazard curves for California in which peak ground motion estimates for ruptures are calculated using wave propagation simulations rather than attenuation relationships. The CyberShake Platform computes synthetic

seismograms for very large ensembles of earthquake ruptures using an efficient algorithm based on the concept of seismic reciprocity. A pseudo-dynamic rupture generator samples all fault-based ruptures of the uniform California earthquake rupture forecast (UCERF2), providing for each fault source multiple realizations. From this rupture set, approximately 880,000 horizontal-component seismograms up to seismic frequencies of 0.5 Hz are calculated at each site of interest. The seismograms are post-processed to obtain single-degree-of-freedom spectral acceleration at various frequencies, and these spectral accelerations are used to compute hazard curves and hazard maps. Earlier CyberShake hazard curves used the CVM-S4 velocity model to represent 3D structure. During this year, CyberShake models were calculated using an alternative pseudo-dynamic rupture generator and the recently released CVM-H v11.2 velocity model.

CyberShake results suggest that the standard attenuation relations used in PSHA, such as the NGA relations used by NSHMP, significantly underestimate the hazard probabilities in the sedimentary basins of the Los Angeles region. We believe this underestimation is due to a strong coupling between source directivity effects and basin amplification effects not captured in the empirical models. The results are significant because most of the population and urban infrastructure, and therefore most of the earthquake risk, is concentrated in the sedimentary basins. Comparisons between CyberShake hazard models indicate that the largest epistemic uncertainty in the hazard curves comes from uncertainties in basin structure, suggesting that more effort should be placed on refining models of basin structure using full-3D tomography and other information.

Broadband CyberShake

During this year, we extended our CyberShake computational capabilities to broadband frequencies by combining two existing SCEC computational capabilities, the CyberShake physics-based PSHA capability, and the Broadband Platform high frequency seismogram calculation. The SCEC Broadband CyberShake Platform can calculate physics-based PSHA hazard curves that contain frequencies up to 10Hz by combining the 0.5Hz deterministic calculations of the CyberShake platform, and the 0.5Hz-10Hz stochastic calculations of the SCEC Broadband Platform. These higher frequency PSHA calculations provide PSHA estimates for higher frequency dependent intensity measures, such as Peak Ground Acceleration (PGA), which are relevant to seismic hazards for stiff structures and precarious rock validation work. The Broad CyberShake platform was used to calculated new PSHA hazard estimates for selected California sites of interest after the Tohoku earthquake in March 2011.

CME High Performance Computing (HPC)

This year's CME research activities were partially funded as part of the NSF PetaApps program that has the explicit goal of preparing science applications that can run at sustained petaflops performance on HPC systems. The research accomplished with this support has positioned SCEC to take advantage of NSF Track 1 and DOE Leadership-class computing systems scheduled to begin operations in 2012-2013. SCEC/CME high performance computing activities during this year include development of highly parallel computational software including AWP-ODC, Hercules, and SORD, as well as extensive automation of computational simulations using scientific workflow technologies.

AWP-ODC

The SCEC AWP-ODC software is a highly parallel, 4th-order, staggered-grid, finite-difference code parallelized for large-scale calculations. By running on several generations of NSF and DOE computer hardware, we have developed AWP-ODC into a highly efficient and scalable code for wide variety of applications, including forward and inverse problems. In 2010, AWP-ODC achieved nearly ideal speedup between 65,610 and 223,074 cores on NCCS Jaguar and exceptional parallel efficiency—nearly 90% on 204,800 Jaguar cores. AWP-ODC was used for the M8 simulations described below, attaining a sustained performance of 220 teraflops in production runs and over 300 teraflops in benchmark runs.

To achieve this level of scalability and performance, SCEC researchers made many software improvements: single-CPU optimization, introducing computation/communication overlap and asynchronous communication, reducing communications at the algorithm level, and optimizing rank placement remapping. Taken together, these optimizations have reduced IO time from 49% of wall clock time to less than 1%.

M8 Study

The SCEC M8 study comprises a set of scenario earthquake simulations of magnitude 8.0 southern San Andreas ruptures. The M8 scenario earthquake is an Mw 8.0 earthquake that ruptures the entire 545-km length of the southern San Andreas Fault,

from Cholame in central California to the southern termination of the San Andreas Fault on the Salton Sea. The SCEC M8 earthquake scenario represents the outer scale required for standard California seismic hazard calculations because there are few, if any, larger ruptures in the existing USGS Unified California Earthquake Rupture Forecast (UCERF 2.0).

Running the M8 earthquake simulation involved a two-step process. First, we ran a dynamic rupture simulation, on NICS Kraken supercomputer, to create a physically realizable slip-time history on the fault. Second, we ran a ground motion simulation, on NCCS Jaguar supercomputer (the world's fastest at the time), to model the anelastic seismic wave propagation from the fault rupture. The latter calculation represented the 3D seismic velocity structure by 436 billion mesh points and ran for 24 hours on Jaguar at full machine scale (more than 223,000 cores), making it the largest-ever earthquake simulation. The M8 simulation team, led by Y. Cui, was recognized as an ACM Gordon Bell Finalist in 2010.

The SCEC M8 simulations show that SCEC's AWP-ODC deterministic 3D wave propagation software can scale to simulate any earthquake in the standard California earthquake rupture forecast up to 2Hz. The M8 simulations show that CME researchers can run well-validated deterministic wave propagation simulations at 2Hz at the scale need to model the "worst-case" seismic hazard earthquake scenarios in current California Earthquake Rupture Forecasts.

The M8 simulation results have led to several significant scientific conclusions: (1) the likelihood that large ruptures on the San Andreas fault will transition from sub-shear speeds during rupture propagation; (2) the importance of directivity and basin effects in ground motion amplification at high frequencies; and (3) the need to model off-fault plastic yielding and non-linear site effects at frequencies above 1 Hz.

The SCEC M8 simulations used an advanced form of earthquake description, one based on dynamic rupture simulation, as input to the simulation. Dynamic rupture simulations model friction-based slip on a fault so dynamic rupture simulations are consistent with known physics of fault ruptures. Less physically-accurate, but less computationally intensive, are kinematic rupture descriptions. Kinematic ruptures are not constrained by friction-based fault slip. Our M8 dynamic rupture simulation progressed quickly into a Supershear rupture, reduced speed, and then returned to Supershear velocity, all during the course of a single M8 earthquake. The fact that we observe Supershear velocities in our most physics-based rupture models suggests that Supershear ruptures are both possible and common. By comparing ground motions from dynamic ruptures and kinematic ruptures we have begun to establish the significant impact that Supershear rupture velocities have on ground motions.

Another important result from the SCEC M8 simulations relates to the important of non-linear site effects. SCEC researchers have significant experience with deterministic simulations up to 1Hz. However, as our M8 simulation work shows, deterministic wave propagation simulation results about 1Hz are significantly less mature. M8 results showed unexpectedly high, near-fault, ground motions. Our analysis of these results point to the need to model less-rigid, more flexible, materials at the surface when simulating seismic waves at frequencies about 1Hz. Indications are that at frequencies above 1Hz, non-linear effects become important. Above 1Hz, deterministic ground motion simulation results begin to diverge from observations especially for intensity measures typically associated with higher frequency motions such as peak acceleration.

These unexpectedly high peak ground motions, at frequencies above 1Hz, indicate a need to model the plastic yielding of near surface layers at higher frequencies. Until now, SCEC deterministic simulations at lower frequencies have not needed to model this additional non-linear behavior. Results from M8 show that SCEC simulations will need to model non-linear behavior as our deterministic simulations reach frequencies above 1Hz.

Hercules

Hercules simulation software, with development led by J. Bielak, is a finite-element parallel code that relies on an Octree-based mesher and solves the anelastic wave equations by approximating the spatial variability of the displacements and the time evolution with piecewise polynomial elements and central differences, respectively. PetaShake project has produced Hercules improvements in the areas of single-processor tuning, and optimization of the communication topology, message sizes, and messaging techniques. Checkpointing was implemented to reinitiate computations after unexpected interruptions. Through these improvements and algorithm improvements, the scalability of Hercules has been established on up to 100,000 compute cores on NICS Kraken, and it has been successfully used in different earthquake validation and verification exercises, such as the ShakeOut scenario.

Recently improved Hercules algorithms have achieved a 3x speed-up over the conventional element-by-element matrix-vector multiplication approach, obtaining a quadratic convergence rate in both time and space. More recently, we have incorporated a quadratic piecewise spatial approximation, which requires fewer nodes per wavelength for a prescribed level of accuracy. The code uses a plane-wave approximation for the absorbing boundary condition and allows either a Rayleigh bulk attenuation mechanism or a viscoelastic relaxation (BKT) model that employs Maxwell and Voigt elements. The solver computes displacements in an element-by-element fashion, scaling the stiffness and lumped mass matrix templates according to the material properties and octant edge-size. This approach allows Hercules to reduce memory requirements considerably relative to standard FEM implementations. We also implemented new Octree-based quadratic elements, which allow the ground motions to be represented much more accurately than the original linear elements with little additional computational effort.

As a part of our Hercules development, we created e-trees of the SCEC Community Velocity Models, CVM-S and CVM-H, up to extraordinary scales (17 billion octants in 2 TB), allowing us to perform earthquake ground motion simulations of large areas (150 km × 100 km) to high seismic frequencies with realistic velocities (~200 m/s) for the soft soil layers. For example, we have simulated the 2008 Chino Hills earthquake with an unprecedented resolution of 4 Hz, spanning frequencies of practical interest for engineered structures. These improvements bring us closer to being able to simulate destructive earthquakes in almost real time, which could be of great importance for emergency response, recovery, and reconstruction activities.

SORD

A CME team, led by G. Ely, has developed a structured FE code called Support Operator Rupture Dynamics (SORD). SORD can simulate dynamic fault ruptures using a logically rectangular hexahedral (structured) mesh that can be distorted to accommodate non-planar ruptures and surface topography. It employs the Kelvin-Voigt model of viscoelasticity. Besides the anelastic energy losses (attenuation) provided by this model during wave propagation, the viscosity helps prevent numerical noise from affecting the nonlinear rupture calculations. Wave motions are computed on a logically rectangular hexahedral mesh, using the generalized finite difference method of support operators. Stiffness and viscous hourglass corrections are employed to suppress zero-energy grid oscillation modes. The fault surface is modeled by coupled double nodes, where the strength of the coupling is determined by a linear slip-weakening friction law. External boundaries may be reflective or absorbing, and the absorbing boundaries are handled using the PML method. SORD code has been enhanced with scalable IO through MPI-IO optimizations, adapted from AWP-ODC IO. The hybrid CPU-GPU has been implemented with external collaboration for efficient speedup on GPU accelerator. SORD is being applied in the SCEC Big Ten simulation project, which uses the CyberShake rupture sets to investigate the most probable large ($M > 7$) ruptures in Southern California with the objective of understanding how source directivity, rupture complexity, and basin effects control ground motions.

CyberShake Workflows

SCEC scientific workflows manage the scheduling, code and file dependencies, and execution of production runs in both high-capability and high-capacity computing environments. The complex, multi-stage, HPC requirements of our CyberShake calculations present our imposing computational challenges, so we have applied workflow technologies to our CyberShake calculation to establish the scale, throughput, and reliability we need to complete CyberShake physics-based PSHA hazard calculations.

To execute the workflows on grid resources, CyberShake uses a software stack including the Pegasus Workflow Management System and Condor. This software enables us to create a generic, high-level workflow description, plan it for execution on a specific computational resource, and submit and monitor the jobs remotely. Large parallel jobs in the CyberShake workflow are submitted directly to the batch scheduler on the remote system using grid protocols. However, using a similar approach for the post-processing workflow resulted in poor performance owing to several factors: (a) grid submission overheads and queue waiting times greatly exceeded the runtimes of the jobs themselves, resulting in low throughput; (b) many computational resources have scheduling policies that limit the number of jobs that can be queued simultaneously, resulting in poor parallelism for serial jobs; and (c) submitting a large number of short-duration jobs often overwhelmed the remote scheduler, resulting in job failures and other errors. Performance for the post-processing CyberShake workflow was improved using two optimization techniques. Using an optimization technique called task clustering, Pegasus is now able to group multiple tasks into a single grid job, reducing the number of jobs to be executed and increasing the average runtime, which reduces the relative scheduling overhead.

Another optimization technique, called resource provisioning, allows CyberShake to allocate resources ahead of workflow execution and assume responsibility for matching jobs with resources. Provisioning for CyberShake is enabled using Condor glide-ins managed by Corral. To provision resources, a glide-in request is submitted to the remote scheduler. Instead of running an application job, the glide-in reserves the resource and starts a condor daemon that can fetch application jobs directly from the workflow management system. This approach bypasses the remote scheduler and reduces scheduling overhead. It also enables one glide-in job to provision multiple resources for a long period, executing many workflow jobs. Finally, giving the workflow system responsibility for resource management enables CyberShake to use custom scheduling policies that result in better performance. Corral automates the complex steps required to create glide-in jobs and automatically resubmits glide-ins as they expire, allowing CyberShake to maintain a fixed-size resource pool over a long period of time.

Earthquake Simulation Visualizations

CME scenario earthquake simulations show how advanced visualizations of earthquake simulations can effectively communicate seismic hazards to scientists, educators, and the public. SCEC earthquake animations, created in collaboration with San Diego Supercomputer Visualization Services have been shown worldwide, and these achievements have garnered a number of scientific visualization awards. During this year, visualizations of the SCEC M8 earthquake simulation won Honorable Mention at International Science & Engineering Visualization Challenges (2010) and SciDAC Office of Advanced Scientific Computing Research (OASCR) Visualization Awards (2011). Links to these award winning scientific visualizations are available through the SCEC web site.

CME Outreach

CME research accomplishments have resulted in several public references to our research. Our Cui et al paper "Scalable Earthquake Simulation on Petascale Supercomputers" describing our M8 simulation was a Gordon Bell Award finalist at SC10. SCEC M8 research was presented at SC10 as part of Thomas H. Jordan's Masterworks presentation. Our M8 and Tera3D research results were presented at American Geophysical Union (AGU) Fall 2010 meeting. M8 research results were used in multiple public press coverage of SCEC M8 at SC10 as well as AGU 2010 meeting. The scientific results and computational achievement of SCEC M8 were described in an SDSC press release and a DOE highlight article. SCEC Broadband Platform developments were presented at multiple NSF geoscience and computer science workshops including SDSC Data Intensive Computing Workshop October 2010 and TeraGrid 2011 meeting.

Draft 2012 Science Plan

SCEC Planning Committee

September 2011

I. Preamble

The Southern California Earthquake Center (SCEC) coordinates basic research in earthquake science using Southern California as its natural laboratory. SCEC emphasizes the connections between information gathering by sensor networks, fieldwork, and laboratory experiments; knowledge formulation through physics-based, system-level modeling; improved understanding of seismic hazard; and actions to reduce earthquake risk and promote resilience. The Center is a consortium of institutions that coordinates earthquake system science within Southern California. SCEC's long-term goal is to understand how seismic hazards change across all time scales of scientific and societal interest, from millennia to seconds. SCEC4 will move earthquake science forward through highly integrated collaborations that are coordinated across scientific disciplines and research institutions and enabled by high-performance computing and advanced information technology. It will focus on six fundamental problems of earthquake physics:

1. Stress transfer from plate motion to crustal faults: long-term fault slip rates.
2. Stress-mediated fault interactions and earthquake clustering: evaluation of mechanisms.
3. Evolution of fault resistance during seismic slip: scale-appropriate laws for rupture modeling.
4. Structure and evolution of fault zones and systems: relation to earthquake physics.
5. Causes and effects of transient deformations: slow slip events and tectonic tremor.
6. Seismic wave generation and scattering: prediction of strong ground motions.

The six fundamental problems constitute the basic-research focus of SCEC. They are interrelated and require an interdisciplinary, multi-institutional approach. Interdisciplinary research initiatives will focus on special fault study areas, the development of a community geodetic model for Southern California, and a community stress model. The latter will be a new platform where the various constraints on earthquake-producing stresses can begin to be integrated. Improvements will be made to SCEC's unified structural representation and its statewide extensions.

Collaboration Plan. On February 1, 2012, the Southern California Earthquake Center (SCEC) transitions from SCEC3 to SCEC4 under joint funding from NSF/EAR and the U.S. Geological Survey. SCEC4 is funded for the period February 2012 through January 2017. This document, referred to as the collaboration plan, solicits proposals from individuals and groups to participate in the first year of the SCEC4 research program.

II. Guidelines for Proposal Submission

A. ***Due Date.*** Friday, November 4, 2011, 5:00 pm PST. Late proposals will not be accepted. Note the different deadline for submitting annual progress reports below.

B. ***Delivery Instructions.*** Proposals must be submitted as PDF documents via the SCEC Proposal web site at *http://www.scec.org/proposals*. Submission procedures, including requirements for how to name your PDF files, will be found at this web site.

C. Formatting Instructions.

Cover Page. The cover page should be headed with the words "2012 SCEC Proposal" and include the project title, Principal Investigator(s), institutional affiliation, amount of request, and proposal categories (from types listed in Section IV). List (in order of priority) three science objectives (Section VII) that your proposal addresses, for example 1a, 3c and 4b. Indicate if the proposal should also be identified with one or more of the SCEC special projects (see Section X). Collaborative proposals involving multiple investigators and/or institutions should list all Principal

Investigators. Proposals do not need to be formally signed by institutional representatives, and should be for one year, with a start date of February 1, 2012.

Technical Description. Describe in up to five pages (including figures) the technical details of the project and how it relates to the short-term objectives outlined in the SCEC Research Priorities and Requirements (Section VII). If you have previously been funded by SCEC, you must include a one page summary of previous research results in this section. This summary is part of the five-page limit. References are not included in the five-page limit. See note below on submission of collaborative proposals.

Budget Page. Budgets and budget explanations should be constructed using NSF categories. Under guidelines of the SCEC Cooperative Agreements and A-21 regulations, secretarial support and office supplies are not allowable as direct expenses.

Current Support. Statements of current support, following NSF guidelines, should be included for each Principal Investigator. Any proposal without a current and pending support statement will not be reviewed.

Final SCEC3 Report. Scientists funded by SCEC in 2011 must submit a report of their progress by 5:00 pm PST February 29, 2012. Submission of this report is critical to preparing the final SCEC3 report to the funding agencies. 2012 proposals approved by the PC will not be funded if this progress report is not submitted on time. Reports should be up to five pages of text and figures. Reports should include bibliographic references to any SCEC publication during the past year (including papers submitted and in review), including their SCEC contribution number. Publications are assigned numbers when they are submitted to the SCEC publication database at *http://www.scec.org/signin*.

Special Note on Workshop Reports. Reports on results and recommendations of workshops funded by SCEC in 2012 are to be submitted no later than 30 days following the completion of the workshop. The reports will be posted on the SCEC web site as soon as possible after review by SCEC directors.

Labeling the Submitted PDF Proposal. PI's must follow the proposal naming convention. Investigators must label their proposals with their last name followed by 2012, e.g., Beroza2012.pdf. If there is more than one proposal, then the file would be labeled as: Beroza2012_1.pdf (for the 1st proposal) and Beroza2012_2.pdf (for the 2nd proposal).

D. ***Principal Investigator Responsibilities.*** PI's are expected to interact with other SCEC scientists on a regular basis (e.g., by attending the annual meeting, workshops and working group meetings), and contribute data, analysis results, and/or models to the appropriate SCEC data center (e.g., Southern California Earthquake Data Center—SCEDC), database, or community model (e.g., Community Velocity Model—CVM). Publications resulting entirely or partially from SCEC funding must include a publication number available at *http://www.scec.org/signin*. By submitting a proposal, investigators are agreeing to these conditions.

E. ***Eligibility.*** Proposals can be submitted by eligible Principal Investigators from:

- U.S. Academic institutions
- U.S. Private corporations
- International Institutions (funding will mainly be for travel and only travel to SCEC sponsored meetings in the US are eligible for support)

F. ***Collaboration.*** Collaborative proposals with investigators from the USGS are encouraged. USGS employees should submit their requests for support through USGS channels. Collaborative proposals involving multiple investigators and/or institutions are strongly encouraged; these can be submitted with the same text, but with different institutional budgets if more than one institution is involved.

A collaborative proposal should be submitted only by the lead PI. Information on all co-PI's (including budgets and current support statements) must be included in one proposal submission. Collaborative proposals may include one extra page per PI to report results of previous research.

G. ***Budget Guidance.*** Typical SCEC grants funded under this Science Plan in the past have fallen in the range of $10,000 to $35,000. This is not intended to limit SCEC to a fixed award amount, nor to a specified number of awards, rather it is intended to calibrate expectations for proposals written by first-time SCEC investigators.

H. ***Award Procedures.*** All awards will be funded by subcontract from the University of Southern California. The Southern California Earthquake Center is funded by the National Science Foundation and the U.S. Geological Survey.

III. SCEC Organization

A. ***Mission and Science Goal.*** SCEC is an interdisciplinary, regionally focused organization with a mission to:

- Gather data on earthquakes in Southern California and elsewhere where such data has direct relevance to southern California (field research investigations outside southern California will not be supported)
- Integrate information into a comprehensive, physics-based understanding of earthquake phenomena
- Communicate understanding to the world at large as useful knowledge for reducing earthquake risk

SCEC's primary science goal is to develop a comprehensive, physics-based understanding of earthquake phenomena in Southern California through integrative, multidisciplinary studies of plate-boundary tectonics, active fault systems, fault-zone processes, dynamics of fault ruptures, ground motions, and seismic hazard analysis.

B. ***Disciplinary Activities.*** The Center sustains disciplinary science through standing committees in seismology, geodesy, geology, and computational science. These committees will be responsible for planning and coordinating disciplinary activities relevant to the SCEC science plan, and they will make recommendations to the SCEC Planning Committee regarding support of disciplinary research and infrastructure. High-priority disciplinary activities are summarized in Section VIII.

C. ***Interdisciplinary Focus Areas.*** Interdisciplinary research is organized within seven science focus areas: 1) Unified Structural Representation (USR), 2) Fault and Rupture Mechanics (FARM), 3) Stress and Deformation Over Time (SDOT), 4) Earthquake Forecasting and Predictability (EFP), 5) Ground Motion Prediction (GMP), 6) Southern San Andreas Fault Evaluation (SOSAFE), and 7) Earthquake Engineering Implementation Interface (EEII). High-priority activities are listed for each of these interdisciplinary focus areas in Section IX.

D. ***Technical Activity Groups.*** Various groups of experts have formed Technical Activity Groups (TAGs) to verify the complex computer calculations needed for wave propagation and dynamic rupture problems, to assess the accuracy and resolving power of source inversions, and to develop geodetic transient detectors and earthquake simulators. TAGs can be thought of as "mini-collaboratories" that pose well-defined “standard problems”, encourage solution of these problems by different researchers using different algorithms or codes, develop a common cyberspace for comparing solutions, and facilitate meetings to discuss discrepancies and potential improvements.

E. ***Communication, Education, and Outreach.*** The theme of the CEO program during SCEC4 is *Creating an Earthquake and Tsunami Resilient California*. CEO will continue to manage and expand a suite of successful activities along with new initiatives, within four CEO interconnected thrust areas:

a. The Implementation Interface connects SCEC scientists with partners in earthquake engineering research, and communicates with and trains practicing engineers and other professionals.

b. The Public Education and Preparedness thrust area educates people of all ages about earthquakes, and motivates them to become prepared.

c. The K-14 Earthquake Education Initiative seeks to improve earth science education and school earthquake safety.

d. Finally, the Experiential Learning and Career Advancement program provides research opportunities, networking, and more to encourage and sustain careers in science and engineering.

Opportunities for participating in the CEO program are described in Section XI.

IV. Proposal Categories

A. ***Data Gathering and Products.*** SCEC coordinates an interdisciplinary and multi-institutional study of earthquakes in Southern California, which requires data and derived products pertinent to the region. Proposals in this category should address the collection, archiving and distribution of data, including the production of SCEC community models that are on-line, maintained, and documented resources for making data and data products available to the scientific community.

B. ***Integration and Theory.*** SCEC supports and coordinates interpretive and theoretical investigations on earthquake problems related to the Center's mission. Proposals in this category should be for the integration of data or data products from Category A, or for general or theoretical studies. Proposals in Categories A and B should address one or more of the goals in Section VII, and may include a brief description (<200 words) as to how the proposed research and/or its results might be used in a special initiative (see Section X) or in an educational or outreach mode (see Section XI).

C. ***Workshops.*** SCEC participants who wish to host a workshop between February 2012 and January 2013 should submit a proposal for the workshop in response to this RFP. This includes workshops that might be organized around the SCEC annual meeting in September. Workshops in the following topics are particularly relevant:

- Organizing collaborative research efforts for the five-year SCEC program (2012-2017). In particular, interactive workshops that engage more than one focus and/or disciplinary group are strongly encouraged.
- Engaging earthquake engineers and other partner and user groups in SCEC-sponsored research.
- Participating in national initiatives such as EarthScope, the Advanced National Seismic System (ANSS), and the George E. Brown, Jr. Network for Earthquake Engineering Simulation (NEES).

D. ***Communication, Education, and Outreach.*** SCEC has developed a long-range CEO plan and opportunities for participation are listed in Section XI. Investigators who are interested in participating in this program should contact Mark Benthien (213-740-0323; *benthien@usc.edu*) before submitting a proposal.

E. ***SCEC/SURE Intern Project.*** If your proposal includes undergraduate funding, please note this on the cover page. Each year SCEC coordinates the SCEC Summer Undergraduate Research Experience (SCEC/SURE) program to support one-on-one student research with a SCEC scientist. See http://www.scec.org/internships for more information. SCEC will be recruiting mentors in the Fall, and will request descriptions of potential projects via email. In December, these descriptions will be published on the SCEC Internship web page to allow applicants to identify their preferred projects.

Mentors are encouraged to provide at least $2500 of the $5000 intern stipend. Mentor contributions can come from any source, including SCEC-funded research projects. Therefore, interested SCEC scientists are encouraged to include support for an undergraduate intern in their 2012 SCEC proposals, and then respond to the recruitment emails. Questions about the SCEC/SURE Intern Project should be referred to Robert de Groot, *degroot@usc.edu*.

F. ***SCEC Annual Meeting participation.*** Investigators who wish to only request funding to cover travel to the annual meeting can participate in a streamlined review process with an abbreviated proposal. Investigators who are already funded to study projects that would be of interest to the SCEC community, and investigators new to SCEC who would benefit from exposure to the Annual Meeting in order to fine-tune future proposals are encouraged to apply.

V. Evaluation Process and Criteria

A. Proposals should be responsive to the RFP. A primary consideration in evaluating proposals will be how directly the proposal addresses the main objectives of SCEC. Important criteria include (not necessarily in order of priority):

1. Scientific merit of the proposed research
2. Competence and performance of the investigators, especially in regard to past SCEC-sponsored research
3. Priority of the proposed project for short-term SCEC objectives as stated in the RFP
4. Promise of the proposed project for contributing to long-term SCEC goals as reflected in the SCEC science plan (see Appendix).
5. Commitment of the P.I. and institution to the SCEC mission
6. Value of the proposed research relative to its cost
7. Ability to leverage the cost of the proposed research through other funding sources
8. Involvement of students and junior investigators
9. Involvement of women and underrepresented groups
10. Innovative or "risky" ideas that have a reasonable chance of leading to new insights or advances in earthquake physics and/or seismic hazard analysis.

B. Proposals may be strengthened by describing:
   1. Collaboration
      - Within a disciplinary or focus group
      - Between disciplinary and/or focus groups
      - In modeling and/or data gathering activities
      - With engineers, government agencies, and others. (See Section XI)
   2. Leveraging additional resources
      - From other agencies
      - From your institution
      - By expanding collaborations
   3. Development and delivery of products
      - Community research tools, models, and databases
      - Collaborative research reports
      - Papers in research journals
      - End-user tools and products
      - Workshop proceedings and CDs
      - Fact sheets, maps, posters, public awareness brochures, etc.
      - Educational curricula, resources, tools, etc.
   4. Educational opportunities
      - Graduate student research assistantships
      - Undergraduate summer and year-round internships (funded by the project)
      - K-12 educator and student activities
        - Presentations to schools near research locations
        - Participation in data collection

C. All research proposals will be evaluated by the appropriate disciplinary committees and focus groups, the Science Planning Committee, and the Center Director. CEO proposals will be evaluated by the CEO Associate Director and the Center Director.

D. The Science Planning Committee is chaired by the Deputy Director and comprises the chairs of the disciplinary committees, focus groups, and special projects. It is responsible for recommending a balanced science budget to the Center Director.

E. Recommendations of the planning committees will be combined into an annual spending plan and forwarded to the SCEC Board of Directors for approval.

F. Final selection of research projects will be made by the Center Director, in consultation with the Board of Directors.

G. The review process should be completed and applicants notified by the end of February, 2012.

VI. Coordination of Research between SCEC and USGS-EHRP

Earthquake research in Southern California is supported both by SCEC and by the USGS Earthquake Hazards Reduction Program (EHRP). EHRP's mission is to provide the scientific information and knowledge necessary to reduce deaths, injuries, and economic losses from earthquakes. Products of this program include timely notifications of earthquake locations, size, and

potential damage, regional and national assessments of earthquakes hazards, and increased understanding of the cause of earthquakes and their effects. EHRP funds research via its External Research Program, as well as work by USGS staff in its Pasadena, Menlo Park, and Golden offices. The EHRP also directly supports SCEC.

SCEC and EHRP coordinate research activities through formal means, including USGS membership on the SCEC Board of Directors and a Joint Planning Committee, and through a variety of less formal means. Interested researchers are invited to contact Dr. Ken Hudnut, EHRP coordinator for Southern California, or other SCEC and EHRP staff to discuss opportunities for coordinated research.

The USGS EHRP supports a competitive, peer-reviewed, external program of research grants that enlists the talents and expertise of the academic community, State and local governments, and the private sector. The investigations and activities supported through the external program are coordinated with and complement the internal USGS program efforts. This program is divided into six geographical/topical 'regions', including one specifically aimed at Southern California earthquake research and others aimed at earthquake physics and effects and at probabilistic seismic hazard assessment (PSHA). The Program invites proposals that assist in achieving EHRP goals.

The EHRP web page, *http://earthquake.usgs.gov/research/external/*, describes program priorities, projects currently funded, results from past work, and instructions for submitting proposals. The EHRP external funding cycle is several months offset from SCEC's, with the RFP due out in February and proposals due in May. Interested PI's are encouraged to contact the USGS regional or topical coordinators for Southern California, Earthquake Physics and Effects, and/or National (PSHA) research, as listed under the "Contact Us" tab.

The USGS internal earthquake research program is summarized by topic at *http://earthquake.usgs.gov/research/topics.php*.

VII. SCEC4 Fundamental Problems of Earthquake Physics: Research Priorities and Requirements

The six fundamental problems constitute the basic-research focus of SCEC4 and are listed in the preamble. They are interrelated and require an interdisciplinary, multi-institutional approach. Interdisciplinary research initiatives will focus on special fault study areas, the development of a community geodetic model for Southern California, and a community stress model. The latter will be a new platform where the various constraints on earthquake-producing stresses can begin to be integrated. Improvements will be made to SCEC's unified structural representation and its statewide extensions.

1. ***Stress transfer from plate motion to crustal faults: long-term fault slip rates.***

   Priorities and Requirements

   1a. Mapping and studying faults for which brittle/ductile transitions have been exposed by detachment faulting or erosion.

   1b. Focused laboratory, numerical, and geophysical studies of the character of the lower crust, its rheol- ogy, stress state, and expression in surface deformation. We will use surface-wave dispersion to im- prove depth resolution relative to teleseismic studies.

   1c. Regional searches for seismic tremor at depth in Southern California to observe if (some) deformation occurs by slip on discrete structures.

   1d. Development of a Community Geodetic Model (CGM) for California, in collaboration with the UNAVCO community, to constrain long-term deformation and fault-slip models.

   1e. Combined modeling/inversion studies to interpret GPS and InSAR geodetic results on postseismic transient deformation without traditional simplifying assumptions.

2. ***Stress-mediated fault interactions and earthquake clustering: evaluation of mechanisms***

   Priorities and Requirements

2a. Improvement of earthquake catalogs, including non-point-source source descriptions, over a range of scales. Traditional aftershock catalogs can be improved through better detection of early aftershocks. Long-term (2000-yr) earthquake chronologies, including slip-per-event data, for the San Andreas Fault system are necessary to constrain long-term clustering behavior.

2b. Improved descriptions of triggered earthquakes. While temporal earthquake clustering behavior (Omori's Law) is well-known, the spatial and coupled temporal-spatial behavior of triggered earth- quakes, potentially key diagnostics, are not well constrained.

2c. Lowered thresholds for detecting aseismic and infraseismic transients, and improved methods for separating triggering by aseismic transients from triggering by other earthquakes.

2d. Development of a Community Stress Model (CSM) for Southern California, based on merging information from borehole measurements, focal mechanisms, paleoslip indicators, observations of damage, topographic loading, geodynamic and earthquake-cycle modeling, and induced seismicity. We will use seismicity to constrain CSM and investigate how stress may control earthquake clustering and triggering. We plan to collaborate with other organizations in fault-drilling projects for in situ hypothesis testing of stress levels.

2e. Development of physics-based earthquake simulators that can unify short-term clustering statistics with long-term renewal statistics, including the quasi-static simulators that incorporate laboratory- based nucleation models.

2f. Better understanding of induced seismicity, specifically induced by geothermal power production in the Salton Sea area, which warrant study as potential hazards. Recent research suggests that microseismicity in the geothermal fields near the Brawley seismic zone may affect and be affected by seismicity on tectonic faults at these distances.

3. Evolution of fault resistance during seismic slip: scale-appropriate laws for rupture modeling

Priorities and Requirements

3a. Laboratory experiments on fault materials under appropriate confining stresses, temperatures, and fluid presence through targeted experiments in collaboration with rock mechanics laboratories.

3b. Search for geological, geochemical, paleotemperature, and hydrological indicators of specific resis- tance mechanisms that can be measured in the field. In particular, we will look for evidence of ther- mal decomposition in exhumed fault zones.

3c. Theoretical and numerical modeling of specific fault resistance mechanisms for seismic radiation and rupture propagation, including interaction with fault roughness and damage-zone properties. At the scale of meters to hundreds of meters, the behavior of the near-fault layer with evolving damage may have to be included in the fault constitutive relations.

3d. Development of parameterized fault rheologies suitable for coarse-grained numerical modeling of rupture dynamics and for simulations of earthquake cycles on interacting fault systems. Currently, the constitutive laws for co-seismic slip are often represented as complex coupled systems of partial differential equations, contain slip scales of the order of microns to millimeters, and hence allow de- tailed simulations of only small fault stretches (Fig. 3.8).

3e. Dynamic rupture modeling to constrain stress levels along major faults, explain the heat-flow para- dox, and understand extreme slip localization and the dynamics of self-healing ruptures. We will use improved seismic slip inversions to constrain the local rupture durations and evolution of fault friction. We will collaborate with other organizations in fault-drilling projects to measure temperature on faults before and after earthquakes and thus constrain co-seismic resistance.

3f. Development of earthquake simulators that can incorporate realistic models of fault-resistance evolution during the earthquake cycle.

4. Structure and evolution of fault zones and systems: relation to earthquake physics

Priorities and Requirements

4a. Establishment of special fault study areas for detailed geologic, seismic, geodetic, and hydrologic investigations of fault complexities

4b. Investigations of along-strike variations in fault roughness and complexity as well as the degree of localization and damage perpendicular to the fault.

4c. Improvements to the CFM using better mapping, including lidar, and precise earthquake relocations. We will also extend the CFM to include spatial uncertainties and stochastic descriptions of fault heterogeneity.

4d. Use of special fault study areas to model stress heterogeneities both deterministically and stochastically. We will integrate the results of these special studies into the CSM.

4e. Use of earthquake simulators and other modeling tools, together with the CFM and CSM, to quantify how large-scale fault system complexities govern the probabilities of large earthquakes and rupture sequences.

5. Causes and effects of transient deformations: slow slip events and tectonic tremor

Priorities and Requirements

5a. Improvement of detection and mapping of the distribution of tremor across southern California by applying better instrumentation and signal-processing techniques to data collected in the special study areas, including the Cholame segment of the San Andreas fault (Area A of Fig. 3.12), where the tectonic tremor was first identified in California and the southern termination of the San Andreas fault near Bombay Beach, which is the locus of an intense swarm activity.

5b. Application of geodetic detectors to the search for aseismic transients across southern California. We will use the CGM as the time-dependent geodetic reference frame for detecting geodetic anomalies.

5c. Collaboration with rock mechanics laboratories on laboratory experiments to understand the mechanisms of slow slip and tremor.

5d. Development of physics-based models of slow slip and tectonic tremor. We will constrain these models using features of tremor occurrence and its relationship to seismicity, geodetic deformation, and tectonic environment, as well as laboratory data.

5e. Use of physics-based models to understand how slow slip events and tremor activity affect earthquake probabilities in Southern California.

6. Seismic wave generation and scattering: prediction of strong ground motions

Priorities and Requirements

6a. Development of a statewide anelastic Community Velocity Model (CVM) that can be iteratively refined through 3D waveform tomography. We will extend current methods of full-3D tomography to include ambient-noise data and to estimate seismic attenuation, and we will develop methods for estimating and representing CVM uncertainties.

6b. Modeling of ruptures that includes realistic dynamic weakening mechanisms, off-fault plastic deformation, and is constrained by source inversions. The priority is to produce physically consistent source models for broadband ground motion simulation. An important issue is how to treat multiscale processes; specifically, does off-fault plasticity regularize the Lorentzian scale collapse associated with strong dynamic weakening? If not, how can adaptive meshing strategies be most effectively used to make full-physics simulations feasible?

6c. Develop stochastic representations of small-scale velocity and attenuation structure in the CVM for use in modeling high-frequency (> 1 Hz) ground motions. We will test the stochastic models with seismic and borehole logging data and evaluate their transportability to regions of comparable geology.

6d. Measure earthquakes with unprecedented station density using emerging sensor technologies (e.g., MEMS). The SCEC Portable Broadband Instrument Center will work with IRIS to make large portable arrays available for aftershock and flexible array studies.

6e. Collaborate with the engineering community in validation of ground motion simulations. We will establish confidence in the simulation-based predictions by continuing to work with engineers in validating the simulations against empirical attenuation models and exploring coherency and other standard engineering measures of ground motion properties.

VIII. Disciplinary Activities

The Center will sustain disciplinary science through standing committees in seismology, geodesy, and geology. These committees will be responsible for planning and coordinating disciplinary activities relevant to the SCEC science plan, and they will make recommendations to the SCEC Planning Committee regarding the support of disciplinary infrastructure. High-priority disciplinary objectives include the following tasks:

A. Seismology

Objectives. The objectives of the Seismology group are to gather data on the range of seismic phenomena observed in southern California and to integrate these data into physics-based models of fault slip. Of particular interest are proposals that foster innovations in network deployments, data collection, real-time research tools, and data processing. Proposals that provide community products that support one or more of the SCEC4 goals or those that include collaboration with network operators in Southern California are especially encouraged. Proposers should consider the SCEC resources available including the Southern California Earthquake Data Center (SCEDC) that provides extensive data on Southern California earthquakes as well as crustal and fault structure, the network of SCEC funded borehole instruments that record high quality reference ground motions, and the pool of portable instruments that is operated in support of targeted deployments or aftershock response.

Research Strategies. Examples of research strategies that support the objectives above include: Enhancement and continued operation of the SCEDC and other existing SCEC facilities particularly the near-real-time availability of earthquake data from SCEDC and automated access. Real-time processing of network data such as improving the estimation of source parameters in relation to known and unknown faults, especially evaluation of the short term evolution of earthquake sequences and real-time stress perturbations on nearby major fault segments. Enhance or add new capabilities to existing earthquake early warning (EEW) systems or provide new EEW algorithms. Develop real-time finite source models constrained by incoming seismic and GPS data to estimate evolution of the slip function and potentially damaging ground shaking. Advance innovative and practical strategies for densification of seismic instrumentation, including borehole instrumentation, in Southern California and develop innovative algorithms to utilize data from these networks. Develop metadata, archival and distribution models for these semi-mobile networks. Develop innovative new methods to search for unusual signals using combined seismic, GPS, and borehole strainmeter data; collaborations with EarthScope or other network operators are encouraged. Investigate near-fault crustal properties, evaluate fault structural complexity, and develop constraints on crustal structure and state of stress. Collaborations, for instance with the ANSS and NEES projects, that would augment existing and planned network stations with downhole and surface instrumentation to assess site response, nonlinear effects, and the ground coupling of built structures. Preliminary design and data collection to seed future passive and active experiments such as dense array measurements of basin structure and large earthquake properties, OBS deployments, and deep basement borehole studies.

Priorities for Seismology in 2012.

1. ***Tremor.*** Tremor has been observed on several faults in California, yet tremor does not appear to be ubiquitous. We seek proposals that explore the distribution and source characteristics of tremor in California and those that explore the conditions necessary for the generation of seismically observable tremor.
2. ***Low-cost seismic network data utilization and archiving.*** Several groups are developing seismic networks that use low-cost MEMS accelerometers. We seek proposals that would address development of seismological algorithms to utilize data from these networks in innovative ways. We also seek proposals that would develop metadata and archiving models for these new semi-mobile networks, as well as archive and serve these data to the SCEC user community.
3. ***The 2010 M7.2 El Mayor-Cucapah Earthquake Sequence.*** The El Mayor sequence ruptured for a distance of more than 120 km, and large data sets were recorded by the SCSN, RESNOM, portable temporary networks, and GPS networks. Proposals that seek to analyze these data and other relevant data sets in the context of SCEC research priorities are welcome.

B. Tectonic Geodesy

Tectonic Geodesy activities in SCEC4 will focus on data collection and analysis that contribute to improved earthquake response and to a better understanding of fault loading and stress transfer, the causes and effects of transient deformation, and the structure and evolution of fault zones and systems. The following are research strategies aimed at meeting these broad objectives:

Contribute to the development of a Community Geodetic Model (CGM).

The goal of this effort is to develop a time-dependent geodetic data product for southern California that leverages the complementary nature of GPS and InSAR time series data. The resulting product will consist of well-constrained, temporally and spatially dense horizontal and vertical displacement time series that can be used in meeting a variety of SCEC4 objectives. This effort will require development of optimal methods for combining GPS and InSAR data, mitigating hydrologic/anthropogenic signals, incorporating new data, and accounting for earthquake effects as needed.

Data collection and analysis designed to address specific questions regarding geodetic/geologic slip rate discrepancies, to assess the role of lower crust/upper mantle processes in driving fault loading, to constrain more physically-realistic deformation models, and to provide input to the development of Community Stress Models are also encouraged, as are studies that pursue integrated use of geodetic, geologic, seismic, and other observations targeting special fault study areas. Proposals for the development of new data products or collection of new data should explicitly motivate the need for such efforts and state how the resulting data or products will be used. Resulting data should be provided for inclusion in the CGM. In compliance with SCEC's data policy, data collected with SCEC funding must be made publically-available upon collection by archiving at an appropriate data center (e.g., UNAVCO).

Improve our understanding of the processes underlying detected transient deformation signals and/or their seismic hazard implications through data collection and development of new analysis tools.

Work that advances methods for near-real-time transient detection and applies these algorithms within the SCEC transient detection testing framework to search for transient deformation in southern California is encouraged. Approaches that can be automated or semi-automated are the highest priority, as is their inclusion in the testing framework now in place at SCEC. Extension of methods to include InSAR and strainmeter data and, when available, the CGM is also a priority.

Targeted collection and analysis of all types of geodetic data to constrain physics-based models of slow slip and tremor are also encouraged.

Develop and apply algorithms that use real-time high-rate GPS data in concert with seismic data for improved earthquake response.

C. Earthquake Geology

Objectives. The Earthquake Geology Disciplinary Group promotes studies of the geologic record of the Southern California natural laboratory that advance SCEC science. Its primary focus is on the Late Quaternary record of faulting and ground motion, including data gathering in response to major earthquakes. Geologic observations provide important contributions, either directly or indirectly, to all six of the fundamental problems in earthquake physics identified in the SCEC4 proposal. Earthquake Geology also fosters research activities motivated by outstanding seismic hazard issues, understanding of the structural framework and earthquake history of special fault study areas (see fundamental problem 4), or will contribute significant information to the statewide Unified Structural Representation. Collaborative proposals that cut across disciplinary boundaries are especially competitive.

Example Research Strategies

- Gathering well-constrained slip-rates on the southern California fault system, with emphasis on major structures (Problem 1).
- Mapping and analysis of fault-zone properties where the seismogenic zone or brittle-ductile transition has been exhumed (Problems 1.a; 3.b).
- Paleoseismic documentation of earthquake ages and displacements, with emphasis on long paleoseismic histories, slip-per-event, and slip-rate histories, including a coordinated effort to develop slip rates and slip-per-event history of southern San Andreas fault system (Problem 2.a, in collaboration with the SoSAFE focus group).
- Studies to improve understanding of special fault study areas (Problem 4.a) or to improve the statewide community fault model, especially that take advantage of high-resolution topographic data sets to better define fault traces, spatial uncertainty, and stochastic heterogeneity of fault geometry (Problem 4.c).

- Quantifying along-strike variations in fault roughness, complexity, strain localization, and damage in relation to the rupture propagation processes, including evaluation of the investigating the processes and likelihood of multi-fault ruptures (Problem 4.b).
- Validation of ground motion prediction through analysis and dating of precariously balanced rocks and other fragile geomorphic features (Problem 6).

Geochronology Infrastructure. The shared geochronology infrastructure supports C-14, optically stimulated luminescence (OSL), and cosmogenic dating for SCEC-sponsored research. The purpose of shared geochronology infrastructure is to allow flexibility in the number and type of dates applied to each SCEC-funded project as investigations proceed. Investigators requesting geochronology support should clearly state in their proposal an estimate of the number and type of dates required. For C-14 specify if sample preparation will take place at a location other than the designated laboratory. For cosmogenic dating, investigators are required to arrange for sample preparation. Sample preparation costs must be included in the proposal budget unless preparation has been pre-arranged with one of the laboratories listed. Investigators are strongly encouraged to contact the investigators at the collaborating laboratories prior to proposal submission. Currently, SCEC geochronology has established relationships with the following laboratories:

- C-14: University of California at Irvine (John Southon, jsouthon@uci.edu) and Lawrence Livermore National Laboratory (Tom Guilderson, tguilderson@llnl.gov).
- OSL: University of Cincinnati (Lewis Owen, lewis.owen@uc.edu) and Utah State University (Tammy Rittenour, tammy.rittenour@usu.edu)
- Cosmogenic: Lawrence Livermore National Laboratory (Dylan Rood, rood5@llnl.gov).

Investigators may alternatively request support for geochronology outside of the infrastructure proposal for methods not listed here or if justified on a cost-basis. These outside requests must be included in the individual proposal budget. Please direct questions regarding geochronology infrastructure to the Earthquake Geology group leader, Mike Oskin (*meoskin@ucdavis.edu*).

Data Reporting Requirements. Studies under Earthquake Geology gather diverse data that are at times challenging to consistently archive per NSF data reporting requirements. Under SCEC4, PIs will be required to provide full reporting of their geochronology samples, including raw data, interpreted age, and geographic/stratigraphic/geomorphic context (what was dated?). This reporting requirement will be coordinated with the geochronology infrastructure program. A priority at the outset of SCEC4 is to do define additional, achievable goals for geology data reporting to be followed by Earthquake Geology community.

Priorities for Earthquake Geology in 2012

- Establishment of special fault study areas and formulation of research strategies for these sites
- Prioritization of research objectives, especially with respect to SoSAFE focus group goals, targets for slip-rate studies, and mechanisms to achieve progress on exhumed fault-zone problems.
- Defining consistent and acheivable data reporting requirements for Earthquake Geology in SCEC4

D. Computational Science

Objectives. The Computational Science group promotes the use of advanced numerical modeling techniques and high performance computing (HPC) to address the emerging needs of SCEC users and application community on HPC platforms. The group works with SCEC scientists across a wide range of topics to take advantage of rapidly changing computer architectures and algorithms. It also engages and coordinates with HPC labs/centers as well as the vendor community in crosscutting efforts enabling SCEC petascale computing milestones. The group encourages research using national supercomputing resources, and supports students from both geoscience and computer science backgrounds to develop their skills in the area.

Research Strategies. Examples of research strategies that support the objectives above include:

1. Assist modelers with porting and optimizing codes on new architectures.

2. Evaluate novel algorithms for earthquake simulation, particularly those that either improve efficiency and accuracy or expand the class of problems that can be solved (e.g., adaptive mesh refinement).
3. Support optimization of earthquake simulators that can resolve the faulting processes across the range of scales required to investigate stress-mediated fault interaction, generate synthetic seismicity catalogs, and assess the viability of earthquake rupture forecasts.
4. Foster and help coordinate a research and development effort utilizing advanced techniques for addressing accelerating technologies such as hybrid MPI/OpenMP, MPI/CUDA, PGAS, and auto-tuning; and preparing the community for sea changes in architecture towards exascale computing.
5. Support development of a community model framework for managing I/O, data repositories, workflow and management, analysis/visualization tools, reliability and resilience capabilities.
6. Identify and develop the necessary tools for data-intensive computing, including but not limited to 3D tomography, cross-correlation algorithms used in ambient noise seismology, and other signal processing techniques used, for example, to search for tectonic tremor.
7. Provide coordinated support to the community on large resource allocation proposals.
8. Participate in major CME projects.

Key Problems in Computational Science

1. Seismic wave propagation
   - Validate SCEC community velocity models.
   - Develop high-frequency simulation methods and investigate the upper frequency limit of deterministic ground motions.
   - Extend existing simulation methodologies to a set of stochastic wavefield simulation codes that can extend the deterministic calculations to frequencies as high as 20 Hz, providing with the capability to synthesize "broadband" seismograms.
2. Tomography
   - Assimilate regional waveform data into the SCEC community velocity models.
3. Rupture dynamics
   - Evaluate proposed fault weakening mechanisms in large-scale earthquake simulations, determine if small-scale physics is essential or irrelevant, and determine if friction law parameters can be artificially enhanced without compromising ground motion predictions.
   - Evaluate different representations of source complexity, including stress heterogeneity, variability in frictional properties, and fault geometrical complexity.
4. Scenario earthquake modeling
   - Model a suite of scenario ruptures, incorporating material properties and fault geometries from the unified structural representation projects.
   - Isolate causes of enhanced ground motion using adjoint-based sensitivity methods.
5. Engineering applications
   - Facilitate the "rupture-to-rafters" modeling capability to transform earthquake risk management into a CS&E discipline.

IX. Interdisciplinary Focus Areas

Interdisciplinary research will be organized into seven science focus areas: 1) Unified Structural Representation (USR), 2) Fault and Rupture Mechanics (FARM), 3) Stress and Deformation Over Time (SDOT), 4) Earthquake Forecasting and Predictability (EFP), 5) Ground Motion Prediction (GMP), 6) Southern San Andreas Fault Evaluation and 7) Earthquake Engineering Interface (EEII).

High-priority objectives are listed below for each of the seven interdisciplinary focus areas. Collaboration within and across focus areas is strongly encouraged.

A. Unified Structural Representation (USR)

The Unified Structural Representation group develops three-dimensional models of active faults and earth structure (velocity, density, attenuation, etc.) for use in fault-system analysis, ground-motion prediction, and hazard assessment. This year's efforts will focus on (1) making improvements to existing community models (CVM, CFM) that will facilitate their uses in SCEC science, education, and post-earthquake response planning and (2) expanding into a new area of emphasis by developing methods to represent smaller scale features, such as the detailed representations needed for the special fault study areas and stochastic variations of seismic velocities and attenuation structure.

- ***Community Velocity Model (CVM).*** Improve the current SCEC CVMs, with emphasis on more accurate representations of Vp, Vs, density, attenuation, and basin structure. Generate improved mantle Vp and Vs models, as well as more accurate descriptions of near-surface properties that can be incorporated into the models' geotechnical layers. Perform 3D waveform tomographic inversions and ambient noise analysis for evaluating and improving the CVMs. Develop and apply procedures (i.e., goodness-of-fit measures) for evaluating the existing and future models with data (e.g., waveforms, gravity) to distinguish alternative representations and quantify model uncertainties; apply these methods for well-recorded earthquakes in southern California to delineate areas where CVM updates are needed. Develop databases, models, and model building tools that will help facilitate expansion of the CVMs to statewide and plate-boundary scale velocity representations. These efforts should be coordinated with the SCEC CME special project.
- ***Community Fault Model (CFM).*** Improve and evaluate the CFM, placing emphasis on defining the geometry of major faults that are incompletely, or inaccurately, represented in the current model. Extend the CFM to include spatial uncertainties and stochastic descriptions of fault heterogeneity. Evaluate the CFM with data (e.g., seismicity, seismic reflection profiles, geodetic displacement fields) to distinguish alternative fault models. Evaluate the new statewide fault model (SCFM), and update the CFM-R (rectilinear fault model) to reflect improvements in the CFM.
- ***Unified Structural Representation (USR).*** Develop better IT mechanisms for delivering the USR, particularly the CVM parameters and information about the model's structural components, to the user community for use in generating and/or parameterizing numerical models. Generate maps of geologic surfaces compatible with the CFM that may serve as strain markers in crustal deformation modeling and/or property boundaries in future iterations of the USR.

B. Fault and Rupture Mechanics (FARM)

The primary mission of the Fault and Rupture Mechanics focus group in SCEC4 is to develop physics-based models of the nucleation, propagation, and arrest of dynamic earthquake rupture. We specifically solicit proposals that will contribute to the six fundamental problems in earthquake physics defined in the SCEC 4 proposal and enhance understanding of fault system behavior through interdisciplinary investigation of special fault study areas. We encourage researchers to address this mission through field, laboratory, and modeling efforts directed at characterizing and understanding the influence of material properties, geometric irregularities and heterogeneities in stress and strength over multiple length and time scales, and that will contribute to our understanding of earthquakes in the Southern California fault system.

Important goals include:

- Investigate the relative importance of different dynamic weakening and fault healing mechanisms, and the slip and time scales over which these mechanisms operate (3a, 3b, 3c, 3e).
- Determine the properties of fault cores and damage zones (1a, 1b, 3a, 3b, 4a, 4b) and characterize their variability with depth and along strike (1a, 1b, 4a, 4b) to constrain theoretical and laboratory studies, including width and

particle composition of actively shearing zones, signatures of temperature variations, extent, origin and significance of on- and off-fault damage, healing, and poromechanical behavior.

- Determine the relative contribution of on- and off-fault damage to the total earthquake energy budget (3c, 4a, 4b), and the absolute levels of local and average stress (3e).
- Develop realistic descriptions of heterogeneity in fault geometry, rock properties, stresses and strains, and tractable ways to incorporate heterogeneity in numerical models of single dynamic rupture events and multiple earthquake cycles (3e, 4b, 4d, 6b).
- Understand the significance of fault zone characteristics and processes on fault dynamics (3a, 3b, 3c) and formulate constitutive laws for use in dynamic rupture models (3d).
- Evaluate the relative importance of fault structure, material properties, interseismic healing, and prior seismic and aseismic slip to earthquake dynamics, in particular, to rupture initiation, propagation, and arrest, and the resulting ground motions (3c, 3d, 3f).
- Characterize earthquake rupture, fault loading, degree of localization, and constitutive behavior at the base of and below the seismogenic zone (1a, 1b, 1e, 4a)
- Develop observations of slow slip events and non-volcanic tremors in southern California and understand their implications for constitutive properties of faults and overall seismic behavior (3a, 5a-5e).
- Assess the predictability of rupture direction and directivity of seismic radiation by collecting and analyzing field and laboratory data (4a, 4b), and conducting theoretical investigations to understand implications for strong ground motion.
- Develop physics-based models that can describe spatio-temporal patterns of seismicity (2e, 4e)

C. Stress and Deformation Over Time (SDOT)

The focus of the interdisciplinary working group Stress and Deformation Over Time (SDOT) is to improve our understanding of how faults are loaded in the context of the wider lithospheric system evolution. SDOT studies these processes on timescales from 10s of Myr to 10s of yrs, using the structure, geological history, and physical state of the southern California lithosphere as a natural laboratory. The objective is to tie the present-day state of stress and deformation on crustal-scale faults and the lithosphere as a whole to the long-term, evolving lithospheric architecture, through 4D geodynamic modeling, constrained by the widest possible range of observables from disciplines including geodesy, geology, and geophysics.

One long-term goal is to contribute to the development of a physics-based, probabilistic seismic hazard analysis for southern California by developing and applying system-wide deformation models of lithospheric processes at time-scales down to the earthquake cycle. These deformation models require a better understanding of a range of fundamental questions such as the forces loading the lithosphere, the relevant rock rheology, fault constitutive laws, and the spatial distribution of absolute deviatoric stress. Tied in with this is a quest for better structural constraints, such as on density, Moho depths, thickness of the seismogenic layer, the geometry of lithosphere-asthenosphere boundary, as well as basin depths, rock type, temperature, water content, and seismic velocity and anisotropy.

Projects solicited for SDOT include:

A. Contributions to our understanding of geologic inheritance and evolution, and its relation to the three-dimensional structure and physical properties of present-day crust and lithosphere. Contributions to efforts of building a 4D model of lithospheric evolution over 10s of Myr for southern California.

B. Seismological imaging of crust, lithosphere and upper mantle using interface and transmission methods with the goal of characterizing the 3D distribution of isotropic and anisotropic wave speed variations.

C. Contributions to the development of a Community Stress Model (CSM), a set of spatio-temporal (4D) representations of the stress tensor in the southern California lithosphere.

D. Geodynamic models of southern California dynamics to allow hypothesis testing, including on issues pertaining to post-seismic deformation, fault friction, rehology of the lithosphere, seismic efficiency, the heat flow paradox, stress and strain transients (A5), fault system evolution, as tied in with stress and deformation measurements across scales.

E. Developments of models of interseismic and earthquake cycle deformation, including efforts to estimate slip rates on southern CA faults, fault geometries at depth, and spatial distribution slip or moment deficits on faults. Assessments of potential discrepancies of models based on geodetic, geologic, and seismic data (A1, A3).

F. Research into averaging, simplification, and coarse-graining approaches across spatio-temporal scales, addressing questions such as the appropriate scale for capturing fault interactions, the adequate representation of frictional behavior and dynamic processes in long-term interaction models, fault roughness, structure, complexity and uncertainty. Modeling approaches may include analytical or semi-analytical methods, spectral approaches, boundary, finite, or distinct element methods, and a mix of these (A10, A3), and there are strong links with all other SCEC working groups, including FARM, Earthquake Simulators, and USR.

D. Earthquake Forecasting and Predictability (EFP)

We seek proposals that will increase our understanding of how earthquakes might be forecast and whether or not earthquakes are predictable. Proposals of any type that can assist in this goal will be considered. In particular, proposals are welcome that will assist in attaining the goals of CSEP (the Collaboratory for the Study of Earthquake Predictability), WGCEP (the Working Group on California Earthquake Probabilities) and SoSAFE (the Southern San Andreas Evaluation).

For research strategies that plan to utilize CSEP, see the description of CSEP under Special Projects to learn of its capabilities. In order to increase the number of earthquakes in the data sets, and so decrease the time required to learn about predictability, proposals are welcome that deal with global data sets and/or include international collaborations. Successful investigators proposing to utilize CSEP would be funded via core SCEC funds to adapt their prediction methodologies to the CSEP framework, to transfer codes to the externally accessible CSEP computers, and to be sure they function there as intended. Subsequently, the codes would be moved to the identical externally inaccessible CSEP computers by CSEP staff who will conduct tests against a variety of data as outlined in the CSEP description. In general, methodologies will be considered successful only if they do better than null hypotheses that include both time-independent and time-dependent probabilities.

Proposals that can lead to understanding whether or not there exists a physical basis for earthquake predictability are welcome, even if they are not aimed toward, or are not ready for, tests in CSEP, or are not aimed toward assisting WGCEP or SoSAFE. We encourage proposals that

- support the development of statistical or physics-based real-time earthquake forecasts,
- utilize and/or evaluate the significance of earthquake simulator results,
- study how to properly characterize various earthquake-related statistical relationships (including the magnitude distribution, Omori law, aftershock productivity, etc.) for use in testing prediction algorithms,
- focus on understanding patterns of seismicity in time and space, as long as they are aimed toward understanding the physical basis of some aspect of extended earthquake predictability,
- develop useful measurement/testing methodology that could be incorporated in the CSEP evaluations, including those that address how to deal with observational errors in data sets.

E. Ground-Motion Prediction (GMP)

The primary goal of the Ground Motion Prediction focus group is to develop and implement physics-based simulation methodologies that can predict earthquake strong-motion waveforms over the frequency range 0-10 Hz. Source characterization plays a vital role in ground-motion prediction. At frequencies less than 1 Hz, the methodologies should deterministically predict the amplitude, phase and waveform of earthquake ground motions using fully three-dimensional representations of Earth structure, as well as dynamic or dynamically compatible kinematic representations of fault rupture. At higher frequencies (1-10 Hz), the methodologies should predict the main character of the amplitude, phase and waveform of the motions using a combination of deterministic and stochastic representations of fault rupture and wave propagation.

Research topics within the Ground-Motion Prediction program include:

- Developing and/or refining physics-based simulation methodologies, with particular emphasis on high frequency (1-10 Hz) approaches. This work could include implementation of simulation methodologies onto the Broadband Simulation Platform (in collaboration with CME).
- Waveform modeling of past earthquakes to validate and/or refine the structure of the Community Velocity Model (CVM) (in collaboration with USR).
- Incorporation of non-linear models of soil response.
- Development of more realistic implementations of dynamic or kinematic representations of fault rupture. This research could also include the examination of current source-inversion strategies and development of robust methods that allow imaging of kinematic and/or dynamic rupture parameters reliably and stably, along with a rigorous uncertainty assessment.
- Verification (comparison against theoretical predictions) and validation (comparison against observations) of the simulation methodologies with the objective of being to develop robust and transparent simulation capabilities that incorporate consistent and accurate representations of the earthquake source and three-dimensional velocity structure. Close collaboration with the Technical Activity Group (TAG) on Ground Motion Simulation Validation (GMSV).

It is expected that the products of the Ground-Motion Prediction group will have direct application to seismic hazard analysis, both in terms of characterizing expected ground-motion levels in future earthquakes, and in terms of directly interfacing with earthquake engineers in the analysis of built structures. Activities within the Ground Motion Prediction group will be closely tied to several special projects, including the GMSV TAG, with particular emphasis on addressing ground motion issues related to seismic hazard and risk (see EEII below).

F. Southern San Andreas Fault Evaluation (SoSAFE)

The SCEC Southern San Andreas Fault Evaluation (SoSAFE) Project has become a SCEC Interdisciplinary Focus Area in SCEC4 and will continue to increase our knowledge of slip rates, paleo-event chronology, and slip distributions of past earthquakes, for the past two thousand years on the southern San Andreas fault system. From Parkfield to Bombay Beach, and including the San Jacinto fault, the objective is to obtain new data to clarify and refine relative hazard assessments for each potential source of a future 'Big One.'

Past SoSAFE workshops have led to a focused research plan that responds to the needs and opportunities identified across existing research projects. We strongly welcome proposals that will:

- Help to improve correlation of ruptures over the past 2000 years. This includes short-term (3-5 earthquake) and slip-per-event data from paleoseismic sites, but can include longer-term rates (60,000 years) in some cases.
- Obtain the best possible measurements of geomorphic slip distributions from past earthquakes using field and LiDAR approaches and to validate the different measures.
- Lengthen existing paleoearthquake chronologies or start new sites in key locations along the fault system.
- Use novel methods for estimating slip rates from geodetic data.
- Investigate methodologies for integrating paleoseismic (including geomorphic measures of slip) and geologic data into rupture histories. For example, studies may improve or inform interactions between SoSAFE results and scenario rupture modeling or rupture forecasts.

It is expected that much support will go towards improved dating (e.g., radiocarbon and OSL) of earthquakes so that event correlations and coefficient of variation in recurrence intervals may be further refined. Requests for geochronology support (e.g., to date 12 radiocarbon samples) are encouraged and shall be coordinated with Earthquake Geology; a portion of SoSAFE funds will be contributed towards joint support for dating. We also welcome proposals that seek to add other data (such as climate variations) to earthquake chronologies, which may be used to improve age control, understanding of the formation of offset features, or site-to-site correlation of events.

Research will address significant portions of the fault system, and all investigators will agree to collaboratively review one another's progress and results. Research by single or multi-investigator teams will be supported to rapidly advance SCEC research towards meeting priority scientific objectives related to the mission of the SoSAFE's Interdisciplinary Focus. SoSAFE

objectives also foster common longer-term research interests and engage in facilitating future collaborations in the broader context of a decade-long series of interdisciplinary, integrated and complementary studies on the southern San Andreas Fault system.

The sixth year of SoSAFE will again be funded at $240K by USGS, although sustained support is contingent upon progress and productivity, effective leveraging of USGS funds with funds from other sources, and the level of available funding and competing demands within the USGS Multi-Hazards Demonstration Project.

G. Earthquake Engineering Implementation Interface (EEII)

The purpose of the EEII Focus Group is to create and maintain collaborations with research and practicing engineers, much as the Seismic Hazard and Risk Analysis focus group did in SCEC3. These activities may include ground motion simulation validation, rupture-to-rafters simulations of building response as well as the end-to-end analysis of large-scale, distributed risk (e.g., ShakeOut-type scenarios). Our goal of impacting engineering practice and large-scale risk assessments require even broader partnerships with the engineering and risk-modeling communities, which motivates the activities described next.

Technical Activity Group (TAG) on Ground Motion Simulation Validation (GMSV)

A TAG focusing on validation of ground motion simulations has been established to develop and implement testing/rating methodologies via collaboration between ground motion modelers and engineering users. A 2011 Workshop on this topic (http://www.scec.org/workshops/2011/gmsv/index.html) identified the following initial efforts as potential priority activities in this area, and proposals on these topics will be reviewed with all other SCEC proposals in January of 2012.

- Validation of simulated ground motions for past earthquakes using elastic and inelastic response spectra.
- Automation of the validation tests. In order to facilitate validation of other/future simulations, develop software modules for the validation of simulated ground motions for past earthquakes in terms of elastic and inelastic response spectra. Implementation into the SCEC Broadband Strong Motion Simulation Platform (http://scec.usc.edu/research/cme/groups/broadband), and/or use of the OpenSees (Open System for Earthquake Engineering Simulation) platform (http://peer.berkeley.edu/products/opensees.html) would be viewed positively.
- Validation of simulated ground motions for past earthquakes for multi-degree-of-freedom (MDoF) nonlinear building systems.
- Compilation of representative structural and geotechnical models and metrics of different types for which the responses to simulated versus recorded seismograms can be compared.
- Comprehensive analysis and documentation of the sensitivity of simulated ground motions to model input parameters and their interactions and uncertainties.
- Development of testing and/or rating metrics for simulated ground motions, perhaps considering testing concepts from the Collaboratory for the Study of Earthquake Predictability (http://www.cseptesting.org).

Improved Hazard Representation

- Develop improved hazard models that consider simulation-based earthquake source and wave propagation effects that are not already well-reflected in observed data. These could include improved methods for incorporating rupture directivity effects, basin effects, and site effects in the USGS ground motion maps, for example. The improved models should be incorporated into OpenSHA.
- Use broadband strong motion simulations, possibly in conjunction with recorded ground motions, to develop ground motion prediction models (or attenuation relations). Broadband simulation methods must be verified (by comparison with simple test case results) and validated (against recorded strong ground motions) before use in model development. The verification, validation, and application of simulation methods must be done on the SCEC Broadband Simulation Platform. Such developments will contribute to the future NGA-H Project.
- Develop ground motion parameters (or intensity measures), whether scalars or vectors, that enhance the prediction of structural response and risk.
- Investigate bounds on the median and variability of ground motions for a given earthquake scenario, in coordination with the Extreme Ground Motion Project.

Ground Motion Time History Simulation

- Develop acceptance criteria for simulated ground motion time histories to be used in structural response analyses for building code applications or risk analysis. This relates closely to the GMSV section above.
- Assess the advantages and disadvantages of using simulated time histories in place of recorded time histories as they relate to the selection, scaling and/or modification of ground motions for building code applications or risk analysis.
- Develop and validate modules for simulation of short period ground motions (< 1 sec) for incorporation in the Broadband Platform.
- Develop and validate modules for the broadband simulation of ground motion time histories close to large earthquakes, and for earthquakes in the central and eastern United States, for incorporation in the Broadband Platform.

Collaboration in Structural Response Analysis

- Tall Buildings and Other Long-Period Structures. Enhance the reliability of simulations of long period ground motions in the Los Angeles region using refinements in source characterization and seismic velocity models, and evaluate the impacts of these ground motions on tall buildings and other long-period structures (e.g., bridges, waterfront structures). Such projects could potentially build on work done in the PEER TBI Project.
- End-to-End Simulation. Interactively identify the sensitivity of structural response to ground motion parameters and structural parameters through end-to-end simulation. Buildings of particular interest include non-ductile concrete frame buildings.
- Reference Buildings and Bridges. Participate with PEER investigators in the analysis of reference buildings and bridges using simulated broadband ground motion time histories. The ground motions of large, rare earthquakes, which are poorly represented in the NGA strong motion data base, are of special interest. Coordination with PEER can be done through Yousef Bozorgnia, yousef@berkeley.edu.
- Earthquake Scenarios. Perform detailed assessments of the results of scenarios such as the ShakeOut exercise, and the scenarios for which ground motions were generated for the Tall Buildings Initiative (including events on the Puente Hills, Southern San Andreas, Northern San Andreas and Hayward faults) as they relate to the relationship between ground motion characteristics and structural response and damage.

Ground Deformation

- Investigate the relationship between input ground motion characteristics and local soil nonlinear response, liquefaction, lateral spreading, local soil failure, and landslides -- i.e., geotechnical hazards. Investigate hazards due to surface faulting and to surface deformation caused by subsurface faulting and folding.

Risk Analysis

- Develop improved site/facility-specific and portfolio/regional risk analysis (or loss estimation) techniques and tools, and incorporate them into the OpenRisk software.
- Use risk analysis software to identify earthquake source and ground motion characteristics that control damage estimates.

Other Topics

- Proposals for other innovative projects that would further implement SCEC information and techniques in seismic hazard, earthquake engineering, risk analysis, and ultimately loss mitigation, are encouraged.

X. Special Projects and Initiatives

The following are special projects for which SCEC has obtained funding beyond the core program. This RFP is not for those funds, which are committed, rather it is for SCEC core funding for research projects that are consonant with these special projects. This is consistent with SCEC policy that requires that special projects be aligned with core SCEC goals.

A. Working Group on California Earthquake Probabilities (WGCEP)

Following the 2008 release of the Uniform California Earthquake Rupture Forecast version 2 (UCERF2), the WGCEP is now working on adding some major enhancements for UCERF3 (due June 2012) and subsequent models. Our primary goals are to

relax segmentation, add multi-fault ruptures, and include spatial-temporal clustering (earthquake triggering). As the latter will require robust interoperability with real-time seismicity information, UCERF3 will bring us into the realm of operational earthquake forecasting (OEF). This model is being developed jointly by SCEC, the USGS, and CGS, in close coordination with the USGS National Seismic Hazard Mapping Program. The following are examples of SCEC activities that could make direct contributions to WGCEP goals:

- Reevaluate fault models in terms of the overall fault inventory, specify more precisely fault endpoints in relationship to neighboring faults, and examine the likelihood of possible multi-fault ruptures. Help specify the extent to which faults represent a well-define surface versus a proxy for a braided deformation zone.
- Reevaluate fault slip rates, especially using more sophisticated modeling approaches (e.g., that include GPS data, generate kinematically consistent results, and perhaps provide off-fault deformation rates as well). This may include how we map simplified block-model results back onto the more complex fault system.
- Help determine the average along-strike slip distribution of large earthquakes, especially where multiple faults are involved (e.g., is there reduced slip at fault connections?)
- Help determine the average down-dip slip distribution of large earthquakes (the ultimate source of existing discrepancies in magnitude-area relationships).
- Contribute to the compilation and interpretation of mean recurrence-interval constraints from paleoseismic data.
- Develop earthquake rate models that relax segmentation and include multi-fault ruptures.
- Develop ways to constrain the spatial distribution of maximum magnitude for background seismicity (for earthquakes occurring off of the explicitly modeled faults).
- Answer the question of whether every small volume of space exhibits a Gutenberg Richter distribution of nucleations?
- Develop methods for quantifying elastic-rebound based probabilities in un-segmented fault models.
- Help quantify the amount of slip in the previous event (including variations along strike) on any major faults in California.
- Develop models for fault-to-fault rupture probabilities, especially given uncertainties in fault endpoints.
- Determine the proper explanation for the apparent post-1906 seismicity-rate reduction (the so-called Empirical Model of previous WGCEPs). How temporally variable are seismicity rates (e.g., more so than implied by aftershock statistics)?
- Develop applicable methods for adding spatiotemporal clustering to the model (e.g., based on empirical models such as ETAS, or derived from physics-based simulators). Are sequence-specific parameters warranted?
- Is there a physical difference between a multi-fault rupture and a separate event that was triggered quickly?
- Develop easily computable hazard or loss metrics that can be used to evaluate and perhaps trim logic-tree branch weights.
- Develop techniques for down-sampling event sets to enable more efficient hazard and loss calculations.
- Develop novel ways of testing UCERF3, especially ones that can be integrated with CSEP.

Further suggestions and details can be found at *http://www.WGCEP.org*, or by speaking with the project leader (Ned Field: *field@usgs.gov*; (626) 644-6435).

B. Collaboratory for the Study of Earthquake Predictability (CSEP)

CSEP is developing a virtual, distributed laboratory—a collaboratory—that supports a wide range of scientific prediction experiments in multiple regional or global natural laboratories. This earthquake system science approach seeks to provide answers to the questions: (1) How should scientific prediction experiments be conducted and evaluated? and (2) What is the intrinsic predictability of the earthquake rupture process? Contributions may include:

1. Establishing rigorous procedures in controlled environments (testing centers) for registering prediction procedures, which include the delivery and maintenance of versioned, documented code for making and evaluating predictions including intercomparisons to evaluate prediction skills;
2. Constructing community-endorsed standards for testing and evaluating probability-based and alarm-based predictions;
3. Developing hardware facilities and software support to allow individual researchers and groups to participate in prediction experiments;
4. Providing prediction experiments with access to data sets and monitoring products, authorized by the agencies that produce them, for use in calibrating and testing algorithms;
5. Intensifying the collaboration between the US and Japan through international projects, and initiating joint efforts with China;
6. Developing experiments to test basic physical principles of earthquake generation (e.g., models for estimating the largest possible earthquake on a given fault are important to earthquake scenarios like ShakeOut and to earthquake hazard models. We seek proposals to develop quantitative tests of such models); and
7. Conducting workshops to facilitate international collaboratories.

A major focus of CSEP is to develop international collaborations between the regional testing centers and to accommodate a wide-ranging set of prediction experiments involving geographically distributed fault systems in different tectonic environments.

Special Note. CSEP global travel grants from 2006 to 2010 were funded with a grant from the W. M. Keck Foundation. The Keck grant ended in early 2011 and future funding for CSEP global travel has not been obtained at the time of the release of this document.

C. Community Modeling Environment (CME)

The Community Modeling Environment is a SCEC special project that develops improved ground motion forecasts by integrating physics-based earthquake simulation software, observational data, and earth structural models using advanced computational techniques including high performance computing. CME projects often use results, and integrate work, from SCEC groups including Interdisciplinary Focus Groups Technical Activity Groups.

The SCEC research community can contribute research activities to CME by providing scientific or computational capability that can improve ground motion forecasts. The following paragraphs briefly describe several current CME computational goals so researchers can propose to develop a needed element that can be integrated into a larger CME calculation.

Examples of CME research requirements include earth structural models, curated data sets to support forecast validation, and scientific software that simulates physical processes in the earth including dynamic ruptures and wave propagation simulations.

CME computational-based research projects include three types of forecast evaluation and testing systems; transient detection and forecast evaluation, earthquake early warning earthquake parameter and ground motion forecast evaluation, and short-term earthquake forecast evaluation.

CME is developing ground motion simulations that produce broadband seismograms. These simulation tools include rupture generators, low frequency wave propagation models, high frequency stochastic models, non-linear site response modules, and validation capabilities including assembled observational strong motion data sets and waveform-matching goodness of fit algorithms and information displays.

Ground motion simulation validation computational and organizational tools are needed to establish repeatable validation of ground motion simulations to engineering standards.

CME is working to improve probabilistic seismic hazard calculations. CME PSHA research requires a high resolution 3D velocity model for California, a pseudo-dynamic rupture generator capable of generating an extended earthquake rupture forecast from UCERF3.0, highly-efficient reciprocity-based seismogram calculations, and probabilistic hazard model information system providing access to calculation results.

D. National Partnerships through EarthScope

The NSF EarthScope project (*http://www.earthscope.org*) provides unique opportunities to learn about the structure and dynamics of North America. SCEC and the NSF EarthScope program encourage proposals that integrate the goals of the SCEC Science Plan with the many overlapping goals of the EarthScope Science Plan. Topics of interest include applying EarthScope observational resources to SCEC science and hazard problems; characterizing the crust and lithosphere of the natural laboratory of Southern California; exploring stress and deformation over time using EarthScope resources (including high resolution topography); testing hypothesis and enhancing models of earthquakes, faulting, and the rheology of the lithosphere; developing innovative contributions to identifying earthquake hazard and community response; and promoting Earth Science literacy in education and outreach in SCEC and EarthScope topic areas. These partnerships should seek to strengthen the connections across the organizations and leverage SCEC and EarthScope resources.

XI. SCEC Communication, Education, and Outreach

SCEC maintains a Communication, Education, and Outreach (CEO) program with four long-term goals:

- Coordinate productive interactions among a diverse community of SCEC scientists and with partners in science, engineering, risk management, government, business, and education.
- Increase earthquake knowledge and science literacy at all educational levels, including students and the general public.
- Improve earthquake hazard and risk assessments
- Promote earthquake preparedness, mitigation, and planning for response and recovery.

Short-term objectives are outlined below. These objectives present opportunities for members of the SCEC community to become involved in CEO activities, which are for the most part coordinated by CEO staff. As project support is very limited, budgets for proposed projects should be on the order of $2,000 to $5,000. Hence proposals that include additional sources of support (cost-sharing, funding from other organizations, etc.) are highly recommended. Smaller activities can be supported directly from the CEO budget and do NOT need a full proposal. Those interested in submitting a CEO proposal should first contact Mark Benthien, associate SCEC director for CEO, at 213-740-0323 or *benthien@usc.edu*. There may be other sources of funding that can be identified together.

CEO Focus Area Objectives

The theme of the CEO program during SCEC4 is Creating an Earthquake and Tsunami Resilient California. CEO will continue to manage and expand a suite of successful activities along with new initiatives, within four CEO interconnected thrust areas:

1. The Implementation Interface connects SCEC scientists with partners in earthquake engineering research, and communicates with and trains practicing engineers and other professionals.
2. The Public Education and Preparedness thrust area educates people of all ages about earthquakes, and motivates them to become prepared.
3. The K-14 Earthquake Education Initiative seeks to improve earth science education and school earthquake safety.
4. Finally, the Experiential Learning and Career Advancement program provides research opportunities, networking, and more to encourage and sustain careers in science and engineering.

These thrust areas present opportunities for members of the SCEC community to partner with CEO staff, however project support is very limited. Limited funding (typically no more than $2000-$5000) may be available as direct payments from SCEC (not subcontracts) for materials or activities and typically does not require a formal proposal. For larger activities, joint proposals with SCEC CEO to potential sources are the best approach. Those interested in partnering with SCEC CEO on activities, submitting a joint proposal, or in submitting a CEO proposal to this RFP should first contact Mark Benthien, associate SCEC director for CEO, at 213-740-0323 or benthien@usc.edu.

Poster Presentations: Group A

Horizon Ballroom & Foyer

Sunday, September 11, 2011
13:00 – 17:00 Poster Set-Up
20:00 – 22:30 Poster Session I

Monday, September 12, 2011
14:30 – 16:00 Poster Session II
16:00 – 21:00 Poster Removal

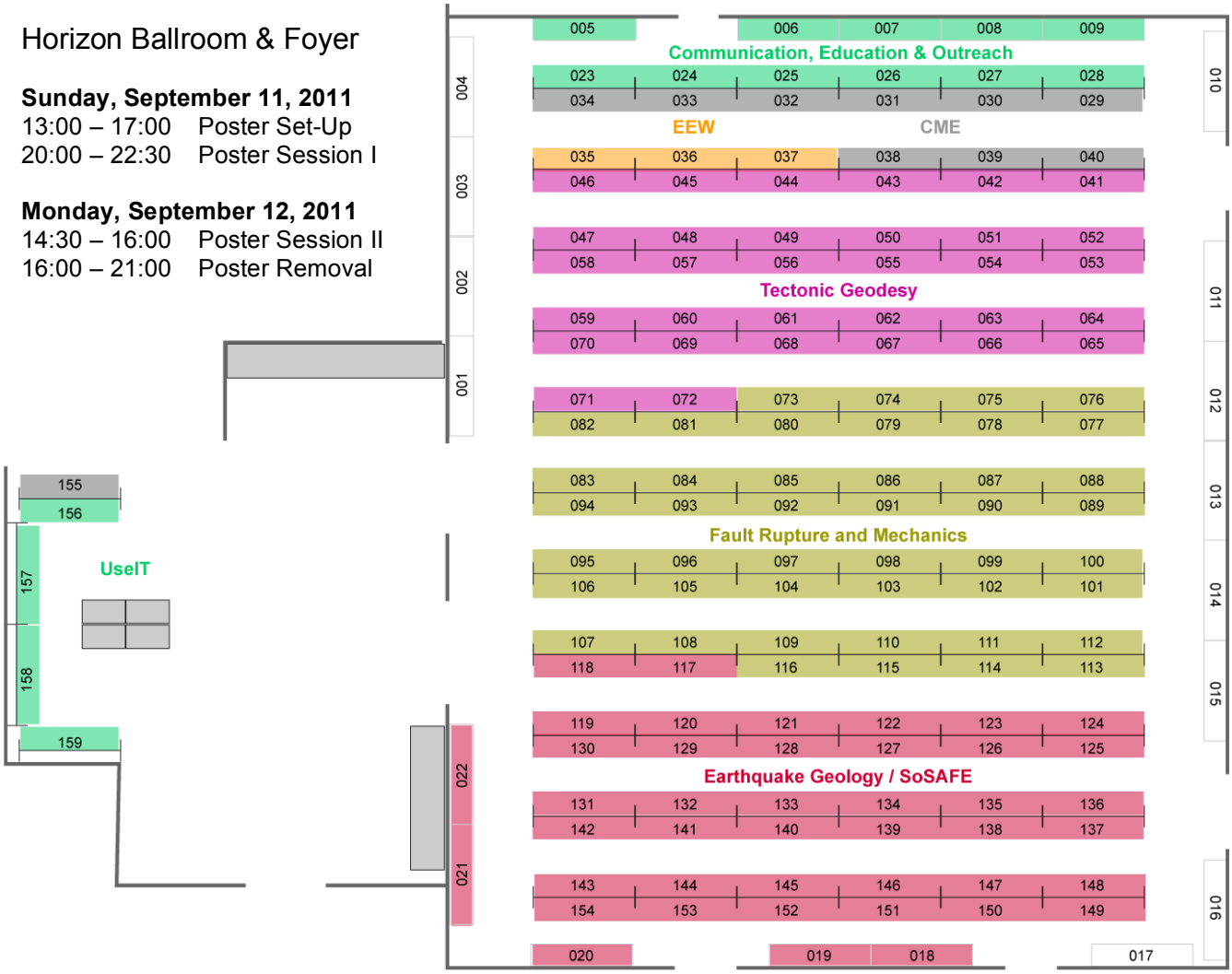

Communication, Education, Outreach (CEO)

A-005 **TEACHERS USING CONTINUOUS GPS DATA TO LEARN ABOUT EARTHQUAKES - SHARING RESEARCH RESULTS IN THE CLASSROOM THROUGH LESSON STUDY**, *R.M. de Groot, S.F. McGill, B. Vargas, R. Ruiz, M. Kline, and S. Wallace*

A-006 **CREATIVE WORLD EARTHQUAKE PREPAREDNESS PROGRAM**, *M.J. Vanegas, R.M. de Groot, and M. Barajas*

A-007 **SHAKEOUT DRILL PLANNING AND EVALUATION AT CSU FULLERTON: A CASE STUDY**, *L.A. Davis, A. Leslie, A. Nguyen, and M.M. Wood*

A-008 **VISUAL COMMUNICATION DESIGN FOR SHAKEOUT RESEARCH DISSEMINATION**, *A. Nguyen*

A-009 **QUAKE CATCHER NETWORK (QCN) SEISMIC SENSOR DEPLOYMENT GAME**, *D.L. Kilb, A. Yang, and D. Rohrlick*

A-023 **CORSSA: COMMUNITY ONLINE RESOURCE FOR STATISTICAL SEISMICITY ANALYSIS - STATUS & OUTLOOK**, *J.D. Zechar, J.L. Hardebeck, A.J. Michael, M. Naylor, S. Steacy, S. Wiemer, and J. Zhuang*

A-024 **VISUALIZING STRUCTURAL RESPONSE AND SITE AMPLIFICATION USING EARTHQUAKE DATA RECORDED AT THE NEES@UCSB FIELD SITES**, *S.H. Seale, J.H. Steidl, L.B. Seale, and A. Chourasia*

A-025 **PRELIMINARY EVALUATION OF THE 2010 SHAKEOUT EARTHQUAKE DRILL**, *A. Leslie, L.A. Davis, M.M. Wood, and R. Green*

A-026 **MAKE YOUR OWN EARTHQUAKE: CURRICULUM DEVELOPMENT FOR GRADES 6 - 12**, *J.P. Trudeau, S.E. Allen, and H.E. Pence*

A-027 **GPS MONITORING OF THE INLAND EMPIRE FOR SLIP-RATE MODELING OF SOUTHERN CALIFORNIA FAULTS: CONTRIBUTIONS FROM HIGH SCHOOL SCIENCE TEACHERS AND THEIR STUDENTS**, *M. Meijer, M. Affadonis, R. Bennett, W. Butscher, E. Carlson, R. de Groot, S. Harris, S. McGill, S. Pearson, A. Pennington, T. Pitruzzello, D. Shafer, J. Spinler, and S. Wallace*

A-028 **PLATE TECTONICS: A NEWLY COMPLETED EXHIBIT IN THE SAN BERNARDINO COUNTY MUSEUM'S HALL OF GEOLOGICAL WONDERS**, *K. Springer, E. Scott, and J.C. Sagebiel*

Community Modeling Environment (CME)

A-029 **SCIENTIFIC VISUALIZATION IN 4D FOR EARTHQUAKE RESEARCH**, *L.H. Kellogg, T. Bernardin, M.I. Billen, E.S. Cowgill, A.J. Elliott, P.O. Gold, C.L. Harwood, O. Kreylos, M.E. Oskin, B. Pellett, D.L. Turcotte, and M.B. Yikilmaz*

A-030 **PEGASUS WMS: POWERING LARGE SCALE SCIENCE THROUGH WORKFLOWS,** *G. Mehta, K. Vahi, E. Deelman, M. Rynge, S. Callaghan, and P. Maechling*

A-031 **AWP-ODC-SGT: WAVE PROPAGATION AND DYNAMIC RUPTURE SIMULATION SOFTWARE WITH STRAIN GREEN'S TENSOR (SGT) CAPABILITIES FOR CYBERSHAKE 2.0**, *J. Zhou, S. Callaghan, S. Song, P. Chen, K. Olsen, R. Graves, P. Small, P. Maechling, Y. Cui, and T. Jordan*

A-032 **FULL-3D WAVEFORM TOMOGRAPHY FOR SOUTHERN CALIFORNIA**, *E. Lee, P. Chen, T.H. Jordan, P.J. Maechling, M. Denolle, and G.C. Beroza*

A-033 **THE CLARK CO. PARCEL MAP AND IMPLICATIONS FOR EARTHQUAKE HAZARD DEFINITION IN SOUTHERN NEVADA**, *J.N. Louie, W. Savran, B. Flinchum, G. Plank, S.K. Pullammanappallil, A. Pancha, and W.K. Hellmer*

A-034 **APPLICATION OF ZH RATIO TO THE URBAN LOS ANGELES REGION FOR SHALLOW S-WAVE VELOCITY STRUCTURE**, *T. Hakamata, T.E. Yano, and T. Tanimoto*

A-038 **BROADBAND CYBERSHAKE PLATFORM: SEISMOGRAM SYNTHESIS FOR BROADBAND PHYSICS-BASED PROBABILISTIC SEISMIC HAZARD ANALYSIS**, *S. Callaghan, P. Maechling, P. Small, K. Milner, R. Graves, T. H. Jordan, and the CyberShake Collaboration*

A-039 **ACCELERATION OF 3D FINITE DIFFERENCE AWP-ODC FOR SEISMIC SIMULATION ON GPU FERMI ARCHITECTURE**, *J. Zhou, Y. Cui, and D. J. Choi*

A-040 **A UNIFIED FINITE ELEMENT METHOD FOR HETEROGENEOUS ELASTIC MEDIA WITH LOW TO HIGH RATIO OF P- TO S-WAVE VELOCITIES**, *H. Karaoglu and J. Bielak*

Earthquake Early Warning (EEW)

A-035 **CISN SHAKEALERT: DEVELOPMENT OF A PROTOTYPE USER DISPLAY FOR PROVIDING EARTHQUAKE ALERTS TO END USERS**, *M. Boese, K. Solanki, T. Heaton, E. Hauksson, and the CISN EEW Team*

A-036 **NEAR REAL-TIME FULL-WAVE CENTROID MOMENT TENSOR (CMT) INVERSION FOR GROUND-MOTION FORECAST IN 3D EARTH STRUCTURE OF SOUTHERN CALIFORNIA**, *E. Lee, P. Chen, T.H. Jordan, and P.J. Maechling*

A-037 **REAL TIME GEODETIC EARLY WARNING SYSTEM FOR EARTHQUAKES**, *H. Tahtinen, Y. Bock, B.W. Crowell, D. Melgar, and M.B. Squibb*

Earthquake Geology / Southern San Andreas Fault Evaluaton (SoSAFE)

A-018 **INVESTIGATIONS OF MICROBIAL LIFE IN THE MUD NEAR THE SALTON SEA, CALIFORNIA**, *S.C. Rosove*

A-019 **HYDROCHEMISTRY OF ACTIVE FAULT ZONES- SALTON SEA, CA AND NORTHERN UTAH**, *K.A. Shervais*

A-020 **FRACTURE NETWORK CHARACTERISTICS, SEALING, AND VELOCITY STRUCTURE OF AN EXHUMED SEISMIC FAULT ZONE; THE GOLE LARGHE FAULT ZONE, ITALIAN ALPS**, *T.M. Mitchell, S.A. Smith, A. Bistacchi, M. Rempe, and G. Di Toro*

A-021 **THE ADVANTAGES OF FIELD WORK**, *M.M. Ponce-Zepeda*

A-022 **SURFACE-EXPOSURE DATING OF SAN ANDREAS EARTHQUAKES**, *W.B. Bull*

A-117 **REMOTE MAPPING OF A LARGE STEPOVER IN THE 4 APRIL 2010 EL MAYOR CUCAPAH EQ**, *A.E. Morelan and M.E. Oskin*

A-118 **STRUCTURAL CONTROLS ON THE SURFACE RUPTURE ASSOCIATED WITH THE MW7.2 EL MAYOR-CUCAPAH EARTHQUAKE OF 4 APRIL 2010: A COMPARATIVE ANALYSIS OF SCARP ARRAY KINEMATICS, ORIENTATION, LITHOLOGY AND WIDTH**, *O.J. Teran, J.M. Fletcher, T.R. Rockwell, K.W. Hudnut, M.E. Oskin, S.O. Akciz, A.J. Elliot, P.O. Gold, L. Liu-Zheng, U.R. Manjarrez, R. Mendoza-Borunda, A.E. Morelan, and R.M. Spelz*

A-119 **OPENTOPOGRAPHY: ONLINE ACCESS TO HIGH-RESOLUTION LIDAR TOPOGRAPHY DATA AND PROCESSING TOOLS IN SUPPORT OF NSF EARTH SCIENCE**, *C.J. Crosby, V. Nandigam, S. Krishnan, C. Baru, and J.R. Arrowsmith*

A-120 **NEAR-FIELD COSEISMIC DEFORMATION QUANTIFIED FROM DIFFERENTIAL AIRBORNE LIDAR OF THE EL MAYOR-CUCAPAH EARTHQUAKE SURFACE RUPTURE**, *M.E. Oskin, J.R. Arrowsmith, A. Hinojosa, A.J. Elliott, O. Teran, J.M. Fletcher, S. Saripali, and D. Banesh*

A-121 **METHODS FOR ANALYZING THE EL MAYOR-CUCAPAH EARTHQUAKE RUPTURE USING LIDAR DATASETS**, *D. Banesh, M.E. Oskin, X. Wang, B. Hamann, and L. Kellogg*

A-122 **RUPTURE PATTERN OF THE 1892 LAGUNA SALADA EARTHQUAKE: A PRECURSOR TO 2010 EL MAYOR-CUCAPAH**, *K. Mueller, T. Rockwell, O. Teran, J. Fletcher, S. Akciz, and P. Patton*

A-123 **STRAIN PARTITIONING IN LOS ANGELES**, *R.S. Yeats and D. Verdugo*

A-124 **CHARACTERIZING THE RECENT BEHAVIOR AND EARTHQUAKE POTENTIAL OF THE BLIND WESTERN SAN CAYETANO AND VENTURA FAULT SYSTEMS**, *L.J. McAuliffe, J.F. Dolan, J. Hubbard, and J.H. Shaw*

A-125 **SEISMIC SOURCE CHARACTERIZATION FOR THE LADWP VAN NORMAN COMPLEX AND ISSUES TO CONSIDER FOR UCERF3 IN THE NORTHERN SAN FERNANDO VALLEY, CA**, *S. Lindvall, C. Kemp, J. Unruh, and D. O'Connell*

A-126 **SUB-SURFACE EVIDENCE OF FAULTING RELATED TO THE COMPTON-LOS ALAMITOS FAULT AND IMPLICATIONS FOR STRAIN PARTITIONING IN THE WESTERN LA BASIN**, *D.M. Verdugo Madugo and R.S. Yeats*

A-127 **NEW CHRONOLOGY AND ESTIMATED RATES OF VERTICAL UPLIFT FOR THE GAVIOTA COAST RAISES ISSUES RELATED TO THE EARTHQUAKE HAZARD**, *E.A. Keller, D.E. DeVecchio, L.D. Gurrola, and L.A. Owen*

A-128 **QUATERNARY CONGLOMERATE DEPOSITION AND IMPLICATIONS ON FAULT EVOLUTION IN THE OJAI AND UPPER OJAI VALLEYS, WESTERN TRANSVERSE RANGES, CA**, *H.L. McKay and R.V. Heermance*

A-129 **COMPILATION OF SLIP IN LAST EARTHQUAKE DATA FOR HIGH-SLIP RATE FAULTS IN CALIFORNIA FOR INPUT INTO SLIP DEPENDENT RUPTURE FORECAST**, *C.L. Madden Madugo, J.R. Arrowsmith, D.E. Haddad, J.B. Salisbury, and R.J. Weldon*

A-130 **LUMINESCENCE DATING AS A TOOL FOR ASSESSING THE VARIABILITY OF FAULT SLIP RATES AND PALEOSEISMIC EVENTS ON TIMESCALES OF 10 TO 100,000 YEARS**, *B.J. Roder, E.J. Rhodes, M.J. Lawson, L. McAuliffe, J.F. Dolan, and S.F. McGill*

A-131 **CHARACTERISTICS OF QUARTZ AND FELDSPAR LUMINESCENCE FROM SOUTHERN CALIFORNIA, USA: IMPLICATIONS FOR PALEOSEISMIC AND FAULT SLIP-RATE STUDIES**, *M.J. Lawson, B.J. Roder, D.M. Stang, E.J. Rhodes, L. McAuliffe, J.F. Dolan, and S.F. McGill*

A-132 **INVESTIGATION OF THE HECTOR MINE EARTHQUAKE SURFACE RUPTURE WITH AIRBORNE LIDAR DATA**, *T. Chen, D.Z. Zhang, S. Akciz, and K.W. Hudnut*

A-133 **PRELIMINARY PALEOSEISMIC RESULTS FROM THE ECHO PLAYA TRENCH SITE ON THE CENTRAL GARLOCK FAULT, CHINA LAKE NAWS, NEAR RIDGECREST, CA**, *R.D. Hartleb, C.D. Kemp, A. Lutz, E.K. Frost, and S.C. Lindvall*

A-134 **PALEOSEISMIC INVESTIGATION OF THE SAN GORGONIO PASS FAULT ZONE NEAR CABEZON, CALIFORNIA**, *S. Ramzan and J.D. Yule*

A-135 **DEPOSITIONAL CONSTRAINTS ON SLIP ALONG THE SAN ANDREAS FAULT WITHIN THE EASTERN SAN GORGONIO PASS REGION, SOUTHERN CALIFORNIA**, *K.J. Kendrick, J.C. Matti, S.A. Mahan, G.P. Landis, and D.P. Miggins*

A-136 **BUILDING HISTORIES OF FAULT SLIP TO OBSERVE SECULAR VARIATION IN SLIP**, *E. Cowgill, R.D. Gold, P.O. Gold, T. Compton, T. Bernardin, and R. Westerteiger*

A-137 **DISCOVERING THE GEOMORPHIC RECORD OF HOLOCENE SLIP ALONG THE MOJAVE SECTION OF THE SAN ANDREAS FAULT, CALIFORNIA**, *T. Compton, E. Cowgill, R. Gold, K. Scharer, R. Westerteiger, and T. Bernardin*

A-138 **OBSERVATIONS OF RECENTLY-EXPOSED FUMAROLE FIELDS NEAR MULLET ISLAND, IMPERIAL VALLEY, CALIFORNIA**, *D.K. Lynch, K.W. Hudnut, P.M. Adams, and L.S. Bernstein*

A-139 **EVALUATING THE RELATIONSHIP BETWEEN LATERAL SLIP AND REPEATED FOLD DEFORMATION ALONG A TRANSTENSIVE STEP-OVER ON THE SAN ANDREAS FAULT AT THE FRAZIER MOUNTAIN SITE**, *A.R. Streig and R.J. Weldon*

A-140 **TRACKING COSMOGENIC 10BE IN MULTIPLE GRAINSIZES DOWN ALLUVIAL SYSTEMS IN ACTIVE OROGENS**, *K.E. McGuire and R.V. Heermance*

A-141 **EARTHQUAKE AGES AND DISPLACEMENTS, FRAZIER MOUNTAIN PALEOSEISMIC SITE**, *K.M. Scharer, R.J. Weldon, B.C. Gibson, and A.R. Streig*

A-142 **PALEOSEISMOLOGY AND SLIP RATE OF THE SAN GORGONIO PASS FAULT ZONE AT MILLARD CANYON: TESTING THE LIKELIHOOD OF THROUGH-GOING SAN ANDREAS RUPTURES**, *J.D. Yule and P.L. McBurnett*

A-143 **MOVIES OF SEISMIC WAVE PROPAGATION THROUGH THE IMPERIAL AND COACHELLA VALLEYS, SOUTHERN CALIFORNIA**, *M. Barba and J.M. Stock*

A-144 **USE OF INTEGRATED MASTER MULTISPECTRAL IMAGERY AND LIDAR DEM FOR ACTIVE FAULT DETECTION AND EVALUATION**, *F.G. Perez, W.A. Bryant, J.A. Treiman, C.R. Real, and S.J. Hook*

A-145 **REVISITING WALLACE CREEK: NEW RADIOCARBON RESULTS AND SLIP RATE ESTIMATES OF THE SAN ANDREAS FAULT IN THE CARRIZO PLAIN**, *S.O. Akciz, D.E. Haddad, W. Bohon, L. Mendes, G. Marliyani, B. Salisbury, T. Sato, L. Grant Ludwig, and J.R. Arrowsmith*

A-146 **STRESS DROP VARIATIONS OF THE SAN ANDREAS FAULT, MOJAVE SEGMENT, OVER THE LAST 2000 YEARS**, *T. Solis and B. Smith-Konter*

A-147 **FAULT ZONE ARCHITECTURE, SAN JACINTO FAULT ZONE, SOUTHERN CALIFORNIA: EVIDENCE FOR FOCUSED FLUID FLOW AND HEAT TRANSFER IN THE SHALLOW CRUST**, *N.M. Morton, G.H. Girty, and T.K. Rockwell*

A-148 **PRELIMINARY PALEOSEISMIC RESULTS FROM SOUTHERN CLARK FAULT, SAN JACINTO FAULT ZONE, SOUTHERN CALIFORNIA; COMPARISON TO THE HOG LAKE PALEOSEISMIC RECORD**, *M.T. Buga, T.K. Rockwell, and J.B. Salisbury*

A-149 **INTERACTIONS BETWEEN THE CLARK STRAND OF THE SAN JACINTO FAULT ZONE AND THE EXTRA-ELMORE FAULT ARRAYS**, *S. Janecke and S. Thornock*

A-150 **TIMING OF LARGE EARTHQUAKES BETWEEN 400 AD TO PRESENT ALONG THE CLAREMONT FAULT, NORTHERN SAN JACINTO FAULT ZONE, FROM MYSTIC LAKE, CALIFORNIA**, *N.W. Onderdonk, T.K. Rockwell, S.F. McGill, and G. Marliyani*

A-151 **SLIP RATE OF THE NORTHERN SAN JACINTO FAULT FROM OFFSET LANDSLIDES IN THE SAN TIMOTEO BADLANDS**, *S.F. McGill, L.A. Owen, E.O. Kent, T.K. Rockwell, and N.W. Onderdonk*

A-152 **SLIP RATES ON THE SOUTHERN SAN JACINTO FAULT AND HOLOCENE-LATE PLEISTOCENE KINEMATICS OF THE PACIFIC-NORTH AMERICAN PLATE BOUNDARY**, *K. Blisniuk, M. Oskin, W. Sharp, T. Rockwell, and K. Fletcher*

A-153 **CRUSTAL THICKENING AND STRIKE-SLIP CONTROLLED GROWTH OF THE NORTHERN COLOMBIAN ANDES**, *M.H. Taylor, G. Veloza, and A. Mora*

A-154 **SEARCHING FOR A PALEOTSUNAMI RECORD IN SOUTHERN CALIFORNIA: LESSON'S FROM THAILAND'S ANDAMAN COAST**, *B.P. Rhodes and M.E. Kirby*

Fault Rupture and Mechanics (FARM)

A-073 **WHAT'S COOKING? EVALUATING FRICTIONAL STRESS USING EXTRACTABLE ORGANIC MATERIAL IN FAULT ZONES**, *P.J. Polissar, H.M. Savage, R.E. Sheppard, E.E. Brodsky, and C.D. Rowe*

A-074 **HOW DOES DAMAGE AFFECT RUPTURE PROPAGATION ACROSS A FAULT STEPOVER?** *H.M. Savage and M.L. Cooke*

A-075 **THE EFFECTS OF INTERMEDIATE FAULT SEGMENTS ON RUPTURE BEHAVIOR AND GROUND MOTION IN STRIKE-SLIP STEPOVERS**, *J.C. Lozos, D.D. Oglesby, J.N. Brune, and K.B. Olsen*

A-076 **THE EFFECT OF BARRIERS ON SLIP PARTITIONING IN AN UPWARD BRANCHING FAULT SYSTEM**, *J. Tarnowski, D. Oglesby, and D. Bowman*

A-077 **JUMPING RUPTURE DEPENDENCE ON FRICTION FORMULATIONS AT STRIKE-SLIP FAULT STEPOVERS**, *K.J. Ryan and D.D. Oglesby*

A-078 **DOES THE TEAR FAULT MATTER?** *Q. Liu, R.J. Archuleta, and R.B. Smith*

A-079 **PROPERTIES OF INELASTIC YIELDING ZONES GENERATED BY IN-PLANE DYNAMIC RUPTURES**, *S. Xu, Y. Ben-Zion, and J.-P. Ampuero*

A-080 **TETEMOKO: AN ADAPTIVE MESH REFINEMENT FRAMEWORK FOR DYNAMIC RUPTURE SIMULATION**, *J.E. Kozdon and E.M. Dunham*

A-081 **ADDITIONAL SHEAR RESISTANCE FROM FAULT ROUGHNESS AND ITS ROLE IN DETERMINING STRESS LEVELS ON MATURE AND IMMATURE FAULTS**, *Z. Fang and E.M. Dunham*

A-082 **CONDITIONS FOR RUPTURE JUMPING TO THE ADJACENT SEGMENTS – A CASE STUDY FOR THE 1992 LANDERS EARTHQUAKE**, *A.J. Delauder, Z. Fang, Y. Klinger, and E.M. Dunham*

A-083 **RECORDING FAULT-ZONE TRAPPED WAVES FROM AFTERSHOCKS OF THE M7.2 DARFIELD AND M6.3 CHRISTCHURCH EARTHQUAKE SEQUENCE FOR DOCUMENT OF SUBSURFACE DAMAGE ZONES**, *Y-G. Li, G. Paucale, D. Gravely, J. Cherrington, and M. Alvarez*

A-084 **A MICROMECHANICS BASED CONSTITUTIVE MODEL FOR BRITTLE FAILURE AT HIGH STRAIN RATES**, *H.S. Bhat, A.J. Rosakis, and C.G. Sammis*

A-085 **VARIABILITY OF SEISMIC SOURCE SPECTRA DERIVED FROM COHESIVE-ZONE MODELS OF A CIRCULAR RUPTURE PROPAGATING AT A CONSTANT SPEED**, *Y. Kaneko and P.M. Shearer*

A-086 **3D SIMULATIONS OF DYNAMIC RUPTURE ON ROUGH FAULTS**, *Z. Shi and S.M. Day*

A-087 **FAULT SLICKENLINES, ROUGHNESS AND INELASTIC DEFORMATION**, *J.D. Kirkpatrick and E.E. Brodsky*

A-088 **THE PERMEABILITY VARIATIONS ON THE WENCHUAN FAULT MEASURED ON THE WATER LEVEL RESPONSE TO SOLID EARTH TIDES**, *L. Xue, E.E. Brodsky, H. Li, H. Wang, and J. Pei*

A-089 **AUTO-ACOUSTIC COMPACTION IN STEADY SHEAR FLOWS: EXPERIMENTAL EVIDENCE FOR SUPPRESSION OF SHEAR DILATANCY BY INTERNAL ACOUSTIC VIBRATION**, *N.J. van der Elst and E.E. Brodsky*

A-090 **TEMPERATURE DEPENDENCE OF FRICTIONAL HEALING: EXPERIMENTAL OBSERVATIONS AND NUMERICAL SIMULATIONS**, *E.K. Mitchell, Y. Fialko, and K.M. Brown*

A-091 **MECHANICAL AND MICROSTRUCTURAL OBSERVATIONS OF DYNAMIC WEAKENING IN SMECTITE-RICH SAFOD GOUGE**, *M.E. French, H. Kitajima, J.S. Chester, and F.M. Chester*

A-092 **STRAIN LOCALIZATION DRIVEN BY THERMAL DECOMPOSITION DURING SEISMIC SHEAR**, *J.D. Platt, N. Brantut, and J.R. Rice*

A-093 **CAUGHT IN THE ACT: EVIDENCE FOR SEISMIC ARREST ON NATURAL FRICTION-MELT-BEARING FAULTS?**, *W.M. Behr and J.P. Platt*

A-094 **THE INFLUENCE OF AMBIENT FAULT TEMPERATURE ON FLASH-HEATING BEHAVIOR**, *F. Passelegue, D.L. Goldsby, T.E. Tullis, and O. Fabbri*

A-095 **RATE/STATE FRICTIONAL NUCLEATION AND DYNAMIC RUPTURE ON LOW-STRESS FAULTS WITH THERMAL WEAKENING EFFECTS**, *S.V. Schmitt, A.M. Bradley, E.M. Dunham, and P. Segall*

A-096 **A PHYSICAL MODEL OF THE MW 6 EARTHQUAKE CYCLE AT PARKFIELD**, *S. Barbot, N. Lapusta, and J. P. Avouac*

A-097 **INTERACTION OF FAULT STRENGTH HETEROGENEITIES AND STRESS REDISTRIBUTION IN MULTIPLE EARTHQUAKE CYCLES ON FAULTS WITH THERMAL PRESSURIZATION**, *J. Jiang and N. Lapusta*

A-098 **ENERGY PARTITION, STRAIN LOCALIZATION AND THERMAL WEAKENING IN A MODEL OF SHEARED GRANULAR MATERIALS**, *A.E. Elbanna, C. Lieou, and J. Carlson*

A-099 **THERMAL FLUID AND FAULT INTERACTIONS AT THE INTERSECTION OF TWO FAULTS, AGUA CALIENTE, CALIFORNIA**, *R.E. Wood and J.P. Evans*

A-100 **NUMERICAL SIMULATION OF SLOW SLIP TRIGGERED TREMOR MIGRATION AND RAPID TREMOR REVERSALS**, *Y. Luo and J.P. Ampuero*

A-101 **COMPARISON OF SIMULATED SLOW SLIP EVENTS WITH OBSERVATIONS**, *H.V. Colella, J.H. Dieterich, and K.B. Richards-Dinger*

A-102 **SLIP DEFICITS, RELEASE AND TRANSIENTS ALONG THE CENTRAL SAF FROM REPEATING MICROEARTHQUAKES**, *R.M. Nadeau, R.C. Turner, and R. Burgmann*

A-103 **IMPACTS OF STATIC AND DYNAMIC STRESS CHANGES ON TREMOR AND CREEP ALONG THE LOWER-CRUSTAL SAN ANDREAS FAULT**, *D.R. Shelly, K.M. Johnson, Z. Peng, D.P. Hill, and C. Aiken*

A-104 **TRIGGERED NON-VOLCANIC TREMOR FOLLOWING THE 2011 TOHOKU-OKI EARTHQUAKE**, *K. Chao, Z. Peng, D.P. Hill, D.R. Shelly, B. Enescu, B. Fry, and C. Aiken*

A-105 **ASSESSMENT OF COSEISMIC SLIP VARIATION FROM TERRESTRIAL LIDAR SCANS OF THE EL MAYOR-CUCAPAH SURFACE RUPTURE**, *P.O. Gold, A.J. Elliott, M.E. Oskin, M.H. Taylor, A. Hinojosa, R. Styron, O. Kreylos, T. Bernardin, E. Cowgill, and A.J. Herrs*

A-106 **A SEQUENCE OF DISTINCT DYNAMIC RUPTURES IN THE EARLY STAGE OF THE 2011 TOHOKU EARTHQUAKE**, *T. Uchide, H. Yao, and P.M. Shearer*

A-107 **DYNAMIC TRIGGERING EVENTS IN HIDA REGION BY THE P WAVE FROM THE 2011 TOHOKU EARTHQUAKE**, *T. Uchide*

A-108 **SHAKING AND FLOODING BY THE TOHOKU-OKI EARTHQUAKE**, *D. Helmberger, S. Wei, J.P. Avouac, H. Kanamori, and J. Jiang*

A-109 **EXPLORING PHYSICAL CONDITIONS THAT CONTROL THE 2011 MW 9.0 TOHOKU-OKI EARTHQUAKE RUPTURE AND SEISMIC RADIATIONS**, *B. Duan*

A-110 **THREE DIMENSIONAL ELASTIC RESPONSE OF COMPLIANT FAULT ZONES TO NEARBY EARTHQUAKES: A THEORETIC STUDY**, *J. Kang and B. Duan*

A-111 **ELASTOSTATIC SOLUTIONS FOR REALISTIC SLIP AND STRESS AROUND MODE II AND III CRACKS**, *V.R. Lambert, S. Barbot, and J. Avouac*

A-112 **IBEM3D: A REMOTE STRESS INVERSION PROGRAM HONORING MECHANICAL RELATIONSHIPS BETWEEN STRESS AND FAULT GEOMETRY**, *E.H. Madden, F. Maerten, and D.D. Pollard*

A-113 **PROPERTIES OF RUPTURE PULSES INDUCED BY DAMAGED FAULT ZONES**, *Y. Huang and J.P. Ampuero*

A-114 **DYNAMIC RUPTURE SIMULATION WITH AN UNSTRUCTURED 3D SPECTRAL ELEMENT METHOD**, *P. Galvez, J.-P. Ampuero, L.A. Dalguer, and T. Nissen-Meyer*

A-115 **THE SCEC-USGS DYNAMIC EARTHQUAKE RUPTURE CODE VERIFICATION EXERCISE**, *R.A. Harris, M. Barall, R. Archuleta, B. Aagaard, J.P. Ampuero, D.J. Andrews, V. Cruz-Atienza, L. Dalguer, S. Day, N. DeDontney, B. Duan, E. Dunham, A.A. Gabriel, P. Galvez, Y. Kaneko, Y. Kase, J. Kozdon, N. Lapusta, S. Ma, P.M. Mai, H. Noda, D. Oglesby, K. Olsen, and S. Somala*

A-116 **REGIONAL BROADBAND WAVEFORM MODELING USING UPGOING AND DOWNGOING WAVE FIELDS**, *S. Wei and D. Helmberger*

Tectonic Geodesy

A-041 **SURFACE DEFORMATION AND SLIP DISTRIBUTION OF THE 1994 NORTHRIDGE EARTHQUAKE DETERMINED FROM INSAR**, *C.M. Severson, G.J. Funning, and S.T. Marshall*

A-042 **IMAGING COSEISMIC SURFACE DEFORMATION AND DAMAGE USING SAR AND GPS: RESULTS FROM ARIA-EQ FROM 2011 M9.0 TOHOKU-OKI AND M6.3 CHRISTCHURCH EARTHQUAKES**, *S.E. Owen, S.H. Yun, A. Moore, E. Fielding, P. Agram, F. Webb, M. Simons, P. Rosen, J. Cruz, and H. Hua*

A-043 **SHARPENED VIEWS OF THE 2011 TOHOKU-OKI EARTHQUAKE FROM SPARSITY BASED OPTIMIZATION**, *E.L. Evans and B.J. Meade*

A-044 **SURFACE RUPTURE AND SLIP VARIATION INDUCED BY THE 2010 EL MAYOR – CUCAPAH EARTHQUAKE, BAJA CALIFORNIA, QUANTIFIED USING COSI-CORR ANALYSIS ON PRE- AND POST-EARTHQUAKE LIDAR ACQUISITIONS**, *S. Leprince, K.W. Hudnut, S. Akciz, A. Hinojosa Corona, and J.M. Fletcher*

A-045 **INTERSEISMIC, COSEISMIC AND POST-SEISMIC GPS OBSERVATIONS OF THE 2010/04/04 EL MAYOR-CUCAPAH EARTHQUAKE**, *M.A. Floyd and G.J. Funning*

A-046 **EL MAYOR CUCAPAH EARTHQUAKE: POSTSEISMIC DEFORMATION FROM INSAR AND GPS OBSERVATIONS**, *A. Gonzalez Ortega, D. Sandwell, Y. Fialko, J. Gonzalez Garcia, J. Fletcher, A. Nava Pichardo, M. Floyd, and B. Lipovsky*

A-047 **VERTICAL DEFORMATION IN THE MEXICALI VALLEY, BEFORE, DURING, AND AFTER THE M=7.2, EL MAYOR – CUCAPAH EARTHQUAKE, FROM INSAR, LEVELING AND GEOTECHNICAL INSTRUMENTS**, *E. Glowacka, O. Sarychikhina, B.B. Robles, F. Suarez, J. Ramírez, F.A. Nava, J. González, A. González, F. Farfán, and B.G. Díaz de Cossío B*

A-048 **HIGH RESOLUTION INTERSEISMIC VELOCITY MODEL OF THE SAN ANDREAS FAULT FROM GPS AND INSAR**, *X. Tong, D.T. Sandwell, and B. Smith-Konter*

A-049 **SAN BERNARDINO GPS NETWORK: TIME SERIES THROUGH 2010**, *E. Upton, S. McGill, R. Bennett, J. Spinler, and A. Torrens-Bonano*

A-050 **DEFORMATION RATES IN THE WESTERN TRANSVERSE RANGES, CALIFORNIA FROM THE SAN ANDREAS TO THE SANTA BARBARA CHANNEL MEASURED WITH GPS AND PERSISTENT SCATTERER INSAR**, *S.T. Marshall, G.J. Funning, and S.E. Owen*

A-051 **INVESTIGATION OF INTERSEISMIC DEFORMATION ALONG THE CENTRAL SECTION OF THE NORTH ANATOLIAN FAULT (TURKEY) USING INSAR OBSERVATIONS AND EARTHQUAKE-CYCLE SIMULATIONS**, *Y. Kaneko, Y. Fialko, X. Tong, D.T. Sandwell, and M. Furuya*

A-052 **GPS CONSTRAINTS ON CRUSTAL DEFORMATION IN THE CENTRAL WALKER LANE AND SIERRA NEVADA FRONTAL FAULT**, *J.M. Bormann, W.C. Hammond, C.W. Kreemer, and G. Blewitt*

A-053 **ASSESSING STRAIN ACCUMULATION RATES ACROSS THE PACIFIC-NORTH AMERICAN PLATE BOUNDARY NEAR SAN BERNARDINO, CALIFORNIA**, *R.F. Mason, E.P. Upton, A. Grijalva, K.L. Muhammad, A. Torrens-Bonano, S.F. McGill, E. Alaniz, J. Spinler, R.A. and Bennett*

A-054 **INVESTIGATING ALONG-STRIKE DEPTH VARIATIONS OF SEISMICITY IN THE SAN ANDREAS FAULT SYSTEM TO BETTER RESOLVE GEODETIC LOCKING DEPTHS**, *C. Del Pardo, B.R. Smith-Konter, D.T. Sandwell, P. Shearer, and Y. Zeng*

A-055 **THREE-DIMENSIONAL MODELING OF INTERSEISMIC DEFORMATION IN TAIWAN**, *B. Rousset, S. Barbot, J.P. Avouac, Y.J. Hsu, and J.C. Lee*

A-056 **KINEMATICS OF ROTATING PANELS OF E-W FAULTS IN THE SAN ANDREAS SYSTEM: WHAT CAN WE TELL FROM GEODESY?**, *J.P. Platt and J.P. Becker*

A-057 **GEODETIC SLIP RATES IN THE SOUTHERN SAN ANDREAS FAULT SYSTEM: INVESTIGATION OF THE EFFECTS OF HETEROGENEOUS ELASTIC STRUCTURE**, *E. Lindsey and Y. Fialko*

A-058 **ONE-DIMENSIONAL ELASTIC MODELING OF FAULT SLIP RATES IN THE SALTON TROUGH, CALIFORNIA**, *E. Alaniz and S.F. McGill*

A-059 **DISCREPANCIES IN OBSERVED VERTICAL MOTION FROM GEODETIC, GEOLOGIC AND GROUNDWATER DATA ALONG THE SOUTHERN SAN ANDREAS FAULT SYSTEM**, *G.M. Thornton, B.R. Smith-Konter, and J.G. Konter*

A-060 **ABSOLUTE STRESS IN SOUTHERN CALIFORNIA CONSTRAINED BY EARTHQUAKE FOCAL MECHANISMS AND MODELS OF STRESS CONTRIBUTIONS FROM TOPOGRAPHY AND FAULT LOADING**, *K.M . Luttrell, D.T. Sandwell, and B.R. Smith-Konter*

A-061 **STATIC DISPLACEMENTS COMPUTED FROM SEISMIC WAVEFIELD SIMULATIONS: VALIDATION TESTS FOR HOMOGENEOUS AND 1D STRUCTURE**, *C. Tape, J.P. Loveless, and B.J. Meade*

A-062 **EVALUATION OF TRANSIENT DEFORMATION FROM TWO DECADES OF CONTINUOUS GPS TIME SERIES ANALYSIS IN SOUTHERN CALIFORNIA**, *Y. Bock, S. Owen, B. Crowell, D. Dong, P. Fang, S. Kedar, Z. Liu, A. Moore, L. Prawirodirdjo, M. Squibb, and F. Webb*

A-063 **DETECTION OF TRANSIENT DEFORMATION IN SOUTHERN CALIFORNIA USING CONTINUOUS AND CAMPAIGN GPS MEASUREMENTS**, *B.W. Crowell and Y. Bock*

A-064 **DETECTION OF ANOMALOUS STRAIN TRANSIENTS USING PRINCIPAL COMPONENT ANALYSIS AND COVARIANCE DESCRIPTOR ANALYSIS METHODS**, *R.A. Granat, J.W. Parker, S. Kedar, and Y. Bock*

A-065 **AUTOMATIC DETECTION OF SHALLOW FAULT CREEP IN INSAR DATA**, *M. Wei, D. Sandwell, and J. McGuire*

A-066 **GPS AND UAVSAR**, *A. Donnellan, J. Parker, S. Hensley, B. Bills, and T. Herring*

A-067 **GPS NETWORK OPERATIONS AT USGS PASADENA**, *D. Determan, A. Aspiotes, K. Hudnut, N. King, and K. Stark*

A-068 **PBO SOUTHWEST REGION: NETWORK OPERATIONS AND BAJA EARTHQUAKE RESPONSE**, *C. Walls, A. Basset, D. Mann, S. Lawrence, C. Jarvis, J. Sklar, K. Feaux, and M. Jackson*

A-069 **IMPROVING GPS STRAIN ESTIMATES ON SUB-DAILY TIMESCALE**, *Y. Reuveni, S. Kedar, S. Owen, and F. Webb*

A-070 **CO-LOCATED PORE PRESSURE AND VOLUMETRIC STRAIN AT PLATE BOUNDARY OBSERVATORY BOREHOLES**, *A.J. Barbour and D.C. Agnew*

A-071 **COMPARISON OF CO-LOCATED PORE PRESSURE AND STRAIN OBSERVATIONS FROM EARTHQUAKES RECORDED AT PBO BOREHOLE STRAINMETER SITES**, *F. Civilini*

A-072 **ANALYZING BUILDING RESPONSE THROUGH THE USE OF GPS & STRONG MOTION DATA FOR THE MONITORING OF INFRASTRUCTURE**, *D. Sanchez, Y. Bock, and D. Melgar*

Undergraduate Studies in Earthquake Information Technology (USEIT)

A-156 **IMPLEMENTATION OF A SEISMIC SEQUENCE VISUALIZATION SYSTEM USING GEOGRAPHIC INFORMATION SYSTEMS**, *B.J. Hellige, M.A. Wagner, and S. Reed*

A-157 **VISUALIZING COMPARATIVE HAZARD VULNERABILITY THROUGH GIS/SHAKEMAP INTEGRATION**, *S.C. Boss, F. Gutierrez, K.Y. Lin, T. Papikyan, and C.M. Valen*

A-158 **IMPLEMENTATION OF GIS LAYERS WITH A SPACE-TIME GRAPHICAL DISPLAY IN SCEC-VDO**, *A. Bernhard, T. Farhat, R. Lacey, A. Lim, S. Paseda, M. Rogers-Martinez, C. Sawyer, T. Jordan, R. de Groot, and N. Rousseau*

A-159 **MEDIA TEAM - ABSTRACT**, *A. Sampson, H. Humpleman, and M. Romano*

Poster Presentations: Group B

Horizon Ballroom

Monday, September 12, 2011
16:00 – 21:00 Poster Set-Up
21:00 – 22:30 Poster Session III

Tuesday, September 13, 2011
14:00 – 15:30 Poster Session IV
21:00 – 22:30 Poster Session V

Wednesdy, September 14, 2011
07:00 – 08:30 Poster Removal

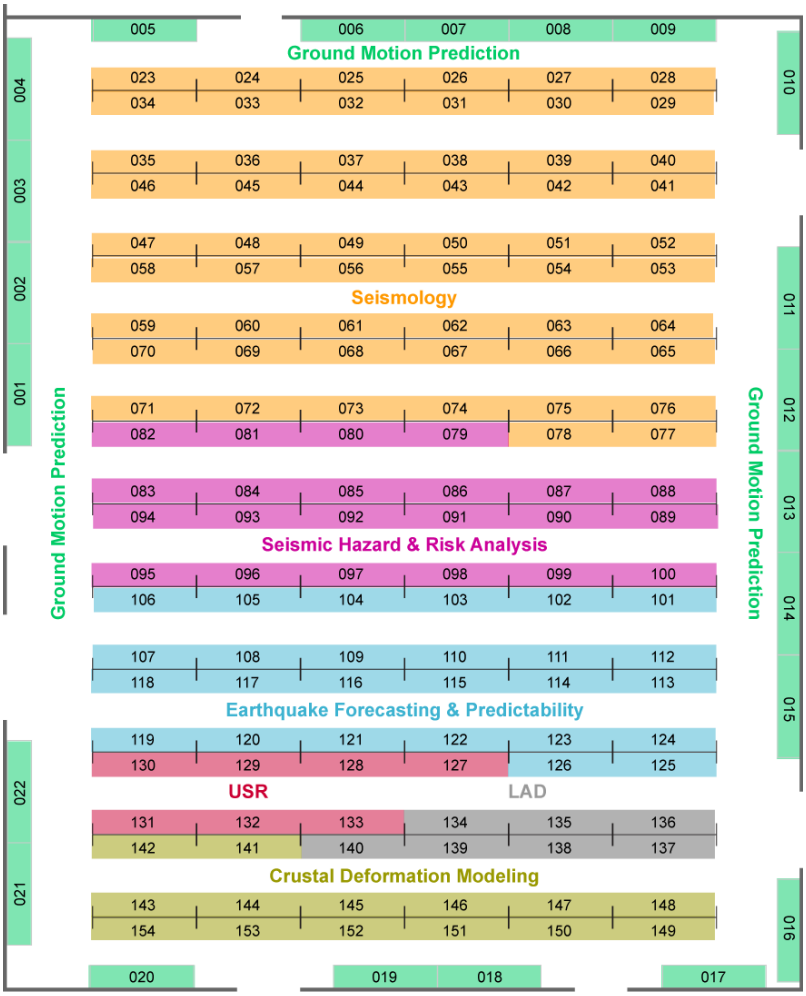

Crustal Deformation Modeling (CDM)

B-141 **SENSITIVITY OF THE SOUTHERN SAN ANDREAS FAULT SYSTEM TO TECTONIC BOUNDARY CONDITIONS**, *J.W. Herbert and M.L. Cooke*

B-142 **STRESS-SLIP BEHAVIOR OF A SHEARED GRANULAR MATERIAL WITH GRAIN BREAKAGE USING THE SHEAR-TRANSFORMATION-ZONE THEORY**, *C.K.C. Lieou, A.E. Elbanna, J.S. Langer, and J.M. Carlson*

B-143 **NEAR REAL-TIME ESTIMATION OF VELOCITY GRADIENT TENSOR FIELDS FOR CONTINUOUS MONITORING IN SOUTHERN CALIFORNIA**, *W.E. Holt, G. Shcherbenko, and E. Caruso*

B-144 **LOW-STRENGTH FRICTIONAL CREEP ON THE LOWER-CRUSTAL EXTENSION OF THE SAN ANDREAS FAULT NEAR PARKFIELD, CA**, *K.M. Johnson, D. Shelly, and A.M. Bradley*

B-145 **NUMERICAL MODELING OF INTERSEISMIC EARTHQUAKE-INDUCED VERTICAL MOTION ASSOCIATED WITH THE SAN ANDREAS FAULT SYSTEM**, *B.P. Hooks, B.R. Smith-Konter, and G. Thornton*

B-146 **MECHANICS OF STRESS TRANSFER FROM PLATE MOTION TO PLATE BOUNDARY FAULTS: DYNAMIC MODELS OF EARTHQUAKE CYCLES ON A STRIKE-SLIP FAULT**, *C.S. Takeuchi and Y. Fialko*

B-147 **INCORPORATING GPS VELOCITIES INTO UCERF3**, *W. Thatcher, P. Bird, J. Bormann, T. Dawson, E. Field, W. Hammond, E. Hearn, K. Johnson, R. McCaffrey, D. Sandwell, and Y. Zeng*

B-148 **ANALYTIC CALCULATION OF STRESSING RATES IN SOUTHERN CALIFORNIA**, *J.P. Loveless and B.J. Meade*

B-149 **MINIMAL MODELS OF FAULT SLIP IN COMPLEX FAULT SYSTEMS**, *B.J. Meade, E.L. Evans, and J.P. Loveless*

B-150 **PYLITH: A FINITE-ELEMENT CODE FOR MODELING QUASI-STATIC AND DYNAMIC CRUSTAL DEFORMATION**, *B. Aagaard, C. Williams, and M. Knepley*

B-151 **HOW DO "GHOST TRANSIENTS" FROM PAST EARTHQUAKES AFFECT GPS SLIP RATE ESTIMATES ON SOUTHERN CALIFORNIA FAULTS?**, *E.H. Hearn, F.F. Pollitz, W.R. Thatcher, and T. Onishi*

B-152 **DO SMALL SURFACE STRAINS IN THE NEW MADRID SEISMIC ZONE REFLECT A PHYSICAL PROCESS?**, *O.S. Boyd, Y. Zeng, L. Ramirez-Guzman, and R. Smalley*

B-153 **SPACE GEODETIC INVESTIGATION OF INTERSEISMIC DEFORMATION DUE TO THE SAN JACINTO FAULT NEAR ANZA, CA**, *V. Sahakian, Y. Fialko, Y. Bock, and T. Rockwell*

Earthquake Forecasting & Predictability (EFP)

B-101 **INJECTING INFORMATION FROM STATIC COULOMB MODELS INTO STATISTICAL AFTERSHOCK MODELS FOR THE CANTERBURY, NEW ZEALAND, EARTHQUAKE SEQUENCE**, *C.A. Williams, M.C. Gerstenberger, and S. Steacy*

B-102 **CORRELATION OF PEAK DYNAMIC AND STATIC COULOMB FAILURE STRESS WITH SEISMICITY RATE CHANGE AFTER THE M7.2 EL MAYOR-CUCAPAH EARTHQUAKE**, *K.B. Withers and K.B. Olsen*

B-103 **THE EFFECTS OF STATIC COULOMB, NORMAL AND SHEAR STRESS CHANGES ON EARTHQUAKE OCCURRENCE IN SOUTHERN CALIFORNIA**, *A.E. Strader and D.D. Jackson*

B-104 **COULOMB STRESS CHANGES IMPARTED BY SIMULATED M>7 EARTHQUAKES TO MAJOR FAULT SURFACES IN SOUTHERN CALIFORNIA**, *J.C. Rollins, G.P. Ely, and T.H. Jordan*

B-105 **HAS THE RISK OF BIG EARTHQUAKES RECENTLY INCREASED?** *P.M. Shearer and P.B. Stark*

B-106 **TOHOKU EARTHQUAKE: A SURPRISE?**, *Y.Y. Kagan and D.D. Jackson*

B-107 **AFTERSHOCK STATISTICS OF THE 1999 CHI-CHI, TAIWAN EARTHQUAKE**, *Y.-T. Lee, D. L. Turcotte, J. B. Rundle, and C.-C. Chen*

B-108 **FREQUENCY-MAGNITUDE DISTRIBUTIONS OF TRIGGERED AND NON-TRIGGERED POPULATIONS OF SEISMICITY**, *S. Hernandez and E.E. Brodsky*

B-109 **COMPARISONS AMONG EARTHQUAKE SIMULATOR RESULTS FOR UCERF2 FAULT MODEL OF CALIFORNIA AND OBSERVED SEISMICITY**, *T.E. Tullis, K. Richards-Dinger, M. Barall, J.H. Dieterich, E.H. Field, E. Heien, L.H. Kellogg, F. Pollitz, J. Rundle, M. Sachs, D.L. Turcotte, S.N. Ward, B. Yikilmaz, and O. Zielke*

B-110 **THE FUTURE OF VIRTUAL CALIFORNIA SIMULATIONS**, *M.B. Yikilmaz, J.B. Rundle, D.L. Turcotte, E.M. Heien, M.K. Sachs, and L.H. Kellogg*

B-111 **PARALLEL SIMULATED ANNEALING APPROACH TO SOLVE FOR UCERF3 RUPTURE RATES**, *K.R. Milner, M.T. Page, and E.H. Field*

B-112 **AN EARTHQUAKE RUPTURE FORECAST INVERSION APPLIED TO FAULT SYSTEMS IN CALIFORNIA**, *M.T. Page, E.H. Field, and K.R. Milner*

B-113 **STOCHASTIC SOURCE MODEL FOR SEISMIC HAZARD ESTIMATION**, *S. Hiemer, Q. Wang, D.D. Jackson, Y.Y. Kagan, S. Wiemer, J.D. Zechar, and J. Woessner*

B-114 **LIDAR-DERIVED MEASUREMENTS OF SLIP IN THE MOST RECENT GROUND-RUPTURING EARTHQUAKES ALONG ELEMENTS OF THE SOUTHERN SAN ANDREAS FAULT SYSTEM**, *D.E. Haddad, C. Madden, J.R. Arrowsmith, J.B. Salisbury, and R.J. Weldon*

B-115 **CONSTANT STRESS DROP FITS EARTHQUAKE SURFACE SLIP-LENGTH DATA**, *B.E. Shaw*

B-116 **EARTHQUAKE SCALING RELATIONSHIPS ESTIMATED FROM A 16 YEAR CATALOG OF PUBLISHED INSAR STUDIES**, *G.J. Funning, J. Weston, J.R. Elliott, A.M.G. Ferreira, and K. Richards-Dinger*

B-117 **CSEP OVERVIEW**, *D. Schorlemmer, M.C. Gerstenberger, N. Hirata, D.D. Jackson, C. Jiang, T.H. Jordan, W. Marzocchi, K.Z. Nanjo, G. A. Papadopoulos, D.A. Rhoades, S. Wiemer, Z. Wu, J.D. Zechar, and CSEP Working Group*

B-118 **NEW DEVELOPMENTS AND FUTURE APPLICATIONS OF THE COLLABORATORY FOR THE STUDY OF EARTHQUAKE PREDICTABILITY (CSEP) TESTING FRAMEWORK**, *M. Liukis, D. Schorlemmer, J. Yu, P. Maechling, J. Zechar, T.H. Jordan, and he CSEP Working Group*

B-119 **RESULTS FROM THE REGIONAL EARTHQUAKE LIKELIHOOD MODELS EXPERIMENT**, *D. Schorlemmer, J.D. Zechar, M.J. Werner, M.C. Gerstenberger, and D.A. Rhoades*

B-120 **AN EVALUATION OF THE RELM TEST FORECASTS**, *M.K. Sachs, Y.T. Lee, D.L. Turcotte, J.R. Holliday, and J.B. Rundle*

B-121 **A TESTABLE EARTHQUAKE LIKELIHOOD MODEL BASED ON PROXIMITY TO KNOWN SOURCES**, *D.A. Rhoades and M.W. Stirling*

B-122 **TESTING SEGMENTATION MODELS**, *D.D. Jackson*

B-123 **ETAS VS. STEP**, *J.D. Zechar, D. Schorlemmer, M.C. Gerstenberger, and D.A. Rhoades*

B-124 **FULL EARTH HIGH-RESOLUTION EARTHQUAKE FORECASTS**, *Y.Y. Kagan and D.D. Jackson*

B-125 **CREATING PROBABILISTIC SEISMIC HAZARD MAPS FROM CSEP DATA**, *J.R. Holliday*

B-126 **ADVANCEMENTS IN PROBABILISTIC SEISMIC NETWORK COMPLETENESS STUDIES**, *D. Schorlemmer*

Ground Motion Prediction (GMP)

B-001 **SEISMICALLY DAMAGED REGOLITH AS SELF-ORGANIZED FRAGILE GEOLOGICAL FEATURE**, *N.H. Sleep*

B-002 **DEVELOPING A PHYSICS-BASED RUPTURE MODEL GENERATOR BASED ON 1-POINT AND 2-POINT STATISTICS OF KINEMATIC SOURCE PARAMETERS**, *S. Song*

B-003 **COMPLEXITY OF THE M6.3 2009 L'AQUILA (CENTRAL ITALY) EARTHQUAKE: SLIP INVERSION AND BROAD-BAND MODELING OF STRONG-GROUND MOTIONS**, *F. Gallovic, J. Zahradnik, G. Ameri, and F. Pacor*

B-004 **A PROGRESS REPORT ON THE ARRA-FUNDED GEOTECHNICAL SITE CHARACTERIZATION PROJECT**, *A. Martin, A. Yong, K. Stokoe, A. Di Matteo, S. Jack, and J. Diehl*

B-005 **DIRECTIVITY-BASIN COUPLING IN THE LOS ANGELES REGION FROM THE CYBERSHAKE HAZARD MODEL**, *F. Wang, T.H. Jordan, S. Callaghan, K. Milner, P. Maechling, R. Graves, and CyberShake Collaboration*

B-006 **3-D FINITE ELEMENT MODELING OF PRECARIOUSLY BALANCED ROCKS**, *S. Veeraraghavan and S. Krishnan*

B-007 **MODELING GROUND MOTION OF A M7+ EARTHQUAKE ON THE SAN ANDREAS FAULT USING THE VIRTUAL EARTHQUAKE APPROACH**, *M. Denolle, G.C. Beroza, E.M. Dunham, and G. Prieto*

B-008 **NEW BE-10 EXPOSURE AGES AND FRAGILITIES FOR PRECARIOUSLY BALANCED ROCKS TEST PSHA AND RUPTURE MODELS IN SOUTHERN CALIFORNIA**, *D.H. Rood, R. Anooshehpoor, G. Balco, J. Brune, R. Brune, L. Grant Ludwig, K. Kendrick, M. Purvance, and I. Saleeby*

B-009 **STOCHASTIC SIMULATION OF EARTHQUAKE GROUND MOTION COMPONENTS FOR SPECIFIED EARTHQUAKE AND SITE CHARACTERISTICS: A TOOL FOR PERFORMANCE-BASED EARTHQUAKE ENGINEERING**, *S. Rezaeian*

B-010 **USING GROUND-BASED LIDAR AND MORPHOMETRIC ANALYSIS TO STUDY THE EVOLUTION OF PRECARIOUSLY BALANCED ROCKS**, *J.E. Harvey and D.H. Rood*

B-011 **BAYESIAN EARTHQUAKE SOURCE VALIDATION FOR GROUND MOTION SIMULATION**, *H.C. Jimenez, P.M. Mai, E. Prudencio, I. Babuska, M. Motamed, and R. Tempone*

B-012 **GENERATING BROADBAND SEISMOGRAMS FOR A SUITE OF SAN ANDREAS EARTHQUAKES**, *R. Mourhatch and S. Krishnan*

B-013 **OPEN-SOURCE GROUND MOTION SELECTION USING THE GENERALIZED CONDITIONAL INTENSITY MEASURE (GCIM) APPROACH**, *B.A. Bradley*

B-014 **STRONG GROUND MOTION IN PORT-AU-PRINCE, HAITI, DURING THE 12 JANUARY 2010 M7.0 HAITI EARTHQUAKE**, *S.E. Hough, T. Taniguchi, J.R. Altidor, D. Angllade, S.L. Mildor, and D. Given*

B-015 **PARTIAL TESTS AND ACID TESTS OF GROUND-MOTION MODELS FOR**

INHIBITION OF VERY STRONG SHAKING, *D.A. Rhoades, G.H. McVerry, and J.X. Zhao*

B-016 **GENERATING STOCHASTIC SOURCE MODELS USING INSIGHTS FROM LABORATORY EARTHQUAKES**, *H. Siriki and S. Krishnan*

B-017 **SPATIAL VARIABILITY OF GROUND MOTION AMPLIFICATION FROM LOW-VELOCITY SEDIMENTS INCLUDING FRACTAL INHOMOGENEITIES WITH SPECIAL REFERENCE TO THE SOUTHERN CALIFORNIA BASINS**, *K.B. Olsen and B.H. Jacobsen*

B-018 **TESTING SCEC 3D SEISMIC VELOCITY MODELS IN THE SAN BERNARDINO AND LOS ANGELES BASIN REGIONS**, *R.W. Graves, A. Plesch, and J. Shaw*

B-019 **GROUND MOTION PREDICTION EQUATIONS FOR DATA RECORDED IN THE IMMEDIATE VICINITY OF THE SAN JACINTO FAULT ZONE**, *I. Kurzon, F.L. Vernon, and Y. Ben-Zion*

B-020 **SCEC BROADBAND PLATFORM STRONG GROUND MOTION SIMULATIONS**, *S. Kumar, S. Callaghan, P.J. Maechling, K.B. Olsen, R. Archuleta, P. Somerville, R. Graves, T.H. Jordan, and the Broadband Platform Working Group*

B-021 **CHARACTERISTICS OF STRONG GROUND MOTION ATTENUATION DURING THE 2010 M7.1 DARFIELD AND 2011 M6.3 CHRISTCHURCH, NEW ZEALAND EARTHQUAKES**, *M. Segou and E. Kalkan*

B-022 **A PERMANENTLY DEPLOYED CROSS-HOLE EXPERIMENT FOR MONITORING DEGRADATION AND RECOVERY OF SHEAR MODULUS AT THE NEES@UCSB GARNER VALLEY FIELD SITE**, *R. Gee, J. Steidl, and P. Hegarty*

Lithospheric Architecture & Dynamics (LAD)

B-134 **THE SALTON SEISMIC IMAGING PROJECT: INVESTIGATING EARTHQUAKE HAZARDS IN THE SALTON TROUGH, SOUTHERN CALIFORNIA**, *G.S. Fuis, M.R. Goldman, R.R. Sickler, R.D. Catchings, M.J. Rymer, E.J. Rose, J.M. Murphy, L.A. Butcher, J.A. Cotton, C.J. Criley, D.S. Croker, I. Emmons, A.J. Ferguson, M.A. Gardner, E.G . Jensen, R. McClearn, C.L. Loughran, C.J. Slayday-Criley, J.R. Svitek, J.A. Hole, J.M. Stock, S. Skinner, N.W. Driscoll, A.J. Harding, J. Babcock, G.M. Kent, A. Kell, and S.H. Harder*

B-135 **MOHO DISCONTINUITY STUDY ALONG SAN ANDREAS FAULT WITH RECEIVER FUNCTIONS**, *P.A. Cox, P.M. Davis, and R.W. Clayton*

B-136 **SEISMIC ANISOTROPY OF THE PELONA SCHIST FROM ELECTRON BACKSCATTER DIFFRACTION (EBSD) MEASUREMENTS OF CRYSTAL PREFERRED ORIENTATIONS (CPOS)**, *K.C. Wagner, S. Brownlee, and B. Hacker*

B-137 **CRUSTAL STRUCTURE OF THE SALTON TROUGH AND SOUTHERN SAN ANDREAS FAULT FROM NEW GRAVITY AND MAGNETIC DATA**, *V.E. Langenheim, D.S. Scheirer, and N.D. Athens*

B-138 **LOWER CRUSTAL ANISOTROPY IN THE MOJAVE DESERT REGION FROM ELECTRON BACKSCATTER DIFFRACTION (EBSD) MEASUREMENTS OF CRYSTAL PREFERRED ORIENTATION (CPO)**, *S.J. Brownlee, K. Wagner, and B.R. Hacker*

B-139 **PRELIMINARY RESULTS ON THE ANALYSIS OF THE DEVIATORIC STRESS FIELD FROM FOCAL MECHANISMS AND SLIP-LINE FIELD FROM CONJUGATE LINEAR SEISMICITY CLUSTERS IN SOUTHERN CALIFORNIA**, *W. Yang and E. Hauksson*

B-140 **STRAIN LOCALIZATION AND CRUSTAL THICKNESS VARIATION ACROSS MAJOR STRIKE SLIP FAULTS IN SOUTHERN CALIFORNIA REVEALED BY RECEIVER FUNCTION STUDIES**, *P. Zhang, M.S. Miller, J.F. Dolan, I.W. Bailey, and D.A. Okaya*

Seismic Hazard & Risk Analysis (SHRA)

B-079 **COMPARISON OF USGS PAGER EMPIRICAL FATALITY RATES TO RECONNAISSANCE OBSERVATIONS AND AN ACCOUNTING OF UNCERTAINTIES IN THE FATALITY MODEL**, *A.H. Olsen, E. So, M. Hearne, K. Jaiswal, and D.J. Wald*

B-080 **ACCURACY OF NON-DESTRUCTIVE TESTING OF PBRS TO ESTIMATE FRAGILITIES**, *J.N. Brune, R. Brune, G.P. Biasi, R. Anooshehpoor, and M.D. Purvance*

B-081 **VECTOR-VALUED FRAGILITIES AND THE STATE OF THE ARCHIVE FOR PRECARIOUSLY BALANCED ROCKS (PBRS) IN SOUTHERN CALIFORNIA**, *G.P. Biasi, J.N. Brune, and A.W. Homan*

B-082 **CAN FAULT MAPS CONSTRAIN FUTURE EARTHQUAKE MAGNITUDES?**, *D.A. Weiser*

B-083 **CHANGE IN STATISTICS FROM A DIMENSIONAL TRANSITION: MEASURING B = 1.5 FOR LARGE EARTHQUAKES**, *M.R. Yoder, J.R. Holliday, D.L. Turcotte, and J.B. Rundle*

B-084 **ANALYZING AMBIENT NOISE USING USB MICRO-ELECTRO-MECHANICAL SYSTEMS (MEMS) ACCELEROMETERS**, *H.J. Potter, A. Chung, and J. Lawrence*

B-085 **NON-LINEAR BUILDING RESPONSE SIMULATIONS USING SCEC SIMULATED GROUND MOTIONS**, *C.A. Goulet and C.B. Haselton*

B-086 **PROBING CALIFORNIA'S COASTLINE TO UNEARTH TRACES OF PALEOTSUNAMIS: IMPLICATIONS FOR THE NEXT USGS MULTI-HAZARDS SCENARIO**, *R. Leeper, N. Graehl, E. Hemphill-Haley, D. Hoirup, B. Jaffe, H. Kelsey, R. Peters, and R. Wilson*

B-087 **PARALLELIZATION OF THE VIRTUAL CALIFORNIA EARTHQUAKE SIMULATOR**, *E.M. Heien, M.B. Yikilmaz, M.K. Sachs, J.B. Rundle, L.H. Kellogg, and D.L. Turcotte*

B-088 **PROBABILISTIC ASSESSMENT OF BUILDING RESPONSE TO SIMULATED AND RECORDED GROUND MOTIONS**, *K.L. Rowe and A.B. Liel*

B-089 **OPENSHA AND THE USGS NATIONAL SEISMIC HAZARD MAPS**, *P.M. Powers*

B-090 **ENGINEERING VALIDATION OF GROUND MOTION SIMULATION: PART 1. ELASTIC AND INELASTIC SPECTRA**, *C. Galasso, F. Zareian, I. Iervolino, and R.W. Graves*

B-091 **ENGINEERING VALIDATION OF GROUND MOTION SIMULATION: PART 2. MAXIMUM INTERSTORY DRIFT RATIO AND CRITICAL STORY SPECTRA**, *C. Galasso, F. Zareian, I. Iervolino, and R.W. Graves*

B-092 **INVESTIGATING THE IMPACT OF SPACE-GEODETIC DATA ON EARTHQUAKE RISK ANALYSES FOR CALIFORNIA**, *C.M. Mak and M. Nyst*

B-093 **UPDATING THE NEW ZEALAND NSHM FROM THE CANTERBURY EARTHQUAKE SEQUENCE**, *M. Gerstenberger, G. McVerry, D. Rhoades, M. Stirling, K. Berryman, and T. Webb*

B-094 **INTEGRATING NONLINEAR SITE RESPONSE MODELS IN BROADBAND GROUND MOTION PREDICTIONS**, *D. Assimaki and W. Li*

B-095 **GROUND MOTION AMPLIFICATION DURING THE M7.0 2010 HAITI EARTHQUAKE: TOPOGRAPHY OR SOIL EFFECTS?**, *D. Assimaki and S. Jeong*

B-096 **FUTURE DIRECTIONS FOR STUDIES OF PRECARIOUSLY BALANCED ROCKS**, *J.G. Anderson, G.P. Biasi, and J.N. Brune*

B-097 **CONSEQUENCES OF THE ASSUMPTIONS REGARDING SEGMENTATION VERSUS NONSEGMENTATION OF THE SHORELINE FAULT WHEN ESTIMATING EARTHQUAKE POTENTIAL AND SEISMIC LOAD FOR DIABLO CANYON NUCLEAR POWER PLANT (DCNPP)**, *A. Bykovtsev and M. Kasimov*

B-098 **TSUNAMI HAZARD MAPPING ACTIVITIES IN SOUTHERN CALIFORNIA**, *R. Wilson, K. Miller, C. Real, J. Goltz, and J. Treiman*

B-099 **A NEW AGE CONSTRAINT FOR A NEAR-FAULT PRECARIOUS LANDFORM IN CENTRAL OTAGO, NEW ZEALAND**, *M. Stirling, D. Rood, G. Balco, and A. Zondervan*

Seismology

B-023 **SEISMIC VELOCITY STRUCTURES IN THE SOUTHERN CALIFORNIA PLATE BOUNDARY ENVIRONMENT FROM DOUBLE-DIFFERENCE TOMOGRAPHY**, *A.A. Allam and Y. Ben-Zion*

B-024 **DEVELOPING A THREE-DIMENSIONAL GEOLOGICAL AND GEOPHYSICAL MODEL OF SIERRA NEGRA VOLCANO OF THE GALAPAGOS**, *L.C. Davidge and C. Ebinger*

B-025 **COMPARISON OF THE LOW-COST MEMS ACCELEROMETERS USED BY THE QUAKE-CATCHER NETWORK AND TRADITIONAL STRONG MOTION SEISMIC SENSORS**, *E.S. Cochran, J.F. Lawrence, A. Kaiser, B. Fry, and A. Chung*

B-026 **GPS AND ACCELEROMETER COMBINATION FOR REAL-TIME SOURCE MODELING AND EARTHQUAKE EARLY WARNING**, *D. Melgar, B.W. Crowell, and Y. Bock*

B-027 **SPATIAL DISTRIBUTIONS OF FORESHOCKS AND AFTERSHOCKS: STATIC OR DYNAMIC TRIGGERING?**, *M.J. Werner and A.M. Rubin*

B-028 **RELATIONS BETWEEN PROPERTIES OF SEISMICITY AND REGIONAL HEAT FLOW IN CALIFORNIA**, *I. Zaliapin and Y. Ben-Zion*

B-029 **IDENTIFYING FAULT HETEROGENEITY THROUGH MAPPING SPATIAL ANOMALIES IN ACOUSTIC EMISSION STATISTICS**, *T.H. Goebel, T. Becker, D. Schorlemmer, S. Stanchits, C. Sammis, E. Rybacki, and G. Dresen*

B-030 **EARTHQUAKE CLUSTERING AND AFTERSHOCK STATISTICS IN SIMULATED CATALOGS**, *J.J. Gilchrist, J.H. Dieterich, and K.B. Richards-Dinger*

B-031 **POTENTIAL MAGNITUDE DEPENDENT QUIESCENCE PRIOR TO THE NORTHRIDGE EARTHQUAKE**, *D.E. Smith and S.I. Sacks*

B-032 **THE MECHANICS OF EARTHQUAKES AND FAULTING IN THE SOUTHERN GULF OF CALIFORNIA**, *D.F. Sumy, J.B. Gaherty, W.-Y. Kim, and T. Diehl*

B-033 **ON THE QUANTIFICATION OF ROBUSTNESS WHEN COMPARING KINEMATIC INVERSION MODELS: A WAVELET APPROACH**, *D. Lavallee, G. Shao, and C. Ji*

B-034 **SOURCE PROCESSES OF MICROEARTHQUAKES AT PARKFIELD, CA, DETERMINED BY NEAR-SOURCE OBSERVATION AT SAFOD MAIN HOLE**, *K. Imanishi and W.L. Ellsworth*

B-035 **INTERACTION BETWEEN EARTHQUAKE GROUND MOTION AND BUILDING MODELS -- A 3D PARAMETRIC STUDY**, *Y.D. Isbiliroglu, R. Taborda, and J. Bielak*

B-036 **CONNECTING THE SPATIAL DISTRIBUTION OF ACOUSTIC EMISSIONS TO FAULT ROUGHNESS DURING STICK-SLIP EXPERIMENTS**, *T.H. Goebel, C. Sammis, and T. Becker*

B-037 **COMPLEX RUPTURE MODES OF THE 2011 MW 9.0 TOHOKU-OKI EARTHQUAKE INFERRED FROM TELESEISMIC AND LOCAL WAVEFORMS**, *H. Yao*

B-038 **LOVE WAVE TRIGGERS TREMOR ALONG SAN JACINTO FAULT IN THE ANZA REGION, CALIFORNIA**, *T.-H. Wang, E.S. Cochran, and D.D. Oglesby*

B-039 **GLOBAL SEARCH FOR DEEP TRIGGERED TREMOR**, *K. Chao, Z. Peng, B. Enescu, C. Wu, and B. Fry*

B-040 **COMPOUND EARTHQUAKES ON A BIMATERIAL INTERFACE AND IMPLICATIONS FOR RUPTURE MECHANICS**, *E. Wang and A.M. Rubin*

B-041 **EARTHQUAKE NUCLEATION MECHANISMS AND DAMAGE IN HETEROGENEOUS FAULT ZONES, PROBED WITH PERIODIC LOADINGS (IN MODELS AND EXPERIMENTS)**, *B.W. Brinkman, Y. Ben-Zion, J.T. Uhl, and K.A. Dahmen*

B-042 **FULL-3D WAVEFORM TOMOGRAPHY FOR NORTHERN CALIFORNIA USING AMBIENT-NOISE CROSS-CORRELATION GREEN'S-FUNCTIONS**, *Z. Xu and P. Chen*

B-043 **STRESS DROP OBSERVATIONS FOR THE 2010 EL MAYOR AFTERSHOCKS WITH $4.0<M_W<5.5$ RECORDED AT THE BORREGO VALLEY DOWNHOLE ARRAY**, *J. Crempien and R. Archuleta*

B-044 **MONITORING TECTONIC TREMORS IN THE SAN-JACINTO FAULT ZONE USING MULTIPLE SMALL-APERTURE SEISMIC ARRAYS**, *A. Inbal, J.P. Ampuero, and J.H. Steidl*

B-045 **MARINE AND LAND ACTIVE-SOURCE SEISMIC INVESTIGATION OF GEOTHERMAL POTENTIAL, TECTONIC STRUCTURE, AND EARTHQUAKE HAZARDS IN PYRAMID LAKE, NEVADA**, *A. Eisses, A. Kell, G. Kent, N. Driscoll, R. Karlin, R. Baskin, J. Louie, K. Smith, and S. Pullammanappallil*

B-046 **AFTERSHOCK RELOCATION IN THE YUHA DESERT FOLLOWING THE 4 APRIL 2010 M7.2 EL MAYOR-CUCAPAH EARTHQUAKE**, *K.A. Kroll, E.S. Cochran, and K.B. Richards-Dinger*

B-047 **IDENTIFYING AND LOCATING TECTONIC TREMOR BENEATH THE SAN ANDREAS FAULT NEAR PARKFIELD, CA, WITH THE PASO ARRAY**, *D. Peterson, C. Thurber, E. Montgomery-Brown, J. Brown, and D. Shelly*

B-048 **EARTHQUAKE MOTIONS RECORDED ON A DENSE 5000-STATION NETWORK IN LONG BEACH, CA**, *M. Barba, R.W. Clayton, and D. Hollis*

B-049 **COSEISMIC SLIP DISTRIBUTION AND HIGH FREQUENCY RADIATION OF THE 2010 MW 7.3 EL MAYOR-CUCAPAH EARTHQUAKE**, *G. Shao, T.E. Yano, X. Zhao, C. Ji, K.M. Larson, K. Hudnut, and T. Herring*

B-050 **MULTIPLE DOUBLE COUPLE ANALYSIS FOR M6-7 EARTHQUAKES**, *X. Li, G. Shao, and C. Ji*

B-051 **PATH CALIBRATION FOR EVENTS IN THE LOWER IMPERIAL VALLEY BASIN**, *X. Tian, S. Wei, Z. Zhan, and D.V. Helmberger*

B-052 **SITE RESPONSE IN THE BÍOBÍO REGION, CHILE USING THE K METHOD**, *C. Neighbors, E.J. Liao, E.S. Cochran, A.I. Chung, J.F. Lawrence, A. Belmonte, M. Miller, H.H. Sepulveda, and C. Christensen*

B-053 **DYNAMIC RUPTURE SIMULATION WITH A HIGH-ORDER DISCONTINUOUS GALERKIN METHOD ON UNSTRUCTURED TETRAHEDRAL MESHES**, *C. Pelties, J. de la Puente, J.-P. Ampuero, G. Brietzke, and M. Käser*

B-054 **STATION-TO-STATION GREEN'S FUNCTIONS EXTRACTED FROM SEISMIC CODA IN SOUTHERN CALIFORNIA**, *E.T. Hirakawa and S. Ma*

B-055 **STRONG GROUND MOTIONS OBSERVED IN THE 22 FEBRUARY 2011 CHRISTCHURCH EARTHQUAKE**, *B.A. Bradley and M. Cubrinovski*

B-056 **A METHOD FOR EARTHQUAKE CYCLE SIMULATIONS: QUASI-STATIC**

EVOLUTION TO DYNAMIC RUPTURE, *B.A. Erickson and E.M. Dunham*

B-057 **EFFECTS OF PARAMETERIZATION ON FINITE SOURCE INVERSIONS WITH DENSE LOCAL DATA**, *S. N. Somala, J. -P. Ampuero, and N. Lapusta*

B-058 **PREPARING TRIAL MODELS OF SPATIAL VARIABILITY IN GEOTECHNICAL VELOCITIES FOR ASSESSING EFFECTS ON GROUND MOTIONS**, *W.H. Savran and J.N. Louie*

B-059 **TELESEISMIC P WAVE CODA OF SUBDUCTION EARTHQUAKES FROM WAVE INTERACTION NEAR TRENCHES**, *W. Wu and S. Ni*

B-060 **AUTO-CORRELATION CLUSTERING EVENT DETECTION APPLIED TO TECTONIC TREMOR**, *A.C. Aguiar and G.C. Beroza*

B-061 **LOCAL AND REGIONAL SEISMIC RESPONSE TO INJECTION AND PRODUCTION AT THE SALTON SEA GEOTHERMAL FIELD, SOUTHERN CALIFORNIA**, *L.J. Lajoie and E.E. Brodsky*

B-062 **WAVEFORM RELOCATED EARTHQUAKE CATALOG FOR SOUTHERN CALIFORNIA (1981 TO 2011)**, *E. Hauksson, W. Yang, and P. Shearer*

B-063 **HIGH-FREQUENCY AMBIENT NOISE TOMOGRAPHY USING INDUSTRIAL SEISMIC ARRAY IN LONG BEACH, CALIFORNIA**, *F. Lin and R.W. Clayton*

B-064 **GEOMETRY OF FAULT SLIP ZONES AT DEPTH FROM QUANTITATIVE ANALYSIS OF SEISMIC CATALOGS: METHOD AND RESULTS FOR THE SAN JACINTO FAULT ZONE**, *Y. Ozakin and Y. Ben-Zion*

B-065 **SALTON SEISMIC IMAGING PROJECT**, *E. Jimenez, J.D. Rodriguez, and J. Stock*

B-066 **PRODUCTS AND SERVICES AVAILABLE FROM THE SOUTHERN CALIFORNIA EARTHQUAKE DATA CENTER (SCEDC) AND THE SOUTHERN CALIFORNIA SEISMIC NETWORK (SCSN)**, *E. Yu, A. Bhaskaran, S. Chen, M.J. Ihrig, F. Chowdhury, S. Meisenhelter, K. Hutton, D. Given, E. Hauksson, and R. Clayton*

B-067 **A GUIDE TO SELECTING EMPIRICAL GREEN'S FUNCTIONS IN REGIONS OF FAULT COMPLEXITY: A STUDY OF DATA FROM THE SAN JACINTO FAULT ZONE, SOUTHERN CALIFORNIA**, *D.L. Kane, D.L. Kilb, and F.L. Vernon*

B-068 **COMPARATIVE STUDY OF SCATTERING AND INTRINSIC ATTENUATION IN CALIFORNIA, MEXICO AND PERU. DOES THE TECTONIC SETTING AFFECT THE FREQUENCY DEPENDENCE?**, *L.A. Dominguez, P.M. Davis, and M. Madrid*

B-069 **DETECTING MISSING EARTHQUAKES ON THE PARKFIELD SECTION OF THE SAN ANDREAS FAULT FOLLOWING THE 2003 MW6.5 SAN SIMEON EARTHQUAKE**, *X. Meng, Z. Peng, and J.L. Hardebeck*

B-070 **DIFFERENTIATING STATIC AND DYNAMIC TRIGGERING NEAR SALTON SEA FOLLOWING THE 2010 MW7.2 EL MAYOR-CUCAPAH EARTHQUAKE**, *X. Meng, Z. Peng, and P. Zhao*

B-071 **STATISTICAL ANALYSIS OF 71 BURSTS IN SOUTHERN CALIFORNIA**, *X. Chen, P.M. Shearer, and R. Abercrombie*

B-072 **FOCAL MECHANISM WITH ERROR ESTIMATION USING REGIONAL WAVEFORMS: A CASE STUDY WITH THE 2008 CHINO HILLS EARTHQUAKE**, *Z. Zhan, S. Wei, and D. Helmberger*

B-073 **APPROACHES FOR HIGH – PERFORMANCE WAVEFORM CROSS CORRELATION**, *R.J. Chen, G.C. Beroza, and W.L. Ellsworth*

B-074 **WIDESPREAD TRIGGERING OF EARTHQUAKES IN THE CENTRAL US BY THE 2011 M9.0 TOHOKU-OKI EARTHQUAKE**, *J.L. Rubinstein and H.M. Savage*

B-075 **THE 2011 MW 9 TOHOKU-OKI EARTHQUAKE: COMPLEXITY OF DYNAMIC RUPTURE AT THE BOTTOM OF A SEISMOGENIC ZONE**, *L. Meng, J.P. Ampuero, and A. Inbal*

B-076 **2011 LONG BEACH/SIGNAL HILL, CA SEISMIC STUDY**, *D.D. Hollis*

B-077 **COMPUTING A LARGE REFINED CATALOG OF FOCAL MECHANISMS FOR SOUTHERN CALIFORNIA (1981 – 2010)**, *W. Yang, E. Hauksson, and P.M. Shearer*

B-078 **RESULTS FROM THE QUAKE-CATCHER NETWORK RAPID AFTERSHOCK MOBILIZATION PROGRAM (QCN-RAMP) IN CHRISTCHURCH, NEW ZEALAND**, *A.I. Chung, E.S. Cochran, C. Christensen, A.E. Kaiser, and J.F. Lawrence*

Unified Structural Representation (USR)

B-127 **SEISMOGRAM-BASED ASSESSMENT OF THE SOUTHERN CALIFORNIA SEISMIC VELOCITY MODEL CVM-H 11.9 WITH 234 REFERENCE EARTHQUAKES**, *C. Tape, E. Casarotti, A. Plesch, and J.H. Shaw*

B-128 **UPDATES FOR THE CVM-H INCLUDING NEW REPRESENTATIONS OF THE OFFSHORE SANTA MARIA AND SAN BERNARDINO BASINS AND A NEW MOHO SURFACE**, *A. Plesch, C. Tape, R. Graves, J.H. Shaw, P. Small, and G. Ely*

B-129 **SCEC UCVM – UNIFIED CALIFORNIA VELOCITY MODEL**, *P. Small, P. Maechling, T. Jordan, G. Ely, and R. Taborda*

B-130 **USING STRUCTURAL CONSTRAINTS ON THE LITTLE SAN BERNARDINO MOUNTAINS TO PETROLOGICALLY AND GEOCHEMICAL ANALYZE THE CRUSTAL VELOCITY MODEL OF SOUTHERN CALIFORNIA**, *C. Symcox and A. Barth*

B-131 **CFM V.4.0: CONTINUED UPGRADES AND IMPROVEMENTS TO THE SCEC COMMUNITY FAULT MODEL AND ITS ASSOCIATED FAULT DATABASE**, *C. Nicholson, A. Plesch, and J.H. Shaw*

B-132 **HIGH-RESOLUTION MAPPING AND ANALYSIS OF BORDERLAND FAULTS USING MULTIBEAM BATHYMETRY DATA**, *M.R. Legg, M. Kohler, D. Weeraratne, and N. Shintaku*

B-133 **FAULT ARCHITECTURE OF THE SALTON SEA THROUGH MULTI-SCALE SEISMIC REFLECTION SURVEYS**, *A.M. Kell, N. Driscoll, G.M. Kent, A. Harding, and R. Baskin*

Poster Abstracts

PYLITH: A FINITE-ELEMENT CODE FOR MODELING QUASI-STATIC AND DYNAMIC CRUSTAL DEFORMATION (B-150)

B. Aagaard, C. Williams, and M. Knepley

We have developed open-source finite-element software for 2-D and 3-D dynamic and quasi-static modeling of crustal deformation. This software, PyLith (current release is version 1.6) can be used for quasi-static viscoelastic modeling, dynamic spontaneous rupture and/or ground-motion modeling. Unstructured and structured finite-element discretizations allow for spatial scales ranging from tens of meters to hundreds of kilometers with temporal scales in dynamic problems ranging from milliseconds to minutes and temporal scales in quasi-static problems ranging from minutes to thousands of years. PyLith development is part of the NSF funded Computational Infrastructure for Geodynamics (CIG) and the software runs on a wide variety of platforms (laptops, workstations, and Beowulf clusters). Binaries (Linux, Darwin, and Windows systems) and source code are available from geodynamics.org. PyLith uses a suite of general, parallel, graph data structures called Sieve for storing and manipulating finite-element meshes. This permits use of a variety of 2-D and 3-D cell types including triangles, quadrilaterals, hexahedra, and tetrahedra.

Current PyLith features include prescribed fault ruptures with multiple earthquakes and aseismic creep, spontaneous fault ruptures with a variety of fault constitutive models, time-dependent Dirichlet and Neumann boundary conditions, absorbing boundary conditions, time-dependent point forces, and gravitational body forces. PyLith supports infinitesimal and small strain formulations for linear elastic rheologies, linear and generalized Maxwell viscoelastic rheologies, power-law viscoelastic rheologies, and Drucker-Prager elastoplastic rheologies. Current software development focuses on coupling quasi-static and dynamic simulations to resolve multi-scale deformation across the entire seismic cycle and the coupling of elasticity to heat and/or fluid flow.

AUTO-CORRELATION CLUSTERING EVENT DETECTION APPLIED TO TECTONIC TREMOR (B-060)

A.C. Aguiar and G.C. Beroza

We exploit the fact that tectonic tremor has been shown to be comprised of frequently occurring and repeating low frequency earthquakes (LFEs) to identify those events. We refer to this approach as the auto-correlation clustering detection method because it builds on the auto-correlation approach of Brown et al. (2008) which detects events based on pair-wise matching. Our method takes advantage of the fact that common signals repeat many times within the tremor signal. This method is applied to 24 hours of data during the April, 2006 tremor episode in the Nankai Trough in SW Japan. We analyze 1-hour periods at a time by auto-correlating 8 s windows shifted 2 samples each. We then shift 20 minutes ahead of the previously analyzed hour and carry detections until the 24 hours of data are completed. We apply a 3-sigma detection threshold to find individual matches, then tally the number of detections for each window and use this as our test statistic. For band-limited Gaussian white noise, the number of detections should follow a binomial distribution governed by the assumed detection threshold. We use this null hypothesis to test the significance of the detection of a candidate LFE family. Our method places the detection of LFE families on a sound statistical basis. It should improve our ability to detect LFEs within weak tremor signals and will likely be applicable to other earthquake swarms.

REVISITING WALLACE CREEK: NEW RADIOCARBON RESULTS AND SLIP RATE ESTIMATES OF THE SAN ANDREAS FAULT IN THE CARRIZO PLAIN (A-145)

S.O. Akciz, D.E. Haddad, W. Bohon, L. Mendes, G. Marliyani, B. Salisbury, T. Sato, L. Grant Ludwig, and J.R. Arrowsmith

Sieh and Jahns (1984) determined the slip rate of the San Andreas fault (SAF) at Wallace Creek in the Carrizo Plain, and thereby provided an anchor for nearly all data-driven models of the southern San Andreas fault behavior. Their landmark study has been referenced hundreds of times and is a critical constraint in many related studies and in hazard estimates for the south-central SAF. Slip rate estimates at Wallace Creek (33.9±2.9 mm/yr) and at Van Matre Ranch site (29.3-35.6 mm/yr; Noriega et al., 2006) agree well within measurement uncertainty, and with the 30–37 mm/yr velocity gradient across the SAF from decadal timescale geodetic measurements (Schmalzle, et al., 2006). Surprisingly, only a few detrital charcoal samples (9 samples at VMR, 8 samples at Wallace Creek) have been used to provide the absolute geochronological constraints. At a third site, Phelan Creeks, located ~ 2.5 km SE of Wallace Creek, 23 trenches were opened and over 400 charcoal samples were collected (Sims et al., unpublished data) to provide additional slip rate constraints, but the detailed study was never published.

New paleoseismologic investigations at the Bidart Fan site, ~5 km SE of Wallace Creek, indicate that southern SAF in the Carrizo Plain has apparently ruptured, on average, every 88 years (45-144 yr for individual intervals) between ~A.D. 1350 and 1857 (Akciz et al., 2010). B4 LiDAR (light detection and ranging) data analysis by Zielke et al. (2010) also found that only ~5.5 m of slip occurred along the SAF in the Carrizo Plain in 1857 and at least since ~A.D. 1400, and none of the earthquakes generated displacements larger than 5 meters (Grant Ludwig et al., 2010).

Slip per event and earthquake timing constraints can be tested against slip rate information to assess the steadiness of slip. Therefore, these new data and the geochronological limitations of the published slip-rate studies emphasize the need to improve, if not confirm, the existing slip-rate estimates by providing additional geochronological constraints. In August, 20111, we re-excavated T7 and T11 from Sieh and Jahns' study, photologged the trench walls (1:10) and collected a total of 30 new detrital charcoal samples from different stratigraphic layers from both of the trenches. Trench logs and radiocarbon results will be presented.

ONE-DIMENSIONAL ELASTIC MODELING OF FAULT SLIP RATES IN THE SALTON TROUGH, CALIFORNIA (A-058)

E. Alaniz and S.F. McGill

We used site velocities from SCEC's Crustal Motion Model 4 (CMM4) to conduct one-dimensional elastic modeling for fault slip rates along a transect across the Pacific-North America plate boundary through the Coachella Valley, southern California. Our best-fitting model has slip rates of 18 and 16 mm/yr for the San Andreas and San Jacinto faults, respectively, with a small amount (2 mm/yr) of right-lateral slip inferred east of the San Andreas fault and 4 mm/yr on the Elsinore fault. Other models that fit the site velocities reasonably well have slip rates ranging from 16-20 mm/yr for the San Andreas and 14-20 for the San Jacinto fault. These results are for the Coyote Creek strand of the San Jacinto fault. Future models will also include the Clark fault.

SEISMIC VELOCITY STRUCTURES IN THE SOUTHERN CALIFORNIA PLATE BOUNDARY ENVIRONMENT FROM DOUBLE-DIFFERENCE TOMOGRAPHY (B-023)

A.A. Allam and Y. Ben-Zion

We present tomographic images of crustal structures in the southern California plate boundary area, with a focus on the San Jacinto Fault Zone (SJFZ), based on double-difference inversions of earthquake arrival times. Absolute arrival times of over 359,410 P- and S- wave phase picks for 5493 earthquakes recorded at 139 stations in Southern California are used. In addition to the absolute event-station traveltimes, the double-difference inversions utilize differential travel times for phases from nearby event pairs. Starting with a layered 1D model, and continuing in later iterations with various updated initial models, we invert the data for Vp and Vs in a 270 km long, 180 km wide and 35 km deep volume around the SJFZ using a space-variable grid with higher density around the SJFZ. The examined volume stretches from Cajon Pass to the northernmost Imperial Fault Zone and includes portions of the southern San Andreas Fault (SAF), the Elsinore Fault, and the Brawley Seismic Zone in the Salton Trough. Because differential traveltimes are most sensitive to near-source structures, we obtain high resolution around the earthquake sources. After 24 iterations we improve the average travel time misfit by a factor of 20. Though ray coverage is limited at shallow depths, we obtain high-resolution images of seismic velocities from 3 to 16 km throughout much of the study area. Our final velocity model shows clear velocity contrasts across the SJFZ and the southern SAF as well as zones of low-velocity and anomalous Vp/Vs ratios associated with various fault strands and sedimentary basins. The NE side of the SJFZ has generally higher velocities than the SW block, and the contrasts of Vp are generally higher (up to 20%) than the contrasts of Vs (up to 15%). Near the San Jacinto valley to the NW, and the SE end of the SJFZ close to the Salton trough, the polarity of the velocity contrast in the shallow crust is reversed. For the southern SAF the NE side is generally the block with lower seismic velocities. The velocity reductions in fault zone regions are generally highest in geometrically complex areas (up to 25% in the top few km), and are higher for Vs than for Vp. The imaged features have important implications for various aspects of earthquake and crustal dynamics in the region.

FUTURE DIRECTIONS FOR STUDIES OF PRECARIOUSLY BALANCED ROCKS (B-096)

J.G. Anderson, G.P. Biasi, and J.N. Brune

In October, 2010, a workshop sponsored by the US Geological Survey discussed applications of precariously balanced rocks (PBR) to the National Hazard Maps (Anderson et al., 2011, Seis. Res. Lett.). A rough consensus of participants is that PBRs are useful to test probabilistic seismic hazard analyses (PSHA). Inconsistencies are a reason to reexamine inputs to the PSHA, but uncertainties in PBR properties could affect the interpretation. Only a few of the hundreds of known rocks have received "state of the art" scrutiny that minimizes uncertainties.

To improve usefulness of PBRs, participants identified several areas for future research. The major issues include dating, fragility, site response, extension to other environments, how to modify input to the PSHA, quantifying the difference between a site-specific PSHA and the USGS hazard curves, and the future of the PBR database.

We are preparing a database linking photos of known PBRs with locations and available information about fragility and age. A protocol for dealing with apparent inconsistencies with a PSHA hazard curve will be needed. We tentatively suggest the following tests:

Review of information about the PBR.

- What are the uncertainties on rocking parameters and fragility?
- What is the toppling direction?
- What are uncertainties on age of the present geometry?
- What are uncertainties in site response?
- Can the inconsistency be resolved within these uncertainties?
- Is the inconsistency supported by nearby PBRs?
- What upper bound on the ground motions vector, and associated rates, would be consistent with the rock?
- Review of input to the PSHA.
- What critical events in the input cause the inconsistency?
- Does data support the existence, magnitude, and rate of the critical events?
- Could the inconsistency be caused by the ergodic assumption? Might single-station or single-station and single-path sigma resolve the inconsistency?
- Is the median of the ground motion prediction equation (GMPE) too high?
- Could a consistent dynamic rupture effect (directivity, super-shear rupture, or step-over of rupture to adjacent faults) in the critical events resolve the inconsistency?
- Could ground motions be consistently polarized, giving smaller amplitudes than the GMPE estimates in the most sensitive toppling direction of the PBR, while motion in a less sensitive direction is stronger?

We propose this checklist to investigate inconsistencies and guide adjusting the input to the PSHA.

INTEGRATING NONLINEAR SITE RESPONSE MODELS IN BROADBAND GROUND MOTION PREDICTIONS (B-094)

D. Assimaki and W. Li

We investigate the empirical relationship between site response nonlinearity, soil properties, and ground motion amplitude and frequency. Our nonlinear site response code developed under the auspices of SCEC is currently being integrated in the Broadband Ground Motion Simulation Platform v11.7, and overarching goal of this work is to quantify when nonlinear analyses should be employed in lieu of empirical amplification factors, thus enabling efficient integration of site response analyses in earthquake ground motion simulations. Due to lack of a statistically significant sample of ground motion recordings, we subject 24 downhole array site profiles with detailed geotechnical information to broadband synthetics that account for nonlinear site response, and use the surface predictions as our ground motion database. We quantify the extent of soil nonlinearity in site-specific response analyses by estimating the divergence between linear and nonlinear ground surface predictions. We show that the parameters controlling the nonlinear response are the weighted averaged shear wave velocity in the top 30m of the soil profile (Vs30), the site amplication at the fundamental frequency, the peak ground acceleration (PGA), and the frequency index (FI), a quantitative measure we define to characterize the proportion of incident seismic energy that is trapped in the near-surface soil layers. Using the synthetic results, we quantitatively describe the error introduced in ground motion predictions when nonlinear effects are not accounted for, and show that the error is both site and

ground motion dependent. Our study indicates that to characterize the susceptibility of a site to nonlinear effects, Vs30 should be complemented by measures of the soil-rock impedance contrast, as well as measures of the ground motion intensity and frequency content.

GROUND MOTION AMPLIFICATION DURING THE M7.0 2010 HAITI EARTHQUAKE: TOPOGRAPHY OR SOIL EFFECTS? (B-095)

D. Assimaki and S. Jeong

Unusually severe structural damage was reported during the 2010 M7.0 Haiti earthquake in the vicinity of Hotel Montana, located on top of a ridge in the district of Pétionville. Prompted by the observations, USGS seismic stations were deployed, and aftershock recordings indicated ground motion amplification on the top of the hill compared to adjacent stations on reference site conditions. The presence of topographic relief has been shown to significantly aggravate the consequences of strong ground motion during past events, and topographic amplification was therefore brought forward to justify the observations. We here investigate the role of ground surface geometry in the recorded ground motions and corresponding damage concentration atop the foothill ridge of Hotel Montana by first conducting site-specific simulations that integrate Digital Elevation Maps (DEM) and shear wave velocity profiles collected at the site. Our analyses show that neither topography nor site amplification predictions alone sufficiently explain the ground motion amplification at the site estimated via aftershock recordings. Numerical simulations of the feature response on homogeneous halfspace quantitatively disagree with the field data both in amplitude and in frequency, while one-dimensional ground response analyses predict amplification in same frequency range as the field data, yet of significantly lower amplitude. We then conduct realistic simulations of the foothill ridge response with soil layering, and qualitatively demonstrate that the recorded amplification can be attributed to coupling of site and topography effects. This effect, referred to as topography-modified site amplification, describes seismic waves trapped in the soft soil layers of the near surface and simultaneously subjected to sediment-induced reverberations as well as diffraction and scattering. Parametric investigations of the topography-soil amplification coupling effects are then conducted, and results show that when accounting for a soil-bedrock interface at 100m depth, predictions are in excellent quantitative agreement with the observed motion.

METHODS FOR ANALYZING THE EL MAYOR-CUCAPAH EARTHQUAKE RUPTURE USING LIDAR DATASETS (A-121)

D. Banesh, M.E. Oskin, X. Wang, B. Hamann, and L. Kellogg

The high-resolution terrestrial LiDAR scans of northern Mexico obtained after the April 2010, Mw7.2 El Mayor-Cucapah earthquake (post-earthquake data), along with aerial LiDAR scans of the same area from before the earthquake (pre-earthquake data), make possible an accurate examination of the shifts in the region due to the event. We present methods for analyzing the various shifts throughout the area. We make two assumptions: (1) at a local level, excluding the area around the fault line, the features have minimal deformation, and (2) any feature was translated no more than five meters, with an optional change in orientation of no more than 15 degrees. We have developed an effective technique, where we iterate though all the points of the pre-earthquake data, using for each point a disc with a radius of 10 meters centered around each sample point, and define a feature based on all the points in this disc. Since the resolution of the pre-earthquake data is less than that of the post-earthquake data, it makes sense to define the features using pre-earthquake points. In the post-earthquake data set, we attempt to find the same feature by searching a ten-by-ten square meter grid centered at the same point as the feature from the pre-earthquake data set. Once a match has been determined, we draw a translation vector from the original position of the feature in the pre-earthquake data to the translated position of the feature in the post-earthquake data. As we draw one vector for each feature, we create a translation vector field that shows the movement caused by the earthquake.

MOVIES OF SEISMIC WAVE PROPAGATION THROUGH THE IMPERIAL AND COACHELLA VALLEYS, SOUTHERN CALIFORNIA (A-143)

M. Barba and J.M. Stock

One of the greatest natural hazards that southern California may face in the future is a 180 km earthquake rupture along the southern segment of the San Andreas Fault. The Salton Seismic Imaging Project, a large-scale active source seismic study of southeastern California, was conducted to improve the understanding of the underground geometry of the San Andreas Fault and surrounding faults and sedimentary basins. In early 2011, temporarily deployed seismometers and permanent seismic stations located in Southern California recorded waveforms from controlled seismic shots. We used the waveforms to create

movies of the propagation of the seismic waves across the region. Deviation from the concentric propagation pattern expected in a 1D velocity model highlights abrupt structural transitions, such as known and concealed faults, dipping layers, or lateral changes in velocity. Also shown are the arrivals and relative amplitudes of various seismic phases as they propagate across the network of seismometers. The movies will ultimately guide the development of the 3D seismic velocity model by identifying the locations and possible types of geological structural disturbances.

EARTHQUAKE MOTIONS RECORDED ON A DENSE 5000-STATION NETWORK IN LONG BEACH, CA (B-048)

M. Barba, R.W. Clayton, and D. Hollis

We present detailed maps and movies of small local earthquakes recorded by a dense seismic network in Long Beach, California. The network consists of approximately 5,000 short-period, vertical sensors spaced an average 100m apart in a 7 by 10 km area. The autonomous network recorded continuously (24 hours/day) for a period of 6 months. The results show local basins and faults, such as the Newport-Inglewood Fault (NIF), strongly focusing and diffracting wave fields, suggesting the existence of fault strands diverging from NIF. The apparent amplification varies significantly over the region. It is also clear that the coda has waves travelling in a wide variety of directions away from the direct path to the epicenter. By combining the maps of peak acceleration from a number of earthquakes, a detailed map of ground amplification can be constructed.

A PHYSICAL MODEL OF THE MW 6 EARTHQUAKE CYCLE AT PARKFIELD (A-096)

S. Barbot, N. Lapusta, and J.P. Avouac

Advances in geophysical monitoring now provide an extensive set of observations of all aspects of the earthquake cycle. Yet, unifying physical models that connect these observations into a coherent picture are lacking. At the same time, laboratory experiments and theoretical developments provide an increasingly detailed understanding of the fault physics, offering the basis for an extrapolation to natural conditions.

In this study, we bridge the gap between observations and fault physics by developing the first model of the full earthquake cycle that explains a number of interesting and robust observations of the crustal dynamics at Parkfield. Despite the similarities between the repeating Mw 6 earthquakes and their short recurrence times (from 12 to 32 years for 5 events until 1966), the latest rupture of 2004 defied the odds by taking place a decade later than anticipated and initiating at the south end to propagate northward, contrarily to all previous events.

We build our model of fault friction using the spatial patterns of microseismicity, the time series of GPS displacements in the 1999-2010 period, the InSAR data, and the GPS offsets of the 2004 earthquake. We also consider the slip distribution of the 1966 event and the historical catalog of recurrence times and hypocenter locations. We show the special role of microseismicity, which marks the transition between stable and unstable friction and circumscribes the seismogenic zone. We use the program BICYLE (Boundary Integral Cycles of Earthquakes) of Lapusta & Liu (2009) to solve the elasto-dynamic equations that govern the fault slip evolution. We obtain a sequence of Mw~6 earthquakes that can explain the observed variability of hypocenters and reproduce the geodetic observations of surface deformation in the co- and postseismic periods associated with the 2004 event. The change of hypocenter between 1966 and 2004 and the delay of the latest event is consistent with the occurrence of a swarm of smaller-magnitude earthquakes during the 1992-1994 period and these two locations being close to the boundary of the seismogenic zone. Our study introduces a methodology capable of integrating seismological and geodetic observations into a coherent physical model of the earthquake cycle. Our approach can serve as an important tool to investigate the effect of other components of earthquake physics and to help understand and mitigate seismic hazards around active faults.

CO-LOCATED PORE PRESSURE AND VOLUMETRIC STRAIN AT PLATE BOUNDARY OBSERVATORY BOREHOLES (A-070)

A.J. Barbour and D.C. Agnew

To establish the viability of pore-pressure instrumentation as a measurement of volumetric deformation in the solid rock matrix, we present initial studies, using Plate Boundary Observatory data, of the relationship between apparent areal strain and pore pressure in the same borehole. The areal strains are given by Gladwin borehole tensor strainmeters (BSM) (and in one case by longbase laser strainmeters). The pore-pressure is measured in a partially sealed, sand-packed region in an uncased section of the borehole containing the BSM. We find parameters relating pore pressure to atmospheric loading and tidal strains. Although these forces explain much of the pressure signal, residual pressures not associated with earthquakes have significant other changes (daily rms signal on the order of 1.5 hPa) attributable to a delay between stress and strain. As

this delay becomes large, or even frequency dependent, the degree of coupling between pore-fluid diffusion and elastic parameters in the rock becomes important. We also find that only very small quantities of non-atmospheric and non-tidal strain energy may be explained by pore pressure variation (roughly 0.1 nanostrain/kPa).

Passing seismic waves that cause volumetric change also affect the pore pressure. Earthquakes at near and intermediate distances cause a postseismic response that decays withing a few days; this might manifest rapid, short-term changes in permeability by pore-sealing/opening, or changes in fracture-conduit flux, but is likely equilibration of pore-fluid diffusion.

Our findings suggest that (1) The pore pressure measurement is stable over hours to weeks. (2) Strainmeters are less sensitive to typical post-seismic transient pressure changes. (3) There may be some level of frequency dependence between the two quantities. A major implication thus follows: Because the pore pressure transducers are apparently stable at long periods and may be more sensitive to fluid-related deformation than strainmeters are, they may be well poised to compliment tectonic deformation studies, assuming site effects may be understood and corrected for the subject of future work.

CAUGHT IN THE ACT: EVIDENCE FOR SEISMIC ARREST ON NATURAL FRICTION-MELT-BEARING FAULTS? (A-093)

W.M. Behr and J.P. Platt

During seismic slip in the earth, frictional work is converted primarily into heat, and may cause melting of the material surrounding the fault plane at depth. The generation of melt will either lubricate the fault by decreasing the dynamic stress relative to the static stress, or it will act as a viscous brake that may impede or arrest the propagating earthquake rupture. Footwall rocks beneath the Whipple detachment fault in eastern California provide an opportunity to examine and potentially quantify this process, as they preserve brittle and ductile features characteristic of both steady-state and transient conditions. We compare natural measurements of static shear stress (τs), from recrystallized grain size paleopiezometry on quartz-rich, brittle-to-ductile shear zones, to natural measurements of the strain-integrated dynamic stress (τf) on adjacent pseudotachylite-bearing faults with measurable displacements. We find that minimum estimates of τf (56 ± 7 MPa) are within error of estimates of τs (60 ± 8 MPa), suggesting that the formation of melt did not cause lubrication and may have caused seismic arrest. The dynamic shear stress measurements are significantly higher than other published natural observations of pseudotachylites, but may be explained by the high clast content present in these fault zones, which would have significantly increased the melt viscosity.

IMPLEMENTATION OF GIS LAYERS WITH A SPACE-TIME GRAPHICAL DISPLAY IN SCEC-VDO (A-158)

A. Bernhard, T. Farhat, R. Lacey, A. Lim, S. Paseda, M. Rogers-Martinez, C. Sawyer, T. Jordan, R. de Groot, and N. Rousseau

The 2011 Undergraduate Studies in Earthquake Information Technology (UseIT) development team was tasked with constructing a seismic sequence visualization system based on SCEC-Virtual Display of Objects (SCEC) and Geographic Information Systems (GIS). Working with the tools of Java3D,the developers implemented space-time earthquake display functionality as well as surface layers for major infrastructure and statistical maps. The space-time plot allows users to display earthquake sequences temporally while still referencing magnitude and geographic location. Other improvements include a more accurate display of topography and greater compatibility with shapefiles (datafiles containing statistical information that can be rendered into graphical displays) and other GIS layers. These advancements will create an informative and easily interpretable display of earthquake sequences, which will improve risk assessment and hazard preparedness.

A MICROMECHANICS BASED CONSTITUTIVE MODEL FOR BRITTLE FAILURE AT HIGH STRAIN RATES (A-084)

H.S. Bhat, A.J. Rosakis, and C.G. Sammis

The micromechanical damage mechanics formulated by Ashby and Sammis [1] and generalized by Desh- pande and Evans [2] has been extended to allow for a more generalized stress state and to incorporate an ex- perimentally motivated new crack growth (damage evo- lution) law that is valid over a wide range of loading rates. This law is sensitive to both the crack tip stress field and its time derivative. Incorporating this feature produces strain-rate sensitivity in the constitutive re- sponse. The model is also experimentally verified by predicting the failure strength of Dionysus-Pentelicon marble over strain rates ranging from ~ 10^{-6} to $10^{3} s^{-1}$. Model parameters determined from from quasi-static experiments were used to predict the failure strength at higher loading rates. Agreement with experimental results was excellent.

VECTOR-VALUED FRAGILITIES AND THE STATE OF THE ARCHIVE FOR PRECARIOUSLY BALANCED ROCKS (PBRS) IN SOUTHERN CALIFORNIA (B-081)

G.P. Biasi, J.N. Brune, and A.W. Homan

Precariously balanced rocks have been recognized as a valuable resource for constraining ground motion extremes at long return times in seismic hazard analyses and seismic hazard maps (e.g., Anderson et al., SRL, 2011).

Rock survival is a non-linear function of rock geometry, size, and angles of contact from the rock center of gravity to the pedestal contact. Relationships of these parameters to rock overturning probabilities were developed through shake-table testing using ensembles of seismograms of varying amplitudes and shapes, and the results summarized in regressions by Purvance et al. (Eqk Eng'g and Struct. Dynam., 2008). Relationships can be displayed as a two-dimensional plot, typically with peak ground acceleration (PGA) on the horizontal axis and an intensity measure such as spectral acceleration (SA: SA1 and SA2 for 1 and 2 s periods, resp.) on another. These plots graphically illustrate combinations of rock ground accelerations and SA required for dynamic overturning.

Parameters for vector valued (VV) overturning probabilities have been developed using 2-D photographic assessment of images in the PBR archive at the University of Nevada Reno. These parameters include rocking angles (alpha 1, 2) and dimensions (R1, R2). There are over 5800 images in the southern California region. We have completed the survey of this collection, and have tabulated 2-D static overturning acceleration estimates on over 1850 of them. The balance are primarily supporting photos of a variety of types. Locations have been tabulated for about 1000 rocks, and a focused effort is underway to complete this aspect of the archive. Based on the 2-D analyses, 580 have one or more directions in which the rock static overturning acceleration is ~1/4 g or less. About 550 rocks have parameters for VV assessment in terms of PGA vs. SA1 and PGA vs. SA2. Some fall outside the range of alphas or rock size in the Purvance et al. regressions. A database has been developed to manage the many overlapping analysis subsets and to support analysis of the combined data volume. We are presently evaluating VV analysis results for application to hazard assessment and seismic hazard mapping.

SLIP RATES ON THE SOUTHERN SAN JACINTO FAULT AND HOLOCENE-LATE PLEISTOCENE KINEMATICS OF THE PACIFIC-NORTH AMERICAN PLATE BOUNDARY (A-152)

K. Blisniuk, M. Oskin, W. Sharp, T. Rockwell, and K. Fletcher

To better understand whether fault strength or loading rate fluctuate over time, we have been testing for slip rate variability on 6 sites across and along the sub-parallel Clark and Coyote Creek fault strands of the southern San Jacinto fault zone (SJFZ). To constrain the late Quaternary slip behavior, we measured and dated the displacement of well-preserved landforms offset on these fault strands at multiple locations and time intervals. Offsets are constrained from field mapping and high-resolution LiDAR topography data, and displaced alluvial fans were dated with U-series on pedogenic carbonate clast-rinds and/or in situ cosmogenic ^{10}Be. Preliminary results presented here in 2010 had suggested an increase in slip rate along the southern SJFZ from the late Pleistocene to the Holocene. New results, including forward modeling of ^{10}Be depth profile ages and ^{10}Be exposure age results on offset late Pleistocene alluvial fans at Anza (A.-S. Meriaux, pers. comm., 2011), indicate that we cannot discern whether slip rates have increased over the late Quaternary. Our results do, however, show a pronounced spatial slip rate variability during the late Quaternary. Over the past 50-30 kyr, slip rates along the Clark fault strand decreased southward from $13.5\ ^{+4.0}/_{-2.6}$ mm/yr at Anza, to 8.9 ± 2.0 mm/yr at Rockhouse Canyon, to 1.5 ± 0.4 mm/yr near Santa Rosa Mountain, as slip is transferred from the Clark fault strand to the Coyote Creek fault strand and to nearby zones of distributed deformation. Slip rates of up to ~14 to 18 mm/yr summed across southern SJFZ suggest that since the latest Pleistocene, the SJFZ may rival the southern San Andreas fault zone (12-22 mm/yr) in accommodating deformation across the Pacific-North America Plate boundary.

EVALUATION OF TRANSIENT DEFORMATION FROM TWO DECADES OF CONTINUOUS GPS TIME SERIES ANALYSIS IN SOUTHERN CALIFORNIA (A-062)

Y. Bock, S. Owen, B. Crowell, D. Dong, P. Fang, S. Kedar, Z. Liu, A. Moore, L. Prawirodirdjo, M. Squibb, and F. Webb

As part of a NASA MEaSUREs project and its contribution to EarthScope, we are producing a combined 24-hour position time series for more than 1000 stations in Western North America based on independent analyses of continuous GPS data at JPL (using GIPSY software) and at SIO (using GAMIT software), using the SOPAC archive as a common source of metadata. Included are all EarthScope/PBO stations as well as stations from other networks still active (SCIGN, BARD and PANGA), and pre-PBO era data some already two decades old. The time series are appended weekly and the entire data set is filtered once a week using a modified principle component analysis (PCA) algorithm. Both the unfiltered and filtered data undergo a

time series analysis with QOCA software. All relevant time series are available through NASA's GPS Explorer data portal and its interactive Java-based time series utility.

After a comprehensive process of re-analysis and quality control, we have evaluated the time series for transient deformation, that is, time series that deviate from linear behavior due to coseismic and postseismic deformation, slow slip events, volcanic events, and strain anomalies. In addition, we have observed non-tectonic effects from hydrologic, magmatic and anthropogenic sources which are manifested primarily in the vertical but sometimes bleed over into the horizontal, making tectonic interpretation and transient detection difficult. We will present an overview of our analysis workflow as well as examples of transient deformation from Southern California, such as Diamond Valley Lake, an important water reservoir in Southern California.

CISN SHAKEALERT: DEVELOPMENT OF A PROTOTYPE USER DISPLAY FOR PROVIDING EARTHQUAKE ALERTS TO END USERS (A-035)

M. Boese, K. Solanki, T. Heaton, E. Hauksson, and the CISN EEW Team

Over the past five years scientists from Caltech, UC Berkeley, ETH Zurich, USC/SCEC and USGS have been working on the development and implementation of a prototype earthquake early warning system for California. CISN ShakeAlert combines the outputs from three independently running algorithms, Tauc-Pd Onsite, Virtual Seismologist, and ElarmS. CISN ShakeAlert provides a continuum of earthquake alert information, including rapid estimates of magnitudes, locations, and expected seismic intensities and their uncertainties. For the rapid visualization of alert information and the notification of users in an easy understandable way, we have developed a Java applet that runs on a user computer and receives xml messages from the ShakeAlert system. This UserDisplay (UD) shows the user location, estimated epicenter of the earthquake, current locations of the P- and S-wave fronts, estimated magnitude, as well as the predicted level of intensity of shaking at the user site and time until this shaking is expected to occur. The UD pops up automatically once an alert message is received. The UD is currently being tested by approximately 30 test users.

GPS CONSTRAINTS ON CRUSTAL DEFORMATION IN THE CENTRAL WALKER LANE AND SIERRA NEVADA FRONTAL FAULT (A-052)

J.M. Bormann, W.C. Hammond, C.W. Kreemer , and G. Blewitt

Between the Walker Lake and Lake Tahoe basins (~38.5-39.5° N latitude), the Walker Lane lacks strike-slip faults optimally oriented to accommodate the 8-10 mm/yr of geodetically observed northwest-directed dextral shear. In this region, geologic studies show that Quaternary active faulting is concentrated in a northwest–trending series of north-striking, normal fault-bounded basins. Geomorphic and paleoseismic studies of the major basin-bounding faults result in normal slip rate estimates between ~0.3-2.5 mm/yr; however, the combined geologically determined slip rates do not sum to fulfill the Walker Lane shear budget.

We use GPS data from UNR's semi-continuous network MAGNET and EarthScope's Plate Boundary Observatory to infer fault slip rates and vertical axis rotations of fault-bounded blocks in the central Walker Lane through an elastic block modeling approach. Comparisons between geodetically and geologically estimated normal slip rates on the basin-bounding faults show that 7 out of 8 geodetic estimates agree with geologic estimates to within uncertainties. However, GPS-based models predict dextral slip rates on the basin-bounding normal faults that are greater than or equal to the estimated normal slip rates, between 0.3-2.0 mm/yr. This prediction is not substantiated by paleoseismic and geomorphic fault studies, suggesting a systemic discrepancy between slip rates estimated from geologic and geodetic datasets.

The sense of deformation across the Sierra Nevada frontal fault system at Mono Basin appears to predict left lateral slip and a higher rate of extension relative to other locations along the range front. The inferred sinistral shear is opposite to the sense of slip observed elsewhere in the Walker Lane. This pattern of anomalous deformation is sensitive to the selection of GPS sites used to define Sierra Nevada/Great Valley (SNGV) microplate, which experiences a low rate of deformation. Postseismic relaxation from historic earthquakes in California and Nevada contributes to SNGV deformation, making it difficult to define a rigid Sierra Nevada reference frame. We explore the effect of various definitions of the SNGV frame and the effect of correcting the GPS velocities for viscoelastic postseismic effects on our results.

VISUALIZING COMPARATIVE HAZARD VULNERABILITY THROUGH GIS/SHAKEMAP INTEGRATION (A-157)

S.C. Boss, F. Gutierrez, K.Y. Lin, T. Papikyan, and C.M. Valen

The 2011 SCEC Undergraduate Studies in Earthquake Information Technology (USEIT) internship program challenged the Data Team to research information on specific earthquake sequences using global earthquake catalogs and incorporate the data into Geographic Information Systems (GIS). The internship focused on being able to integrate GIS into SCEC-Virtual Display of Objects (SCEC-VDO) software. The Data Team compiled information about six global earthquake sequences: the 2010 Maule sequence in Chile, the 2010 Port-au-Prince sequence in Haiti, the 2011 Tohoku sequence in Japan, the 2010 El Mayor-Cucapah sequence in Mexico, the 2010 Canterbury sequence in New Zealand, and the 2004 Indonesian trench sequence in Sumatra. Information on population density, transportation routes, and infrastructure was located for each of the six countries and California. Data on hospitals, major airports, major roads, railways, and nuclear power plants was displayed onto maps in GIS. This information can be used to assess the hazards and the impact an earthquake could have on society. In addition, California data included locations of schools, fire stations, and police stations.

The Data team also incorporated earthquake catalogs that were used to gather information on each sequence as well as focal mechanisms. Each earthquake sequence included the mainshock, aftershocks, and foreshocks. The global earthquake catalogs that were used included the National Earthquake Information Center Preliminary Determination of Epicenters (NEIC PDE) and the Global CMT (Global Centroid Moment Tensor). The Institute of Geologic and Nuclear Science (GNS) catalog was used to gather earthquake information in New Zealand. Research was also conducted on the ShakeMaps that SCEC created. All of the resulting information was then posted on the data team's own website, which is organized by corresponding countries.

DO SMALL SURFACE STRAINS IN THE NEW MADRID SEISMIC ZONE REFLECT A PHYSICAL PROCESS? (B-152)

O.S. Boyd, Y. Zeng, L. Ramirez-Guzman, and R. Smalley

We reevaluate GPS data over the decade from 2000–2010 and model the resulting observations with local deformation mechanisms: viscoelastic relaxation subsequent to the 1811–1812 New Madrid, MO, earthquakes and slip across deeply buried finite dislocations to represent interseismic strain accumulation. The reevaluation of the GPS data accounts for outliers, offsets in the position time-series, and annual and bi-annual seasonal variations. Site velocities are found from the slope of the position time-series and are relative to a reference, which is the stack of all position time-series for a given component. We find that relative site velocities have a standard deviation of about 0.2 mm/yr with uncertainties on the order of 0.1 to 0.2 mm/yr or more. Uncertainty is difficult to estimate directly because the random walk component of noise, which contributes most to uncertainty in long geodetic time series, cannot be distinguished from the flicker and white noise components.

Multiple models can account for some of the variance in the GPS data. A viscoelastic response of the crust from the 7 February 1812 earthquake on the Reelfoot fault can account for 41% of the variance in the data. We perform an F-test and find that such a model has a 99% chance of being better able to match the data than does a null hypothesis. In this model, viscosity and slip are directly correlated such that increasing the viscosity by an order of magnitude requires an increase in slip by an order of magnitude to generate the same surface deformation. A viscoelastic response due to an earthquake on the Cottonwood Grove fault does not significantly improve our ability to model the data, but the lack of significance may be partly due to data limitations. Alternatively, a lower crustal right-lateral dislocation along the Cottonwood Grove fault slipping between 2 and 3 mm/yr from 20 to 40 km depth can account for 25% of the variance and has a 70% chance of being better able to match the data than does a null hypothesis, while slip on a down-dip extension of the Reelfoot fault cannot significantly reduce the variance of the GPS data. These results suggest that having a good estimate of the subsurface rheology might allow for estimation of mean slip and magnitude of the 1811–1812 earthquakes as well as ongoing loading of the seismic zone.

OPEN-SOURCE GROUND MOTION SELECTION USING THE GENERALIZED CONDITIONAL INTENSITY MEASURE (GCIM) APPROACH (B-013)

B.A. Bradley

The increasing use of time domain analysis is seismic assessment has resulted in a frequent requirement for site-specific ground motions. Many heuristic ground motion selection approaches have been proposed, and the use of a range of such methods has been shown to result a in large range of seismic performance statistics. A theoretically-founded ground motion selection methodology, based on the generalized conditional intensity measure (GCIM) approach, is presented. Both as-recorded and simulated ground motions can be selected using a semi-automated algorithm that requires only the specification

of a 'weight vector' which quantifies the hierarchy of importance of various ground motion intensity measures. A simple method allows an estimation of bias in seismic response analysis results due to improper ground motion selection. The methodology has been implemented in the open-source software OpenSHA to improve uptake in practice. The theoretical foundation of the methodology leads to the consistent computation of the seismic demand hazard, irrespective of the adopted conditioning intensity measure.

STRONG GROUND MOTIONS OBSERVED IN THE 22 FEBRUARY 2011 CHRISTCHURCH EARTHQUAKE (B-055)

B.A. Bradley and M. Cubrinovski

On 22 February 2011 at 12:51pm local time, a moment magnitude M_w6.3 earthquake occurred beneath the city of Christchurch, New Zealand, causing an unparalleled level of damage and human causalities in the country's history. Compared to the preceding 4th September 2010 M_w 7.1 Darfield earthquake, which occurred approximately 30km to the west of Christchurch, the close proximity of the 22 February event lead to ground motions of significantly higher amplitude in the densely populated regions of Christchurch. As a result of these significantly larger ground motions, structures in general, and commercial structures in the central business district in particular, were subjected to severe seismic demands and, combined with the event timing (12:51pm), structural collapses accounted for the majority of the 181 causalities.

A preliminary assessment of the near-source ground motions recorded in the Christchurch region is conducted. Particular attention is given to the observed spatial distribution of ground motions which is interpreted based on source, path and site effects. Comparison is also made of the observed ground motion response spectra with those of the 4 September 2010 Darfield earthquake and those used in seismic design in order to emphasise the amplitude of the ground shaking and also elucidate the importance of local geotechnical and deep geologic structure on surface ground motions.

EARTHQUAKE NUCLEATION MECHANISMS AND DAMAGE IN HETEROGENEOUS FAULT ZONES, PROBED WITH PERIODIC LOADINGS (IN MODELS AND EXPERIMENTS). (B-041)

B.W. Brinkman, Y. Ben-Zion, J.T. Uhl, and K.A. Dahmen

We study the response to stress oscillations of different periods and amplitudes in models and experiments, in order to improve the understanding of nucleation processes and evolving seismicity. The basic question is whether monitoring changes in observed seismicity can be used to identify the operative nucleation mechanism (or combination of mechanisms). We use a simple earthquake model (Ben-Zion 2008; Dahmen et al., 2009) to explain the frequency and amplitude dependence of slip nucleations seen in acoustic emission experiments on sheared rocks (Lockner 1999, Beeler 2003). We show comparisons of analytical results, numerics, and experiments. The results suggest new ways to estimate the rate at which frictional slips or earthquakes are nucleated. The application to earthquake faults suggests that seasonal stresses may be more likely to trigger large earthquakes than tidal stresses.

References:

Beeler, N.M., D.A. Lockner (2003). „Why earthquakes correlate weakly with the solid Earth tides: effects of periodic stress on the rate and probability of earthquake occurrence." J. Geophys. Res.-Solid Earth 108.

Ben-Zion, Y. (2008). Collective Behavior of Earthquakes and Faults: Continuum-Discrete Transitions, Evolutionary Changes and Corresponding Dynamic Regimes, Rev. Geophysics, 46, RG4006, doi:10.1029/2008RG000260.

Dahmen, K.A., Y. Ben-Zion, and J.T. Uhl (2009). A micromechanical model for the deformation in solids with universal predictions for stress-strain curves and slip avalanches, Phys. Rev. Lett. 102, 175501.

Lockner, David A. and Nick M. Beeler (1999). Premonitory slip and tidal triggering of earthquakes, J. Geophys. Res. 104, 20,133-20,151.

LOWER CRUSTAL ANISOTROPY IN THE MOJAVE DESERT REGION FROM ELECTRON BACKSCATTER DIFFRACTION (EBSD) MEASUREMENTS OF CRYSTAL PREFERRED ORIENTATION (CPO) (B-138)

S.J. Brownlee, K. Wagner, and B.R. Hacker

Seismic anisotropy is commonly used to infer flow directions in the mantle, but anisotropy in the mid and lower crust can be much more difficult to measure and to interpret. By measuring the crystal preferred orientations (CPOs) of minerals in lower crustal rocks we can calculate the anisotropic seismic properties of the aggregate using mineral single-crystal elastic constants

and the Christoffel equation. This allows prediction of the expected lower crustal contribution to seismic anisotropy and improves our ability to interpret crustal anisotropy in terms of composition as well as deformation mechanisms. In the Mojave Desert region of southern California the crust is under-plated by the Pelona Schist, which due to its high mica content is expected to have significant seismic anisotropy. We measured mineral CPOs in 10 samples of the Pelona Schist using electron backscatter diffraction (EBSD) and then 148c148a148l148c148u148l148a148t148e148d148 148t148h148e148i148r148 148 a 148 n 148 i 148 s 148 o 148 t 148 r 148 o 148 p 148 i 148 c 148 148 s 148 e 148 i 148 s 148 m 148 i 148 c 148 148 p 148 r 148 o 148 p 148 e 148 r 148 t 148 i 148 e 148 s 148 . 148 148 T 148 h 148 e 148 148 P 148 e 148 l 148 o 148 n 148 a 148 148S148c148h148i148s148t148 148d148i148s148p148l148a148y148s148 148a148 148r148a148n148g148e148 148o148f148 148c148a148l148c148u148l148a148t148e148d148 148a148n148i148s148o148t148r148o148p148y148:148 148~1485148 148 14831480148%148 148i148n148 148V148p148,148 148a148n148d148 148~1487148 148 14841480148%148 148i148n148 148V148s148 148(148s148e148e148 148a148l148s148o148 148a148b148s148t148r148a148c148t148 148b148y148 148W148a148g148n148e148r148,148 148K148)148.148 148T148h148e148 148m148a148g148n148i148t148u148d148e148 148 o 148 f 148 148 a 148 n 148 i 148 s 148 o 148 t 148 r 148 o 148 p 148 y 148 148 i 148 s 148 148 m 148 o 148 s 148 t 148 148 c 148 l 148 o 148 s 148 e 148 l 148 y 148 148 r 148 e 148 l 148 a 148 t 148 e 148 d 148 148 t 148 o 148 148 t 148 h 148 e 148 148 a 148 m 148 o 148 u 148 n 148 t 148 148 o 148 f 148 148 m 148 i 148 c 148 a 148 148 i 148 n 148 148 t 148 h 148 e 148 148s148a148m148p148l148e148.148 148N148e148a148r148l148y148 148a148l148l148 148s148a148m148p148l148e148s148 148h148a148v148e148 148a148p148p148r148o148x148i148m148a148t148e148l148y148 148u148n148i148a148x148i148a148l148 148 s 148 y 148 m 148 m 148 e 148 t 148 r 148 y 148 148 i 148 n 148 148 t 148 h 148 e 148 i 148 r 148 148c148a148l148c148u148l148a148t148e148d148 148v148e148l148o148c148i148t148i148e148s148,148 148w148i148t148h148 148a148 148u148n148i148q148u148e148 148s148l148o148w148 148a148x148i148s148.148 148T148h148i148s148 148i148s148 148a148 148c148o148m148m148o148n148 148a148s148s148u148m148p148t148i148o148n

ACCURACY OF NON-DESTRUCTIVE TESTING OF PBRS TO ESTIMATE FRAGILITIES (B-080)

J.N. Brune, R. Brune, G.P. Biasi, R. Anooshehpoor, and M.D. Purvance

Prior studies of Precariously Balanced Rocks (PBRs) have involved various methods of estimating fragilities. These have included non-destructive testing (NDT) methods such as photomodeling, and potentially destructive testing (PDT) such as forced tilt tests. PDT methods have the potential of damaging or disturbing the rock or its pedestal so that the future usefulness of the PBR is compromised. To date we have force-tilt tested approximately 28 PBRs, and of these we believe 7 have been compromised. We suggest here that NDT methods are now sufficiently advanced as to be adequate for comparison with Ground Motion Prediction Equations (GMPEs) and seismic hazard maps (SHMs). We compare tilt-test static toppling estimates to three non-destructive methods: (1) 3-D photographic modeling (2) profile analysis assuming the rock is 2-D, and (3) expert judgments from photographs.

3-D modeling uses the commercial Photomodeler program and photographs in the field taken from numerous directions around the rock. The output polyhedral shape is analyzed in Matlab determine the center of mass and in Autocad to estimate the static overturning angle alpha.

For the 2-D method we chose the photograph in profile looking perpendicular to the estimated direction of toppling. The rock is outlined as a 2-D object in Matlab. Rock dimensions, rocking points, and a vertical reference are supplied by the photo analyst to estimate the center of gravity and static force overturning angles. For the expert opinion method we used additional photographs taken from different directions to improve the estimates of the center of mass and the rocking points.

We used 7 rocks for comparisons. The error in estimating tan alpha from 3-D modeling, 2-D estimates, and expert opinion are about 0.05, 0.1, and 0.06, respectively. Tilt-testing differs materially in one case from 3-D (*) because an irregular base on the rock allowed the rock to begin to tilt at a lower angle onto a second rocking point with higher alpha. 2-D methods generally perform well enough to use as a screening method for the larger archive. The following is a list of the tan alpha data:

Method:	Tilt,	3-D,	2-D,	Expert	
Grass Valley 2:	.31*,	.50,	.50,	.47	
Lovejoy Buttes 5(NE):		.33,	.34,	.20,	.31
Mead Valley West:		.53,	.53,	.55,	.53
Pacifico:	.22,	.18,	.29,	.27	

Perris2: .17, .16, .20, .23

PRELIMINARY PALEOSEISMIC RESULTS FROM SOUTHERN CLARK FAULT, SAN JACINTO FAULT ZONE, SOUTHERN CALIFORNIA; COMPARISON TO THE HOG LAKE PALEOSEISMIC RECORD (A-148)

M.T. Buga, T.K. Rockwell, and J.B. Salisbury

We present preliminary results from a new paleoseismic site on the Clark strand of the San Jacinto Fault Zone in Clark (Dry) Lake, western Salton Trough, southern California. Based on morphological evidence, previous workers mapped multiple strands of the fault through Clark Lake. We excavated trenches across two of the prominent lineaments and found only minor cracking but no faults. In contrast, a trench across the most prominent lineament with a surface scarp exposed a major fault with clear evidence of recurrent activity. Based on these observations, it appears that most late Holocene slip along the Clark fault at Clark Lake is localized within a narrow zone. The main strand of the fault juxtaposes mid-Holocene lake deposits against late Holocene, inter-bedded lake and alluvial deposits. We identified past surface ruptures by the presence of filled fissures, upward fault terminations, angular unconformities, presence of growth strata, and abrupt vertical separations, from which we identify evidence for six surface ruptures that have occurred in the past 1600 years, yielding an average recurrence interval of 250-300 years. The two most recent events are likely the November 1800 and ca 1550 earthquakes, and correlate to events 1 and 2 at Hog Lake, ~50 km to the NW, based on mapping of small geomorphic offsets along the Clark fault. The 3 earliest events are constrained to have ruptured between about 400 and 1250 AD and likely correlate to events 6, 7 and 8 at Hog Lake. Thus, we recognize only 1 event at Clark Lake that corresponds to the cluster of 3 events at Hog Lake, suggesting that some of the ruptures in the Hog Lake cluster correspond to rupture of the northern part of the zone, similar to the 1918 rupture.

SURFACE-EXPOSURE DATING OF SAN ANDREAS EARTHQUAKES (A-022)

W.B. Bull

Precise, accurate dating of prehistoric earthquakes provides verification of 40 years of stratigraphic dating at trenches excavated across the southern San Andreas fault. Radiocarbon dating of trench organic material, created before or after times of surface ruptures, is much improved – thanks to being able to date many small-size samples, and to Bayesian modeling. Limits to what can be done were noted by Biasi and Weldon (2009, p. 496) who said "Dating precision alone is unlikely to ever be adequate to demonstrate correlations, especially among events relatively close in time." But surface-exposure dating gives us a breakthrough to easily distinguish between two seismic shaking events in a decade, with a dating precision of ± 5 years.

We now can date "seismically induced landslides (that are) induced at extraordinary distances" (Keefer, 1984; Harp, et al, 1993). Freshly exposed block and outcrop surfaces are colonized by lichens with known growth rates. I measure the largest lichen on many rockfall blocks at sites susceptible to seismic shaking, but not snow avalanches and rainstorms. Rockfalls 400 km away in Yosemite date to the times of southern San Andreas earthquakes of 1857 and 1812 AD. Previous Sierra Nevada work defined growth rates for four lichen genera that were used to date rockfall events in diverse altitudes and climatic settings. These four genera grow at the same rate in the San Jacinto, San Gabriel, and San Bernardino Mountains.

Icehouse Canyon (San Gabriel Mountains) lichen sizes cluster nicely in separate peaks that date back to ~815 AD. Most of these seismic shaking events emanated from earthquakes that have been C_{14} dated at eight trench sites between Carrizo and Indio. Closely spaced, distinct lichen-size peaks date as ~1503 and ~1490 AD (Also C_{14} dated at Thousand Palms as ~1503 and at Wrightwood as ~1487 AD).

Future work will collect data from many sites. Seismic shaking, and rockfall abundance, decrease away from an earthquake epicenter. Regional data modeling will map prehistoric seismic shaking of San Andreas events >Mw 7, and may assess the relative importance of earthquakes generated by the San Jacinto and Transverse Range fault zones.

CONSEQUENCES OF THE ASSUMPTIONS REGARDING SEGMENTATION VERSUS NONSEGMENTATION OF THE SHORELINE FAULT WHEN ESTIMATING EARTHQUAKE POTENTIAL AND SEISMIC LOAD FOR DIABLO CANYON NUCLEAR POWER PLANT (DCNPP) (B-097)

A. Bykovtsev and M. Kasimov

The CALIFORNIA ENERGY COMMISSION held a day-long workshop "California Nuclear Power Plant Issues" in Sacramento on July 26, 2011. One of the main questions for discussion on Section 1 "Seismic/Tsunami Scenarios and Uncertainties for Diablo Canyon…" was "A recent USGS study in April 2011 concluded that, "There's no objective evidence for any discontinuities or segmentation of the Shoreline Fault," in contrast to PG&E's conclusion in January 2011 the Shoreline

Fault is segmented. An important "unanticipated" phenomenon in relation to the Mw 9.0 earthquake in Japan was that five segments along the subduction zone ruptured together, rather than independently as scientists had earlier predicted. What are the expected consequences of the assumptions regarding segmentation versus nonsegmentation of the Shoreline Fault when estimating earthquake potential?" Unfortunately, presenters were unable provide clear answers on situation related to the assumptions.

The emergency in Japan (March 2011) provides as an important wake-up call for contribution. Tools and knowledge for the proper Seismic Hazard Analysis(SHA) nuclear plants located in California exist, and we cannot afford to ignore new information. During the last 6 months have spent our own money, time and effort we achieved preliminary results about assumptions regarding segmentation versus non-segmentation of the Shoreline Fault zone(SFZ) and San Luis Bay Fault Zone(SLBFZ) when estimating earthquake potential for DCNPP.

Effect of SFZ and SLBFZ segmentations on simulation of long-period seismic motions (LPSM) and seismic load will be presented for DCNPP. As a result of the our analysis it is possible to conclude, that for the DCNPP site the segmentations of SFZ and SLBFZ introduce additional extremes for LPSM and effects of vibratory ground motion should be properly estimated in SHA and included in design of seismic load for DCPP. LPSM with multiple oscillations can cause severe nonlinear structural response and have become a crucial consideration in proper SHA of DCNPP due to cyclic load. The nature of such cyclic loading induces progressive alteration in the bearing capacity and head displacement of the foundation. This may lead to disastrous consequences (for example Japan- 2011 lessons). These findings should be investigated more accurately for proper SHA of DCNPP. We have very strong concerns about seismic issues at DCNPP and proper estimate of ground motions based on existing assumptions and approaches.

BROADBAND CYBERSHAKE PLATFORM: SEISMOGRAM SYNTHESIS FOR BROADBAND PHYSICS-BASED PROBABILISTIC SEISMIC HAZARD ANALYSIS (A-038)

S. Callaghan, P. Maechling, P. Small, K. Milner, R. Graves, T.H. Jordan, and the CyberShake Collaboration

Researchers at the Southern California Earthquake Center (SCEC) have developed the CyberShake computational platform to perform probabilistic seismic hazard analysis (PSHA) in the Los Angeles region (Graves et al., 2010) using deterministic wave propagation simulations at frequencies up to 0.5 Hz. CyberShake uses seismic reciprocity to calculate synthetic seismograms for a suite of more than 600,000 rupture realizations. From this set of seismograms we compute intensity measures, which are then combined into a PSHA hazard curve for the site of interest.

Here we report on expanded CyberShake capabilities. We have integrated the high-frequency computational capabilities of the SCEC Broadband Platform into CyberShake, producing the Broadband CyberShake Platform. The Broadband CyberShake Platform extends the frequency range up to 10 Hz by combining low frequency deterministic synthetic seismograms with higher frequency stochastic seismograms. We can now calculate physics-based seismograms and PSHA hazard curves for intensity measures such as PGA that are strongly dependent on higher frequency ground motions.

We are applying our new broadband computational capabilities of the Broadband CyberShake Platform at southern California sites selected to support validation of this newly developed PSHA computational technique. This includes calculation of Broadband CyberShake seismograms and hazard curves at precariously balanced rock sites to validate our technique and to investigate the impact of higher frequencies on these fragile geological structures.

We have also added functionality to calculate CyberShake seismograms using CVM-H v11.2 as well as CVM-S4. This enables us to compare seismograms and hazard curves generated with the two velocity models and determine the impact the choice of velocity model has on the predicted hazard. We have calculated seismograms and PSHA curves for southern California sites selected to improve our understanding of the contribution velocity model has on seismic hazard.

TRIGGERED NON-VOLCANIC TREMOR FOLLOWING THE 2011 TOHOKU-OKI EARTHQUAKE (A-104)

K. Chao, Z. Peng, D.P. Hill, D.R. Shelly, B. Enescu, B. Fry, and C. Aiken

Non-volcanic tremor triggered by teleseismic surface waves was recently discovered in many different types of tectonic boundaries, mainly around major subduction zones around the Pacific Rim and the San Andreas Fault system in California. Here we present the observations of tremor around the world triggered by the 2011 Mw9.0 Tohoku-Oki, Japan earthquake. We identified clear tremor signals recorded at many stations at Parkfield of the San Andreas Fault in central California. The tremor begins around the ~100-sec period S-wave arrival with a minor burst coinciding with the SH-SH arrival as recorded on the nearby broadband station PKD. A more pronounced burst coincides with the Love arrival followed by a spike in tremor

amplitude with the Rayleigh wave. The triggered tremor was located at depths between 20 and 30 km beneath the surface trace of the fault with the burst coincident with the S wave centered beneath the fault 25 km NW of Parkfield. Most of the subsequent activity, including the tremor coincident the SH-SH arrival, was concentrated beneath a stretch of the fault extending from 10 to 40 km SE of Parkfield. Peak dynamic Coulomb stresses on the fault at tremor depths computed from peak amplitudes on the PKD station are in the range of 2 to 6 kPa. In comparison, only weak tremor signals were observed during the large-amplitude surface waves around the San Jacinto Fault (SJF) in southern California. The surface wave amplitudes and pre-event background noises in these two regions are similar, yet the triggered tremor amplitudes differ by nearly an order of magnitude. As was found in our previous studies (Chao et al., BSSA, 2011), we suggest that such difference could be related to different ambient tremor rate or tremor triggering threshold in these regions. In addition, we also identified clear triggered tremor in southwest Japan and southern Central Range in Taiwan during the Tohoku-Oki mainshock and some large aftershocks. In comparison, the triggered tremor signals are relatively weak in northern Central Range in Taiwan, and the North Island in New Zealand. We plan to investigate in details possible controlling factors that affect the tremor triggerability in these regions.

GLOBAL SEARCH FOR DEEP TRIGGERED TREMOR (B-039)

K. Chao, Z. Peng, B. Enescu, C. Wu, and B. Fry

Deep "non-volcanic" tremor has been observed at many major plate-boundary faults. Recent studies have shown that triggered tremor occurs on the same fault patches as ambient tremor and can be used as a proxy to estimate background tremor activity. Following our previous studies, here we conduct a global search for tremor triggered by teleseismic earthquakes with Mw ≥ 7.5 between 2001 and 2011. We focus on regions in southwest Japan and the North Island of New Zealand. In southwest Japan, we found a total of 16 teleseismic earthquakes associated with clear triggered tremor during the passing surface waves. Using standard envelope cross-correlation techniques, we found that the triggered tremor is located close to the regions where ambient tremor is identified previously. Thus far, in New Zealand, we have only identified 4 events associated with triggered tremor in the North Island. Next, we calculate the dynamic stress loading and compare the stress threshold of triggering with the following regions: the Parkfield section of the San Andreas Fault in central California (CC), the Calaveras Fault in northern California (NC), the San Jacinto Fault in southern California (SC), the southern and northern Central Range in Taiwan, and the Vancouver Island in Cascadia. The apparent triggering threshold in southwest Japan is around 3-4 KPa, close to the triggering threshold at Parkfield (2-3 KPa) and southern Central Range in Taiwan (7-8 KPa). Our systematic survey of triggered tremor around the world not only helps to better clarify the relationship between triggered and ambient tremor, but also provide a clue to understand the necessary conditions and underlying physics of tremor generation.

INVESTIGATION OF THE HECTOR MINE EARTHQUAKE SURFACE RUPTURE WITH AIRBORNE LIDAR DATA (A-132)

T. Chen, D.Z. Zhang, S. Akciz, and K.W. Hudnut

The 16 October 1999 Hector Mine earthquake (Mw7.1) generated significant surface rupture along the Lavic Lake Fault through almost 60 kilometers of sparsely vegetated, relatively barren desert terrain. It was the first large earthquake for which post-earthquake airborne LiDAR, collected to image the fault surface rupture, exists. Despite the lack of pre-earthquake high-resolution topographic data, we were able to make both horizontal and vertical displacement measurements, which complement published field investigation results that include ~254 data points (164 of which are within LiDAR coverage area). We made 255 new horizontal and 83 vertical displacement measurements using a 0.5 m DEM generated from the LiDAR dataset. The maximum horizontal offset value is 6.6±1.1 m, and is located approximately ~700 m south of the maximum horizontal offset observed during the field work. The average horizontal offset value from LiDAR measurements is ~2.27 m, whereas the average calculated from field data is ~2.5 m. The maximum vertical displacement is ~1.2 m, and the average vertical offset value is less than 1 m. No consistent trends are apparent in the sense of the vertical component, except in the north of the mountainous section, which is predominated by east-side-down measurements.

Compared to field data, LiDAR-based measurements (a) have larger measurement uncertainties, (b) have slightly higher values, (c) do not include many measurements of offsets <1 m due to the DEM resolution, and (d) are spatially denser. The field investigation produced measurements of higher quality in alluvial deposits (e.g. tire tracks, offset rock or pebble lineaments) which are not typically visible with 0.5 m resolution DEMs unless a piercing feature has a very large or clear offset. LiDAR measurements included more geomorphic features with larger measurement uncertainties, which may not have been measured in the field due to their proximity to higher quality measurements. However, along the section of the fault that traverses exposed rhyolite bedrock, LiDAR data provided additional measurements because it is possible to visualize the data

from different angles to better identify possible offset features. Overall, the LiDAR measurements compare well within a reasonable level of expectation with the field observations. The objective of attempting to attain a greater number of observations was achieved, but the measurements had more uncertainty than did the field observations.

STATISTICAL ANALYSIS OF 71 BURSTS IN SOUTHERN CALIFORNIA (B-071)

X. Chen, P.M. Shearer, and R. Abercrombie

We analyze 69 out of the 71 bursts in Southern California from Vidale and Shearer [2006] with LSH catalog locations. We apply a weighted least- squares method to model the spatial migration behavior, finding the best- fitting migration directions and velocities. We then compute a statistical migration significance s_m with a bootstrap resampling method for each burst. We define 37 bursts with $s_m \geq 0.8$ as the migration group, and 32 bursts with $s_m < 0.8$ as the non-migration group. To better distinguish the two groups, we compute a set of parameters including effective stress drop $\Delta\sigma$ (ratio between total moment and radius), skew of moment release time series μ, timing of largest event t_{max}, and distance separation between the first half and second half of the sequence (d_s). As expected, the migration group features higher d_s and lower $\Delta\sigma$, consistent with higher migration significance. It also features lower μ and higher t_{max}, similar to swarms in the Salton Trough [Chen and Shearer, 2011], while the non-migration group is more similar to mainshock-aftershock sequences. To explore possible fluid involvement, we model the migration behavior with the fluid diffusion equation, and identify 18 bursts with diffusion coefficients ranging from 0.01 to 0.8 m^2/s, with the majority below 0.16 m^2/s. The 18 bursts are mostly associated with normal faulting mechanisms, while the non-migration group has the most reverse faulting mechanisms, indicating a possible link between sequence type and focal mechanism.

APPROACHES FOR HIGH – PERFORMANCE WAVEFORM CROSS CORRELATION (B-073)

R.J. Chen, G.C. Beroza, and W.L. Ellsworth

Repeating earthquakes and low-frequency earthquakes exhibit very similar seismograms. Comparing waveform similarity is an essential task for detecting either events, but it is computationally expensive due to enormous amounts of continuous data needed to be analyzed. In this study, we examine seismograms from earthquakes on the San Andreas Fault near Parkfield and test the efficiency of several algorithms for measuring waveform similarity. We start with the standard similarity measure, where we take a window of a sample seismogram as a template and compare it with another seismogram using the correlation coefficient as our benchmark. To test this, we use several approaches. First, we decrease the computations required by using only alternate data points in the analysis to see if the results are sufficiently accurate. We then try another approach in which we parameterize the seismograms using only the peaks and troughs as the basis for a different similarity measure that might have sufficient accuracy. Our goal in these approaches is to develop algorithms that are sufficiently efficient to apply to continuous waveform data.

RESULTS FROM THE QUAKE-CATCHER NETWORK RAPID AFTERSHOCK MOBILIZATION PROGRAM (QCN-RAMP) IN CHRISTCHURCH, NEW ZEALAND (B-078)

A.I. Chung, E.S. Cochran, C. Christensen, A.E. Kaiser, and J.F. Lawrence

Following the 4 September 2010 M7.1 Darfield earthquake in New Zealand, we initiated a QCN Rapid Aftershock Mobilization Program (RAMP). 180 low-cost 14-bit USB accelerometers were quickly installed to record as many aftershocks as possible. Earlier in 2010, the QCN team deployed about 100 accelerometers in Chile following the M8.8 earthquake there and began experimenting with our rapid earthquake detection and characterization program. Following the New Zealand RAMP deployment, we continued to test this program with the more densely spaced Christchurch QCN array.

When the Christchurch event occurred on 22 February 2011, QCN sensors recorded the M6.3 event and calculated its magnitude, location and created a map of estimated shaking intensity within 7 seconds of the earthquake. Successive iterations improved the calculations and within 24 seconds of the earthquake, magnitude and location values comparable to those provided from GNS were calculated.

Using the wealth of data from this event as well as the following aftershocks, we have been able to improve our detection and identification algorithms. Whilst still in the development stages, our preliminary results from the data collected from these and other QCN stations around the world suggest that MEMS sensors installed in homes, schools, and offices provide a way to dramatically increase the density of strong motion observations for use in seismic hazard analysis and earthquake early warning. We are continuing to expand our network and have recently started deploying QCN sensors to the San Francisco Bay Area and Los Angeles areas.

COMPARISON OF CO-LOCATED PORE PRESSURE AND STRAIN OBSERVATIONS FROM EARTHQUAKES RECORDED AT PBO BOREHOLE STRAINMETER SITES. (A-071)

F. Civilini

Water level fluctuations in response to earthquakes and tidal strains have been observed in wells for many decades. The relationship between water level and dilatation can be used to characterize the well as a type of strainmeter. The correlation between the water level of an aquifer and the induced strain due to the earth tidal force is a well documented relationship, and can be used to calibrate various constitutive equations of a poroelastic medium to obtain Skempton's coefficient, a variable describing the effect of induced strain on pore pressure. The pore pressure response of the October 1999 Hector Mine earthquake (Mw 7.1) at the Garner Valley Downhole Array (GVDA) is compared to pore pressure and strain observations from two stations of the EarthScope Plate Boundary Observatory (PBO) for three magnitude 4.9 and above earthquakes in 2010: an El Mayor-Cucapah aftershock Mw 5.7 and two events of Mw 4.9 and Mw 5.4. These earthquakes were recorded at distances of ~97 Km, ~20 Km, and ~14 Km, respectively. Sudden pore pressure steps, both positive and negative, ranging from 500 Pa to 10 KPa are observed in all but one of the records, with the later being a more gradual decrease. The strain records for the same earthquakes reveal sharp and sustained changes of strain matching the pore pressure behavior. This suggests that in at least some of the cases, the observed pore pressure responses correspond to tectonic deformation caused by the strain field associated with the earthquakes. The similarity of the pore pressure step during the 1999 Hector Mine event to those of the 2010 earthquakes suggests that a this response was also related to the co-seismic tectonic strain field.

COMPARISON OF THE LOW-COST MEMS ACCELEROMETERS USED BY THE QUAKE-CATCHER NETWORK AND TRADITIONAL STRONG MOTION SEISMIC SENSORS (B-025)

E.S. Cochran, J.F. Lawrence, A. Kaiser, B. Fry, and A. Chung

Accelerometers based on low-cost micro-electro-mechanical systems (MEMS) have improved swiftly, making the rapid deployment of dense seismic arrays possible. For example, the Quake-Catcher Network (QCN) makes use of MEMS-based tri-axial sensors installed in homes and businesses to record earthquakes, with almost 2000 participants worldwide. QCN utilizes an open-source distributed-computing system, called the Berkeley Open Infrastructure for Network Computing (BOINC), to retrieve waveforms from continuous or triggered recordings back to the QCN server. Furthermore, the QCN approach can also be used to augment existing seismic networks for rapid-earthquake detection purposes, as well as studies on seismic source- and site-related phenomena.

Following the 3 September 2010 Mw7.1 Darfield earthquake, 192 QCN stations were installed in a dense array to record the on-going aftershock sequence in and around the city of Christchurch. We examine the peak ground motions recorded during a M5.1 aftershock and find that peak ground acceleration (PGA) is spatially variable, but with a clear decay in amplitude with distance. In general, closely located GeoNet and QCN stations report similar PGA. Several QCN stations were located within 1 km of existing GeoNet stations, providing an opportunity to compare time series and amplitude spectra. For these closely spaced pairs of stations, the amplitude spectra observed from the horizontal components are highly correlated with average cross-correlation coefficients of 0.9 or higher. In addition, we find the correlation coefficient decreases with increasing distance between station pairs.

COMPARISON OF SIMULATED SLOW SLIP EVENTS WITH OBSERVATIONS (A-101)

H.V. Colella, J.H. Dieterich, and K.B. Richards-Dinger

We model slow slip events (SSEs) after those observed along the Cascadia subduction zone using the 3D simulation code, RSQSim, which employs rate- and state-dependent constitutive properties appropriate to the mode of fault slip. For computational efficiency we impose the slip speed for SSEs, otherwise the simulations are fully deterministic in the nucleation, propagation speed, extent of slip, and final distribution of slip. To develop robust statistical characterizations of slow slip events, we generate long histories consisting of more than 105 events (spanning ~300-500 yrs). The simulated catalogs of SSEs span a large range of moments, most of which would be too small to detected geodetically. The largest simulated SSEs (Mw6.3-7.0) are in broad agreement with SSEs observed in Cascadia with a quasi-periodic recurrence interval ~10 months, durations of 10-40 days, and a mean slip of ~3 cm. Results also show spontaneous, but transient, segmentation of SSEs. The simulations also produce slip propagation characteristics similar to complex tremor patterns observed in Cascadia (i.e. rapid tremor reversals and along-dip streaking). Stressing rates at the base of the seismogenic zone, directly adjacent to the region in which SSEs occur, may be as much as 100x more than the stressing rate between events. This suggests a potential for triggering of mega-thrust earthquakes by SSEs.

DISCOVERING THE GEOMORPHIC RECORD OF HOLOCENE SLIP ALONG THE MOJAVE SECTION OF THE SAN ANDREAS FAULT, CALIFORNIA (A-137)

T. Compton, E. Cowgill, R. Gold, K. Scharer, R. Westerteiger, and T. Bernardin

Constructing long (10-100 kyr) records of fault slip is important for advancing our understanding of fault-system behavior and temporal variations in strain release. Paleoseismic data along the Mojave section of the San Andreas fault (MSAF) suggest temporal variations in strain release over the last 2 kyr, but more offsets are needed to extend the slip history back in time. We use virtual-reality analysis of LiDAR data and field observations to discover a more complete record of potential piercing points from offset Holocene landforms along the MSAF. Compilation of previously reported landform offsets reveals four gaps in the Holocene slip record at: 30-40m, 50-90m, 100-120m, and 130-360m of cumulative offset. Using new virtual-reality visualization software Crusta, we studied a 100km-long section of the B4 airborne LiDAR dataset to identify offset landforms within these offset intervals. Crusta is a virtual globe application that displays large (>60GB) LiDAR digital elevation models, merging the mapping functionality of ArcMap with the terrain visualization of GoogleEarth. The slicer tool in Crusta allows the user to interactively reconstruct fault slip by defining a piecewise linear fault plane and incrementally moving one block relative to the other in any direction on the plane. This tool has been helpful in identification, evaluation and reconstruction of landform offsets. Using Crusta, we have remotely identified 80+ landform offsets from 20 to 300m along the MSAF. Assuming an average Holocene slip rate of ~3cm/yr, these offsets span the Holocene. A majority (54) of the offsets cluster in displacements of <100m, with one half between 20-50m and the other between 51-100m. We find several channel offsets along the fault that are particularly promising for further analysis with offsets of 30m, 90m, 115m, and 260m, which fall within the data gaps noted above. At these locations, both the fault trace and offset are clear, and our preliminary analysis suggests the landforms are dateable. To evaluate geologic and geomorphic relationships in the field we will conduct terrestrial laser scanning (TLS) surveys and field-based mapping of select sites. This proposed work will provide the necessary foundation for geochronologic measurements and is the critical next step in constructing the MSAF slip history.

BUILDING HISTORIES OF FAULT SLIP TO OBSERVE SECULAR VARIATION IN SLIP (A-136)

E. Cowgill, R.D. Gold, P.O. Gold, T. Compton, T. Bernardin, and R. Westerteiger

Faults show temporal variations in slip at time scales ranging from the hours following a major rupture to the millions of years over which plate boundaries reorganize. One long-term behavior is secular variation in slip (SVS): a pulse of accelerated strain release along a single fault that occurs with a frequency that is more than an order-of-magnitude longer than the recurrence interval of surface ruptures within the pulse. Although numerous mechanical models have been proposed to explain SVS, it has proven much harder to measure long (5-500 kyr) records of fault displacement. Here we describe a method we are developing to determine such histories by measuring suites of piercing points defined by faulted landforms. To rapidly identify populations of faulted landforms, we use the virtual-reality based data visualization tool Crusta. Crusta is a virtual-globe that we developed to support interactive visualization of massive (> 1 TB), high-resolution topographic data sets such as from airborne LiDAR. Using this tool, we have identified > 80 potential piercing points along a ~100-km-long reach of the Mojave section of the San Andreas fault, California. To evaluate such sites, we have expanded the conceptual understanding of potential sources of epistemic uncertainty in the combined structural and geomorphic reconstruction of faulted landforms. To reduce such uncertainties, we use ground-based LiDAR to image faulted landforms and determine the 3D slip vector and its associated uncertainty via Monte Carlo analysis. Such analysis has yielded error envelopes at two sites studied along the Dixie Valley fault in Nevada that were 16% and 83% of offset uncertainties previously reported. Finally, we have developed a Monte Carlo approach for determining slip histories from suites of faulted landforms that allows us to determine both precise average slip rates and evaluate the extent to which such rates varied over time. Application of this method to data we collected along the central Altyn Tagh fault, China, reveals a pulse of accelerated strain release in the mid Holocene, with ~20 m of slip being released from ~6.7 to ~5.9 ka at a short-term rate (~28 mm/yr) that is 3 times greater than the average rate (~9 mm/yr). We interpret this pulse to represent a cluster of two to six, Mw > 7.2 earthquakes. To our knowledge, this is the first possible pre-historic earthquake cluster detected using slip-history analysis.

MOHO DISCONTINUITY STUDY ALONG SAN ANDREAS FAULT WITH RECEIVER FUNCTIONS (B-135)

P.A. Cox, P.M. Davis, and R.W. Clayton

We have calculated radial and transverse teleseismic receiver functions at 25 seismic stations along San Andreas Fault (SAF) between Eastern San Gabriel Mountains and Salton Sea. Near 8 km large offsets on the Moho beneath the SAF in the Eastern San Gabriel Mountains were observed (Yan & Clayton 2007), but no clear evidence for the offsets beneath the SAF have been

found at other stations. Our objective is to extend the study to Salton Sea rift zone along the SAF using more recent data and newly installed stations, and to examine topographic structure of the Moho and its variation across the fault. The purpose of this study is to understand earthquakes by determining seismic properties of the lithosphere. If sharp topography can be observed on the Moho, that will be evidence of lower crust having enough strength to hold vertical offsets. Our data shows 30 to 37 km depth Moho beneath the Eastern San Gabriel Mountains, and much shallower Moho depth of 14 to 20 km beneath Salton Sea. Moho depth seems to vary as a function of azimuth, becoming less north to south. We are testing whether the variation is due to offsets, dip or anisotropy.

References: Yan, Z., Clayton, R.W., 2007, A notch structure on the Moho beneath the Eastern San Gabriel Mountains: Earth and Planetary Science Letters 260 (2007) 570-581

STRESS DROP OBSERVATIONS FOR THE 2010 EL MAYOR AFTERSHOCKS WITH $4.0<M_W<5.5$ RECORDED AT THE BORREGO VALLEY DOWNHOLE ARRAY (B-043)

J. Crempien and R. Archuleta

Using P waves, Shearer et al. (2006) estimated stress drops for ~65,000 earthquakes with $1.6<M_w<3.1$ in southern California. In their map of smoothed stress drops, the stress drop decreases going from west (near the Elsinore Fault) —with values near 1.6 to 2.5MPa— to east near the southern extension of the San Jacinto and Imperial Faults —with values near 0.6MPa.

The northern end of the El Mayor earthquake was particularly active in producing earthquakes with $M_w>4$. The epicenters are in a region where one would expect stress drops to be as low as ~0.6 MPa. These aftershocks, with $4.0<M_w<5.5$ are well recorded at the Borrego Valley Downhole Array (BVDA) (Steidl, 2006). BVDA has accelerometers at different depths. We use the accelerograms recorded at depth to compute the spectra of the S waves from which we determine the corner frequency and stress drops using Brune's (1970, 1971) relations. Shearer et al. used Madariaga's (1976) relationship between corner frequency and source radius. Madariaga's relation amplifies the stress drop by 5.5 compared to Brune's, which would imply that the stress drop observations for the southern portion of the San Jacinto and Imperial faults would be approximately ~0.1MPa, if one were to use Brune's relationship. This assumes that stress-drops computed P wave corner frequencies are equivalent to stress drops computed using the corner frequencies determined from S waves.

We have analyzed 27 events of the 2010 El Mayor aftershock sequence with magnitudes between $4.0<M_w<5.5$. Although the epicentral distance ranges between 80 and 190km, the backazimuth is nearly constant. For each epicentral distance, we used the observed average Q to eliminate path effects. We used accelerograms at the bedrock depth of 238m to avoid site effects. After correcting for Q we used a nonlinear least square method to find the best fitting ω^2 model to the source displacement amplitude spectrum for each horizontal component. From the original 27 events, we selected 14 events, which had a good fit of the ω^2 model to the observed displacement spectrum. Using the corner frequency from the best fit and converting the catalog magnitude to seismic moment, we determined the stress drop of each event. In this preliminary investigation we find an average stress drop of approximately 1.1MPa, a value almost ten times that reported by Shearer et al. (2006) for this region, considering that their stress drops (~0.6MPa) were computed using Madariaga's relationship.

OPENTOPOGRAPHY: ONLINE ACCESS TO HIGH-RESOLUTION LIDAR TOPOGRAPHY DATA AND PROCESSING TOOLS IN SUPPORT OF NSF EARTH SCIENCE (A-119)

C.J. Crosby, V. Nandigam, S. Krishnan, C. Baru, and J.R. Arrowsmith

High-resolution topography data acquired with lidar (light detection and ranging) technology are revolutionizing the way we study the Earth's surface and overlying vegetation. These data, acquired from airborne or tripod-mounted scanners, have emerged as a fundamental tool for research on a variety of topics ranging from earthquake hazards to hillslope processes.

However, along with the scientific potential of lidar topography comes challenges associated with the massive volume and complexity of data that the technology generates. A single lidar data acquisition may produce terabytes of data in the form of point clouds, digital elevation models (DEMs), and derivative imagery. Further complicating matters is the fact that in many cases these large datasets are a community resource that must be made accessible to users with variable expertise, computing and software resources, and scientific applications.

The National Science Foundation-funded OpenTopography Facility (*http://www.opentopography.org*) is an online system designed to democratize access to Earth science-oriented lidar topography data. OpenTopography provides free, Web-based access to lidar data in a number of forms, including lidar point cloud data and associated geospatial processing tools for customized analysis. OpenTopography also delivers standard DEM products, and easily accessible Google Earth visualizations.

Presently, OpenTopography has approximately 16,500 km2 of data available – a total of 79 billion lidar returns – including coverage of many active faults in southern California collected through various community and PI-driven initiatives (e.g., B4, EarthScope, post-El Mayor-Cucapah earthquake). With several thousand active users, OpenTopography is an excellent example of a mature cyberinfrastructure system that is enabling access to challenging data for research, education and outreach.

This poster will provide an update on the OpenTopography Facility, including processing capabilities and resources, examples from scientific use cases, a snapshot of system and data usage thus far, and a discussion of ongoing and planned work.

DETECTION OF TRANSIENT DEFORMATION IN SOUTHERN CALIFORNIA USING CONTINUOUS AND CAMPAIGN GPS MEASUREMENTS (A-063)

B.W. Crowell and Y. Bock

Detection of small regional transient deformation remains an elusive problem within GPS geodesy, and automated detection of such events has proven to be more difficult. Here we report on an analysis of 10 years of continuous and campaign GPS data throughout southern California from 2000-2010, with the main areas of focus in the Imperial and Coachella Valleys. We first investigate small changes in yearly interseismic velocities in continuous GPS records compared to their long term interseismic estimates and compute the resulting change in the strain rate over a given year. Using this methodology, we are able to identify a number of known events such as the 2005 Obsidian Buttes and 2009 Bombay Beach seismic swarms. We take this further by utilizing campaign GPS measurements before and after the 2005 Obsidian Buttes seismic swarm to further constrain the extent of deformation. Our second approach utilizes a spatio-temporal principal component analysis (PCA) on a 100 day moving window of continuous GPS data over a radius of 250 km. Using this approach, we are able to pick out smaller scale changes on the GPS time series, when compared with basic least-squares time series parameter estimation, by looking at the ratio of the first two eigenvalues of the PCA. Our spatio-temporal PCA analysis has the added benefit of potentially contributing to an automated anomaly (e.g., offsets) detection algorithm during modeling and quality control of continuous GPS time series.

DEVELOPING A THREE-DIMENSIONAL GEOLOGICAL AND GEOPHYSICAL MODEL OF SIERRA NEGRA VOLCANO OF THE GALAPAGOS (B-024)

L.C. Davidge and C. Ebinger

Basaltic shield volcanoes in the Western Galapagos Island chain are among the most rapidly deforming volcanoes in the world, but little has been done to visualize the geological deformation of the area and to study the consequent subsurface microfaulting. By implementing the iterative double-difference earthquake relocation algorithm (Waldhauser & Ellsworth, 2000), high-resolution hypocentral locations of local quakes can be determined. The seismic data that was analyzed was recorded by seismometers deployed around the caldera of the Sierra Negra volcano between 2009 and 2011. Both catalogue arrival times and cross-correlated arrival times were used to relocate the hypocenters. Additionally, SCEC-VDO was used to visualize these high-resolution earthquakes and this visualization was supplemented with preexisting bathymetry and INSAR images of the region. The resulting visualization facilitates a more accessible analysis of the earthquakes occurring along the southeast flank of the shield complex, and it also allows for better visualization of zones interpreted as hydrofracture along the margins of magma chamber(s). The subsurface imaging does not resolve the angle of reverse faults, which have near-vertical and shallow focal planes. The time-dependent visualization of earthquakes in this area produced with SCEC-VDO also enables non-experts to gain an understanding of geohazards in the Galapagos region and relates findings of regional research in a way that is more visually appealing to the general public.

SHAKEOUT DRILL PLANNING AND EVALUATION AT CSU FULLERTON: A CASE STUDY (A-007)

L.A. Davis, A. Leslie, A. Nguyen, and M.M. Wood

Development of the California ShakeOut earthquake scenario in 2008 by the USGS provided a foundation for conducting earthquake drills. Since that time, ShakeOut earthquake drills have been conducted annually by an unprecedented number of individuals and organizations, including colleges and universities. California State University Fullerton (CSUF) is one such institution attempting to maximize the impact of the ShakeOut drills under the direction of an ad hoc planning group consisting of CSUF faculty, staff, and administrators. Efforts have been made to improve future campus ShakeOut events through review and evaluation of previous CSUF ShakeOut activities. Recommendations were developed through review of prior ShakeOut questionnaires and evaluation reports; review of qualitative evaluation data; and informal interviews conducted with members of the ShakeOut Evaluation subcommittee, ShakeOut stakeholders, and Southern California Earthquake Center staff. Recommendations include developing a logic model to guide program design and evaluation, expanding collaboration and drill-integration with community groups, mapping pre-event and post-event staged messaging, and conducting a campus-specific survey of administrators, faculty, staff, and students. These efforts may foster the development of a prototype that can be used by other campuses to facilitate their own ShakeOut planning and evaluation.

TEACHERS USING CONTINUOUS GPS DATA TO LEARN ABOUT EARTHQUAKES - SHARING RESEARCH RESULTS IN THE CLASSROOM THROUGH LESSON STUDY (A-005)

R.M. de Groot, S.F. McGill, B. Vargas, R. Ruiz, M. Kline, and S. Wallace

This EarthScope-funded project is a collaboration between high school science teachers and their students, undergraduate and graduate students, and faculty from California State University San Bernardino (CSUSB), University of Arizona, and the Southern California Earthquake Center (SCEC). As high school teachers and their students work alongside one another, they are exposed to and contribute to an authentic research process that will lead to publishable results. The scientific goal of this project is to measure plate tectonic movement within the San Bernardino mountain area and the Inland Empire region of Southern California utilizing the Global Positioning System (GPS). Teachers and high school students collected survey-mode GPS data from 11 sites (among a total of 25 sampled by the larger group of participants) during a 5-day campaign in July 2011. The information obtained will be useful for understanding and characterizing seismic hazards in that region of Southern California. To enhance this experience, all of the teachers and their students have been invited to present their results at the SCEC Annual Meeting in September 2011. As part of the classroom implementation phase of the program the teachers are introduced to the Lesson Study approach. Lesson Study is a professional development process where teachers systematically examine their practice with the goal of becoming more effective. This process centers on teachers working collaboratively on a small number of Research Lessons. First, they identify the areas where their students are encountering challenges in learning standards-based content. The challenging areas are identified through results from standardized exams or other assessment tools. To address areas of difficulty the teachers develop, test, and improve an instructional experience that promotes student learning of that standards-based material. Lesson Study is different from "lesson planning" because it focuses on what teachers want students to learn rather than on what teachers plan to teach. The 2011 teachers divided into three groups and each group is developing a Research Lesson. One of each of the group members teaches the lesson while the others observe the student learning. After the Research Lesson is taught the entire group comes together to debrief the lesson, make revisions, and another member of the group re-teaches the lesson (at a later date and at a different school) to incorporate what has been learned.

INVESTIGATING ALONG-STRIKE DEPTH VARIATIONS OF SEISMICITY IN THE SAN ANDREAS FAULT SYSTEM TO BETTER RESOLVE GEODETIC LOCKING DEPTHS (A-054)

C. Del Pardo, B.R. Smith-Konter, D.T. Sandwell, P. Shearer, and Y. Zeng

Accurate estimates of maximum fault locking depth along the San Andreas Fault System (SAFS) are fundamental in estimating the seismic moment accumulation rate of active faults. As geodetic estimates of fault locking depth are dependent upon model fault geometry and segmentation resolution, proper representation of each active fault segment of the SAFS is critical. In this study, we re-evaluate the along-strike segmentation of the San Andreas, San Jacinto, Elsinore and Eastern California Shear Zone faults in Southern California using variations in depths of seismicity from the earthquake hypocenter catalog of Lin et al. [2007]. We use the UCERF3 fault segmentation as a first-order model of major fault segments and examine seismicity profiles as a function of depth for each segment. To achieve robust depth estimates that are insensitive to occasional stray earthquake locations at large depth, we assign a cutoff percentile depth at 99% to define the maximum depth of seismicity. For segments that have significant along-strike variations in maximum depth of seismicity, or gaps in seismicity, we refine the fault segmentation to accommodate these observed variations. Previous work suggests that the inclusion of earthquakes within 5 km of each fault trace provides a reasonable representation of the active fault zone, however we also investigate the sensitivity of fault depth to the width of the seismicity window. Lastly, we assess the range of appropriate along-strike segment lengths that are resolvable with the current geodetic array in Southern California. Ultimately, this analysis will contribute a more refined fault segmentation model to be used for complimentary UCERF3 fault slip rate and locking depth analyzes.

CONDITIONS FOR RUPTURE JUMPING TO THE ADJACENT SEGMENTS – A CASE STUDY FOR THE 1992 LANDERS EARTHQUAKE (A-082)

A.J. Delauder, Z. Fang, Y. Klinger, and E.M. Dunham

Multifault rupture occurs when the rupture on one fault “jumps” to another fault thus triggering a rupture on the second fault. This phenomenon has interested seismologists for years and continues to be a growing field of study. The 1992 Landers earthquake is a classic example of multifault rupture through a geometrically complex fault system.

Previous models of the Landers rupture process have included multiple nonplanar fault segments, but the off-fault response was assumed to be ideally elastic. Our prior studies of dynamic ruptures on idealized nonplanar faults have highlighted the importance of accounting for inelastic deformation to bound otherwise unreasonable stress concentrations that develop around structural complexities. Building on that modeling framework, we present a dynamic rupture model of the Landers earthquake that incorporates plastic deformation in addition to the realistic nonplanar geometry. Simulations show that a rupture cannot jump over one kilometer without the presence of a linking fault, at least for the specific geometries and parameters we studied. Since the main segments of the complex Landers fault system are almost 5 kilometers apart, we speculate that minor connecting faults must play a key role in rupture propagation spanning multiple segments.

To gain more insight, we have studied three typical but simplified fault geometries: parallel (two faults 5 km apart with no overlap), overlapping, and linked (two overlapping faults connected by a linking fault). The linked geometry was the only one of the three tested geometries that allowed the rupture to jump from the first fault to the second. This confirms our speculation, and brings attention to the often-neglected linking faults in complex fault systems. We expect that our findings will help seismologists better understand both the physics behind and the probability of multifault rupture on large, complex fault systems.

MODELING GROUND MOTION OF A M7+ EARTHQUAKE ON THE SAN ANDREAS FAULT USING THE VIRTUAL EARTHQUAKE APPROACH (B-007)

M. Denolle, G.C. Beroza, E.M. Dunham, and G. Prieto

The utility of empirical ground motion prediction equations is limited by the scarcity of large events. Physics-based simulations provide an important way to overcome this data scarcity, provided they accurately take into account the complexity of the source, the crustal elastic and anelastic structure and the local site effects. Our incomplete knowledge on crustal structure is an important source of uncertainty in ground motion simulations. We use the ambient seismic field to validate ground motion predictions at long periods. We compute the impulse responses of the Earth in between specific seismic station pairs with ambient seismic field analysis. Comparison of impulse responses with earthquake records from moderate earthquakes confirms that this process preserves relative amplitude. The distribution of the noise sources is not homogeneous, however, and this has the potential to bias amplitude variations.

We can achieve a better control on the source of seismic energy with the coda-wave interferometry. We use the aftershocks of the April 4th, 2010, M7.2, El Mayor-Cucapah earthquake and southern California earthquakes with magnitudes exceeding 4. If the direction of the microseism and the earthquakes are complementary in some directions and improve the stability of the amplitude, they also improve the quality of the asymmetric impulse responses. We then correct the impulse responses with simple analysis on the dispersion of the surface waves to account for the depth-dependence of excitation as well as radiation pattern of a double couple point source and directivity effects of an extended finite source. We use a spectral collocation method using Chebyshev polynomials to evaluate the depth-dependence of the fundamental mode surface-wave excitation for complex crustal structure. After validating this technique with moderate Californian earthquakes, we apply our approach to a temporary seismic network that was deployed along the southern segment of the San Andreas Fault (SAVELA experiment). To simulate an extended finite source and capture directivity effects, we superimpose the impulse responses from all the station sources that represent parts of the fault. As predicted by large-scale computer simulations strong ground motion amplification in the Los Angeles sedimentary basin is clearly observed in the scenarios we study for a large M7+ strike-slip earthquake on the reach of the San Andreas Fault near San Gorgonio Pass.

GPS NETWORK OPERATIONS AT USGS PASADENA (A-067)

D. Determan, A. Aspiotes, K. Hudnut, N. King, and K. Stark

The US Geological Survey Pasadena field office operates 104 permanent, continuously-operating Global Positioning System (GPS) stations in southern California. These stations are primarily located throughout the urban Los Angeles area and along the southern San Andreas fault. The construction and in159s159t159a159l159l159a159t159i159o159n159 159o159f159 159t159h159e159 159s159t159a159t159i159o159n159s159 159b159e159g159a159n159 159i159n159 159115991599159415 9159a159n159d159 159c159o159n159t159i159n159u159e159s159 159t159o159d159a159y159.159 159 159T159h159e159 159m159a159j159o159r159i159t159y159 159o159f159 159t159h159e159 159s159i159t159e159s159 159w159e159r159e159 159c159o159n159s159t159r159u159c159t159e159d159 159a159s159 159p159a159r159t159 159o159f159 159t159h159e159 159 S 159 o 159 u 159 t 159 h 159 e 159 r 159 n 159 159 C 159 a 159 l 159 i 159 f 159 o 159 r 159 n 159 i 159 a 159 159 I 159 n 159 t 159 e 159 g 159 r 159 a 159 t 159 e 159 d 159 159 G 159 P 159 S 159 159 N 159 e 159 t 159 w 159 o 159 r 159 k 159

160(160S160C160I160G160N160)160 160p160r160o160j160e160c160t160 160i160n160 160t160h160e160 160l160a160t160e160 160116091609160 0160s160 160t160h160r160o160u160g160h160 160216001600160 1160.160 160T160e160n160 160n160e160w160 160s160t160a160t160i160o160n160s160 160h160a160v160e160 160b160e160e160n160 160a160d160d160e160d160 160s160i160n160c160e160 160216001600160 9160.160 160 160S160e160v160e160r160a160l160 160h160a160v160e160 160 b 160 o 160 t 160 h 160 160 s 160 e 160 i 160 s 160 m 160 i 160 c 160 160 a 160 n 160 d 160 160 G 160 P 160 S 160 160 i 160 n 160 s 160 t 160 r 160 u 160 m 160 e 160 n 160 t 160 a 160 t 160 i 160 o 160 n 160 . 160 160 I 160 n 160 160c160o160o160p160e160r160a160t160i160o160n160 160w160i160t160h160 160t160h160e160 160L160o160s160 160A160n160g160e160l160e160s160 160D160e160p160a160r160t160m160e160n160t160 160o160f160 160W160a160t160e160r160 160 a 160 n 160 d 160 160 P 160 o 160 w 160 e 160 r 160 , 160 160 w 160 e 160 160 r 160 e 160 c 160 e 160 n 160 t 160 l 160 y 160 160i160n160s160t160a160l160l160e160d160 160c160o160-160l160o160c160a160t160e160d160 160s160e160i160s160m160i160c160 160 a 160 n 160 d 160 160 G 160 P 160 S 160 160 e 160 q 160 u 160 i 160 p 160 m 160 e 160 n 160 t 160 160 a 160 t 160 160 E 160 l 160 i 160 z 160 a 160 b 160 e 160 t 160 h 160 160 L 160 a 160 k 160 e 160 160 T 160 u 160 n 160 n 160 e 160 l 160 160 S 160 o 160 u 160 t 160 h 160 , 160 160 a 160 160 c 160 r 160 i 160 t 160 i 160 c 160 a 160 l 160 160i160n160f160r160a160s160t160r160u160c160t160u160r160e160 160s160i160t160e160 160t160h160a160t160 160m160o160n160i160t160o160r160s160 160t160h160e160 160i160n160t160e160g160r160i160t160y160 160o160f160 160t160h160e160 160f160r160e160s160h160 160w160a160t160e160r160 160t160u160n160n160e160l160 160t160h160a160t160 160c160r160o160s160s160e160s160 160t160h160e160 160S160a160n160 160A160n160d160r160e160a160s160.160 160T160h160e160 160P160a160s160a160d160e160n160a160 160f160i160e160l160d160 160o160f160f160i160c160e160 160c160u160r160r160e160n160t160l160y160 160o160p160e160r160a160t160e160s160 160t160h160r160e160e160 160t160y160p160e160s160 160o160f160 160g160e160o160d160e160t160i160c160 160g160r160a160d160e160 160G160P160S160 160e160q160u160i160p160m160e160n160t160:160 160t160h160e160 160A160s160h160t160e160c160h160 160Z160-160X160I160I1603160,160 160t160h160e160 160T160r160i160m160b160l160e160 160N160e160t160R160S160,160 160a160n160d160 160t160h160e160 160T160O160P160C160O160N160 160N160e160t160-160G1603160A160.160 160 160 T 160 h 160 e 160 160 T 160 O 160 P 160 C 160 O 160 N 160 160 N 160 e 160 t 160 - 160 G 160 3 160 A 160 160r160e160c160e160i160v160e160r160s160 160w160e160r160e160 160a160c160q160u160i160r160e160d160 160i160n160 160216001601160 0160,160 160t160h160r160o160u160g160h160 160f160u160n160d160i160n160g160 160f160r160o160m160 160t160h160e160 160A160m160e160r160i160c160a160n160 160R160e160c160o160v160e160r160y160 160a160n160d160 160R160e160i160n160v160e160s160t160m160e160n160t160 160A160c160t160.160

COMPARATIVE STUDY OF SCATTERING AND INTRINSIC ATTENUATION IN CALIFORNIA, MEXICO AND PERU. DOES THE TECTONIC SETTING AFFECT THE FREQUENCY DEPENDENCE? (B-068)

L.A. Dominguez, P.M. Davis, and M. Madrid

We compare seismic attenuation results for three broadband seismic networks: the Integrate Seismic Network (CI) in California, the Middle America Seismic Experiment (MASE) in Mexico, and the Peru Seismic Experiment (PERUSE). We obtained independent measurements of scattering and intrinsic attenuation using the Multiple Lapse Time Window (MLTW) by Hoshiba (1991). We chose California as a reference frame due to the availability of similar published studies and the ready access to the data through the SCEC data center. Unlike California, Mexico and Peru networks are located along two distinctive subduction zones. Peru is characterized by a thick crust ~80km above a dipping subducting slab whereas Mexico shows a flat subducting slab that extends for about ~250km from the trench and a crust of ~40km. We discuss the implications that the tectonic setting has on the the measurements of seismic attenuation. Our results from Peru and Mexico show remarkable differences from published results in California. In particular, measurements of seismic albedo (ratio between scattering attenuation and total attenuation) show low frequency dependence for the subduction zones in contrast with California. We suggest that waveguide effects play a significant role in the interpretation of the results. While in California most of the earthquakes occur at shallow depth and can experience total internal reflection, Mexico and Peru earthquakes occur at greater depths beneath the crust. This difference can potentially lead to reflection of energy to the mantle when seismic waves encounter the Moho and transmitted waves into the crust remain at sub-critical angles. Our results provide new evidence for the interpretation of attenuation studies and origin of coda.

GPS AND UAVSAR (A-066)

A. Donnellan, J. Parker, S. Hensley, B. Bills, and T. Herring

The 4 April 2010, M 7.2 El Mayor-Cucapah earthquake was observed by continuous GPS and with UAVSAR beginning in October of 2009. Several UAVSAR acquisitions following the earthquake provide detailed co-seismic and postseismic images

of surface deformation. UAVSAR data were first collected for the Salton Trough experiment along the border on October 20, 2009. Repeat data were collected on April 12 and 13, 2010 about one week after the M 7.2 El Mayor-Cucapah earthquake, and on July 1 of 2010. The coseismic data can be fit fairly well by a single fault along the length of the rupture and much smaller left-lateral conjugate faults. Disturbance can be seen on the Superstition Hills fault, though there is no observable offset in the UAVSAR data. The GPS data suggest up to 2 cm of regional uplift in the Imperial Valley. Observed UAVSAR postseismic motions indicate a left step in the mainshock rupture that continues northward, consistent with the M 5.7 aftershock that occurred on June 15, 2010.

EXPLORING PHYSICAL CONDITIONS THAT CONTROL THE 2011 MW 9.0 TOHOKU-OKI EARTHQUAKE RUPTURE AND SEISMIC RADIATIONS (A-109)

B. Duan

Seismic and geodetic recordings are routinely used to invert for kinematic source models of large earthquakes, which provide us with detailed images of slip distribution and rupture evolution on causative faults. To gain insight into physical conditions that control earthquake rupture and seismic radiations, we resort to dynamic source models that obey physical laws in continuum mechanics and rock friction. Published kinematic models of the 2011 Mw 9.0 Tohoku-Oki earthquake reveal several features of the rupture, including 1) high static stress drop with large amounts of slip in a small area, 2) a weak initial phase, down-dip rupture for the first 40 seconds, extensive shallow rupture during 60 to 70 seconds, and continuing deeper rupture lasting more than 100 seconds, and 3) systematically down-dip high-frequency radiation with respect to the hypocenter. In this study, we use spontaneous rupture models to explore what physical conditions can produce these features, so that we can gain some physical insights into controls on this megathrust earthquake.

Dynamic rupture simulations of this shallow dipping megathrust faulting at reasonable spatial and temporal resolutions require parallel computing on supercomputers. Our newly parallelized finite element method algorithm EQdyna allows us to simulate a large suite of spontaneous rupture models. In model setup, we use depth-dependence principal stresses and take into account variations in pore fluid pressure and frictional properties associated with subducted seafloor features such as seamounts. Our preliminary results suggest followings. First, a high strength and high stress drop patch (probably a subducted seamount or seamout chains) just above the hypocenter on the fault plane can delay up-dip rupture and result in a concentrated large slip area. Second, significantly negative stress drop on the shallow portion of the subducting fault associated with the active accretionary prism is needed to reduce the amplitude of shallow slip and to confine shallow slip in a small area near the trench just up-dip of the region of maximum fault slip. Third, heterogeneities in the seismic strength parameter S down-dip of the hypocenter, probably due to both heterogeneous stresses from previous earthquakes and heterogeneous friction properties at the brittle and ductile transition zone, can produce large amounts of high-frequency radiations.

MARINE AND LAND ACTIVE-SOURCE SEISMIC INVESTIGATION OF GEOTHERMAL POTENTIAL, TECTONIC STRUCTURE, AND EARTHQUAKE HAZARDS IN PYRAMID LAKE, NEVADA (B-045)

A. Eisses, A. Kell, G. Kent, N. Driscoll, R. Karlin, R. Baskin, J. Louie, K. Smith, and S. Pullammanappallil

Preliminary slip rates measured across the East Pyramid Lake fault, or the Lake Range fault, help provide new estimates of extension across the Pyramid Lake basin. Multiple stratigraphic horizons spanning 48 ka were tracked throughout the lake, with layer offsets measured across all significant faults in the basin. A chronstratigraphic framework acquired from four sediment cores allows slip rates of the Lake Range and other faults to be calculated accurately. This region of the northern Walker Lake, strategically placed between the right-lateral strike-slip faults of Honey and Eagle Lakes to the north, and the normal fault bounded basins to the southwest (e.g., Tahoe, Carson), is critical in understanding the underlying structural complexity that is not only necessary for geothermal exploration, but also earthquake hazard assessment due to the proximity of the Reno-Sparks metropolitan area. In addition, our seismic CHIRP imaging with submeter resolution allows the construction of the first fault map of Pyramid Lake. The Lake Range fault can be obviously traced west of Anahoe Island extending north along the east end of the lake in numerous CHIRP lines. Initial drafts of the fault map reveal active transtension through a series of numerous, small, northwest striking, oblique-slip faults in the north end of the lake. A previously field mapped northwest striking fault near Sutcliff can be extended into the west end of Pyramid Lake. This fault map, along with the calculated slip rate of the Lake Range, and potentially multiple other faults, gives a clearer picture into understanding the geothermal potential, tectonic regime and earthquake hazards in the Pyramid Lake basin and the northern Walker Lane. These new results have also been merged with seismicity maps, along with focal mechanisms for the larger events to begin to extend our fault map in depth.

ENERGY PARTITION, STRAIN LOCALIZATION AND THERMAL WEAKENING IN A MODEL OF SHEARED GRANULAR MATERIALS (A-098)

A.E. Elbanna, C. Lieou, and J. Carlson

Ample field observations and seismic imaging results show that mature faults fail along very thin primarily slip zones with no significant evidence of melting. This is usually taken as an indication that the dynamic friction during sliding is much lower than its static counterpart. Here we explore the problem of dynamic weakening of frictional faults within the framework of the shear transformation zone (STZ) theory. Manning et al. (2007,2009), using the STZ theory, showed that strain localizes and long lived shear banding zone forms for a wide range of strain rates and initial conditions relevant to the earthquake problem. Here we further consider the problem of shear deformation in granular gouge in the presence of temperature-dependent material properties; both the yield stress and the shear modulus of the gouge material are assumed to decrease with increasing temperature. As the two surfaces of the fault move relative to each other, part of the change in strain energy is consumed in raising the temperature of the gouge particles which in turn leads to a reduction in the gouge strength and stiffness. We find that this feedback between the thermal softening and the irreversible shear rearrangements of the gouge particles lead to i)a smaller slip-weakening distance; ii) a lower steady state sliding friction; and iii) a smaller fraction of the total energy being dissipated as frictional heat than in the athermal case. Finally, we briefly discuss some constraints on the width of the shear banding zone as well as the maximum achievable temperatures predicted by our model.

A METHOD FOR EARTHQUAKE CYCLE SIMULATIONS: QUASI-STATIC EVOLUTION TO DYNAMIC RUPTURE (B-056)

B.A. Erickson and E.M. Dunham

The goal of our project has been the development of a time-stepping methodology to understand and simulate full earthquake cycles with multiple events on geometrically complex faults, with rate-and-state friction and off-fault plasticity. This framework requires numerical methods to advance the model over long interseismic periods using the quasi-static equations, and through dynamic rupture using the elastodynamic formulation. In order to handle geometric complexities and off-fault plasticity, a volume discretization is required. During the quasi-static phase, we neglect inertia and the system evolves due to slow tectonic loading. Once inertial effects become significant we switch to solving the equations of elastodynamics. This switching method has been implemented in 1D, taking large time steps through the interseismic period and much smaller time steps in order to fully resolve coseismic rupture. In 2D we have solved the quasi-static equations for the antiplane problem by imposing constant creep at the downdip extension of the fault, intended to capture the effect of slow loading during the interseismic period. We have concurrently begun to use 2D plane strain models with off-fault plasticity to approximate multiple earthquake ruptures on rough faults. The initial conditions prior to the first event are sufficient to immediately nucleate dynamic rupture. Once the rupture has terminated and slip velocity is sufficiently small, fault strength evolves according to the aging law and the system is loaded by a constant increment in shear stress in the medium. This incremental method is an easy implementation that allows us to generate earthquake cycles on rough faults, but it is an approximation in the sense that it may overlook effects such as creep and afterslip during an interseismic time step. For the time being it may be a useful tool for incorporating the basic effects of interseismic load accumulation and to study how heterogenous residual stresses affect subsequent ruptures. However, it will be important to see what additional effects are captured once we implement the quasi-static evolution on rough faults with off-fault plasticity via our switching method.

SHARPENED VIEWS OF THE 2011 TOHOKU-OKI EARTHQUAKE FROM SPARSITY BASED OPTIMIZATION (A-043)

E.L. Evans and B.J. Meade

Understanding the relationship between strain accumulation and release in subduction zones is limited by our ability to resolve and compare spatial patterns of coseismic slip and interseismic slip deficit. In earthquake geodesy, estimates of fault slip are traditionally determined by regularized least squares minimization. Implicit in this approach is the assumption that slip distributions vary smoothly. However, if boundaries to fault slip are sharp in nature, smooth solutions given by traditional least squares estimation may artificially smear fault slip beyond physical boundaries. Resolving sharp variations in fault slip may be achieved with techniques such as basis pursuit denoising that incorporate L1 minimization of the state vector. Minimizing the L1 norm reduces the number of nonzero state vector elements resulting in a sparse, and therefore sharp, solution. We investigate two methods combining least squares minimization of residual velocities with L1 minimization of the state vector. We apply these techniques to geodetic data in Japan to image interseismic coupling prior to the 2011 Mw=9.0 Tohoku-oki earthquake and coseismic slip during the event and quantitatively assess the extent to which they are co-located.

ADDITIONAL SHEAR RESISTANCE FROM FAULT ROUGHNESS AND ITS ROLE IN DETERMINING STRESS LEVELS ON MATURE AND IMMATURE FAULTS (A-081)

Z. Fang and E.M. Dunham

The majority of crustal faults host earthquakes at $\tau/(\sigma - p) \sim 0.6$, while mature plate-boundary faults, like the San Andreas Fault (SAF), host earthquakes at $\tau/(\sigma - p) \sim 0.2$. A leading explanation for the weakness of the SAF is the existence of dynamic weakening, which, on planar faults, allows self-sustaining rupture at a critical background stress level $\tau^{pulse}/(\sigma - p) \sim 0.25$. Provided that dynamic weakening also occurs on less mature faults, which seems likely given the ubiquity of dynamic weakening in high velocity friction experiments, the stress levels on the less mature faults are puzzling. We offer a self-consistent explanation for the relatively high stress levels on immature faults that is compatible with dynamic weakening and low coseismic strength of all faults. Our explanation is that increased geometrical complexity of less mature faults introduces an additional resistance to slip that must be overcome in order for the fault to host ruptures. Lab and field observations suggest that faults are self-similar surfaces with amplitude-to wavelength ratio α in the range of 10^{-3} (mature faults) to 10^{-2} (immature faults). Slip on such faults induces huge stress perturbations near the fault. Projection of these stress perturbations back onto the rough fault surface results in an additional shear resistance to slip, the 'roughness drag' τ^{drag}, that exists even if the fault is frictionless. A perturbation analysis, accurate to second order in α, shows that $\tau^{drag} = 8\pi^3\alpha^2[G/(1-\nu)][\Delta u/\ \lambda_{min}]$, in which G is shear modulus, ν is Poisson's ratio, Δu is the amount of slip, and λ_{min} is the minimum wavelength of roughness. Estimates indicate that τ^{drag} is negligible on mature faults ($\alpha \sim 10^{-3}$) but can become substantial on immature faults ($\alpha \sim 10^{-2}$). We expect that the finite strength of the off-fault material ultimately bounds τ^{drag} to a value determined by the internal friction coefficient of the material. To test our hypothesis, we model dynamic rupture propagation on hundreds of randomly generated rough faults. The model includes dynamic weakening of fault strength and off-fault plasticity. Simulation results consistently indicate that rough faults require background stress levels $\tau^b \approx \tau^{pulse} + \tau^{drag}$ to host sizable ruptures. There are thus two limiting cases of fault behavior: For mature faults, $\tau^{drag} << \tau^{pulse}$, such that $\tau^b \approx \tau^{pulse} \sim 0.25(\sigma - p)$; while for immature faults, $\tau^{drag} \sim \tau^{pulse}$, thus requiring much higher $\tau^b \sim 0.6/(\sigma - p)$ to host earthquakes.

INTERSEISMIC, COSEISMIC AND POST-SEISMIC GPS OBSERVATIONS OF THE 2010/04/04 EL MAYOR-CUCAPAH EARTHQUAKE (A-045)

M.A. Floyd and G.J. Funning

We present reprocessed solutions of survey GPS data from 1993 onwards in the area surrounding the El Mayor-Cucapah rupture zone. Pre-earthquake survey data from the UNAVCO and S163C163E163C163 163a163r163c163h163i163v163e163s163 163a163r163e163 163c163o163m163b163i163n163e163d163 163w163i163t163h163 163P163B163O163 163a163n163d163 163o163t163h163e163r163 163c163o163n163t163i163n163u163o163u163s163 163G163P163S163 163d163a163t163a163 163t163o163 163p163r163o163d163u163c163e163 163e163s163t163i163m163a163t163e163s163 163o163f163 163t163h163e163 163 r 163 a 163 t 163 e 163 s 163 163 o 163 f 163 163 i 163 n 163 t 163 e 163 r 163 s 163 e 163 i 163 s 163 m 163 i 163 c 163 163d163e163f163o163r163m163a163t163i163o163n163 163i163n163 163t163h163e163 163r163e163g163i163o163n163.163

163 G 163 P 163 S 163 163 d 163 a 163 t 163 a 163 163 a 163 r 163 e 163 163 p 163 r 163 o 163 c 163 e 163 s 163 s 163 e 163 d 163 163 u 163 s 163 i 163 n 163 g 163 163 t 163 h 163 e 163 163 G 163 A 163 M 163 I 163 T 163 / 163 G 163 L 163 O 163 B 163 K 163 163s163u163i163t163e163.163 163A163l163l163 163a163v163a163i163l163a163b163l163e163 163d163a163t163a163 163a163r163e163 163v163e163r163i163f163i163e163d163 163f163o163r163 163m163e163t163a163d163a163t163a163 163e163r163r163o163r163s163 163b163e163f163o163r163e163 163p163r163o163c163e163s163s163i163n163g163,163 163o163u163t163l163i163e163r163s163 163a163r163e163 163r163e163m163o163v163e163d163 163b163y163 163e163x163a163m163i163n163i163n163g163 163t163i163m163e163 163s163e163r163i163e163s163,163 163n163o163i163s163e163 163c163h163a163r163a163c163t163e163r163i163s163t163i163c163s163 163o163f163 163t163i163m163e163 163s163e163r163i163e163s163 163a163r163e163 163a163l163s163o163 163a163s163s163e163s163s163e163d163 163t163o163 163i163m163p163r163o163v163e163 163e163s163t163i163m163a163t163e163s163 163o163f163 163u163n163c163e163r163t163a163i163n163t163i163e163s163 163i163n163 163v163e163l163o163c163i163t163y163,163 163a163n163d163 163a163 163f163i163n163a163l163 163(163p163r163e163-163e163a163r163t163h163q163u163a163k163e163)163 163v163e163l163o163c163i163t163y163 163s163o163l163u163t163i163o163n163 163p163r163o163d163u163c163e163d163 163t163h163r163o163u163g163h163 163t163h163e163 163K163a163l163m163a163n163 163f163i163l163t163e163r163 163w163i163t163h163 163n163o163i163s163e163 163i163n163c163l163u163d163e163d163.163

164W164e164 164e164x164t164r164a164p164o164l164a164t164e164 164t164h164e164s164e164 164r164e164s164u164l164t164s164 164i164n164 164t164i164m164e164 164t164o164 164t164h164e164 164d164a164t164e164 164o164f164 164t164h164e164 1642164016411640164 164e164a164r164t164h164q164u164a164k164e164 164i164n164 164o164r164d164e164r164 164t164o164 164c164o164n164s164t164r164a164i164n164 164t164w164o164 164q164u164a164n164t164i164t164i164e164s – 164t164h164e164 164 c 164 o 164 s 164 e 164 i 164 s 164 m 164 i 164 c 164 164 d 164 i 164 s 164 p 164 l 164 a 164 c 164 e 164 m 164 e 164 n 164 t 164 164 f 164 i 164 e 164 l 164 d 164 , 164 164 w 164 h 164 i 164 c 164 h 164 164 a 164 c 164 t 164 s 164 164 a 164 s 164 164 t 164 h 164 e 164 164 i 164 n 164 i 164 t 164 i 164 a 164 l 164 164 c 164 o 164 n 164 d 164 i 164 t 164 i 164 o 164 n 164 164 o 164 f 164 164 t 164 h 164 e 164 164 p 164 o 164 s 164 t 164 - 164 s 164 e 164 i 164 s 164 m 164 i 164 c 164 164 d 164 e 164 f 164 o 164 r 164 m 164 a 164 t 164 i 164 o 164 n 164 , 164 164 a 164 n 164 d 164 164 t 164 h 164 e 164 164 p 164 o 164 s 164 t 164 - 164 s 164 e 164 i 164 s 164 m 164 i 164 c 164 164 d 164 e 164 f 164 o 164 r 164 m 164 a 164 t 164 i 164 o 164 n 164 164 i 164 t 164 s 164 e 164 l 164 f 164 , 164 164 i 164 n 164 c 164 l 164 u 164 d 164 i 164 n 164 g 164 164 d 164 e 164 f 164 i 164 n 164 i 164 n 164 g 164 164 a 164 n 164 164 a 164 p 164 p 164 r 164 o 164 p 164 r 164 i 164 a 164 t 164 e 164 164 i 164 n 164 t 164 e 164 r 164 s 164 e 164 i 164 s 164 m 164 i 164 c 164 164r164e164f164e164r164e164n164c164e164

MECHANICAL AND MICROSTRUCTURAL OBSERVATIONS OF DYNAMIC WEAKENING IN SMECTITE-RICH SAFOD GOUGE (A-091)

M.E. French, H. Kitajima, J.S. Chester, and F.M. Chester

We present the results of high-speed rotary shear experiments on gouge from the Central Deforming Zone (CDZ) of the San Andreas Fault (SAF). Core from the CDZ, which currently creeps aseismically, was recovered during Phase 3 drilling of the San Andreas Fault Observatory at Depth (SAFOD). The sample tested is a well-foliated smectite – rich gouge that contains clasts of serpentine, quartz, feldspar, and opaques. The sample was flaked to ~600 μm to preserve the clay fabric; a ~1 mm thick layer was sheared between gabbro blocks 25 mm in diameter and semi-sealed with a press-fit Teflon ring. Experiments were conducted at a constant normal stress of 0.3 - 1.5 MPa, velocity of 0.1 - 1.3 m/s, and displacement up to 20 m (we refer to the local condition at 2/3 the sample radius). We tested room-dry and water-saturated gouge at room temperature and measured the gouge temperature on a representative suite of samples. Microstructural analyses were conducted on radial cut thin sections which show slip-perpendicular structures formed under spatial gradients in velocity and displacement.

The CDZ gouge weakens with an increase in velocity. The steady-state coefficient of friction of the wet gouge varies from μ= 0.40 at 0.1 m/s to μ= 0.14 at 1.3 m/s. Temperature within the gouge layer exceeds the water-vapor phase transition in the water-saturated gouge sheared at 0.35-1.3 m/s. In general, the coefficient of friction and temperature of the dry gouge are greater than that of the wet gouge. Microstructures show a progression in deformation mechanisms with increasing displacement and velocity. A clay-foliation develops by ~1 m of displacement. Under the highest velocity and/or displacement conditions poorly-foliated to nonfoliated regions develop parallel and oblique to the foliation. In some cases the non-foliated, disaggregated gouge cross-cuts and disrupts adjacent foliated zones and contains fragments of foliated material. The disrupted zones occur in regions of different displacement and velocity conditions where the temperatures may have risen high enough to promote pore fluid pressurization and vaporization. Because these experiments are essentially vented, we expect greater weakening in-situ where fluid escape is limited. Thus, although previous studies have shown this material to be velocity-strengthening at sub-seismic slip rates, the creeping segment of the SAF and similar clay-rich faults may be capable of propagating seismic rupture.

THE SALTON SEISMIC IMAGING PROJECT: INVESTIGATING EARTHQUAKE HAZARDS IN THE SALTON TROUGH, SOUTHERN CALIFORNIA (B-134)

G.S. Fuis, M.R. Goldman, R.R. Sickler, R.D. Catchings, M.J. Rymer, E.J. Rose, J.M. Murphy, L.A. Butcher, J.A. Cotton, C.J. Criley, D.S. Croker, I. Emmons, A.J. Ferguson, M.A. Gardner, E.G . Jensen, R. McClearn, C.L. Loughran, C.J. Slayday-Criley, J.R. Svitek, J.A. Hole, J.M. Stock, S. Skinner, N.W. Driscoll, A.J. Harding, J. Babcock, G.M. Kent, A. Kell, and S.H. Harder

The Salton Seismic Imaging Project (SSIP) is a collaborative effort between academia and the U.S. Geological Survey to provide detailed, subsurface 3-D images of the Salton Trough of southern California and northern Mexico. From both active- and passive-source seismic data that were acquired both onshore and offshore (Salton Sea), the resulting images will provide insights into earthquake hazards, rift processes, and rift-transform interaction at the southern end of the San Andreas Fault system. The southernmost San Andreas Fault (SAF) is considered to be at high-risk of producing a large damaging earthquake, yet the structure of this and other regional faults and that of adjacent sedimentary basins is not currently well understood.

Seismic data were acquired from 2 to 18 March 2011. One hundred and twenty-six borehole explosions (10-1400 kg yield) were detonated along seven profiles in the Salton Trough region, extending from area of Palm Springs, California, to the southwestern tip of Arizona. Airguns (1500 and 3500 cc) were fired along two profiles in the Salton Sea and at points in a 2-D array in the southern Salton Sea. Approximately 2800 seismometers were deployed at over 4200 locations throughout the Salton Trough region, and 48 ocean-bottom seismometers were deployed at 78 locations beneath the Salton Sea. Many of the onshore explosions were energetic enough to be recorded and located by the Southern California Seismograph Network.

The geometry of the SAF has important implications for energy radiation in the next major rupture. Prior potential field, seismicity, and InSAR data indicate that the SAF may dip moderately to the northeast from the Salton Sea to Cajon Pass in the Transverse Ranges. Much of SSIP was designed to test models of this geometry.

EARTHQUAKE SCALING RELATIONSHIPS ESTIMATED FROM A 16 YEAR CATALOG OF PUBLISHED INSAR STUDIES (B-116)

G.J. Funning, J. Weston , J.R. Elliott, A.M.G. Ferreira, and K. Richards-Dinger

The question of how moment release in earthquakes scales to other earthquake source parameters, such as fault length and average slip, is a long-standing controversy in earthquake science. The question has wide practical implications (e.g. in estimating seismic hazard due to known unruptured fault segments) and also theoretical implications (e.g. in the debate about self-similarity of earthquakes across all magnitudes). Here we use a catalog of earthquake source parameters derived from published InSAR earthquake studies to address this question. InSAR data may be considered preferable for this purpose over traditional sources such as aftershock data and seismic inversion models, as several key source parameters – in particular, the fault length – can in many cases be measured directly from the data.

We have compiled fault length, width, average slip and seismic moment estimates from over 70 published studies of 57 individual earthquakes. Using linear regressions, we find the best best-fitting trends and their uncertainties between these quantities, treating all events together and also separately by mechanism type (strike-slip, thrust and normal). Our preliminary results suggest: 1) The best-fitting single scaling relationship between moment and length has a slope of 1.76 in log-log space. This is more consistent with the 'L model' scaling which predicts a slope of 2, than 'W model' scaling, which requires linear scaling (Scholz, 1982). This relationship does not vary significantly with earthquake mechanism. 2) The data do not require a change of scaling regime around M7.2 as suggested previously (e.g. Romanowicz, 1992). 3) Ratios of average slip to length fall broadly into two fields – high slip-to-length events (1–3 x 10**-4) and low slip-to-length events (0.4–4 x 10**-5). The low slip-to-length category includes subduction earthquakes and events occurring on strike-slip faults with fast slip rates (> 2 mm/yr); the high slip-to-length category includes several blind faulting earthquakes, typically occurring on faults with low slip rates (<2 mm/yr). We will discuss these results in the light of recent results from earthquake simulator models that provide a means of testing the frictional and/or constitutive relationships that may control the scaling behavior of faults.

ENGINEERING VALIDATION OF GROUND MOTION SIMULATION: PART 1. ELASTIC AND INELASTIC SPECTRA. (B-090)

C. Galasso, F. Zareian, I. Iervolino, and R.W. Graves

Design of new structures or assessment of existing ones may be complicated by the inherent rareness or total absence of suitable real (i.e. recorded) accelerograms for the earthquake scenarios that dominate the seismic hazard at a given site. Thereby, synthetic records generated by seismologists are an attractive alternative with respect to real accelerograms as input to nonlinear dynamic analyses of both existing and new structures. However, to date, there are some concerns among engineers regarding the fact that simulated records are equivalent to real records (considered as a benchmark by many and herein) with respect to estimation of the seismic demand.

The study presented in this poster (which is the first of a set of two) addresses the issue of engineering validation of ground motion simulation in terms of elastic and post-elastic structural response. A number of single degree of freedom (SDOF) systems were selected considering: (1) twenty oscillation periods between 0.1s and 10s; (2) four non-linearity levels, from mildly inelastic to severely inelastic structures; (3) two hysteretic behaviors, namely non-degrading and non-evolutionary and both degrading and evolutionary. For each horizontal component of ground motion, demand spectra in term of peak and cyclic response were derived for four historical earthquakes; i.e., 1979 M 6.5 Imperial Valley earthquake, 1989 M 6.8 Loma Prieta earthquake, 1992 M 7.2 Landers earthquake and 1994 M 6.7 Northridge earthquake. For each earthquake, a hybrid broadband ground motions simulation methodology was used, which combines a deterministic and rigorous approach at low frequencies with a semi-stochastic approach at high frequencies (> 1Hz).

Results of this study show that, for certain structural systems, simulated accelerograms may produce median inelastic demand (at a collection of stations for each earthquake) different from a similar estimate using corresponding recorded motions. This difference is especially observed in the case of degrading and evolutionary systems at high non-linearity levels, and if cyclic response is of concern. Moreover, simulated records tend to produce nonlinear demands that are generally less heterogeneous compared to those caused by real records. The amount of this variability reduction depends on the structural period, the non-linearity level and the hysteretic model used. Further investigation is needed to prove the statistical significance of these results and identify their source.

ENGINEERING VALIDATION OF GROUND MOTION SIMULATION: PART 2. MAXIMUM INTERSTORY DRIFT RATIO AND CRITICAL STORY SPECTRA (B-091)

C. Galasso, F. Zareian, I. Iervolino, and R.W. Graves

The study presented in this poster complement the first one addressing the issue of ground motion simulation engineering validation in terms of elastic seismic response of multiple degrees of freedom (MDOF) systems. MDOF buildings considered in this study are modeled as equivalent continuum structures consisting of a combination of a flexural cantilever beam coupled with a shear cantilever beam (both with uniform mass distribution). Such models are useful tools for approximate analysis of structures, especially those tall, ranging from moment-resisting frames to shear walls systems and for which the higher-mode contributions may become important.

In order to study dynamic response of a wide range of buildings, a number of simplified continuum systems were selected considering: (1) twenty oscillation periods between 0.1s and 10s; (2) three shear to flexural deformation ratios to represent respectively shear walls structures, dual systems, and moment-resisting frames; (3) two stiffness distribution along the height of the systems; i.e., uniform and linear. Demand spectra in term of maximum interstory drift (IDR) and critical story (i.e., the height of maximum interstory drift) were derived for the same four historical earthquakes of the first poster; i.e., 1979 M 6.5 Imperial Valley earthquake, 1989 M 6.8 Loma Prieta earthquake, 1992 M 7.2 Landers earthquake and 1994 M 6.7 Northridge earthquake. In addition, for same selected case study structures, the IDR distribution over the height and the modal contributions are obtained and compared for both recorded and simulated time histories.

Some differences between median estimate of IDR demand obtained by using real records and that obtained by simulations were observed, over a certain frequency range throughout the regions surrounding the event epicenter. These differences vary with the considered event and the structural period while they are fairly independent of the type of structure. Moreover, the record-to-record variability of seismic demand produced by simulated and recorded motions may be different. Further analysis is underway to explain the effect of various ground motion simulation parameters on the discrepancy found and to prove the statistical significance of these results.

COMPLEXITY OF THE M6.3 2009 L'AQUILA (CENTRAL ITALY) EARTHQUAKE: SLIP INVERSION AND BROAD-BAND MODELING OF STRONG-GROUND MOTIONS (B-003)

F. Gallovic, J. Zahradnik, G. Ameri, and F. Pacor

Strong ground motion recordings of the M6.3 2009 L'Aquila (central Italy) earthquake are analyzed by a newly proposed inversion technique. The source model consists of Multiple Finite-Extent (MuFEx) subsources. Each subsource is characterized by an individual set of trial nucleation positions, rupture velocities and nucleation times. In addition to the best-fitting model, grid-searching all combinations of the subsource parameters allows also the uncertainty analysis. The MuFEx model requires a preliminary setup based on a technique free of strong constraints (constant rupture velocity over the whole fault, etc.). Here we used two published approaches of such a type, the truncated singular value decomposition and the iterative multiple-point source deconvolution. Final adjustment of the MuFEX model can be performed by repeating the analysis while varying the dimensions and locations of the subsources. Both the best-fitting model and the uncertainty analysis of the low-frequency L'Aquila records suggest that the event consisted of two major episodes, one with the rupture propagating immediately after the nucleation in the up-dip direction, while the other being delayed by 3-4s and characterized by the dominant propagation towards SE along the deeper part of the fault. We point out that the data cannot distinguish between a temporal rupture arrest and a partial slow-down of the rupture, the latter suggested in other published 'smooth' models. We also present broad-band (0.1 - 10 Hz) modeling of strong ground motions constraining the source model by MuFEx inversion. The modeling allows linking distinct features of the observed wavefield to particular source and propagation effects and provides insights on strong-motion complexity from this moderate magnitude event. We utilize a hybrid integral-composite approach based on a k-square kinematic rupture model, combining low-frequency coherent and high-frequency incoherent source radiation and

providing omega-squared source spectral decay. Synthetic Green's functions are calculated in a 1D-layered crustal model including 1D soil profiles to account for site-specific response (where available). The results show that although the local site effects improve the modeling results, the observed spatial broad-band ground-motion variability is to large extent controlled by the rupture kinematics revealed by the low-frequency inversion.

DYNAMIC RUPTURE SIMULATION WITH AN UNSTRUCTURED 3D SPECTRAL ELEMENT METHOD (A-114)

P. Galvez, J.-P. Ampuero, L.A. Dalguer, and T. Nissen-Meyer

Natural faults are not planar, but can have curvature, roughness, branches, kinks and steps. Fault geometry is one of the important factors that affect earthquake rupture. To model dynamic rupture in realistic fault geometries, while including heterogeneous crustal structures and non-linear rheologies, we have implemented the capability of simulating dynamic earthquake rupture in an unstructured 3D spectral element (SEM) solver. Our implementation follows the principles introduced by Ampuero (2002) and Kaneko et al. (2008) and involves encapsulated modules plugged on the 3D open source code SPECFEM3D-SESAME. Our current implementation provides the possibility of modeling dynamic rupture for multiple, non-planar faults governed by slip-weakening friction. The modularity of the code allows the implementation of different friction laws and non-linear constitutive laws off the fault (damage or plasticity) or other physical processes related to dynamic rupture. High flexibility to represent the geometrical complexity of real fault systems with unstructured meshes of hexahedral elements is provided by CUBIT, a general-purpose state-of-the-art mesh generation software. Meshing with progressive coarsening away from the fault pushes away the absorbing boundaries to allow an accurate resolution of the static field. We successfully verified the code in several SCEC benchmark problems, including a 3D problem with branched faults. We also ran simulations of rupture on a subduction megathrust with a splay fault, finding results comparable to published results. The code also allows the simulation of kinematic finite sources which can be incorporated in source inversion procedures. We will report on our efforts to model the complex dynamic rupture of the 2001 M9 Tohoku, Japan, earthquake.

A PERMANENTLY DEPLOYED CROSS-HOLE EXPERIMENT FOR MONITORING DEGRADATION AND RECOVERY OF SHEAR MODULUS AT THE NEES@UCSB GARNER VALLEY FIELD SITE (B-022)

R. Gee, J. Steidl, and P. Hegarty

Cross-hole tests are often used in site characterization studies to provide in situ estimates of shear-wave velocity at a particular depth by measuring the travel time from an active source deployed at depth in one well casing, to geophones located at the same depth in other well casings. Knowing the travel time and the distance between receiver casings, an estimate of the velocity can be made. The NEES@UCSB Garner Valley facility was recently enhanced to include a permanent cross-hole array that includes two geophones and a solenoid-activated dual-direction hammer source at 5 meters depth. A second set of geophones at 2 meters depth is deployed directly above the 5-meter geophones in the same casings. The system is set to trigger once per day automatically with both upward and downward hammer strikes, thus providing the capability to measure shear-wave velocity on a daily basis. In addition, the system is set to automatically activate the hammer source at shorter time intervals immediately following a large earthquake. This cross-hole experiment is unique in that these velocity measurements will be able to capture the decrease and recovery of shear wave velocity after a large event, and thus the degradation of shear modulus and its recovery with time at the same level in the soil. In combination with the permanent vertical array of accelerometers already deployed at Garner Valley, this new cross-hole experiment should provide a level of detail never before achieved in the observation of dynamic soil behavior during and following large earthquakes. In the mean time, as we wait for the earth to provide larger motions, the once daily hammer strikes are recorded and analyzed for potential temporal changes in velocity with seasons. The shear-wave velocity is determined by cross-correlation of the signals between the geophones of equal depth, separated by 4.82 meters. Initial analysis performing this cross correlation on the 5-meter sensors yields a shear wave velocity ~220 m/s. We present the results of approximately one year's worth of daily hammer strikes to determine if there is seasonal variation of shear-wave velocity at the site related to variations in soil saturation and water table depth.

UPDATING THE NEW ZEALAND NSHM FROM THE CANTERBURY EARTHQUAKE SEQUENCE (B-093)

M. Gerstenberger, G. McVerry, D. Rhoades, M. Stirling, K. Berryman, and T. Webb

The Canterbury, New Zealand, earthquake sequence began in September 2010 with the Mw 7.1 Darfield earthquake which caused significant structural damage. It has continued with a damaging sequence of aftershocks including the Mw 6.3

earthquake in February, which caused the loss of more than 180 lives, and the June Mw 6.0 earthquake; both of these major aftershocks occurred directly under the city of Christchurch. The sequence of events is occurring in what is a moderate hazard area in the New Zealand National Seismic Hazard Model (NSHM). With significant rebuilding effort required due to the damage from the sequence, a reinvestigation of the NSHM was requested in terms of the NZ building code, and in terms of probabilities of future liquefaction. Initially a very tight time frame (on the order of weeks) was given for the update to the model. On this short schedule, modifications were made to both the ground motion prediction equation and to the source models.

All larger earthquakes in the sequence to date have had large apparent stresses based on energy magnitudes; we have scaled the predicted ground-motions to account for this. Additionally we have developed a composite source model of differing clustering scales that consists of four sub-models: 1) the NSHM fault model including conditional probabilities of rupture on key faults; 2) a short-term clustering model to account for immediate aftershock clustering; 3) a medium-to-long-term clustering model to account for more distant and clustering on a longer time scale; and 4) a smoothed seismicity model based on a non-declustered catalog to allow for the expectation of increased seismicity in the coming decades. This preliminary work has resulted in an increase in the official building code requirements by about 1/3. The work is currently being re-evaluated with additional alternatives and uncertainties being considered. Due to the nature of the sequence, and the fact that the hazard is dominated by events with M<6.5, some particular aspects being investigated are: minimum-magnitude included in the hazard calculations; maximum source distance; stress-drop scaling; existing structural performance in earthquakes of this magnitude; and alternative source models. An expert panel is now being coordinated, with a final model using an expert elicitation panel based on the method of Cooke expected in October.

EARTHQUAKE CLUSTERING AND AFTERSHOCK STATISTICS IN SIMULATED CATALOGS (B-030)

J.J. Gilchrist, J.H. Dieterich, and K.B. Richards-Dinger

We employ the 3D boundary element code RSQSim with a California fault model to investigate clustering of large earthquakes. The simulations incorporate rate-state fault constitutive properties, and the synthetic catalogs include foreshocks, aftershocks and large event clusters. Simulated foreshocks and aftershocks have reasonable Omori values (-0.93 to -0.96) and the inter-event-time and space-time statistics of smaller earthquakes in the RSQSim catalogs are in good agreement with California catalogs. Therefore, we believe that the RSQSim catalogs provide an appropriate basis for investigation of large-event clustering. The majority of clusters are event pairs consisting of only two events with occasional three and four event clusters. Here we define a large event cluster as two or more M≥7 events within four years of each other. Most clustered events are closely grouped in space as well as time. Among potential indicators of large event clusters are highly productive aftershock sequences where the aftershock locations of the first events in a cluster appear to correlate with the location of the next large event in the cluster. We quantify the aftershock productivity, including the timescale of decay and magnitude-frequency dependence of all large events, in order to compare characteristics of clustered to non-clustered events. We find that the aftershock productivity of the first event of the large event clusters is roughly double that of the non-clustered events and that aftershock rate is a proxy for the stress state of the faults. We also find that deviation of the inter-event waiting times from the Poisson fit indicates fluctuating event rates and that more geometrically complex faults and fault systems show more clustering behavior.

VERTICAL DEFORMATION IN THE MEXICALI VALLEY, BEFORE, DURING, AND AFTER THE M=7.2, EL MAYOR – CUCAPAH EARTHQUAKE, FROM INSAR, LEVELING AND GEOTECHNICAL INSTRUMENTS (A-047)

E. Glowacka, O. Sarychikhina, B.B. Robles, F. Suarez, J. Ramírez, F.A. Nava, J. González, A. González, F. Farfán, and B.G. Díaz de Cossío B

Over many years strong subsidence in the Mexicali Valley has been observed from leveling, InSAR, and geotechnical instruments data. The area of subsidence is controlled by tectonic faults which limit the Cerro Prieto pull apart basin, while the amplitude of subsidence seems to be controlled by the extraction volume of geothermal fluids in the Cerro Prieto Geothermal Field.

Since 1996, CICESE has been operating a network of geotechnical instruments for continuous recording of deformation related to tectonic (seismic and interseismic) phenomena, as well as anthropogenic deformation caused by the deep fluid extraction at the geothermal field. The instruments are installed along the faults which limit the Cerro Prieto pull-apart basin, at distances from 8 to 15 km from the M=7.2 epicenter. Information gathered from instruments, InSAR and leveling is important for

understanding the physics of the subsidence process, the role of faults, the geohydrology of the local aquifers, and the mechanism of creep on the faults, as well as for decision-making for future investments in the Mexicali Valley.

Before the earthquake, faults were slipping vertically few centimeters per year, a rate of about half the subsidence rate observed in the nearest subsidence bowl. Coseismic slip observed from the instruments and from manual measurements was of the order of centimeters, suggesting a strong consolidation effect triggered by seismic waves. One year after the earthquake, vertical slip observed on the Saltillo fault has been slower, while vertical slip on the Cerro Prieto fault ceased.

A precision leveling survey in the Mexicali Valley had been done 2 months before the earthquake and was repeated two months after the earthquake. As expected for this earthquake, an uplift of about 30 cm towards the NE was observed along a 38 km line in the SW-NE direction. Three subsidence bowls differ from this general pattern. While two bowls lay within the limits of subsidence area observed before the earthquake, the deepest one, with 36 cm relative depth, is situated to the southwest outside of the subsidence zone. All the subsidence bowls are probably associated with liquefaction observed in the area, with more liquefaction observed close to the epicenter.

We checked the subsidence pattern after the earthquake using InSAR images. The small number of available images does not allow drawing definite conclusions, but suggests that the subsidence process continues at the previous rate.

IDENTIFYING FAULT HETEROGENEITY THROUGH MAPPING SPATIAL ANOMALIES IN ACOUSTIC EMISSION STATISTICS (B-029)

T.H. Goebel, T. Becker, D. Schorlemmer, S. Stanchits, C. Sammis, E. Rybacki, G. Dresen

Frictional properties of fault surfaces fundamentally influence the local strength of the seismogenic crust. We investigate the relationship between fault asperities and the creation of micro-cracks and damage by analyzing acoustic emission (AE) events emitted during sliding of fractured Westerly granite surfaces in the laboratory. We developed a three stage procedure, for which rock samples are initially fractured under triaxial loading, followed by fault locking due to pressure increase and a final stage of fault reactivation. We observed three different types of behavior: (1) frictional sliding with decreasing differential stress (creeping fault) (2) linear and non linear stress increase, slow as well as abrupt stress drops (3) approximately linear stress increase followed by abrupt stress drop events between 10 to 300 MPa (stick slips with saw tooth pattern). We performed a detailed spatial analysis of event clusters before and after stick slips, primarily focusing on their b-values, seismic moment release and AE event densities. AE hypocenter distributions showed a high degree of spatial clustering close to low b-value regions. Slip events and the connected acoustic emission "aftershocks" nucleated within or at the periphery of areas of low b. To identify larger scale geometric asperities we combined fault structural information from post-experimental CT-scans with AE statistics. Asperities were connected seismically to low b-value regions, high moment release and increased AE event density and structurally to anomalous thin fault parts and point contacts of the host rock walls.

The rough fracture surfaces during laboratory experiments, strongly favor the creation of spatial and temporal distinct AE clusters which have similar characteristics to seismicity observed on crustal scales. Specific crustal seismicity anomalies may be an expression of fault heterogeneity and mark areas of increased seismic hazard.

CONNECTING THE SPATIAL DISTRIBUTION OF ACOUSTIC EMISSIONS TO FAULT ROUGHNESS DURING STICK-SLIP EXPERIMENTS (B-036)

T.H. Goebel, C. Sammis, and T. Becker

Most continental earthquakes occur on or close to narrow fault zones within the seismogenic crust. Variations in size and spatial distribution of seismic events are likely influenced by differences in roughness and degree of heterogeneity of faults. The understanding of controlling factors of seismicity distributions around natural faults is limited due to largely unknown crustal stress, fault zone structure and roughness. Unlike field studies, high pressure laboratory stick-slip experiments enable the investigation of earthquake analog systems under controlled conditions. We connected spatial distributions of acoustic emissions (AEs) to post-experimental fault structure and slip surface roughness of previously faulted and saw-cut Westerly granite samples.

To create stick-slip events we locked the specimen by increasing the confining pressure and resumed axial loading. Our experimental set-up enables the creation of a series of stick-slip events on a single fault plane. AEs were recorded and located with high speed and accuracy using 14 piezo-ceramic sensors attached directly to the rock sample. We analyzed the degree of localization of AEs with increasing stress level leading up to slip events. AE hypocenter distributions were quantified by computing the fractal dimension of spatial AE distributions and the activity fall-off with fault normal distance. Fault structure

and slip surface roughness were determined from post-experimental computer tomography scans and sets of roughness profiles parallel and perpendicular to the direction of slip. We observed a high degree of localization at high differential stresses before slip events. Increasing power-law exponents of fault normal activity fall-offs indicated fault smoothening with successive slip events. Naturally faulted and saw-cut surfaces exhibited distinct characteristics of AE distributions. Saw cut surfaces with higher roughness exhibited slower activity fall-offs with fault normal distance.

Thus both the initial roughness of the fault plane and the changes in roughness during one experiment due to, e.g., new surface creation seemed to be detectable through variations in spatial AE statistics.

Understanding the connection between micro-seismicity and fault roughness may have important implications on the seismic hazard connected to specific fault zones or fault segments. The nucleation points of large earthquake ruptures may be connected to rough fault patches or asperities.

ASSESSMENT OF COSEISMIC SLIP VARIATION FROM TERRESTRIAL LIDAR SCANS OF THE EL MAYOR-CUCAPAH SURFACE RUPTURE (A-105)

P.O. Gold, A.J. Elliott, M.E. Oskin, M.H. Taylor, A. Hinojosa, R. Styron, O. Kreylos, T. Bernardin, E. Cowgill, and A.J. Herrs

We assess the slip distribution at four sites along the El Mayor-Cucapah (EMC) earthquake surface rupture with cm-resolution terrestrial lidar (TLS). Slip distributions based on field measurements typically show abrupt variation (0.5-2 m) over short along-strike distances (10 to 100 m), implying large along-fault strains (>10-2). While some of this variation may be real, the degree to which it can be attributed to measurement uncertainty is not well known because accurately assessing uncertainties in the field is difficult. We quantify this uncertainty by evaluating the repeatability of virtual field measurements using TLS datasets in an immersive 3D-cave environment. The TLS scans, collected 12 to 18 days following the EMC earthquake, capture fault displacements in a range of geologic and geomorphic settings. We build slip distributions by measuring individual displaced landforms and by summing vertical offsets along strike-perpendicular profiles. For comparison, we also measure orientations of free-face striations where observable in the scans. We construct composite slip distributions using 15 sets of repeat measurements from each suite of offsets at each site. The variability in individual offset measurements defines uncertainties of 2% to 25% of the total offset distance. In all cases, net along-strike gradients in the displacement curve cannot be solely explained by uncertainties in offset measurements. However, these uncertainty measurements are significant enough to confirm that true fault slip is less abruptly variable than commonly portrayed by slip distribution curves. We also find that the displacement curve may not be accurately represented by the envelope of displacement maxima, as is the common practice. In addition, repeat TLS scans collected ~1 year after the EMC earthquake expand on the initial scans and will enable future expansion of the slip distribution curves, as well as quantification of post-event surface change by comparing datasets.

EL MAYOR CUCAPAH EARTHQUAKE: POSTSEISMIC DEFORMATION FROM INSAR AND GPS OBSERVATIONS (A-046)

A. Gonzalez Ortega, D. Sandwell, Y. Fialko, J. Gonzalez Garcia, J. Fletcher , A. Nava Pichardo, M. Floyd, and B. Lipovsky

El Mayor Cucapah earthquake ocurred on April 4, 2010, rupturing several previously mapped as well as unidentified faults, including the Pescadores, Borrego and Paso Superior faults in Cucapah Mountains, and Indiviso fault in the Mexicali valley. We conducted several campaign GPS surveys of pre-existing and newly established benchmarks within 30 km of the earthquake rupture. Most of the benchmarks were occupied within days after the earthquake, allowing us to capture the entire postseismic transient.

GPS timeseries indicate a gradual decay in postseismic velocities having the same sense as the coseismic displacements. We also analyzed available Synthetic Aperture Radar (SAR) data from ENVISAT and ALOS satellites. The main deformation features seen in the line of sight displacement maps indicate subsidence in the southern and northern part of the Indiviso and Paso Superior faults, respectively. We investigate to which extent GPS and InSAR observations can be explained by commonly assumed mechanisms of postsesimic deformation. In particular, we present a best-fitting afterslip model for the time period of 6 months after the earthquake.

NON-LINEAR BUILDING RESPONSE SIMULATIONS USING SCEC SIMULATED GROUND MOTIONS (B-085)

C.A. Goulet and C.B. Haselton

Although substantial progress has been made in physics-based ground motion simulations in the recent years, the engineering community is still reluctant to use simulated time series for design. One of the reasons for this is a lack of understanding of how simulated ground motions compare to recorded ground motions, especially when it comes to their impact on structural response. There are on-going efforts of validation and verification of simulated ground motions, but these tend to be focused on record properties or on the response of single-degree-of-freedom systems. We are proposing a different approach: we plan to compare the nonlinear structural response of buildings subjected to recorded and simulated ground motions, given that both sets have similar spectral shapes.

The responses of buildings to recorded motions have already been processed in a project recently completed by the PIs. The recorded set is representative of a magnitude 7 earthquake, rupturing within 20 km from a site with a Vs30 of 400 m/s (average shear wave velocity of the upper 30 meters of the soil column). We selected SCEC simulated records (for the same type of event and site conditions) with spectral shapes that were consistent with the recorded set previously used by the PIs. We then performed the structural simulations and compared the response results from both sets of time series (recorded and simulated). We present the summary of the approach used and the structural response results we have obtained for recorded and simulated ground motion records.

DETECTION OF ANOMALOUS STRAIN TRANSIENTS USING PRINCIPAL COMPONENT ANALYSIS AND COVARIANCE DESCRIPTOR ANALYSIS METHODS (A-064)

R.A. Granat, J.W. Parker, S. Kedar, and Y. Bock

We have tested two classes of anomalous transient detectors that are completely independent of each other in origin, logic and implementation. Principal Component Analysis (PCA) has been successfully implemented in tectonic geodesy for regional filtering and common mode removal. Covariance Descriptor based detection methods are relatively recent technologies that have seen considerable success in the field of computer vision, and are predominantly used to detect statistically significant, spatially correlated anomalies in images. The two techniques examine the data in a fundamentally different and complementary way. The one (PCA) detecting common fundamental modes of ground motion across the array, and the other (CDA) detecting statistically significant common anomalies in a space-time "image" composed of deformation time series.

The advantage of the PCA technique lies in its ability to resolve temporal transients that although common to a particular region, are not necessarily of the same amplitude across it. In addition, examination of higher residual modes highlights whether or not the transient has propagated across the network in time.

Covariance descriptor methods are typically used in image analysis applications, where a set of filters is applied to an image, and the outputs of these filters form a feature vector for each pixel. The covariance matrices of the feature vectors for different image regions are calculated (these are termed the covariance descriptors for the regions), and then compared using a distance metric. The generalized covariance distance between regions that resemble one another (in the chosen feature space) will be small, while that between regions that are dissimilar will be relatively large. In this manner anomalies or matches between regions can be identified. This method can be readily extended to tectonic time series analysis, where the "image" regions are simply time windows, while the feature vectors are the tectonic displacement time series measurements themselves. The covariance descriptor of the time series as a whole is calculated and compared with covariance descriptors of localized time windows. Descriptors for localized windows that are far from the descriptor for the entire time series are likely anomalous.

We present results from synthetic cases, where these methods were tested using an iterative approach, in which the output of one technique was used to fine-tune the input to the other.

TESTING SCEC 3D SEISMIC VELOCITY MODELS IN THE SAN BERNARDINO AND LOS ANGELES BASIN REGIONS (B-018)

R.W. Graves, A. Plesch, and J. Shaw

The 2001 Mw 4.6 Big Bear Lake earthquake was recorded at over 180 broadband sites of the Southern California Seismic Network throughout the greater Los Angeles region of southern California. At periods longer than about 1 sec, the ground motions in the San Bernardino, San Gabriel and Los Angeles basins have significantly larger amplitudes and extended durations relative to sites outside the basins. To model the longer period (T > 1 sec) near-source motions, Graves (2008) developed a 3D representation of the basin structure in the San Bernardino region based on the potential field modeling of Anderson et al. (2000). This study extends the previous analysis by modeling the motions across the San Gabriel, Chino and Los Angeles basins using two Southern California Earthquake Center three-dimensional seismic velocity models (CVM-S4 and

CVM-H64). CVM-H64 (released as CVM-H 11.9 at the meeting) is a recent revision of the CVM-Harvard model, which includes a newly developed representation of the San Bernardino basin using the basement surface from Anderson et al. (2000) adjusted to match interpretations of seismic reflection data (Stephenson et al., 2002) which also constrain the sediment velocities. The simulations use a minimum shear velocity of 400 m/sec and a grid spacing of 80 m to yield a bandwidth resolution limit of T > 1 sec. Both models perform reasonably well at reproducing the observed waveforms, amplitudes, and durations, especially in the San Bernardino and Los Angeles basins at periods of 3 sec and longer. At shorter periods (1–2 sec), the fit to the recorded motions is less well resolved for both models. This reinforces the conclusions of Graves (2008) that deterministic modeling at periods approaching 1 sec in regions of complex geology involves more than simply reducing the minimum velocity threshold, but also requires knowledge of the subsurface structure and distribution of seismic velocities at relatively short length scales.

LIDAR-DERIVED MEASUREMENTS OF SLIP IN THE MOST RECENT GROUND-RUPTURING EARTHQUAKES ALONG ELEMENTS OF THE SOUTHERN SAN ANDREAS FAULT SYSTEM (B-114)

D.E. Haddad, C. Madden, J.R. Arrowsmith, J.B. Salisbury, and R.J. Weldon

Tectonically displaced geomorphic markers record the surface manifestation of earthquake-induced ground ruptures. Of particular interest to earthquake forecast models is the slip produced during the most recent ground-rupturing earthquake. High-resolution digital topography from light detection and ranging (LiDAR) is a powerful tool for measuring the most recent meter-scale slip along fault zones. We present surface slip measurements of recent ground-rupturing earthquakes along the Garlock, Owens Valley, Elsinore, and Blackwater-Calico fault zones. Fault scarp traces were mapped using LiDAR-derived digital elevation models (DEMs), local topographic gradient and relief maps, and aerial photography. An individual slip measurement was made for each offset feature (or landform element such as thalweg, channel margin, etc.) by iteratively reconstructing the topography on either side of the fault and finding the best-matching vertically backslipped offset values. A goodness-of-fit approach was then used to calculate the best laterally backslipped displacements using a combination of vertical backslips, horizontal backslips, and topographic scaling. Along-strike, reach-averaged surface displacement distributions of the most recent earthquakes were then generated from the LiDAR-derived offsets and compared to published field-derived offset measurements. For the eastern section of the Garlock fault, our LiDAR-derived offsets compared well with published field measurements and attained an R^2 value of 0.9. Reach-averaged slip in the last event of 4.2 m ±0.7 m for Searles Valley (2.7 km reach; n = 9), 4.6 m +0.7/-0.9 m for Pilot Knob Valley (24.7 km reach; n = 41), and 3.5 m +0.8/-0.9 m for Leach Lake and Avawatz Mountains (12.6 km reach; n = 57). LiDAR-derived offset measurements compare well with field measurements in the comprehensive documentation of along-strike surface slip distributions of the most recent earthquakes. Furthermore, our results demonstrate the utility of LiDAR-derived offset measurements for fault zones that do not have sufficient documentation of slip in the last event. These data provide critical input parameters for seismic hazard analyses and earthquake rupture forecasts that rely on surface slip measurements to physically constrain the occurrences and magnitudes of ground-rupturing earthquakes (e.g., the Uniform California Earthquake Rupture Forecast).

APPLICATION OF ZH RATIO TO THE URBAN LOS ANGELES REGION FOR SHALLOW S-WAVE VELOCITY STRUCTURE (A-034)

T. Hakamata, T.E. Yano, and T. Tanimoto

In order to predict seismic ground motion, the model Vs30 serves an important role to provide very shallow structure. However, in order to predict long-period ground motions (~ 0.1 Hz), the depth range must be extended from 30 m to a much deeper depth. We developed a method that uses Rayleigh-wave ellipticity data, estimated from seismic noise (the ZH method), to derive shallow S-wave structure (< 10 km in depth) in the Los Angeles area, using broadband data (about 150 stations) recorded at local dense SCSN network.

Using two years (2002 and 2003) of continuous data, we tested an approach that analyzes microseisms about 0.1-0.3 Hz which are dominated by Rayleigh waves. In fact, we observe strong systematic geographic variations in the ZH ratios between the LA basin and outside of this basin. Depth sensitivity of the ZH ratios of fundamental Rayleigh wave is confined to approximately 10 km. With the ZH ratios, we thus have a clean data set to derive shallow S-wave structure for the upper 10 km of the Earth.

Application to the urban Los Angeles region indicates that systematic perturbations in S-wave velocity structure are required up to about 50% of the reference velocity model for the region (the SCEC Community Velocity Models). This systematic perturbation implies that patterns of surface ground motion by large earthquakes in the region may dramatically change.

We will present the systematic difference of ZH ratio measurements depending on the different area and S-wave structure due to the inversion using ZH ratio measurements.

THE SCEC-USGS DYNAMIC EARTHQUAKE RUPTURE CODE VERIFICATION EXERCISE (A-115)

R.A. Harris, M. Barall, R. Archuleta, B. Aagaard, J.P. Ampuero, D.J. Andrews, V. Cruz-Atienza, L. Dalguer, S. Day, N. DeDontney, B. Duan, E. Dunham, A.A. Gabriel, P. Galvez, Y. Kaneko, Y. Kase, J. Kozdon, N. Lapusta, S. Ma, P.M. Mai, H. Noda, D. Oglesby, K. Olsen, and S. Somala

We summarize recent progress by the SCEC-USGS Dynamic Rupture Code Verification Group. In February 2011 we held our most recent workshop where we examined how SCEC and USGS researchers spontaneous-rupture computer code results agree (or disagree) when computing benchmark scenarios for dynamic earthquake rupture. Our recent benchmarks were a 2D case of thermal pressurization and 2D and 3D cases of slip-weakening friction on branched vertical strike-slip faults set in an elastic medium.

Since our February 2011 workshop, we have officially archived the results of the TPV12 and TPV13 Extreme Ground motion normal-fault benchmarks that were used in our new paper Harris, R.A., M. Barall, D.J. Andrews, B. Duan, E.M. Dunham, S. Ma, A.-A. Gabriel, Y. Kaneko, Y. Kase, B. Aagaard, D. Oglesby, J.-P. Ampuero, T.C. Hanks, N. Abrahamson, Verifying a Computational Method for Predicting Extreme Ground Motion, Seismological Research Letters, Vol. 82, No. 5, September/October 2011. The online archive allows newcomers (and veterans) to conduct new TPV12 and TPV13 extreme ground motion simulations while at the same time we are preserving the results that are described in our journal publication, for scientific repeatability.

In the fall of 2011, our group will embark on our next benchmark exercises, both of which will assume a slip-weakening framework. One new benchmark will involve heterogeneous initial stresses on a planar vertical strike-slip fault set in an elastic medium, using a stress-conditions methodology that is updated from the 2010 100-runs exercise. A second new benchmark will involve more-homogeneous initial stresses on branching faults that are this time set in a medium that allows for plastic yielding.

For more information please visit our website: scecdata.usc.edu/cvws

PRELIMINARY PALEOSEISMIC RESULTS FROM THE ECHO PLAYA TRENCH SITE ON THE CENTRAL GARLOCK FAULT, CHINA LAKE NAWS, NEAR RIDGECREST, CA (A-133)

R.D. Hartleb, C.D. Kemp, A. Lutz, E.K. Frost, and S.C. Lindvall

Investigation of a new paleoseismic trench site along the central Garlock fault at Echo Playa on the China Lake Naval Air Weapons Station exposed evidence for at least four, and as many as six, surface-rupturing earthquakes. The Echo Playa site is located within a roughly 150-m-wide and 1.5-km-long transtensional step-over that has formed a closed basin fringed by alluvial fan and colluvial deposits that grade basinward into laterally continuous playa sediments. Numerous subdued north- and south-facing fault scarps are recognized between the playa edge and the ridges of the step-over. These faults generally deform bedrock or coarse alluvial fans, although two fault strands have formed low scarps along the playa margin. Two trenches opened at Echo Playa across these playa margin faults exposed roughly 5 m of generally conformable stratigraphy, recording several episodes of fan progradation and lacustrine/palustrine transgression along the playa margin.

Evidence for four surface-rupturing earthquakes is preserved within a roughly 30-m-wide zone of distributed deformation where correlative sets of faults and fissure fills terminate upward at the base of laterally continuous stratigraphic horizons. The distributed nature of deformation here has produced very small individual offsets that indicate different combinations of lateral and normal slip components. Age estimates for strata that bracket each rupture are pending radiocarbon analyses of detrital charcoal and optically stimulated luminescence analyses of fine-grained playa deposits. Initial age estimates based on an assumption of reasonable sedimentation rates and the observed lack of soil development suggest that these four to six surface-rupturing earthquakes occurred during the Holocene.

Echo Playa is the easternmost paleoseismic trench site along the Garlock fault, and data from this site are expected to provide a basis for developing an earthquake chronology for the eastern Garlock fault, which is currently not well characterized. These data also will provide an important opportunity to refine estimates of earthquake chronology, fault rupture length, and recurrence intervals along the central and western Garlock fault, contributing to an improved understanding of seismic hazard in southern California.

USING GROUND-BASED LIDAR AND MORPHOMETRIC ANALYSIS TO STUDY THE EVOLUTION OF PRECARIOUSLY BALANCED ROCKS (B-010)

J.E. Harvey and D.H. Rood

Precariously balanced rocks (PBRs) are fragile geologic features that can be destroyed by ground motion during earthquakes. Measuring the fragility of PBRs yields an estimate of unexceeded ground motion, which, when combined with an estimate of the duration of PBR exposure, allows us to test the USGS National Seismic Hazard Maps (NSHM). However, the age of such fragile features is poorly known because we lack a detailed understanding of the geomorphic processes acting to exhume corestone PBRs.

Here we use ground-based LiDAR to study the geomorphic evolution of PBRs in the Mojave desert, and use this information to constrain unexceeded ground motion near the San Andreas Fault. Lovejoy Buttes is an inselberg rising above a broad pediment east of Palmdale, CA. At this site, PBRs are granitic corestones that form as a result of weathering along joint surfaces at depth before being subsequently exhumed by fluvial and hillslope processes incision. We use terrestrial laser scanning to generate a high resolution (~1-2 m) DEM of the studied catchment, allowing us to explore the relation of erosional processes to the location of studied PBRs. PBRs are sampled for cosmogenic Be-10 along a vertical profile. These exposure ages are corrected for shielding by the rock itself, and fed into a forward model to yield the most likely exhumation history for each PBR (Balco et al., 2011, Quaternary Geochronology).

Preliminary results of this ongoing work suggest that PBRs in the studied catchment at Lovejoy Buttes were exhumed after the last glacial maxmimum (~20 ka). PBR age is likely a combination of proximity to an incising drainage and position relative to major knickpoints along channels. Future work will include expanding the study to another site in the Mojave characterized by lower landscape relief and greater distance to major faults. This study is improving our understanding of the geomorphic evolution of PBRs and helping to place realistic constraints on the numerical models used in the interpretation of PBR ages from Be-10 data.

WAVEFORM RELOCATED EARTHQUAKE CATALOG FOR SOUTHERN CALIFORNIA (1981 TO 2011) (B-062)

E. Hauksson, W. Yang, and P. Shearer

The Pacific North-America plate tectonic deformation is the main process that causes small and large earthquakes in southern California. Secondary processes such as geothermal exploitation, extensional gravitation collapse, or crustal delamination also cause ongoing seismicity. The overall pattern of waveform relocated seismicity shows the familiar prominent features such as mainshock-aftershock sequences of the 1992 Landers, 1999 Hector Mine, 1994 Northridge, and 2010 El Mayor-Cucapah superimposed on a high level of background seismicity near the late Quaternary faults. In particular, the background seismicity along the San Andreas fault, capable of generating the largest earthquakes, is diffuse and the background rate is low.

In addition, to the aftershock zones, other regions that are driven by secondary processes such as the southern Sierra, Banning Pass, Coso regions, and the Salton Trough exhibit high levels of seismicity. As an example, the Banning Pass region is characterized by numerous west to northwest trending alignments of seismicity, which are both mainshock and swarm like sequences, suggesting the presence of multiple tectonic processes.

For the first time, we are able to resolve new detailed seismicity patterns at the north end of the 2010 El Mayor-Cucapah aftershock zone, where the majority of the aftershocks occurred. The occurrence of aftershocks is not simply related to the principal slip surfaces of faults that accommodate the bulk of the slip. As two other examples also show, the 1992 Landers and 1999 Hector Mine earthquake sequences, aftershock distributions exhibit heterogeneous spatial distribution, which may be related to heterogeneous stress release in the region. Geometrical complexities such as step-overs or push-ups, as mainshock slip transfers from one fault segment to the next, also contribute to complexity of aftershock productions.

Adjacent to the US Mexico boarder, the background seismicity patterns exhibit interaction of northeast and northwest trending fault segments. Particularly in the Salton Trough region, the relocated seismicity exhibits spatial distributions that are much tighter than what is observed with the routine catalog. These refined distributions often align with late Quaternary faults or other tectonic features. In some cases they suggest the presence of previously unmapped faults.

HOW DO "GHOST TRANSIENTS" FROM PAST EARTHQUAKES AFFECT GPS SLIP RATE ESTIMATES ON SOUTHERN CALIFORNIA FAULTS? (B-151)

E.H. Hearn, F.F. Pollitz, W.R. Thatcher, and T. Onishi

Elastic block models are generally used to infer slip rates on fault segments in tectonically complex areas, such as southern California (e.g. McCaffrey, 2005: Meade et al., 2005). These models implicitly assume steady-state deformation. However, owing to viscoelastic effects of past large earthquakes, deformation rates and patterns around major faults are expected to vary with time. Where viscoelasticity has been incorporated into block models, differences in inferred slip rates have resulted (Johnson et al.,2007). Here, we investigate the extent to which viscoelastic velocity perturbations (or "ghost transients") from individual earthquakes affect elastic block model-based inferences of fault slip rates from the southern California GPS velocity field. First, we calculate average velocities and time-dependent perturbations relative to this average at all GPS sites due to repeated large earthquakes on a particular fault segment. (We deal with perturbations because to recover the velocities, we would have to compute and sum cycle-average velocities and perturbations for all fault segments in the region.) Next, we invert two GPS velocity fields for slip rates using an elastic block modeling approach: one field that has been corrected for the perturbation, and one which has not, and we compare the resulting slip rates. For now, the viscoelastic models are simple (layered, with linear rheologies), and locking depth in the block models is fixed. We find that if asthenosphere viscosities are low enough (3 x 10**18 Pa-s) the current GPS velocity field is significantly perturbed by the 1857 M 7.9 San Andreas Fault (SAF) earthquake sequence; that is, current strain rates around the SAF are lower than their average values. Correcting the GPS velocity field for this perturbation adds up to about 5 mm/yr to the SAF slip rate along the Mojave and San Bernardino segments, consistent with the results of Johnson et al. (2007). The GPS velocity perturbation due to the most recent, large Garlock Fault earthquake (assumed to be an M 7.5 event in 1640) is smaller. In this case, inversions of the corrected and uncorrected GPS velocity fields yield near-identical slip rates for all of the faults in our block model. This suggests that the discrepancy between geodetic and geologic slip rates for the Garlock Fault is not due to a ghost transient.

PARALLELIZATION OF THE VIRTUAL CALIFORNIA EARTHQUAKE SIMULATOR (B-087)

E.M. Heien, M.B. Yikilmaz, M.K. Sachs, J.B. Rundle, L.H. Kellogg, and D.L. Turcotte

Virtual California is an earthquake simulation program designed to help analyze the behavior of fault systems over long time periods. These simulations can be computationally intensive due to the stress calculations that occur during long term fault movement and the multiple rupture propagation calculations that occur during each earthquake. In order to handle fault models with high resolution, we parallelized Virtual California using MPI and OpenMP. Here we demonstrate the effectiveness of these techniques in providing up to a 15.9x speedup for the core calculation on 16 processors. We also show where further work can ameliorate the effects of communication which reduces total simulation speedup on 16 processors to a factor of 5.8x.

IMPLEMENTATION OF A SEISMIC SEQUENCE VISUALIZATION SYSTEM USING GEOGRAPHIC INFORMATION SYSTEMS (A-156)

B.J. Hellige, M.A. Wagner, and S. Reed

The VDO Production team addressed the Grand Challenge with the goal of producing eight movies using SCEC Virtual Display of Objects (SCEC-VDO). A separate final VDO product was generated for each of the following earthquake sequences: the Tohoku (Japan), Canterbury (New Zealand), El Mayor-Cucapah (Mexico), Maule (Chile), Haiti, and Indonesian trench sequences. Each movie begins with the relevant earthquake sequence animation (at depth) to give the viewer perspective of the breadth of the sequence. The sequence animates in two views: 1) an overhead map view on the left, and 2) space-time on the right. This feature introduces the viewer to earthquake sequences relative to the dimensions of space and time. The movie then showcases the added Geographic Information Systems (GIS) capabilities by overlaying earthquake sequences and ShakeMaps with GIS layers that highlight population density, nuclear power plants, and hospitals. A seventh VDO with GIS information and rupture simulations displays potential risks associated with earthquake hazards in Southern California, along the San Andreas fault. Additionally, an eighth VDO was created to show seismicity in Southern California and Northern Mexico over the last 20 years. This video uses a space-time plot to show where and when earthquakes occurred in California from 1991-2010. Successfully producing these seven VDOs with space-time plots and GIS was the final goal for the 2011 USEIT Grand Challenge.

SHAKING AND FLOODING BY THE TOHOKU-OKI EARTHQUAKE (A-108)

D. Helmberger, S. Wei, J.P. Avouac, H. Kanamori, and J. Jiang

Large subduction zone earthquakes pose one of the greatest nature hazards to mankind, either by shaking down structures and/or flooding. Rupture properties of these rare events are poorly understood, especially tsunamigenic earthquakes with

little pre-shaking such as the 1896 Sanriku earthquake. The well recorded Tohoku-Oki earthquake sheds some new light on these issues. Here we document the history of the rupture from the inversion of accelerometric waveform data and high-rate GPS data. Our results demonstrate that the flooding was caused by the shallow ruptured (Mw~9) portion close to the trench while the shaking came from ruptures at depth >30km with a relatively small magnitude (Mw~8.5). Several deep pockets of high frequency energy release can be resolved, which correspond to locations predicted from back-projection. The Peak Ground Velocity (PGV) recorded by over 1400 strong motions and ~400 high rate GPS stations is nicely correlated with geological structure (topography). Separation of the wavefield into upgoing and downgoing energy indicates that the shaking on the island is mainly controlled by upgoing energy. Forward calculation indicates that the shallow basin structure could amplify the ground shaking and some of the high frequency arrivals could be explained by using a modified source time function which suggests a pulse like rupture.

SENSITIVITY OF THE SOUTHERN SAN ANDREAS FAULT SYSTEM TO TECTONIC BOUNDARY CONDITIONS (B-141)

J.W. Herbert and M.L. Cooke

The southern Big Bend of the San Andreas fault incorporates numerous non-vertical, non-planar, and intersecting active surfaces. Our three-dimensional Boundary Element Models incorporate complex fault geometries from the Southern California Earthquake Center's Community Fault Model and a range of tectonic boundary conditions from Global Positioning System studies of the region (45-50mm/yr and 320˚-325˚). We also test the sensitivity of fault slip rates to the magnitude and orientation of plate velocity applied to the model. Consequently our models provide a range of fault slip rates associated with present-day uncertainties on plate motion rather than a single slip rate. Model slip rates match most of the available geologic slip rates and discrepancies may owe to inaccurate fault geometries. More northerly plate velocity (325˚) produces greater transpression along the San Andreas Fault system. This is associated with greater uplift of the San Bernardino Mountains, greater reverse-slip along range bounding reverse thrust faults, lower strike-slip rates along the San Andreas Fault and greater strike-slip rates along the Eastern California Shear Zone and Garlock fault. These results suggest that the degree of regional transpression controls the partitioning of deformation between local uplift, slip along the San Andreas system and slip along the ECSZ. A northerly shift in plate velocity orientation could account for the abandonment of the Mill Creek strand of the San Andreas fault ~120 ka.

FREQUENCY-MAGNITUDE DISTRIBUTIONS OF TRIGGERED AND NON-TRIGGERED POPULATIONS OF SEISMICITY (B-108)

S. Hernandez and E.E. Brodsky

Large dynamic strains carried by seismic waves are known to trigger seismicity far from their source region. This effect has been attributed to several mechanisms including Coulomb frictional failure and induced changes in fault strength and pore pressures in the far field. As a harbinger of seismicity rate change however, it is as yet unconfirmed whether the passage of dynamic surface waves can also induce societally significant earthquake changes. To test for such changes, we utilize the inter-event time ratio R to identify populations of seismicity that contain larger than average proportions of triggered earthquakes. The inter-event time ratio, or R-ratio, is computed in California for the time period 1 Jan 1984 - 15 Apr 2011 and utilizes the ANSS catalogue, nominally complete down to M2.1. In particular, R-ratios for spatial grids of 0.1x0.1 degrees are calculated with respect to each potential far field trigger, defined as any event with imposed strain greater than 1e-8 and epicentral distance greater than 800 km from source. The bias introduced by finite catalog effects is corrected using 2 techniques: 1) directly estimating the deviation from homogenous (i.e., Poissonian) behaviour using randomized simulations of local seismicity catalogs, and 2) restricting local seismicity catalogs to symmetric windows of 1, 2, and 5 years around each potential far field trigger. We then measure the Gutenberg-Richter (GR) frequency-magnitude distributions for 2 broad classes of seismicity: those that include many triggered events ($R < 0.484$, or ~10% rate change or greater) and those that include very few or possibly negative rate change ($R > 0.484$). In general, we find that the distribution of b-values for both types of datasets show significant overlap and persists when both techniques for eliminating our time-dependent finite catalog bias are applied. For populations with low R, GR b-values are 1.13 +/- 0.15. For high R populations, GR b-values are 1.09 +/- 0.09. Additionally, neither b-values nor mean maximum magnitude show any correlation with respect to calculated peak dynamic strain. In terms of hazard estimates, our results indicate an inability to resolve societally significant induced changes in Gutenberg-Richter frequency-magnitude distributions within California at various temporal scales.

STOCHASTIC SOURCE MODEL FOR SEISMIC HAZARD ESTIMATION (B-113)

S. Hiemer, Q. Wang, D.D. Jackson, Y.Y. Kagan, S. Wiemer, J.D. Zechar, and J. Woessner

We are developing a stochastic earthquake source model appropriate for intermediate to long-term forecasts, expressed in terms of earthquake rate per unit area-time-magnitude-focal mechanism direction. We start with what is known best: the frequency-magnitude distribution, slip rates on major faults, long-term strain rate, and instrumentally recorded and historic earthquake catalogs. We illustrate our approach with an application to California. We use the stochastic earthquake source model to simulate hazard-relevant earthquakes. The resulting simulated earthquakes are represented by spatially tapered ruptures on hypothetical rectangular fault planes with specified length, width, strike, dip, and rake. Their locations and orientations approximate those of mapped faults based on empirical studies as well as historical and instrumental seismicity records. Many mapped faults are located only after major earthquakes occur on them, and many 20th century earthquakes occurred on previously unrecognized faults. We identify testable features of the model and devise quantitative prospective and/or retrospective tests as appropriate for parameter optimization.

STATION-TO-STATION GREEN'S FUNCTIONS EXTRACTED FROM SEISMIC CODA IN SOUTHERN CALIFORNIA (B-054)

E.T. Hirakawa and S. Ma

It has been demonstrated recently that correlation of seismic diffuse field (ambient noise and coda) recorded at two stations leads to deterministic station-to-station Green's functions. The theory requires a homogeneous distribution of uncorrelated sources or scatters. However, this condition is not satisfied by the ambient noise data, which is dominated by the microseisms. In this study, we will explore the seismic coda recorded in southern California for over 10 years. In contrary to ambient seismic noise, coda waves, generated by multiple scattering by small-scale heterogeneities, are independent of the sources that generate them. The Green's function extracted from coda waves should approach more closely to the true Green's functions. These Green's functions will provide a way to quantify the bias in these two different data sets. We will also explore the frequency content and amplitude of coda-wave Green's functions and compare them with numerical Green's functions based on the current Community Velocity Models of southern California.

CREATING PROBABILISTIC SEISMIC HAZARD MAPS FROM CSEP DATA (B-125)

J.R. Holliday

One of the loftier goals in seismic hazard analysis is the creation of an end-to-end earthquake prediction system: a "rupture to rafters" work flow that takes a prediction of fault rupture, propagates it with a ground shaking model, and outputs a damage or loss profile at a given location. So far, the initial prediction of an earthquake rupture (either as a point source or a fault system) has proven to be the most difficult and least solved step in this chain. However, this may soon change.

The Collaboratory for the Study of Earthquake Predictability (CSEP) has amassed a suite of earthquake source models for assorted testing regions worldwide. These models are capable of providing rate-based forecasts for earthquake (point) sources over a range of time horizons. Furthermore, these rate forecasts can be easily refined into probabilistic source forecasts. While it's still difficult to fully assess the "goodness" of each of these models, progress is being made: new evaluation procedures are being devised and earthquake statistics continue to accumulate. The scientific community appears to be heading towards a better understanding of rupture predictability. It is perhaps time to start addressing the second step in the earthquake prediction system.

In this poster, I show how a simple ground shaking model can be constructed and applied directly to CSEP formatted source output. As a case study, I present probabilistic seismic hazard maps for peak ground acceleration (PGA) in the state of California using sixteen models supplied to the Regional Earthquake Likelihood Models (RELM) experiment. Furthermore, I give a full PGA exceedance profile for Palm Springs as calculated by each of the sixteen input models.

2011 LONG BEACH/SIGNAL HILL, CA SEISMIC STUDY (B-076)

D.D. Hollis

Presented is an overview, maps and data of a recent active and passive seismic study recorded by a dense seismic network in Long Beach, California. The network consists of approximately 5,000 short-period vertical sensors covering a 7 by 10 km area, with an average station spacing of 100m. The network recorded continuously (24 hours/day) for a period of 6 months. The primary goal of the survey was to collect 3D reflection seismic data over the Long Beach Oil Field. Another goal of the survey was to collect passive seismic for basic earthquake and exploration seismology research.

NEAR REAL-TIME ESTIMATION OF VELOCITY GRADIENT TENSOR FIELDS FOR CONTINUOUS MONITORING IN SOUTHERN CALIFORNIA (B-143)

W.E. Holt, G. Shcherbenko, and E. Caruso

We present test results of a geodetic network processing system designed to detect anomalous strain transients. This work is a first step in the development of a continuous, near-real-time monitoring system for Southern California. The modeling procedure consists of interpolating velocities within a region to estimate the velocity gradient tensor field. These velocities are time-dependent estimates of velocity obtained from CGPS data using a simple moving average filter, while also removing seasonal signal estimates. Time dependent velocities can be output at any regular time interval (e.g., daily, weekly) and the associated velocity gradient tensor field for Southern California can then be estimated for each respective epoch. Regularization of the solution for Southern California consists of obtaining the sharpest estimate of strain rates possible that can be supported by the CGPS data. The smoothing of the strain rate solution is controlled through optimization of a functional in a formal least-squares inversion. Both the transient detection exercise results, along with results from real CGPS data, are presented. Results to date suggest that the method is well-suited for uncovering transients following past real earthquakes, as well as transients within the blind test exercise that involve extended periods of slow slip over long-time periods of several years. Presently further testing and refinement of the methodology is necessary to enable detection of transients that occur over shorter time periods of 2 – 6 months.

NUMERICAL MODELING OF INTERSEISMIC EARTHQUAKE-INDUCED VERTICAL MOTION ASSOCIATED WITH THE SAN ANDREAS FAULT SYSTEM (B-145)

B.P. Hooks, B.R. Smith-Konter, and G. Thornton

An accurate representation of vertical motion along active plate boundaries is a critical component of earthquake hazard models, as the accumulation of strain and vertical displacement can greatly affect the strength of the crust, and therefore, the associated seismic hazard. However, analysis of vertical deformation is rarely done due to the large uncertainty in the geodetic datasets. Here we present 3D numerical models that reproduce the strain patterns associated with the San Andreas and subsidiary faults. Our models utilize a commercial finite difference code (FLAC3D) that simulates the deformation of Earth material using mechanical and thermal constitutive relationships. We use a temperature-dependent viscous model for the lower crust (> 350 C) and plastic upper crust (Mohr-Coulomb with strain softening criteria). Model temperature controls the thickness of the upper crust and the viscosity of the lower crust, and therefore the overall strength of the model. Deformation, including the formation of large-scale fault systems, is driven by a basal shear consistent with the SCEC Crustal Motion Model. The model reproduces first-order characteristic horizontal velocities, strain rates, and stress rates associated with the San Andreas Fault System that compare favorably to reported measurements and previous modeling results. Additionally, vertical displacement and velocity results reproduce first-order vertical offset marker and tide gauge datasets and agree well with interseismic vertical deformation produced by a 3D semi-analytical model that applies geologic strike-slip rates along active faults. Both models suggest three primary areas of the San Andreas Fault System where vertical motion is significant: the Salton Trough, Death Valley, and the Big Bend. The Salton Trough and Death Valley are areas of subsidence controlled by crustal transtension resulting in thinned and weakened crust with in a lower potential to accumulate large stresses. The Big Bend region has uplifted due to a transpressional restraining bend. The substantial uplift and evolving crustal stress conditions within this area would have thickened and strengthened the crust resulting in relatively larger stress accumulation. The long-term effect of the non-linear feedbacks between vertical deformation, thermal advection, and crustal rheology causes a dynamic link between geomorphic signal, strain accumulation and long-term seismicity.

STRONG GROUND MOTION IN PORT-AU-PRINCE, HAITI, DURING THE 12 JANUARY 2010 M7.0 HAITI EARTHQUAKE (B-014)

S.E. Hough, T. Taniguchi, J.R. Altidor, D. Angllade, S.L. Mildor, and D. Given

No strong motion records are available for the 12 January 2010 M7.0 Haiti earthquake. We use recordings of M3.5-4.5 aftershocks as well as detailed considerations of damage to estimate the severity and distribution of mainshock shaking in Port-au-Prince. Relative to ground motions at a hard-rock reference site, peak accelerations are amplified by a factor of approximately 2 at sites on low-lying deposits in central Port-au-Prince and by a factor of 2.5-3.5 on a steep foothill ridge in the southern Port-au-Prince metropolitan region. The observed amplification along the ridge cannot be explained by sediment-induced amplification, but the observed amplitude, predominant periods, variability, and polarization are consistent with predicted topographic amplification by a steep, narrow ridge. Although damage was largely a consequence of poor construction, the damage pattern inferred from analysis of remote sensing imagery provides evidence for a correspondence between small-scale (0.1-1.0 km) topographic relief and high damage. Mainshock shaking intensity can be estimated crudely from a consideration of macroseismic effects: in the areas of Port-au-Prince that experienced relatively light damage, we estimate PGA on the order of 0.10-0.15g (MMI VI). We further present detailed, quantitative analysis of the marks left on a tile floor by an industrial battery rack displaced during the mainshock, at the location where we observed the highest weak motion amplifications. Results of this analysis indicate that mainshock shaking was significantly higher at this location (~0.5g, MMI VIII) relative to the shaking in parts of Port-au-Prince that experienced relatively light damage. This estimate of PGA is consistent with that estimated independently using the weak-motion amplification factors together with the estimate for shaking intensity apart from local amplification. Our results illustrate how well-documented observations of rigid body horizontal displacement during earthquakes can be used to estimate peak ground accelerations in the absence of instrumental recordings of ground motion.

PROPERTIES OF RUPTURE PULSES INDUCED BY DAMAGED FAULT ZONES (A-113)

Y. Huang and J.P. Ampuero

Low-velocity fault zones (LVFZ) are found in most mature faults. They are usually 100-400 m wide and have ~20%-60% wave velocity reductions relative to the country rock. To study the effect of LVFZs on earthquake rupture and the radiated wavefield, we conduct 2D spectral element simulations of dynamic rupture on faults that bisect a LVFZ, considering a range of velocity reductions and widths. Most earthquakes apparently have slip rise times much shorter than their overall rupture duration. A number of dynamic mechanisms for such pulse-like ruptures have been proposed, including frictional self-healing, fault strength heterogeneities and bimaterial effects. We find that ruptures in LVFZs with strong enough wave velocity contrast behave as pulses. These pulses are generated by fault locking induced by waves reflected from the boundaries of the LVFZ. Their rise time is proportional to the wave travel time across the LVFZ. Pure pulse-like rupture is favored by high velocity reduction and narrow width of the LVFZ. This mechanism of pulse generation is robust to variations of initial stress, smoothness of the LVFZ structure, rupture mode and exclusion of frictional healing.

Moreover, we find that LVFZs can generate complex rupture patterns. LVFZs with low velocity reduction induce multiple rupture fronts involving co-existing pulses and cracks. LVFZs with certain widths can accelerate the transition to supershear rupture speed. The LVFZ can also induce repeated nucleation of pulses in front of a crack. These additional effects of LVFZs on dynamic rupture can have characteristic signatures on the radiated wavefield and contribute especially to high frequency ground motions. Given the natural existence of LVFZ and the generality of the pulse generation mechanism presented, it seems unlikely for earthquakes to propagate as pure cracks.

To further analyze the relation between wavefield and rupture healing fronts, we are analyzing the dynamic fault stresses generated by elementary kinematic sources inside a LVFZ. Our goal is to identify which wave phase (such as S or SS) plays the dominant role in the process of pulse generation and. By studying the amplitude and timing of this phase as a function of velocity reduction and width of the LVFZ, we can rationalize the effect of fault zone properties on the induce pulses, including their conditions of existence, their rise time and their supershear transition.

SOURCE PROCESSES OF MICROEARTHQUAKES AT PARKFIELD, CA, DETERMINED BY NEAR-SOURCE OBSERVATION AT SAFOD MAIN HOLE (B-034)

K. Imanishi and W.L. Ellsworth

Near-source observation of earthquakes in deep boreholes and mines provides significant opportunities to enhance our understanding of the source properties of earthquakes. Short hypocentral distances and a high-Q environment make it

possible to observe earthquake processes that cannot be seen in shallow boreholes or at the surface. The SAFOD Main Hole is a 3.2 km-deep inclined borehole that crosses the active traces of the San Andreas Fault. A 3-component 15 Hz GS-20DM geophone was deployed within the fault zone at depths between 2350 and 2750 m. Because of the close proximity to earthquake sources, we routinely observed earthquakes with Mw < 0 with high signal-to-noise ratio. Events were recorded at three different sampling rates (1000, 2000, and 4000 sps) depending on observation period (2005 - 2011). This study focuses on earthquakes with S-P time differences shorter than 0.5s, corresponding to hypocentral distance less than 3 km. We determined source parameters by the Multi-Window Spectral Ratio (MWSR) method (Imanishi and Ellsworth, 2006). The key step in the method is to stack the ratios calculated from moving windows taken along the record starting with the direct waves. We confirmed that stacking better suppresses the random noise due to differences in path than single-window methods, producing a better estimate of the source spectral ratio. For Mw>-1, the calculated stress drops range between 0.1 and 100 MPa. These observations indicate that there is no breakdown in stress drop scaling for Mw>-1. The stacked spectral ratios show that corner frequencies of events for Mw<-1 are generally beyond the upper limit of the frequency range of the data, so that we could not estimate their static stress drops. We notice that the stress drops for any given cluster are consistent within one order of magnitude, while mean stress drop across all clusters vary by about three orders of magnitude. This spatial variability must reflect different material properties and/or source processes along the fault. Extrapolation of in-situ stress magnitudes to the depth of our events predicts shear stresses resolved onto the San Andreas Fault of about 20 MPa under hydrostatic pore pressure conditions. The SAFOD result shows that microearthquakes with stress drops near the strength of the fault occur on the creeping section of the San Andreas Fault, implying the existence of fault surfaces juxtaposing normal crustal rocks where repeating earthquakes occur.

MONITORING TECTONIC TREMORS IN THE SAN-JACINTO FAULT ZONE USING MULTIPLE SMALL-APERTURE SEISMIC ARRAYS (B-044)

A. Inbal, J.P. Ampuero, and J.H. Steidl

Non-volcanic tremors provide a unique opportunity to explore complex mechanical processes occurring at the roots of crustal faults. While spontaneous tremors are routinely observed along many subduction zones, similar observations for continental transforms are scarce, and have so far been limited to the Parkfield segment of the San-Andreas Fault. Motivated by recent findings of spontaneous tremors along the San-Jacinto Fault (SJF) by Hillers and Ampuero (submitted paper, 2011), we have deployed three dense small-aperture seismic arrays in that area. Each array is composed of 15 to 25 3-component short-period sensors over aperture of few hundred meters. Our goal is to capture the spatio-temporal distribution of tremors along the SJF.

The detection scheme is carried out semi-automatically and is based on data from the 6 nearby PBO borehole seismometers. We first calculate the energy envelopes of their horizontal traces, then we compute the coherency between the available envelope pairs. True detections are defined as windows with increased energy in the 2-5 Hz frequency band that are coherent across this local network. We find that tremor-like signals occur regularly in the study area, with periods of intense activity that may last up to several weeks. During such periods we observe tremor bursts whose duration varies between a few hundred seconds to several hours. We utilize array analysis to compute the slowness and back-azimuth of wavefronts arriving at the arrays for consecutive time windows containing tremor. Preliminary results suggest that the apparent velocities during the tremor episodes are stable and consistent with body-wave velocities from deep sources. In some cases tremor activity seems to be confined to isolated fault segments located a few kilometers north of the Anza valley. We also observe occasions in which tremor migrates along strike at velocities of about 100 km/hour, similar to migration speeds obtained for the Parkfield tremor. In order to estimate the tremor depths we back-project rays from the arrays onto the SJF plane using a regional 1-D velocity modal. The resulting focal depths range between 10-20 kilometers, consistent with estimates of the base of the seismogenic zone in our study area.

INTERACTION BETWEEN EARTHQUAKE GROUND MOTION AND BUILDING MODELS -- A 3D PARAMETRIC STUDY (B-035)

Y.D. Isbiliroglu, R. Taborda, and J. Bielak

This study deals with the effects of the built environment on the earthquake ground motion, and with how individual buildings interact with the surrounding soil and with each other. We conduct a parametric study using Hercules, the parallel octree-based finite element earthquake simulator developed by the Quake Group at Carnegie Mellon University. Because of the necessity of performing repeated ground motion simulations , our analysis is based on the Domain Reduction Method (DRM), a modular two-step finite element methodology for modeling earthquake ground motion in highly heterogeneous localized regions. Buildings are included by modifying Hercules' finite-element meshing routines so that they are

incorporated as additional block elements that are adjusted to emulate the general geometric and dynamic characteristics of buildings in city-like arrangements. We conduct our study in the greater Los Angeles basin using the main shock of 1994 Northridge earthquake for frequencies up to 2 Hz and a domain size of 85 x 85 x 42.5 km^3 as the first step of the DRM. Then, we reduce the size of the region to a small subdomain of 2 x 2 x 1 km^3 within the downtown Los Angeles region and introduce the building structures, for the second step of the DRM, in order to perform the repeated simulations of the parametric study.

TESTING SEGMENTATION MODELS (B-122)

D.D. Jackson

Many hazard models and earthquake forecasts assume that large earthquakes occur on fault segments whose boundaries are effective in stopping or impeding rupture. A corollary is that the end points of rupture should lie "at" the segment boundaries. Here I propose a test that segment boundaries do in fact affect earthquake rupture. The test requires that faults and segment boundaries be defined in advance by map polygons, and that an objective procedure be specified for defining the end points of a future earthquake rupture. A segmentation model will then be judged successful to the extent that rupture termini fall into the boundary polygons in greater proportion than their relative area. Polygons are required in order to judge whether rupture ends "at" a boundary, and the polygons' sizes should reflect the uncertainties of the estimated boundary locations. Retrospective testing is useful but will not be definitive because it requires arbitrary a-posteriori data selection. Prospective testing is a challenge because it requires precise definitions and rules for selecting data for future earthquakes. Some seismic hazard models, such as those prepared by the Working Group on California Earthquake Probabilities, imply the rate at which rupture termini should land in prescribed segment boundary zones. A simple null hypothesis is that rupture termini occur with equal probability anywhere on a fault.

INTERACTIONS BETWEEN THE CLARK STRAND OF THE SAN JACINTO FAULT ZONE AND THE EXTRA-ELMORE FAULT ARRAYS (A-149)

S. Janecke and S. Thornock

The Clark fault is currently mapped as terminating north of the Extra fault in unfaulted middle Quaternary deposits. We mapped the San Sebastian Marsh area between the tip of the Clark fault and the Superstition Hills to assess the possible SEward continuation of the Clark fault that appears in InSAR-based inversions. One field season, extensive mapping on imagery, landscape analysis, and correlation of mapped fault traces with of published InSAR, gravity and magnetic data suggest that NE-striking left-lateral faults dominate in the shallow crust whereas the nascent Clark fault persists under or through the crossing left-lateral network at deeper levels. Mapping produced more evidence for active NE-striking left-lateral faults than of NW-striking dextral faults. NE-striking faults form a continuous, curving and dense array between the Coyote Creek fault zone and the Salton Sea and are in line with previously mapped faults beneath the Sea. Most ENE to NNE-striking faults are steep, preserve more horizontal slickenlines than dip-slip slickenlines due to left- and left-oblique slip. These numerous fault zones, which include the Extra, Elmore Ranch, and Kane Spring faults, produce uplifts along their traces, and cut Holocene sediment of Lake Cahuilla. The main strand of the Extra fault zone cuts Holocene lakebeds, generated colluvial wedges, but is lapped by ~900 yrs BP sand dunes and 1-2 deep lake cycles of Lake Cahuilla.

Only one of the 4 larger strands of the Clark fault in the San Felipe Hills continues SE as small-offset dextral faults. This strand projects to similar small offset dextral faults in the Superstition Hills, with a possible gap near the marsh. There is also a suggestion of an en-echelon left-stepping dextral zone that steps to the east side of the Superstition Hills and the NW tip of the Imperial fault. Despite the limited expression of the Clark fault zone at the surface, we infer that it persists SEward to the Superstition Hills fault in the subsurface because it is axial to a major hourglass-shaped uplift of basin fill that stretches from the SE tip of the Santa Rosa Mountains to the New River. Major strands of the San Jacinto fault zone form the "spine" of this uplift except in its narrow waist around San Sebastian Marsh where a blind fault is likely. The uplift is so large and active that it traps all the sediment of the San Felipe and Carrizo Wash drainage basins on its upslope side. Further study will test these working hypotheses.

INTERACTION OF FAULT STRENGTH HETEROGENEITIES AND STRESS REDISTRIBUTION IN MULTIPLE EARTHQUAKE CYCLES ON FAULTS WITH THERMAL PRESSURIZATION (A-097)

J. Jiang and N. Lapusta

Natural faults are characterized by geometric complexities, variations in hydraulic and frictional properties, and non-uniform prestress. In simulations of isolated dynamic rupture, these heterogeneities are used to produce complex earthquake scenarios, and often fault prestress and frictional strength are assigned independently. However, simulations of multiple earthquake

cycles (e.g., Lapusta and Liu, 2009) show that fault prestress and strength are physically related through stress redistribution due to prior slip. Considering the interplay of stress redistribution and fault strength heterogeneity is important for understanding earthquake cycle patterns and characteristics of dynamic ruptures.

Here we study long-term slip on faults with large-scale heterogeneous fault strength due to non-uniform normal stress and/or frictional properties, which could be related to geometric and/or material complexity. Using BICycle algorithm in 2D (Noda and Lapusta, 2011), we simulate the entire earthquake cycles, including fully dynamic seismic rupture and aseismic tectonic loading, on faults governed by Dieterich-Ruina rate-and-state friction with thermal pressurization. Initial shear stresses are pre-assigned and developed into physically-consistent distribution over multiple cycles.

In our simulations, incorporation of thermal pressurization enables the fault to operate at lower average stress level. Increasing heat production, and hence larger co-seismic weakening at the places of higher normal confinement, tends to partially compensate for the effect of heterogeneous static strength. The sequences are characterized by occasional large fault-spanning seismic events and many smaller events that rupture across only part of the fault. Shear stresses evolve and get redistributed on the entire fault during the major events, in accordance with the fault strength, to reduce the effect of the introduced heterogeneity in dynamic rupture in long-term fault behavior. Intermittent smaller events complexify the stress level.

Our current work is directed towards quantifying the interaction of the extent of fault strength heterogeneities with earthquake sequences and dynamic ruptures. It would be used to: (1) draw implications for the state of stress on heterogeneous faults and how it would affect earthquake nucleation conditions; and (2) understand the effect of stress redistribution on rupture propagation, with consequences for ground shaking.

BAYESIAN EARTHQUAKE SOURCE VALIDATION FOR GROUND MOTION SIMULATION (B-011)

H.C. Jimenez, P.M. Mai, E. Prudencio, I. Babuska, M. Motamed, and R. Tempone

Design parameters in building codes require reliable ground-motion predictions. They depend on realistic source models controlled by several parameters, such as fault dimensions, hypocenter location, stress field, rupture speed, rise time, etc. In this project we initially consider simple kinematic earthquake rupture models to simulate near-field ground-motions that produce the smallest misfit between Ground Motion Prediction Equations (GMPE) and predicted quantities of interest (QoI, e.g. peak ground velocity or spectral acceleration at different periods). Based on the experience with simple kinematic rupture models we will move toward more realistic, pseudo-dynamic rupture models. The key question we would like to address using a Bayesian approach is: "How much source complexity is needed to adequately reproduce GMPE's".

In the first stage, we consider 1D velocity structures and simplistic kinematic models in which we sequentially perturb a single source parameter (slip heterogeneity, rise time, rupture speed, hypocenter location) in the framework of a "calibration & validation experiment" using a Bayesian updating approach. Including also data uncertainties of the QoI's, both in GMPE's and in recent observations, we seek to (a) map the sensitivities of the QoI's to rupture-model parameterization, and (b) quantify the required rupture-model complexity for kinematic source models that best reproduces the QoI's given by GMPE's.

In later stages of this project, we will also include 3D velocity structures and more realistic (pseudo-)dynamic rupture models. Using a Bayesian modeling approach we aim at being able to rigorously define the level of complexity needed in ground-motion source modeling for satisfying observational constraints and engineering requirements for seismic safety.

SALTON SEISMIC IMAGING PROJECT (B-065)

E. Jimenez, J.D. Rodriguez, and J. Stock

The Salton Seismic Imaging Project is an active-source seismic study of the southeastern region of the San Andreas Fault crossing the Salton Trough. The study used explosives to radiate seismic waves, which were detected by portable seismometers (vertical-component ?Texans? and 3-component RT-130s) near the explosions as well as by permanent seismic stations in the region of Southern California. The survey was divided into lines, with Line 1 crossing from South to North along the axis of the Salton Trough, lines 8 and 9 parallel to line 1 on the edges of the Salton Sea and the other lines perpendicular across much of the first line. Ocean-bottom seismometers also recorded the explosions but those data are not used in this study because we are concentrating on the structure in the region south of the Salton Sea. We analyzed the first arrivals on the two sets of seismometers and compared them to identify with more precision the structure of the region. The network arrivals yielded late origin times for shots within the southern Imperial Valley indicating the need for a more detailed

velocity model in this region. We made detailed picks of first arrivals from the vertical-component portable stations in the southern Imperial Valley and used these to determine more detailed 2-D velocity models here.

These structure velocity models will help in predicting characteristics of seismic wave transmission based on our new, more detailed knowledge of the thickness of the layers and the behavior of seismic waves as they pass through them.These studies may help us understand more clearly the effects expected from small and large earthquakes in the Southern California region.

LOW-STRENGTH FRICTIONAL CREEP ON THE LOWER-CRUSTAL EXTENSION OF THE SAN ANDREAS FAULT NEAR PARKFIELD, CA (B-144)

K.M. Johnson, D. Shelly, and A.M. Bradley

Understanding how seismogenic faults in the upper brittle layer of the crust are coupled to time-dependent inelastic deformation in the viscous lower crust and upper mantle is important for achieving a better understanding of earthquake nucleation processes. Field and laboratory studies indicate that deformation in the lower crust tends to localize into narrow shear zones. A number of studies of postseismic deformation following large earthquakes infer rapid rate of deformation across shear zones extending into the lower crust below the earthquake rupture and lasting for years to decades. However, less is known about how seismogenic faults are loaded from below by deformation in the lower crust during the interseismic period, after the rapid period of postseismic deformation. Until recently, evidence for interseismic activity on the lower crustal extension of large active strike slip faults like the San Andreas Fault has remained elusive. Recent observations of tremor in the lower crust near Parkfield, CA (e.g., Nadeau and Dolenc, 2005; Shelly, 2010) provide the first hint of active faulting in the lower crust below nominally seismogenic depths. Shelly (2010) cites these observations as evidence that the San Andreas fault exists as a localized structure extending at least to the bottom of the crust. Shelly and Johnson (2011) suggest that tremor transients triggered by static stress changes on the fault induced by the nearby 2003 M6.7 San Simeon Earthquake and the 2004 M6.0 Parkfield earthquake indicate transient fault creep. However, these inferences of deep fault creep remain circumstantial because any slip associated with the tremor activity would be too small to detect with instruments at the ground surface. Because the deep fault slip cannot be observed directly, umerical modeling is required to link tremor to fault slip. In this study we show that these transient tremor episodes are indeed consistent with model predictions of triggered fault creep on the lower crustal extension of the San Andreas fault. We show that the deep SAF is presently sliding at conditions consistent with model results from tremor and slip studies of subduction zones [Liu and Rice (2009)]: low effective normal stress and frictional properties consistent with laboratory measurements on Gabbro.

TOHOKU EARTHQUAKE: A SURPRISE? (B-106)

Y.Y. Kagan and D.D. Jackson

We consider three issues related to the 2011 Tohoku earthquake:

(1) Why was the magnitude limit for the Tohoku region so badly underestimated, and how can we estimate realistic limits for subduction zones in general?

(2) How frequently can such large events occur off Tohoku?

(3) Could short-term forecasts have offered effective guidance for emergency preparation?

Two methods can be applied to estimate the maximum earthquake size in any region: statistical analysis of available earthquake records, and the moment conservation principle -- how earthquakes release tectonic deformation. We have developed both methods since 1991. For subduction zones, the seismic record is usually insufficient (in fact it failed badly for Tohoku), because the largest earthquakes are so rare. However, the moment conservation principle yields consistent estimates for all subduction zones. Various measurements imply maximum moment magnitudes of the order 9.0--9.7. A comparison of the inter-earthquake secular strain accumulation and its release by the coseismic slip implies a similar maximum earthquake size estimate.

Beginning in 1999 we used our statistical short- and long-term earthquake forecasts, based on the GCMT catalog, for the western Pacific, including Japan. We have posted them on the web and included expected focal mechanisms as well. Long-term forecasts indicate that the average frequency for magnitude 9 earthquakes in the Tohoku area is about 1/400 years. We have archived several forecasts made before and after the Tohoku earthquake. As expected, the Tohoku mega-earthquake changed the forecasted long-term rate by just a few percent. However, the magnitude 7.5 foreshock increased the short term

rate to about 100 times the long-term rate, and the magnitude 9 event increased it briefly to more than 1000 times the long-term rate. These results could well justify the development of an operational earthquake forecasting plan.

FULL EARTH HIGH-RESOLUTION EARTHQUAKE FORECASTS (B-124)

Y.Y. Kagan and D.D. Jackson

Since 1977 we have developed statistical short- and long-term earthquake forecasts to predict earthquake rate per unit area, time, and magnitude. The forecasts are based on smoothed maps of past seismicity and assume spatial and temporal clustering. Our new program forecasts earthquakes on a 0.1 degree grid for a global region 90N--90S latitude. We use the PDE catalog that reports many smaller quakes (M>=5.0). For the long-term forecast we test two types of smoothing kernels based on the power-law and on the spherical Fisher distribution. We employ adaptive kernel smoothing which improves our forecast both in seismically quiet and active areas. Our forecasts can be tested within a relatively short time period since smaller events occur with greater frequency. The forecast efficiency can be measured by likelihood scores expressed as the average probability gains per earthquake compared to spatially or temporally uniform Poisson distribution. The other method uses the error diagram to display the forecasted point density and the point events.

A GUIDE TO SELECTING EMPIRICAL GREEN'S FUNCTIONS IN REGIONS OF FAULT COMPLEXITY: A STUDY OF DATA FROM THE SAN JACINTO FAULT ZONE, SOUTHERN CALIFORNIA (B-067)

D.L. Kane, D.L. Kilb, and F.L. Vernon

We examine the appropriateness of applying the empirical Green's function (EGF) method to constrain the source properties of target M > 3 mainshock events in regions of complex faulting. A key aspect of our analyses is testing a broad range of trial EGFs to identify the transition separating appropriate EGF events from other local events that do not satisfy the assumptions of the EGF method. We use data (>183,000 seismograms from ~56,000 earthquakes) recorded by the ANZA seismic network (12 seismic stations), which spans the San Jacinto Fault Zone (SJFZ) in southern California. The SJFZ provides a good testing ground because of its heterogeneous fault structure, high seismicity rate, and diverse distribution of earthquake sources and locations. We define a M > 3 mainshock catalog of 52 events, and for each mainshock we identify a suite of potential EGF events that locate within 10 km. For all possible mainshock/EGF pairs, we estimate the preferred corner frequency of the source spectrum signal that results after spectral division of the EGF spectrum from the mainshock spectrum. We assume that an ideal EGF choice will result in similar corner frequency estimates at all stations in the array. To quantify this similarity, we measure the standard deviation of the corner frequency estimates across all stations for each mainshock/EGF pair. Our results show the preferred EGF events are at least one magnitude unit smaller than the mainshock magnitude. Importantly, we find a limiting maximum hypocentral separation between the mainshock and EGF of ~2 km (based on a relocated catalog), above which the results are indistinguishable from pairs with greater separation (e.g., 2-10 km). The EGF event selection can also be significantly improved by testing for matching first motion polarities and high correlation between the mainshock and EGF waveforms at each station. Waveform correlation degrades considerably at separation distances greater than 1 km. To select the most appropriate EGF events, we suggest using only EGF events located within 1 km of the mainshock. However, EGF events at distances up to 2 km can be considered if one verifies that the mainshock/EGF pair have similar waveforms and polarities. When sufficient data exists, we suggest applying these pairwise constraints to obtain optimal source parameter estimates using the EGF method.

INVESTIGATION OF INTERSEISMIC DEFORMATION ALONG THE CENTRAL SECTION OF THE NORTH ANATOLIAN FAULT (TURKEY) USING INSAR OBSERVATIONS AND EARTHQUAKE-CYCLE SIMULATIONS (A-051)

Y. Kaneko, Y. Fialko, X. Tong, D.T. Sandwell, and M. Furuya

We present high-resolution measurements of interseismic deformation along the central section of the North Anatolian fault (NAF) in Turkey using L-band Interferometric Synthetic Aperture Radar (InSAR) data collected by the Advanced Land Observing Satellite (ALOS) of the Japan Aerospace Exploration Agency. We generated satellite line-of-sight (LOS) velocities for the three ascending ALOS tracks (603-605) covering the NAF between 31.2-33.2 deg. East. LOS velocity maps for each track were obtained by averaging 15 to 30 radar interferograms spanning a time period of 4 years between 2007 and 2010. The average LOS velocities reveal discontinuities of up to ~6 mm/year across the geologically mapped fault trace. Assuming that these discontinuities are due to horizontal surface motion, they imply fault creep at a rate of ~10 mm/year, accounting for nearly half of the relative plate motion accommodated by this segment of the NAF. The inferred lateral extent of significant shallow creep is in excess of 60 km. These inferences are broadly consistent with previously reported trilateration surveys and

InSAR results based on C-band ERS data (Cakir et al., 2005) that suggested that the NAF segment near Ismetpasa may be only partially locked. If so, the deeper locked portion of the fault must be characterized by a higher stressing rate, and presumably shorter recurrence interval. We are modeling available InSAR and GPS data using numerical simulations of spontaneous earthquake sequences that incorporate laboratory-derived rate-and-state friction laws. The goal of these simulations is to constrain key parameters of fault friction such as the depth extent of the velocity-strengthening and velocity-weakening layers, the long-term fault slip rate, and stress evolution in the seismogenic crust.

VARIABILITY OF SEISMIC SOURCE SPECTRA DERIVED FROM COHESIVE-ZONE MODELS OF A CIRCULAR RUPTURE PROPAGATING AT A CONSTANT SPEED (A-085)

Y. Kaneko and P.M. Shearer

Static stress drop of earthquakes is often estimated from far-field body-wave spectra using measurements of corner frequencies, together with seismic moment, which can be computed from the low-frequency part of the spectrum. Corner frequencies are used to infer the source dimension based on a specific theoretical model. The most widely used model is from Madariaga (1976), which considered a bilateral rupture expanding at a constant speed on a circular fault. This model assumes that the rupture front is characterized by an abrupt change of fault strength from a uniform initial prestress to a kinetic frictional stress, and hence the stress is singular at the rupture front. In this study, we investigate variability of source spectra derived from dynamic models of expanding bilateral ruptures on a circular fault with a cohesive zone that prevents a stress singularity at the rupture front. We study the dependence of far-field body-wave spectra on the rate of frictional weakening (which controls the cohesive zone size), rupture speed, and dynamic stress drop. For each source model, we compute far-field body-wave displacement synthetics for a homogeneous elastic space using the representation theorem (Aki and Richards, 2002). Our results show that P- and S-wave corner frequencies of displacement spectra are systematically larger than those predicted by Madariaga (1976) and generally depend on the rate of frictional weakening in the source model, which affects the fracture-energy-density distribution on the fault. For a given rupture speed, the average of corner frequencies over the focal sphere is larger for source models with larger fracture energy. For ruptures propagating at 90 percent of the S-wave speed, the azimuthal average of P-wave corner frequencies in the case with the smallest fracture energy is about 20 percent larger than that of Madariaga (1976), which corresponds to about a factor of two difference in the inferred stress drop. Thus for these ruptures, application of the Madariaga model overestimates stress drops by factors of two or more, depending upon the fracture energy. We also find that the takeoff angle dependence of the corner frequencies for supershear ruptures is systematically different from that for subshear ruptures due to the difference in radiated wave fields for supershear and subshear ruptures.

THREE DIMENSIONAL ELASTIC RESPONSE OF COMPLIANT FAULT ZONES TO NEARBY EARTHQUAKES: A THEORETIC STUDY (A-110)

J. Kang and B. Duan

Compliant fault zones have been detected along active faults by seismic

investigations (trapped waves and travel time analysis) and InSAR observations. However, the width and depth extent of compliant fault zones are still under debate in the community. Numerical models of dynamic rupture build a bridge between theories and the geological and geophysical observations. Theoretical 2D plane-strain studies of elastic and inelastic response of compliant fault zones to nearby earthquake have been conducted by Duan [2010] and Duan et al [2010]. In this study, we further extend the experiments to 3D with a focus on elastic response. We are specifically interested in how residual displacements depend on the structure and properties of complaint fault zones, in particular on the width and depth extent. We conduct numerical experiments on various types of fault-zone models, including fault zones with a constant width along depth, with decreasing widths along depth, and with Hanning taper profiles of velocity reduction. . Our preliminary results suggest 1) the width of anomalous horizontal residual displacement is only indicative of the width of a fault zone near the surface, and 2) the vertical residual displacement contains information of the depth extent of compliant fault zones.

A UNIFIED FINITE ELEMENT METHOD FOR HETEROGENEOUS ELASTIC MEDIA WITH LOW TO HIGH RATIO OF P- TO S-WAVE VELOCITIES (A-040)

H. Karaoglu and J. Bielak

This study reports on a mixed finite element formulation that overcomes certain limitations faced by low-order primal-based formulations. A primal-based formulation with displacement as the variable is a widely used method to solve wave-

propagation problems. It has been observed, however, that its accuracy deteriorates badly with increasing contrast between the P- and S-wave velocities.

By using a dual-based formulation, we develop a method that is robust within the entire range of an elastic solid medium with moderate to high contrast of the P- and S-wave velocities. By solving a constrained variational problem with the Lagrange-Multiplier Method, we developed the dual-based (mixed) formulation with pressure and displacement as the variables.This is similar to earlier mixed displacement-pressure formulations, except that we introduce the methodology as a global one applicable to different domains rather than being limited to certain extreme cases. The variational problem makes a wider range of interpolation functions permissible for pressure including discontinuous functions across element boundaries.

We illustrate the validity of the method by solving a range of idealized problems with moderate to high contrast of P- to S-wave velocity, and compare the performance of different types of elements. We verify the method and illustrate the general principles with an application in Southern California of the 1994 Northridge earthquake.

FAULT ARCHITECTURE OF THE SALTON SEA THROUGH MULTI-SCALE SEISMIC REFLECTION SURVEYS (B-133)

A.M. Kell, N. Driscoll, G.M. Kent, A. Harding, and R. Baskin

Two sets of seismic reflection images collected in the Salton Sea, California in May 2010 and April 2011 highlight a longstanding episode of extension-related deformation within the Salton Sea pull-apart system. These data are part of a continued multi-scale network of seismic studies of the faults within the Salton Trough. In 2010, we collected ~350 line-km of data using a 75-m-long, 24-channel streamer and a 1.6kJ "sparker" source fired at 1.2 sec intervals. These images document a series of south-east dipping normal faults that are related to the current pull-apart geometry; this configuration appears to persist for only the past 20-40 ka. Newly acquired low fold images (~150 line-km) collected using a 300-m-long, 48-channel streamer and a Generator Injector (GI) airgun source firing at 1 min intervals show that the same structures seen in the higher resolution (2010) data as well as high-resolution seismic CHIRP images collected in 2007 (Brothers et al., 2009, 2010) continue to depths of >2.5 km. From this deeper imagery, we infer that the structures seen in the very shallow CHIRP data are through-going to seismogenic depths and play a dominant role in strain partitioning from the Imperial Fault to the San Andreas Fault through the Brawley Seismic Zone. The 2011 reflection and refraction data are part of a larger collaborative project involving Cal Tech, Virginia Tech, the USGS, University of Nevada, Reno and Scripps Institution of Oceanography. Within this study we seek to understand the mechanisms of how crustal thinning and rifting develops. The fault dip imaged at both scales is ~50-60° and show vertical offsets (sub-meter to tens of meters) distinguishable to the limits of our imaging resolution. These multi-scale data offer a unique opportunity to calculate the timing and mode of motion in the most actively deforming portion of the Salton Trough. The insights gained through these data allow a greater understanding of the tectonics and seismic hazards inherent in Southern California.

NEW CHRONOLOGY AND ESTIMATED RATES OF VERTICAL UPLIFT FOR THE GAVIOTA COAST RAISES ISSUES RELATED TO THE EARTHQUAKE HAZARD (A-127)

E.A. Keller, D.E. DeVecchio, L.D. Gurrola, and L.A. Owen

Marine terraces are useful for quantifying surface uplift and thus earthquake hazard. Surprisingly, numerical dates are few along the Gaviota Coast, which extends westward for 50 km from Ellwood (west of Santa Barbara) to Point Conception. Previously estimated rates of vertical uplift of marine terraces along the Gaviota Coast and elsewhere in Southern California tend to be relatively low at 0.1 to 0.3 m/ka. An exception is within the Santa Barbara and Ventura fold belts, where uplift rates are 1 to 2 m/ka and 8 m/ka, respectively. Our research in the Santa Barbara fold belt (SBFB) indicates the rate of uplift increases toward the west from More Mesa toward Isla Vista and Ellwood, where the first emergent terrace, correlated to Marine Isotope Stage 3a (MIS3a), is at an elevation of 10 m above mean sea level; for this marine terrace to be present requires a rate of uplift exceeding 2 m/ka. Existing chronology in southern California consists largely of amino acid racemization (AAR) ages from 3 decades ago. We have dated and estimated terrace age at More Mesa, Isla Vista, and Ellwood using multiple techniques (OSL, U-series, 14C, and oxygen isotope ratios on small mollusks). The MIS3a terrace appears continuous along much of the Gaviota coastline, where the first emergent terrace has been previously interpreted to be MIS5a. If our chronology is correct, this calls in question the previous chronology and rates of uplift from Ellwood west across the south branch of the Santa Ynez fault. Low marine terraces at UCSB Point (and other locations) are ~ 2+ m above mean sea level. Two hypotheses have been presented to explain these low marine terraces. The terraces either represent a mid-Holocene maximum sea level highstand or in an active tectonic setting like the SBFB the terrace may represent coseismic uplift, which we prefer.

We have observed higher marine terraces at La Mesa and Ellwood that do not correlate to sea level highstands, which we interpret to be earthquake terraces. In order to have uplift of 2 m, the earthquake would have to have had a magnitude of 7.0+, which is worrisome because several hundred thousand people live there today and urbanization is increasing. Additional dating of Holocene and late Pleistocene terraces along the Gaviota Coast will improve assessment of the earthquake hazard of the region.

SCIENTIFIC VISUALIZATION IN 4D FOR EARTHQUAKE RESEARCH (A-029)

L.H. Kellogg, T. Bernardin, M.I. Billen, E.S. Cowgill, A.J. Elliott, P.O. Gold, C.L. Harwood, O. Kreylos, M.E. Oskin, B. Pellett, D.L. Turcotte, and M.B. Yikilmaz

Three major earthquakes over the past two years have provided the opportunity to study the rupture process in unprecedented detail: the 2010 Haiti, 2010 El Mayor-Cucupah, and 2011 Tōhoku earthquake. Here we both demonstrate the use of virtual-reality based data visualization and analysis in rapid scientific response and investigations of earthquake processes and illustrate their potential use following future events. After the Haiti and El Mayor-Cucupah earthquakes, rapid data collection efforts were deployed, and high resolution LIDAR made it possible to map the fault zones and detect changes. To manage, assess, and interpret the large 3D and 4D datasets collected during and after these earthquakes, we used interactive scientific visualization tools developed in the W. M. Keck Center for Active Visualization in Earth Sciences (KeckCAVES). Software based on the Virtual Reality User Interface (VRUI) makes it possible to view, interact with, and select data, and rapidly carry out geologic mapping tasks in a immersive VR environments ranging from a desktop computer to a CAVE. The EarthViewer software allowed us to visualize foreshock and aftershock sequences from the Tōhoku earthquake which reveal the structure of the rupture surface. LIDARViewer made it possible to rapidly process and interpret airborne and tripod LIDAR data collected after the Haiti and El Mayor-Cucupah, while Crusta permitted virtual geologic mapping on the resulting high-resolution topographic models.

DEPOSITIONAL CONSTRAINTS ON SLIP ALONG THE SAN ANDREAS FAULT WITHIN THE EASTERN SAN GORGONIO PASS REGION, SOUTHERN CALIFORNIA (A-135)

K.J. Kendrick, J.C. Matti, S.A. Mahan, G.P. Landis, and D.P. Miggins

A nested alluvial complex within the Mission Creek (MC) drainage records fault-activity histories of the Mission Creek and Mill Creek strands of the San Andreas Fault (SAF) in the San Gorgonio Pass (SGP) region. We have investigated six surface remnants using geologic mapping, morphometric and stratigraphic analysis, geochronology of fills (IRSL) and surfaces (CRN), and pedogenic analysis. The surfaces cap distinct alluvial fills having clasts that we associate with sources in the Mission Creek drainage in the nearby San Bernardino Mtns. We have distinguished and correlated the disconnected surface remnants, based on morphometric analysis, including their longitudinal profiles, surface texture and drainage density. The degree of soil-profile development, when compared to other regional pedons that have been independently dated, constrains the timing of tectonic evolution. Pedogenic properties useful for age appraisals include tiron-extractable pedogenic silica, soil-development indices, increase in clay volume, and iron-oxide composition and content. Correlation to regional soil chronosequences indicates that the oldest MC surfaces are significantly older than 500 ka, although this age range (>500 ka) is particularly difficult to constrain with available geochronologic methods. IRSL dates of 106 and 95 Ka from (respectively) 5 and 4 m beneath the youngest pedon are consistent with age estimates based on soil-profile development. The oldest surfaces in the alluvial complex occur on deposits formed prior to movement along the Mill Creek strand of the SAF, and have been displaced approximately 8 km from their source across both the Mill Creek and Mission Creek fault strands in SGP. This is the same as a total slip estimate for the Mill Creek strand elsewhere in SGP, and indicates that there has been no movement on the Mission Creek strand since the emplacement of this deposit. The youngest deposits within this complex accumulated following cessation of movement along both the Mission Creek and Mill Creek strands, and mark the time after which slip had transferred onto the Banning and Garnet Hill strands. Summing total lateral slip accumulated on the fault strands in the eastern San Gorgonio Pass region, including the Mission Creek (0 km), Mill Creek (8 km), Banning and Garnet Hill (2-3 km), during the past approximately 500 ka results in a maximum long-term slip rate of 20 – 22 mm/yr. This agrees well some models of tectonic evolution, but not others.

QUAKE CATCHER NETWORK (QCN) SEISMIC SENSOR DEPLOYMENT GAME (A-009)

D.L. Kilb, A. Yang, and D. Rohrlick

The Kinect technology allows for hands-free game play, greatly increasing the accessibility of gaming for those uncomfortable using controllers. How it works is the Kinect camera transmits invisible near-infrared light and measures its "time of flight" to

reflect off an object, allowing it to distinguish objects within 1 centimeter in depth and 3 mm in height and width. The middleware can also respond to body gestures and voice commands. Here, we use the Kinect Windows SDK software to create a game that mimics how scientists deploy seismic instruments following a large earthquake. The educational goal of the game is to allow the players to explore 3D space as they learn about the Quake Catcher Network's (QCN) Rapid Aftershock Mobilization Program (RAMP). Many of the scenarios within the game are taken from factual RAMP experiences. To date, only the PC platform (or a Mac running PC emulator software) is available for use, but we hope to move to other platforms (e.g., Xbox 360, iPad, iPhone) as they become available. The game is written in programming language C# using Microsoft XNA and Visual Studio 2010, graphic shading is added using High Level Shader Language (HLSL), and rendering is produced using XNA's graphics libraries. Key elements of the game include selecting sensor locations, adequately installing the sensor, and monitoring the incoming data. During game play aftershocks can occur unexpectedly, as can other problems that require attention (e.g., power outages, equipment failure, and theft). The player accrues points for quickly deploying the first sensor (recording as many initial aftershocks as possible), correctly installing the sensors (orientation with respect to north, properly securing, and testing), distributing the sensors adequately in the region, and troubleshooting problems. One can also net points for efficient use of game play time. Setting up for game play in your local environment requires: (1) the Kinect hardware (~$145); (2) a computer with a Windows operating system (Mac users can use a Windows emulator); and (3) our free QCN game software (available from http://quakeinfo.ucsd.edu/~dkilb/WEB/QCN/Downloads.html).

FAULT SLICKENLINES, ROUGHNESS AND INELASTIC DEFORMATION (A-087)

J.D. Kirkpatrick and E.E. Brodsky

Repeated measurements show that fault roughness is self affine with anisotropic scaling exponents within typical exposure length scales. Displacement across a geometrically matched, bumpy fault requires some deformation of the wall rocks for the opposing sides of the fault to remain in contact. Strain in the wall rock induces stresses that, when resolved onto the fault surface, cause the maximum shear stress direction to deflect from the direction imposed by the tectonic load. In the slip-parallel direction, a Hurst exponent of 0.6 predicts that the strains required to flatten small amplitude, short bumps are greater than those for larger amplitude, long bumps. Short length scales should therefore induce the greatest stresses in the wall rock and deflect shear stresses the most. We measure the orientation of slickenlines that form parallel to the maximum shear stress direction on fault surfaces using ground-based LiDAR. Slickenlines defined in the field are compared to the curvature of the fault surface. Consistent principal curvature directions closely match the field measurements, and provide a basis for measuring slickenline orientations across large areas of fault surfaces. Deflection of the slickenlines from the mean orientation is limited to a few degrees in all faults analyzed. In addition, there is no correlation between the amount of deflection and the local fault topography. We explore the spatial structure of fault surface roughness and show that the strain from flattening bumps at short length scales exceeds the typical yield strain of rock. This implies that the material fails inelastically in small bumps. The lack of slickenline deflection suggests short length scales consequently support little stress. Because the roughness is self-affine there must be a cross-over length scale at which the strain remains below the yield value. Peak strains estimated from the amplitude (~0.1-0.3m) of the biggest bumps in exposed fault surfaces (lengths ~10-20m in the slip direction) is of the order of 0.01. Elastic stresses therefore become important at length scales of a few tens of meters and the roughness at shorter scales is the product of inelastic deformation. Models of earthquake rupture that incorporate laboratory-scale constitutive laws should also include the inelastic yielding of the wallrock that occurs at length scales up to tens of meters.

TETEMOKO: AN ADAPTIVE MESH REFINEMENT FRAMEWORK FOR DYNAMIC RUPTURE SIMULATION (A-080)

J.E. Kozdon and E.M. Dunham

Tetemoko is an adaptive mesh refinement (AMR) code in development for dynamic rupture simulations. The main promise of AMR is that grid resolution is dynamically allocated in response to the local resolution needs of the solution. For dynamic rupture simulations these resolution needs are largely dictated by the nearly-singular nature of the solution around the propagating rupture front. When laboratory measured friction parameters are used, sub-meter grid spacing is required to resolve the solution. This has forced the modelling community to artificially enhance the frictional parameters used in large-scale earthquake simulations. It is largely unknown what is lost by this procedure, and one of the goals of this project is to address this.

In past meetings we have outlined the AMR framework for dynamic rupture simulations and have validated our code against the SCEC TPV205 problem (slip-weakening friction and a homogeneous half-space). Here we present an extension of the code to include rate-and-state friction and plasticity. This combination will enable us to determine if the occurrence of plasticity

near the rupture front prevents development of the extreme gradients in stress and velocity, thereby lessening the resolution needs. The AMR simulation with Tetemoko results are validated by comparison with a high-order finite difference method.

AFTERSHOCK RELOCATION IN THE YUHA DESERT FOLLOWING THE 4 APRIL 2010 M7.2 EL MAYOR-CUCAPAH EARTHQUAKE (B-046)

K.A. Kroll, E.S. Cochran, and K.B. Richards-Dinger

Following the 4 April 2010 El Mayor-Cucapah earthquake, 8 temporary seismometers were installed in the Yuha Desert region north of the Mexican border. During the deployment period, between 6 April and 14 June 2010, over 4,000 aftershocks, within a 20km by 14km study area in the Yuha Desert, are reported in the SCEDC catalog. We relocate the aftershocks and also determine shallow crustal anisotropy to illuminate the complex fault structure in this region.

We compute the double difference hypocenter relocations using hypoDD with both manually picked P and S phase arrivals and waveform cross-correlations. We test three velocity models based on the Imperial Valley profile from the SCEC Community Velocity Model, Version 4 (CVM-S4), including the original profile and the profile with a 10% and 20% velocity reduction in Vp/Vs. We use a jackknife test in which the relocations are recomputed with one of the 13 stations removed in each test to estimate horizontal and vertical relative errors. By comparison with the LSQR errors of hypoDD, we find that scaling the LSQR errors by the jackknife/ LSQR error ratio provides a better error estimate. We find that the Imperial Valley profile with a 10% velocity reduction results in the lowest location errors. The absolute and relative relocation errors were reduced by at least an order of magnitude when compared to the original SCEDC catalog locations. We then use statistical uncertainties in the data to identify simple structures in the cloud of earthquake relocations. This modified collapsing method employs principal component analysis to identify three types of structures that a set of closely located events is most likely associated with: point, line or plane. With this method, collapsed locations provide insight to the poorly understood geologic structures in the Yuha Desert.

SCEC BROADBAND PLATFORM STRONG GROUND MOTION SIMULATIONS (B-020)

S. Kumar, S. Callaghan, P.J. Maechling, K.B. Olsen, R. Archuleta, P. Somerville, R. Graves, T.H. Jordan, and the Broadband Platform Working Group

The Southern California Earthquake Center (SCEC) Broadband Platform is a collaborative software development project involving SCEC researchers, graduate students, and the SCEC Community Modeling Environment. The goal of the SCEC Broadband Simulation Platform is to generate broadband (0-10 Hz) ground motions for earthquakes using deterministic low-frequency and stochastic high-frequency simulations. SCEC developers have integrated complex scientific modules for rupture generation, low-frequency deterministic seismogram synthesis, high-frequency stochastic seismogram synthesis, and non-linear site effects calculation into a system that supports easy on-demand computation of broadband seismograms. The SCEC Broadband platform has two primary modes of operation, validation mode, and scenario mode. In validation mode, the earthquake modeling software calculates broadband seismograms for one of three earthquakes, Northridge, Loma Prieta, or Landers at sites with observed strong motion data. Then, the platform calculates goodness of fit measurements that quantify how well the model-based broadband seismograms match the observed seismograms for each event. In scenario mode, the user can specify a scenario earthquake and a list of sites and calculate ground motions at each site for the scenario event. In February 2011, SCEC released Broadband Platform 11.2 as an open-source scientific software distribution. Since that time, we have continued development of the platform by adding a new site response module and new goodness of fit measures by Mayhew and Olsen. Along with a source code distribution of the Broadband Platform, we now offer a virtual software image distribution of the platform to support its use on a variety of computing hardware and operating systems.

GROUND MOTION PREDICTION EQUATIONS FOR DATA RECORDED IN THE IMMEDIATE VICINITY OF THE SAN JACINTO FAULT ZONE (B-019)

I. Kurzon, F.L. Vernon, and Y. Ben-Zion

We present a new set of empirical Ground Motion results for horizontal Peak Ground Acceleration (PGA) and Peak Ground Velocity (PGV) that include data from the immediate vicinity of the San Jacinto fault zone. The results to date are based on earthquakes in the magnitude range of $1 < M < 5.5$ recorded by up to 60 stations at distances ranging from the fault zone itself up to 120km. The data are examined and compared against several models of Ground Motion Prediction Equations (GMPE). The New Generation Attenuation (NGA) project was focused on a magnitude range of $M > 5$ (e.g., Campbell & Bozorgnia 2006, Boore & Atkinson 2006); therefore, our main comparison is with the ShakeMap system results (Quitoriano 2003 for $M < 5.3$) and with Cua & Heaton (2008) GMPE accounting for a magnitude range of $2 < M < 8$.

The data employed so far involves several aftershock sequences on small and known fault segments. These constrains allow for better consideration of the path and site effects, including the path in the near vicinity of the source. Therefore, as opposed to most models (using either the epicentral distance for low magnitude events or the closest surface projection of the fault for stronger events) we consider the hypocentral source-receiver distance as controlling both the geometrical spreading and the inelastic path effects. This approach is not only more physical for M < 5 events, but also reveals the upper crustal heterogeneity (< 20km) in the San Jacinto Fault Zone area. The continuing work will focus on incorporating more data as it becomes available, and using the results to develop updated Ground Motion Prediction Equations. The results will be useful for earthquake engineering and for exploring the crustal heterogeneity around active faults.

LOCAL AND REGIONAL SEISMIC RESPONSE TO INJECTION AND PRODUCTION AT THE SALTON SEA GEOTHERMAL FIELD, SOUTHERN CALIFORNIA (B-061)

L.J. Lajoie and E.E. Brodsky

California hosts both the largest geothermal resource capacity and highest seismicity rate in the nation. With plans to increase geothermal output, and proven earthquake triggering in the vicinity of geothermal power plants worldwide, it is important to determine the local and regional effects of geothermal power production. This study focuses on relating the volume of fluid extracted from and re-injected into wells at the Salton Sea geothermal field (SSGF) in Southern California to local seismicity rate and increased probability of larger events on nearby faults such as the San Andreas and Imperial faults. Seismic data is obtained from the publicly available Advanced National Seismic System (ANSS) catalog and SSGF injection and production data from the State of California Department of Conservation. We identify triggered earthquakes in the catalog by modeling seismicity in a 15km radius around the SSGF according to an Epidemic-Type Aftershock Sequence (ETAS) method. The model seeks to fit the cumulative seismicity curve from our dataset by optimizing five seismic parameters in accordance with Gutenberg-Richter and Omori's law. The modeled curve is then removed from the dataset to isolate the non-ETAS, or production-triggered, signal. We then formulate a constitutive law to relate the seismicity rate to the driving stress (i.e. volumetric strain in the reservoir). Defining the local stressing rate provides a tool for predicting the effects that production has on regional seismicity rates.

The largest spike in SSGF net production volume over the past 30 years is accompanied by the one of the largest increases in both seismicity rate and moment release within the geothermal field. This indicates a direct coupling between net fluid production volume (volume extracted minus volume re-injected) and seismicity rate and cumulative seismic moment in the field. Three dimensional plots of hypocentral earthquake locations show that seismicity is concentrated on an approximately NW-SE striking plane that dips shallowly to the west. Numerous inactive low angle normal faults with the same orientation have been mapped within and bounding the Salton Trough, suggesting the fault underlying the SSGF could be a reactivated detachment fault. Elevated seismicity rates on the detachment increases the probability of a larger earthquake on the fault that could directly trigger an event on the San Andreas fault.

ELASTOSTATIC SOLUTIONS FOR REALISTIC SLIP AND STRESS AROUND MODE II AND III CRACKS (A-111)

V.R. Lambert, S. Barbot, and J. Avouac

A common practice for analyzing the displacement and stress caused by slip on buried faults is to discretize the fault area into finite size patches of assumed uniform slip and use the corresponding Green's functions to predict strain at the surface or within the bulk of the medium. This formalism is commonly used to invert observation of co-seismic deformation for fault slip, in afterslip analyses, stress transfer studies and in numerical models of the seismic cycle, such as the Uniform California Earthquake Rupture Forecast (UCERF). The discretization of the fault into areas of uniform slip introduces stress singularities at the edges of each patch, which might make the results quite sensitive to the choice of the discretization scheme. Yet, little attention has been paid to this issue so far. Here, we derive analytic expressions of the Green's functions, for which the Okada's solution is a special case. We derive a full-space formulation for linearly interpolated fault slip distributions, which allows discretization of any fault slip distributions without introducing stress singularities. We investigate the case of a finite crack with a uniform distribution of stress on the fault. We show that the Okada solution provides an inadequate representation of the stress distribution for mode II and III cracks, even in the limit of infinitely small discretization. We introduce a critical size of fault discretization below which stress singularities dominate and bias the distribution. Our tapered-slip solution does not suffer from these shortcomings, suppresses all singularities and converges to a uniform stress with smaller discretization. Our results demonstrate the need to resolve the areas of stress concentration in our models of fault slip evolution.

CRUSTAL STRUCTURE OF THE SALTON TROUGH AND SOUTHERN SAN ANDREAS FAULT FROM NEW GRAVITY AND MAGNETIC DATA (B-137)

V.E. Langenheim, D.S. Scheirer, and N.D. Athens

Gravity and magnetic data shed light on the subsurface structure of the southern San Andreas fault and Salton Trough. Regional gravity features include a prominent narrow gravity low in Coachella Valley that decreases in amplitude to the southeast near the north shore of the Salton Sea. At the south end of the Salton Sea, the gravity low has become a large gravity high that has been attributed to crustal thinning and mafic lower crust. The northeast margin of the gravity low is linear and coincides with the San Andreas fault and with a significant magnetic high that is sourced by crystalline basement rocks of the Little San Bernardino Mountains. The southwest margin is also marked by a gravity gradient, but is not linear in plan view and the gradient is generally less steep. The gradient mimics the irregular contact of pre-Cenozoic basement rocks and Cenozoic basin fill.

New gravity data were collected to augment existing data along transects of the Salton Seismic Imaging Project. Measurement spacing averaged about 800 m, except along the high-resolution seismic line near Salt Creek, where a grid of gravity measurements spaced about 400 m is supplemented by ground magnetic transects. The detailed geophysical data suggest the San Andreas fault zone that is about 500-1000 m wide. Between Indio and Salt Creek, the fault is located near the base of the southwest-facing steep gravity gradient, indicating a steep northeast dip of the basement contact, with higher-density rocks northeast of the fault. North of Indio, the gradient becomes more diffuse, suggestive of a gentler northeast dip. About 5 km south of Salt Creek, the fault changes its position relative to the gravity field and is located at the top of a northeast-facing gravity gradient. This is also suggestive of a northeast dip, but instead places high-density material on the southwest side against low-density rocks on the northeast side of the fault. A northwest-trending, 20-km-long gravity low northeast of the San Andreas fault could speculatively reflect a basin formed by a right step between the San Andreas and the Hot Springs fault. In this region, the active San Andreas fault curves to the south into the Brawley Seismic Zone and large positive gravity and magnetic anomalies indicate intrusions of mafic material.

ON THE QUANTIFICATION OF ROBUSTNESS WHEN COMPARING KINEMATIC INVERSION MODELS: A WAVELET APPROACH (B-033)

D. Lavallee, G. Shao, and C. Ji

The Source Inversion Validation (SIV) project (Mai et al. 2011; *http://siv.usc.edu/*) is an ongoing effort to assess the reliability and consistency of earthquake source inversion. In this project, multiple inversion codes are used to constrain slip models from synthetic ground motions generated from a synthetic model. Researchers attempt to understand the resolution of fault inversions by comparing the inverted models and the synthetic model. Apparently, the algorithms that quantitatively evaluate the similarity between two 2D models are crucial for such a task. In view of the intrinsic scale and position dependent nature of the slip distribution, a 2D wavelet based procedure is developed to study the interdependence between the different slip spatial distributions as a function of the spatial resolution. Quantification of the interdependence can then be used to assess the quality of the fit between slip models.

Decomposition of a 2D data set with a 2D discrete wavelet transform provides four sets of coefficients. One set of coefficients essentially consists of a rescaled version of the original data and is used to compute additional wavelet coefficients at lower resolutions. The three other sets of coefficients are designed to capture the diagonal, horizontal and vertical patterns, respectively, embedded in the 2D data set. The basic idea of the procedure is to pair the synthetic model with a computed slip inversion and compare the match of their diagonal, horizontal and vertical patterns. For instance, the quantification of the matching of the diagonal patterns is achieved by computing the correlation between the wavelet coefficients characterizing the diagonal patterns. This operation is repeated at different resolutions. The same procedure is applied to the wavelet coefficients characterizing the horizontal and vertical patterns.

To account for the presence of additional constants in the computed slip inversion, we also compare the square norm of the wavelet coefficients of both slip distributions as a function of the resolution. This investigation provides the (relative) weight of the dominant patterns in the data sets. The square norm is computed for the wavelet coefficients characterizing the diagonal, horizontal and vertical patterns.

The procedure discussed above is applied to different pairs of slip models taken from a bank of slip models computed by Ji and Shao (2010) (*http://adsabs.harvard.edu/abs/2010AGUFM.S53C1994J*).

CHARACTERISTICS OF QUARTZ AND FELDSPAR LUMINESCENCE FROM SOUTHERN CALIFORNIA, USA: IMPLICATIONS FOR PALEOSEISMIC AND FAULT SLIP-RATE STUDIES (A-131)

M.J. Lawson, B.J. Roder, D.M. Stang, E.J. Rhodes, L. McAuliffe, J.F. Dolan, and S.F. McGill

Southern California comprises a wide range of diverse landscapes and environments, from high mountains with glacial and periglacial sediments to deserts with large sand dunes, extensive alluvial fans and ephemeral playas. Highly active tectonic processes have exposed ancient (c. 2 Ga) plutonic and metamorphic basement from deep within the crust, while similar Paleozoic and Mesozoic rocks are also common. A rich array of volcanic lithologies extending into the late Quaternary complement many thick sedimentary sequences that formed in equally diverse ancient environments typical of an accreting active continental margin. In some locations, notably in the Coachella Valley close to Palm Springs and the Salton Sea, low OSL sensitivity and poor characteristics restrict the application of quartz to date late Pleistocene and Holocene fluvial sediments, leading to increased age uncertainties in comparison to other places. In other locations such as the Malibu coastline, high sensitivity of the quartz OSL signal is observed. Problems of poor quartz characteristics, along with uncertainty in predicting quartz OSL behaviour for future dating campaigns poses a problem for projects, in particular for neotectonic contexts, including paleoseismic and fault slip-rate studies. While K-feldspar has been used extensively to date eolian and fluvial sediments in southern California, little information regarding signal stability is available. We explore the characteristics of both quartz and feldspar subsamples from alluvial fan contexts, in addition to eolian, fluvial, lacustrine environments, in order to help develop mineral selection criteria for optical dating applications and clarify these issues. Key issues include signal bleachability (how rapidly the signals are reset by light exposure), signal sensitivity, the presence of fading after laboratory irradiation and the reproducibility of age estimates. The importance of dose quenching in quartz grains recently eroded from bedrock, and the role of wildfire in enhancing OSL sensitivity are considered. The relative bleachability of quartz and feldspar fractions, along with thermal stability considerations are discussed, as part of a process designed to select an optimal approach for dating sediments typically encountered as part of paleoseismic and fault slip-rate studies. This presentation represents fundamental research being conducted as part of SCEC award #11198.

FULL-3D WAVEFORM TOMOGRAPHY FOR SOUTHERN CALIFORNIA (A-032)

E. Lee, P. Chen, T.H. Jordan, P.J. Maechling, M. Denolle, and G.C. Beroza

Our full-3D tomography (F3DT) uses 3D SCEC Community Velocity Model Version 4.0 (CVM4) in Southern California as initial model, a staggered-grid finite-difference code to simulate seismic wave propagation and the sensitivity (Fréchet) kernels are calculated based on the scattering integral and adjoint methods to iteratively improve the model. We use both earthquake recordings and ambient noise Green's function data, stacking of station-to-station correlations of ambient seismic noise, in our F3DT inversions. To reduce errors of earthquake sources, the epicenters and source parameters of earthquakes used in our F3DT are inverted based on full-wave method. In the first two iterations, we used scattering integral to construct sensitivity (Fréchet) kernels of broadband phase-delay measurements and LSQR algorithm to invert 3D perturbations. In first iteration, we only used waveforms from regional earthquakes and the waveforms of updated model generally provide better fit to the observed waveforms. In second iteration, we only used ambient noise Green's function data in inversion and the synthetic waveforms generated by updated model not only improved ambient noise Green's function waveform fittings but also earthquake waveform similarities. Since the waveform fittings of earthquake waveforms and ambient noise Green's function data are improved after first two iterations, we start to combine frequency dependent measurements made on waveforms of earthquake and ambient noise Green's function data and to use adjoint method for structure perturbations. After six iterations, the current model reduced the variance of the waveform misfit more than 55%.

NEAR REAL-TIME FULL-WAVE CENTROID MOMENT TENSOR (CMT) INVERSION FOR GROUND-MOTION FORECAST IN 3D EARTH STRUCTURE OF SOUTHERN CALIFORNIA (A-036)

E. Lee, P. Chen, T.H. Jordan, and P.J. Maechling

Accurate and rapid CMT inversion is important for seismic hazard analysis. We have developed an algorithm for very rapid full-wave CMT inversions in a 3D Earth structure model and applied it on earthquakes recorded by the Southern California Seismic Network (SCSN). The procedure relies on the use of receiver-side Green tensors (RGTs), which comprise the spatial-temporal displacements produced by the three orthogonal unit impulsive point forces acting at the receiver. We have constructed a RGT database for 219 broadband stations in Southern California using an updated version of the 3D SCEC Community Velocity Model (CVM) version 4.0 and a staggered-grid finite-difference code. Finite-difference synthetic seismograms for any earthquake in our modeling volume can be simply calculated by extracting a small, source-centered

volume from the RGT database and applying the reciprocity principle. We have developed an automated algorithm that combines a grid-search for suitable epicenter and focal mechanisms with a gradient-descent method that further refines the grid-search results. In this algorithm, the CMT solutions are inverted near real-time by using waveform in a 3D Earth structure. Comparing with the CMT solutions provided by the Southern California Seismic Network (SCSN) shows that our solutions generally provide better fit to the observed waveforms. Our algorithm may provide more robust CMT solutions for earthquakes in Southern California. In addition, the rapid and accurate full-wave CMT inversion has potential to extent to accurate near real-time ground motion prediction based on 3D structure model for earthquake early warning purpose. When combined with real-time telemetered waveform recordings, our algorithm can provide (near) real-time ground-motion forecast.

AFTERSHOCK STATISTICS OF THE 1999 CHI-CHI, TAIWAN EARTHQUAKE (B-107)

Y.-T. Lee, D.L. Turcotte, J.B. Rundle, and C.-C. Chen

We analyze the three scaling laws for the aftershock sequences from the Chi-Chi earthquake in Taiwan. The aftershocks are in good agreement with the Gutenberg-Richter law for frequency-magnitude scaling and the Chi-Chi aftershock decay rates satisfy the modified Omori's law. We also consider the statistics of interoccurrence times for Chi-Chi aftershocks. The observed statistics of interoccurrence times for the Chi-Chi earthquake sequence has a power-law dependence on the times between successive aftershocks over several orders of magnitude. In this study, we also apply the concept of Omori times to analyze the interoccurrence times for the Chi-Chi aftershock sequence. We calculate the mean interoccurrence interval over a fixed number of aftershocks N = 25, 50, 100, 200, and compare the Chi-Chi aftershocks with a combination of Omori decay and a steady-state background. We consider the Omori times result for the full seismic cycle from 1994 to 2008. Compare seismicity for the six years period prior to Chi-Chi earthquake with the seismicity for the eight years period following the Chi-Chi earthquake. Apparently the aftershocks of Chi-Chi earthquake still exist.

PROBING CALIFORNIA'S COASTLINE TO UNEARTH TRACES OF PALEOTSUNAMIS: IMPLICATIONS FOR THE NEXT USGS MULTI-HAZARDS SCENARIO (B-086)

R. Leeper, N. Graehl, E. Hemphill-Haley, D. Hoirup, B. Jaffe, H. Kelsey, R. Peters, and R. Wilson

Paleotsunami data along the California coast are rare and the data that do exist are limited to northern California. For a better understanding of the tsunami threat throughout central and southern California, prehistoric data need to be unearthed and documented in these regions. To accomplish this, the USGS Multi-Hazards Demonstration Project (MHDP) has brought together scientists from the USGS, California Geological Survey (CGS), and Humboldt State University to identify traces and develop a prehistoric tsunami inundation chronology. These data will provide geologic evidence to support the next MHDP scenario, which will consider the effect on California of a tsunami generated by a major earthquake in the eastern Aleutian Islands.

Research sites were determined by reviewing previous paleotsunami reconnaissance and research, considering coastal geomorphology and historic site-disturbance, and use of tsunami run-up data from the latest numerical tsunami models. These models were developed collaboratively by the CGS, California Emergency Management Agency, and the Tsunami Research Center at the University of Southern California. In response to a major earthquake in the eastern Aleutian Islands, one scenario results in wave elevations in excess of 9 m at some locations along the central and northern California coast, and 4 m in portions of southern California. In late July 2011, reconnaissance fieldwork commenced in northern California south of Point Area and will continue southward along California's coast throughout 2011.

Results of the paleotsunami reconnaissance will set the stage for more in-depth research, which will get underway in early 2012. The final results of the study will be used by the State to better assess its tsunami hazard, especially for probabilistic tsunami hazard assessment, and incorporated by the MHDP into the next scenario.

HIGH-RESOLUTION MAPPING AND ANALYSIS OF BORDERLAND FAULTS USING MULTIBEAM BATHYMETRY DATA (B-132)

M.R. Legg, M. Kohler, D. Weeraratne, and N. Shintaku

We have processed new high-resolution swath bathymetry data to map active Borderland fault structures and provide more accurate estimation of offshore earthquake and tsunami potential. The new data obtained during deployment of a large OBS array last year are combined with existing data offshore southern California to produce more comprehensive maps of the seafloor morphology. Four areas of gridded bathymetry maps at 100-m grid spacing were developed. The first area covers

most of the northern Borderland from Point Arguello to the southern San Diego Trough offshore Baja California. The second area covers the northern part of the Inner Borderland and eastern Outer Borderland from San Nicolas Island to Oceanside centered around Catalina Basin and Santa Catalina Island. The third area covers the northern Outer Borderland, south of the Channel Islands and south of the San Nicolas Island escarpment. The fourth area covers the central Outer Borderland from San Nicolas Island to Velero Basin west of northern Baja California. New multibeam bathymetry tracklines were chosen to follow major seafloor escarpments where active faulting is expressed by scarps and other lineaments in the seafloor morphology. Area 2 (Catalina) provides coverage of the major San Clemente fault system including triple junctions (fault wedge tips of Crowell, 1974) where major active faults intersect at each end of the Catalina Ridge. Area 3 (North Ferrelo) provides coverage of the major Ferrelo fault zone that extends to the southeast from Santa Rosa Island for more than 300-km into Mexican waters. The northern section of the East Santa Cruz Basin fault zone (ESCB) lies within the third area. Area 4 (South Ferrelo) provides coverage of the southern two-thirds of the Ferrelo fault zone that lies within U.S. waters–existing data provide some coverage of this fault zone in Mexican waters to the south. The southern sections of the ESCB fall within the South Ferrelo map area. The transverse San Nicolas Island escarpment is covered by both Ferrelo map areas, with the southern map providing coverage of the intersection with the ESCB to the east and the northern map covering the intersection with the Ferrelo fault zone to the west. In preliminary analysis, we have identified numerous seafloor channels inferred to result from turbidite flows and deposition that may provide important piercing points where active faults are crossed, such as the San Diego Trough and San Pedro Basin fault zones.

SURFACE RUPTURE AND SLIP VARIATION INDUCED BY THE 2010 EL MAYOR – CUCAPAH EARTHQUAKE, BAJA CALIFORNIA, QUANTIFIED USING COSI-CORR ANALYSIS ON PRE- AND POST-EARTHQUAKE LIDAR ACQUISITIONS. (A-044)

S. Leprince, K.W. Hudnut, S. Akciz, A. Hinojosa Corona, and J.M. Fletcher

One-hundred and three years after the publication of the Lawson report on the Great 1906 earthquake, accurate documentation of surface deformation along the entire length of an earthquake is still challenging. Analysis of pre- and post-earthquake topographic data provides an opportunity to deliver the full 3D displacement field of the ground's surface. However, direct differencing of a pre- and post-earthquake digital topography model (DEM) generally leads to biased estimation of the vertical component of the deformation. Indeed, if the earthquake also produced significant horizontal motion, or if the pre- and post-earthquake DEM acquisitions exhibit non-negligible horizontal mis-registration, the vertical offset measured by direct differencing will be biased by the local topography gradient. To overcome this limitation, we use the COSI-Corr sub-pixel correlation algorithm to estimate the relative horizontal offset between the pre- and post- 2010 El Mayor – Cucapah earthquake high resolution LiDAR acquisitions. Compensating for the horizontal offset between the two LiDAR acquisitions allows us to estimate unbiased measurements of the vertical component of the surface fault rupture induced by the El Mayor – Cucapah earthquake. We will also show the limitations of the available dataset, such as aircraft jitter artifacts, which impaired accurate measurements of the horizontal component of the surface deformation. This analysis shows an unprecedented view of the complete vertical slip component of the rupture induced by the Mw 7.2 2010 El Mayor – Cucapah earthquake, sampled at every 5 m, over a length of about 100 km, and with a vertical accuracy of a few centimeters. Using sampling bins as narrow as 150 m and 1.5 km long, variations in the vertical component of an oblique slip earthquake are presented, with breaks along multiple fault-strands showing opposite dip directions and diffuse boundaries. Vertical displacement profiles across the entire fault rupture and selective horizontal displacement profiles will be shown. With the availability of high precision pre- and post-earthquake data, COSI-Corr has the ability to accurately document the variability of 3D surface slip along strike of an earthquake rupture. Such data can be used to investigate the causes of this variability, and improve our understanding of its influence on the pattern of ground shaking.

http://www.tectonics.caltech.edu/slip_history/spot_coseis/

PRELIMINARY EVALUATION OF THE 2010 SHAKEOUT EARTHQUAKE DRILL (A-025)

A. Leslie, L.A. Davis, M.M. Wood, and R. Green

An annual ShakeOut earthquake drill has been held in California since 2008. Evaluation of such efforts is essential to confirming successful implementation, assessing program effectiveness, and determining whether resources have been used efficiently. Evaluation activities have taken place for each of the ShakeOuts to date. Following the most recent ShakeOut in October of 2010, an internet survey was conducted with registrants 3 -7 weeks following the drill. A volunteer sample (N=1,879 of 8,726 registrants with valid email addresses; 22%) of registered ShakeOut participants was recruited to participate in the survey via email. The survey sample consisted of respondents who were California residents who were registered as

individuals (30%), organizations (46%), K-12 schools (16%), school districts (5%), and colleges/universities (3%). Process and outcome results will be reported and are being organized into a final report which will be made available to stakeholders and drill participants. The final report will include information such as respondent demographics, drill implementation, and preparedness actions taken both before and after conduct of the drill. This information can be utilized by drill participants to evaluate their own ShakeOut methods and to provide feedback for future drill improvements.

RECORDING FAULT-ZONE TRAPPED WAVES FROM AFTERSHOCKS OF THE M7.2 DARFIELD AND M6.3 CHRISTCHURCH EARTHQUAKE SEQUENCE FOR DOCUMENT OF SUBSURFACE DAMAGE ZONES (A-083)

Y-G. Li, G. Paucale, D. Gravely, J. Cherrington, and M. Alvarez

The M6.3 Christchurch earthquake struck the Canterbury region in NZ's South Island on 22 February 2011, following ~6 months after the Sept. 4, 2010 M7.1 Darfield earthquake in the same region. It is not know clearly whether the later M6.3 event is technically an aftershock because of its relationship to the ongoing activity since September last year, or it is a separate event, given its location on a separate fault system. In order to study the complicated subsurface structure of the damage zones caused by this sequence of earthquakes in NZ, under the support of NSF-RAPID Program, we deployed 12 PASSCAL seismographs in two ~300-m long seismic lines across the Greendale fault where the horizontal right-lateral slip of 4.5 m and vertical slip of 1.6 m were caused by the 2010 M7.2 Darfield earthquake and the aftershock zone of the M6.3 Christchurch earthquake, respectively, to record fault-zone trapped waves (FZTWs) generated by aftershocks, starting from May 5th, 2011. Two arrays have recorded the data for more than 300 M>3 aftershocks and more than ~1000 small aftershocks not located yet but with good signal-to-noise ratio. The data include M5.3, M6, M5.4 and M5.1 aftershocks with clustered events at depths of 10-15 km. Preliminary examination of the waveform data shows FZTWs clearly at stations located within the 50-75-m wide rupture zone with high density of en-echelon cracks on the ground surface along the Greendale fault. 3-D finite-difference simulations of these FZTWs show a distinct low-velocity zone (LVZ) at seismogenic depth, indicating that the Greendale fault has undergone strong dynamic stresses and pervasive cracking during the M7.2 Darfield earthquake. We interpret this LVZ as being a remnant of damage zone in dynamic ruptures that accumulated damage from historical earthquakes, but mainly from the most recent M7.2 mainshock. The zone co-seismically weakens in the mainshock subsequently heals (partially) during the interseismic period. More detailed results coming from a systematical analysis and modeling of the entire waveform data recorded in our RAMP experiment help us to document (1) the material property (width, velocity reduction, Q value and depth extension of damage zones of M7.2 Darfield and M6.3 Christchurch earthquakes, (2) the subsurface geometry of their principal slip planes, segmentation and connection, and (3) the procession of co-seismic damage and post-mainshock healing of fault zone rocks during this earthquake sequence.

MULTIPLE DOUBLE COUPLE ANALYSIS FOR M6-7 EARTHQUAKES (B-050)

X. Li, G. Shao, and C. Ji

We develop a Multiple Double Couple (MDC) source inverse algorithm to quickly explore the potential complex source with the same or different focal mechanisms of an earthquake. We have applied this method to study the global large earthquakes (Mw>8) using long-period records and obtained a couple of dependable results. In this study, low frequency signals recorded at near field broadband or/and strong motion stations are implemented to probe the source complexity of smaller earthquake based on our MDC method. Inversion speed is highly accelerated by employing OpenMP technique and we can typically obtain the results in a few minutes. Uncertainty of inverted parameters is explored by searching the ensemble of models with acceptable fit to the data. We first test this code using the well-studied 1999 M7.1 Hector Mine, California earthquake and then apply this method to study the complex 2010 Mw7.2 El Mayor-Cucapah earthquake, which is dominant by strike-slip motion but has a significant normal component.

STRESS-SLIP BEHAVIOR OF A SHEARED GRANULAR MATERIAL WITH GRAIN BREAKAGE USING THE SHEAR-TRANSFORMATION-ZONE THEORY (B-142)

C.K.C. Lieou, A.E. Elbanna, J.S. Langer, and J.M. Carlson

With an eye towards geophysical applications, we study the stress-slip behavior and energy dissipation in a sheared granular material with breakage through a reformulation of the shear-transformation-zone (STZ) theory of plastic deformation Our new theory accomodates the occurrence of grain breakage by means of a constitutive law, based on dimensional analysis alone, for the time evolution of the average grain size as a result of grain fragmentation. Our numerical results indicate that grain

breakage weakens the ability of a granular material to support a shear stress, even though grain breakage accounts for only a small fraction of the total energy dissipation.

HIGH-FREQUENCY AMBIENT NOISE TOMOGRAPHY USING INDUSTRIAL SEISMIC ARRAY IN LONG BEACH, CALIFORNIA (B-063)

F. Lin and R.W. Clayton

The ambient noise cross-correlation method has now routinely being applied to study shallow earth structure. Here we present the preliminary result of such application on an industrial array in Long Beach, California. The data was recorded by NodalSeismic Inc. The pilot study contains about 150 stations with 72 hours of data on each of the four local streets (Cherry Ave., Redonde Ave., Spring St., and Willow St.). After temporal normalization and spectrum whitening, cross-correlations are calculated and clear signals, which can be associated with air waves and surface waves, are observed between 1 and 20 Hz frequency. We perform frequency-time analysis (FTAN) to study the dispersion property of the observed signals. Besides demonstrating the applicable of the ambient noise method in a suburban area, we also present potential complexities in observed cross-correlations due to persistent regional noise sources.

GEODETIC SLIP RATES IN THE SOUTHERN SAN ANDREAS FAULT SYSTEM: INVESTIGATION OF THE EFFECTS OF HETEROGENEOUS ELASTIC STRUCTURE (A-057)

E. Lindsey and Y. Fialko

We investigate the importance of fault geometry and crustal heterogeneity on estimates of slip rates and locking depths of the Southern San Andreas fault (SAF) and San Jacinto fault (SJF). Previous estimates of geodetic slip rates in the Salton Sea region based on dislocation models have generally inferred a higher slip rate on the SAF (21-26 mm/yr) compared to the SJF (12-19 mm/yr). The inferred geodetic slip rate on the SAF is higher than recent geologic estimates representing average slip rates on time scales of 10^4-10^6 years. We investigate to what extent the geodetically inferred slip rate might be biased by incorrect assumptions about the fault geometry and neglect of spatial variations in crustal rigidity. To address this issue, we use a forward model that incorporates heterogeneous elastic moduli computed from the SCEC CVM-H seismic tomography model of Southern California. In our inversions we allow for a non-vertical SAF and a "blind" segment of the SJF, the previously suggested southern continuation of the Clark fault. The models are compared to surface velocities derived from a combination of all available continuous and campaign GPS sites in the region, processed in a consistent North American fixed frame (NAFD), and InSAR data spanning 18 years (1992-2010). These data sources are strongly complementary: while InSAR provides higher spatial resolution in the near-fault region, we find that GPS sites located more than 10 locking depths from the fault are required to resolve the trade-off between locking depth and fault slip rate. The parameter space is examined using an efficient Monte Carlo algorithm which approximates the joint probability distribution for the model parameters and allows for a formal evaluation of uncertainties and trade-offs. We estimate slip rates of 15(+/-2) mm/yr for the Southern San Andreas fault and a total of 23(+/-3) mm/yr for the two closely spaced branches of the southern San Jacinto fault, in reasonable agreement with geologic estimates. The locking depths are estimated at 9(+/-3) km and 16(+/-3) km for the SAF and SJF, respectively. The incorporation of realistic elastic properties serves to increase the estimated locking depths on both faults by 2-3 km, and decreases the estimated slip rate on the San Andreas fault by several mm/yr in comparison to a homogeneous elastic model.

SEISMIC SOURCE CHARACTERIZATION FOR THE LADWP VAN NORMAN COMPLEX AND ISSUES TO CONSIDER FOR UCERF3 IN THE NORTHERN SAN FERNANDO VALLEY, CA (A-125)

S. Lindvall, C. Kemp, J. Unruh, and D. O'Connell

A new seismic source model was developed to support the seismic hazard evaluation of the Los Angeles Department of Water & Power (LADWP) existing and proposed water storage, treatment, and conveyance facilities at the Van Norman Complex (VNC) located in the northern San Fernando Valley. The LADWP is the largest municipal utility in the USA and nearly 75% of the city's annual water supply flows through the VNC, which makes these reservoir, embankment, water treatment, and pipeline facilities critical to the City of Los Angeles. The VNC site, which lies in one of the most tectonically complex areas of the Transverse Ranges, has experienced strong near-field ground motions in both the 1971 M6.7 San Fernando and 1994 M6.7 Northridge earthquakes that ruptured faults adjacent to and beneath the VNC. The new seismic source characterization focused on detailed assessments of these and several other local fault sources that contribute most significantly to the VNC seismic hazard. The new seismic source characterization included the reprocessing and interpretation of nine oil-industry seismic reflection profiles in the northeastern San Fernando Valley to map subsurface strands of the Verdugo, Mission Hills,

and Northridge Hills faults. Integration of these subsurface seismic data with an analysis of tectonic geomorphology suggests that these three faults are continuous and represent a larger fault system. The new source model also added the Mission Hills and Santa Susana East faults as new sources, both of which define geomorphically expressed range fronts. These relatively short faults have not been included in recent regional source models (e.g., UCERF2) due to their relatively small dimensions. However, including these smaller faults is critical to the site hazard as they represent moderate magnitude, single-fault ruptures, as well as fill in gaps of potentially larger, multi-fault seismic sources. In an effort to capture a greater uncertainty in segmentation and fault behavior, the model allows for multi-fault ruptures for several sources, including the Santa Susana-Sierra Madre-Cucamonga fault system.

DOES THE TEAR FAULT MATTER? (A-078)

Q. Liu, R.J. Archuleta, and R.B. Smith

Faults are not planar; the geometry of the fault has introduced extra dimension of complexity into the earthquake physics problem. (Scholz, 1998; Wesnousky 2006) Dynamic triggering between adjacent faults could lead to cascading earthquakes thus changing the seismic hazard estimation dramatically. Previous work has address the multi-fault dynamic rupture problem in terms of piece-wise planar fault system (e.g. Harris and Day, 1993; Magistrale and Day, 1999). We are trying to study a similar but more realistic case with the Wasatch Fault. The Salt Lake City segment of the Wasatch Fault (SLCWF) is a curved normal fault, which poses a serious threat to the surrounding communities due to the potential of a Mw 7+ earthquake. In the middle of the segment there is a potential tear fault that would separate the northern and southern segments. We want to answer the following question: to what extent does the possible tear fault impact the dynamic rupture process. This problem needs a careful investigation about not only the rupture dynamic on a non-planar fault, but also several ingredients in dynamic rupture problems, such as hypocenter location, initial stress distribution, etc. We use a finite element method (Ma & Liu, 2006) to simulate the dynamics of a propagating rupture on SLCWF both with and without the tear fault.

NEW DEVELOPMENTS AND FUTURE APPLICATIONS OF THE COLLABORATORY FOR THE STUDY OF EARTHQUAKE PREDICTABILITY (CSEP) TESTING FRAMEWORK (B-118)

M. Liukis, D. Schorlemmer, J. Yu, P. Maechling, J. Zechar, T.H. Jordan, and he CSEP Working Group

Southern California Earthquake Center (SCEC) began development of the Collaboratory for the Study of Earthquake Predictability (CSEP) in January of 2006 with funding provided by the W. M. Keck Foundation. Since that time, scientists and software engineers have applied the scientific and computational principles of CSEP to develop several operational testing centers. The W. M. Keck Foundation Testing Center at SCEC, designed to conduct computational earthquake forecast experiments in California, began operations on September 1, 2007 and has been improved, optimized, and extended over the past four years. The implementation of the SCEC Testing Center has been guided by four design goals proposed by the Regional Earthquake Likelihood Models (RELM) working group: (1) Controlled Environment, (2) Transparency, (3) Comparability, and (4) Reproducibility. By meeting these goals, the CSEP testing framework can provide clear descriptions of how all registered earthquake forecasts are produced and evaluated. As of August 2011, there are four testing centers established around the globe, with 224 models under test. CSEP software is also available for personal use by scientists to perform independent study and evaluation of their model prior submitting it to the Testing Center (*http://northridge.usc.edu/trac/csep/wiki/MiniCSEP*). The SCEC Testing Center hosts intermediate-term and short-term alarm-based and rate-based forecasts for California, the Western Pacific, and a global testing region. We describe how the CSEP Testing Center at SCEC has been constructed to meet the design goals; we also present recent developments of the Testing Center and share our experiences operating the center since its inception. Additionally, we discuss how the CSEP infrastructure will be applied to geodetic transient detection, earthquake early warning and ground motion prediction experiments.

THE CLARK CO. PARCEL MAP AND IMPLICATIONS FOR EARTHQUAKE HAZARD DEFINITION IN SOUTHERN NEVADA (A-033)

J.N. Louie, W. Savran, B. Flinchum, G. Plank, S.K. Pullammanappallil, A. Pancha, and W.K. Hellmer

Clark County, Nevada has completed the nation's very first effort to map earthquake hazard class systematically through an entire urban area. The Parcel Map contains measurements of geotechnical shear velocity to 30 m depth obtained using SeisOpt® ReMi™ (© Optim, 2011) at over 10,000 separate sites in urban and urbanizing Clark County and the City of Henderson. These municipalities use the Parcel Map to assure compliance with the NEHRP provisions of the International Building Code. Leveraging the unprecedented detail of the Parcel Map, our multi-institutional collaboration is developing

"Next-Level ShakeZoning" procedures tailored for defining earthquake hazards in the Intermountain West. Current federally sponsored tools- the USGS hazard maps and ShakeMap, and FEMA HAZUS- were developed as statistical summaries to match earthquake data from California, Japan, and Taiwan. The 2008 Wells and Mogul events in Nevada showed in particular that the generalized statistical approach taken by ShakeMap cannot match actual data on shaking from earthquakes in the Intermountain West, even to first order. Next-Level ShakeZoning relies on physics and geology to define earthquake shaking hazards, rather than statistics. It follows theoretical and computational developments made over the past 20 years, to capitalize on detailed and specific local data sets and more accurately model the propagation and amplification of earthquake waves through the multiple geologic basins of the Intermountain West. Using the new Parcel Map in computing shaking in Las Vegas Valley for scenario earthquakes is crucial for obtaining realistic predictions of ground motions. In an educational element of the project, a dozen undergraduate students are computing 50 separate earthquake scenarios affecting Las Vegas Valley, using the Next-Level ShakeZoning process. Despite affecting only the upper 30 m, the Vs30 geotechnical shear-velocity from the Parcel Map shows clear effects on even the longer-wavelength 0.1-Hz to 0.5-Hz shaking predictions. The fully 3-d Next-Level ShakeZoning scenarios show many areas of shaking amplification and de-amplification that USGS ShakeMap scenarios cannot predict.

ANALYTIC CALCULATION OF STRESSING RATES IN SOUTHERN CALIFORNIA (B-148)

J.P. Loveless and B.J. Meade

During the interseismic phase of the earthquake cycle stresses on faults evolves in response to elastic strain accumulation driven by tectonic plate motions. Because earthquake cycle processes induce non-local stress changes, the interseismic stress accumulation rate on one fault is influenced by the behavior of all nearby faults. Here we calculate stressing rates throughout the upper crust in southern California using a three-dimensional fault system model constrained by GPS observations. Stressing rates on all faults are calculated analyticallying used dislocation theory without the need to spatially differentiate GPS velocity observations. Notably, the total interseismic elastic strain field generated by fault interactions within the southern California may increase stressing rates on the Mojave and San Bernardino sections of the San Andreas fault within the Big Bend region by up to 38% relative to estimates from isolated San Andreas models. Assuming steady fault system behavior since the 1857 Fort Tejon earthquake, stress accumulated on these sections due only to interaction with faults other than the San Andreas reaches 1 MPa, ~3 times larger than the coseismic and postseismic stress changes induced by recent southern California earthquakes.

THE EFFECTS OF INTERMEDIATE FAULT SEGMENTS ON RUPTURE BEHAVIOR AND GROUND MOTION IN STRIKE-SLIP STEPOVERS (A-075)

J.C. Lozos, D.D. Oglesby, J.N. Brune, and K.B. Olsen

Stepovers in natural faults are complex regions of deformation, fracturing, and smaller faulting; they rarely consist of two planar fault segments, as they are often modeled. While conducting dynamic models of completely realistically complex stepover systems is still computationally prohibitive, the present study investigates one common complexity: the presence of smaller intermediate fault segments between the two main faults. We investigate the effects of these segments on rupture behavior and ground motion in the stepover region using the three-dimensional finite element method. We align the intermediate segment with the projected point at which rupture jumps from main segment to main segment, so as to maximize its effect. We test intermediate segments of several different lengths and depths, and we test both extensional and compressional systems. For each of these geometries, we test two stress states: one in which rupture will jump the stepover in an analogous system with no intermediate segment, and one in which rupture does not jump in such a system. We find that, depending on the regional stress field and the size of the intermediate fault segment, the presence of this segment may either promote or inhibit throughgoing rupture at the stepover, and may either increase or decrease peak ground motion. The dependence of ground motion on intermediate fault size is not monotonic, and is can be different between extensional and compressional stepovers. These results may appear somewhat counterintuitive, but they may have important implications for fault-to-fault rupture probabilities, ground motion prediction, and overall seismic hazard calculation.

NUMERICAL SIMULATION OF SLOW SLIP TRIGGERED TREMOR MIGRATION AND RAPID TREMOR REVERSALS (A-100)

Y. Luo and J.P. Ampuero

Recently discovered slow-slip events (SSE) and non-volcanic tremors have greatly enriched the spectrum of earthquake behavior. These phenomena offer a unique window into the mechanics of the bottom of the seismogenic zone of active faults.

In an emergent view, this transition region has heterogeneous frictional properties, and is composed of frictionally unstable, velocity-weakening patches embedded in a frictionally stable fault region. Tremor swarms are viewed as the collective response of brittle asperities interacting through transient aseismic slip in their surroundings. A hierarchy of migration patterns of tremors has now been observed in the Cascadia subduction zone, including large-scale along-strike tremor propagation at ~10km/day and rare swarms that propagate 10 times faster in the opposite direction ('rapid tremor reversals'). A cascade of brittle asperity failures mediated by transient creep is an appealing model to explain these migration patterns. We performed a quantitative study of this model through numerical simulations of heterogeneous rate-and-state faults under the quasi-dynamic approximation, solved by a Boundary Element Method. We conveniently generated SSEs, propagating at ~10 km/day, by adopting an ad hoc rate-and-state friction law with a transition from velocity-weakening to strengthening. Brittle asperities are defined as small patches of velocity-weakening friction with shorter characteristic slip distance Dc, larger friction parameters a and b or higher effective normal stress (sigma) than their surroundings. The state variable is governed by the 'slip law', which allows conditionally stable behavior. A collection of brittle asperities is distributed along the fault. We studied the effect of their size and spacing and of the contrast of a*sigma and Dc with respect to the background. We successfully simulated both observed migration patterns. The slow forward migration is obviously due to tremor triggering near the leading front of the propagating SSE pulse. Less trivially, our model also produces RTRs with similar characteristics as in Cascadia: spatially scattered swarms back-propagating at fast speed ~100 km/day. These RTRs are rare because they nucleate at the asperities with largest Dc. While our model reproduces key features of the complex spatio-temporal organization of tremors as observed in Cascadia and Japan, this comes at the cost of tuning some model parameters. We will report the results of our parametric study.

ABSOLUTE STRESS IN SOUTHERN CALIFORNIA CONSTRAINED BY EARTHQUAKE FOCAL MECHANISMS AND MODELS OF STRESS CONTRIBUTIONS FROM TOPOGRAPHY AND FAULT LOADING (A-060)

K.M. Luttrell, D.T. Sandwell, and B.R. Smith-Konter

Earthquake focal mechanisms in southern California may be used as in situ indicators of the 3-D orientation of the stress field. This stress field is heterogeneous, as reflected by the presence of strike-slip, reverse, and normal faulting mechanisms in close proximity to one another. We attempt to reproduce these observations by accounting for the stress fields from three sources: 1) the 3-D crustal stress associated with the support of local topography (i.e., wavelengths less than ~350 km) at both the surface and Moho, as constrained by gravity observations; 2) the 3-D earthquake cycle stress accumulated on locked fault segments; and 3) a 2-D regionally uniform stress field representing plate boundary scale tectonic driving stress. The magnitude and orientation of the regional stress field are varied to obtain the best possible fit to the stress orientations indicated by earthquake focal mechanisms. For southern California, we find the non-lithostatic component of regional driving stress must consist of at least 30 MPa compression oriented at N15E. However the magnitude of the orthogonal component must be varied along the fault in order to simultaneously reproduce both the strike-slip and thrust mechanisms. This indicates that there is an additional E15S compressional stress in the big bend region that is not accounted for by the weight of topography and the earthquake cycle stress.

OBSERVATIONS OF RECENTLY-EXPOSED FUMAROLE FIELDS NEAR MULLET ISLAND, IMPERIAL VALLEY, CALIFORNIA (A-138)

D.K. Lynch, K.W. Hudnut, P.M. Adams, and L.S. Bernstein

New field observations, lidar measurements, aerial imaging and preliminary laboratory measurements of mud samples are reported of three formerly submerged fumarole fields in the Salton Trough near Mullet Island in southeastern California, USA. The fumarole fields have recently been exposed as the Salton Sea level has dropped. The largest of the three fields visited in January 2011 is irregular in outline with a marked northeast elongation. It is roughly 400 meters long and 120 meters wide. The field consists of approximately one hundred warm to boiling hot (100° C) mud volcanoes (0.1 – 2 m in height), several hundred mud pots, and countless CO2 gas vents. Unusual shaped mud volcanoes in the form of vertical tubes with central vents were observed in many places. Lidar measurements were obtained in the time period Nov 9-13, 2010 using an Optech Orion 200M lidar from an elevation 800 m AGL. They reveal that the terrain immediately surrounding the two fields that are above water level reside on a low (~0.5 m high) gently sloping mound about 500 m across that shows no evidence of lineaments indicative of surface faulting. With other geothermal features, the fumaroles define a well-defined line marking the probable trace of the Calipatria fault. Although the precise locations is uncertain, it appears to define a straight line 4 km long between the Davis-Schrimpf mud volcanoes and Mullet Island. Mullet Island is one of five late Quaternary rhyolitic volcanic

necks in the immediate area of the fumaroles. The Calipatria fault is subparallel to the San Andreas and Imperial faults and only one of many verified or suspected faults (including cross faults) in the complex tectonic setting of the Salton Trough. Mud from several volcanoes was analyzed using scanning electron microscopy (SEM), and energy dispersive X-ray spectroscopy (EDS). One sample contained boussingaultite, (NH4)2Mg(SO4)2·6(H2O), a rare mineral that is known to sublime under fumarolic conditions, possibly by ammoniation of hydrated MgSO4.

As the Salton Sea level continues to drop, the third fumarole field is expected to surface in the next couple of years. It is also likely that as more land emerges, many of the CO2 gas seeps currently under water will begin to form mud volcanoes and mud pots, most of them along the same NW trending axis as the others. At about the same time a land bridge will form to Mullet Island, the first in about 60 years.

IBEM3D: A REMOTE STRESS INVERSION PROGRAM HONORING MECHANICAL RELATIONSHIPS BETWEEN STRESS AND FAULT GEOMETRY (A-112)

E.H. Madden, F. Maerten, and D.D. Pollard

Aftershocks have been correlated spatially with changes to the Coulomb shear stress on optimally orientated planes (e.g. Stein and Lisowski, 1983; King et al, 1994) and static stress change on nodal planes inferred from focal mechanisms (e.g. Hardebeck et al, 1998; Seeber and Armbruster, 2000) due to slip on planar mainshock faults. The orientations of individual aftershocks have been mechanically related to the perturbed stress field from slip on non-planar faults, with distinct fault geometries producing the best-fit model Coulomb planes at aftershock hypocenters, as well as honoring the recorded slip distribution at Earth's surface (Madden and Pollard, 2011, submitted). However, stress inversions generally overlook these connections between aftershocks, fault geometry and stress perturbations. New inversion software, iBem3D (Maerten, 2010), uses a homogeneous remote stress with one principal axis vertical to drive slip on non-planar faults and determines the resulting stress state at all aftershock locations. The orientation and remote principal stress magnitudes that minimize the 'cost' or misfit between aftershock focal mechanisms and model Coulomb plane orientations or slip vectors are converged upon iteratively, over multiple model runs. The cost of individual aftershocks may be analyzed for systematic effects on inversion results of aftershock characteristics such as magnitude, distance in time and space from the mainshock, and focal mechanism uncertainty, or to determine locations where mainshock fault geometry may be incorrect, producing a cluster of aftershocks with large misfits. The sum of all individual costs quantitatively assesses the relative performance of inversions executed with different model geometries or subsets of aftershocks. In addition, relative costs are used to select one nodal plane, from the two provided by the aftershock focal mechanism, for inclusion in the inversion. Other observed data, such as the orientations of slickenlines, veins, or secondary faults, may be used to constrain the inversion, either in addition to, or instead of, aftershock focal mechanisms; the only change to iBem3D procedure is adjustment of the cost function applied.

COMPILATION OF SLIP IN LAST EARTHQUAKE DATA FOR HIGH-SLIP RATE FAULTS IN CALIFORNIA FOR INPUT INTO SLIP DEPENDENT RUPTURE FORECAST (A-129)

C.L. Madden Madugo, J.R. Arrowsmith, D.E. Haddad, J.B. Salisbury, and R.J. Weldon

Slip in the last earthquake along a fault, in conjunction with the application of appropriate recurrence models, can be used to estimate the timing and size of future ground-rupturing earthquakes. Surface slip measurements are relatively easy to acquire along highly active faults because offsets from the last event are often well preserved by geomorphic features in the landscape. We present a comprehensive database of slip measurements for high slip rate strike-slip and dip-slip faults in California for input into the slip-dependent 2011 Uniform California Earthquake Rupture Forecast (UCERF 3). Our database includes historic, paleoseismic, and geomorphic data on slip in the last event and multi-event offsets. Faults were prioritized by highest slip rates and longest time since the last event relative to average recurrence interval. Slip rate, timing of the last event, and recurrence interval were obtained from past reports by the Working Group on California Earthquake Probabilities, unless more recently published data were available. A literature search determined the availability of offset data for the highest priority faults. We contacted authors of published slip studies to ascertain whether additional data exist in unpublished archives, gray literature, or publications in preparation. Lack of consistency in existing schemes to rate offset quality led us to develop a new semi-quantitative method to asses feature and tectonic quality for new and existing data. Recent analyses of newly available, high-resolution LiDAR topography for micro-geomorphic offsets have substantially increased the number of slip measurements available for our compilation. For faults with LiDAR coverage, but limited offset data, we identified reaches with high potential to preserve geomorphic offsets and calculated slip measurements. The methodology for our geomorphic analyses has been developed and implemented successfully in recent studies along the central San Jacinto Fault and 1857 earthquake reach of the San Andreas Fault. Last, we compiled data collected from our literature search and LiDAR

analysis into a geodatabase. Our database contains multiple measurements for the same features using different techniques, making it a powerful tool to test the repeatability of slip measurements. Our compilation reveals that despite local variation, slip values tend to cluster around a reach averaged-mean, and slip can be similar at a point over multiple events.

INVESTIGATING THE IMPACT OF SPACE-GEODETIC DATA ON EARTHQUAKE RISK ANALYSES FOR CALIFORNIA (B-092)

C.M. Mak and M. Nyst

California is monitored by a dense network of GPS stations, producing a high resolution velocity field of the Earth's surface. One way of translating this velocity field into crustal deformation parameters that can be used in PSHA is the 'Block Model'. In the block model the crust is parameterized as a number of elastically deforming blocks, bounded by surfaces that represent the major active faults. Based on differences in underlying methods and assumptions they produce significant differences in terms of fault slip rates, geometry of the building blocks and location of the faults.

This study focuses on the impact of the inclusion of block models on earthquake risk in California. Earthquake risk combines earthquake hazard and building vulnerability to estimate the probable damage and loss of property and/or life. We look at the impact of space-geodetic data on risk by comparing loss results from traditional risk models, based on earthquake and geology data, with loss results from block models. More specifically, we will present what the impact of a geodetic deformation model on residential earthquake risk.

DEFORMATION RATES IN THE WESTERN TRANSVERSE RANGES, CALIFORNIA FROM THE SAN ANDREAS TO THE SANTA BARBARA CHANNEL MEASURED WITH GPS AND PERSISTENT SCATTERER INSAR (A-050)

S.T. Marshall, G.J. Funning, and S.E. Owen

We combine data from 52 continuous GPS sites in the Plate Boundary Observatory network with a persistent scatterer InSAR data set formed from ENVISAT ASAR data to determine the rates of seasonal, anthropogenic, and tectonic deformation in the western Transverse Ranges of southern California. To characterize seasonal motions, we independently estimate phases and amplitudes of annual and semiannual motions for each GPS time series. We remove these seasonal terms, and then perform Principal Component Analysis on the residual time series to remove any common-mode errors. The final time series are dominantly linear with a significant reduction in root-mean squared error, suggesting that the seasonal motions have been successfully removed. To determine if any of the remaining motions are non-tectonic in origin, we use a persistent scatterer InSAR (PSI) data set comprised of 21 ENVISAT scenes. The PSI data show potential anthropogenic deformation in the form of subsidence in the Oxnard/Ventura area as well as at a location just south of the Oak Ridge. No GPS stations are located near the areas of suspected anthropogenic motion, and so the GPS velocities are unlikely to be contaminated by non-tectonic motions. The relative lack of anthropogenic contamination of permanent GPS motion in the western Transverse Ranges is in stark contrast to the nearby Los Angeles basin where many permanent GPS stations record significant anthropogenic motions. To determine the local (within-basin) deformation rates, we remove strain associated with the nearby San Andreas fault using a rectangular dislocation model. The resultant velocity field shows dominantly north-northwest directed contraction. The central Ventura basin shows the fastest contraction rates with approximately 6 mm/yr of shortening. To the east, approaching the San Andreas fault, contraction rates slow to about 2 mm/yr Contraction rates across the Santa Barbara Channel appear to monotonically decrease westward from approximately 6 mm/yr at the longitude of Anacapa Island to 2 mm/yr at the longitude of San Miguel island. We estimate a regional strain rate tensor of approximately 100 nanostrains/yr oriented approximately north-south. Mismatches between the estimated regional strain and the strain estimated locally highlight areas of localized tectonic contraction.

A PROGRESS REPORT ON THE ARRA-FUNDED GEOTECHNICAL SITE CHARACTERIZATION PROJECT (B-004)

A. Martin, A. Yong, K. Stokoe, A. Di Matteo, S. Jack, and J. Diehl

For the past 18 months, the 2009 American Recovery and Reinvestment Act (ARRA) has funded geotechnical site characterizations at 189 seismographic station sites in California and the central U.S. This ongoing effort applies methods involving surface-wave techniques, which include the horizontal-to-vertical spectral ratio (HVSR) technique and one or more of the following: spectral analysis of surface wave (SASW), active and passive multi-channel analysis of surface wave (MASW) and passive array microtremor techniques. From this multi-method approach, shear-wave velocity profiles (Vs) and the time-averaged shear-wave velocity of the upper 30 meters (Vs30) are estimated for each site. To accommodate the variability in

local conditions (e.g., rural and urban soil locales, as well as weathered and competent rock sites), conventional field procedures are often modified ad-hoc to fit the unanticipated complexity at each location. For the majority of sites (>80%), fundamental-mode Rayleigh wave dispersion-based techniques are deployed and where complex geology is encountered, multiple test locations are made. Due to the presence of high velocity layers, about five percent of the locations require multi-mode inversion of Rayleigh wave (MASW-based) data or 3-D array-based inversion of SASW dispersion data, in combination with shallow P-wave seismic refraction and/or HVSR results. Where a strong impedance contrast (i.e. soil over rock) exists at shallow depth (about 10% of sites), dominant higher modes limit the use of Rayleigh wave dispersion techniques. Here, use of the Love wave dispersion technique, along with seismic refraction and/or HVSR data, is required to model the presence of shallow bedrock. At a small percentage of the sites, surface wave techniques are found not suitable for stand-alone deployment and site characterization is limited to the use of the seismic refraction technique. A USGS Open File Report--describing the surface geology, Vs profile and the calculated Vs30 for each site--will be prepared after the completion of the project in November 2011.

ASSESSING STRAIN ACCUMULATION RATES ACROSS THE PACIFIC-NORTH AMERICAN PLATE BOUNDARY NEAR SAN BERNARDINO, CALIFORNIA (A-053)

R.F. Mason, E.P. Upton, A. Grijalva, K.L. Muhammad, A. Torrens-Bonano, S.F. McGill, E. Alaniz, J. Spinler, R.A. and Bennett

The goal of this project was to achieve a more precise understanding of the strain accumulation rates of the various faults that make up the Pacific and North American plate boundaries in Southern California. We are particularly interested in the San Andreas Fault (SAF) and the San Jacinto Fault (SJF), which are likely sources of impending large earthquakes in Southern California. To do this, we used precise Global Positioning System (GPS) surveying equipment to measure site positions at 26 pre-established benchmarks throughout the San Bernardino Mountains and surrounding area. Using a spreadsheet, we then conducted one-dimensional elastic modeling of our velocity data, along with site velocities from SCEC's Crustal Motion Model 4 (CMM4), within a transect across the plate boundary passing through the San Bernardino Mountains. We tested about 3.2 million slip-rate combinations to find which ones produced a good fit to the measured site velocities. From the combinations that produced the best-fitting curves, we concluded that the SJF accounts for more movement (~12 mm/yr) along the plate boundary than does the SAF (~10 mm/yr). From combinations producing the reasonably well-fitting curves, our results show that the faults west of the SJF system could have slip-rates between 6-12 mm/yr, the SAF and SJF combined could have rates between 18-28 mm/yr (with most reasonable fits between 20-24mm/yr), and the ECSZ could have rates between 12-16 mm/yr.

CHARACTERIZING THE RECENT BEHAVIOR AND EARTHQUAKE POTENTIAL OF THE BLIND WESTERN SAN CAYETANO AND VENTURA FAULT SYSTEMS (A-124)

L.J. McAuliffe, J.F. Dolan, J. Hubbard, and J.H. Shaw

We are studying the activity and paleoearthquake history of the blind Ventura and western San Cayetano faults through a multidisciplinary analysis of strata that have been folded above the fault tiplines. These two thrust faults form the middle section of a >200-km-long, east-west belt of large, interconnected reverse faults that extends across southern California. Although each of these faults represents a major seismic source in its own right, we are exploring the possibility of even larger-magnitude, multi-segment ruptures that may link these faults to other major faults in the Transverse Ranges system. The proximity of this large reverse-fault system to several major population centers emphasizes the importance of understanding the behavior of these faults for seismic hazard assessment.

During the summer of 2010 we used a mini-vibrator source to acquire four, one- to three-km-long, high-resolution seismic reflection profiles. The profiles were collected along the locus of active folding above the blind, western San Cayetano and Ventura faults - specifically, across prominent fold scarps that have developed in response to recent slip on the underlying thrust ramps.

Our initial efforts to document the earthquake history and slip-rate of this large, multi-fault reverse fault system focus on a site above the blind, western San Cayetano thrust ramp. At Briggs Road ~14 km east of Ventura, a high-resolution profile across the locus of recent folding reveals a well-defined north-dipping active synclinal axial surface in growth strata that extends to the surface at a prominent south-facing fold scarp lying at the topographic range front. During August 2011, we drilled 11 hollow-stem boreholes and cone-penetrometer tests along the same alignment as the reflection profile, providing overlap between the data sets. Preliminary analysis of the borehole data reveals a fine-grained section dominated by thinly bedded

silts and sands. The absence of any well-developed soils within the upper 20 m, coupled with at least 15 m of structural growth within this section, suggests a rapid slip rate that we will quantify with radiocarbon dating of detrital charcoal and several buried organic-rich A horizons. Collectively, we anticipate that these borehole and high-resolution seismic reflection data will allow us to reconstruct the paleoseismic history of the underlying blind thrust ramp.

SLIP RATE OF THE NORTHERN SAN JACINTO FAULT FROM OFFSET LANDSLIDES IN THE SAN TIMOTEO BADLANDS (A-151)

S.F. McGill, L.A. Owen, E.O. Kent, T.K. Rockwell, and N.W. Onderdonk

A small restraining bend in the Claremont fault (northern San Jacinto fault zone) has produced basement uplift in the northern San Timoteo badlands. Bouldery debris has been shed from this basement uplift northeastward across the fault, through landslide and/or debris flow processes. These deposits, which we refer to as the Quincy Ridge debris fan, are now offset about 1.0 to 1.6 km across the San Jacinto fault, although further mapping is needed to fully constrain this offset. Be-10 dates from 6 boulders on the Quincy Ridge debris fan range from 16 to 68 ka. We regard the oldest date as closest to the true age of the landslide because the remaining boulders may have been more recently exhumed by surface deflation. This interpretation is confirmed by soil pits excavated next to the 68 ka boulder and next to one of the younger (26 ka) boulders. The 68 ka boulder may itself underestimate the age of the landslide. The soil pit next to this boulder revealed a silica-cemented horizon over-printed with clay-lined fractures below the main argillic horizon. The silica likely formed during a semi-arid climatic period (probably the last interglacial), and the translocated clay lining the fractures in the silica horizon likely formed during the last glacial period. This suggests that the debris fan may be as old as 100-125 ka. For a preliminary slip-rate estimate, we assume the 68 ka age is a minimum, which yields a maximum slip rate of 15-24 mm/yr. If the true age turns out to be ~ 100 ka, as the soils suggest, this rate would reduce to 10-16 mm/yr. Dates from three additional boulders, as well as OSL and Be-10 dates from a depth profile near the 68 ka boulder are pending

A younger landslide, the Ebenezer Canyon slide, is sourced from older landslide or debris-flow deposits and has been offset 270 100 m. Three boulders from the head scarp have Be-10 ages of 9 ka, 10 ka and 21 ka. The headscarp was suddenly exposed by the landslide event but may have continued unraveling over time. Thus, all three ages are likely to be minima, and we use 21 ka as a minimum age for the Ebenezer Canyon slide. The Be-10 ages of six boulders from the slide deposit itself range from 14 ka to 93 ka, with a cluster of three dates between 30-37 ka. We use the weighted average of these three dates (35.4 ka) as our preferred age of the Ebenezer Canyon slide. This yields a slip rate of about 10 mm/yr, with a 95% confidence interval of 5-18 mm/yr.

TRACKING COSMOGENIC 10BE IN MULTIPLE GRAINSIZES DOWN ALLUVIAL SYSTEMS IN ACTIVE OROGENS (A-140)

K.E. McGuire and R.V. Heermance

The concentration of cosmogenic 10Be in alluvial sediments can be used to interpret catchment-scale erosion rates. We have applied this method in two tectonically active catchments in the Transverse Ranges, Southern California: the upper Ventura River catchment and Millard Canyon within the Topatopa and San Bernardino Mountains, respectively. We use 10Be concentrations in multiple grain-sizes to determine the erosion rates, and understand geomorphic process and the implications of clast size variable 10Be concentrations by sampling spatially separated transects. Within the Ventura River drainage, spatially separated samples of both sand (0.25-0.50 mm) and pebbles (70-100 mm) were collected from the active channel and below Late Pleistocene and Holocene terrace surfaces. Results indicate average paleo-erosion rates for the Holocene to present from the sand size fraction are 180 ± 20 mm/ka, but rates determined from pebbles are 1010 ± 100 mm/ka, and Late Pleistocene pebble erosion rates are 530 ± 100 mm/ka. Pebbles imply at least a five times greater erosion rate than sand for the Holocene to present. Millard Canyon was sampled in the active channel in three locations over 4.7km near the catchment mouth over four grain sizes (0.25-0.500 mm, 1-2 mm, 11-22 mm, 100-250 mm). Clast size variable 10Be concentrations were not measured at or above the catchment mouth. Thus, the erosion rate using the average 10Be concentration from all grain sizes at the catchment mouth is 740 mm/ka. The 10Be concentration beyond the catchment mouth in the midfan 0.250-0.500mm sand fraction is enriched 1.4x the catchment mouth fraction; the midfan sand fraction is enriched 1.4x the midfan pebble concentration. These data show how 10Be concentration varies as a function of grain-size in the midfan transect. Incorporation of older sediment can alter the measured 10Be inventory; a sediment mixing model was used to determine the percentage of sediment of a known age that must be present in the active channel to return the observed concentrations. Results considering adjacent surface sediment suggests between 18-44 ± 9% of sediment in active channel is sourced from surfaces. The most likely pathway is aeolian saltation of grains. Our data indicate that 10Be concentration, and

thus erosion rates and exposure ages, vary with grain size and suggest sediment transport pathways and sources of sediment outside the catchment should be considered in any cosmogenic 10Be study.

QUATERNARY CONGLOMERATE DEPOSITION AND IMPLICATIONS ON FAULT EVOLUTION IN THE OJAI AND UPPER OJAI VALLEYS, WESTERN TRANSVERSE RANGES, CA (A-128)

H.L. McKay and R.V. Heermance

Ojai and Upper Ojai Valleys are intermontane basins in the western Transverse Ranges filled with Quaternary conglomerate (Ojai Conglomerate) that records a rare record of fault slip, uplift of surrounding ranges, evolution of the drainage system, and landscape development since mid Quaternary time. Here we combine mapping and stratigraphy of exhumed strata in the hanging walls of the Arroyo Parida-Santa Ana and La Vista faults and in the footwall of the Devil's Gulch/Lion fault with subsurface well data to document late-Quaternary provenance changes, depositional settings, and geometry of the basin fill. New measured sections, clast counts, paleocurrent measurements, and mapping suggest that an E-W paleodrainage system was present and sourced from the Topatopa Mountains to the north. Assymetrical depocenters 240 and 550 m deep in Ojai and Upper Ojai Valleys, respectively, are preserved beneath the valleys implying complex paleotopography was present during conglomerate deposition. At least 300 and 220 m of displacement must have occurred on the Lion and Santa Ana Faults, respectively, based on offset of the base of the conglomerate unit. Lion Creek flows through incised meanders in Lion Canyon that expose the basal contact of the basin fill and provide evidence for a much wider and flatter E-W paleovalley in the past between the Lion and Santa-Ana Faults. Age constraints on the conglomerate are limited. As evidenced by the cross cutting relationship between the deformed conglomerate and terrace surfaces, the fill must be older than the oldest terrace surface (~92,000 y.b.p). Although previously interpreted as correlative with mid-Quaternary Saugus Formation (200,000-800,000 y.b.p.), the local deposition, E-W directed paleocurrents, and buttress unconformity between the Quaternary conglomerate and Neogene basement suggests that the basin fill in Ojai and Upper Ojai valleys are a separate entity from the rest of the Ventura Basin stratigraphy. We therefore consider the onset of deposition of Ojai Conglomerate to be middle-late Pleistocene, prior to or contemporaneous with uplift of Sulphur Mountain. Further constraining the age of the Ojai Conglomerate, are overlying lacustrine deposits in Upper Ojai Valley with ages of >46,000 to <13,000 y.b.p determined from radiocarbon dating of detrital charcoal. Our work highlights the complex interaction between faulting and landscape evolution, and places minimum fault-slip values on these fault at 10^4-10^5 years.

MINIMAL MODELS OF FAULT SLIP IN COMPLEX FAULT SYSTEMS (B-149)

B.J. Meade, E.L. Evans, and J.P. Loveless

Active deformation in the southern California fault system may, or may not, occur on all of the large number of mapped structures. A major goal of tectonic geodesy is to identify which faults are most active and how quickly they slip. These calculations are complicated by the fact that representations of fault system geometry are typically simplified before models are run rather than as a part of the estimation process. Here we utilize a "knockout" algorithm to form 15,000 different possible fault network configurations in the Eastern California Shear zone. For each of these configurations we estimate fault slip rates using a kinematically consistent block model and find that the frequency distribution of estimated slip rates is exceptionally broad. This broad covariance between fault slip rates suggests asking the question, "What is the simplest active fault system configuration that can explain the geodetic data?" Answering this question, and identifying minimal models of fault system activity, is possible through the use of optimization algorithms such as basis pursuit denoising that simultaneously minimize model residuals and maximize the sparsity of the state vector. We demonstrate that this approach can be used to successfully develop models of minimal fault system activity within synthetic models of complex fault systems.

PEGASUS WMS: POWERING LARGE SCALE SCIENCE THROUGH WORKFLOWS. (A-030)

G. Mehta, K. Vahi, E. Deelman, M. Rynge, S. Callaghan, and P. Maechling

Pegasus WMS is a Workflow Management System that can manage large-scale scientific workflows across local, Grid and Cloud resources. Pegasus WMS has been used for the SCEC Cybershake analysis, powering 2 production runs, in 2007 and 2009 resulting in a hazard map. The 2009 hazard map run consisted of computing hazard curves for 223 sites in the Los Angeles area, running approximately 189 million tasks and producing 11TB of output seismograms and peak acceleration values. These runs were run on the USC campus cluster as well as National Cyberinfrastructure like Teragrid. Cybershake is gearing up to use Pegasus in its next production run involving 70 sites and running over 150 million tasks using a new velocity model (CVM-H) as well as using Strain Green Tensors in all 3 dimensions.

Pegasus WMS provides a means for representing the workflow of an application in an abstract form, agnostic of the resources available to run it and the location of data and executables. It then, compiles these workflows into executable workflows by querying catalogs and sending the computations to the different resources using the Condor DAGMan as a workflow executor. Pegasus WMS optimizes the execution as well as data movement by leveraging existing Grid and Cloud technologies via a flexible pluggable interface. Pegasus also provides advanced features such as reusing existing data, automatic cleanup of generated data, job clustering.

The latest Pegasus 3.1.0 version has several new features like the recursive hierarchal workflows with deferred planning, allowing a task in a workflow to be another workflow that is planned right at the point of execution thus allowing Pegasus to use updated information from resources. Another new feature is the ability to add notifications for an entire workflow or for each individual task, which can report back on task or workflow, start, end, error success etc. via flexible notification scripts. Major improvements have also been made in the monitoring capability of Pegasus, helping scientists to accurately monitor, analyze, debug and measure performance of their workflows.

Pegasus currently supports production workflows in other large-scale experiments from the astrophysics domain like LIGO, ATLAS of Periodograms as well as the bioinformatics domain like Brain Span and the Cancer Atlas. Pegasus has also enabled smaller projects from diverse domains like astronomy, chemistry, biology, ocean modeling and others.

GPS MONITORING OF THE INLAND EMPIRE FOR SLIP-RATE MODELING OF SOUTHERN CALIFORNIA FAULTS: CONTRIBUTIONS FROM HIGH SCHOOL SCIENCE TEACHERS AND THEIR STUDENTS (A-027)

M. Meijer, M. Affadonis, R. Bennett, W. Butscher, E. Carlson, R. de Groot, S. Harris, S. McGill, S. Pearson, A. Pennington, T. Pitruzzello, D. Shafer, J. Spinler, and S. Wallace

A week-long GPS campaign coordinated by California State University, San Bernardino and funded by NSF's EarthScope program, was conducted from July 13-19, 2011. The 44 researchers included 6 SCEC interns, 7 other undergraduate students, 9 local high school Earth science and physics teachers and 22 high school students. Campaign GPS data were collected from 26 sites in the San Bernardino Mountains, Inland Empire and high desert. These data will be processed by the University of Arizona group using GAMIT/GLOBK. Following the GPS data collection campaign, participants analyzed results from the 2010 campaign, constructing time-series plots of the north, east, and vertical position for each site. Each site was determined to be moving at horizontal rates ranging from 20.0-33.0 mm/year (relative to stable North America) in a horizontal direction ranging from N21.3W to N46.4W. Velocities consistently increased for sites located farther southwest, consistent with elastic strain accumulation between the Pacific and North American plates. Slip rates for the San Andreas and 10 surrounding faults were modeled using a two-dimensional elastic model, with locking depths set to 15 km. In one afternoon of ad-hoc testing, the best-fitting curves found by the group had a slip-rate range of 6-10 mm/year for the San Andreas Fault and 8-12 mm/year for the San Jacinto Fault. However, a wide range of possible slip rates for the San Andreas Fault (0-17.5 mm/yr) was found that fit the GPS velocities relatively well. More systematic testing of slip rates was conducted by the SCEC interns over the remainder of the summer, and their results are shown in a separate poster. The high school teachers will continue their involvement by collaboratively developing and testing related Earth science or physics lessons during Fall 2011.

GPS AND ACCELEROMETER COMBINATION FOR REAL-TIME SOURCE MODELING AND EARTHQUAKE EARLY WARNING (B-026)

D. Melgar, B.W. Crowell, and Y. Bock

Real-time GPS networks provide the perfect complement to seismic networks, which operate with lower noise and higher sampling rates than GPS networks, but only measure accelerations or velocities, putting them at a disadvantage for ascertaining the full extent of slip during a large earthquake in real-time. Real-time GPS networks also have the advantage of capturing motions throughout the entire earthquake cycle (interseismic, seismic, coseismic, postseismic). Here we report on three examples of rapid modeling of recent large earthquakes near large regional real-time GPS networks and combined GPS/seismic networks. The first utilizes 416 stations in Japan's GEONET during the 2003 Mw 8.3 Tokachi-Oki earthquake about 100 km offshore Hokkaido Island, the second investigates the 2010 Mw 7.2 El Mayor-Cucapah earthquake recorded by 95 stations in the California Real Time Network and the final one examines the 2011 Mw 9.0 Tohoku-Oki earthquake recorded by over 800 stations in GEONET. We first employ a simulated real-time centroid moment tensor (CMT) determination algorithm showing that a solution can be obtained within 2-3 minutes of origin time. We also present two inverse approaches and one forward approach to ascertain the extent of fault-slip in a simulated real-time environment. The first inverse approach uses predefined fault planes from a catalogue of generalized faults while the second one computes fault planes from the CMT

inversion that operates once per second. The forward approach runs a grid search over a suite of possible 2-D Gaussian slip distributions. In all three approaches we are able to roughly characterize all three earthquakes using about a 2-3 minutes of data, greatly enhancing the time to obtain fault slip and moment release during medium-to-large earthquakes by almost an order of magnitude. We investigate gains made through combined analysis of GPS and seismic instruments (accelerometers) within rapid modeling versus GPS-only modeling with respect to the aforementioned methodologies as well as peak ground displacement scaling relationships.

DETECTING MISSING EARTHQUAKES ON THE PARKFIELD SECTION OF THE SAN ANDREAS FAULT FOLLOWING THE 2003 MW6.5 SAN SIMEON EARTHQUAKE (B-069)

X. Meng, Z. Peng, and J.L. Hardebeck

Large shallow earthquakes are typically followed by increased seismic activity, known as "aftershocks". However, whether aftershocks are triggered by static or dynamic stress changes is still in debate. Previous studies on aftershock triggering mostly utilize earthquakes listed in earthquake catalogs, which could be incomplete immediately after moderate to large earthquakes. In this study, we apply the recently developed matched filter technique to detect missing microearthquakes along the Parkfield section of the San Andreas Fault (SAF) around the occurrence time of the 2003 Mw6.5 San Simeon earthquake. Previous studies have found the San Simeon mainshock induced ~10 kPa positive Coulomb stress changes on the SAF, which is inconsistent with the observation of a decrease in seismicity rate around Parkfield immediately after the mainshock according to Northern California Seismic Network (NCSN) catalog. Here we use waveforms of ~3000 earthquakes recorded by 12 High Resolution Seismic Network (NRSN) stations around Parkfield as templates, and scan through the continuous data 48 hours before and 30 hours after the San Simeon mainshock. We band-pass filtered waveforms of 10-25 Hz to depress the effects of large aftershocks from the San Simeon rupture. A total of 158 events are detected, of which only 8 are listed in the NCSN catalog. The seismicity rate from the newly detected events shows a clear increase around Parkfield immediately after the San Simeon mainshock. In comparison, swarm-like activity at south of Gold Hill started about 2 days before and turned off immediately ~6 hours before the mainshock, which resulted in a decrease of seismicity rate. No detections are found further north in the creeping section of the SAF either before or after the mainshock, despite the fact that there are many templates in this region. Our observations suggest that the SAF near Parkfield was positively loaded by the San Simeon mainshock. This is consistent with the Coulomb stress calculation and triggered right-lateral creep observed by the USGS creepmeters, although we cannot rule out the possibility of dynamic triggering at this stage.

DIFFERENTIATING STATIC AND DYNAMIC TRIGGERING NEAR SALTON SEA FOLLOWING THE 2010 MW7.2 EL MAYOR-CUCAPAH EARTHQUAKE (B-070)

X. Meng, Z. Peng, and P. Zhao

Whether static or dynamic triggering is the dominant triggering mechanism in near field is currently under heated debate. Previous studies on earthquake triggering mostly examined seismicity rate changes around the occurrence time of large earthquakes based on existing earthquake catalogs. However, such catalogs could be incomplete immediately after the mainshock, which may cause apparent seismicity rate changes that are unrelated to stress changes. In this study, we focus on Salton Sea geothermal region following the 2010 Mw7.2 El Mayor-Cucapah earthquake, mainly because of its abundant background seismicity, dense network coverage and being in the stress shadow of the mainshock, which is the key factor to differentiate static and dynamic triggering. According to the Southern California Seismic Network (SCSN) catalog, the seismicity rate near Salton Sea increased immediately after the mainshock. It dropped below the pre-mainshock level within a few days and remained low for another few months. To check whether such patterns are caused by catalog incompleteness, we are currently applying a waveform-based matched filter technique to detect possible missing events around Salton Sea. With more completed catalog, we can identify the genuine seismicity rate changes for better comparison with the stress changes. Static and dynamic stress changes could also affect seismic velocity in the upper crust in the way similar to seismicity rate. Thus, monitoring seismic velocity can further help differentiate the triggering mechanisms. In our preliminary study, we apply the ambient noise cross-correlation technique to monitor the seismic velocity near Salton Sea 10 days before and after the mainshock. We find that immediately after the mainshock, seismic velocity reduced up to 0.4% and followed by a fast recovery in the next three days. From 5 to 10 days after the mainshock, the velocity changes remained ~0.2% lower than the pre-shock level. Such co-seismic decrease was most likely caused by the widespread damages induced by strong ground motion, suggesting that dynamic stress changes were dominant in the short term. We are currently applying the same technique at later times to check whether the velocity change returns back to the pre-mainshock or not.

THE 2011 MW 9 TOHOKU-OKI EARTHQUAKE: COMPLEXITY OF DYNAMIC RUPTURE AT THE BOTTOM OF A SEISMOGENIC ZONE (B-075)

L. Meng, J.P. Ampuero, and A. Inbal

The 2011 Mw 9 Tohoku-Oki earthquake, recorded by over 1000 near-field stations and multiple large-aperture arrays, is by far the best recorded earthquake in the history of seismology and provides unique opportunities to address fundamental issues in earthquake source dynamics. We achieved high resolution source imaging of the high frequency (1 Hz) aspects of the rupture process by back-projecting teleseismic P waves recorded by the USarray and the European seismic network. The mutually consistent results from both arrays reveal rupture complexity with unprecedented resolution, involving phases of diverse rupture speed and intermittent high frequency bursts within slow speed phases. The high frequency radiation is generated mainly at the down-dip edge of the principal slip regions constrained by geodesy. Moreover, its location coincides with the down-dip limit of interplate seismicity and encompasses regions where the background seismicity contains repeating earthquakes. The high frequency sources initially propagated down-dip, with a slow initiation phase followed by sustained propagation at speeds of 3 km/s. The rupture then slowed down to less than 1 km/s for 60 seconds. A rich sequence of bursts was generated along the down-dip rim of this slow rupture front. Before the end of the slow phase an extremely fast rupture front detached towards the North, with apparent speed of about 5 km/s . Finally a rupture front propagated towards the South running at about 2.5 km/s for over 100 km. Key features of the rupture process are confirmed by the strong motion data recorded by K-net and KIK-net. The energetic high frequency radiation episodes within a slow rupture phase suggests a patchy image of the brittle-ductile transition zone, composed of discrete brittle (velocity-weakening) asperities within a ductile (velocity-strengthening) fault zone matrix.

PARALLEL SIMULATED ANNEALING APPROACH TO SOLVE FOR UCERF3 RUPTURE RATES (B-111)

K.R. Milner, M.T. Page, and E.H. Field

We present a parallel approach to the classic simulated annealing algorithm (Kirkpatrick 1983) in order to solve for the rates of earthquake ruptures in California's complex fault system, being developed for the 3rd Uniform California Earthquake Rupture Forecast (UCERF3). Through the use of distributed computing, we have achieved substantial speedup when compared to serial simulated annealing. We will describe the parallel simulated annealing algorithm in detail, as well as the parallelization parameters used and their effect on speedup (time to convergence, or alternatively a specified energy level) and communications efficiency. Additionally we will discuss the correlation between performance of the parallel algorithm and the degree of constraints on the solution. We will present scaling results to hundreds of processors, and experiences with the MPJ Express Java Message Passing Library (Baker 2006) on the University of Southern California's High Performance Computing and Communications cluster.

References:

Mark Baker, Bryan Carpenter, and Aamir Shafi. MPJ Express: Towards Thread Safe Java HPC, Submitted to the IEEE International Conference on Cluster Computing (Cluster 2006), Barcelona, Spain, 25-28 September, 2006.

S. Kirkpatrick, C. D. Gelatt, Jr., and M. P. Vecchi. Optimization by Simulated Annealing. Science 13 May 1983: 220 (4598), 671-680. [DOI:10.1126/science.220.4598.671]

FRACTURE NETWORK CHARACTERISTICS, SEALING, AND VELOCITY STRUCTURE OF AN EXHUMED SEISMIC FAULT ZONE; THE GOLE LARGHE FAULT ZONE, ITALIAN ALPS (A-020)

T.M. Mitchell, S.A. Smith, A. Bistacchi, M. Rempe, and G. Di Toro

The Gole Larghe Fault Zone (GLFZ) in the Italian Southern Alps has been extensively studied as a natural laboratory for seismic faulting. Cataclasites and pseudotachylytes formed along pre-existing magmatic cooling joints over a fault zone width of ~500m, at ambient conditions of 9-11km depth and 250-300°C. We synthesize field measurements and laboratory data collected in the past three years that concern the architecture, sealing history, and seismic velocity and permeability structure of the GLFZ.

The GLFZ contains three structural zones: 1) a southern damage zone ~250m wide; 2) a central zone ~100m wide bordered by the two thickest cataclastic faults (~1m) identified to date, and; 3) a northern damage zone >150m thick. In the southern damage zone, macroscopic fracture density (faults + joints) increases gradually from background wall-rock values towards the central zone where it remains relatively high throughout. Despite a similar overall fracture density, the boundary between the wall rocks and the southern damage zone defined by an abrupt transition from joints to cataclasite- and pseudotachylyte-

bearing faults as the dominant fracture type. Fracture density drops off sharply within the northern damage zone, resulting in a highly asymmetric damage structure on a km-scale. Although fracture density is higher in the central zone, syn-tectonic sealing of both micro- and macro-fractures by epidote, K-feldspar, and chlorite minerals was pervasive, resulting in low permeabilities (~10-21m2). Fracture density is lower in the damage zones, and partial healing results in higher sample permeabilities (~10-18m2). Laboratory P-wave velocities correlate well with both the architecture and sealing characteristics of the fault zone. P-wave velocities are uniformly high (up to 6km/s) both within and immediately surrounding the central zone, consistent with pervasive sealing of fractures and low sample permeability. In the damage zones P-wave velocities are much lower (3-4km/s) due to the presence of open fractures. Such relationships highlight the close interplay between fracturing, fluid flow, mineralization, and the strength of large fault zones. Importantly, they demonstrate that seismic wave velocities and permeability depend on both fracture density and the degree of fracture sealing, which has implications for the interpretation of active fault zone structure based on geophysical data.

TEMPERATURE DEPENDENCE OF FRICTIONAL HEALING: EXPERIMENTAL OBSERVATIONS AND NUMERICAL SIMULATIONS (A-090)

E.K. Mitchell, Y. Fialko, and K.M. Brown

We performed a series of slide-hold-slide experiments on Westerly granite using a direct shear apparatus at ambient temperatures between 20-550 ºC. We measured changes in static coefficient of friction after a period of time over which the sample was held in nominally stationary contact. Friction increases in proportion to the logarithm of hold time at a rate of about .02 per decade, similar to findings of previous studies conducted at room temperature. Friction also linearly increases with temperature at about .02 per 140 ºC. We found that temperature has little effect on the rate of change in static friction with hold time. We interpret these results using a numerical model that incorporates viscoelastoplastic rheology and a fractal geometry of contact surfaces. We explore to what extent the observed time and temperature dependence of static friction can be explained in terms of increases in the true contact area due to creep at highly stressed microasperities. We performed finite element simulations of a contact consisting of a fractional Brownian surface pressed against a rigid flat surface. Changes in contact area between the surfaces with respect to an initial contact area are compared to changes in static friction coefficient with respect to its initial (reference) value. We find that the power-law rheology with stress exponent n = 3 (e.g., expected of dislocation creep) does not fit the experimental data. It fails to generate an increase in the contact area over short (< 1000 s) timescales; once the highly stressed contacts begin to relax, they do so too quickly. For the power-law rheology to provide a reasonable fit to the data, the stress exponent needs to be increased to n = 45. In this case, significant (up to 500 degrees) changes in contact temperature have little effect on the rate of increase in contact area.

REMOTE MAPPING OF A LARGE STEPOVER IN THE 4 APRIL 2010 EL MAYOR CUCAPAH EQ (A-117)

A.E. Morelan and M.E. Oskin

The 4 April 2010 MW 7.2 El Mayor Cucapah earthquake has been valuable to study because of its rich rupture exposure and preservation. This dextral-oblique normal event ruptured on the NW-striking Pescadores, Borrego, Paso Inferior and Paso Superior faults in the Sierra El Mayor and Sierra Cucapah mountain ranges, part of the active Pacific-North America plate boundary between the northern tip of the Gulf of California and US- Mexico border. In total, the rupture consists of six major faults, ~120 km in total length. Initial field work mapped the rupture across an 11 km left stepover in rugged terrain between the Pescadores and Borrego faults. If accurate, this rupture would violate many accepted theories concerning the mechanics of how ruptures terminate through stepovers; 11km is thought too great a distance for rupture to jump in a single event. Although most models for stepovers use pure strike- slip motion on faults, this fault ruptured in a dextral- oblique normal fashion with the ratio between normal and dextral motion between ~2- 3:1. This rupture characteristic may explain the somewhat odd nature of this large stepover. Our remote mapping using high-resolution airborne LiDAR topographic data, collected soon after the event, has yielded 2010 rupture on previously unidentified faults within the stepover. The distance between rupture in the stepover, based on this new mapping, is 4km significantly less than the previously mapped 11km. Abundant bedrock scarps were also remotely mapped in this rugged accommodation zone and are interpreted as rupture on faults that pre-date the 2010 earthquake. These features turn out to be quite important because they beg the question of whether or not this event was typical of this fault system. An 1892 event on the Laguna Salada fault ruptured along the western range front of the Sierra Cucapah in a west- down motion, in an opposite sense of the 2010 event. Observation of and comparison with such previous ruptures in the same region can increase our knowledge about the evolution of rupture style along this fault system. Our remote mapping documents patterns of distributed faulting and displacement that allows us to better understand strain accommodation and fault continuity during large oblique earthquakes. The airborne LiDAR dataset

has proved to be an invaluable tool in this investigation of an unusually large stepover and will continue to yield interesting scientific results about the event.

FAULT ZONE ARCHITECTURE, SAN JACINTO FAULT ZONE, SOUTHERN CALIFORNIA: EVIDENCE FOR FOCUSED FLUID FLOW AND HEAT TRANSFER IN THE SHALLOW CRUST (A-147)

N.M. Morton, G.H. Girty, and T.K. Rockwell

We report results of a new study of the San Jacinto fault zone architecture in Horse Canyon, SW of Anza, California, where stream incision has exposed a near-continuous outcrop of the fault zone at ~0.4 km depth. The fault zone at this location consists of a fault core, transition zone, damage zone, and lithologically similar wall rocks. We collected and analyzed samples for their bulk and grain density, geochemical data, clay mineralogy, and textural and modal mineralogy. Progressive deformation within the fault zone is characterized by mode I cracking, subsequent shearing of already fractured rock, and cataclastic flow. Grain comminution advances towards the strongly indurated cataclasite fault core. Damage progression towards the core is accompanied by a decrease in bulk and grain density, and an increase in porosity and dilational volumetric strain. Palygorskite and mixed-layer illite/smectite clay minerals are present in the damage and transition zones and are the result of hydrolysis reactions. The estimated percentage of illite in illite/smectite increases towards the fault core where the illite/smectite to illite conversion is complete, suggesting elevated temperatures that may have reached 150°C. Chemical alteration and elemental mass changes are observed throughout the fault zone and are most pronounced in the fault core. We conclude that the observed chemical and mineralogical changes can only be produced by the interaction of fractured wall rocks and chemically active fluids that are mobilized through the fault zone by thermo-pressurization during and after seismic events. Based on the high element mobility and absence of illite/smectite in the fault core, we expect that greatest water/rock ratios occur within the fault core. These results indicate that hot pore fluids circulate upwards through the fractured fault core and into the surrounding damage zone. Though difficult to constrain, the site studied during this investigation may represent the top of a narrow, ephemeral hydrothermal circulation cell that dissipates heat generated from rupture events at deeper levels (> 4 km).

GENERATING BROADBAND SEISMOGRAMS FOR A SUITE OF SAN ANDREAS EARTHQUAKES (B-012)

R. Mourhatch and S. Krishnan

We examine a method for generating broadband ground motions for a suite of San Andreas earthquakes (6.0-8.0 Mw) using a hybrid of empirical & deterministic methods of ground motion simulations. We use finite source models from past earthquakes resampled to a 0.5km x 0.5km grid to generate the earthquakes. The low frequency content (<0.5Hz) of the ground motions are generated using a wave propagation software package called SPECFEM3D(Ver.2). This package incorporates the regional 3D-velocity structure (SCEC,CVM-H) with its resolution enabling the software to accurately propagate waves with periods greater than 2 seconds. The results for this period range have been extensively validated in previous studies. The low frequency will be superposed with high frequency ground motions determined using empirical green's function (EGF) approach. The basic principle involving the EGF method is generating ground motions using seismograms from smaller earthquakes (sub-events) as green's functions for a large earthquake. The high frequency motion for a given San Andreas earthquake scenario is generated using the following steps taken to best capture the path & local site effects: (i) Seismograms from actual historic events in the magnitude range 2.5-5.0 that have occurred along the entire rupture length of the given scenario are collected and highpass-filtered with a corner at 2s. For each sub-fault we have identified small earthquake that best matches the location of the sub-fault. (ii) Each of the seismograms is scaled by the ratio of assigned sub-fault moment to the sub-event moment. (iii) For a given analysis site of interest, the seismogram recorded at the seismic station that is closest in distance is used. (iv) The effect of geometric spreading & the delay in arrival of the waves is accounted by additional scaling and shifting. (v) The earthquake records corresponding to the rupture of all the sub-faults participating in the given earthquake scenario are combined after due scaling and shifting. The key advances in this work are the use of rupture scenario-specific events as EGFs & the use of small magnitude earthquakes for generating high frequency synthetics for large magnitude earthquakes. The main challenge is the low signal-to-noise ratio of the seismic waveforms from small magnitude earthquakes at large distances. The approach is being validated against recorded ground motions from the 2004 Parkfield (Mw 6.0) & the 1992 Landers (M 7.3) Earthquakes.

RUPTURE PATTERN OF THE 1892 LAGUNA SALADA EARTHQUAKE: A PRECURSOR TO 2010 EL MAYOR-CUCAPAH (A-122)

K. Mueller, T. Rockwell, O. Teran, J. Fletcher, S. Akciz, and P. Patton

As part of the SCEC response effort and analysis of surface deformation produced by the 2010 El Mayor-Cucapah earthquake, we measured fault displacement and larger-scale rupture patterns from the 1892 Mw 7.2 Laguna Salada precursor earthquake. Our goal was to understand the interaction between rupture segmentation in 1892 and 2010 and its implications for connectivity between the two fault zones. Comparison between the 1892 and 2010 ruptures suggests that both earthquakes activated distinct fault segments separated by 1-3 km gaps except for the much larger Puerta accommodation zone in 2010. Interestingly, the 9 km-wide Puerta gap ruptured previously in 1892 as part of a longer segment on the Laguna Salada fault. In contrast, this pattern is not apparent where another transfer zone further north at Paso Superior behaved similarly in both 1891 and 2010. The greatest difference between the 1892 and 2010 ruptures is the sense of slip at the rupture endpoints. While both 1892 and 2010 fed oblique slip into pure dextral offset towards their respective northern and southern endpoints, the Laguna Salada fault terminated abruptly at the rapidly slipping Canon Rojo normal fault. The proportion of dextral to normal slip, or slip budget along 1892 rupture segments is not necessarily consistent with fault strike except across the right angle bend at Canon Rojo. We postulate the difference is due to strain release at longer timescales than is apparent from just the 2010 and 1892 events.

SLIP DEFICITS, RELEASE AND TRANSIENTS ALONG THE CENTRAL SAF FROM REPEATING MICROEARTHQUAKES (A-102)

R.M. Nadeau, R.C. Turner, and R. Burgmann

To better understand interactions between seismic and aseismic deformation at seismogenic depths, deep aseismic fault slip rates (Vd) from characteristically repeating microearthquake seqeunces (CSs) along the central San Andreas Fault (SAF) are compiled and analyzed. Using repeating CS data, spatial and temporal variations in Vd can be resolved over large contiguous regions, in diverse tectonic settings, and back in time to well before the advent of satalite based geodesy (e.g., GPS, InSAR). Previous studies have also revealed systematics in Vd indicative of slip transients associated with post-seismic deformation, slow-slip events, quasi-periodic slip pulsing, and regions of slip-deficit accumulation. We present results of Vd from 343 CSs (~3000 repeated microearthquakes) along a 200 km stretch of the SAF in central California occurring over a 27+ year period between 1984 and mid-2011. The spatio-temporal mapping of CS inferred Vd covers the section of the SAF between the the 1989 M6.9 Loma Prieta (LP) earthquake and the inferred northern terminus of the 1857 M7.8 Ft. Tejon (FT) earthquake. This mapping includes pre- and post- seismic periods of the LP and 2004 M6.0 Parkfield earthquakes. In the study zone we find large (several 100%), broadly distriubted (several 10s of kms), and systematic variations in Vd associated with the occurrence of moderate to large earthquakes (i.e., low preseismic rates and large postseismic transients) and in the SAF creeping section (e.g., quasi-periodic slow-slips) where moderate to large events did not occur. We also show that the a slip deficit that had accumulated in the Parkfield area was fully released northwest of Parkfield in the 2004 M6 mainshock, but was only partially released to the southeast adjacent to the locked Cholame segment of the SAF.

SITE RESPONSE IN THE BÍOBÍO REGION, CHILE USING THE K METHOD (B-052)

C. Neighbors, E.J. Liao, E.S. Cochran, A.I. Chung, J.F. Lawrence, A. Belmonte, M. Miller, H.H. Sepulveda, and C. Christensen

We assess local site response in the Bíobío region of Chile utilizing seismograms recorded by the Quake-Catcher Network (QCN) micro-electro-mechanical system (MEMS) accelerometers during the aftershock sequence that followed the February 27, 2010 Mw 8.8 Maule earthquake. The earthquakes were captured by over 70 QCN low-resolution (10, 12, and 14-bit) seismometers from March 1 to June 1, 2010. Site effects are caused by the local amplification of seismic energy due to subsurface structures and geologic materials, which often result in spatially variable patterns of surface damage following an earthquake.

In this study we estimate kappa, κ, which models the decay of the acceleration spectra to characterize strong ground motion at high frequencies (> 1 Hz). We calculated the Fourier spectra and κ for each station following the method of Douglas et al. (2010). During the aftershock deployment, the QCN network recorded over 229 earthquakes of magnitude 4.5 and greater. Of these recordings, we determine that 57 earthquakes (25%) have sufficient signal-to-noise quality for use in site response analysis, as determined by visual inspection. Preliminary results indicate κ values between 0.03 and 0.06 s. These values suggest that the Bíobío region of Chile is sharply attenuating and likely consists of less competent rock, as expected.

Preliminary results also suggest that kappa has a positive correlation with source-station distance as high frequency waves become more attenuated with distance from source.

Further comparison of κ values between stations will highlight the influence of local geology on observed seismic records at individual sites in the Bíobío region. As a result of the site response analysis, we highlight areas of the Bíobío region that may be more susceptible to greater ground shaking following future large earthquakes.

VISUAL COMMUNICATION DESIGN FOR SHAKEOUT RESEARCH DISSEMINATION (A-008)

A. Nguyen

Preventing earthquakes from becoming disasters requires behavior change on the part of everyone at risk. This project seeks to apply professional design to research dissemination and to information, education and communication (IEC) outreach materials.

Risk RED, in cooperation with Earthquake Country Alliance, Western Washington University, and California State University, Fullerton has developed a participant survey used in connection with annual community-wide ShakeOut drills worldwide. This project focuses on communicating the results of these surveys by making the research findings understandable and interesting, based on enhancing their visual appeal.

Deliverables are:

- Design of a full range of re-usable icons to highlight both research results and risk reduction concepts
- Development of Excel/Microsoft Word templates for a dozen infographics to convey research results in bar and pie chart formats.
- Design for a re-usable Microsoft Word template for an annual research report.

Icons, infographics, charts, and templates were created with the intent of better visualization, maintaining a balance between simple details and successful communicative imagery. The effort to support information with clear and appealing graphics is expected to enhance research utilization as well as reinforcing disaster risk reduction education messages.

CFM V.4.0: CONTINUED UPGRADES AND IMPROVEMENTS TO THE SCEC COMMUNITY FAULT MODEL AND ITS ASSOCIATED FAULT DATABASE (B-131)

C. Nicholson, A. Plesch, and J.H. Shaw

We are completing a major upgrade to the SCEC Community Fault Model (CFM v.4.0) which incorporates improvements in 3D fault representations, a detailed fault surface trace layer, and a new naming and numbering scheme for individual 3D fault models that allows for closer links to the USGS/CGS Quaternary Fault database (Qfaults) and other SCEC data sets. Fault representations in CFM are now referenced to the modern WG84 datum and the new surface layer in CFM allows 3D fault models to be registered to the more detailed, mapped Qfaults and other digital fault maps. A systematic revision of CFM 3D fault segments was triggered by unexpected discrepancies between some previous CFM fault representations and the newer Qfaults surface traces, as well as by the availability of extensive catalogs of relocated earthquake hypocenters to better define the subsurface geometry of active faults. New 3D fault representations for major fault zones, including the San Andreas from San Gorgonio Pass to the Salton Sea, the subparallel Mecca Hills, the San Jacinto, the Elsinore-Laguna Salada (including El Mayor-Cucapah), and the San Fernando/Sierra Madre fault systems are being added that allow for more non-planar, multi-stranded 3D fault geometry. These new revised 3D fault models and interpretations help characterize a more complex pattern of fault interactions at depth between various fault sets and linked fault systems. In addition, a new SCEC fault database hierarchical naming and numbering scheme is implemented that provides unique identifiers (number, name, abbreviation) for each level of the fault hierarchy under which a particular fault segment is classified. Levels of fault hierarchy include Fault Area, Fault Zone or System, Fault Section, Fault Name, Fault Strand or Model, and Fault Component, which can be easily shortened to Fault System identifier and Fault Name (e.g., SJFZ-Clark fault). These additional fault hierarchical levels allow for more flexible database searches and easier identification of fault components, alternative representations, and possible system-level associations of individual 3D fault elements that comprise CFM. This hierarchical scheme also allows for grouping related individual faults under a higher level fault system (e.g., Southern Frontal Fault System for the Raymond, Hollywood, Santa Monica, and Malibu Coast faults) to help facilitate identification of potentially larger earthquake ruptures between such kinematically linked fault segments.

SPATIAL VARIABILITY OF GROUND MOTION AMPLIFICATION FROM LOW-VELOCITY SEDIMENTS INCLUDING FRACTAL INHOMOGENEITIES WITH SPECIAL REFERENCE TO THE SOUTHERN CALIFORNIA BASINS (B-017)

K.B. Olsen and B.H. Jacobsen

Many state-of-the-art area-specific velocity models (e.g., the Southern California Earthquake Center (SCEC) Community Velocity Model (CVM) V.4.0) include a wealth of geophysical data, such as tomographc results, and gravity, reflection and well-log data. However, these CVMs usually poorly resolve near-surface small-scale amplification effects. Toward characterizing the variability of shallow sediment amplification, we have investigated the effects of inhomogeneities with fractal distributions augmented onto the shallow seismic velocity structure derived from the SCEC CVM V.4.0. Our analysis used linear 0-2 Hz 3D visco-elastic finite-difference wave propagation with grid spacings of 25 m or less. We find that even simple and rather weak fractal stochastic inhomogenities imply significant variations in ground motion amplifications (up to a factor of four), including bands of strong amplification aligned along the average ray path from a horizontally-propagating SH-wave source. We show that these patterns depend strongly on the incidence angle of the main wavefront. For vertically-incident planar SH-wave sources we find that the largest contribution to the site effects from small-scale heterogeneities arise from those included in the upper ~100 m of the sediment column. Finally, it is important to tune the statistical model (scattering Q) with anelastic attenuation (intrinsic Q), where a tradeoff appears to persist.

COMPARISON OF USGS PAGER EMPIRICAL FATALITY RATES TO RECONNAISSANCE OBSERVATIONS AND AN ACCOUNTING OF UNCERTAINTIES IN THE FATALITY MODEL (B-079)

A.H. Olsen, E. So, M. Hearne, K. Jaiswal, and D.J. Wald

The U.S. Geological Survey's Prompt Assessment of Global Earthquakes for Response (PAGER) system estimates fatalities and economic losses typically within thirty minutes of a significant earthquake. Emergency responders, governmental and aid agencies, and the media are the primary users of this information. The operational PAGER fatality model combines: estimates of shaking intensities (in the form of a ShakeMap); estimates of the populations exposed to the shaking (from LandScan); and fatality rates as a function of intensity, specific to a country or set of countries. The fatality-rate model is empirical, developed from observations of total fatalities in past events of the last several decades. The first part of this study compares the existing fatality-rate model to additional data on observed fatalities from municipality- and district-level reconnaissance surveys. This comparison is not straightforward because the intensity value associated with a fatality is not always known or known with certainty. The second part of this study identifies the sources of uncertainty in the empirical fatality model, and it proposes a method to combine the sources of uncertainty for a prediction of fatalities. Since this work is in progress, we present here only our methodology and some preliminary results.

TIMING OF LARGE EARTHQUAKES BETWEEN 400 AD TO PRESENT ALONG THE CLAREMONT FAULT, NORTHERN SAN JACINTO FAULT ZONE, FROM MYSTIC LAKE, CALIFORNIA. (A-150)

N.W. Onderdonk, T.K. Rockwell, S.F. McGill, and G. Marliyani

Additional trench exposures and radiocarbon dating over the past year have refined the timing of pre-historic earthquakes along the northern San Jacinto fault zone at the Mystic Lake paleoseimic site. Seven events are recorded in the upper 1.8 meters of strata, which spans approximately 1600 years. The ages of the events are constrained by 50 radiocarbon dates from detrital charcoal and are as follows:

Event 1: 1738 to 1853 AD

Event 2: 1670 to 1828 AD

Event 3: 1521 to 1616 AD

Event 4: 1349 to 1445 AD

Event 5: 1076 to 1258 AD

Event 6: 807 to 961 AD

Event 7: 579 to 845 AD

The recurrence interval for the last 7 events ranges from 159 to 210 years and based on historical data it has been at least 200 years since the last ground-rupturing earthquake on the northern San Jacinto fault.

Comparison of this new event history on the Claremont fault with the Hog Lake site along the Clark segment of central San Jacinto fault shows some overlaps in event ages from 3 events. The strongest correlation is between Event 3 at Mystic Lake and Event 2 at Hog Lake, both of which are constrained to within 100 years. This may be evidence that some events can jump the San Jacinto Valley releasing step-over, or that events on one fault can trigger closely timed events on the other fault. Comparison of the Mystic Lake data with event histories from sites along the San Andreas fault north and south of its juncture with the northern San Jacinto fault show that some events north of the juncture overlap better with events at Mystic Lake than with events at sites on the San Andreas fault to the south of the juncture (Events 5 and 6). This leaves open the possibility that ruptures may have jumped from the San Andreas fault to the San Jacinto fault (or vice versa) in the past.

NEAR-FIELD COSEISMIC DEFORMATION QUANTIFIED FROM DIFFERENTIAL AIRBORNE LIDAR OF THE EL MAYOR-CUCAPAH EARTHQUAKE SURFACE RUPTURE (A-120)

M.E. Oskin, J.R. Arrowsmith, A. Hinojosa, A.J. Elliott, O. Teran, J.M. Fletcher, S. Saripali, and D. Banesh

We analyze a high-resolution (9 to 18 returns/sq. m) airborne LiDAR topographic survey of the 4 April 2010 M7.2 El Mayor-Cucapah surface rupture to quantify fault slip and the amount and style of distributed near-field deformation. This is the first LiDAR survey to capture a fresh rupture in a sparsely vegetated region with pre-earthquake lower-resolution (5m-pixel) LiDAR data. The amount of distributed deformation we observe suggests the frequency of large earthquakes on secondary fault arrays may often be underestimated from geologic observations of prehistoric fault slip.The earthquake produced a 120 km-long, complex multi-segment rupture with dextral-normal slip through northernmost Baja California, Mexico. The post-event survey reveals numerous surface ruptures, including subtle distributed slip above previously undocumented faults within the Colorado River delta. Differential elevations from comparison of pre- and post-event topography quantify distributed deformation surrounding fault ruptures in the Sierra Cucapah. Folding strains up to 1000 microstrains occur in the absence of visible faulting. Shear with opposite sense to adjacent faulting demonstrates that these strains were, at least initially, elastic. Changes in shallow stress that accompanied this strain may be comparable to the coseismic stress drop at seismogenic depth. We speculate that distributed mechanisms, such as granular deformation and velocity strengthening creep on small faults, relaxed these stresses post-seismically and rendered this shallow, distributed deformation into permanent fault-related folding.

IMAGING COSEISMIC SURFACE DEFORMATION AND DAMAGE USING SAR AND GPS: RESULTS FROM ARIA-EQ FROM 2011 M9.0 TOHOKU-OKI AND M6.3 CHRISTCHURCH EARTHQUAKES (A-042)

S.E. Owen, S.H. Yun, A. Moore, E. Fielding, P. Agram, F. Webb, M. Simons, P. Rosen, J. Cruz, and H. Hua

The Advanced Rapid Imaging and Analysis for Earthquakes (ARIA-EQ) project is a joint JPL/Caltech effort to automate geodetic imaging capabilities for hazard response. Geodetic imaging's unique ability to capture the surface deformation in high spatial and temporal resolution allow us to resolve the earthquake fault geometry and fault slip in correspondingly high spatial & temporal detail. In addition, remote sensing with radar provides change detection and damage assessment capabilities that can image even at night or through clouds. However, since these data sets are still essentially hand-crafted, they are not generated rapidly and reliably enough to be useful for informing decision-making agencies and the public following an earthquake. We are building an end-to-end prototype geodetic imaging data system that would integrate InSAR, GPS, seismology, and modeling to deliver actionable science and situational awareness products.

We will present our recent results generating products for 2011 M9.0 Tohoku-oki and M6.3 Christchurch earthquakes. In response to the Tohoku-oki event, we have processed GPS data supplied by Japan's Geospatial Information Authority to generate measurements of coseismic and postseismic deformation. These coseismic results enabled several research groups to better constrain models of the earthquake shortly after the event, helping to understand where this unexpectedly large earthquake had occurred along a well-studied subduction zone fault. We processed radar data from several SAR platforms and mosaicked interferograms show spectacular coseismic and aftershock deformation.

We have also developed a prototype algorithm to detect surface property change caused by natural or man-made damage using InSAR coherence change. The algorithm was tested on construction sites in Pasadena, California. The developed algorithm performed significantly better, producing 150 % higher signal-to-noise ratio, than a standard coherence change detection method. We applied the algorithm to 2011 M6.3 Christchurch earthquake in New Zealand using ALOS PALSAR data. In Christchurch area we detected three different types of damage: liquefaction, building collapse, and landslide. These detected damage sites were confirmed with Google earth images provided by GeoEye. Larger-scale damage pattern also

agrees well with the ground truth damage assessment map indicated with polygonal zones of 3 different damage levels, compiled by the government of New Zealand.

GEOMETRY OF FAULT SLIP ZONES AT DEPTH FROM QUANTITATIVE ANALYSIS OF SEISMIC CATALOGS: METHOD AND RESULTS FOR THE SAN JACINTO FAULT ZONE (B-064)

Y. Ozakin and Y. Ben-Zion

We develop a quantitative method for estimating the geometry of active fault zones at seismogenic depth using typical entries of earthquake catalogs. In contrast to prior methods that make various assumptions on geometrical properties of the structure (e.g. sets of planes or fractal network), our method does not presuppose any shape. Each recorded earthquake is assigned a Gaussian likelihood function with central coordinates and standard deviations in different directions corresponding to the hypocenter location and errors. The likelihood function is given a weight corresponding to the event size. The sum of the likelihoods of all earthquakes reported for a given region, with normalization to account for different event numbers in different locations, provides a likelihood field for the occurrence of slip patches in the examined volume. High contiguous regions of likelihood values represent large fault zone sections. Synthetic catalogs are used to develop and test normalization methods that account for typical spatio-temporal variations of seismicity, and to identify characteristic likelihood shapes corresponding to typical types of structural heterogeneities (e.g. stepovers, parallel faults). In the present application the method is applied to estimate geometrical properties of the seismicity in the San Jacinto fault zone environment. Preliminary results show high general complexity and a dipping trend with increasing depth of seismic slip patches along a NW-SE direction. The continuing work will focus on performing in-depth analysis of segmentation and continuity along different sections of the fault, and especially the trifurcation area and Hemet stepover region.

AN EARTHQUAKE RUPTURE FORECAST INVERSION APPLIED TO FAULT SYSTEMS IN CALIFORNIA (B-112)

M.T. Page, E.H. Field, and K.R. Milner

Previous fault-based rupture forecasts for California have been plagued with magnitude "bulges" and fail to simultaneously fit all available data. We present results from an inversion-based methodology being developed for the 3rd Uniform California Earthquake Rupture Forecast (UCERF3) that simultaneously satisfies available slip-rate, paleoseismic event-rate, and magnitude-distribution constraints. Using a parallel simulated-annealing algorithm, we solve for the rates of all ruptures that extend through the seismogenic thickness on major mapped faults in California. This inverse approach eliminates the need for expert-opinion voting on rupture rates themselves, allowing for more transparent and reproducible results than previous earthquake rupture forecasts. The inversion methodology also allows for the incorporation of multi-fault ruptures, which eliminates the magnitude-distribution misfits that were present in earlier models. Furthermore, we show that the inversion solutions match slip-rate and paleoseismic event-rate data better than previous models.

THE INFLUENCE OF AMBIENT FAULT TEMPERATURE ON FLASH-HEATING BEHAVIOR (A-094)

F. Passelegue, D.L. Goldsby, T.E. Tullis, and O. Fabbri

Recent friction experiments demonstrate that rocks become dynamically weak due to extreme heating and thermal degradation of the strength of microscopic asperity contacts on a slip surface – i.e., due to 'flash' heating. Here we test the effect of an increase of ambient temperature Tf of a slip surface, up to those occurring at the base of the seismogenic zone, on the flash-heating behavior of quartzite, India gabbro and Westerly granite. Experiments were performed in a 1-atm rotary-shear apparatus at ambient humidity, wherein a fixed annulus was slid against a rotating plate of the same material at a normal stress of 5 MPa. Samples were heated by hot plates adjacent to the annulus and plate. Average sliding surface temperatures were monitored with thermocouples in contact the annulus and plate, and with a handheld IR detector. The sliding velocity was initially stepped from 10 μm/s to ~0.36 m/s, then subsequently decreased to ~0.25 m/s over ~45 mm of slip, then to zero within several mm of slip at the end of the test. The friction coefficient below a critical weakening velocity Vw of 0.10 - 0.15 m/s obtained values of 0.6 - 0.9 depending on the rock type. Above Vw, a dramatic 1/V decrease in friction with velocity was observed, with values of the friction coefficient as low as 0.4 for quartzite and 0.5 for granite and gabbro at the highest slip rate. The experiments demonstrate that increasing values of Tf cause 1) an increase in friction coefficient at quasi-static slip rates, 2) an increase in the value of Vw, and 3) an increase in the value of the weakened friction coefficient observed for a given velocity V > Vw. The unexpected increase in Vw with increasing values of Tf is consistent with flash-heating theory (Rice, 2006) when appropriate higher-T values of thermal conductivity, heat capacity and contact stress in the theoretical expression for Vw are adopted.

DYNAMIC RUPTURE SIMULATION WITH A HIGH-ORDER DISCONTINUOUS GALERKIN METHOD ON UNSTRUCTURED TETRAHEDRAL MESHES (B-053)

C. Pelties, J. de la Puente, J.-P. Ampuero, G. Brietzke, and M. Käser

We will present recent developments concerning the extensions of the arbitrary high-order derivative Discontinuous Galerkin (ADER-DG) method to solve three dimensional dynamic rupture problems on unstructured tetrahedral meshes. First of all, we verify our implementation by comparing results of the SCEC test case with other numerical methods. An important result of the benchmark is that the ADER-DG method avoids spurious high-frequency contributions in the slip rate spectra and therefore does not require artificial Kelvin-Voigt damping or a posteriori filtering of synthetic seismograms.

To demonstrate the capabilities of the high-order accurate ADER-DG scheme on unstructured meshes we use the 1992 Landers earthquake as an example. It represents a complex fault system including branching and six curved fault segments. Furthermore, topography is respected in the discretized model to capture the surface waves correctly. Strong mesh coarsening or refinement at areas of interest is applied to keep the computational costs feasible. Finally current problems and further developments will be discussed.

USE OF INTEGRATED MASTER MULTISPECTRAL IMAGERY AND LIDAR DEM FOR ACTIVE FAULT DETECTION AND EVALUATION (A-144)

F.G. Perez, W.A. Bryant, J.A. Treiman, C.R. Real, and S.J. Hook

Displacement caused by surface fault rupture associated with large earthquakes not only disrupts infrastructure and damages natural and built environments, but also constitutes a life safety hazard. The California Geological Survey (CGS) has the authority and responsibility, under the Alquist-Priolo Earthquake Fault Zoning Act, to identify and map active faults in California for the purpose of surface rupture hazard identification and mitigation through regulatory zoning.

Mapping and evaluation of active faults is generally accomplished through conventional aerial photo interpretation and field mapping, which rely on recognizing fault-related geomorphic features and juxtaposition of contrasting rocks, soil, and geologic structure. Faults covered by vegetation or concealed by young alluvium will most likely not be detected by this method. Furthermore, spatial accuracy of photo-interpreted fault traces is limited to the accuracy, scale, and method of transfer to conventional topographic base maps, which generally lack the spatial accuracy of geolocated imagery.

The inherent limitations of conventional active fault mapping are expected to be overcome by using integrated MASTER and LiDAR data. MASTER is a multispectral imagery with 50 spectral bands ranging from visible to thermal region of the electromagnetic spectrum. LiDAR on the other hand is a laser-based technology with very high positional accuracy, sub-meter resolution and capability to filter out vegetation. MASTER and LiDAR are integrated via data transformation/fusion and the resulting fused imagery are utilized to interpret active faults through recognition of fault features associated with different distinctive properties related to geology, drainage, vegetation, hydrology, thermal, anthropogenic, and topography. The completeness and accuracy of the fault interpretation is gauged by overlaying it to a baseline data of previously mapped fault traces.

The research study, supported by a NASA grant, evaluated a well-mapped, 26-km reach of the southern San Andreas Fault Zone in the Antelope Valley near Palmdale.

IDENTIFYING AND LOCATING TECTONIC TREMOR BENEATH THE SAN ANDREAS FAULT NEAR PARKFIELD, CA, WITH THE PASO ARRAY (B-047)

D. Peterson, C. Thurber, E. Montgomery-Brown, J. Brown, and D. Shelly

Tectonic tremor is a weak but persistent shaking of the Earth that was first discovered in subduction zones and later found beneath the San Andreas Fault (SAF). Tremor events represent spasmodic slip on the deep extension of the SAF, occurring at a depth of about 20-25 kilometers. Tremor occurs deeper than the nearby regular earthquakes, which can be found at maximum depths of 12-15 kilometers. Tremor is characterized by bursts of low frequency and/or very low frequency earthquakes (LFE/VLF) with dominant energy in the 1-10 Hz range. Tremor tells us about fault slip at depth in both space and time by illuminating the fault down to about the base of the crust.

In the pursuit of deriving information about deep fault behavior and crustal structure, we are analyzing continuous data from the previously untapped Parkfield Area Seismic Observatory (PASO) temporary array, operated in 2000-2002 and 2004-2006. We started the identification process by correlating templates of known events from a nearby station array based on an

existing catalog of tremor events. Using the dense PASO array and various correlation methods, including autocorrelation (Brown et. al. 2008), a scanning algorithm (Rowe, 2005), and cross correlation of template events (Shelly et al., 2007), we will refine the locations of these known events and seek to identify undiscovered clusters of LFEs and tremor. After generating an updated catalog initially for the month of September 2002, we will use S-wave arrivals from the 59 stations comprising the PASO array to provide strong constraints on the locations of identified events.

KINEMATICS OF ROTATING PANELS OF E-W FAULTS IN THE SAN ANDREAS SYSTEM: WHAT CAN WE TELL FROM GEODESY? (A-056)

J.P. Platt and J.P. Becker

Panels of E-W-trending sinistral and/or reverse faults occur in various locations within the San Andreas system, and are commonly associated with paleomagnetic evidence for clockwise rotations over geologic time. These panels commonly cut across the trend of active dextral faults, posing questions as to how displacement is transferred across them. Geodetic data indicate that they lie within an overall dextral shear field, and the data are commonly interpreted to indicate little or no slip on the E-W faults.

We model these faults and fault panels as rotating by bookshelf slip in a dextral shear field. This allows prediction of rates of slip, rotation, fault-parallel extension, and fault-normal shortening. We decompose the geodetically determined velocity field into these components, and compare them with our predictions,as illustrated by the following two examples. (1) The velocity field around the central section of the Garlock fault is consistent with a combination of long-term sinistral slip rate of ~7.5 mm/yr on a locked fault, and a counterclockwise rotation rate of 5.2°/m.y. The resultant field comprises a dominant component of dextral shear at a rate of 90 nanostrain/yr, and a residual component of fault-parallel motion that reflects the elastic strain around the locked fault. (2) The E-W trending faults of the western Transverse Ranges currently lie at ~50° to the Pacific – North America plate motion vector, having been rotated clockwise into this orientation during the since early Miocene time. In this orientation the rate of sinistral slip is small, but they are still rotating at ~2.5°/m.y. Strike-parallel extension at 4 mm/yr is also clearly detectable in the velocity field, as well as strike-normal shortening at up to 6mm/yr. The rate of strike-normal shortening decreases westward, reflecting transfer of displacement from Inner Borderland dextral faults south of the Transverse Ranges onto faults within the Salinia block.

These two examples demonstrate firstly, that significant sinistral slip on rotating E-W trending faults may only be detectable through second-order elastic effects; and secondly, that previously active sinistral faults may become inactive because of rotation, but may still define a discrete panel deforming by other mechanisms.

STRAIN LOCALIZATION DRIVEN BY THERMAL DECOMPOSITION DURING SEISMIC SHEAR (A-092)

J.D. Platt, N. Brantut, and J.R. Rice

De Paola et al. [2008] analyzed a series of faults in the Northern Apennines, Italy, hosted in anhydrite and dolomite rocks. They found a highly localized band of less than 100 microns, contained within a broader damage zone. Recent High-Velocity Friction (HVF) experiments on kaolinite-bearing gouge samples (Brantut et al. [2008]) have also shown extreme localization in samples undergoing thermal decomposition. They performed microstructural analysis on HVF samples and found an "ultralocalized deformation zone", less than ten microns wide, interpreted to be the main slipping zone in the experiment. By measuring relative humidity in the sample chamber they were also able to observe the thermal dehydration of kaolinite. These laboratory and field observations indicate that straining is extremely localized in fault materials where thermal decomposition reactions may occur.

During thermal decomposition reactions pore fluid is released, leading to increases in pore pressure, and a corresponding drop in frictional heating. The reactions are endothermic, so heat is also absorbed as the reactions progress. Previous work by Sulem and Famin [2009] has investigated how these effects influence the evolution of pore pressure and temperature in a uniformly sheared gouge layer. They found that accounting for thermal decomposition reactions leads to significant pore pressure increases, and that the endothermic nature of the reaction acts to cap the maximum temperature achieved.

In previous work (Platt, Rudnicki and Rice [2010]) we investigated strain localization using a model for shearing of a fluid-saturated gouge material, finding a formula for the localized zone width as a function of physical properties of the gouge. We now extend this model to include thermal decomposition. Using linear stability methods and an idealized reaction kinetic we infer a new localized zone width when decomposition is accounted for. Numerical simulations then allow us to compare this prediction to results obtained using a realistic Arrhenius kinetic relation for the reaction. We find qualitative agreement

between our two methods and find that thermal decomposition is important when attempting to predict the severity of strain localization. The presence of the reaction localizes the deformation to zones as narrow as a few microns. This extreme localization leads to dramatic dynamic weakening, suggesting thermal decomposition reactions may play an important role in earthquake mechanics.

UPDATES FOR THE CVM-H INCLUDING NEW REPRESENTATIONS OF THE OFFSHORE SANTA MARIA AND SAN BERNARDINO BASINS AND A NEW MOHO SURFACE (B-128)

A. Plesch, C. Tape, R. Graves, J.H. Shaw, P. Small, and G. Ely

We deliver an updated version of the Community Velocity Model to the SCEC UCVM as version 11.9. Major improvements include a newly compiled Moho surface, addition of the offshore Santa Maria basin, a new detailed representation of the San Bernardino basin, and a much smoother transition between the low resolution area and high resolution area at the southern border of the Los Angeles basin.

The new Moho surface was compiled by Tape et al. from a large number of data sources, including global data sets, receiver functions and and active-source studies. In replacing this surface care was taken to ensure that the depth intervals around the revised Moho level both in the crustal and in the mantle data grids of the model were properly assigned to crust or mantle, and consequently parametrized with velocities extrapolated from the underlying mantle model or from the crustal background model.

In the offshore Santa Maria basin we extended the definition of the basement surface using reflection seismic data (McIntosh et al., 1991) to the very western margin of the model, as well as to the north. This offshore basin addition removed an abrupt transition from the basin to the background model. We smoothly extrapolated sediment velocities from the onshore model into this new offshore basin area.

We also added a basin representation for the San Bernardino basin to the model. The basement surface is based on gravity data (Anderson, 2000) and seismic reflection data (Stephenson et al., 2004). To the west the relatively small basin is connected by a thin veneer of sediments to the Los Angeles basin whereas to the ESE the basin is represented as gradually tapering out keeping in mind that the data there allow for other interpretations. The velocity structure (Vp) in the basin is defined by stacking velocities (Stephenson et al., 2004) and a 1D velocity profile (Graves, 2008) combined to a basin thickness-depth-velocity function. Vs is derived from Vp using Brocher (2004).

Finally, we revised the transition from the high to the low resolution models, removing a discrepancy in the velocity structure between the southern margin of the high resolution model in the Los Angeles area and the surrounding low resolution model. We modified the high resolution area by introducing a smooth N-S gradient in the previously existing delta between the low and high resolution models in a region at its southern margin.

WHAT'S COOKING? EVALUATING FRICTIONAL STRESS USING EXTRACTABLE ORGANIC MATERIAL IN FAULT ZONES (A-073)

P.J. Polissar, H.M. Savage, R.E. Sheppard, E.E. Brodsky, and C.D. Rowe

Determining the absolute stress on faults during slip is one of the major goals of earthquake physics as this information is necessary for full mechanical modeling of the rupture process. One indicator of absolute stress is the total energy dissipated as heat through frictional resistance. The heat results in a temperature rise on the fault that is potentially measurable and interpretable as an indicator of the absolute stress. We present a new paleothermometer for fault zones that utilizes the thermal maturity of extractable organic material to determine the maximum frictional heating experienced by the fault. As a rock is heated, temperature-sensitive molecules degrade, increasing the abundance of refractory organic molecules. On the short timescales involved in fault heating, these reactions are strongly temperature dependent and therefore track the maximum temperature achieved during fault slip. Furthermore, because there are no retrograde reactions in these organic systems, the maximum heating signature is preserved. We investigate four fault zones. According to a variety of organic thermal maturity indices, the thermal maturity of the wall rocks falls within the range of heating expected from the bounds on burial depth and time, indicating that the method is robust and in some cases improving our knowledge of burial depth.

Only the Pasagshak Point Megathrust, AK, which is also pseudotachylyte-bearing, shows differential heating between the fault and off-fault samples. Our finding confirms that this rapid heating is sufficient to measurably alter the thermal maturity of organic molecules. However, most of the faults did not get hotter than the surrounding rock during slip. Simple temperature models coupled to the kinetic reactions for organic maturity let us constrain certain aspects of the fault during

slip such as fault friction, maximum slip in a single earthquake, the thickness of the active slipping zone and the effective normal stress. Because of the significant length of these faults, we find it unlikely that they never sustained large earthquakes. Therefore we focus on the implications that either 1) some faults undergo dynamic weakening, at least during large earthquakes, or 2) that slip is not confined to very thin localized zones during earthquakes.

THE ADVANTAGES OF FIELD WORK (A-021)

M.M. Ponce-Zepeda

Peer-driven fieldwork transformed student to investigators by challenging them to be responsible for the success of the entire group. Fellow investigators were responsible for managing a detailed field notebook, sampling, planning routes, level logger maintenance, x-ray diffractometer analysis interpretation, and constantly troubleshooting. Mentorship from and challenges proposed by the USU faculty further built on this scaffolding of field experience.

First hand fieldwork provides a battery of beneficial skills that many undergraduate geology students, at the two-year college level, rarely participate in. The advantage of including two-year college students allows for dynamic research from an untapped resource. The East Los Angeles College (ELAC) Geology Club, a student-run club at an inner city community college, facilitated data collection from gryphons and mudpots in the Salton Trough. Students tested temperature, pH, electrical conductivity, and total dissolved solids in the field. This collaborative effort is symbiotic as sharing responsibilities allowed USU to save funds and provided ELAC with the opportunity to participate in research. The collaboration allowed all students to gain confidence in new sampling skills, and collaborate in an ongoing study. By sharing the opportunity to conduct fieldwork more students are able to engage in the learning process and contribute to scientific discovery.

ANALYZING AMBIENT NOISE USING USB MICRO-ELECTRO-MECHANICAL SYSTEMS (MEMS) ACCELEROMETERS (B-084)

H.J. Potter, A. Chung, and J. Lawrence

Collecting data for building stability analysis is typically cost prohibitive using traditional (large and expensive) seismometers. If inexpensive (<$150) micro-electro-mechanical systems (MEMs) accelerometers become sensitive enough to detect ambient noise, then low-cost building stability analyses could be achieved. This would reduce a key barrier to collecting vast quantities of data important for earthquake engineering. The data are collected through the Quake-Catcher Network (QCN), a volunteer distributed computing network that allows host computers to relay data measured from the USB accelerometer to the QCN server through the internet.

In this study, we compare the noise floor of four different USB accelerometers (12-bit O-navi, 14-bit JoyWarrior, 16-bit O-navi, and 24-bit O-navi) deployed on the fourth floor of the Mitchell building at Stanford University. We first examined if ambient noise differed by floor by comparing data collected on seven different floors with the same type of sensor (14-bit JoyWarrior). We Fast Fourier transform ten-minute durations of acceleration data to create power spectral density (PSD) distributions for each sensor. The PSD's of the four different sensor types showed that the newer O-navi sensors have lower noise floor than the older Joy Warrior sensors. Similarly, PSDs of the Joy Warrior sensor deployed on different floors showed that the instrument in the basement had lower noise floor. Small spikes seen in a few of the PSDs could not be correlated with other sensors, indicating that the spikes were mostly caused by instrument noise. Unfortunately, the current sensors used in this experiment cannot be used in ambient noise analysis; however, the next generation sensor should have a lower noise floor capable of detecting high amplitude ambient noise.

OPENSHA AND THE USGS NATIONAL SEISMIC HAZARD MAPS (B-089)

P.M. Powers

The USGS is currently preparing for the next release of the National Seismic Hazard Maps (NSHM), due out in 2014. With each 6-year release cycle, the logic trees behind the maps that balance the best available science and expert opinion have become increasingly complex. This complexity is reflected in the source code used to generate the maps. I am therefore investigating the viability of OpenSHA as an alternate platform for generating the national maps. OpenSHA is an open-source, Java-based platform for performing seismic hazard analysis (*http://www.opensha.org*). It is under active development and has a broad user base that spans both academia and industry. The Global Earthquake Model (GEM) has adopted OpenSHA as the hazard engine of choice, and the 2014 NSHM will be developed in parallel using OpenSHA and updated versions of the 2008 Fortran codes. To demonstrate the viability of OpenSHA and verify the national maps in the process, I generate versions of the 2008 NSHM (at return periods of 2% and 10% in 50 years and for several common spectral periods: PGA, 0.2 sec, 1.0 sec, and

3.0 sec). In the worst cases, the OpenSHA maps agree to within 5% of the values determined using the 2008 Fortran codes; generally the discrepancy is much lower. There are two primary contributors to the observed discrepancies. The first arises from how each codebase handles fault geometry: given a fault source and an associated magnitude frequency distribution, there is no established best practice for representing floating events on a fault surface. The second arises from optimizations in the Fortran code. Whereas OpenSHA is currently not optimized, the Fortran codes make use of numerous precalculated lookup arrays for ground motions, distance approximations, hanging-wall effects and the like. While speeding up the code significantly, the mean hazard at a point can be slightly different than it would be in the absence of such approximations. Regardless of what platform is used in the future, this exercise provides an opportunity to cross-verify and debug each codebase, as well as identify key issues related to fault and point source model definition, selection, and implementation.

PALEOSEISMIC INVESTIGATION OF THE SAN GORGONIO PASS FAULT ZONE NEAR CABEZON, CALIFORNIA (A-134)

S. Ramzan and J.D. Yule

The discontinuous nature of the San Andreas fault at San Gorgonio Pass has led to competing models about whether or not large earthquakes can rupture through this structurally complex region. To test these models we excavated trenches across the San Gorgonio Pass fault zone (SGPFZ) near Cabezon as part of a larger effort (also see McBurnett and Yule, this volume). Our site is located ~100 m to the east of a site excavated in 1997 by Yule where trenches uncovered evidence for at least one earthquake 500-700 yrs ago. At the 1997 site heavy bioturbation and low sedimentation rates hampered efforts to distinguish events. The new site, located where two alluvial fans merge, was selected for its higher sedimentation rates and excellent stratigraphy. Excavations at the new site show weak soil layers that subdivide the stratigraphy into six units (units 100 to 600, from base to top of the section). The units form tabular to wedge-shaped layers up to ~1 m thick. In general, the base of each unit consists of yellowish-gray, thin- to medium-bedded sand and pebbly sand, with occasional gravel lenses and mud and silt interlayers. The tops of each unit are more massive; they locally contain numerous burrows and display a slight orange-red oxidized soil (?) horizon. A distinct angular unconformity lies at the base of unit 400. Units that underlie the unconformity (100-300) are cut by a fault that strikes N35-50° E and dips 15-30° NW. The fault shows 1.0 to 1.5 m of vertical separation, equivalent to 2.5 to 6 m of slip resolved parallel to a N45°W slip vector. Unit 400 is up to 1 m thick at the south end of the trench and pinches out against the fault scarp on the north. A channel fill sequence in unit 500 caps the scarp. The stratigraphic (onlap) and structural (faulting) relations clearly restrict the most recent event (MRE) to have occurred post- and pre-deposition of units 300 and 400, respectively. Radiocarbon ages (n=12) from detrital charcoal fragments constrain the timing of this earthquake to between ~600-800 yrs BP. We suspect that the story here is incomplete because, due to a road that we could not excavate, we did not extend the trenches across the entire fault zone. However, results from this and the 1997 study (which trenched the complete fault zone) suggest that the MRE occurred 600-700 yrs BP. Evidence from Cabezon therefore supports a model with infrequent ruptures (by San Andreas fault standards) in San Gorgonio Pass and rare through-going events.

IMPROVING GPS STRAIN ESTIMATES ON SUB-DAILY TIMESCALE (A-069)

Y. Reuveni, S. Kedar, S. Owen, and F. Webb

The study of the strain field resulting from active plate boundary deformations across active plate boundary zones is one of the primary scientific objectives of global GPS-based geodetic measurements. Furthermore, observations of aseismic strain accumulation are required for advancing our understanding of the earthquake cycle, which is the main motivation for the establishment of GPS networks such as SCIGN, PBO and GEONET in Japan. Here, we present an improved GPS analysis strategy that enables us to reduce the noise level of GPS-based sub-daily strain measurements up to a factor of 10. This will allow the monitoring of sub-daily deformation, and provide exceptional spatial coverage for monitoring sub-daily strain deformation improved sub-daily resolution of positions and baseline estimates is maintained through GPS analysis approach, which reduces the key sources of error such as diurnal path effects, path delays caused by reflections and refractions of the GPS signal near the receiver (multipath), and the ionosphere and troposphere. We will present analysis of the resolution power of sub-daily baseline estimates as a function of baseline lengths and frequency.

STOCHASTIC SIMULATION OF EARTHQUAKE GROUND MOTION COMPONENTS FOR SPECIFIED EARTHQUAKE AND SITE CHARACTERISTICS: A TOOL FOR PERFORMANCE-BASED EARTHQUAKE ENGINEERING (B-009)

S. Rezaeian

A method for generating an ensemble of orthogonal ground motion components for specified earthquake and site characteristics is presented (Rezaeian and Der Kiureghian, 2011). The generated synthetic ground motions can be used in performance-based earthquake engineering when a large number of recordings is required and real recorded motions are scarce or lacking. The method employs a parameterized stochastic model that is based on a time-modulated filtered white-noise process with the filter having time-varying characteristics. Whereas the input white-noise excitation describes the stochastic nature of the ground motion, the forms of the modulating function and the filter and their parameters characterize the evolutionary intensity and nonstationary frequency content of the ground motion. The stochastic model is fitted to a database of recorded horizontal ground motion component pairs that are rotated into their principal axes, a set of orthogonal axes along which the components are statistically uncorrelated. Model parameters are identified for each ground motion component in the database. Using these data, predictive equations are developed for the model parameters in terms of earthquake and site characteristics: faulting mechanism, earthquake magnitude, source-to-site distance, and site conditions. Furthermore, correlation coefficients between parameters of the two components are estimated. Given a design scenario specified in terms of earthquake and site characteristics, the results of this study allow one to generate realizations of correlated model parameters and use them along with simulated white-noise processes to generate synthetic pairs of horizontal ground motion components along the principal axes. The proposed simulation method can be easily extended to the vertical component. It does not require any seed recorded ground motion and therefore is ideal for use in performance-based earthquake engineering. This simulation method has been validated by comparing the resulting synthetic motions with real recorded motions and by comparing the statistics of their elastic response spectra with the values predicted by the Next Generation Attenuation ground motion prediction equations.

Rezaeian and Der Kiureghian. Simulation of orthogonal horizontal ground motion components for specified earthquake and site characteristics. Earthquake Engineering & Structural Dynamics, Published online (Early View): May 17, 2011. DOI: 10.1002/eqe.1132.

PARTIAL TESTS AND ACID TESTS OF GROUND-MOTION MODELS FOR INHIBITION OF VERY STRONG SHAKING (B-015)

D.A. Rhoades, G.H. McVerry, and J.X. Zhao

Abrahamson and Wooden (2010) (AW) pointed out that the Rhoades et al. (2008) (RZM) test for inhibition of very strong shaking in ground-motion models assumes independence of total residual; it does not allow for correlation in the total residuals resulting from the inclusion of both inter-event and intra-event error terms in the models. Therefore, for a highly unbalanced sample, such as that chosen for fitting the Abahamson and Silva Next Generation Attenuation (AS-NGA) models, the test does not give a reliable estimate of the statistical significance of deviations of the expected number of exceedances of very strong ground-motion levels from the actual number in the sample. AW proposed replacing the RZM test by two partial tests, in which either the random inter-event or intra-event errors are regarded as fixed effects, and found that the AS-NGA model passed these partial tests. This shows that the model can be confidently applied to future earthquakes where one of these error terms is known exactly in advance, but does not show how the model can be expected to perform in the realistic case where both of the error terms are random. Here, using a simulation approach, we adapt the RZM test to take account of correlation in the total residuals, and apply it to test for inhibition in the Zhao et (2006) and AS-NGA models for peak ground acceleration.

A TESTABLE EARTHQUAKE LIKELIHOOD MODEL BASED ON PROXIMITY TO KNOWN SOURCES (B-121)

D.A. Rhoades and M.W. Stirling

Known earthquake sources include mapped faults and past earthquakes. We propose a long-term earthquake likelihood model which makes use of both types of source, but does not invoke the concepts of fault segments or characteristic earthquakes. The model has two components, one based on proximity to past earthquakes, taking into account the magnitude of each, and another based on proximity to mapped faults, taking into account the slip-rate of each. The Gutenberg-Richter law is invoked for earthquake magnitudes and an inverse power law for the diminution of earthquake rate density with

distance from past earthquakes and mapped faults. The parameters of each component are optimised using a target catalogue, and the rate density of the combined model is estimated as an optimal linear combination of the two components. The model has been applied to the New Zealand region using the active fault database and the earthquake catalogue since 1964. In a retrospective analysis, the combined model has an informative gain (log likelihood increase) per earthquake of about 0.15 over each of its components. The model is suitable for comparison with other long-term models in the testing centers of the Collaboratory for the Study of Earthquake Predictability.

SEARCHING FOR A PALEOTSUNAMI RECORD IN SOUTHERN CALIFORNIA: LESSON'S FROM THAILAND'S ANDAMAN COAST. (A-154)

B.P. Rhodes and M.E. Kirby

In 2004, no paleotsunami deposits were known from the Andaman Coast of Thailand; in 2011, southern California likewise has no confirmed paleotsunami deposits. In the case of Thailand, a flurry of research followed the 2004 tsunami. After several months of futile searching in favorable environments by several research teams, candidate deposits were finally located. Subsequent research confirmed paleotsunami deposits at 2 locations: in a mangrove forest at Klong Thap Lamu (KTL)(Rhodes et al., 2011); and in swales in a wide beach plain at Koh Prathong (Jankaew et al., 2008). At KTL, cores located a buried layer of coral and shell rubble within peat with a lateral extent that closely matched the location of the 2004 tsunami rubble layer. We interpreted this event horizon as a paleotsunami deposit, with an age between 2720 and 4290 cy BP. Shortly after the discovery at KTL, Jankaew et al. (2008) discovered a sequence of at least 3 sand sheets sandwiched between peaty soil layers within wet swales at Koh Prathong. In order to expand this discovery, and better date the events, we have spent > 20 days on Koh Prathong north of the earlier discovery. We have identified at least 7 additional sites with a spatially heterogeneous distribution of between 1 and 4 sand layers. The dates (in progress) should allow correlation of the sand layers between swales and will establish a tsunami chronology for this area.

During our search in Thailand, we learned important lessons that should help locate paleotsunami deposits elsewhere. We propose to search for deposits in the wetlands of southern California. The following lessons will inform our search: 1) Paleotsunami deposits are heterogeneous in thickness and extent. Cores taken in widely spaced sites could miss a significant deposit; 2) Quantitative physical sedimentology, including grain size analyses, magnetic susceptibility, organic content, and microfossils can not only characterize the paleotsunami deposit, but also can identify the environment of deposition of the encasing sediment; 3) Bioturbation can mix a tsunami sand in with the encasing muddy, organic-rich sediment; the sandy layer may not be "visible" except via quantitative grain size analysis; and, 4) In the organic rich sediments where paleotsunami deposits are typically found, 14C dating can be frustrated by sediment reworking by the tsunami, and by modern roots. Bracketing dates must be obtained from abundant and carefully chosen samples.

LUMINESCENCE DATING AS A TOOL FOR ASSESSING THE VARIABILITY OF FAULT SLIP RATES AND PALEOSEISMIC EVENTS ON TIMESCALES OF 10 TO 100,000 YEARS (A-130)

B.J. Roder, E.J. Rhodes, M.J. Lawson, L. McAuliffe, J.F. Dolan, and S.F. McGill

The Mojave Desert, California, USA, is crossed by a number of major active fault systems that have played an important role in landscape development and represent a significant seismic hazard. Critical questions include the degree to which fault slip is clustered into episodes of more rapid movement, followed by periods of reduced activity, and whether slip is accommodated by different sub-parallel faults within a single system. These issues are important for understanding fault dynamics and improving earthquake risk assessment. While radiocarbon dating, terrestrial cosmogenic nuclides and U-series dating of carbonate overgrowths can help constrain the timing of events, an absence of organic matter, thin or pulsed deposition along with problems of signal inheritance, and unpromising depositional conditions can render each of these techniques ineffective.

OSL (optically stimulated luminescence) and IRSL (infrared stimulated luminescence) dating have a key role to play. These techniques rely on the gradual trapping of electrons in the crystal lattice of quartz and feldspar grains by interaction with environmental ionizing radiation during burial. This follows zeroing of the signal by daylight exposure as sediment grains are transported by surface processes. Despite significant advances in OSL dating of quartz over the past decade, in many tectonically active areas, the luminescence characteristics of quartz grains are not well-suited for the determination of precise age estimates. Here, we explore the potential for using OSL and IRSL signals to provide age control for the paleoseismic record and morphological features associated with the Garlock fault, a major left-lateral fault that extends for 250 km in a broad east-west arc across the northern edge of the Mojave block. Slip rate determinations are based on the direct dating of

offset depositional features on small alluvial fans. Age determination of samples from the El Paso Peaks paleoseismic site provides the opportunity to compare OSL and IRSL age estimates to an established radiocarbon chronology based on 31 dates. We present preliminary OSL and IRSL age estimates measured as part of SCEC award #11198, clearly demonstrating the great potential of this dating approach.

COULOMB STRESS CHANGES IMPARTED BY SIMULATED M>7 EARTHQUAKES TO MAJOR FAULT SURFACES IN SOUTHERN CALIFORNIA (B-104)

J.C. Rollins, G.P. Ely, and T.H. Jordan

To study static stress interactions between faults in southern California and identify cases where one large earthquake could trigger another, we select fourteen M>7 events simulated by the SCEC/CME CyberShake project and calculate the Coulomb stress changes those events impart to major fault surfaces in the UCERF2 fault model for the region. CyberShake simulates between 6 and 32 slip distributions for each event at a slip sampling resolution of 1 km, and we calculate stress changes on fault surfaces at the same resolution, a level of detail which is unprecedented in studies of stress transfer and which allows us to study the way that variabilities in slip on the source can affect imparted stress changes. We find that earthquakes rupturing the southern San Andreas fault generally decrease Coulomb stress on right-lateral faults in the Los Angeles basin, while M>7 events on the San Jacinto, Elsinore, Newport-Inglewood and Palos Verdes faults generally decrease stress on parallel right-lateral faults but increase Coulomb stress on the Mojave or San Bernardino sections of the San Andreas. Stress interactions between strike-slip and thrust faults and between the San Andreas and Garlock faults depend on the rupture area of the source. Coulomb stress changes imparted by simulated SAF events to locations on the San Jacinto and Garlock faults within ~8 km of the San Andreas appear to be influenced more by the nearby distribution of high and low slip on the San Andreas than by the overall slip distribution across the entire rupture. Using a simplified model, we calculate that an area of no slip surrounded by high slip on a rupture imparts strong Coulomb stress increases ≤7 km to either side of the source fault, possibly explaining the apparent ~8-km range of influence of local slip on the San Andreas. Additionally, we devise a method for evaluating uncertainty values in Coulomb stress changes caused by uncertainties in the strike, dip and rake of the receiver fault. These findings may be useful in understanding stress interactions between faults of different orientations and rakes, stress transfer and variability at short distances from the source fault, and applications of uncertainty values to Coulomb stress changes.

NEW BE-10 EXPOSURE AGES AND FRAGILITIES FOR PRECARIOUSLY BALANCED ROCKS TEST PSHA AND RUPTURE MODELS IN SOUTHERN CALIFORNIA (B-008)

D.H. Rood, R. Anooshehpoor, G. Balco, J. Brune, R. Brune, L. Grant Ludwig, K. Kendrick, M. Purvance, and I. Saleeby

Currently, the only empirical tool available to test maximum earthquake ground motions spanning timescales of 10 ky-1 My is the use of fragile geologic features, including precariously balanced rocks (PBRs). The ages of PBRs together with their areal distribution and mechanical stability ("fragility") constrain probabilistic seismic hazard analysis (PSHA) over long timescales; pertinent applications include the USGS National Seismic Hazard Maps (NSHM) and tests for ground motion models (e.g., Cybershake). Until recently, age constraints for PBRs were limited to varnish microlamination (VML) dating techniques and sparse cosmogenic nuclide data; however, VML methods yield minimum limiting ages for individual rock surfaces, and the interpretations of cosmogenic nuclide data were ambiguous because they did not account for the exhumation history of the PBRs or the complex shielding of cosmic rays. We have recently published a robust method for the exposure dating of PBRs combining Be-10 profiles, a numerical model, and a three-dimensional model for each PBR constructed using photogrammetry (Balco et al., 2011, Quaternary Geochronology). Here, we use this method to calculate new exposure ages and fragilities for 4 PBRs near the San Andreas, San Jacinto, and Elsinore faults at the Lovejoy Buttes, Round Top, Pacifico, and Beaumont South sites (in addition to the recently published age of 18.7 +/- 2.8 ka for a PBR at the Grass Valley site). We combine our ages and fragilities for each PBR, and use these data to test the USGS 2008 NSHM PGA with 2% in 50 year probability, USGS 2008 PSHA deaggregations, and basic hazard curves from USGS 2002 NSHM data.

INVESTIGATIONS OF MICROBIAL LIFE IN THE MUD NEAR THE SALTON SEA, CALIFORNIA (A-018)

S.C. Rosove

Thermal springs can be an area where microorganisms can thrive, an aspect of studying the gryphons and mud pots we examined near the Salton Sea was to identify potential microbes. The idea is that since the type of environment is borderline extremophiles, with high temperatures, the smell of sulfur, salt precipitating in some areas, and black mud. Through collecting mud samples we would plate them onto potato based agar plates to attempt to grow anything present in the mud. The

colonies would be characterized in terms of how they appeared (colour and texture), and isolated to try to genetically identify them. We found that microorganisms do live in the mud, but with the agar we used very few culturable organism came to fruition. We were unable to genetically identify them as their DNA was not amplified. The next steps of the project are to continue trying to amplify the DNA for genetic analysis, perhaps using different methods. Also, using different types of agar plates to plate the mud on to see if different types of organisms appear instead of the small set obtained. It would be interesting to use media with higher sulfur and salt concentrations, as this was prominent in the environment.

THREE-DIMENSIONAL MODELING OF INTERSEISMIC DEFORMATION IN TAIWAN (A-055)

B. Rousset, S. Barbot, J.P. Avouac, Y.J. Hsu, and J.C. Lee

The Taiwan Island, a complex orogenic system at the intersect between an arc-continent collision and a subduction zone, is a much studied area. The 1999 Chi-Chi earthquake, the latest of a series of Mw 7+ earthquakes, was a reminder of the active tectonics shaping the island. Yet, the structure of the fault system at crustal depths, responsible for the sequence of devastating earthquakes, is not fully resolved. In this study, we establish the fault structure of Taiwan in its entirety that reconciles many geophysicals observations (seismicity, tomography and structural analyses) and explains the pattern of secular deformation. We optimise and complement the fault geometry at crustal depths using data from several GPS networks, including island-wide continuous measurements and regional campaigns. The inversion of the entire velocity field in Taiwan can be challenging because a large portion of the convergence is taking place on deep décollements, far below the surface, for which a precise geometry is unknown. We develop a new inversion scheme where we use the difference between nearby GPS stations to constrain slip rate on faults. We show that the method allows for a much finer optimization of fault geometry and is particularly fitted for a complex faulting environment such as Taiwan. We find that the Chihshang segment of the Longitudinal Valley Fault is sliping at a rate of ~30 mm.yr-1 whereas the Yumei segment to the north appears locked. The Chelungpu Fault and the Shuangtung Fault also appear locked, but the décollement subjacent is inferred to move at a rate of 20 to 30 mm.yr-1. The Chuckou system, which originated 10 earthquakes of Mw 6+ in the past 100 years seems locked at the surface and loaded from below at a rate of ~20 mm.yr-1. The Hsincheng fault, 50 km to the south of Taipei seems loaded from below at a rate of 12 mm.yr-1. The GPS data alone are not sufficient to determine uniquely the degree and area of locking and, but if completely locked, such a fault could host an earthquake of Mw 6.2 with a recurrence time of ~40 yr. The integration of decades of GPS surveys, previous fine-scale structural analyses, seismic and tomography imaging allows for a refined three-dimensional fault structure for Taiwan. Our study reveals areas under active loading, which could represent substantial seismic hazards around the regions of Hualien, Jhudong, Fongyuan and Chiayi.

PROBABILISTIC ASSESSMENT OF BUILDING RESPONSE TO SIMULATED AND RECORDED GROUND MOTIONS (B-088)

K.L. Rowe and A.B. Liel

This study examines the seismic response of buildings subjected to both physics-based ground motion simulations and recorded ground motions time histories. Nonlinear dynamic analysis is used to evaluate the response of six archetypical reinforced concrete (RC) frame buildings to a set of three simulated and three recorded earthquakes. Using probabilistic analysis, building response is examined and statistically compared to determine whether the broadband ground motion simulations and the recorded ground motion time histories yield similar distributions for building response, focusing especially on the likelihood of earthquake induced collapse. Important aspects of the ground motion time histories that may cause differences in building response are then examined to attempt and explain the source of these dissimilarities in response. This study also examines the potential of applying the probabilistic analysis outlined in this study to the broader area of seismic risk analysis by using response results from recorded or simulated ground motions to predict regional collapse risks. This offers a new framework with which to evaluate building vulnerability to seismic events. Results indicate that, when examined based on the elastic spectral response, there are significant differences in building response. These differences are attributed in part to the long-period energy (T>1sec) content of the ground motions, and can be captured if ground motion intensity is quantified in terms of inelastic spectral displacement. Higher mode effects, earthquake duration, energy content and rate of energy accruement were not found to have a significant effect on differences in building response.

WIDESPREAD TRIGGERING OF EARTHQUAKES IN THE CENTRAL US BY THE 2011 M9.0 TOHOKU-OKI EARTHQUAKE (B-074)

J.L. Rubinstein and H.M. Savage

The strong shaking of the 2011 M9.0 off-Tohoku earthquake triggered tectonic tremor and earthquakes in many locations around the world. We analyze broadband records from the USARRAY to identify triggered seismicity in more than 10 different locations in the Central United States. We identify triggered events in many states including: Kansas, Nebraska, Arkansas, Minnesota, and Iowa. The locally triggered earthquakes are obscured in broadband records by the Tohoku-Oki mainshock but can be revealed with high-pass filtering. With the exception of one location (central Arkansas), the triggered seismicity occurred in regions that are seismically quiet. The coincidence of this seismicity with the Tohoku-Oki event suggests that these earthquakes were triggered. The triggered seismicity in Arkansas occurred in a region where there has been an active swarm of seismicity since August 2010. There are two lines of evidence to indicate that the seismicity in Arkansas is triggered instead of part of the swarm: (1) we observe two earthquakes that initiate coincident with the arrival of shear wave and Love wave; (2) the seismicity rate increased dramatically following the Tohoku-Oki mainshock. Our observations of widespread earthquake triggering in regions thought to be seismically quiet remind us that earthquakes can occur in most any location. Studying additional teleseismic events has the potential to reveal regions with a propensity for earthquake triggering.

JUMPING RUPTURE DEPENDENCE ON FRICTION FORMULATIONS AT STRIKE-SLIP FAULT STEPOVERS (A-077)

K.J. Ryan and D.D. Oglesby

It is well known that fault stepovers can under some circumstances allow through-going rupture, and under other circumstances cause rupture termination (e.g., Harris and Day, 1993; Kase and Kuge, 1998; Duan and Oglesby, 2006). However, the effects of different friction law formulations on jumping rupture have not been extensively explored. In this study we investigate how 4 different frictional parameterizations affect the ability of rupture to jump a stepover. We compare linear slip weakening friction (Ida, 1972) and 3 forms of rate- and state-dependent friction (Dieterich, 1978, 1979; Ruina, 1983): ageing law, slip law, and slip law with strong rate-weakening (e.g., Rice, 1999, 2006; Beeler and Tullis, 2003; Rojas et al., 2009). We use the dynamic finite element method (Barall, 2008) to model earthquake rupture along 2-D strike-slip stepovers, in both extensional and compressional settings. We consider frictional effects on systems with large and small absolute stress fields, with large and small stress drops, respectively. We have found that for parameterizations with the same effective slip-weakening distance, the functional form of the friction law can greatly effect whether or not rupture is likely to jump and continue along the secondary fault segment. In particular, we find that the slip law, which has lower fracture energy for a given effective slip-weakening distance than the aging law or the linear slip-weakening law, allows rupture to jump larger stepover widths than the aging or slip-weakening law. We also investigate the effect of the Linker-Dieterich (Linker and Dieterich, 1992) dependence of state variable on normal stress. We find through preliminary models that adding normal stress dependence to the state variable delays nucleation on the secondary fault segment when compared to normal-stress independent state evolution laws. Nucleations along the secondary segments occur in areas of decreased normal stress, in both compressional and dilational stepovers. However, state-variable dependent normal stress results in an increase in state variable (fault strength) in those same areas, thereby hindering rupture. Thus, we illustrate that the ability of rupture to jump a stepover can depend strongly on the formulation of the friction law. In the future we will investigate the effects of friction law formulation on other fault geometries including dip-slip faults.

AN EVALUATION OF THE RELM TEST FORECASTS (B-120)

M.K. Sachs, Y.T. Lee, D.L. Turcotte, J.R. Holliday, and J.B. Rundle

The RELM test of earthquake forecasts in California was the first competitive evaluation of earthquake forecasts of future earthquakes. Participants submitted forecast probabilities of occurrence of $M \geq 5$ earthquakes in $0.1° \times 0.1°$ cells for the period 1 January 2006 to 31 December 2010. During this period 31 test earthquakes occurred in 22 test cells. This seismic activity was dominated by earthquakes associated with the $M = 7.2$ El Mayor-Cucapah earthquake. Forecasts of the number of earthquakes and their locations are considered separately. The five forecasts for the entire test region are evaluated in several ways. In addition we evaluated thirteen forecasts for southern California.

SPACE GEODETIC INVESTIGATION OF INTERSEISMIC DEFORMATION DUE TO THE SAN JACINTO FAULT NEAR ANZA, CA (B-153)

V. Sahakian, Y. Fialko, Y. Bock, and T. Rockwell

We performed campaign GPS measurements of near-field interseismic deformation in the Anza section of the San Jacinto fault zone. Our survey occupied 27 benchmarks within 4 km of the fault trace, including a 400-m long alignment array established across the fault in 1990 by SDSU investigators. To constrain the fault slip rate and locking depth, we used SCEC CMM4 velocities in addition to our near field campaign GPS measurements. We inverted GPS velocities using a non-linear Monte-Carlo algorithm. The best-fitting slip rate and fault locking depths are 14 ± 2 mm/yr and 16 ± 3 km, respectively. We also investigated the occurrence of shallow creep on the fault by comparing GPS positions of the alignment array monuments to the total station measurements conducted in the early 1990's. This comparison yields a maximum rate of rotation of .002 degrees per year within the array. We combined these observations with simple models of shallow creep to place an upper bound on the amount of surface creep. The data appear to rule out shallow creep at a rate greater than 0.5 mm/yr. This upper bound is well below predictions of models of interseismic deformation on rate-and-state faults assuming a two to three kilometer deep velocity-strengthening layer.

MEDIA TEAM - ABSTRACT (A-159)

A. Sampson, H. Humpleman, and M. Romano

At the University of Southern California, nineteen students from across the nation are brought together to study earthquake behavior at the Southern California Earthquake Center (SCEC). These students, coming from a wide range of academic interests, compose the intern class for the Undergraduate Studies in Earthquake Information Technology (UseIT). Each intern class is presented with a Grand Challenge - a task that can only be completed by combining each interns' knowledge of computer science and geology - and it is the Media Team's responsibility to record this collaboration and development throughout the entirety of the internship.

In order to accomplish this, the Media Team was in constant dialogue with each of the separate groups working on different aspects of the Grand Challenge. They collected multiple interviews with interns and supervisors each week and wrote the voice over narration for the documentary as the interviews were clipped. Shooting footage to be paired with the interviews in the documentary was a constant process, as was logging and editing the footage filmed. As the Media Team experienced the internship, they decided UseIT would be best represented by having both a scientific documentary and more light-hearted intern experience video.

ANALYZING BUILDING RESPONSE THROUGH THE USE OF GPS & STRONG MOTION DATA FOR THE MONITORING OF INFRASTRUCTURE (A-072)

D. Sanchez, Y. Bock, and D. Melgar

Major earthquakes constantly remind us of the vulnerability of structures to ground vibrations and motion. Accelerometers are currently being used to collect ground motions in order to estimate displacements of the ground and of structures. However, this approach has its limitations, providing poor accuracy at low frequencies. With the innovations in GPS sensor technologies, their contribution in collecting data from earthquakes along with accelerometers has led to obtaining a more accurate method in estimating ground displacements via a Kalman filter, a signal processing methodology not common in seismology or earthquake engineering. The advantage of this new methodology is that it takes the strengths of both, seismic and geodetic networks in order to provide a more precise record of ground motion from an earthquake, resolving the problems encountered in the low frequencies of the accelerometer data, which are of great interest in tall structures. In this study, a Kalman filter is being explored using both GPS and accelerometer earthquake engineering data obtained from two sources: An earthquake simulation testing at UCSD's Large High-Performance Outdoor Shake Table, which enables us to compare the results with the true ground-motion that was simulated, ensuring the Kalman filter's accuracy and data from the April 2010 Mw 7.2 El Mayor-Cucapah earthquake to test the method in a real world setting. The goal is to investigate these new displacement records of strong ground motion to determine if a response spectra of higher accuracy can be developed across a wider range of frequency values and have a better representation of the effects in low frequency building response due to strong ground motions.

HOW DOES DAMAGE AFFECT RUPTURE PROPAGATION ACROSS A FAULT STEPOVER? (A-074)

H.M. Savage and M.L. Cooke

We investigate the potential for fault damage to influence earthquake rupture at fault step-overs using a mechanical numerical model that explicitly includes the generation of cracks around faults. We compare the off-fault fracture patterns and slip profiles generated along faults with a variety of frictional slip-weakening distances and step-over geometry. Models with greater damage facilitate the transfer of slip to the second fault. Increasing separation and decreasing the overlap distance reduces the transfer of slip across the step over. This is consistent with observations of rupture stopping at step-over separation greater than 4 km (Wesnousky, 2006). In cases of slip transfer, rupture is often passed to the second fault before the damage zone cracks of the first fault reach the second fault. This implies that stresses from the damage fracture tips are transmitted elastically to the second fault to trigger the onset of slip along the second fault. Consequently, the growth of damage facilitates transfer of rupture from one fault to another across the step-over. In addition, the rupture propagates along the damage-producing fault faster than along the rougher fault that does not produce damage. While this result seems counter to our understanding that damage slows rupture propagation, which is documented in our models with pre-existing damage, these model results are suggesting an additional process. The slip along the newly created damage may unclamp portions of the fault ahead of the rupture and promote faster rupture. We simulate the M7.1 Hector Mine Earthquake and compare the generated fracture patterns to maps of surface damage. Because along with the detailed damage pattern, we also know the stress drop during the earthquake, we may begin to constrain parameters like the slip-weakening distance along portions of the faults that ruptured in the Hector Mine earthquake.

PREPARING TRIAL MODELS OF SPATIAL VARIABILITY IN GEOTECHNICAL VELOCITIES FOR ASSESSING EFFECTS ON GROUND MOTIONS (B-058)

W.H. Savran and J.N. Louie

The Clark County Parcel Map provides us with a data set of geotechnical velocities in Las Vegas Valley, at an unprecedented level of detail. Las Vegas Valley is a basin with similar geologic properties to some areas of Southern California. We first analyze elementary spatial statistical properties of the Parcel Map. We then investigate the same spatial statistics from the peak ground velocity r226e226s226u226l226t226s226 226c226o226m226p226u226t226e226d226 226f226r226o226m226 226 o 226 n 226 e 226 226 m 226 o 226 d 226 e 226 l 226 226 (226 B 226 l 226 a 226 c 226 k 226 226 H 226 i 226 l 226 l 226 s 226 226F226a226u226l226t226)226 226t226h226a226t226 226i226n226c226o226r226p226o226r226a226t226e226 226t226h226e226 226P226a226r226c226e226l226 226M226a226p226 226a226s226 226p226a226r226a226m226e226t226e226r226s226.226 226 W 226 e 226 226 c 226 o 226 n 226 f 226 i 226 g 226 u 226 r 226 e 226 226 f 226 i 226 n 226 i 226 t 226 e 226 - 226 d 226 i 226 f 226 f 226 e 226 r 226 e 226 n 226 c 226 e 226 226 s 226 e 226 i 226 s 226 m 226 i 226 c 226 226 w 226 a 226 v 226 e 226 226p226r226o226p226a226g226a226t226i226o226n226 226m226o226d226e226l226s226 226a226t226 2260226.2265226 226H226z226 226w226i226t226h226 226L226L226N226L226s226 226E2263226D226 226c226o226d226e226,226 226u226t226i226l226i226z226i226n226g226 226t226h226e226 226P226a226r226c226e226l226 226M226a226p226 226a226s226 226i226n226p226u226t226 226p226a226r226a226m226e226t226e226r226s226 226t226o226 226c226o226m226p226u226t226e226 226a226 226P226G226V226 226d226a226t226a226 226s226e226t226 226f226r226o226m226 226t226h226e226 226e226a226r226t226h226q226u226a226k226e226 226s226c226e226n226a226r226i226o226.226 226 226T226h226e226 226r226e226s226u226l226t226i226n226g226 226P226G226V226 226i226s226 226f226r226a226c226t226a226l226 226o226v226e226r226 226t226h226e226 226s226a226m226e226 226s226p226a226t226i226a226l226 226f226r226e226q226u226e226n226c226i226e226s226 226a226s226 226t226h226e226 226V226s22632260226 226d226a226t226a226 226s226e226t226s226 226a226s226s226o226c226i226a226t226e226d226 226w226i226t226h226 226t226h226e226i226r226 226r226e226s226p226e226c226t226i226v226e226 226m226o226d226e226l226s226.226 226 226T226h226e226 226f226r226a226c226t226a226l226 226d226i226m226e226n226s226i226o226n226 226i226s226 226s226y226s226t226e226m226a226t226i226c226a226l226l226y226 226l226o226w226e226r226 226i226n226 226a226l226l226 226o226f226 226t226h226e226 226P226G226V226 226m226a226p226s226 226a226s226 226o

EARTHQUAKE AGES AND DISPLACEMENTS, FRAZIER MOUNTAIN PALEOSEISMIC SITE (A-141)

K.M. Scharer, R.J. Weldon, B.C. Gibson, and A.R. Streig

The Frazier Mountain paleoseismic site is located on a poorly understood section of the southern San Andreas fault, mid-way between the well-known Carrizo Plain and Mojave sites of Bidart Fan and Pallett Creek. Emerging paleoseismic evidence indicates that earthquakes along this stretch repeat at a similar pace, with an average interval of ~122 years between A.D. 1000

and 1857. Individual intervals vary considerably, including an interval of ~325 years between the sixth and fifth earthquakes back, followed by two intervals lasting less than 50 years each. We modeled slip required to gently fold the sediments during three of the earthquakes with a 2D, optimized trishear inverse model that uses a simulated annealing algorithm. Due to the orientation of the trenches and broad shape of the folds, the slip estimate (3 m total in 3 events) is a minimum yet indicates an average magnitude of at least M7 using standard regressions. In combination, paleoseismic evidence appears similar to the historic record: individual events can be separated by less than 50 or greater than 150 years, and slip data suggest that large ≥M7 events often bridge the Carrizo and Mojave sections of the San Andreas fault.

RATE/STATE FRICTIONAL NUCLEATION AND DYNAMIC RUPTURE ON LOW-STRESS FAULTS WITH THERMAL WEAKENING EFFECTS (A-095)

S.V. Schmitt, A.M. Bradley, E.M. Dunham, and P. Segall

It is believed that faults sustain large shear stresses during the nucleation phase, but slip at much lower stresses during earthquakes. Nucleation is typically characterized by rate- and state-dependent friction, in which slip accelerates after shear stress τ grows to about 0.6 to 0.9 times the effective normal stress σ. During earthquakes, dynamic weakening mechanisms such as shear heating-induced thermal pressurization of pore fluid and flash heating of asperity contacts allow for slip to occur at much lower values of τ. Since 0.6σ is ~100 MPa at seismogenic depths with hydrostatic pore pressure, earthquakes likely nucleate in regions of elevated τ/σ and propagate outward into regions of low τ/σ. Noda & others [JGR, 2009] investigated this issue with numerical simulations in which they included both flash weakening and thermal pressurization. They initiated ruptures with a sudden perturbation in τ on a weakly stressed fault. Flash heating quickly dominated the fault strength, with thermal pressurization contributing a modest amount of additional weakening. Recent work has shown that thermal pressurization may, however, become the dominant weakening mechanism during quasi-static nucleation, well before the onset of seismic radiation [Schmitt & others, JGR, 2011]. We present more physically-motivated simulations of early rupture that model fault weakening mechanisms through nucleation and into the dynamic slip phase. The initial τ/σ heterogeneities remain idealized, but we now consider two types. The first type is a region of elevated τ with uniform σ, while the other type has uniform τ with a low-strength region of diminished σ. We use a quasi-static code to model fault slip from well below steady-state to the early stages of nucleation. Late in nucleation, we switch to a fully dynamic code that otherwise solves the same equations for friction and coupled thermal effects. Our results indicate that there are differences between ruptures on high-stress and low-strength heterogeneities. In rate/state frictional nucleation, slip zones capable of accelerating above steady state have a minimum length dimension L. Heterogeneities must be of greater size than a few L in order to host instability at low background stress, and since $L \propto 1/\sigma$, nucleation under low strength conditions requires a much larger heterogeneity. Thermal weakening effects are also affected by the heterogeneity; they are subdued in the low-strength case because of reduced heating with low τ.

CSEP OVERVIEW (B-117)

D. Schorlemmer, M.C. Gerstenberger, N. Hirata, D.D. Jackson, C. Jiang, T.H. Jordan, W. Marzocchi, K.Z. Nanjo, G. A. Papadopoulos, D.A. Rhoades, S. Wiemer, Z. Wu, J.D. Zechar, and CSEP Working Group

The Collaboratory for the Study of Earthquake Predictability (CSEP) established 4 earthquake forecast testing centers around the world. These centers are rigorously testing more than 100 earthquake forecast models in a truly prospective manner. Centers are operating in Los Angeles (US), Wellington (NZ), Tokyo (JP), and Zurich (CH), covering many different regions and tectonic environments: California, New Zealand, Western Pacific, Japan, and Italy. Besides new upcoming regional earthquake forecast testing, CSEP has started a global testing program which is targeting the magnitude range of destructive earthquakes that are relevant for seismic hazard and risk. This program is the first link in the chain of facilities that aim to test seismic hazard and risk models and their underlying hypotheses. To complement the current activities, CSEP is developing methods for assessing the reliability of earthquake early warning algorithms, for understanding the uncertainties and limits of earthquake source inversions, and for the prospective testing of ground motion prediction models. CSEP researchers are also working on creating testable models for many seismological hypotheses, e.g. characteristic earthquakes, maximum magnitude to fault length relation. CSEP is collaborating with large modeling efforts like the Uniform California Earthquake Rupture Forecast (UCERF3) and the Global Earthquake Model (GEM). We present the ongoing activities and give perspectives for the future development of CSEP and its global collaboration.

RESULTS FROM THE REGIONAL EARTHQUAKE LIKELIHOOD MODELS EXPERIMENT (B-119)

D. Schorlemmer, J.D. Zechar, M.J. Werner, M.C. Gerstenberger, and D.A. Rhoades

One of the primary objectives of the Regional Earthquake Likelihood Models (RELM) working group was to formalize earthquake occurrence hypotheses in the form of prospective earthquake rate forecasts for California. RELM scientists developed more than a dozen time-invariant five-year forecasts for the period 1 January 2006-1 January 2011; they also outlined a performance evaluation method and provided a conceptual description of a Testing Center in which to perform this forecast experiments. Subsequently, researchers working within the Collaboratory for the Study of Earthquake Predictability (CSEP) have begun implementing Testing Centers in different locations worldwide, and the RELM forecast experiment-a truly prospective earthquake prediction effort-was conducted within the U.S. branch of CSEP. The experiment, designed to compare this set of forecasts is now complete. Here, we present the forecasts under evaluation and the results of this experiment. We also evaluate the sample of observed target earthquakes in the context of historical seismicity within the testing region. Finally, we discuss the implications of the results for California hazard assessment and for further experiments.

ADVANCEMENTS IN PROBABILISTIC SEISMIC NETWORK COMPLETENESS STUDIES (B-126)

D. Schorlemmer

An important characteristic of any seismic network is its detection completeness, which should be considered a function of space and time. Many researchers rely on robust estimates of detection completeness, especially when investigating statistical parameters of earthquake occurrence.

We present the Probability-based Magnitude of Completeness (PMC) method for computing the spatial variation and temporal evolution of detection capability of seismic networks based on empirical data only: phase data, station information, and the network specific attenuation relation. New developments are extending this method to complex 3D structures like mining environments.

We present studies of regional networks from California, Switzerland, Italy, Japan, New Zealand, and compare the result with estimated completeness levels of other methods. We report on the time evolution of monitoring completeness in these regions. Scenario computations show the impact of different possible network failures and offer estimates of possible network optimization strategies. Optimizations are reducing the necessary processor time for computing. All presented results are published on the CompletenessWeb (*www.completenessweb.org*) from which the user can download completeness data from all investigated regions, software codes for reproducing the results, and publication-ready and customizable figures.

VISUALIZING STRUCTURAL RESPONSE AND SITE AMPLIFICATION USING EARTHQUAKE DATA RECORDED AT THE NEES@UCSB FIELD SITES (A-024)

S.H. Seale, J.H. Steidl, L.B. Seale, and A. Chourasia

We present animation created with data recorded at the Garner Valley Downhole Array field site (GVDA) from two events. The two events were both located directly below GVDA. The M3.1 event occurred on 3 June 2011 and the M3.6 event occurred on 14 June 2011. Both of these events were recorded by all channels in the boreholes at GVDA and on the Soil-Foundation-Structure-Interaction (SFSI) structure. Animation of the SFSI structure was created with Blender (*http://www.blender.org/*), an open source 3D content creation suite.

The animation shows distinct characteristics of the braced and unbraced SFSI structure. Resonance of the unbraced roof of the structure after the arrival of the S-wave can clearly be seen.

The greatest displacements occur in the horizontal plane compared to the vertical component. Rocking modes excited by the earthquake are also clearly visible. Visualization Services group at the San Diego Supercomputer Center created animation of the ground excitation. Using data recorded in the boreholes at GVDA, the animation clearly shows the amplification of the signal in the near surface materials. These visualizations created from actual earthquake data provide new insight into ground and structural response to strong motion. The animations will be used as teaching tools for college-level engineering courses.

CHARACTERISTICS OF STRONG GROUND MOTION ATTENUATION DURING THE 2010 M7.1 DARFIELD AND 2011 M6.3 CHRISTCHURCH, NEW ZEALAND EARTHQUAKES (B-021)

M. Segou and E. Kalkan

M7.1 Darfield earthquake, occurred 40 km west of Christchurch on September 4th 2010, and it was followed by another M6.3 event on 21st February 2011. These events had disastrous effects in the city's center and suburbs within the Canterbury region. Processed data, corresponding to peak ground acceleration (PGA) and 5% damped spectral acceleration (SA) values at 0.3, 1, 3 s, were used for evaluating the performance of global ground motion prediction equations (GMPEs) to estimate peak and spectral values. The selected GMPEs are: Graizer and Kalkan (2007 and 2009) (GK07), and Next Generation of Attenuation (NGA) models of Abrahamson and Silva (2008) (AS08), Boore and Atkinson (2008) (BA08), Campbell and Bozorgnia (2008) (CB08), and Chiou and Youngs (2008) (CY08). To rank the relative performance of the GMPEs, we followed a traditional residual analysis and an information theoretic approach, suggested by Scherbaum et al. (2009). For the Darfield earthquake, we observed an overestimation of predicted ground motion at short periods (PGA and SA at 0.3 s). The overestimation is evident in the NGA models at 70 km and beyond, and it is very prominent for the case of CB08 model. The GK07 model performs as well as the NGA models. For the Christchurch earthquake the overestimation begins around 40 km for all GMPEs, and it is less pronounced for the GK07 and CY08. At longer periods (SA at 1 s and 3 s), the overall trend of the overestimation is suppressed, possibly due to large amplitudes of ground motions associated with the basin amplification and Moho reflection. At 1 s, BA08 and CB08 perform better for distances less than 50 km, than for greater distances. The ranking results

for both events show that the performance of the GK07, BA08 and CY08 models are equal, while the CB08 and AS08 models show relatively poorer performance.

SURFACE DEFORMATION AND SLIP DISTRIBUTION OF THE 1994 NORTHRIDGE EARTHQUAKE DETERMINED FROM INSAR (A-041)

C.M. Severson, G.J. Funning, and S.T. Marshall

The January 17, 1994 M6.7 Northridge earthquake occurred in the densely populated suburbs northwest of Los Angeles, California. Occurring on a previously unknown blind thrust fault, it was the most costly earthquake in United States history causing 60 deaths and ~20 billion dollars in damage. Since the earthquake, several other blind thrusts have been identified in the area. In order to quantify the influence, in terms of stress changes, of the Northridge event on surrounding faults, detailed knowledge of the location, orientation and amount of fault slip is important. Existing Interferometric Synthetic Aperture Radar (InSAR) models of this earthquake were developed by fitting the pattern of displacements by trial and error, and were therefore somewhat subjective. In the 15 years since the original studies were published a number of new modeling tools and community data products have been developed that should enable us to produce more detailed, and robust results.

We measure the coseismic deformation of this earthquake using InSAR. A pair of descending images from the European Space Agency's ERS-1 satellite, containing the earthquake are processed using the ROI_PAC software, and show uplift of up to ~45 cm centered on 118.508°W, 34.321°N. Using this data, we first employ a nonlinear inversion to determine the parameters of the single rectangular dislocation that best fits the data. The best-fitting fault has strike: 110°, dip: 40.6° to the southwest, length: 14.2 km, width: 8.5 km, top fault depth: 6.7 km, slip: 2m, and moment: 1.1*1019 Nm. These results are relatively consistent with other published geodetic work, and the global CMT moment estimate.

However, slip on a single rectangular dislocation does not completely model the observed deformation. Residual deformation to the west of our best-fitting dislocation suggests that additional fault segments may have ruptured. In order to investigate this, we solve for a detailed slip distribution for the event in a non-negative least squares sense, using a non-planar triangular element fault mesh modified from the SCEC CFM and the Poly3D code to calculate model displacements. This model shows a main asperity, with peak slip of ~3 m, bounded at its western edge by a geometrical barrier, a down-dip parallel corrugation in the fault. Secondary slip of about 0.6 m to the west of this feature is also present, and is the likely source of the residual deformation in our original single dislocation model.

COSEISMIC SLIP DISTRIBUTION AND HIGH FREQUENCY RADIATION OF THE 2010 MW 7.3 EL MAYOR-CUCAPAH EARTHQUAKE (B-049)

G. Shao, T.E. Yano, X. Zhao, C. Ji, K.M. Larson, K. Hudnut, and T. Herring

We investigated the slip history of the 2010 Mw 7.3 El Mayor-Cucapah earthquake by jointly inverting near-field strong motion records, teleseismic broadband waves, long-period surface waves, along with GPS static observations and high rate GPS waveforms. Our inversion results reveal a complex rupture process of the 2010 event. The rupture initiated at a depth of 7.3 km on a so-called El Mayor-Hardy fault dipping 57 degrees to the east. It first propagated upward along the fault with dominant normal motions in the beginning 12 s, and then triggered the strike slip on the other two high-angle faults with the Sierra Cucapah fault in northwest and the Indiviso fault in southeast. The rupture propagated on those three faults simultaneously and released about 90% of the total seismic moment between 12 s and 40 s. The fault rupture had a total duration of about 60 s and released a total seismic moment of 1.31×10^{20} N.m. Our estimation to the average rupture velocity is relatively low, only 1.2 km/s. This earthquake is dominated by the right-lateral strike-slip motion but with significant normal motion below the hypocenter region, resulting a large (31%) CLVD component. The slip distribution on the northwest fault segment is well constrained by extensive high rate GPS waveforms in California. The heterogeneous rupture on the northwest segment, changing from oblique motion to pure strike-slip and to oblique motion from the epicenter to the northwest, is consistent with surface observations. However, the slip distribution on the southeast Indiviso fault is poorly constrained because of lack of near field observations.

In addition to the finite fault slip model constrained by the low-frequency (> 2s) data, we also study the high frequency radiation of the 2010 El Mayor-Cucapah by using a recently developed back-propagation method. The novel feature of our approach is to consider the propagation and radiation difference among stations by computing the deconvolution of theoretical Green's functions and to use a stacking approach instead of nonlinear inversions to image high frequency radiations.

CONSTANT STRESS DROP FITS EARTHQUAKE SURFACE SLIP-LENGTH DATA (B-115)

B.E. Shaw

Slip at the surface of the Earth provides a direct window into the earthquake source. A longstanding controversy surrounds the scaling of average surface slip with rupture length, which shows the puzzling feature of continuing to increase with rupture length for lengths many times the seismogenic width. Here we show that a more careful treatment of how ruptures transition from small circular ruptures to large rectangular ruptures combined with an assumption of constant stress drop provides a new scaling law for slip versus length which

(1) does an excellent job fitting the data,

(2) gives an explanation for the large crossover lengthscale at which slip begins to saturate, and

(3) supports constant stress drop scaling which matches that seen for small earthquakes.

We additionally discuss how the new scaling can be usefully applied to seismic hazard estimates.

HAS THE RISK OF BIG EARTHQUAKES RECENTLY INCREASED? (B-105)

P.M. Shearer and P.B. Stark

The above-average rate of earthquakes of magnitude 8 and larger in recent years has prompted speculation that this reflects a true change in the underlying rate of earthquake activity rather than simply expected fluctuations in a homogeneous random process. Temporal clustering, including aftershock sequences, is well known at regional scales. Similar rate changes at global scales would have important implications for assessments of seismic hazard and our understanding of how faults interact. We examine large (magnitude M 7.5 to 9.6) earthquakes in the PAGER and PDE catalogs from 1900 to present. Because local clustering is not at issue, we decluster the catalog by removing events for which larger earthquakes occur within 3 years and 1000 km. The smoothed (5-yr averaged) annual rate of $M \geq 8$ earthquakes has been at a record high roughly since 2004, but rates have been almost as high before, and the rate of $7.5 \leq M < 8$ earthquakes is close to its historical average. Moreover, computer simulations show that the recent clustering in large earthquakes is not surprising for a homogeneous process defined by the observed average occurrence rates. The high recent rates of $M \geq 8$ and $M \geq 8.5$ earthquakes are expected to occur at least once during the 111-year history of the catalog.

A more general question is whether the earthquake catalog (after removing local clustering) is statistically distinguishable from a realization of a homogenous Poisson process. We estimate the p-value (the chance of observing such large inhomogeneity if seismicity arose from a homogeneous Poisson process) to be 57% for the locally declustered events of $M \geq 8$ and 96% for $7.5 \leq M < 8$ events. Thus the evidence against the Poisson hypothesis is quite weak. Although the underlying process might have changed, the observed fluctuations would not be surprising if seismicity followed a Poisson process with constant expected rate. It is also difficult to explain why a change in physical processes would increase the rate of the largest earthquakes but not the rate of smaller earthquakes. This suggests that the global risk of large earthquakes is no higher today than it has been in the past.

IMPACTS OF STATIC AND DYNAMIC STRESS CHANGES ON TREMOR AND CREEP ALONG THE LOWER-CRUSTAL SAN ANDREAS FAULT (A-103)

D.R. Shelly, K.M. Johnson, Z. Peng, D.P. Hill, and C. Aiken

Tremor activity along the central San Andreas fault near Parkfield is strongly affected by small stress changes induced by other earthquakes. Tremor responds both to permanent (static) stress changes from nearby earthquakes as well as to temporary (dynamic) stresses from passing seismic waves. We examine the impacts of the nearby 2003 M 6.5 San Simeon and 2004 M 6.0 Parkfield earthquakes, as well as triggering by numerous regional and teleseismic earthquakes.

We find major changes in tremor activity rates associated with the nearby earthquakes. For the San Simeon event, this includes a stress shadow north of Parkfield that persists for about 1 month following the earthquake, consistent with the modeled static shear stress change. On the other hand, tremor activity following the Parkfield earthquake is increased both north and south of Parkfield, especially at shallow sources close to the rupture. Again, this behavior is consistent with the static shear stress imparted by the event. These elevated activity rates persist for more than a year in some places. Together with a growing understanding of tremor as a reflection of fault creep, these observations allow us to track the spatial and temporal evolution of lower-crustal afterslip (see Shelly and Johnson, 2011).

Dynamic stresses also produce notable effects on tremor activity, and we observe triggering by regional events as small as M 5.4. While observations of triggering and modulation of tremor during passing surface waves are now relatively common, we also observe accompanying migration of tremor along the fault. Furthermore, we find that some triggered episodes persist for hours or days after the waves have passed. We interpret this behavior as reflecting small, prolonged fault creep episodes, also known as slow slip events. Although the prevalence of this phenomenon in other areas is unknown, we note that since creep events can trigger earthquakes, this mechanism provides a possible explanation for observations of delayed dynamic earthquake triggering (see Shelly et al., 2011).

References:

Shelly, D. R. and K. M. Johnson (2011), Tremor reveals stress shadowing, deep postseismic creep, and depth-dependent slip recurrence on the lower-crustal San Andreas fault near Parkfield, Geophys. Res. Lett., L13312.

Shelly, D. R., Z. Peng, D. P. Hill, and C. Aiken (2011), Triggered creep as a possible mechanism for delayed dynamic triggering of tremor and earthquakes, Nature Geoscience, 4, 384-388.

HYDROCHEMISTRY OF ACTIVE FAULT ZONES- SALTON SEA, CA AND NORTHERN UTAH (A-019)

K.A. Shervais

We examined 12 mud pots and mud volcanoes in the Salton Sea region and 30 + thermal springs (within a half mile of a fault) in Northern Utah and Southern Idaho. The following analyses were performed on samples from both locations: GIS, water composition, gas composition, microbiological influence, and on-going temperature and water level statistics. We then used geothermometers (equations based on Na-K-Ca values) to examine the predicted temperature maximum each sample reached. This was cross-referenced with geothermal gradient data to hypothesize the depth from which each sample came for both Utah an California samples. The on-going temperature data as well as the on-going water level statistics were cross-referenced with earthquake data in the region to mark any correlation. This temperature and water-level data was also examined to note any time-dependent trends which will be shown in figures. The last major analysis was the examination of pH over time; pH in the Salton Sea region seems to be decreasing over the past 20 years at least. Gas sample analysis is currently ongoing; finding a lab that does the analyses we requested has proved difficult. The ultimate goal, which is currently being examined is finding commonality between the Utah and California field area with the intent of creating a set of characteristics universal to water near faults.

3D SIMULATIONS OF DYNAMIC RUPTURE ON ROUGH FAULTS (A-086)

Z. Shi and S.M. Day

Natural faults during their evolution stages manifest varying degrees of geometric complexities over a broad range of scales spanning from larger-scale features such as branching and segmentation to smaller-scale features such as topographic variations on the slip surface. At a mic 232 r 232 o 232 s 232 c 232 o 232 p 232 i 232 c 232 232 s 232 c 232 a 232 l 232 e 232 , 232 232 s 232 u 232 r 232 f 232 a 232 c 232 e 232 232 r 232 o 232 u 232 g 232 h 232 n 232 e 232 s 232 s 232 232 a 232 f 232 f 232 e 232 c 232 t 232 s 232 232 t 232 h 232 e 232 232 f 232 r 232 i 232 c 232 t 232 i 232 o 232 n 232 a 232 l 232 232 p 232 r 232 o 232 p 232 e 232 r 232 t 232 i 232 e 232 s 232 232 t 232 h 232 r 232 o 232 u 232 g 232 h 232 232 i 232 t 232 s 232 232 r 232 o 232 l 232 e 232 232 i 232 n 232 232 t 232 h 232 e 232 232 d 232 i 232 s 232 t 232 r 232 i 232 b 232 u 232 t 232 i 232 o 232 n 232 232 a 232 n 232 d 232 232 e 232 v 232 o 232 l 232 u 232 t 232 i 232 o 232 n 232 232 o 232 f 232 232 c 232 o 232 n 232 t 232 a 232 c 232 t 232 232 a 232 r 232 e 232 a 232 s 232 232 o 232 f 232 232 t 232 h 232 e 232 232 s 232 l 232 i 232 d 232 i 232 n 232 g 232 232 s 232 u 232 r 232 f 232 a 232 c 232 e 232.232 232 A 232 t 232 232 a 232 232 l 232 a 232 r 232 g 232 e 232 r 232 232 s 232 c 232 a 232 l 232 e 232 , 232 232 t 232 h 232 e 232 232 g 232 e 232 o 232 m 232 e 232 t 232 r 232 i 232 c 232 232 i 232 r 232 r 232 e 232 g 232 u 232 l 232 a 232 r 232 i 232 t 232 i 232 e 232 s 232 232 o 232 f 232 232 t 232 h 232 e 232 232 f 232 a 232 u 232 l 232 t 232 232 a 232 f 232 f 232 e 232 c 232 t 232 s 232 232 t 232 h 232 e 232 232 i 232 n 232 t 232 e 232 r 232 - 232 s 232 e 232 i 232 s 232 m 232 i 232 c 232 232 a 232 n 232 d 232 232 p 232 o 232 s 232 t 232 - 232 s 232 e 232 i 232 s 232 m 232 i 232 c 232 232 s 232 t 232 a 232 t 232 i 232 c 232 232 s 232 t 232 r 232 e 232 s 232 s 232 232 d 232 i 232 s 232 t 232 r 232 i 232 b 232 u 232 t 232 i 232 o 232 n 232 232 t 232 h 232 a 232 t 232 232 i 232 s 232 232 r 232 e 232 s 232 p 232 o 232 n 232 s 232 i 232 b 232 l 232 e 232 232 f 232 o 232 r 232 232 e 232 a 232 r 232 t 232 h 232 q 232 u 232 a 232 k 232 e 232 232 n 232 u 232 c 232 l 232 e 232 a 232 t 232 i 232 o 232 n 232 . 232 232 O 232 u 232 r 232 232 s 232 t 232 u 232 d 232 y 232 , 232 232 h 232 o 232 w 232 e 232 v 232 e 232 r 232 , 232 232 f 232 o 232 c 232 u 232 s 232 e 232 s 232 232 o 232 n 232 232 t 232 h 232 e 232 232 f 232 u 232 n 232 d 232 a 232 m 232 e 232 n 232 t 232 a 232 l 232 232 r 232 o 232 l 232 e 232 232 t 232 h 232 a 232 t 232 232 s 232 u 232 r 232 f 232 a 232 c 232 e 232 232 r 232 o 232 u 232 g 232 h 232 n 232 e 232 s 232 s 232 232 p 232 l 232 a 232 y 232 s 232 232 i 232 n 232 232 t 232 h 232 e 232 232 d 232 y 232 n 232 a 232 m 232 i 232 c 232 232 p 232 r 232 o 232 c 232 e 232 s 232 s 232 e 232 s 232 232 o 232 f 232

233 e 233 a 233 r 233 t 233 h 233 q 233 u 233 a 233 k 233 e 233 233 r 233 u 233 p 233 t 233 u 233 r 233 e 233 233p233r233o233p233a233g233a233t233i233o233n233 233a233n233d233 233r233e233s233u233l233t233a233n233t233 233 g 233 r 233 o 233 u 233 n 233 d 233 233 m 233 o 233 t 233 i 233 o 233 n 233 233 u 233 s 233 i 233 n 233 g 233 233n233u233m233e233r233i233c233a233l233 233s233i233m233u233l233a233t233i233o233n233s233 233o233f233 2333233D233 233 d 233 y 233 n 233 a 233 m 233 i 233 c 233 233 r 233 u 233 p 233 t 233 u 233 r 233 e 233 . 233 233 A 233 s 233 233 h 233 a 233 v 233 e 233 233 b 233 e 233 e 233 n 233 233 s 233 h 233 o 233 w 233 n 233 233 i 233 n 233 233 s 233 e 233 v 233 e 233 r 233 a 233 l 233 233 p 233 r 233 e 233 v 233 i 233 o 233 u 233 s 233 233 2 233 D 233 233 n 233 u 233 m 233 e 233 r 233 i 233 c 233 a 233 l 233 233s233t233u233d233i233e233s233,233 233d233y233n233a233m233i233c233 233r233u233p233t233u233r233e233s233 233p233r233o233p233a233g233a233t233i233n233g233 233a233l233o233n233g233 233r233o233u233g233h233 233f233a233u233l233t233 233s233u233r233f233a233c233e233 233c233a233n233 233e233x233c233i233t233e233 233h233i233g233h233-233f233r233e233q233u233e233n233c233y233 233r233a233d233i233a233t233i233o233n233 233a233s233 233 t 233 h 233 e 233 y 233 233 a 233 c 233 c 233 e 233 l 233 e 233 r 233 a 233 t 233 e 233 233 a 233 n 233 d 233 233d233e233c233e233l233e233r233a233t233e233 233f233r233o233m233 233i233n233t233e233r233a233c233t233i233o233n233 233 w 233 i 233 t 233 h 233 233 g 233 e 233 o 233 m 233 e 233 t 233 r 233 i 233 c 233 233 i 233 r 233 r 233 e 233 g 233 u 233 l 233 a 233 r 233 i 233 t 233 i 233 e 233 s 233 . 233 233 A 233 l 233 s 233 o 233 233 p 233 e 233 r 233 t 233 u 233 r 233 b 233 a 233 t 233 i 233 o 233 n 233 233 o 233 f 233 233 l 233 o 233 c 233 a 233 l 233 233 d 233 y 233 n 233 a 233 m 233 i 233 c 233 233 s 233 t 233 r 233 e 233 s 233 s 233 233 d 233 u 233 e 233 233 t 233 o 233 233 r 233 o 233 u 233 g 233 h 233 n 233 e 233 s 233 s 233 233 c 233 o 233 n 233 t 233 r 233 i 233 b 233 u 233 t 233 e 233 s 233 233 t 233 o 233 233 t 233 h 233 e 233 233 h 233 e 233 t 233 e 233 r 233 o 233 g 233 e 233 n 233 e 233 o 233 u 233 s 233 233d233i233s233t233r233i233b233u233t233i233o233n233s233 233o233f233 233s233l233i233p233 233r233a233t233e233 233a233n233d233 233s233l233i233p233 233o233v233e233r233

GENERATING STOCHASTIC SOURCE MODELS USING INSIGHTS FROM LABORATORY EARTHQUAKES (B-016)

H. Siriki and S. Krishnan

We present a method for generating a suite of stochastic source models for high magnitude (Mw 6.0 - 8.0) strike-slip earthquakes. Slip, rupture-velocity & rise-times across the 2-D fault area are parameters that define these models. Laboratory earthquakes by Mello et al. & Lu 2008 point to two preferred rupture velocities, one in the sub-Rayleigh regime (~ 0.87* Vs) & the other in the super-shear regime (~ 1.414* Vs), depending upon the initial level of pre-stress on the fault. To determine the rupture velocity in our model, we calculate pre-stress across the fault using the orientation between fault plane & maximum principal stress. The orientation is calculated as average of stochastic realizations of a distribution fit to data from the World Stress Map project. We generate slip distributions based on a hierarchy model in which the rupture area is divided into two sub-segments (here on referred to as sub-seg) recursively until a dimensional aspect-ratio close to 1.0 is reached for each sub-seg. Each sub-seg is discretized into a number of smaller sub-faults. Slip values are assigned randomly to sub-faults using a Gaussian distribution with a mean equal to the average-slip of its sub-seg. The standard deviation (s.d.) for the distribution is calculated from seismic-moment (mo) of its corresponding sub-seg using a relation between s.d & mo. We developed this relation with data from finite-source models (inversions) of historic earthquakes. A filter is applied to smooth the distribution of slip across the fault thus preventing any drastic variations in the values of slip between intermittent points. We calculate rise-time for each sub-fault using slip to rise-time ratios that are generated as linearly independent realizations of a probability model for these ratios. This model is inferred from the aforementioned laboratory earthquake measurements. We select only those stochastic source models such that the 1-D power spectral density along strike & dip decays as a power (2.0-4.0, Lavallee et al. 2006) of wave number. We discard the source model if this condition is not satisfied. We have written a program that unifies all the aforementioned process & generates stochastic source models that could be used to address uncertainties about future earthquakes. We will use the ground motions generated from these source-models to quantify the risk to tall buildings (sensitive to long-period ground motions) from San Andreas earthquakes over the next 30 years

SEISMICALLY DAMAGED REGOLITH AS SELF-ORGANIZED FRAGILE GEOLOGICAL FEATURE (B-001)

N.H. Sleep

Repeated strong earthquakes damage shallow brittle regolith reducing its shear modulus to a value where little Coulomb failure occurs at the peak ground velocity (PGV) in later strong earthquakes. The shear modulus (and S-wave velocity) as a function of depth thus evolve to the value where the rock just exceeds its Coulomb elastic limit in typical strong strain events. Near-field dynamic motion of strike-slip faults is amenable to scaling relationships. Type A velocity pulses of Makris and

Black (2004) last over a second. Motion is mostly horizontal and fault parallel as with a Love wave. Deep stiff rocks determine the dynamic strain in the shallow regolith; the deep dynamic strain is the measured particle velocity (PGV) divided by the deep S-wave velocity. The shallow dynamic stress is the shallow shear modulus times the dynamic strain. Dynamic shear traction exists on vertical planes all the way to the surface. Coulomb failure thus occurs at shallow depths where the rock is sufficiently stiff with the imposed strain. S-wave velocities in sandstone near Cajon Pass (Anderson et al.) increase with depth as expected for dynamic strain of 1.e-3 and 2 m/s dynamic velocity (PGV). Such damage may trigger observed downslope sackung movement near Wrightwood on modest 19° slopes. Conversely, shallow stiff intact rocks indicate that strong shaking (high PGV) did not occur.

SCEC UCVM – UNIFIED CALIFORNIA VELOCITY MODEL (B-129)

P. Small, P. Maechling, T. Jordan, G. Ely, and R. Taborda

The SCEC Unified California Velocity Model (UCVM) is a software framework for a state-wide California velocity model. UCVM provides researchers with two new capabilities: (1) the ability to query Vp, Vs, and density from any standard regional California velocity model through a uniform interface, and (2) the ability to combine multiple velocity models into a single state-wide model. These features are crucial in order to support large-scale ground motion simulations and to facilitate improvements in the underlying velocity models.

UCVM provides integrated support for the following standard velocity models: SCEC CVM-H, SCEC CVM-S and the CVM-SI variant, USGS Bay Area (cencalvm), Lin-Thurber Statewide, and other smaller regional models. New models may be easily incorporated as they become available. Two query interfaces are provided: a Linux command line program, and a C application programming interface (API). The C API query interface is simple, fully independent of any specific model, and MPI-friendly. Input coordinates are geographic longitude/latitude and the vertical coordinate may be either depth or elevation. Output parameters include Vp, Vs, and density along with the identity of the model from which these material properties were obtained.

In addition to access to the standard models, UCVM also includes a high resolution statewide digital elevation model, Vs30 map, and an optional near-surface geo-technical layer (GTL) based on Ely's Vs30-derived GTL. The elevation and Vs30 information is bundled along with the returned Vp,Vs velocities and density, so that all relevant information is retrieved with a single query. When the GTL is enabled, it is blended with the underlying crustal velocity models along a configurable transition depth range with an interpolation function.

Multiple, possibly overlapping, regional velocity models may be combined together into a single state-wide model. This is accomplished by tiling the regional models on top of one another in three dimensions in a researcher-specified order. No reconciliation is performed within overlapping model regions, although a post-processing tool is provided to perform a simple numerical smoothing. Lastly, a 3D region from a combined model may be extracted and exported into a CVM-Etree. This etree may then be queried by UCVM much like a standard velocity model but with less overhead and generally better performance due to the efficiency of the etree data structure.

POTENTIAL MAGNITUDE DEPENDENT QUIESCENCE PRIOR TO THE NORTHRIDGE EARTHQUAKE (B-031)

D.E. Smith and S.I. Sacks

Seismic quiescence 1-3 years prior to the mainshock is observed for several major Japanese earthquakes including the 1982 Urakawa-Oki quake [Taylor et al., 1992] and the 1994 Hokkaido-Toho-Oki quake [Takanami et al., 1996]. Quiescence is magnitude and location dependent, where the region surrounding the future rupture becomes significantly depleted in Mw >3.0 earthquakes a few years prior to the event. Within the future mainshock region, smaller magnitude quakes become more abundant at a slightly later time.

In this study, we observe a magnitude dependent quiescence signal with the relatively high stress drop 1994 Northridge earthquake. However, when we apply the same quiescence detection procedure to the lower stress drop 2010 Laguna Salada earthquake, we find a null result.

We compare these two recent CA earthquakes to the 1982 Urakawa-Oki earthquake. For Urakawa-Oki, Mw >3.0 earthquakes in the surrounding region start to vanish approximately 2 years before the mainshock, and small magnitude events in the fault core increase about 1 year prior to the mainshock. For Northridge, a quiescence signal begins approximately 7 years prior to the mainshock for Mw >3.0 events. Small magnitude events near the future fault rupture increase about 3-4 years prior to the

mainshock, but the signal is less well resolved than Urakawa-Oki. For Laguna Salada, no magnitude dependent seismic quiescence is observed; however, approximately 3-4 years before the earthquake, seismicity increases in the fault core region across many magnitudes.

The physics of dilatancy theory [Nur, 1972; Whitcomb et al., 1973; Scholz et al., 1973] is proposed as an explanation for seismic quiescence [Takanami et al., 1996; Scholz, 2000]. As the fault is loaded toward failure and stress increases, if stress is sufficiently high, the rock can begin to dilate. As dilation causes an increase in the rock volume, pore pressure decreases, effective normal stress increases, and the fault core strengthens [Rice, 1975]. Because the fault core supports more of the stress, seismicity of the surrounding region will decrease, which is consistent with seismic quiescent observations for Urakawa-Oki or Northridge. Over time (~2-20 years) the water will percolate back into the fault core from the surrounding region. Pore pressure in the fault core increases again, normal stress decreases, and failure is encouraged.

STRESS DROP VARIATIONS OF THE SAN ANDREAS FAULT, MOJAVE SEGMENT, OVER THE LAST 2000 YEARS (A-146)

T. Solis and B. Smith-Konter

There is significant evidence suggesting that repeating earthquakes on a single fault segment are not periodic in time nor do they generate equivalent amounts of coseismic slip or stress drop. Earthquake cycle models also show that stress accumulation and stress drop are a complex function of space and time. In this study we investigate earthquake cycle stress variations from (1) a 3-D viscoelastic crustal deformation model and (2) paleoseismic slip measurements, where stress drop is traditionally estimated using the ratio of the coseismic fault slip to an appropriate scale length (fault length, fault depth, or a combination of these). Here we focus on the Wrightwood paleoseismic site, located along the Mojave segment of the San Andreas fault and use published slip estimates from 15 paleo-events to calculate a sequence of stress drops over the last 2000 years. Resulting paleoseismic slip-derived stress drops range from ~0.2-1.7 MPa (std 0.49 MPa) assuming a scale length representing the along-strike fault length. Using the 3-D model, we simulate 14 earthquake cycles of interseismic stress accumulation, coseismic stress drop, and postseismic stress relaxation from the same paleoseismic dataset, assuming a constant slip rate of 33 mm/yr and a stress drop to zero for each event. Model-derived stress drops range from 0.2-2.5 MPa (std 0.7 MPa). In the model, the stress field is distributed along the fault depth and is influenced by postseismic relaxation and neighboring fault interactions, which may contribute to the stress drop differences. To better approximate the pattern of paleoseismic stress drops and further investigate the implications of such variations at Wrightwood, we develop a model with slip rates that are adjusted over each earthquake cycle to match the recorded paleoseismic offsets. This model yields a stress drop pattern coincident with the paleoseismic data, but with larger magnitudes, ranging from 0.1-3.2 MPa (std 0.94 MPa). A better match to this model is provided by paleoseismic stress drops calculated using a characteristic scale length that reflects both the fault depth and length. While there is no obvious stress threshold for which Mojave segment earthquakes rupture, it does seem that all stress drops have been relatively small and large variations in slip rate are required to reproduce the paleoseismic data. Current work is aimed at applying this method to several other fault segments of the SAF with a rich paleoseismic history.

EFFECTS OF PARAMETERIZATION ON FINITE SOURCE INVERSIONS WITH DENSE LOCAL DATA (B-057)

S. N. Somala, J. -P. Ampuero, and N. Lapusta

The recent 2011 M9 Tohoku, Japan, earthquake was recorded by thousands of sensors at near-fault distance, orders of magnitude more than previous earthquakes. This event provides a unique opportunity to obtain high resolution images of earthquake rupture processes. Current projects of network densification, based on low-cost sensors or on remote sensing, aim at obtaining even denser coverage of future earthquakes. In order to enable the exploitation of such immense amounts of data we are developing a scalable source inversion procedure based on time-reversal adjoint inversion. We study in great detail a synthetic earthquake scenario of a vertical strike-slip fault embedded in an elastic, isotropic, homogenous half-space, with very dense data sampled every 100 m on the free surface, at near source distances, but limited to frequencies lower than 1 Hz. We adopt the linear formulation of the source inversion problem, in terms of slip rate. An iterative finite source inversion procedure is performed, involving one time-reversal (adjoint) and one forward simulation in each iteration. The finite frequency band of the data imposes a resolution limit on the source inversion. We explore the question of the optimal resolution length scale of the source parameterization. Upon inverting for localized (Gaussian) sources at several depths, we determine that a length scale of the order a few kms represents the data (f<1Hz) accurately. Furthermore, a 2 km coarsening of source parameters gives ground motions very similar to our original finely sampled source (100 m) indicating that such fineness in source parameterization is redundant. We also present the sensitivity of our source inversion to other coarser

resolutions. Overall, coarsely parameterized source reduces storage drastically, though a gain in computational time requires an equivalent coarsening of the data, and the mean slip during the adjoint iterations converges towards the mean slip of the true source (projected in the coarser mesh) in about 9 iterations.

DEVELOPING A PHYSICS-BASED RUPTURE MODEL GENERATOR BASED ON 1-POINT AND 2-POINT STATISTICS OF KINEMATIC SOURCE PARAMETERS (B-002)

S. Song

A finite-fault earthquake rupture model generator (SongRMG, Ver 1.0) has been developed, based on 1-point and 2-point statistics of key kinematic source parameters such as slip, rupture velocity, slip velocity and duration. 1-point statistics define a marginal probability density function for a certain source parameter at a given point on a fault. 2-point statistics, i.e. auto- and cross-coherence between source parameters, control the heterogeneity of each source parameter and their coupling, respectively. Sequential Gaussian simulation with simple kriging (SK) was initially adopted to perform stochastic modeling (Song and Somerville, 2010), but it was replaced with a new algorithm based on the Cholesky factorization because it is conceptually simpler to implement and also more closely linked to earthquake source inversion in the Bayesian framework, which is an important tool in constraining the 1-point and 2-point statistics of source parameters from data. Currently the 1-point variability of source parameters follows the Gaussian distribution, but it is straightforward to transform it to any other non-Gaussian distributions if desired. This transform will break the multi-Gaussian distribution assumed in the stochastic modeling, but the target covariance matrix (or correlation structure) will be preserved as long as the transformed distribution has a monotonically and smoothly increasing cumulative density function (CDF). The non-stationarity of the 1-point statistics can also be easily implemented if necessary, such as depth dependency of the 1-point variability. Following studies will focus on constraining input parameters in the stochastic model by dynamic rupture modeling, kinematic source inversion, and laboratory experiments, etc., and understanding their effects on near-fault ground motion characteristics. Additionally since the rupture model generator constrains a possible range of rupture scenarios for future events and quantify their variability within the range, it can be used as a basis to develop an extended earthquake rupture forecast model (eERF) for full-waveform-simulation-based hazard analysis.

PLATE TECTONICS: A NEWLY COMPLETED EXHIBIT IN THE SAN BERNARDINO COUNTY MUSEUM'S HALL OF GEOLOGICAL WONDERS (A-028)

K. Springer, E. Scott, and J.C. Sagebiel

The San Bernardino County Museum (SBCM) in Redlands, California is completing a suite of exhibits in our new Hall of Geological Wonders. One of the first to be realized is "Plate Tectonics". Throughout the Hall, the theme imbued in every exhibit is the process of science, inviting visitors to ask us "How do we know?" In that vein, we have positioned the theory of Plate Tectonics as the bedrock for all modern geologic studies and its development of the theory as one of the best examples of the scientific method. We initially introduce plate tectonics to the public in a series of quotations, ideas and observations of the earth from the likes of Aristotle, Native Americans, Darwin and Ben Franklin. The scientific method is introduced, explaining that scientific inquiry strives to understand how things work, objectively and without bias. The exhibit then seques to quotes from Wegener, Longwell, and Hess, finally culminating in "The Lines of Evidence", displayed as a touchable scaled giant bronze globe of the Earth's topography along with mini globes that discuss continental drift (its rock and fossil evidence), sea-floor spreading and paleomagnetism, culminating in the unified theory of plate tectonics.

"Plate Tectonics" is the scaffolding for a suite of future exhibits on earthquake science that reveal the origin of southern California's striking topography and our most notorious geologic feature, the San Andreas fault system, as the culprit. Visitors will observe the San Andreas Fault zone from our "Earth's Cylinder" – below ground in a re-created paleoseismic trench across the fault, exhibited next to a Pallet Creek and a Wrightwood fault peel, and above ground from a viewing tower. Visitors will experience a simulated earthquake in our immersive "ShakeOut Cabin", while receiving earthquake preparedness information. These exhibits explore the importance of science in everyday life, emphasizing science as a process and encouraging visitors to become a part of this process. "Did You Feel It?" and the "Quake Catcher Network" are interactives that simulate a real-time earthquake experience in a museum exhibit setting, and the "Active Earth" touch-screen kiosk provides nested online information on earthquake science. Additionally, a video of SCEC researchers will inspire visitors to explore science. This collection of exhibits will provide a unique introduction to scientific inquiry, earthquake science and earthquake preparedness for our visitors.

A NEW AGE CONSTRAINT FOR A NEAR-FAULT PRECARIOUS LANDFORM IN CENTRAL OTAGO, NEW ZEALAND (B-099)

M. Stirling, D. Rood, G. Balco, and A. Zondervan

In recent years, studies of precariously balanced rocks (PBRs) in New Zealand were focused on age determinations of features at near-fault sites. Until recently, efforts to interpret exposure ages from Be-10 data on PBRs in central Otago, an area with an equivalent climate to that of coastal central-to-northern California, were unable to resolve whether the rocks are of the order 10^3-10^4 or 10^4-10^5 years of age. Resolution of these age differences is critical to determining the utility of PBRs for constraining seismic hazard models at long return periods. Reinterpretation of cosmogenic Be-10 data for "Clyde 6", a near-fault PBR that has had eight Be-10 analyses undertaken in recent years (and three additional analyses on nearby outcrops), is possible using the methodology of Balco et al (2011). Samples collected from a vertical profile are used to interpret the rate of exhumation and thus an age for the PBR. The dating method combines measured Be-10 concentrations with a numerical model that accounts for nuclide production before, during, and after exhumation of the PBR from the subsurface. A three-dimensional model constructed from photogrammetry is used to correct for the shielding of cosmic rays due to the shape of the feature. Using all 8 Be-10 samples from Clyde 6 (and assuming zero rock erosion since exhumation), the results suggest that the "tipping age" (time at which the rock was exhumed and free to topple) is ~40 ka. The best fit model is fairly well fit to observed Be-10 concentrations, except for one sample; however, the misfit for this sample can be reduced if modest post-exhumation rock erosion (e.g. spalling) occurred at this sample location. The results also suggest that the feature sat in the subsurface for a long time period, consistent with the site being part of an exhumed Tertiary peneplain (i.e., a landform characterised by low rates of erosion). The interpreted age of Clyde 6 allows 4-6 Dunstan Fault earthquakes to have occurred since the rock was exhumed. Combined with the fragility of the feature (alpha=6 degrees), these data suggest that ground motions in these earthquakes did not exceed 0.11-0.14g (Stirling and Anooshehpoor, 2006) at this site.

THE EFFECTS OF STATIC COULOMB, NORMAL AND SHEAR STRESS CHANGES ON EARTHQUAKE OCCURRENCE IN SOUTHERN CALIFORNIA (B-103)

A.E. Strader and D.D. Jackson

Deng & Sykes (1997) found a strong correlation between receiver earthquake location and positive increase in Coulomb stress (ΔCFF). Assuming a coefficient of friction of 0.6, and resolving stresses onto assumed fault planes with uniform orientation parallel to average Pacific-North American plate motion, they found that only 15% of receiver earthquakes occur in "stress shadows" where the Coulomb stress change should impede faulting. We extended their study by adding two source earthquakes (Hector Mine, 1999 and El Mayor-Cucupah, 2010), and calculating the stress changes at the locations of 134 receiver earthquakes with magnitude 4.4 and greater after 1999. We examined shear stress, normal stress, and Coulomb stress, resolving stresses onto four different hypothetical fault planes: optimally oriented planes, a weighted average of nearby fault-plane orientations, and the two nodal planes of weighed average moment tensors of nearby earthquakes. We also computed shear, normal, and Coulomb stress histories oriented according to the four choices of fault orientation., and we tested the effect of total stress change on receiver earthquake magnitude.

Our chi square test results indicate that, with 95% confidence, receiver earthquakes do not tend to avoid stress shadows, and that the choice of plane onto which stress is resolved does not affect the result. On average, 39% of earthquakes occur at the time of maximum stress at the event location, with no significant variation depending on the choice of rupture plane or type of stress change. We found no correlation between earthquake magnitude and total stress change at the events' locations. These results suggest that instantaneous cumulative Coulomb stress, as we and Deng & Sykes modeled it, does not strongly control the locations of future earthquakes. The lack of correlation between Coulomb stress change and magnitude suggests that modeled Coulomb stress change does not control the size of earthquakes once they nucleate.

EVALUATING THE RELATIONSHIP BETWEEN LATERAL SLIP AND REPEATED FOLD DEFORMATION ALONG A TRANSTENSIVE STEP-OVER ON THE SAN ANDREAS FAULT AT THE FRAZIER MOUNTAIN SITE (A-139)

A.R. Streig and R.J. Weldon

Transtensive step-overs known as sags are among the most ubiquitous features of strike slip faults. These structures create closed depressions that collect sediment, are often wet and thus preserve organic material that can be used to date the section. It is clear from historical ruptures that these depressions grow incrementally with each earthquake. We are developing methods to carefully document and separate individual folding events, and to relate the amount of folding to the amount of horizontal slip creating the sag, with the goal of generating slip per event chronologies. This will be useful as sags are often the best sites for preserving evidence of earthquake timing, and determining slip at these sites will eliminate ambiguity inherent in tying earthquake age data from micro-stratigraphic sites to nearby undated sites with good micro-geomorphic slip evidence. We apply this approach to the Frazier Mountain site on the Southern San Andreas fault.

Approximately 20 trenches show the main active trace of the San Andreas fault right stepping ~30 m over ~100 m along strike producing two small synclinal sags that dramatically thicken the stratigraphic section. The northwest sag is about 50 m long, 15 m wide, and the southwest sag measures 20 m long and 8 m wide. Frazier has yielded good earthquake chronologies, and relationships between fold deformation and surface fault rupture for the last 6 earthquakes. We observe that the degree of sagging in the synclines varies along strike for each feature, but that the ratio of fold deformation between earthquake horizons remains constant in both sags. The penultimate earthquake, E2, produced a depression that was infilled by gravel which was subsequently folded in the most recent earthquake in 1857. Fine-grained alluvial units overlie the gravel and fill the 1857 depression such that the current surface is relatively horizontal. E2 has double the observed folding associated with the 1857 event in the core of the NW syncline. Ratios of fold deformation between events are E2 = 2*E1, E6 = 3*E2, and E6 = 2*E3.

We plan to model the folding to quantitatively assess the lateral offset, but to date we have only been able to establish minimum offset values (Scharer, Gibson, Weldon, Streig, this meeting). Qualitatively, the relative amounts of folding suggest all slip events are similar to 1857, which had ~5 meters slip at this site.

THE MECHANICS OF EARTHQUAKES AND FAULTING IN THE SOUTHERN GULF OF CALIFORNIA (B-032)

D.F. Sumy, J.B. Gaherty, W.-Y. Kim, and T. Diehl

Accurate earthquake locations and their focal mechanisms can illuminate the distribution and mode of deformation at rifted continental margins. The Pacific-North America plate boundary within the Gulf of California (GoC) provides an excellent opportunity to explore such rifting, as continental extension in the north transitions to seafloor spreading in the south. From October 2005 to October 2006, an array of fourteen four-component ocean-bottom seismographs were deployed in the GoC to record earthquakes and other natural seismic signals as part of the Sea of Cortez Ocean-Bottom Array (SCOOBA) experiment. By combining the data from this deployment with that from the on-shore NARS-Baja array, we detect and locate ~700 earthquakes (Mw 2.5-6.6) mainly located on the NW-SE striking transform faults that delineate the plate boundary. The earthquakes occur mainly during short-term swarm events that cluster predominantly around the inside corner of ridge-transform intersections, with events occurring on both the strike-slip and normal faults within the system. We use the waveforms of 31 events with high signal-to-noise long-period Rayleigh waves (Mw 3.45-4.92) to calculate regional deviatoric moment tensors and determine the focal mechanisms of these earthquakes. Most of these events exhibit right-lateral strike-slip focal mechanisms along the transform faults; however, several oblique and rotated mechanisms reveal a more complex structure within the gulf. In addition, we capture a swarm of events on Baja California along an apparent right-lateral NW-SE striking fault, which may be evidence of an extension of the Carmen fracture zone across the Baja California peninsula. A calculation of seismic coupling using data from global earthquake catalogs combined with our dataset illuminates regions of active deformation along broad regions of the gulf and individual transform segments, respectively. The combination of high-resolution earthquake locations, with the broad distribution of event focal mechanisms and an estimate of seismic coupling improves our understanding of the distribution of seismic deformation within the greater extensional zone in the southern GoC.

USING STRUCTURAL CONSTRAINTS ON THE LITTLE SAN BERNARDINO MOUNTAINS TO PETROLOGICALLY AND GEOCHEMICAL ANALYZE THE CRUSTAL VELOCITY MODEL OF SOUTHERN CALIFORNIA. (B-130)

C. Symcox and A. Barth

Recent years have seen great advances in subsurface velocity model data stemming from an increased density and sophistication of global seismic networks, resulting in improved models of crustal structure. Crustal velocity models are critical for accurately calculating earthquake hypocenters and understanding how crustal architecture influences the development of faults. Using a tilted crustal cross section in the Little San Bernardino Mountains, we aim to compare what we see petrologically and geochemically in the region to the CVMH, a crustal velocity model created by the Southern California Earthquake Center (SCEC) and Harvard. Our focus is predominantly two-fold: to finding the "average" rock that best describes the crust in the region by comparing the data provided in the CVMH to what we see on the ground knowing the convenient structural architecture of the region, and to search out inconsistencies between what is seen in the velocity model and what geologists see in outcrop. Other focuses in the coming weeks may include analyses of crystal structure and composition, anisotropy, and radiogenic heat production to compare what we see geologically in the rock to what the CVMH tells us what we should see.

REAL TIME GEODETIC EARLY WARNING SYSTEM FOR EARTHQUAKES (A-037)

H. Tahtinen, Y. Bock, B.W. Crowell, D. Melgar, and M.B. Squibb

Every second, new positions are calculated for all GPS stations within the California Real Time Geodetic Network (*http://sopac.ucsd.edu/projects/realtime/*). When a medium or large earthquake does occur in the region, the displacements will be quite visible in the recorded data in all three directions (north, east, up or x, y, z). We report on a redesign of our processing methodology by using Delaunay Triangulation to break up the large network of GPS sites (~100) can be broken into sub-networks each of which contain one reference station and two moving stations; in conjunction with the network redesign. The principal components of 2-D strain rate are computed for each triangle. If strain exceeds a pre-set threshold, a network adjustment is performed to reconstitute the entire network; this process detects and extracts outliers and references the positions of all sites with respect to the coordinates of a single CRTN site. The study area contains two networks, one in northern California including BARD (*http://seismo.berkeley.edu/bard/*) and PBO (*http://pboweb.unavco.org/?pageid=107*) sites, while the other is in southern California. The reason to have a network that covers such a large spatial extent is because when an earthquake initiates, the rupture will be able to be observed from its start to end along many possible faults, in particular the

San Andreas fault system, and an earthquake early warning can be issued. We show results from the southern Californian CRTN sites during the 2010 Mw 7.2 El Mayor-Cucapah earthquake. The data collected showed significant ground motions in the Imperial Valley a few seconds after the initial earthquake and for a few minutes, the movement reverberated across all of southern California (Bock et al., 2011). The SOPAC group is working on rapid determination of earthquake location, magnitude and fault plane using the site displacements computed by the network adjustment (Crowell et al., 2009; Melgar et al., 2011).

MECHANICS OF STRESS TRANSFER FROM PLATE MOTION TO PLATE BOUNDARY FAULTS: DYNAMIC MODELS OF EARTHQUAKE CYCLES ON A STRIKE-SLIP FAULT (B-146)

C.S. Takeuchi and Y. Fialko

Existing models of interseismic deformation are predominantly kinematic: loading is applied by prescribing slip on dislocations, either at a constant rate below the seismogenic layer (the Savage-Burford model) or quasi-periodically in the seismogenic layer on top of a viscoelastic substrate (the Elsasser model). These loading mechanisms are not physically consistent. In particular, kinematic viscoelastic cycle models produce absolute stresses on the seismogenic fault that are opposite to the sense of tectonic loading. We consider dynamic (stress-controlled) models of strike-slip faults that are driven by far-field tractions due to relative plate motion. We use antiplane strain finite element models to simulate quasi-periodic earthquakes on a fault in a brittle crust underlain by a viscoelastic medium. Each model is driven by far-field plate motion at a rate of 4 cm/yr, similar to the San Andreas Fault (SAF) in California. Slip occurs when the shear stress on the fault exceeds a prescribed threshold. We analyze stresses, strain rates, and surface deformation for models assuming various rheologies of a ductile substrate, including a) linear Maxwell rheology, b) power law temperature dependent rheology assuming a given linear geotherm, and c) power law temperature dependent rheology with thermo-mechanical coupling. The latter class of models gives rise to a permanent localized shear zone due to the interaction of viscous dissipation and heat conduction. An initial temperature perturbation is generated via a kinematically-driven thermal "maturation" of the fault at a constant slip rate over "geological" (millions of years) time scales. Strain localization in the power law viscoelastic medium due to thermo-mechanical coupling is used as a proxy for all strain-weakening mechanisms (including e.g. grain-size reduction). Simulations are performed for "dry" and "wet" rheological endmembers for the viscoelastic substrate. We compare the predicted surface velocities and strain rates to available observations from the SAF. We find that a dry temperature-dependent power law rheology best reproduces time-dependent surface deformation and generates reasonable deviatoric stresses in the crust and upper mantle.

STATIC DISPLACEMENTS COMPUTED FROM SEISMIC WAVEFIELD SIMULATIONS: VALIDATION TESTS FOR HOMOGENEOUS AND 1D STRUCTURE (A-061)

C. Tape, J.P. Loveless, and B.J. Meade

Earthquake 240 240 c 240 y 240 c 240 l 240 e 240 240 p 240 r 240 o 240 c 240 e 240 s 240 s 240 240 i 240 n 240 240 s 240 o 240 u 240 t 240 h 240 e 240 r 240 n 240 240 C 240 a 240 l 240 i 240 f 240 o 240 r 240 n 240 i 240 a 240 240 a 240 r 240 e 240 240 c 240 o 240 m 240 m 240 o 240 n 240 l 240 y 240 240 i 240 n 240 f 240 e 240 r 240 r 240 e 240 d 240 240 f 240 r 240 o 240 m 240 240 m 240 o 240 d 240 e 240 l 240 s 240 240 o 240 f 240 240 g 240 e 240 o 240 d 240 e 240 t 240 i 240 c 240 240 d 240 a 240 t 240 a 240 240 a 240 s 240 s 240 u 240 m 240 i 240 n 240 g 240 240 t 240 h 240 a 240 t 240 240 t 240 h 240 e 240 240 u 240 p 240 p 240 e 240 r 240 240 c 240 r 240 u 240 s 240 t 240 240 c 240 a 240 n 240 240 b 240 e 240 240 t 240 r 240 e 240 a 240 t 240 e 240 d 240 240 a 240 s 240 240 a 240 240s240i240m240p240l240e240 240h240o240m240o240g240e240n240e240o240u240s240 240e240l240a240s240t240i240c240 240h240a240l240f240s240p240a240c240e240.240 240H240o240w240e240v240e240r240,240 240i240t240 240i240s240 240w240e240l240l240 240k240n240o240w240n240 240t240h240a240t240 240m240a240t240e240r240i240a240l240 240p240r240o240p240e240r240t240i240e240s240 240(240f240o240r240 240e240x240a240m240p240l240e240,240 240V240s240 240o240r240 240V240p240)240 240v240a240r240y240 240b240y240 240m240o240r240e240 240t240h240a240n240 240a240n240 240o240r240d240e240r240 240o240f240 240m240a240g240n240i240t240u240d240e240,240 240f240r240o240m240 240 l 240 o 240 w 240 240 w 240 a 240 v 240 e 240 240 s 240 p 240 e 240 e 240 d 240 s 240 240 i 240 n 240 240u240n240c240o240n240s240o240l240i240d240a240t240e240d240 240s240e240d240i240m240e240n240t240s240 240t240o240 240h240i240g240h240 240w240a240v240e240 240s240p240e240e240d240s240 240i240n240 240t240h240e240 240u240p240p240e240r240m240o240s240t240 240m240a240n240t240l240e240 240b240e240l240o240w240 240t240h240e240 240M240o240h240o240.240 240T240h240i240s240 240r240a240n240g240e240 240o240f240 240w240a240v240e240 240s240p240e240e240d240s240 240i240s240 240p240r240e240s240e240n240t240 240w240i240t240h240i240n240 240c240r240u240s240t240a240l240 240m240o240d240e240l240s240 240i240n240 240s240o240u240t240h240e240r240n240

241 C 241 a 241 l 241 i 241 f 241 o 241 r 241 n 241 i 241 a 241 , 241 241 a 241 n 241 d 241 241 t 241 h 241 e 241 s 241 e 241 241m241o241d241e241l241s241 241h241a241v241e241 241b241e241e241n241 241v241a241l241i241d241a241t241e241d241 241 w 241 i 241 t 241 h 241 241 s 241 e 241 i 241 s 241 m 241 i 241 c 241 241 w 241 a 241 v 241 e 241 f 241 i 241 e 241 l 241 d 241 241s241i241m241u241l241a241t241i241o241n241s241 241o241f241 241h241u241n241d241r241e241d241s241 241o241f241 241 l 241 o 241 c 241 a 241 l 241 241 e 241 a 241 r 241 t 241 h 241 q 241 u 241 a 241 k 241 e 241 s 241 . 241 241 T 241 h 241 e 241 241s241t241r241u241c241t241u241r241a241l241 241c241o241m241p241l241e241x241i241t241i241e241s241 241a241r241e241 241 m 241 a 241 n 241 i 241 f 241 e 241 s 241 t 241 e 241 d 241 241 i 241 n 241 241 s 241 t 241 r 241 i 241 k 241 i 241 n 241 g 241 241m241a241n241n241e241r241 241w241i241t241h241i241n241 241s241e241i241s241m241o241g241r241a241m241s241 241 i 241 n 241 241 t 241 h 241 e 241 241 f 241 o 241 r 241 m 241 241 o 241 f 241 241 b 241 a 241 s 241 i 241 n 241 241r241e241s241o241n241a241n241c241e241 241a241n241d241 241m241u241l241t241i241p241a241t241h241i241n241g241 241e241f241f241e241c241t241s241.241 241H241o241w241e241v241e241r241,241 241t241h241e241 241e241f241f241e241c241t241 241 o 241 f 241 241 t 241 h 241 e 241 241 s 241 t 241 r 241 u 241 c 241 t 241 u 241 r 241 a 241 l 241 241 c 241 o 241 m 241 p 241 l 241 e 241 x 241 i 241 t 241 i 241 e 241 s 241 241 o 241 n 241 241 s 241 t 241 a 241 t 241 i 241 c 241 241o241f241f241s241e241t241s241 241i241s241

SEISMOGRAM-BASED ASSESSMENT OF THE SOUTHERN CALIFORNIA SEISMIC VELOCITY MODEL CVM-H 11.9 WITH 234 REFERENCE EARTHQUAKES (B-127)

C. Tape, E. Casarotti, A. Plesch, and J.H. Shaw

Pervasive moderate earthquakes (M > 3) in southern California provide an excellent means for independently testing seismic velocity models of the crust and uppermost mantle. It is possible to obtain a seismic data set that is potentially sensitive to all details in a complex structural setting by using a large number of earthquakes, considering the full length of three-component seismograms, and examining different period ranges. We quantitatively assess the crustal and upper mantle model CVM-H 11.9 by performing seismic wavefield simulations based on unstructured hexahedral meshing (GEOCUBIT) and the spectral-element method (SPECFEM3D). We generate a database of synthetic seismograms for 234 reference earthquakes in southern California. These synthetic seismograms are filtered over different period ranges and then compared with observed seismograms using a variety of misfit functions. The misfit analysis provides an earthquake-based perspective of the quality of CVM-H 11.9, and it can be used to improve future model versions.

THE EFFECT OF BARRIERS ON SLIP PARTITIONING IN AN UPWARD BRANCHING FAULT SYSTEM (A-076)

J. Tarnowski, D. Oglesby, and D. Bowman

The finite element method and slip-weakening friction are employed to investigate dynamic rupture propagation on a branched fault system. The system consists of an oblique-normal fault at depth connected to vertical and dipping fault branches 5km from the surface. The branches accommodate predominately strike-slip and dip-slip motion, respectively. When rupture is nucleated on the oblique fault at depth, dynamic unclamping favors rupture propagation to the vertical fault, with no rupture on the dipping fault. However, when a zone of doubled normal stress, referred to as a barrier, is located on the vertical fault, rupture is delayed on the vertical fault, causing shear stress to increase and normal stress to decrease along the corresponding area of the dipping fault. Consequently, the dynamic nature of the stresses facilitates slip on both segments. There is a correlation between barrier area and the ease with which an earthquake at depth propagates to both upper branches, suggesting a critical patch size for nucleation on the dipping fault. Increasing the slip-weakening distance by a factor of $\sqrt{2}$ necessitates the use of a critical barrier area that is increased by a factor of ~2, which is consistent with the critical patch size relationship suggested by Day (1982). Further numerical models show that the behavior above is relatively general, and does not require finely-tuned stress and frictional parameters.

CRUSTAL THICKENING AND STRIKE-SLIP CONTROLLED GROWTH OF THE NORTHERN COLOMBIAN ANDES (A-153)

M.H. Taylor, G. Veloza, and A. Mora

Neotectonic field mapping, seismic reflection profiles, and cosmogenic nuclide surface exposure dating aid in estimating the style and rate of recent shortening across the eastern foothills of the Colombian Andes. Active structures include the east-directed Guicarimo thrust fault that folds Cretaceous, Paleogene, Neogene and Quaternary sediments, and the east-directed Cusiana thrust fault – both structures are seismically active and are considered to sole at depth into a common decollement. Uplifted, folded and entrenched Quaternary alluvium are cut by active thrust faults with resulting entrenchment mainly

occurring across folds and faults suggesting abandonment of the terrace surfaces are likely tectonically controlled. Seismic reflection data reveals the along-strike subsurface geometry and shortening magnitude of the active thrust faults. Our preliminary analysis suggests shortening magnitude increases northward from Yopal in the south to the actively growing Tame anticline in the north. We use cosmogenic 10Be depth profiles in quartz-rich fluvial sand in weakly eroded sites with well-developed soils on uplifted terrace surfaces to estimate shortening rates at several locations along the active thrust system. The active northwest-striking left-slip Bucaramanga fault system kinematically links the subduction zone megathrust in the northwest with the active thrust belt of the eastern Cordillera to the southeast. The regional geometry and kinematics of the active fault systems suggests crustal thickening must have been coupled with strike-slip controlled growth of the Northern Colombian Andes.

STRUCTURAL CONTROLS ON THE SURFACE RUPTURE ASSOCIATED WITH THE MW7.2 EL MAYOR-CUCAPAH EARTHQUAKE OF 4 APRIL 2010: A COMPARATIVE ANALYSIS OF SCARP ARRAY KINEMATICS, ORIENTATION, LITHOLOGY AND WIDTH. (A-118)

O.J. Teran, J.M. Fletcher, T.K. Rockwell, K.W. Hudnut, M.E. Oskin, S.O. Akciz, A.J. Elliot, P.O. Gold, L. Liu-Zheng, U.R. Manjarrez, R. Mendoza-Borunda, A.E. Morelan, and R.M. Spelz

The Mw 7.2 El Mayor-Cucapah earthquake revealed the existence of a previously unidentified plate-margin fault system that extends 120 km from the northern tip of the Gulf of California to the international border. The system is composed of at least 6 major faults linked by numerous smaller faults. Kinematics on individual faults vary systematically with fault orientation. Faults with strikes ranging from N72W-N68W, N67W-N13W, N12W-N08W and N07W-N47E have kinematics dominated by dextral, oblique-dextral normal, normal, and oblique normal-sinistral shear, respectively. Stress inversion of the kinematic data yields high phi values (0.65-0.8) with sigma-1 close in magnitude to sigma-2 and sigma-3 oriented sub-horizontally with an azimuth of S80W. This demonstrates that kinematic variations of the 2010 rupture are most strongly controlled by regional stress related to transtensional plate margin.

Detailed mapping of the surface rupture through the Sierra Cucapah demonstrates that scarp array width (SAW) or total local width of the rupture zone ranges from 5 to 400 m and varies systematically with rock type, fault orientation, and fault kinematics. We classified 71 discrete fault segments according to the lithologies they juxtapose and in general SAW increases in the following order: basement-on-basement, sediment-on-basement and sediment-on-sediment faults. Dips of the master faults vary from 30° to 85° and this parameter shows the strongest correlation with SAW, which increases dramatically with more shallowly dipping master faults. When faults are classified by both lithology and dip, interesting patterns emerge to show systematic variations in SAW with strike. Sediment-on-sediment faults that dip greater than 45° show a sinusoidal variation of strike versus SAW. SAW is minimized with faults that strike ~N68W and ~N08W, which correspond well with the orientations of pure dextral and pure normal slip, respectively. SAW is maximized with faults that strike ~N30W, which correspond well with the orientations of oblique dextral-normal slip. Therefore, SAW increases with the increasing kinematic complexity of oblique slip. Based on stress inversion, the oblique slip segments have higher shear stress, which we conclude is an important factor controlling SAW. The predictive power resulting from this parametric analysis may allow refined assessments of future fault surface rupture hazards for critical facilities and lifeline fault crossings.

INCORPORATING GPS VELOCITIES INTO UCERF3 (B-147)

W. Thatcher, P. Bird, J. Bormann, T. Dawson, E. Field, W. Hammond, E. Hearn, K. Johnson, R. McCaffrey, D. Sandwell, and Y. Zeng

UCERF3 aims to incorporate space geodetic constraints on fault slip rates and off-fault strain rates. A subgroup was formed to undertake this task and forge a consensus on space geodetic results that could be confidently applied to UCERF3 goals. With support from both SCEC and the California Earthquake Authority (CEA), this activity was initiated in 2010. The activities included 2-day workshops in April 2010 and June 2011 to solicit comments and guidance from the space geodetic community. The culmunitation of the efforts is a suite of kinematic inversions of GPS velocities and geologic slip rate data for the distribution of fault slip rates and off-fault strain rates in California. In this poster we summarize the suite of inversion results using five different kinematic block and non-block models.

DISCREPANCIES IN OBSERVED VERTICAL MOTION FROM GEODETIC, GEOLOGIC AND GROUNDWATER DATA ALONG THE SOUTHERN SAN ANDREAS FAULT SYSTEM (A-059)

G.M. Thornton, B.R. Smith-Konter, and J.G. Konter

Geodetic and geologic measurements of vertical deformation in southern California record localized zones of uplift and subsidence associated with tectonic motions of the San Andreas Fault System (SAFS) and several other factors like ground water pumping and hydrocarbon extraction. Moreover, investigating the relationship between geodetic and geologic vertical data is nontrivial, as these datasets differ in geographic coverage area, spatial resolution, signal source, and associated uncertainties. Here we compare 888 geodetic velocities (from EarthScope PBO) that range from -11.1 to 7.6 mm/yr (average uncertainty of 1.7 mm/yr) and 1627 geologic velocities (from the SCEC Vertical Motion Database) that range from -3.5 to 3.6 mm/yr (average uncertainty of 0.13 mm/yr). The geodetic data are evenly distributed over a relatively large region, while the geologic data are very closely spaced over small areas. Thus, as these datasets are not spatially co-located, several different interpolation techniques (surfacing, masking, Delaunay triangulation) were utilized for optimal analysis of the data. While the number of available data points for each comparison largely depends on the chosen interpolation technique, all methods suggest that the relationship between geologic and geodetic vertical data is not 1:1, and in several locations the observations are even anticorrelated. Since anthropogenic effects may contaminate some of the geodetic data signal, a vertical velocity crustal deformation model of the SAFS was used to help identify locations where tectonic motions should dominate the data signals. To further improve the data-model misfit, a first-order groundwater correction was developed to isolate groundwater deformation recorded in the geodetic data. A ground subsidence/groundwater level change ratio of 0.006 was derived from published measurements and applied to changes in groundwater levels from regional well log data. Applying the groundwater correction improved the data-model fit by 33% and also doubled the correlation between the geodetic and geologic data. As we continue to explore the vertical motion discrepancies of the SAFS using regional tide gauge records along the California coast, we emphasize the fundamental importance of correcting vertical deformation data for ground water pumping and hydrocarbon extraction, and encourage future deployment of geodetic arrays in locations complimentary to existing geologic observations.

PATH CALIBRATION FOR EVENTS IN THE LOWER IMPERIAL VALLEY BASIN (B-051)

X. Tian, S. Wei, Z. Zhan, and D.V. Helmberger

The Imperial Valley below the US-Mexican border has few seismic stations but many significant earthquakes. Many of these events, such as the recent El Mayor-Cucapah event, have complex mechanisms involving a mixture of strike-slip and normal slip patterns with over 30 aftershocks with magnitudes over 4.5. Unfortunately, many earthquake records from the Southern Imperial Valley display a great deal of complexity, i.e., strong Rayleigh wave multipathing and extended codas. In short, regional recordings in the US are too complex to easily separate source properties from complex propagation. Here we present a hybrid method of using a combination of travel times including surface waves to locate events as well as determine their mechanisms. This is accomplished by assuming two pure-path models: one basin and one usual SoCal model, and a combination of Ambient Seismic Noise (ASN) and well located earthquakes. In particular, there was a broadband station NE70 (NARS array) in the vicinity of the epicenters, which enables us to use ASN calibration. We are finding the lags of phases of correlated surface waves relative to the reference model is consistent with the time shifts obtained in the cut-and-paste (CAP) routine. We cross-correlate the stations in the basin with the TriNet stations and measure the time delays of surface waves, which can be used to reduce the uncertainty of the source mechanisms and locations for earthquakes in the Lower Imperial Valley Basin without a detailed crustal structure. We will report on both the aftershocks and historic events.

HIGH RESOLUTION INTERSEISMIC VELOCITY MODEL OF THE SAN ANDREAS FAULT FROM GPS AND INSAR (A-048)

X. Tong, D.T. Sandwell, and B. Smith-Konter

We recover the interseismic deformation along the entire San Andreas Fault System (SAFS) at a spatial resolution of 200 meters by combining InSAR and GPS observations using a dislocation model. Previous efforts to compare 17 different GPS-derived strain rate models of the SAFS shows that GPS data alone cannot uniquely resolve the rapid velocity gradients near faults, which are critical for understanding the along-strike variations in stress accumulation rate and associated earthquake hazard.

To improve the near-fault velocity resolution, we integrate new GPS observations with InSAR observations, initially from ALOS (Advanced Land Observation Satellite launched by Japan Aerospace Exploration Agency) ascending data (spanning 2006.5-2010), using a remove/restore approach. More than 1100 interferograms were processed with the newly developed InSAR processing software GMTSAR. The integration uses a dislocation-based velocity model to interpolate the Line-Of-Sight (LOS) velocity at the full resolution of the InSAR data in radar coordinates. The residual between the model and InSAR LOS velocity are stacked and high-pass filtered, then added back to the model. This LOS velocity map covers almost entire San

Andreas Fault System (see Figure 1) from Maacama Fault to the north to the Superstition Hills Fault to the south. The average standard deviation of the LOS velocity model ranges from 2 to 4 mm/yr.

Our initial results show previously unknown details in along-strike variations in surface fault creep. Moreover, the high resolution velocity field can resolve asperities in these creeping sections that are important for understanding moment accumulation rates and seismic hazards. We find that much of the high resolution velocity signal is related to non-tectonic processes (e.g., ground subsidence and uplift) sometimes very close to the fault zone. The near-fault deformation signal extracted from this velocity map can provide tighter constraints on fault slip rates and locking depths of the major fault segments along the SAFS.

"MAKE YOUR OWN EARTHQUAKE: CURRICULUM DEVELOPMENT FOR GRADES 6 - 12" (A-026)

J.P. Trudeau, S.E. Allen, and H.E. Pence

Public understanding of earthquakes is important when it comes to preparing a community for a seismic event. In California, the interval between earthquakes is 50 to 100 years so the question becomes not if but when will the next one occur (Press and Siever 1982). Development of a curriculum to educate students on earthquakes is important. Having knowledge on how and why an earthquake occurs will help prevent casualties and panic when the next seismic event occurs. The Make Your Own Earthquake (MYOE) is an Educational Outreach and Training activity (EOT) that originally required university educators to go to local schools with expensive and heavy equipment. With the development of the Quake Catcher Network (QCN) device teacher can now use this accelerometer to show students acceleration in the x, y, and z axis. The main focus of this research was the development of a K-12 activities.

References:

Press, F., and Siever, R. (1982). "Earth, 3rd Ed.", W. H. Freeman and Company, San Francisco.

COMPARISONS AMONG EARTHQUAKE SIMULATOR RESULTS FOR UCERF2 FAULT MODEL OF CALIFORNIA AND OBSERVED SEISMICITY (B-109)

T.E. Tullis, K. Richards-Dinger, M. Barall, J.H. Dieterich, E.H. Field, E. Heien, L.H. Kellogg, F. Pollitz, J. Rundle, M. Sachs, D.L. Turcotte, S.N. Ward, B. Yikilmaz, and O. Zielke

We compare simulated histories generated by five different earthquake simulators with one another and with what is known about actual earthquake history in order to evaluate the usefulness of the simulator results for anticipating the probabilities of future earthquakes and for contributing to public policy decisions. Although sharing common features, our simulators differ from one another in their details in many important ways. All simulators use the same fault geometry and the same ~15,000, 3x3 km elements to represent the all strike-slip and thrust faults in California, excluding Cascadia. The set of faults and the input slip rates on them are essentially those of the UCERF2 fault and deformation model; we will switch to the UCERF3 model once it is available. All simulators use the boundary element method to compute stress transfer between elements. Differences between the simulators include how they represent fault friction and what assumptions they make to promote rupture propagation from one element to another.

The behavior of the simulators is encouragingly similar and the results are similar to what is known about real earthquakes, although some refinements are being made to some of the simulators to improve these comparisons as a result of our initial results. The frequency magnitude distributions of simulated events from M6 to M7.5 for a 30,000 year simulated history agree with instrumental observations for all of California. Scaling relations, as seen on plots of slip vs. rupture length, magnitude vs. rupture area, and magnitude vs rupture length, are similar for the different simulators. On these plots, overlaying results from several studies characterizing actual earthquake scaling shows good agreement with the simulator results. Importantly, moment rates and event rates for M7+ events show variations by factors of 3 in 100-yr moving averages throughout the 30,000 year simulated histories, with event rates for M6+ events correlating with M7+ event rates and 200 year periods being too short to characterize the moment and event rates. This suggests that in California our observational instrumental and historical record is too short to characterize seismicity rates adequately. For fault sections where paleoseismic data exist to constrain interevent times, fault stress drops assumed by the simulators can be adjusted to agree with observations. Lacking constraining data the simulated interevent times may be off, perhaps by up to a factor of 2.

A SEQUENCE OF DISTINCT DYNAMIC RUPTURES IN THE EARLY STAGE OF THE 2011 TOHOKU EARTHQUAKE (A-106)

T. Uchide, H. Yao, and P.M. Shearer

The 2011 M9 Tohoku earthquake gives us numerous mysteries. One of them is the exceptionally huge shallow slip of up to 30-40 m close to the Japan Trench. This massive slip is inferred from seismic, geodetic, and tsunami slip inversions, and is also implied by ocean bottom GPS observations [Sato et al., 2011]. The shallow slip started about 40 s after the onset. Such large shallow slip was not found in the 2004 Sumatra and the 2010 Chile earthquakes. What enabled the huge shallow slip in Tohoku? Although there are issues related to how the required strain energy accumulated for hundreds of years, this study attempts only to address the question how the source process evolved around the hypocenter in the first 40 s and its relationship with the shallow slip event.

Seismic slip inversions and back-projection studies suggest that the initial slip rate and rupture velocity are small. Two possibilities exist: (1) the slip rate and rupture velocity are actually small, or (2) a sequence of individual subevents is seen as apparently slow continuous rupture due to a lack of resolution. Since these two models have different physical interpretations, we investigate the early stage in some detail.

An iterative back projection (IBP) method [Yao et al., this meeting] detects bursts of high-frequency radiation, which may represent individual subevents or rapid changes in the rupture velocity [e.g., Spudich and Frazer, 1984]. In the first 40 s, many high-frequency radiation sources are found within 30 km of the hypocenter at a variety of azimuths from the hypocenter.

Multiscale slip inversion [Uchide and Ide, 2007] reveals the rupture process both in the early stage and the entire rupture process. In the early stage, the rupture propagated westward first, then from 20 s propagated eastward. This is consistent with the IBP result. Both the slip rate of about 1 m/s and the westward propagating rupture velocity are comparable to results from other earthquakes.

These results imply that the early stage until 40 s is a sequence of distinct dynamic ruptures, which do not spread linearly from the hypocenter, rather than continuous slip with a low slip rate and a low rupture velocity. The rupture may grow by

triggering subevents around the hypocenter by dynamic and static stress transfer. Resolving the details of this process should help in understanding what triggered the large shallow slip event.

DYNAMIC TRIGGERING EVENTS IN HIDA REGION BY THE P WAVE FROM THE 2011 TOHOKU EARTHQUAKE (A-107)

T. Uchide

Seismicity rates in the Hida region of central Japan, located about 400 km west of the source area of the 2011 M9 Tohoku earthquake, significantly increased at a time coincident with the passage of the Tohoku's P-wave. These local events are clearly identifiable in 8 Hz high-pass filtered Hi-net data in the region. Here, I systematically search for P-wave triggered events in the Hida region using a matched filter analysis. I examine data spanning 600 s before to 600 s after the origin time of the Tohoku mainshock, which nets 887 events, of these 82% occurred on or after the Tohoku P-wave arrival. I hypothesize the passage of the mainshock generated P-wave played an important role in raising the seismicity rate in the Hida region. Using 50s of waveform data, starting at the time of the mainshock's' P-wave arrival, I estimate the dynamic Coulomb stress change induced by the M9 mainshock reaches a maximum level of 1 - 10 kPa in the Hida region. This value, although on the low end, is comparable to other triggering thresholds. The immediacy of remote earthquake triggering at the time of the P-waves passage indicates secondary triggering processes, such as fluid movement or stress recalibration, are not necessarily required to remotely triggered earthquakes in this region.

SAN BERNARDINO GPS NETWORK: TIME SERIES THROUGH 2010 (A-049)

E. Upton, S. McGill, R. Bennett, J. Spinler, and A. Torrens-Bonano

As the Pacific plate slides past the North American plate along the San Andreas Fault (SAF) it exerts stress upon the fault. Although there has been no major earthquake in San Bernardino along the SAF in the past two centuries, the plates are in constant motion, moving a small amount every year. Yearly Global Positioning System (GPS) monitoring at benchmark sites around the SAF and other faults allows us to calculate the velocity of the Pacific plate in relation to stable North America. These calculations allow us to test hypotheses regarding the slip rate of the SAF as well as other faults. This year we conducted GPS monitoring at 25 locations. The data collected this summer is currently being processed at the University of Arizona. This poster summarizes the data collected in 2010 and previous years into a set of time series plots for 34 locations around the San Bernardino area. Our analysis shows the horizontal motion of the benchmarks is bounded by a minimum of 11.6 mm/yr (Site 7211, in the San Bernardino Mountains) and a maximum of 33.8 mm/yr (Site NORC, in Norco). Our results also show a distinct northwesterly trend of movement for stations in the San Bernardino GPS Network. The benchmarks display a direction of motion of between N17.6˚W (Site RICU, near Landers) and N56.7˚W (Site LACY, near Hemet). Furthermore, there is a noticeable increase in plate velocity the farther to the west as one moves from the North American plate onto the Pacific plate. Although they lie on a stable plate, there are locations on the North American plate are moving in the direction of the Pacific plate—northwest—due to the deformation of the plate boundaries along the locked SAF. While sites on the stable North American plate are moving to the northwest, sites located on the Pacific plate are moving to the northwest at greater velocities. Site NORC, which is the westernmost site of our survey, has a horizontal velocity of 33.8 mm/yr. In comparison, site RICU, located the farthest to the east, shows a horizontal motion of 16.2 mm/yr. Both sites are moving to the northwest but the locations on the Pacific plate are moving at a greater speed.

AUTO-ACOUSTIC COMPACTION IN STEADY SHEAR FLOWS: EXPERIMENTAL EVIDENCE FOR SUPPRESSION OF SHEAR DILATANCY BY INTERNAL ACOUSTIC VIBRATION (A-089)

N.J. van der Elst and E.E. Brodsky

Granular shear flows are intrinsic to many geophysical processes, ranging from landslides and debris flows to earthquake rupture on gouge-filled faults. The rheology of a granular flow depends strongly on the boundary conditions and shear rate. Earthquake rupture involves a runaway transition from quasi-static to rapid shear rates. Understanding the rheology of the granular flow in this transition is therefore crucial for understanding the rupture process and the coseismic strength of faults. Here we explore this transition experimentally using a commercial torsional rheometer. We measure the dilatation of a steady-state shear flow at velocities ranging between 10^{-3} and 10^{2} cm/s, and observe that dilatation is suppressed at intermediate velocities (0.1 - 10 cm/s) for angular particles, but not for smooth glass beads. The maximum reduction in thickness is on the order of 10% of the active shear zone thickness, and scales with the amplitude of shear-generated acoustic vibration. By examining the response to externally applied vibration, we confirm that the intermediate-velocity compaction represents a feedback between internally generated acoustic vibration and flow rheology. We link this phenomenon to that of acoustic

compaction of a dilated granular medium, and formulate an empirical model for the steady-state thickness of a shear-zone based on a balance between shear induced dilatation and "auto-acoustic" compaction. This mechanism is activated when the acoustic pressure is on the order of the confining pressure, and results in a velocity-weakening granular flow regime at shear rates four orders of magnitude below the range traditionally associated with the inertial transition to dispersive granular flow.

CREATIVE WORLD EARTHQUAKE PREPAREDNESS PROGRAM (A-006)

M.J. Vanegas, R.M. de Groot, and M. Barajas

Created in partnership with the California Science Center (CSC), SCEC, and the Earthquake Country Alliance (ECA), this 15-minute interactive program covers key concepts of earthquake science and preparedness. Beginning in fall 2011 this program will be offered as a Science Spectacular!™ show at the CSC with the goal of implementing it in other free-choice learning institutions especially with members of the Earthquake Education and Public Information Center (EPIcenter) Network. Part of the ECA, the EPIcenter Network is a collaborative of free-choice learning institutions devoted to enhancing earthquake education programs and exhibits. EPIcenters are found in a variety of venues such as museums, science centers, parks, libraries, and universities. The main goals of the presentation are to raise public awareness of earthquakes and seismic risk throughout California and to stimulate public interest (especially among children ages 6 - 12) in earth science. The presentation focuses on three key learning points: the geology of earthquakes, disaster preparedness, and earthquake survival. One of the challenges of creating such a presentation is communicating complex concepts of geology and natural disasters in a way that promotes understanding, interest, and ultimately action. Research for this project consisted of a literature review on effective teaching strategies in informal environments. The presentation, script, and interactive activities were reviewed by the management and staff of the CSC Education Department. The first half of the presentation discusses the relationship between the earth's composition, plate tectonics, and earthquakes. The second half focuses on creating a disaster supplies kit and why it is important to be prepared for a natural disaster. The interactive portions of the presentation include having volunteers participate in demonstrations such as fault movement using blocks, sorting through an unsatisfactory disaster supplies kit, and proper earthquake survival techniques (drop, cover, and hold on).

3-D FINITE ELEMENT MODELING OF PRECARIOUSLY BALANCED ROCKS (B-006)

S. Veeraraghavan and S. Krishnan

Many Precariously Balanced Rocks (PBRs) have been found in California. Since these rocks have been precariously placed for thousands of years, they can help in providing a constraint on the maximum ground shaking experienced by that region during the age of the PBR. Shake table tests and field tests have been conducted on some rocks to establish the importance of PBRs. Since most of the rocks are either very large or present in unapproachable locations, these tests cannot be conducted on majority of the rocks. Therefore, we are creating detailed 3-D finite element models of some of the PBRs that have been imaged using Terrestrial Laser Scanning techniques. We have validated the methodology by creating a FEM model of Housner's rectangular block. To establish the proof of concept, we are modeling the Echo Cliff PBR which is located in the Western Santa Monica Mountain. We model the rock by generating the mesh on MatLab and then analyze its response to various ground motions using LS-Dyna. The Echo Cliff PBR survived the 1994 Northridge earthquake and we will use this ground motion to validate the rock model. The success of this prototype study will provide an impetus to 3-D imaging and analysis of hundreds of PBRs. The ultimate goal is to arrive at probabilistic constraints on region-wide ground shaking intensity by combining the results of this study with cosmogenic dating of these rocks. Besides providing a better constraint on the US Seismic Hazard maps,this could also help in improving the ground motion simulations.

SUB-SURFACE EVIDENCE OF FAULTING RELATED TO THE COMPTON-LOS ALAMITOS FAULT AND IMPLICATIONS FOR STRAIN PARTITIONING IN THE WESTERN LA BASIN (A-126)

D.M. Verdugo Madugo and R.S. Yeats

Recent structural models for the Los Angeles (LA) Basin attribute deformation along the Compton-Los Alamitos fault (CLA) to fault-bend folding above a NE-dipping ramp rather, than to a near-surface fault, as had been interpreted in earlier studies. Our discovery last year of repeated stratigraphic sections on oil well logs across the northwestern CLA, however, support the earlier interpretation. To test whether the fault we observe represents a significant structure, rather than localized fold-related faulting, we focused our efforts this year on confirming our earlier work, and extending our study further southeast along the CLA. Our new analysis of exploratory well data, petroleum industry seismic lines, and cross-sections of seismicity across the central and southeastern CLA (generously provided by Shaw/Plesch and Yang/Hauksson, respectively) reveal a complex fault that cannot be explained by folding. According to seismic lines, truncated reflectors on the section north of the LA River

extend to about 600 m below the surface, and well data shows evidence of faulting at ~4 km, dipping towards the NIFZ. The southeastern 5 km of this section of the fault, between the LA River and Long Beach Blvd, corresponds to the deepest part of the LA Basin, as contoured in Wright, 1991, and truncates reflectors to within 200 m of the surface, exhibiting the greatest deformation along the CLA and defining perhaps oldest section of the fault. Newly relocated seismicity by Yang and Hauksson reveal primarily reverse focal solutions below this section of the CLA. South of the LA River, seismic lines and well data reveal truncated reflectors up to depths of 5-1.5 km and gently warped basinal stratigraphy, exhibiting less apparent vertical separation than observed on the northwestern section of CLA. Newly relocated seismicity shows the fault coincides with southwest-dipping strike-slip foci. This southeastern section of the CLA also corresponds to the easternmost extent of uplift measured by Gilluly and Grant after the 1933 Long Beach earthquake. Repeated evidence of faulting in seismic lines and well data suggests the CLA is a significant fault. Its proximity to the eastern boundary of uplift measured in the Long Beach earthquake by Gilluly and Grant and oblique strike-slip focal mechanisms calculated by Yang and Hauksson suggest a structural connection between the southeastern extent of the CLA and NIFZ, implying a strain-partitioning relationship between the two faults.

SEISMIC ANISOTROPY OF THE PELONA SCHIST FROM ELECTRON BACKSCATTER DIFFRACTION (EBSD) MEASUREMENTS OF CRYSTAL PREFERRED ORIENTATIONS (CPOS) (B-136)

K.C. Wagner, S. Brownlee, and B. Hacker

Seismic Anisotropy of the mid to lower crust is difficult to measure in the field by seismologists. Using a scanning electron microscope (SEM) to obtain crystal preferred orientations (CPO's) of mineral grains from samples taken from this region allows us to calculate seismic anisotropy theoretically using published mineral elastic constants. Calculations are made according to methods described in Mainprice et. al. (1990). Polished thin sections from the Pelona Schist were analyzed using electron back scatter diffraction (EBSD) in an SEM. The slide was tilted 70 degrees from horizontal. The samples included: 4 mica schists that were cut parallel to foliation, 3 corresponding mica schists cut perpendicular to foliation, and 2 xenoliths with high amphibole content. The 4 mica schists had max Vp's that ranged from 6.44 to 7.26 km/s; Vp anisotropies that ranged from 4.8% to 29.2%; and max Vs anisotropies from 7.0% to 42.6%. The 3 corresponding mica schists had max Vp's that ranged from 6.26 to 6.61 km/s; Vp anisotropies from 3.1% to 7.9%; and Vs anisotropies from 4.9% to 6.61%. In samples that were cut orthogonal to foliation biotite is difficult to index using the automated indexing routine and had to be found manually to improve calculations. This may account for significant differences in anisotropy between corresponding samples. The xenoliths had max Vp's of 6.14 and 6.48 km/s; their Vp anisotropies were both 6.5%; and their Vs anisotropies were 8.35 and 8.37. Our calculations give slightly higher maximum Vp than the average Vp reported in Pellerin and Christensen (1997) for similar rock types from the area. Calculated anisotropies are comparable to Pellerin and Christensen (1997). Samples with large amounts of mica had the highest anisotropy. On average, the calculated velocities have approximately hexagonal symmetry with a unique slow axis. In contrast, one sample contained significant plagioclase that caused velocities to be fast perpendicular to foliation. An assumption of hexagonal symmetry with a unique slow axis is a valid assumption for the Pelona Schist.

PBO SOUTHWEST REGION: NETWORK OPERATIONS AND BAJA EARTHQUAKE RESPONSE (A-068)

C. Walls, A. Basset, D. Mann, S. Lawrence, C. Jarvis, J. Sklar, K. Feaux

M. Jackson

The SW region of the Plate Boundary Observatory consists of 455 continuously operating GPS stations located principally along the transform system of the San Andreas fault and Eastern California Shear Zone. In the past year network uptime exceeded an average of 97% with greater than 99% data acquisition. Communications range from CDMA modem (307), radio (92), Vsat (30), DSL/T1/other (25) to manual downloads (1). Sixty-three stations stream 1 Hz data over the VRS3Net typically with <0.5 second latency. Over 620 maintenance activities were performed during 316 onsite visits out of approximately 368 engineer field days. Within the past year there have been 7 incidences of minor (attempted theft) to moderate vandalism (solar panel stolen) with one total loss of receiver and communications gear. Security was enhanced at these sites through fencing and more secure station configurations. In the past 12 months, 4 new stations were installed to replace removed stations or to augment the network at strategic locations.

Following the M7.2 El Mayor-Cucapah earthquake CGPS station P796, a deep-drilled braced monument, was constructed in San Luis, AZ along the border within 5 weeks of the event. In addition, UNAVCO participated in a successful University of Arizona-led RAPID proposal for the installation of six SDBM GPS stations for post-seismic observations. Six stations are

installed and telemetered through a UNAM relay at the Sierra San Pedro Martir. Four of these stations have Vaisala WXT520 meteorological sensors. An additional site in the Sierra Cucapah (PTAX) that was built by CICESE, an Associate UNAVCO Member institution in Mexico, and Caltech has been integrated into PBO dataflow. The stations will be maintained as part of the PBO network in coordination with CICESE.

UNAVCO is working with NOAA to upgrade PBO stations with WXT520 meteorological sensors and communications systems capable of streaming real-time GPS and met data. The real-time GPS and meteorological sensor data streaming support watershed and flood analyses for regional early-warning systems related to NOAA's work with California Department of Water Resources. Currently 19 stations are online and streaming with 7 more in preparation.

DIRECTIVITY-BASIN COUPLING IN THE LOS ANGELES REGION FROM THE CYBERSHAKE HAZARD MODEL (B-005)

F. Wang, T.H. Jordan, S. Callaghan, K. Milner, P. Maechling, R. Graves, and CyberShake Collaboration

The coupling between source directivity effects and basin amplification effects can substantially enhance the low-frequency seismic hazards in sedimentary basins. These effects have been qualitatively illustrated by TeraShake (Olsen et al., 2006), ShakeOut (Graves et al., 2008), and other earthquake scenarios simulated by the Southern California Earthquake Center. In this study, we use version 1 of the CyberShake Hazard Model (CSHM-1) for the Los Angeles region (Graves et al., 2010) to quantify directivity-basin effects in low-frequency response spectra. The CyberShake computational platform employs the reversal symmetries of linear wave propagation (seismic reciprocity) to numerically simulate suites of synthetic time-histories large enough for the probabilistic mapping of shaking intensities. In CSHM-1, a set of more than 600,000 rupture realizations was generated that stochastically sample the Uniform California Earthquake Rupture Forecast (UCERF2); horizontal-component seismograms were computed at 250 sites in the Los Angeles region, and hazard curves and hazard maps were constructed from the UCERF2 probabilities. We use the response spectra calculated from these seismograms in the band 0.1-0.3 Hz to analyze the dependence of strong-motion amplitudes on basin and source geometry, from which we extract measures of directivity-basin coupling. These measures indicate how directivity-basin coupling is enhanced by the tectonic branching structure of the San Andreas system. Additionally, we analyze the dependence of this coupling on source complexity and earth structure.

LOVE WAVE TRIGGERS TREMOR ALONG SAN JACINTO FAULT IN THE ANZA REGION, CALIFORNIA (B-038)

T.-H. Wang, E.S. Cochran, and D.D. Oglesby

We investigate the stress amplitude required to trigger tremor along the San Jacinto fault. We examine continuous broadband recordings from 11 Southern California Seismic Network (SCSN) stations located near Anza, California, of 41 Mw>=7.0 teleseismic events that occurred between 2001 andn 2009. These events occurred at a wide range of backazimuths and hypocentral distances. An initial visual inspection of 2 to 8 Hz bandpassed time series reveals only one clear episode of triggered tremor, during the 3 November 2002 Mw 7.8 Denali earthquake. The triggered tremor episode is 300 seconds long and composed of 12 tremor bursts around 15 km depth. We compare the frequency spectra of tremor, local earthquakes, and background noise. We find that the tremor at Anza lacks high frequency energy above 1 Hz compared to local earthquakes. Such a frequency characteristic is similar to tremor observed in other regions. The start of the tremor episode correlates well with surface wave particle motions primarily in the transverse direction, suggesting that Love wave may have triggered tremor.

We tested the hypothesis that similar, but lower amplitude episodes of tremor occurred during the teleseismic earthquakes. We manually identify high amplitude bursts, or low frequency earthquakes (LFEs), that occur during the Denali tremor episode, cross-correlate these LFE templates with the continuous time series of the 41 teleseismic events, and stack the correlation coefficients across 11 stations. We find sufficiently high correlation values only in the Denali earthquake wavetrains. We examine the amplitude and the dominant period of the posited triggering surface waves for all the teleseismic events. We find that the Denali earthquake had the highest amplitude surface waves but similar spectral shape to other teleseismic events, suggesting that the amplitude of the incoming surface wave primarily controls triggering of tremor on the San Jacinto fault. In addition, since the backazimuth of the Denali surface wave is parallel to strike of the near-vertical San Jacinto fault, the shear stress applied to the fault by the radial-direction gradients in the Love wave particle displacement is maximized.

COMPOUND EARTHQUAKES ON A BIMATERIAL INTERFACE AND IMPLICATIONS FOR RUPTURE MECHANICS (B-040)

E. Wang and A.M. Rubin

Rubin and Ampuero [2007] simulated slip-weakening ruptures on a 2-D (line fault) bimaterial interface and observed differences in the timescales for the two edges to experience their peak stress after being slowed by barriers. The barrier on the "negative" side reached its peak stress when the P-wave stopping phase arrives from the opposite end, which takes ~20 ms for a 100 m event. This may be long enough for a potential secondary rupture to be observed as a distinct subevent. In contrast, the same timescale for a barrier at the "positive" front is nearly instantaneous, possibly making a secondary event there indistinguishable from the main rupture. Rubin and Gillard [2000] observed that 5 of a family of 72 similar earthquakes along the San Andreas fault in Northern California are compound and in all cases the second event was located on the negative (NW) side of the main event. Based on their simulations, Rubin and Ampuero interpreted this as being due to the above-mentioned asymmetry in the dynamic stressing-rate history on the two sides of a rupture on a bimaterial interface.

In this study, we search more systematically for secondary arrivals within 0.15 s of the first P arrival for microearthquakes on the San Andreas. Using an iterative deconvolution method described in Kikuchi & Kanamori [1982], we deconvolve the first 0.64 s following the P arrival of a target event using a nearby Empirical Green's Function (EGF). When the EGF is a simple earthquake and the target is compound, the deconvolution result is expected to show two positive spikes, corresponding to the main and secondary events. A subevent is considered robust only when the difference between the waveforms of the target event and the aligned and scaled EGF is similar enough to the EGF at multiple stations. The azimuthal consistency of delays between the main and secondary arrivals is more convincing evidence that the target is a compound event.

Using these criteria we temporarily identified ~70 compound events out of ~8300 in our catalog. Future work will include improving the quality of the inter-event delay time by using Monte Carlo simulations to allow the amplitudes and arrival times of both spikes (as opposed to just the second spike) to vary. Accurate relative locations and times can improve our understanding of the triggering mechanism of the subevents and perhaps the longer-timescale aftershock asymmetry observed in this region as well.

AUTOMATIC DETECTION OF SHALLOW FAULT CREEP IN INSAR DATA (A-065)

M. Wei, D. Sandwell, and J. McGuire

Fault creep in Southern California mostly occurs at the shallow part of a fault with clear surface breakage. Monitoring and observing these shallow fault creep is important for regional seismic hazard assessment and improving our understanding of fault mechanics. Many fault creep occurred in remote area where no other observation instruments nearby. Even on faults with creepmeters, partial creep on sections that do not coincide with the creepmeter becomes undetectable. InSAR has been used to study fault creep in this region. However, as the volume of InSAR data has increased dramatically, over ~1000 scenes in California, and will continue to increase as future missions such as DESDynI start, searching for fault creep manually in InSAR data becomes time consuming and unrealistic. An automatic detector of fault creep in InSAR data is called for.

Here, we developed an automatic detector using pattern recognition algorithm developed for road detection in SAR data to find shallow fault creep in InSAR data. The main workflow includes: process InSAR data, make gradient image of the phase image, detect linear features, and report possible fault creep. We tested this detector in Salton Trough with ERS, ENVISAT and ALOS data. Our method successfully detected most fault creep, mainly on the Superstition Hills Fault and San Andreas Fault. Limitations of the method include: prefer flat area with little sharp topography change; only be able to detect displacement larger than ~1 cm; can't detect deep fault creep. Nevertheless, this detector is a useful tool for monitoring shallow fault creep.

REGIONAL BROADBAND WAVEFORM MODELING USING UPGOING AND DOWNGOING WAVE FIELDS (A-116)

S. Wei and D. Helmberger

3D crustal structure usually complicates the modeling of regional waveforms. The Cut and Paste (CAP) waveform inversion method, on the other hand, is much less sensitive to velocity models and lateral crustal variation, because it breaks the waveforms into Pnl and Surface waves and inverts them separately, allowing different time shifts to align the data and the synthetics for different portions of the waveform. These time shifts represent the difference between the 1D structure and the real earth. Similar idea is applied to the upgoing and downgoing wave fields, where we use different time adjustments for upgoing and downgoing waveforms to improve the broadband waveform fits. Furthermore, different source-time-functions

are adopted for upgoing and downgoing phases to take into account of the directivity effect of the source process in vertical direction. The sensitivity tests indicate that, the separation with adjustable time shifts can better fit the waveforms especially the depth phases. The improved method is applied to the 2003 Big Bear sequence to derive lateral crustal structure.

CAN FAULT MAPS CONSTRAIN FUTURE EARTHQUAKE MAGNITUDES? (B-082)

D.A. Weiser

Can one use an existing fault map to accurately determine maximum magnitude for earthquakes in a region? It is generally assumed that fault traces constrain the location, orientation, and size of future earthquakes. Yet many earthquakes, like the M7.3, 1992 Landers, CA and M7.9, 1999 Denali, AK earthquakes, rupture beyond previousl 251 y 251 251 m 251 a 251 p 251 p 251 e 251 d 251 251 t 251 r 251 a 251 c 251 e 251 s 251 251 o 251 r 251 251 a 251 r 251 e 251 251 t 251 r 251 a 251 n 251 s 251 f 251 e 251 r 251 r 251 e 251 d 251 251 o 251 n 251 t 251 o 251 251 a 251 251 s 251 p 251 l 251 a 251 y 251 251 f 251 a 251 u 251 l 251 t 251 . 251 251 O 251 t 251 h 251 e 251 r 251 251 e 251 v 251 e 251 n 251 t 251 s 251 , 251 251 l 251 i 251 k 251 e 251 251t251h251e251 251M2516251.2517251,251 251125192519251425 1 251N251o251r251t251h251r251i251d251g251e251,251 251C251A251,251 251t251h251e251 251M2517251.2510251 251225102511251025 1 251D251a251r251f251i251e251l251d251,251 251N251e251w251 251Z251e251a251l251a251n251d251,251 251a251n251d251 251M2516251.2513251 251225102511251125 1 251C251h251r251i251s251t251c251h251u251r251c251h251,251 251N251e251w251 251Z251e251a251l251a251n251d251 251 e 251 a 251 r 251 t 251 h 251 q 251 u 251 a 251 k 251 e 251 s 251 , 251 251 s 251 e 251 r 251 v 251 e 251 251 a 251 s 251 251 a 251 d 251 d 251 i 251 t 251 i 251 o 251 n 251 a 251 l 251 251 e 251 v 251 i 251 d 251 e 251 n 251 c 251 e 251 251 t 251 h 251 a 251 t 251 251 l 251 a 251 r 251 g 251 e 251 251 e 251 a 251 r 251 t 251 h 251 q 251 u 251 a 251 k 251 e 251 s 251 251 c 251 a 251 n 251 251 a 251 n 251 d 251 251d251o251 251o251c251c251u251r251 251w251h251e251r251e251 251n251o251 251f251a251u251l251t251 251h251a251d251 251 b 251 e 251 e 251 n 251 251 i 251 d 251 e 251 n 251 t 251 i 251 f 251 i 251 e 251 d 251 . 251 251 251 T 251 h 251 i 251 s 251 251 i 251 s 251 251 i 251 m 251 p 251 o 251 r 251 t 251 a 251 n 251 t 251 251 b 251 e 251 c 251 a 251 u 251 s 251 e 251 251 r 251 e 251 g 251 r 251 e 251 s 251 s 251 i 251 o 251 n 251 s 251 251 b 251 e 251 t 251 w 251 e 251 e 251 n 251 251 m 251 a 251 g 251 n 251 i 251 t 251 u 251 d 251 e 251 251 a 251 n 251 d 251 251 r 251 u 251 p 251 t 251 u 251 r 251 e 251 251 d 251 i 251 m 251 e 251 n 251 s 251 i 251 o 251 n 251 s 251 251 a 251 r 251 e 251 251 b 251 a 251 s 251 e 251 d 251 251 o 251 n 251 251p251o251s251t251-251e251a251r251t251h251q251u251a251k251e251 251m251a251p251s251 251o251f251 251t251h251e251 251 s 251 u 251 r 251 f 251 a 251 c 251 e 251 251 r 251 u 251 p 251 t 251 u 251 r 251 e 251 251 a 251 n 251 d 251 251 i 251 n 251 s 251 t 251 r 251 u 251 m 251 e 251 n 251 t 251 a 251 l 251 251 d 251 a 251 t 251 a 251 . 251 251 T 251 h 251 e 251 s 251 e 251 251 r 251 e 251 g 251 r 251 e 251 s 251 s 251 i 251 o 251 n 251 s 251 251 a 251 r 251 e 251 251 t 251 h 251 e 251 n 251 251 e 251 m 251 p 251 l 251 o 251 y 251 e 251 d 251 251 t 251 o 251 251 e 251 s 251 t 251 i 251 m 251 a 251 t 251 e 251 251 m 251 a 251 g 251 n 251 i 251 t 251 u 251 d 251 e 251 251 o 251 f 251 251 f 251 u 251 t 251 u 251 r 251 e 251 251e251a251r251t251h251q251u251a251k251e251s251,251 251u251s251i251n251g251 251e251x251i251s251t251i251n251g251 251f251a251u251l251t251 251m251a251p251s251.251 251S251i

SPATIAL DISTRIBUTIONS OF FORESHOCKS AND AFTERSHOCKS: STATIC OR DYNAMIC TRIGGERING? (B-027)

M.J. Werner and A.M. Rubin

In recent years, the spatial distributions of foreshocks and aftershocks have been scrutinized for evidence supporting either triggering by static stress changes induced by the permanent deformation from prior earthquakes or triggering by the dynamic stresses from seismic waves. Felzer & Brodsky (2006) identified mainshocks and triggered aftershocks, stacked the distances between these pairs and observed a single power-law decay with distance that extends beyond the zone traditionally thought to be affected by static stress changes. On this basis, they argued that dynamic stresses are responsible for triggering 251 e 251 a 251 r 251 t 251 h 251 q 251 u 251 a 251 k 251 e 251 s 251 . 251 251 R 251 i 251 c 251 h 251 a 251 r 251 d 251 s 251 - 251 D 251 i 251 n 251 g 251 e 251 r 251 251 e 251 t 251 251 a 251 l 251 . 251 251 (251 2 251 0 251 1 251 0 251) 251 251 a 251 n 251 d 251 251 o 251 t 251 h 251 e 251 r 251 251 s 251 t 251 u 251 d 251 i 251 e 251 s 251 , 251 251 h 251 o 251 w 251 e 251 v 251 e 251 r 251 , 251 251h251a251v251e251 251p251r251e251s251e251n251t251e251d251 251s251e251v251e251r251a251l251 251l251i251n251e251s251 251 o 251 f 251 251 e 251 v 251 i 251 d 251 e 251 n 251 c 251 e 251 251 t 251 h 251 a 251 t 251 251 s 251 u 251 g 251 g 251 e 251 s 251 t 251 251 o 251 t 251 h 251 e 251 r 251 w 251 i 251 s 251 e 251 . 251 251 O 251 n 251 e 251 251 c 251 r 251 u 251 c 251 i 251 a 251 l 251 251 q 251 u 251 e 251 s 251 t 251 i 251 o 251 n 251 251 i 251 s 251 251 w 251 h 251 e 251 t 251 h 251 e 251 r 251 251 t 251 h 251 e 251 251s251t251a251c251k251e251d251 251d251i251s251t251a251n251c251e251s251 251o251f251 251p251a251i251r251s251 251 o 251 f 251 251 e 251 a 251 r 251 t 251 h 251 q 251 u 251 a 251 k 251 e 251 s 251 , 251 251 r 251 e 251 p 251 r 251 e 251 s 251 e 251 n 251 t 251 i 251 n 251 g 251 251 e 251 i 251 t 251 h 251 e 251 r 251

252 m 252 a 252 i 252 n 252 s 252 h 252 o 252 c 252 k 252 - 252 a 252 f 252 t 252 e 252 r 252 s 252 h 252 o 252 c 252 k 252 252 o 252 r 252 252f252o252r252e252s252h252o252c252k252-252m252a252i252n252s252h252o252c252k252 252p252a252i252r252s252,252 252 a 252 r 252 e 252 252 i 252 n 252 252 f 252 a 252 c 252 t 252 252 c 252 o 252 r 252 r 252 e 252 c 252 t 252 l 252 y 252 252 i 252 d 252 e 252 n 252 t 252 i 252 f 252 i 252 e 252 d 252 252 a 252 n 252 d 252 252 n 252 o 252 t 252 252 m 252 i 252 s 252 a 252 t 252 t 252 r 252 i 252 b 252 u 252 t 252 e 252 d 252 , 252 252 u 252 n 252 r 252 e 252 l 252 a 252 t 252 e 252 d 252 252e252a252r252t252h252q252u252a252k252e252s252.252 252T252h252i252s252 252q252u252e252s252t252i252o252n252 252i252s252 252e252s252p252e252c252i252a252l252l252y252 252i252m252p252o252r252t252a252n252t252 252i252n252 252t252h252e252 252c252r252i252t252i252c252a252l252 252d252i252s252t252a252n252c252e252 252r252a252n252g252e252 252 o 252 f 252 252 s 252 e 252 v 252 e 252 r 252 a 252 l 252 252 t 252 o 252 252 t 252 e 252 n 252 s 252 252 o 252 f 252 252 e 252 a 252 r 252 t 252 h 252 q 252 u 252 a 252 k 252 e 252 252 r 252 a 252 d 252 i 252 i 252 , 252 252 o 252 v 252 e 252 r 252 252 w 252 h 252 i 252 c 252 h 252 252 s 252 t 252 a 252 t 252 i 252 c 252 252 s 252 t 252 r 252 e 252 s 252 s 252 e 252 s 252 252 a 252 r 252 e 252 252t252h252o252u252g252h252t252 252t252o252 252b252e252 252t252o252o252 252s252m252a252l252l252 252t252o252 252 a 252 f 252 f 252 e 252 c 252 t 252 252 s 252 e 252 i 252 s 252 m 252 i 252 c 252 i 252 t 252 y 252 . 252 252 I 252 f 252 252 e 252 a 252 r 252 t 252 h 252 q 252 u 252 a 252 k 252 e 252 252 p 252 a 252 i 252 r 252 s 252 252 i 252 n 252 252 t 252 h 252 i 252 s 252 252 r 252 a 252 n 252 g 252 e 252 252 a 252 r 252 e 252 252 n 252 o 252 t 252 252 c 252 a 252 u 252 s 252 a 252 l 252 l 252 y 252 252r252e252l252a252t252e252d252,252 252t252h252e252n252 252t252h252e252 252h252i252s252t252o252g252r252a252m252 252o252f252 252f252o252r252e252s252h252o252c252k252-252m252a252i252n252s252h252o252c252k252 252a252n252d252 252m252a252i252n252s252h252o252c252k252-252a252f252t252e252r252s252h252o252c252k252 252p252a252i252r252s252 252 s 252 h 252 o 252 u 252 l 252 d 252 252 b 252 e 252 252 i 252 d 252 e 252 n 252 t 252 i 252 c 252 a 252 l 252 . 252 252P252r252e252l252i252m252i252n252a252r252y252 252r252e252s252u252l252t252s252 252u252s252i252n252g252 252 s 252 o 252 u 252 t 252 h 252 e 252 r 252 n 252 252 C 252 a 252 l 252 i 252 f 252 o 252 r 252 n 252 i 252 a 252 252s252e252i252s252m252i252c252i252t252y252 252r252o252u252g252h252l252y252 252r252e252p

INJECTING INFORMATION FROM STATIC COULOMB MODELS INTO STATISTICAL AFTERSHOCK MODELS FOR THE CANTERBURY, NEW ZEALAND, EARTHQUAKE SEQUENCE (B-101)

C.A. Williams, M.C. Gerstenberger, and S. Steacy

The Canterbury earthquake sequence began with the Mw 7.1 Darfield earthquake in September, 2010, and continues to the present. This event was followed by events in February, 2011 (Mw 6.3) and June, 2011 (Mw 6.0), causing severe damage to the city of Christchurch, where the level of seismic hazard was previously thought to be moderate. The occurrence of these events, as well as numerous smaller aftershocks, will obviously perturb the pre-existing stress field in this vicinity. We are exploring methods of estimating these stress changes and then using this information to revise existing statistical models of earthquake occurrence. The problem is made more difficult by the uncertainties involved in Coulomb stress calculations. These uncertainties involve both the source fault parameters (e.g., fault geometry and slip distribution) and target fault parameters (orientation, frictional properties, etc.). We address these problems by allowing the different parameters to vary, thus providing a suite of possible models. Using this suite of models, we can then compute the mean and variance of the computed Coulomb stresses and use this as the input for the modified statistical models. We use the estimated stress changes in two different ways. In the first approach, we use a rate and state model to forecast aftershock probabilities. In the second, we use a simplified approach that uses only the polarity of the stress changes to redistribute the forecasts from statistical aftershock models. Using these approaches, we plan to provide revised aftershock probabilities for the Canterbury region.

TSUNAMI HAZARD MAPPING ACTIVITIES IN SOUTHERN CALIFORNIA (B-098)

R. Wilson, K. Miller, C. Real, J. Goltz, and J. Treiman

The California Geological Survey (CGS) and its partner agency in the state tsunami program, the California Emergency Management Agency (CalEMA), have completed a number of tsunami hazard mapping products and plan additional work in southern California over the next several years. Funded by the National Tsunami Hazard Mitigation Program (NTHMP), CGS, CalEMA, and the University of Southern California – Tsunami Research Center completed work on 130 tsunami inundation maps for emergency response planning that cover all at-risk communities within the state (maps on www.tsunami.ca.gov). These maps are based on extreme, but realistic scenarios from forty local and distant sources, and cover all at-risk, populated areas along the coast, including over 90% of the southern California coast. New maps for Catalina Island will be completed within by the end of 2011.

Additional tsunami hazard mapping activities by CGS and CalEMA include: 1) production of tsunami hazard zone maps for land-use planning under the 1990 Seismic Hazard Zonation Act; 2) production of tsunami current hazard maps and offshore

safety zones for the maritime community; 3) completion of a tsunami deposit and tsunami source database; and, 4) formation of pre-tsunami field teams to observe and collect data during and after a tsunami. A pilot project for the land-use planning maps, which will require a probabilistic tsunami hazard analysis, has been initiated in the City of Huntington Beach. The maritime community maps, which will include in-harbor tsunami hazard maps and offshore safety zone, have also been initiated with likely "pilot" locations in Ventura Harbor, the Ports of Los Angeles and Long Beach, and San Diego Bay. The two tsunami databases for deposits and sources will be completed by 2012 to help evaluate existing tsunami hazard mapping products and guide future products for both emergency response and land-use planning. During and after the March 11, 2011 tsunami, which caused over $50-million in damage to two dozen harbors in the state, data collected by the pre- and post-tsunami field team will also help evaluate the tsunami modeling and mapping methods used by the state, especially as they relate to strong tsunami currents within harbors.

CORRELATION OF PEAK DYNAMIC AND STATIC COULOMB FAILURE STRESS WITH SEISMICITY RATE CHANGE AFTER THE M7.2 EL MAYOR-CUCAPAH EARTHQUAKE (B-102)

K.B. Withers and K.B. Olsen

We have investigated the relation between the April 4 Mw7.2 El Mayor-Cucapah earthquake and seismicity rate changes in southern California and northern Baja California in the months following the mainshock. Specifically, we use dynamic rupture models with observational constraints for the event simulated in the SCEC 3D CVM4.0 (Roten and Olsen, 2009) to calculate the resulting static (ΔCFS) and dynamic Coulomb failure stress changes, ΔCFS(t), parameterized by its largest positive amplitude (peak ΔCFS(t)). The seismicity rate changes are estimated using the Z-value (Haberman, 1983) using both undeclustered and declustered datasets (with a magnitude of completeness equal to 1.5), and show varying goodness of fit values with different time periods after the mainshock (ranging from a day to 1 year). We employ different methods to measure the correlation between the seismicity rate change and both ΔCFS and peak ΔCFS(t) in time and space, in order to estimate the most efficient triggering parameter for the aftershocks, including a ternary map comparison (as used by Kilb et. al, 2002) and cross-correlation. We perform this analysis using both CVM-4 and CVM-H, investigating, in particular, which model better describes the increased seismicity NW of the rupture. We have rotated the stress changes onto focal mechanisms of several Mw5 aftershocks as well as onto optimum oriented planes (King, 1994). We find that increases in static stress changes closer to the fault can explain nearby aftershocks, while the triggering of those farther away are more likely attributed to dynamic stress changes, where static stress change is nearly zero. We attempted to define an estimate of potential threshold level of static and dynamic stress change required to trigger earthquakes/aftershocks of different magnitude, but thus far have found no definitive relation.

THERMAL FLUID AND FAULT INTERACTIONS AT THE INTERSECTION OF TWO FAULTS, AGUA CALIENTE, CALIFORNIA (A-099)

R.E. Wood and J.P. Evans

Agua Caliente Springs lies at a unique intersection between the NNW-trending Elsinore fault and the 40° northeast-dipping, likely inactive West Salton detachment fault; it provides an opportunity to study damage zone geometry, fault behavior in crystalline rocks, a left-stepover, microseismicity, and the influence of thermal fluids on rock deformation. The Elsinore fault bounds the northwestern flank of the Tierra Blanca Mountains with strike-slip and normal motion; the detachment fault wraps around the northernmost portion of the mountains. Damage along the Elsinore ranges in thickness from a narrow slip plane to > 100 m along the eastern flank of the Tierra Blanca Mountains. Subsidiary faults trend northeast and southeast, and slip orientations vary from normal to strike-slip horizontal motion. Thermal fluids (~30°C) emerge at the intersection of the West Salton detachment and Elsinore faults actively alter the 94 Ma La Posta tonalite pluton, already fractured and crushed during fault slip, to a fine-grained white to orange powder through mineral re-equilibration. Grain sizes decrease with closer proximity to the faults. Fault cores contain thin dark green zones of chlorite ± epidote, and fault surfaces are coated with a thin layer of the same. Origin of the mineralization may be from reworked biotite crystals. We present water chemistry data from the hot springs at Agua Caliente in conjunction with geochemical and petrographic analysis of the surrounding rock. Water analyses include cation and anion measurements, bicarbonate, stable isotopes, tritium, and a multi-month recording of spring conductivity, water level, and temperature fluctuations. Cation geothermometry shows the fluids are enriched in Na, Ca, Mg, K, and Si from broken down quartz, plagioclase, and orthoclase. Water level and temperature data are compared to seismicity during the logging interval; temperatures so far have diurnal fluctuations indicating air temperature plays a larger role than anticipated for the subsurface fluids. Conductivity also displays daily cycles. We propose a larger scale map of the intersection of the two faults and the continuation of the Elsinore farther south showing the current extent and probable growth of the

damage and alteration as more slip occurs. Spring flow increases post seismic events, and we believe by monitoring fluid chemistry and comparing seismicity along the faults we will see precursors to and effects from fault motion.

TELESEISMIC P WAVE CODA OF SUBDUCTION EARTHQUAKES FROM WAVE INTERACTION NEAR TRENCHES (B-059)

W. Wu and S. Ni

Teleseismic P waves are essential for imaging rupture processes of great earthquakes, either in the back projection method or in finite fault inversion method involving of quantitative waveform modeling. In these studies, P waves are assumed to be direct P waves generated by localized patches of the ruptured fault. However these methods fail to produce accurate rupture models when some portion of the P waves are later arrivals generated by structural complexities such as mantle discontinuities or rapid lateral variation. For ~M7 earthquakes near the 2011 M9 Tohoku-Oki earthquake, we observed strong long period (10~20s) signals between P and PP on seismic network in eastern and central US. These P wave coda signals show strong coherence and are frequency dependent. The coda's amplitudes are comparable with those of the direct P wave in the 10-20s band and are much weaker in shorter period. With array analysis, we find that the coda's slowness is very close to that of the direct P wave, suggesting that they are generated near the source region. There have been reports of the coherent P wave coda interpreted as the P wave converted or reflected in the upper mantle discontinuities, but their amplitudes should be much smaller than those of the direct P wave. As the earthquakes occur near the Japan trench featuring rapid variation in bathymetry, we hypothesize that the coda waves are converted from surface waves at the trench.

To investigate the effects of the bathymetry on P wave coda, we apply ray theory to interface full wave field from spectral-element simulation to get the teleseismic P waves. With this approach, computation efficiency is greatly improved. The simulation results demonstrate that the surface wave can be severely scattered by the trench structure and coherent P waves are generated. We find that the coda's amplitudes are mainly controlled by the focal mechanism and depth. The frequency dependent feature from our simulation is also consistent with the observation that P coda is strongest in the 10-20s band. Thus, the coherent long period P codas are confirmed to be generated by the rapid variation of bathymetry near the trenches. Our study argues that the topography/bathymetry effect should be taken into account when imaging rupture processes of mega thrust earthquakes with teleseismic P waves.

PROPERTIES OF INELASTIC YIELDING ZONES GENERATED BY IN-PLANE DYNAMIC RUPTURES (A-079)

S. Xu, Y. Ben-Zion, and J.-P. Ampuero

We investigate the spatial distribution and intensity of off-fault yielding, the local orientation of the expected microfractures inside the yielding zone, and scaling relations or correlations among different measurable quantities. The study employs simulations of in-plane dynamic ruptures on a frictional fault governed by slip-weakening and rate-and-state friction laws, with a Mohr-Coulomb type off-fault inelastic response and a possible contrast of elasticity across the fault. The results indicate in agreement with previous studies that the location and spatial pattern of the yielding zones are strongly affected by the angle \Psi of the background maximum compressive stress relative to the fault. The yielding extent depends strongly on rupture mode (crack- or pulse-like), the seismic S ratio representing the initial stress level relative to failure, and the value of rock cohesion c. For cracks, the yielding zone thickness T linearly increases with the rupture distance L and the ratio of T/L is inversely proportional to the square of S. For pulses, the local T positively correlates with the maximum slip velocity at the point, while the average T along-strike approaches a constant for a range of S values (although it can change for other S levels). The yielding zone thickness for both rupture modes is reduced by increasing c. The magnitude of plastic strain decays logarithmically with fault normal distance, while its maximum value close to the fault approaches a constant along strike as the rupture speed is gradually stabilized. The local angle to the fault of the expected microfractures (assumed to be tensile) inferred from the distributed plastic strain is generally shallower and steeper than \Psi in the compressional and tensional quadrants, respectively. With a velocity contrast across the fault, ruptures can have preferred propagation direction that is the same as the slip in the compliant medium (positive direction) or opposite propagation direction, depending on a competition between dynamic changes of normal stress across the bimaterial interface and generation of off-fault yielding. With large values of \Psi representing large strike-slip faults, the off-fault yielding enhances the bimaterial effect and promotes propagation in the positive direction, with larger rupture and slip velocities, and with a more prominent off-fault yielding zone.

FULL-3D WAVEFORM TOMOGRAPHY FOR NORTHERN CALIFORNIA USING AMBIENT-NOISE CROSS-CORRELATION GREEN'S-FUNCTIONS (B-042)

Z. Xu and P. Chen

We cross-correlate the vertical components of ambient seismic noise data recorded on USArray broadband stations in the northern California area to estimate inter-station Green's functions.These ambient-noise Green's functions are then compared with synthetic Green's functions computed using the finite-difference method in a hybrid 3D reference model obtained by combining the California state-wide 3D seismic velocity model provided by Lin et al. (2010) with the USGS 3D seismic velocity model for the San Francisco Bay Region. The adjoint method is adopted to construct the gradient of the misfit functional, which is defined in terms of the frequency-dependent phase-delay measurements made on time-localized surface waves on the ambient-noise Green's functions and the synthetics computed using our 3D starting model. The first iteration of our inversion involves nearly 3200 inter-station paths that provide good coverage of northern California. After the first iteration, the updated 3D seismic velocity model provides nearly 50% reduction in the misfit functional. By carrying out more iterations and including more waveforms from ambient-noise Green's functions as well as waveforms from natural earthquakes, our studies will gradually improve the regional seismic velocity model in northern California.

THE PERMEABILITY VARIATIONS ON THE WENCHUAN FAULT MEASURED ON THE WATER LEVEL RESPONSE TO SOLID EARTH TIDES (A-088)

L. Xue, E.E. Brodsky, H. Li, H. Wang, and J. Pei

The mechanics of slip during an earthquake depends critically on the hydrologic properties. The in situ fault zone hydrological properties are difficult to measure and have never directly been constrained on the fault zone immediately after a large earthquake. In this work, we analyze 1.5 years of continuous data from the Wenchuan Fault Zone which was the site of the Mw 7.9 Wenchuan earthquake. We find that the hydraulic diffusivity D of Wenchuan Fault Zone is 0.03 m2/s, which is two orders of magnitude larger than pump test values on the Chelungpu Fault which is the site of the Mw 7.6 Chi-Chi earthquake. This measurement at Wenchuan was made by continuously monitoring the response of the well to the solid Earth tides. The solid earth tides impose a dilatational strain on the formation that pumps water cyclically in and out of the well. By measuring the phase and amplitude response, we can constrain the transmissivity and storage of the damage zone at 200-600 m form the principal slip zone assuming an isotropic, homogenous and laterally extensive aquifer. We evaluated the phase and amplitude responses for solid Earth tide in both frequency domain and time domain, and these two separate methods yield almost identical results. The average phase lag is 25 degree, and the average amplitude response is 6x10-7 strain/m. According to the Heish model, we solve for storage coefficient S 2.2x10-4 and transmissivity T 6.6x10-6 m2.

Calculation for the hydraulic diffusivity D with D=T/S, yields the reported value of D is 0.03 m2/s,which is a high number compared with the thermal diffusivity 10-6 m2/s.If the value is representative of the fault zone,then this means the hydrology processes should have an effect on the earthquake rupture process.One advantage of this tidal response method is that it is passive and so the D is accurately recording the in situ permeability undisturbed by the potential effects of a pump test. In the previous studies, Kitagawa et al.,[2002] reported the permeability of Nojima Fault decreased 50% over three years and Brenguier et al.,[2008] observed seismic velocity decreased by 0.08% immediately after the Parkfield earthquake and posetseismic velocity remained low for 3 years.We did not observe a significant healing signal recorded in the well after the 2008 Wenchuan earthquake. It seems that permeability of Wenchuan Fault does not follow expected healing behavior. This poses constraints on any geochemically-based model of fault zone healing.

COMPUTING A LARGE REFINED CATALOG OF FOCAL MECHANISMS FOR SOUTHERN CALIFORNIA (1981 – 2010) (B-077)

W. Yang, E. Hauksson, and P.M. Shearer

We calculate focal mechanisms for earthquakes that occurred in the southern California region from 1981 to 2010 using the HASH method and locations derived from waveform cross-correlation. Each focal mechanism is obtained from grid searching for the best-fitting double-couple focal mechanism solution to both the P-wave first motion records that were picked by network analysts, and the S/P amplitude ratios computed from three-component seismograms. We process more than 410,000 earthquakes, and analyze the statistical features of the whole data set. As more S/P amplitude ratios become available after 2000, the average focal plane uncertainty decreases significantly compared with solutions that include only P-wave first motions. We filter the preliminary data set with criteria associated with mean fault plane uncertainty and azimuthal gap, and obtain a high quality focal mechanisms catalog with approximately 179,000 earthquakes. In general the parameters of the focal mechanisms have been stable during the three decades. The dominant style of faulting is high angle right-lateral strike-slip faulting with the most likely strike angle centered at 150°/330°. For earthquakes of M < 2.5, there are more normal faulting

events than reverse faulting events while the opposite holds for M>2.5 events. A comparison of 23,000 common earthquakes shows our results generally agree with the focal mechanism catalog obtained by Hardebeck and Shearer (2003). Using 211 moment tensor solutions in Tape et al (2010) as benchmarks, we compare the focal plane rotation angles of common events in the catalog. 69% of common earthquakes in both catalogs match well, with rotation angles less than 35°. The common events with relatively large rotation angles are either located around the edge of the SCSN network or poorly recorded.

PRELIMINARY RESULTS ON THE ANALYSIS OF THE DEVIATORIC STRESS FIELD FROM FOCAL MECHANISMS AND SLIP-LINE FIELD FROM CONJUGATE LINEAR SEISMICITY CLUSTERS IN SOUTHERN CALIFORNIA (B-139)

W. Yang and E. Hauksson

We analyze the spatial and temporal variations of the deviatoric stress field and the geometric properties of conjugate linear seismicity clusters in the southern California region using earthquake data recorded by the SCSN from 1981 to 2011. Using a data set with about 179,000 high quality focal mechanisms that were determined from P first motions and S/P amplitude ratios, we invert for the variation in the stress field in time and space using the SATSI method. The inversion results match with results from prior studies with a predominant NS to NNE orientation of maximum horizontal stress, but our results reveal the stress field at higher level of resolution because we use a larger data set than was available before. The results show that the stress field exhibits minimal regional temporal variations, but some variations exist in small areas close to large mainshocks. Similarly, localized depth variations in the stress field suggest the possible existence of vertical strain partitioning. We determine a data set with approximate 8,000 seismicity clusters using waveform cross-correlation and a clustering method. We calculate the geometrical properties of clusters. Pairs of conjugated linear clusters exist across southern California. The angles between conjugate linear clusters in the direction of maximum shortening range from 80 [deg] to 160 [deg], with a median value of 120 [deg] and a mode value of 115 [deg]. The bisection of conjugate linear clusters in the direction of maximum shortening generally match with the maximum horizontal stress orientation, which implies a relation between orientation of the stress field and the orientation of clusters. We infer that the variation of conjugate angles is associated with brittle and ductile deformation, and apply slip-line field theory to interpret such observations. Overall, our observations provide new understanding of the kinematic crustal process in southern California.

COMPLEX RUPTURE MODES OF THE 2011 MW 9.0 TOHOKU-OKI EARTHQUAKE INFERRED FROM TELESEISMIC AND LOCAL WAVEFORMS (B-037)

H. Yao

The 2011 Mw 9.0 Tohoku-Oki earthquake occurred in the offshore Tohoku region in Japan, the Western Pacific subduction zone. It had very large coseismic slip (30-40 m) in the up-dip region close to the trench and tens of thousands of aftershocks dominantly in the down-dip region close to the coast. We have analyzed broadband teleseismic P-wave data from about 500 stations in the central and western US as well as local strong-motion waveforms from F-net and KiK-net in Japan to infer the rupture characteristics. We apply the newly developed time-domain iterative back-projection (IBP) method (with subevent waveform stripping and subevent relocation) to investigate the spatiotemporal distribution of subevents (P-wave energy radiation) in the source region in two frequency bands (0.2-1 and 0.05-0.2Hz). We also use a new frequency-domain method for sparse source inversion, compressive sensing (CS), to study the spatiotemporal distribution of P-wave energy radiation in four frequency bands between 0.05 and 1 Hz. In addition, we resolve slip details from finite-fault slip inversion of strong motion data from F-net and KiK-net in the low frequency band (0.005-0.05 Hz). Our results suggest a complicated rupture process, which is not well described by a constant velocity rupture from the hypocenter. Our results suggest that most high-frequency seismic energy was radiated near the epicenter for at least the first 80 s. Although the rupture was bilateral, significant southward rupture mainly occurred after 100 s, as seen from the spatiotemporal distribution of subevents or energy radiation in both low and high-frequency bands. Our analyses show that the earthquake has frequency-dependent rupture modes. Radiated high-frequency energy mainly came from the down-dip region, which is similar to the aftershock distribution pattern. However, radiated low-frequency energy was dominant in the up-dip (offshore) region, which is consistent with much larger slip in the up-dip region from the low-frequency seismic slip inversion. This frequency-dependent rupture may be caused by differences in rupture behavior (more intermittently at high frequencies and more continuous at low frequencies) at the plate interface due to heterogeneous friction properties.

STRAIN PARTITIONING IN LOS ANGELES (A-123)

R.S. Yeats and D. Verdugo

The Whittier fault offsets major streams in the foothills of the Puente Hills, and it presents a hazard from a strike-slip earthquake. However, the fault has reverse separation, north-side-up, and its footwall is uplifted by folding imaged by oil-well data supported by shallow instrumental seismicity from Yang and Hauksson (2011). The Whittier fault masks an anticline deformed on an underlying blind reverse fault that poses a separate hazard.

Similarly, the earthquake hazard from the Newport-Inglewood fault has been limited previously to right-lateral strike slip, similar to the 1933 Long Beach earthquake. However, Gilluly and Grant (1949) documented coseismic uplift immediately east of the fault in 1933, suggesting a reverse-fault subevent northwest of the strike-slip mainshock near Newport Beach. In addition, Hauksson (1987) documented reverse-fault-plane solutions, particularly in the northern half of the onshore fault trace. In addition, the discontinuous strike-slip fault traces in this part of the Newport-Inglewood zone extend along the crest of the broad Central Uplift anticline, bounded on the northeast by the active Compton-Los Alamitos reverse fault. We suggest that this deformation, like the Whittier fault system, involves strain partitioning.

The Palos Verdes fault has a right-lateral strike-slip rate of 2.7-3.8 mm/yr in Los Angeles Harbor. However, marine terraces in the Palos Verdes Hills show reverse-oblique slip along the fault of 3.0-3.7 mm/yr. Brankman and Shaw (2009) identified a southwest-dipping reverse-oblique-slip fault with a long-term oblique-slip rate of 4 mm/yr.

The next earthquake on one of these faults, then, could be a strike-slip fault like the 1933 Long Beach earthquake, a reverse-slip earthquake like the aftershocks of the 2010 Léogâne earthquake, or an oblique-reverse-slip event like the 1989 Loma Prieta earthquake. Each of these possibilities should be considered in the Community Fault Model.

THE FUTURE OF VIRTUAL CALIFORNIA SIMULATIONS (B-110)

M.B. Yikilmaz, J.B. Rundle, D.L. Turcotte, E.M. Heien, M.K. Sachs, and L.H. Kellogg

The Virtual California (VC) simulation code produces a long term synthetic catalog of earthquakes on major faults in California. The input is the slip rates and the recurrence intervals on the faults. At the present time the simulations produce complexity and statistical distribution of earthquakes on major faults. Straight forward future studies can:

1) Produce fault to fault correlations of activity (cross-correlations)

2) Produce maps of shaking for California based on the long term synthetic catalogs available from VC.

3) It is desirable to include the extension of displacements beneath the seismogenic zone. This is particularly important for fault to fault jumps.

4) Currently, fault jumps are inhibited by the stiff elastic region between faults. It may be necessary to introduce damage zone to enhance transfer of stress.

CHANGE IN STATISTICS FROM A DIMENSIONAL TRANSITION: MEASURING B = 1.5 FOR LARGE EARTHQUAKES (B-083)

M.R. Yoder, J.R. Holliday, D.L. Turcotte, and J.B. Rundle

We identify two distinct scaling regimes in the frequency-magnitude distribution of global earthquakes. Specifically, we measure the scaling exponent b = 1.0 for "small" earthquakes with $5.5 < m < 7.6$ and b = 1.5 for "large" earthquakes with $7.6 < m < 9.0$. This transition at mb = 7.6, can be explained by geometric constraints on the rupture. In conjunction with supporting literature, this corroborates theories in favor of fully self-similar and magnitude independent earthquake physics. We also show that the scaling behavior and abrupt transition between the scaling regimes implies that earthquake ruptures have compact shapes and smooth rupture-fronts.

PRODUCTS AND SERVICES AVAILABLE FROM THE SOUTHERN CALIFORNIA EARTHQUAKE DATA CENTER (SCEDC) AND THE SOUTHERN CALIFORNIA SEISMIC NETWORK (SCSN) (B-066)

E. Yu, A. Bhaskaran, S. Chen, M.J. Ihrig, F. Chowdhury, S. Meisenhelter, K. Hutton, D. Given, E. Hauksson, and R. Clayton

Currently the SCEDC archives continuous and triggered data from nearly 8400 data channels from 425 SCSN recorded stations, processing and archiving an average of 6.4 TB of continuous waveforms and 12,000 earthquakes each year. The SCEDC provides public access to these earthquake parametric and waveform data through its website www.data.scec.org and through client applications such as STP and DHI. This poster will describe the most significant developments at the SCEDC during 2011.

- The SCEDC has revamped its website. The changes make it easier for users to search the archive, discover updates and new content.
- Post processing on El Mayor Cucapah 7.2 sequence continues. To date there have been 11847 events reviewed. Updates are available in the earthquake catalog immediately.
- A double difference catalog (Hauksson et. al 2011) spanning 1981 to 6/30/11 will be available for download at www.data.scec.org and available via STP.
- A focal mechanism catalog determined Yang et al. 2011 is available for distribution at *www.data.scec.org*.
- Waveforms from Southern California NetQuake stations are now being stored in the SCEDC archive and available via STP as event associated waveforms.
- As part of a NASA/AIST project in collaboration with JPL and SIO, the SCEDC will receive real time 1 sps streams of GPS displacement solutions from the California Real Time Network (*http://sopac.ucsd.edu/projects/realtime*; Genrich and Bock, 2006, J. Geophys. Res.). These channels will be archived at the SCEDC as miniSEED waveforms, which then can be distributed to the user community via applications such as STP.
- STP sac output now includes picks from the SCSN.
- The SCEDC is exploring the feasibility of archiving and distributing waveform data using cloud computing such as Google Apps. A month of continuous data from the SCEDC archive will be stored in Google Apps and a client developed to access it in a manner similar to STP. The data is stored in miniseed format with gzip compression. Time gaps between time series were padded with null values, which substantially increases search efficiency by make the records uniform in length.
- In the past year, the SCEDC has collaborated with with NCEDC and USGS Golden, and IRIS to review the StationXML schema, make suggested changes, and and determine what software would be needed to develop StationXML writers and readers. Information on StationXML can be found at *http://www.data.scec.org/xml/station/*

PALEOSEISMOLOGY AND SLIP RATE OF THE SAN GORGONIO PASS FAULT ZONE AT MILLARD CANYON: TESTING THE LIKELIHOOD OF THROUGH-GOING SAN ANDREAS RUPTURES (A-142)

J.D. Yule and P.L. McBurnett

Understanding the San Andreas fault (SAF) behavior in San Gorgonio Pass is essential to assess earthquake and hazard risks in southern California. Within the San Gorgonio Pass region the SAF system becomes complex and diffuse. Here, strike-slip segments to the north and south intersect with the thrust-dominated San Gorgonio Pass fault zone (SGPFZ). Two end-member hypotheses explain this 20 km wide, left-stepping zone in terms large earthquake behavior. The 'enabler' model suggests a through going rupture of M7.8 that ruptures from the Salton Trough to the Mojave Desert whereas the 'barrier' model forecast < M7.5 ruptures to the north and south that are arrested by the complexity of SGPFZ. Trenches excavated at the northern Millard Canyon site test these competing hypotheses by constraining the timing of large ruptures on the SGPFZ and comparing them chronologies on the SAF to the north and south of the Pass.

Two ~55 m-long and 2-5 m-deep trenches cross a 2.5 m-high scarp that cuts an abandoned terrace riser. Paleoearthquakes are recognized by growth strata relations and secondary reverse faults. On lapping sequences buttress ground surface rupture events with intervals of unconformities between each on lapping unit. Ample detrital charcoal was present allowing dating of on lapping sequences constraining rupture timing and uplift rates. Displacement in Trench 1 shows growth folding of fluvial material with minor faulting. Preliminary total displacement measurements suggest ~9 m of total offset within the last ~2700 yrs giving an average slip rate of 3 mm/yr. Four individual faulting events can be seen implying recurrence intervals of ~600-700 yrs.

Our preferred model is the 'enabler' which allows SAF ruptures to propagate through the SGPFZ. Recurrence intervals change from ~100-200 yrs, as is common throughout the SAF, to intervals of ~600-700 yrs coinciding with lower slip rates. The SGPFZ complex structure may discourage through going ruptures, as with the 1812 rupture ending in Burro Flats, with through going ruptures occurring every 600-700 yrs on average. We also cannot rule out local ruptures contained within the SGPFZ as a possible source of faulting without surface rupture continuing north or south of the zone. Since 1906 most segments of the

SAF have had a major rupture event with the exception of the southern SAF. With no historical record or rupture on this segment of the SAF within the last 600-700 yrs, a rupture event may be imminent.

RELATIONS BETWEEN PROPERTIES OF SEISMICITY AND REGIONAL HEAT FLOW IN CALIFORNIA (B-028)

I. Zaliapin and Y. Ben-Zion

This work continues exploration of the relations between dynamics of seismicity and physical properties of the lithosphere. We establish quantitative connections between the existence and productivity of different types of seismicity (foreshocks, aftershocks, background activity, swarms) and regional heat flow in California. Methodologically, we first represent the seismicity as a sequence of statistically significant clusters using the approach of Zaliapin et al. [PRL, 2008]. The multi-event clusters largely correspond to individual foreshock-mainshock-aftershock sequences or swarms. Within each cluster we compute the number, total seismic moment, and rupture area of events. We demonstrate that the heat flow is positively correlated with (i) total offspring number, seismic moment, and rupture area, (ii) foreshock production relative to that of aftershocks, measured by number, moment, or rupture area, and (iii) average duration of foreshock and aftershock series (absolute as well as normalized by the mainshock magnitude). In addition, the heat flow is (iv) negatively correlated with average distance between offsprings and the respective mainshock (absolute as well as normalized by the mainshock magnitude), and (v) the local b-value is negatively correlated with the heat flow. The above results are obtained in two consecutively more detailed approaches: (i) for spatio-temporal averages, and (ii) for time-averaged space intensities. To study the second case, we introduce a novel methodology for quantifying coupling between two (multidimensional) intensities or between intensity and a point field. The proposed methodology is focused on detecting non-linear relations and is shown to have particular advantages on the likelihood approach and classical correlation. The presented methodology and results contribute to better understanding of detailed non-universal relations between time-space-size varying features of seismicity and physical properties of a region. The results can be used to develop improved region-specific estimates of earthquake hazard assessment.

CORSSA: COMMUNITY ONLINE RESOURCE FOR STATISTICAL SEISMICITY ANALYSIS - STATUS & OUTLOOK (A-023)

J.D. Zechar, J.L. Hardebeck, A.J. Michael, M. Naylor, S. Steacy, S. Wiemer, J. Zhuang

Statistical seismology is critical to the understanding of seismicity, the evaluation of proposed earthquake prediction and forecasting methods, and the assessment of seismic hazard. Unfortunately, despite its importance to seismology—especially to those aspects with great impact on public policy—statistical seismology is mostly ignored in the education of seismologists, and there is no central repository for the existing open-source software tools. To remedy these deficiencies, and with the broader goal to enhance the quality of statistical seismology research, we have begun building the Community Online Resource for Statistical Seismicity Analysis (CORSSA, *www.corssa.org*). We anticipate that the users of CORSSA will range from beginning graduate students to experienced researchers.

More than 20 scientists from around the world met for a week in Zurich in May 2010 to kick-start the creation of CORSSA: the format and initial table of contents were defined; a governing structure was organized; and workshop participants began drafting articles. CORSSA materials are organized with respect to six themes, each will contain between four and eight articles. CORSSA now includes seven articles with an additional six in draft form along with forums for discussion, a glossary, and news about upcoming meetings, special issues, and recent papers. Each article is peer-reviewed and presents a balanced discussion, including illustrative examples and code snippets. Topics in the initial set of articles include: introductions to both CORSSA and statistical seismology, basic statistical tests and their role in seismology; understanding seismicity catalogs and their problems; basic techniques for modeling seismicity; and methods for testing earthquake predictability hypotheses. We have also begun curating a collection of statistical seismology software packages.

ETAS VS. STEP (B-123)

J.D. Zechar, D. Schorlemmer, M.C. Gerstenberger, and D.A. Rhoades

Since September 2007, there has been an experiment in California to test and evaluate two models that yield next-day seismicity forecasts: the Epidemic-Type Aftershock Sequence, or ETAS, model and the Short Term Earthquake Probability, or STEP, model. ETAS and STEP are statistical models that incorporate well-studied empirical relations such as the Gutenberg-Richter magnitude distribution and the Omori-Utsu relation for the temporal decay of "aftershock" activity. The objective of

the experiment is for each model to generate a forecast that specifies the expected number of earthquakes for the next 24 hours in bins specified by ranges of latitude, longitude, and magnitude. The spatial cells are 0.1 degrees by 0.1 degrees, and the models target all earthquakes with magnitude greater than or equal to 3.95 in bins of 0.1 units. We examined the first three years of results; during this time, 270 target earthquakes occurred in the testing region, including a swarm in Baja California throughout February 2008 and the April 2010 M 7.2 El Mayor-Cucapah earthquake.

Through the testing component of this experiment, we discovered a flaw in the STEP implementation; it was corrected, and we evaluated forecasts based on the revised implementation. To evaluate the models, we conducted investigations of consistency (each model relative to the observation) and comparison (each model relative to the other). Based on joint log-likelihood measures, we found that both models are reasonably consistent with the observations of interest: the number of earthquakes, their spatial distribution, their magnitude distribution, and the joint distribution. To compare the models, we computed the rate-corrected average information gain per earthquake; this is the natural logarithm of the probability gain. STEP had an average information gain of 0.43 relative to ETAS; in other words, STEP had, on average, a 54% higher forecast rate than ETAS in bins where target earthquakes occurred, indicating that STEP was superior in this experiment.

FOCAL MECHANISM WITH ERROR ESTIMATION USING REGIONAL WAVEFORMS: A CASE STUDY WITH THE 2008 CHINO HILLS EARTHQUAKE (B-072)

Z. Zhan, S. Wei, and D. Helmberger

Earthquake focal mechanisms are now routinely reported using regional records. However, due to difficulties in fitting seismograms with inadequate velocity model, and the usually non-linear inverse methodology, error estimation of focal mechanism is not a trivial problem. Here we explore the potential of using the bootstrapping method to estimate the error of focal mechanism from Cut-And-Paste (CAP). CAP first cuts the regional seismograms into Pnl wave and surface wave segments, then fits them allowing different time shifts, period bands and weights. CAP finds the best waveform-fitting focal mechanism by grid-searching the whole model space so we have the full information about each station's waveform misfit for every possible focal mechanism. This information naturally goes into the bootstrapping method. We validate this technique with the 2008 Chino Hills earthquake, which is well recorded and studied with the dense regional data from the TriNet. We also test the possibility to correct Amplitude Amplification Factors (AAFs) for each station using the information from the large number of bootstrapping solutions. Tests with both synthetic test and real data show largely reduced errors of focal mechanism parameters.

STRAIN LOCALIZATION AND CRUSTAL THICKNESS VARIATION ACROSS MAJOR STRIKE SLIP FAULTS IN SOUTHERN CALIFORNIA REVEALED BY RECEIVER FUNCTION STUDIES (B-140)

P. Zhang, M.S. Miller, J.F. Dolan, I.W. Bailey, and D.A. Okaya

The degree to which faults are localized or distributed within the continental lithosphere has been a controversial subject for decades. Reflection and refraction studies indicate that the San Andreas fault (SAF) extends into the lower crust as a narrow fault zone in northern California and along the Mojave segment of the fault. However, the discretness of lithospheric deformation along the southernmost segments of the SAF system (e.g., the Elsinore, the San Jacinto and the Coachella segment of the San Andreas) remains unclear. We have begun a detailed study of how the distribution of strain at depth is in southern California using P receiver functions to image crustal and lithospheric thickness variations. We specifically focus on the depths of the Moho and lithosphere-asthenosphere boundary (LAB) underneath the major faults. Our results for the geometry of crustal and lithospheric interfaces provide insight into the strain localization in this region. Our preliminary results using events recorded by Southern California Seismic Network and USarray reveal complex crustal and lithospheric structure in this region. A SW-NE profile across the Elsinore, San Jacinto, and and San Andreas faults indicates that the Moho dips to the southwest. Moreover, receiver gathers at certain stations near the faults show a strong back-azimuthal variation. Using simple velocity models to project the Ps conversions to depth, we find that some of the back-azimuth variation can be related to different sides of the faults. These back-azimuthal variations of the Moho signal indicate three-dimensional complexity beneath the central San Jacinto fault that may suggest strain localization at these depths.

AWP-ODC-SGT: WAVE PROPAGATION AND DYNAMIC RUPTURE SIMULATION SOFTWARE WITH STRAIN GREEN'S TENSOR (SGT) CAPABILITIES FOR CYBERSHAKE 2.0 (A-031)

J. Zhou, S. Callaghan, S. Song, P. Chen, K. Olsen, R. Graves, P. Small, P. Maechling, Y. Cui, and T. Jordan

CyberShake (Graves, et al., 2008/2011) is a SCEC research project to develop a physics-based computational approach to create a probabilistic seismic hazard analysis (PSHA). CyberShake uses fully 3D wave propagation simulations to forecast

ground motions which is expected to produce significantly more accurate PSHA estimates as compared to those conventionally produced by attenuation relationships. In the planned CyberShake 2.0 project, SCEC plans to include multiple Community Velocity Models with state-wide capabilities for frequencies up to 1Hz. Toward this goal we are in the process of implementing and verifying strain green's tensor (SGT) creation, seismogram synthesis, and error minimization from numerical differentiation (Zhao, et al., 2006) in AWP-ODC, a SCEC community software package which simulates earthquake dynamic rupture and wave propagation using a fourth-order accurate staggered grid finite difference scheme. The use of AWP-ODC for CyberShake 2.0 is based on the need for maximum computational efficiency in the waveform modeling of the project. AWP-ODC has demonstrated its petascale scalability by successfully simulating a magnitude-8 earthquake on the southern San Andreas fault up to 2 Hz using 223,074 cores on NCCS Jaguar (Cui et al., 2010).

ACCELERATION OF 3D FINITE DIFFERENCE AWP-ODC FOR SEISMIC SIMULATION ON GPU FERMI ARCHITECTURE (A-039)

J. Zhou, Y. Cui, and D.J. Choi

AWP-ODC, a highly scalable parallel finite-difference application, enables petascale 3D earthquake calculations. This application generates realistic dynamic earthquake source description and detailed physics-based anelastic ground motions at frequencies pertinent to safe building design. In 2010, the code achieved M8, a full dynamical simulation of a magnitude-8 earthquake on the southern San Andreas fault up to 2-Hz, the largest-ever earthquake simulation.

Building on the success of the previous work, we have implemented CUDA on AWP-ODC to accelerate wave propagation on GPU platform. Our CUDA development aims on aggressive parallel efficiency, optimized global and shared memory access to make the best use of GPU memory hierarchy. The benchmark on NVIDIA Tesla C2050 graphics cards demonstrated many tens of speedup in single precision compared to serial implementation at a testing problem size, while an MPI-CUDA implementation is in the progress to extend our solver to multi-GPU clusters. Our CUDA implementation has been carefully verified for accuracy.

Meeting Participants

AAGAARD *Brad*, USGS
ABERS *Geoffrey*, LDEO
ABRAHAMSON *Norman*, PG&E
AFFADONIS *Mikkail*, Terrace Hills MS
AGUIAR *Ana*, Stanford
AKCIZ *Sinan*, UC Irvine
ALANIZ *Emigdio*, ELAC
ALLAM *Amir*, USC
ALLEN *Richard*, UC Berkeley
ALLEN *Sean*, UNR
AMPUERO *Jean Paul*, Caltech
ANDERSON *Robert*, California Earthquake Authority
ANDERSON *John*, UNR
ANDREWS *Dudley*, USGS-retired
ARCHULETA *Ralph*, UCSB
ARROWSMITH *J Ramon*, ASU
ASPIOTES *Aris*, USGS
ASSIMAKI *Dominic*, Georgia Tech
ATKINSON *Gail*, U Western Ontario
BAILEY *Iain*, USC
BAKER *Jack*, Stanford
BANESH *Divya*, UC Davis
BARBA *Magali*, UC Berkeley
BARBOT *Sylvain*, Caltech
BARBOUR *Andrew*, UCSD
BARRETT *Sarah*, Stanford
BAYLESS *Jeff*, URS
BEAUDOIN *Bruce*, IRIS PASSCAL
BECKER *Thorsten*, USC
BEHR *Whitney*, Brown
BEN-ZION *Yehuda*, USC
BENNETT *Richard*, U Arizona
BENTHIEN *Mark*, SCEC/USC
BEROZA *Gregory*, Stanford
BEUTIN *Thomas*, GFZ Potsdam
BHAT *Harsha*, USC/Caltech
BIASI *Glenn*, UNR
BIELAK *Jacobo*, CMU
BILHAM *Roger*, Colorado
BIRD *Peter*, UCLA
BLANPIED *Michael*, USGS
BLISNIUK *Kimberly*, UC Davis
BOESE *Maren*, Caltech
BOHON *Wendy*, ASU
BOORE *David*, USGS
BORMANN *Jayne*, UNR
BORSA *Adrian*, UNAVCO
BOSS *Stephanie*, LMU
BOWMAN *David*, CSU Fullerton
BOYD *Oliver*, USGS
BRADLEY *Brendon*, U Canterbury
BRIDGES *Peter*, UMass
BROCHER *Thomas*, USGS
BRODSKY *Emily*, UC Santa Cruz
BROWN *Justin*, Stanford
BROWNLEE *Sarah*, UCSB
BRUNE *James*, UNR
BUGA *Michael*, SDSU
BULL *William*, U Arizona
BUTCHER *Amber*, Cal Poly Pomona
BUTSCHER *William*, Bloomington HS
BWARIE *John*, USGS
BYDLON *Samuel*, Penn State
BYKOVTSEV *Alexander*, Regional Acad of Natural Sciences
CADENA *Ana*, CWU
CALLAGHAN *Scott*, SCEC/USC
CARLSON *Erica*, Hesperia HS
CASTRO *Raúl*, CICESE
CATCHINGS *Rufus*, USGS
CATO *Kerry*, Cato Geoscience
CHAO *Kevin*, Georgia Tech
CHEN *Shang-Lin*, Caltech
CHEN *Tao*, China Earthquake Administration / USGS
CHEN *Raymond*, UCLA
CHEN *Xiaowei*, UCSD
CHEN *Po*, U Wyoming
CHESTER *Judith*, Texas A&M
CHIOU *Ray*, NAVFAC
CHOI *Dong Ju*, SDSC
CHUANG *Yun-Ruei*, Indiana
CHUNG *Angela*, Stanford
CIVILINI *Francesco*, UCSB
CLAYTON *Robert*, Caltech
COCHRAN *Elizabeth*, USGS
COLELLA *Harmony*, UC Riverside
COMPTON *Tracy*, UC Davis
COOKE *Michele*, UMass
COON *Ethan*, LANL
COWGILL *Eric*, UC Davis
COX *Paul*, UCLA
CREMPIEN *Jorge*, UCSB
CROSBY *Christopher*, SDSC/UCSD
CROWELL *Brendan*, UCSD
CRUZ JIMENEZ *Hugo*, KAUST
CUI *Yifeng*, SDSC
CURRIE *Trevor*, Caltech
DAHMEN *Karin*, Illinois
DAVATZES *Nicholas*, Temple U
DAVIDGE *Lindsey*, USC
DAVIS *Lindsay*, Colorado State
DAVIS *Paul*, UCLA
DAWSON *Timothy*, CGS
DAY *Steve*, SDSU
DE CRISTOFARO *Jason*, USGS
DE GROOT *Robert*, SCEC/USC
DEL PARDO *Cecilia*, UTEP
DELAUDER *Audra*, U Virginia
DENOLLE *Marine*, Stanford
DETERMAN *Daniel*, USGS
DIEHL *John*, GEOVision
DIETERICH *James*, UC Riverside
DMOWSKA *Renata*, Harvard
DOLAN *James*, USC
DOMINGUEZ *Luis*, UCLA
DONNELLAN *Andrea*, NASA JPL
DONOVAN *Jessica*, USC
DRISCOLL *Neal*, SIO
DUAN *Benchun*, Texas A&M
DUNHAM *Eric*, Stanford
EISSES *Amy*, UNR
ELBANNA *Ahmed*, UCSB
ELLIOTT *Austin*, UC Davis
ELLSWORTH *William*, USGS
ELY *Geoffrey*, Argonne National Lab
ERICKSON *Brittany*, Stanford
EVANS *Eileen*, Harvard
FANG *Zijun*, Stanford
FARHAT *Tarana*, Hampton
FENNING *Neil*, USGS
FERGUSON *Alex*, USGS
FIALKO *Yuri*, UCSD
FIELD *Edward*, USGS
FILSON *John*, USGS-Retired
FLETCHER *John*, CICESE
FLOYD *Michael*, MIT
FREEMAN *Stephen*, GeoPentech
FRENCH *Melodie*, Texas A&M

FREYMUELLER *Jeffrey*, U Alaska Fairbanks
FUIS *Gary*, USGS
FUNNING *Gareth*, UC Riverside
GALASSO *Carmine*, UC Irvine
GALETZKA *John*, Caltech
GALLOVIC *Frantisek*, Charles Univ in Prague
GARDNER *Max*, USGS
GAVILLOT *Yann*, Oregon State
GEE *Robin*, UCSB
GERSTENBERGER *Matthew*, GNS Science
GERSTOFT *Peter*, UCSD
GILCHRIST *Jacquelyn*, UC Riverside
GLOWACKA *Ewa*, CICESE
GOEBEL *Thomas*, USC
GOLD *Peter*, UC Davis
GOLDBERG *Daniel*, USC
GOLDMAN *Mark*, USGS
GOLTZ *James*, CalEMA
GONZALEZ-ORTEGA *Alejandro*, CICESE
GOODING *Margaret*, LSA Assoc
GORMLEY *Deborah*, SCEC/USC
GOULET *Christine*, UC Berkeley
GRANAT *Robert*, NASA JPL
GRANT LUDWIG *Lisa*, UC Irvine
GRAVES *Robert*, USGS
GREENWOOD *Rebecca*, Cal Poly Pomona
GRIJALVA *Ashley*, UTEP
GULOTTA *Bryan*, UC Riverside
HADDAD *David*, ASU
HAKAMATA *Tomohiro*, UCSB
HALLER *Kathleen*, USGS
HANKS *Audra*, Cal Poly Pomona
HARDEBECK *Jeanne*, USGS
HARDY *Gregory*, SGH
HARRIS *Sheri*, Arlington HS
HARRIS *Sharon*, QuakeSafeKits
HARRIS *Bob*, QuakeSafeKits
HARRIS *Ruth*, USGS
HARVEY *Jonathan*, UCSB
HAUKSSON *Egill*, Caltech
HEARN *Elizabeth*, UBC
HEATON *Thomas*, Caltech
HEERMANCE *Richard*, CSUN
HEIEN *Eric*, UC Davis
HELLIGE *Bridget*, USC
HELMBERGER *Donald*, Caltech
HENRY *Pamela*, Fault Line
HERBERT *Justin*, UMass
HERNANDEZ *Stephen*, UC Santa Cruz
HERRING *Thomas*, MIT
HILL *David*, USGS
HINOJOSA-CORONA *Alejandro*, CICESE
HIRAKAWA *Evan*, SDSU
HOGAN *Phillip*, Fugro Consultants
HOLDEN *Caroline*, GNS Science
HOLE *John*, Virginia Tech
HOLLIDAY *James*, UC Davis
HOLLIS *Daniel*, NodalSeismic
HOLT *William*, SUNY-Stony Brook
HOOKS *Benjamin*, UTM
HOUGH *Susan*, USGS
HUANG *Yihe*, Caltech
HUBBARD *Judith*, Harvard
HUDNUT *Kenneth*, USGS
HUMPLEMAN *Heather*, USC
HUYNH *Tran*, SCEC/USC
IMANISHI *Kazutoshi*, GS Japan
INBAL *Asaf*, Caltech
ISBILIROGLU *Yigit*, CMU
JACKSON *David*, UCLA
JANECKE *Susanne*, Utah State
JI *Chen*, UCSB
JIANG *Junle*, Caltech
JIMENEZ *Ernesto*, PCC
JOHANSON *Ingrid*, UC Berkeley
JOHNSON *Kaj*, Indiana
JOHNSON *Marilyn*, PCC
JONES *Andrea*, USC
JONES *Lucile*, USGS
JORDAN *Thomas*, SCEC/USC
JORDAN, JR. *Frank*, John R Byerly
KAGAN *Yan*, UCLA
KANEKO *Yoshihiro*, UCSD
KANG *Jingqian*, Texas A&M
KARAOGLU *Haydar*, CMU
KEDAR *Sharon*, NASA JPL
KELL *Annie*, UNR
KELLER *Edward*, UCSB
KELLER *Brenton*, USC
KELLOGG *Louise*, UC Davis
KENDRICK *Katherine*, USGS
KENT *Graham*, UNR
KENT *Tyler*, UNR
KILB *Debi*, UCSD
KIM *Hyun-Tae*, ASU
KING *Nancy*, USGS
KIRBY *Matthew* , CSU Fullerton
KIRKPATRICK *James*, UC Santa Cruz
KITAJIMA *Hiroko*, Penn State
KLEIN *Mark*, Banning HS
KNOWLTON *Michael*, SCE/SONGS
KNUDSEN *Keith*, USGS
KOHLI *Arjun*, Stanford
KOZDON *Jeremy*, Stanford
KRISHNAN *Swaminathan*, Caltech
KROLL *Kayla*, UC Riverside
KUMAR *Sandarsh*, SCEC/USC
KURZON *Ittai*, UCSD
LAJOIE *Lia*, UC Santa Cruz
LAMBERT *Valère*, Caltech
LANGENHEIM *Victoria*, USGS
LAPUSTA *Nadia*, Caltech
LAVALLEE *Daniel*, UCSB
LAVIER *Luc*, UT Austin
LAWSON *Michael*, UCLA
LEE *Ya Ting*, NCU Taiwan
LEE *En-Jui*, U Wyoming
LEEPER *Robert*, USGS
LEGG *Mark*, Legg Geophysical
LEKIC *Vedran*, Brown
LEMERSAL *Elizabeth*, USGS
LEMME *Nathan*, NAVFAC ESC/US Navy
LEMNITZER *Anne*, UC Irvine
LEPRINCE *Sebastien*, Caltech
LI *Xiangyu*, UCSB
LI *Yong-Gang*, USC
LIAO *Eric*, UCR
LIEOU *Charles*, UCSB
LILLIE *Robert*, Oregon State
LIM *Amy*, PCC
LIN *Fan-Chi*, Caltech
LIN *Kevin*, USC
LINDSEY *Eric*, SIO/IGPP
LINDVALL *Scott*, Fugro Consultants
LINO *Susana*, Cal Poly Pomona
LIPOVSKY *Brad*, Stanford
LIPPOLDT *Rachel*, Oregon
LIU *Zaifeng*, Texas A&M
LIU *Qiming*, UCSB
LIU *Xin*, USC

LIUKIS *Maria*, SCEC/USC
LLENOS *Andrea*, USGS
LOGAN *John*, Oregon
LOHMAN *Rowena*, Cornell
LONG *Kate*, CalEMA
LOUIE *John*, UNR
LOZOS *Julian*, UCR
LUCERO *Jaron*, UCSB
LUCO *Nicolas*, USGS
LUI *Ka Yan Semechah*, Caltech
LUO *Yingdi*, Caltech
LUTHER *Amy*, New Mexico Tech
LUTTRELL *Karen*, USGS
LYDEEN *William*, USGS
LYNCH *David*, USGS
LYNETT *Patrick*, USC
MA *Shuo*, SDSU
MACCARTHY *Dawn*, USGS
MADDEN *Elizabeth*, Stanford
MADDEN MADUGO *Christopher*, Oregon State
MAECHLING *Philip*, SCEC/USC
MAI *P. Martin*, KAUST
MAK *Chi Ming*, PCC
MANJARREZ *Uriel*, CICESE
MARLIYANI *Gayatri*, ASU
MARQUIS *John*, SCEC/USC
MARSHALL *Scott*, Appalachian State
MASON *Robert*, PCC
MATTI *Jonathan*, USGS
MAZZONI *Silvia*, Degenkolb
MCAULIFFE *Lee*, USC
MCBURNETT *Paul*, CSUN
MCCAFFREY *Robert*, Portland State
MCCARTHY *Christine*, Columbia
MCCARTHY *Jill*, USGS
MCGILL *Sally*, CSU San Bernardino
MCGUIRE *Kathleen*, CSUN
MCKAY *Hannah*, CSUN
MCLELLAN *Mary*, PCC
MCRANEY *John*, SCEC/USC
MEADE *Brendan*, Harvard
MEHTA *Gaurang*, USC/ISI
MEIJER *Michelle*, Eleanor Roosevelt HS
MELGAR *Diego*, SIO/UCSD
MELTZER *Anne*, Lehigh
MELTZNER *Aron*, Nanyang Tech U
MENCIN *David*, UNAVCO
MENDES *Laura*, ASU/UFR Rio de Janeiro
MENG *Lingsen*, Caltech
MENG *Xiaofeng*, Georgia Tech
MENGES *Christopher*, USGS
MERRIAM *Martha*, Caltrans
MICHAEL *Andrew*, USGS
MILETI *Dennis*, U Colorado
MILLER *Meghan*, USC
MILLINER *Chris*, USC
MILNER *Kevin*, SCEC/USC
MINSTER *Jean*, UCSD
MITCHELL *Thomas*, Bochum
MITCHELL *Erica*, UCSD
MOONEY *Walter*, USGS
MORELAN *Alexander*, UNR
MORESI *Louis*, Monash University
MORI *James*, Kyoto University
MORTON *Nissa*, SDSU
MOURHATCH *Ramses*, Caltech
MUELLER *Karl*, U Colorado
MUHAMMAD *Kaliymah*, CSU San Bernardino
MURPHY *Janice*, USGS
NADEAU *Robert*, UC Berkeley
NAEIM *Farzad*, John A Martin & Associates
NALE *Stephanie*, UC Santa Cruz
NEIGHBORS *Corrie*, UCR
NI *Sidao*, U Science & Tech of China
NICHOLSON *Craig*, UCSB
NISSEN *Edwin*, ASU
NYST *Marleen*, RMS
OGLESBY *David*, UC Riverside
OKAYA *David*, USC
OLSEN *Kim*, SDSU
OLSEN *Anna*, USGS
ONDERDONK *Nate*, CSU Long Beach
ORTEGA *Gustavo*, CALTRANS-LA
OSKIN *Michael*, UC Davis
OWEN *Susan*, NASA JPL
OZAKIN *Yaman*, USC
PACE *Alan*, Petra Geotechnical
PAGE *Morgan*, USGS
PAPIKYAN *Tatev*, UCLA
PARKER *Jay*, NASA JPL
PASEDA *Sulaimon*, Howard
PATTON *Patrick*, Colorado
PEARSON *Eric*, La Sierra HS
PELTIES *Christian*, LMU Munich
PENG *Zhigang*, Georgia Tech
PENNINGTON *Alan*, Valley View HS
PEREZ *Florante*, CGS
PERRY *Suzanne*, USGS
PETAL *Marla*, Risk RED
PETERSEN *Mark*, USGS
PETERSON *Dana*, UW Madison
PITARKA *Arben*, URS
PITRUZELLO *Trey*, Martin Luther King HS
PLATT *John*, Harvard
PLATT *John*, USC
PLESCH *Andreas*, Harvard
POLET *Jascha*, Cal Poly Pomona
PONCE-ZEPEDA *Moises*, ELAC
PORTER *Keith*, U Colorado
POTTER *Hannah*, Cal Poly Pomona
POWELL *Robert*, USGS
POWERS *Peter*, USGS
PRUDENCIO *Ernesto*, UT Austin
PURASINGHE *Rupa*, CSU Los Angeles
PURASINGHE *Ruwanka*, UC Davis
RAMZAN *Shahid*, CSUN
REUVENI *Yuval*, NASA JPL
REZAEIAN *Sanaz*, USGS
RHOADES *David*, GNS Science
RHODES *Brady*, CSU Fullerton
RHODES *Edward*, UCLA
RICE *James*, Harvard
RICHARDS-DINGER *Keith*, UC Riverside
ROCKWELL *Thomas*, SDSU
RODER *Belinda*, UCLA
RODRIGUEZ-CASTRO *David*, Puerto Rico at Mayaguez
ROGERS-MARTINEZ *Marshall*, Columbia
ROLLINS *John*, USC
ROMANO *Mark*, USC
ROOD *Dylan*, LLNL
ROSE *Elizabeth*, USGS
ROSOVE *Sari*, UBC
ROSS *Zachary*, USC
ROSS *Stephanie*, USGS
ROUSSEAU *Nick*, SCEC/USC
ROUSSET *Baptiste*, Caltech
ROWE *Kristen*, U Colorado
ROWSHANDEL *Badie*, CGS/CEA
RUBINO *Vito*, Caltech
RUBINSTEIN *Justin*, USGS

RUIZ *Ricardo*, Chaffey HS
RUNDLE *John*, UC Davis
RYAN *Kenny*, UC Riverside
RYNGE *Mats*, USC/ISI
SACHS *Michael*, UC Davis
SAHAKIAN *Valerie*, UCSD
SALISBURY *James*, ASU
SANCHEZ *Dominga*, UCSD
SANDWELL *David*, UCSD
SATO *Tsurue*, ASU
SAVAGE *Heather*, LDEO
SAVRAN *William*, UNR
SAWYER *Christine*, SBCC
SCHARER *Katherine*, USGS
SCHMANDT *Brandon*, Caltech
SCHMITT *Stuart*, Stanford
SCHORLEMMER *Danijel*, USC/GFZ
SCOTT *Eric*, San Bernardino County Museum
SEALE *Sandra*, NEES@UCSB
SEDKI *Ziad*, CSULB
SEGALL *Paul*, Stanford
SEGOU *Margarita*, USGS
SELIGSON *Hope*, MMI Engineering
SEVERSON *Chad*, UC Riverside
SHAFER *Debora*, Hesperia HS
SHAO *Guangfu*, UCSB
SHAW *John*, Harvard
SHAW *Bruce*, LDEO
SHEARER *Peter*, UCSD
SHELLY *David*, USGS
SHERVAIS *Katherine*, Wesleyan
SHI *Zheqiang*, SDSU
SHOME *Nilesh*, RMS
SICKLER *Robert*, USGS
SIRIKI *Hemanth*, Caltech
SLEEP *Norman*, Stanford
SMALL *Patrick*, SCEC/USC
SMITH *Deborah*, CIW
SMITH-KONTER *Bridget*, UTEP
SOLIS *Teira*, UTEP
SOMALA *Surendra*, Caltech
SOMERVILLE *Paul*, URS
SONG *Seok Goo*, ETH Zurich
SONG *Shiyu*, UCSD
SPELZ *Ronald*, UABC
SPINLER *Joshua*, U Arizona
SPRINGER *Kathleen*, San Bernardino County Museum
STARK *Keith*, SCIGN
STEIDL *Jamison*, UCSB
STERN *Aviel*, UC Santa Cruz
STIRLING *Mark*, GNS Science
STOCK *Joann*, Caltech
STRADER *Anne*, UCLA
STREIG *Ashley*, Oregon
STUBAILO *Igor*, UCLA
SU *Feng*, US Bureau of Reclamation
SUMY *Danielle*, USGS
SYMCOX *Carl*, Dartmouth
TABORDA *Ricardo*, CMU
TAHTINEN *Hillary*, UCSD
TAKEUCHI *Christopher*, UCSD
TAPE *Carl*, U Alaska Fairbanks
TARNOWSKI *Jennifer*, UCR
TAYLOR *Michael*, U Kansas
TERAN *Orlando*, CICESE
THATCHER *Wayne*, USGS
THIO *Hong Kie*, URS
THOMAS *Marion*, Caltech
THOMAS *Helen*, USGS
THORNOCK *Steve*, Utah State
THORNTON *Garrett*, UTEP
THURBER *Clifford*, UW Madison
TIAN *Xiangyan*, Caltech
TINSLEY *John*, USGS
TODD *Erin*, UC Santa Cruz
TOKE *Nathan*, Utah Valley U
TONG *Xiaopeng*, IGPP/SIO
TORRENS-BONANO *Angel*, Puerto Rico at Mayaguez
TRAER *James*, UCSD
TREIMAN *Jerome*, CGS
TRUDEAU *Joseph*, UCSB
TSAI *Victor*, Caltech
TULLIS *Terry*, Brown
TURCOTTE *Donald*, UC Davis
TURKLE *Katharine*, USGS
UCHIDE *Takahiko*, UCSD
UPTON *Elizabeth*, Occidental
VALEN *Christina*, UCSD
VAN DER ELST *Nicholas*, UC Santa Cruz
VANEGAS *Michelle*, PCC
VARGAS *Bernadette*, Etiwanda HS
VARGAS *Bernadette*, Etiwanda HS
VEERARAGHAVAN *Swetha*, Caltech
VERDUGO MADUGO *Danielle*, Earth Consultants International
VIDALE *John*, U Washington
WAGNER *Kelsey*, USC
WAGNER *Max*, USC
WALKER *Brendon*, SDSU
WALLACE *Seth*, Bloomington HS
WALLS *Christian*, UNAVCO
WALTERS *Randi*, Stanford
WANG *Enning*, Princeton
WANG *Tien-Huei*, UCR
WANG *Feng*, USC
WARD *Steven*, UC Santa Cruz
WEI *Shengji*, Caltech
WEI *Meng*, WHOI
WEISER *Deborah*, UCLA and USGS
WELDON *Ray*, Oregon
WERNER *Maximilian*, Princeton
WESNOUSKY *Steven*, UNR
WESSON *Rob*, USGS
WHITCOMB *James*, NSF
WICKER *Cary*, CSULB
WILLIAMS *Charles*, GNS Science
WILLIAMS *Patrick*, SDSU
WILLS *Chris*, CGS
WILSON *Rick*, CGS
WITHERS *Kyle*, SDSU
WONG-ORTEGA *Victor Manuel*, CICESE
WOOD *Michele*, CSU Fullerton
WOOD *Rebekah*, Utah State
WU *Wenbo*, U Science & Tech of China
WYATT *Frank*, UCSD
XU *Zhiguo*, China Earthquake Administration
XU *Xiaohua*, UCLA
XU *Shiqing*, USC
XUE *Lian*, UC Santa Cruz
YANG *Wenzheng*, Caltech
YANO *Tomoko*, UCSB
YAO *Huajian*, SIO/UCSD
YE *Lingling*, UC Santa Cruz
YEATS *Robert*, Oregon State
YIKILMAZ *Mehmet*, UC Davis
YODER *Mark*, UC Davis
YONG *Alan*, USGS
YOUNG *Karen*, USC
YU *Ellen*, Caltech
YU *John*, SCEC/USC
YULE *Doug*, CSUN
YUN *Sang-Ho*, JPL
ZALIAPIN *Ilya*, UNR

ZANZERKIA *Eva*, NSF
ZAREIAN *Farzin*, UC Irvine
ZECHAR *Jeremy*, ETH Zurich
ZENG *Yuehua*, USGS
ZHAN *Zhongwen*, Caltech
ZHANG *Panxu*, USC
ZHOU *Jun*, SDSC